




ADVERTIMENT. L'accés als continguts d'aquesta tesi queda condicionat a l'acceptació de les condicions d'ús establertes per la següent llicència Creative Commons:  http://cat.creativecommons.org/?page_id=184

ADVERTENCIA. El acceso a los contenidos de esta tesis queda condicionado a la aceptación de las condiciones de uso establecidas por la siguiente licencia Creative Commons:  <http://es.creativecommons.org/blog/licencias/>

WARNING. The access to the contents of this doctoral thesis it is limited to the acceptance of the use conditions set by the following Creative Commons license:  <https://creativecommons.org/licenses/?lang=en>

Increasing biomass production in bioreactors applying metabolic analysis and engineering tools

Pere Comas Sanchez

Universitat Autònoma de Barcelona

Department of Chemical, Biological and Environmental
Engineering

December 2020



Supervisors:

Jordi Joan Cairó Badillo
Iván Martínez Monge
Antoni Casablanques Mira

JORDI JOAN CAIRÓ BADILLO, professor titular del Departament d'Enginyeria Química de la Universitat Autònoma de Barcelona, ANTONI CASABLANCAS MIRA, Tècnic superior de suport a la recerca de la Universitat Autònoma de Barcelona i IVÁN MARTÍNEZ MONGE, Postdoc at The Novo Nordisk Foundation Center for Biosustainability (Technical University of Denmark).

CERTIFIQUEM:

Que el graduat Pere Comas Sanchez ha dut a terme sota la nostra direcció, en els laboratoris del Departament d'Enginyeria Química, Biològica i Ambiental de la Universitat Autònoma de Barcelona, el treball que, amb el títol de "Increasing biomass production in bioreactors applying metabolic analysis and engineering tools", es presenta en aquesta memòria, la qual constitueix la seva Tesi per optar al grau de Doctor en Biotecnologia.

I perquè en prengueu coneixement i tingui els efectes que corresponguin, presentem davant de l'Escola de Doctorat de la Universitat Autònoma de Barcelona l'esmentada Tesi signada aquesta certificació a

Bellaterra, Desembre de 2020

Jordi Joan Cairó Badillo

Iván Martínez Monge

Antoni Casablanças Mira

Summary.....	1
Resumen.....	8
Resum.....	16

Chapter 1. Overall introduction

1.1	Biotechnology and red biotechnology.....	23
1.2	Bioprocess engineering and volumetric productivity.....	30
1.3	Physiology and Metabolism.....	31
1.4	Bioprocess design.....	41
1.4.1	Bioprocess strategies.....	44
1.4.2	Bioreactor.....	48
1.5	System biology and Omics.....	49
1.6	Genome-scale metabolic models as example of fluxomics.....	52
1.7	References.....	55

<u>Chapter 2. Objectives</u>	61
---	----

Chapter 3. Physiology and metabolism of *Escherichia coli*

3.1	Nomenclature.....	63
3.2	Introduction.....	64
3.3	Results (I) – Analysis and modelling of <i>E. coli</i> M15 (K cell line): glucose/acetate metabolism in batch culture	
3.3.1	Experiment in batch culture with the <i>E. coli</i> M15.....	65
3.3.2	Study of <i>E. coli</i> M15 carbon metabolism by means of metabolic flux balance analysis.....	68
3.3.3	Study of <i>E. coli</i> M15 Energy metabolism by means of use of a metabolic model.....	71
3.4	Results (II) - Analysis and modelling of <i>E. coli</i> BL21 (B cell line): glucose/acetate metabolism in batch and continuous cultures	
3.4.1	Experiment in batch culture with <i>E. coli</i> BL21.....	74
3.4.2	Study of <i>E. coli</i> BL21 carbon metabolism by means of the use of a metabolic model.....	76

3.4.3	Study of <i>E. coli</i> BL21 energy metabolism by means of the use of a metabolic model.....	79
3.5	Results (III) - Metabolic Model Comparison between <i>E. coli</i> BL21 and <i>E. coli</i> M15: carbon metabolism.....	80
3.6	Results (IV) - Metabolic Model Comparison between <i>E. coli</i> BL21 and <i>E. coli</i> M15: energy metabolism.....	84
3.7	Results (V) – Analysis and modelling of continuous cultures in <i>E. coli</i> BL21.....	88
3.7.1	Metabolic Model Comparison between each stationary states: carbon metabolism.....	95
3.7.2	Metabolic Model Comparison between each stationary states: energy metabolism.....	99
3.8	Discussion and Conclusions.....	103
3.9	Materials and Methods.....	105
3.10	References.....	116

Chapter 4. Physiology and metabolism of *Saccharomyces cerevisiae*

4.1	Nomenclature.....	120
4.2	Introduction.....	121
4.3	Results (I) - Analysis and modeling the carbon metabolism of <i>S. cerevisiae</i> : glucose /ethanol metabolism and Crabtree Effect in batch cultures	
4.3.1	Experiment in batch culture with <i>S. cerevisiae</i>	123
4.3.2	Study of <i>S. cerevisiae</i> carbon metabolism by means of Flux Balance Analysis.....	126
4.3.3	Study of <i>S. cerevisiae</i> energy metabolism by means Flux Balance Analysis.....	130
4.4	Results (II) - Analysis and modeling the carbon metabolism of <i>Pichia pastoris</i> : glucose metabolism in aerobic batch cultures.	
4.4.1	Experiment in batch culture with <i>P. pastoris</i>	133
4.4.2	Study of <i>P. pastoris</i> carbon metabolism by means of FBA.....	136
4.4.3	Study of <i>P. pastoris</i> energy metabolism by means of use of a metabolic model.....	139
4.5	Results (III) - Metabolic comparison between <i>S. cerevisiae</i> and <i>P. pastoris</i> – carbon metabolism models.....	141
4.6	Results (IV) - Metabolic comparison between <i>S. cerevisiae</i> and <i>P. pastoris</i> – energy metabolism model.....	147

4.7	Results (V) - Analysis and modelling of <i>S. cerevisiae</i> in continuous glucose-based media cultures.....	152
4.7.1	Metabolic comparison between steady states regarding the carbon metabolism.....	159
4.7.2	Energetic Metabolism Comparison between the different steady states - ATP distribution.....	163
4.8	Discussion and conclusions.....	167
4.9	Materials and Methods.....	170
4.10	References.....	180

Chapter 5. Physiology and metabolism of animal cells

5.1	Nomenclature.....	184
5.2	Introduction.....	185
5.3	Results (I) - Analysis of the physiological parameters for HEK293 and hybridoma KB26.5 when glucose is used as a carbon source.	
5.3.1	HEK293.....	187
5.3.2	Hybridoma KB26.5.....	189
5.4	Results (II) - Description of the HEK293 and hybridoma KB26.5 carbon metabolism by means of metabolic models.....	191
5.4.1	HEK293.....	191
5.4.2	Hybridoma KB26.5.....	196
5.5	Results (III) - Reason behind the lactate production in HEK293 and hybridoma KB26.5 and its difference.	
5.6	Results (IV) - Reducing the lactate production in both cell lines.....	203
5.6.1	Reducing the lactate production by means of changing the carbon source.	205
5.6.2	Metabolic comparison of HEK293 cultured on glucose, fructose and fructose supplemented with lactate.....	226
5.6.3	Reducing the lactate production by means of expressing an anti-apoptotic gen (BHRF1) using hybridoma KB26.5.....	235
5.6.4	Metabolic model comparison between hybridoma KB26.5 and hybridoma KB26.5 – BHRF1.....	244
5.7	Discussion and conclusions.....	251
5.8	Materials and Methods.....	254
5.9	References.....	260

Chapter 6. From metabolomics to bioprocess definition

6.1.	The “shared” metabolism.....	264
6.2.	The metabolic and physiologic story.....	265
6.3.	Stepping to bioprocess definition.....	272
6.4.	References.....	274

Chapter 7. *Escherichia coli* bioprocess definition

7.1	Nomenclature.....	275
7.2	Introduction.....	276
7.3	Batch strategies	
7.3.1	Batch.....	278
7.3.2	Fortified Batch.....	282
7.4	Fed batch strategies.....	286
7.4.1	Fed batch based on exponential feeding.....	289
7.4.2	Fed-batch feeding based on CER evolution.....	293
7.4.3	Fed-batch feeding based on alkali buffer addition.....	298
7.4.4	Fed Batch feeding based on non-metabolism related parameter.....	303
7.5	Study of the induction phase of a recombinant protein.....	307
7.5.1	Batch cultures.....	309
7.5.2	Fed-batch induction strategy.....	316
7.6	Discussion and conclusions.....	320
7.7	Materials and Methods.....	323
7.8	References.....	334

Chapter 8. *Saccharomyces cerevisiae* bioprocess definition

8.1	Nomenclature.....	336
8.2	Introduction.....	337
8.3	Results (I) - Batch strategies	
8.3.1	Batch.....	339

8.3.2	Fortified Batch.....	341
8.4	Results (II) - Fed batch strategies.....	346
8.4.1	Fed batch based on exponential feeding.....	348
8.4.2	Fed-batch feeding strategy based on a non-metabolic tool.....	357
8.5	Results (III) - Study of the induction phase of a recombinant protein.....	364
8.5.1	The auxotrophic GFP-producer <i>S. cerevisiae</i>	365
8.6	Discussion and conclusions.....	369
8.7	Materials and methods.....	372
8.8	References.....	382

Chapter 9. Animal cell bioprocess definition

9.1	Nomenclature.....	384
9.2	Introduction.....	385
9.3	Results (I) - Batch culture.....	386
9.4	Results (II) - Fed batch strategy.....	388
9.4.1	Feeding media definition.....	389
9.4.2	Fed batch based on exponential feeding.....	392
9.5	Results (III) - Perfusion strategies.....	401
9.5.1	Perfusion feeding based on OUR monitoring.....	403
9.6	Discussion and conclusions.....	410
9.7	Materials and Method.....	412

Chapter 10. General conclusions and future work

Chapter 11. Appendix

APPENDIX A: <i>E. coli</i> M15 and <i>E. coli</i> BL21 metabolic model.....	432
APPENDIX B: <i>S. cerevisiae</i> metabolic model.....	450
APPENDIX C: <i>P. pastoris</i> metabolic model.....	460
APPENDIX D.: Hybridoma KB26.5 and hybridoma KB26.5-BHRF1 metabolic model.....	470
APPENDIX E: HEK293 metabolic models.....	486

Summary

All the high added-value proteins with both diagnostic and therapeutic applications are produced by expression platforms that can be divided mainly into three groups of organisms: bacteria, yeast and animal cells. The difference between them lays in the cellular capacity to perform complex post-translational modifications in order to produce biologically active proteins. About 60% including monoclonal antibodies, viral vaccines and gene therapy vectors are produced in mammalian cells, due its capacity to produce complex Post-translational Modifications (PtM), while the rest are produced in bacteria or yeast depending on the required PtM. However, even if the use of each expression platform is defined by what product is expressed, all of them share the same bioprocess feature, the volumetric productivity obtained when the protein production is transferred to industrial scale. On this basis, this work is focused on increasing the volumetric productivity of bacteria, yeast and animal cells in bioreactors. In order to do that, several culture methodologies are studied based on their capacity to add carbon source and the main nutrients when it is required and to optimize the carbon conversion towards biomass formation.

In this context, the thesis is divided into two main sections, in order to approach the two main fields that the biotechnology-based industry is directing the current efforts in order to increase the volumetric productivity: the systems biology and the bioprocess engineering. In other words, beginning by understanding the cell metabolism in culture and then using this knowledge to develop new monitoring and controlling systems to improve the processes performance. In addition, the understanding of the metabolism allows the detection of possible genetic modifications, in order to enhance cell lines performance from synthetic biology point of view. Getting deep into the work developed, one of the most important limitations of bacteria, yeast and animal cells is the deregulation of the metabolism in front of different environmental situations, characterized by the consumption of large quantities of substrates and concomitant production of by-products, like acetate in the case of bacteria, ethanol in yeast and lactate in animal cells. The minimization of the by-product production is an issue of a high interest and it has been tackled from a myriad of different approaches. Significant reduction of acetate and ethanol accumulation has been achieved, but it has never been completely avoided without affecting growth rate. Interestingly, we have observed that under certain culture conditions bacteria and yeast are able to regulate the uptake of carbon source while the specific growth rate remained constant. As a result, the carbon conversion towards biomass formation is optimized. In the case of lactate generation for animal cells, a significant reduction has been

achieved, although it has never been completely depleted without modifying the growth rate. However, we have observed that under certain culture conditions mammalian cells are able to co-consume lactate as carbon source along with another secondary carbon source without lactate being produced while the growth was unaffected.

Chapter 1 constitutes an introduction to the overall microorganism-based bioprocesses and the state of the art of bioprocess engineering and systems biology. Afterwards, in **chapter 2** the goals of the thesis are established to focus the results chapters on the challenges declared.

Chapter 3 is centred on the presentation of the glucose and acetate metabolism in cultures of *Escherichia coli* (*E. coli*) M15, as an acetate producer, and *E. coli* BL21, as a non-acetate producer. In order to perform a deeper study of the reasons behind the acetate production, an analysis of the intracellular flux distribution for each strain have been performed by means of Flux Balance Analysis (FBA). FBA shows that, when *E. coli* M15 is compared with *E. coli* BL21, the acetate production is due to the appearance of a carbon flux unbalance between the glycolytic pathway and the Tricarboxylic Acid Cycle (TCA). Specifically, the reaction step that internalizes the acetyl-CoA in the TCA. As a result, acetate is produced to balance the rate between glycolysis and TCA at acetyl-CoA level. In contrast, in the case of *E. coli* BL21, acetate is not produced because all the acetyl-CoA produced is able to be internalized by the TCA. Moreover, it is observed that the glucose consumption of *E. coli* BL21 can be modified while the growth is unaffected and as a result, the conversion of glucose to biomass is optimized when it is cultured using a continuous culture strategy. Thus, this metabolism becomes very interesting from bioprocess point of view, owing to the carbon conversion could be optimize to obtain more biomass with the same amount of substrate.

Chapter 4 is centred on presenting the relation between the glucose metabolism and production of ethanol and glycerol in two yeasts: *S. cerevisiae*, as an ethanol producer, and *P. pastoris*, as a low ethanol producer. In order to perform a deeper study behind the ethanol and glycerol production, the intracellular flux distribution is analysed for each strain by means of Flux Balance Analysis (FBA). The FBA shows that when *S. cerevisiae* is compared with *P. pastoris*, the ethanol production is related to a unbalance in the cytoplasmic redox potential caused by the difference between the flux on top of NADH production from the glycolytic pathway and the mitochondrial shuttles capacity responsible for its regeneration. As a result, ethanol and glycerol are produced to regenerate the cytoplasmic NADH. In the case of *P. pastoris*, the low flux of NADH from the glycolytic pathway is almost regenerated using mitochondrial shuttles and only a small amount

of ethanol is produced. On the contrary, *S. cerevisiae* has a high flux of NADH from glycolytic pathway, which is not able to be regenerated via mitochondrial shuttles. Consequently, the ethanol and glycerol production is required to balance the cytoplasmic NADH. Moreover, a study based on the describing of the relation between the specific consumption rate of glucose and the glucose media availability when *S. cerevisiae* is cultured on continuous strategies. A decrease in the glycolytic pathway's rate is observed that optimize the conversion of glucose to biomass by reducing the ethanol production while glycerol is not produced. As it is mentioned before, this metabolism becomes very interesting from bioprocess point of view, owing to the carbon metabolism became more efficient in regard with the biomass production.

Chapter 5 is centred on describing the lactate metabolism in animal cell cultures of HEK293 and hybridoma KB26.5, two cell lines widely used in the industry. Lactate is the main by-product of glucose metabolism, representing since 90% of the glucose consumed. In order to perform a deeper study of the glucose conversion to lactate, an analysis of the intracellular flux distribution has been performed for both cell lines through using the FBA methodology. FBA demonstrates that lactate is produced due to an unbalance in the cytoplasmic redox potential caused by the difference between the flux of NADH from the glycolytic pathway and the flux of NADH regenerated from mitochondrial shuttles. Afterwards, the reduction of the glucose conversion is carried out based on two approaches: via changing the carbon source or via genetic modification.

It is observed that when HEK293 consumes fructose instead of glucose, the lactate production is avoided, although, the growth is affected. However, the supplementation of lactate to fructose-based media is able to provide the amount of carbon required for obtaining the same growth observed in the glucose-based media. Therefore, it was possible the completely elimination of lactate while the growth remains unaffected.

In relation with hybridoma KB26.5, the consumption of other carbon source is not accomplished because hybridoma KB26.5 can solely grow on glucose-based media. However, it is possible to reduce the lactate production through genetic modification by means of the expression of the anti-apoptotic gene BHRF1. In addition to the antiapoptotic effect, its expression provokes the improvement of both the growth and the conversion of glucose to biomass.

In **chapter 6**, an overall hypothesis of the metabolic traits observed in bacteria, yeast and animal cells is developed in order to have a “bridge” between metabolism studies and bioprocess definition. In respect to acetate production in bacteria, it is proposed that the carbon unbalance observed between glycolysis and TCA is related to the biochemical evolution from anaerobiosis

to aerobiosis in ancient bacteria. These ancient bacteria were anaerobic heterotrophs that were capable to evolve to heterotrophs aerobics by addition of TCA to glycolysis. The coexistence of both metabolisms in the same cell provokes the carbon unbalance because the carbon rates and energy generation in both pathways is quite different.

Regarding yeast and animal cells ethanol and lactate generation, it is proposed that all the metabolic unbalances in redox metabolism observed in those cases are related to the evolutionary formation of the Eukarya domain. Although several theories explain the formation of Eukarya domain, in this work the endosymbiotic one is used. It exposes that the formation of the first mitochondria-based microorganism is related to the endosymbiosis of two bacteria whose carbon consumption rates are different. The resulting microorganism of the endosymbiosis, due to the metabolic characteristics of its predecessors, expresses both metabolisms at the same time. Consequently, a redox unbalance in the union point between both metabolisms should be observed.

Regarding yeast and animal cells, the formation of the first eukaryote (based on the endosymbiosis of two microorganism, one of them was the predecessor of a mitochondria) can explain both the ethanol and glycerol metabolism in yeast and the lactate metabolism in animal cells. Each of them is the result of the cell compartmentalization and the difference in carbon consumption rate for both predecessors. Considering this, the cytoplasmic NADH unbalance caused by a high glucose consumption and a restriction in the mitochondrial shuttles when ethanol, glycerol and lactate are produced can be explained.

Furthermore, using the evolution theory, it can be state that the continuity of living beings over the time is related to its interaction with the environment and its capacity to change the environmental conditions and adapt to them.

Lastly, the biomass optimization in bioprocesses that consists on changing the interaction between the environment and the microorganism is proposed. This optimization is based on the description of the carbon metabolism related to all the selected microorganisms. Therefore, it is used to design bioprocess strategies whose main aim is to increase the volumetric productivity via increasing the biomass concentration. In connection with bioprocess development and optimization, fed-batch and perfusion cultures are generally considered more attractive choices for the industry than batch processes. However, the efficient application of these processes requires the availability of reliable on-line measuring systems for cell density and cell metabolic activity estimation. To this end, several on-line monitoring tool are developed based on the estimation of a biomass profile by means of the monitoring of physiological variables.

In **chapter 7**, the definition of a culture strategy whose aim is to increase the biomass concentration of the *E. coli* BL21 is described. First, the description of a batch culture as a reference is carried out. Secondly, to increase the biomass obtained, a fortification media is developed from the reference media. As a result, the biomass is increased by 2,48-fold, although the addition of maximum available carbon source is accomplished. Lastly, to further increase the biomass concentration, fed-batch strategies are developed. The study analyses five feeding algorithms that use the optimal conversion of glucose to biomass determined in **chapter 3** in order to calculate the optimal feeding profile.

The first fed-batch used as a reference is based on a theoretical exponential growth to calculate the feeding profile. As a result, the biomass concentration increased by 5,75-fold. However, a growth limitation due to the underestimation of the optimal feeding profile is observed. The error in the feeding profile is caused by the difference between the experimental biomass profile and the theoretical one. In order to solve this problem; the next three feeding profiles are developed based on the relation between a physiological parameter and the carbon metabolism in order to predict the biomass concentration:

- A relation between the buffer alkali addition caused by from compounds that are products or substrate in relation with the carbon metabolism.
- A relation between the Oxygen Uptake Rate (OUR) and the oxygen consumed as the electron acceptor in the carbon metabolism.
- A relation between the Carbon Evolution Rate (CER) and the carbon dioxide produced by the oxidation of the carbon source via the carbon metabolism.

At early stages of fed-batch, the three proposed feeding profiles follow the biomass concentration. However, the unpredictable changes in the carbon metabolism during the mid and late phases of the fed-batch provoke both the underestimation of the biomass concentration and underestimation or overestimation of the feeding profile. This error is explained by the fact that the feeding profile requires metabolic parameters for its calculation and they are supposed to be constant during the course of the experiment. As it is observed, those parameters are not constant during the fed-batch phase. Therefore, in order to overcome the incapacity to predict the metabolic behaviour, a feeding algorithm that is not based on the estimation of the biomass or the usage of a metabolic parameter is developed. As a result, the biomass concentration increase by 5,37-fold, while *E. coli* BL21 grow at the optimal rate.

Moreover, in order to test this new feeding profile, a fed-batch strategy with an induction phase of a model recombinant protein is carried out. The idea behind this procedure is to observe if the variation induced by the inconstancy of the carbon metabolism during the induction phase, can be followed by the new algorithm. Therefore, the new methodology is tested in the worst conditions possible: the production of a recombinant GFP via IPTG induction. The fed-batch with an induction phase is carried out and the feeding profile is available to satisfy the carbon requirements during the growth and induction phase without limiting the growth rate.

In **chapter 8**, the definition of a culture strategy whose aim is to increase the biomass concentration of the *S. cerevisiae* is described. First, the description of a batch culture as a reference is carried out. In order to increase the biomass obtained, a fortification media is developed. As a result, the biomass is increased by 3,43-fold. Afterwards, fed-batch strategies are developed to further increase the biomass concentration. Due to the conclusions obtained in relation with the feeding profiles developed in **chapter 7**, this study analyses a fed-batch that is based on a theoretical exponential growth in order to determine if the metabolic parameters can be maintained during the feeding addition. Moreover, the optimal conversion of glucose to biomass determined in **chapter 4** is used in the calculation of the feeding profile.

It is observed that during the fed-batch phase the metabolic parameters are changing depending on environmental conditions. On this basis, the next fed-batch strategy carried out is the one that does not use the estimation of the biomass concentration or metabolic parameters. Regarding the other feeding profiles, they are discarded due to the fact that it makes no sense using a feeding profile that solely can adjust to the carbon requirement in the early stages of the fed-batch strategy. Due to the appearance of growth inhibition conditions at the last stage in the two fed-batch done, the fortification strategy and the fed-batch strategy achieve the same biomass concentration. However, the use of fed-batch strategies decrease the carbon conversion towards ethanol by 50 % because the metabolic data from **chapter 4** is used to calculate the feeding profile.

Moreover, the induction of a model protein during a fed-batch strategy is proposed. In contrast with what is made in **chapter 7**, the protein is produced using an auxotrophic marker with *S. cerevisiae* expressing several auxotrophies instead of an antibiotic selection marker. Due to a growth limitation observed in the auxotrophic *S. cerevisiae* in comparison with the wild type strain, this specific work is closed. The alternative proposed is based on expressing the GFP on a *S. cerevisiae* wild type that is selected by an antibiotic; although it is not further developed.

In **chapter 9**, the definition of a culture strategy whose aim is to increase the biomass concentration of hybridoma KB26.5-BHRF1 is described. First, the description of a batch culture as a reference is carried out. To increase the biomass obtained, fed-batch strategies are developed. This study analyses a fed-batch that is based on a theoretical exponential growth in order to determine if the metabolic parameters can be maintained during the feeding addition. As a result, the biomass is increased by 1,43-fold. Principally, two facts are observed during the fed-batch phase: a growth inhibition that take place during the fed-batch phase and the variation of the metabolic parameters depending on the environmental conditions. On this basis, to further increase the biomass concentration, the next strategy carried out is a perfusion strategy that assures constant environmental conditions while the growth inhibitors are retired from the culture's media. As a result, the inhibition conditions are avoided and the biomass concentration is increased by 6,46-fold.

Substantial contributions have been made in both systems biology and bioprocess engineering. However, this thesis intended to be and starting point to better understand the cell metabolism to further be applied in bioprocess development. To this end, **chapter 10** has been included with the aim of wrapping up the general conclusions of the thesis and the future work that could be interesting to carry out.

Resumen

Todas las proteínas de alto valor añadido con aplicaciones tanto diagnósticas como terapéuticas, son producidas por plataformas de expresión que se pueden dividir en tres grupos principales de organismos: bacterias, levaduras y células animales. La diferencia entre ellas radica en la capacidad celular de realizar complejas modificaciones post-traduccionales para producir proteínas biológicamente activas. Alrededor del 60% de todos los biofármacos - incluidos los anticuerpos monoclonales, las vacunas virales y los vectores de la terapia génica - se producen en las células de mamíferos debido a su capacidad de producir complejas modificaciones post-traduccionales (PtM). El 40 % restante es producido por bacterias y levaduras dependiendo de la complejidad de la PtM deseada. Sin embargo, aunque el uso de cada plataforma está definido por el producto expresado, todos ellos comparten la misma problemática en relación con su producción a escala industrial. Dependen de la productividad volumétrica obtenida en su bioproceso y de la capacidad específica de la plataforma para producir la proteína deseada y la biomasa alcanzada. En este caso, mi trabajo se centra en el aumento de la concentración de biomasa obtenida al final del proceso mediante la capacidad de añadir una fuente de carbono cuando sea necesario y de optimizar la conversión de carbono hacia la formación de biomasa.

Sobre esta base, la tesis presentada se centra en mejora de la productividad volumétrica de cultivos de bacterias, levaduras y células animales en bioreactores. En este contexto, con el objetivo de acercarse a los dos campos en los cuales la industria de base biotecnológica está dirigiendo gran parte de los esfuerzos actuales para aumentar la productividad de los bioprocesos, la tesis se divide en dos secciones principales: la biología de sistemas y la ingeniería de bioprocesos. Se empezó por la comprensión del metabolismo del carbono y nutrientes principales, utilizando luego este conocimiento para desarrollar nuevos sistemas de monitoreo y control para mejorar el rendimiento de los procesos. Además, la comprensión del metabolismo del carbono permite detectar posibles modificaciones genéticas para mejorar las líneas celulares desde el punto de vista de la biología sintética.

Profundizando en el trabajo desarrollado, una de las limitaciones más importantes del mismo es el ineficiente metabolismo de las bacterias, levaduras y células animales, caracterizado por el gran consumo de grandes cantidades de carbono y la producción concomitante de cantidades similares de subproductos metabólicos, como el acetato en el caso de las bacterias, el etanol en relación con la levadura y el lactato en lo que respecta a las células animales. La minimización de la producción subproductos es una cuestión de gran interés y se ha abordado desde una

multitud de enfoques diferentes. Se ha logrado una reducción significativa de la acumulación de acetato y etanol, pero nunca se ha suprimido por completo en las células en crecimiento sin cambiar la tasa de crecimiento específica o mediante modificaciones genéticas. Curiosamente, hemos observado que bajo ciertas condiciones de cultivo las bacterias y la levadura son capaces de regular la absorción de la fuente de carbono, mientras que la tasa de crecimiento específico se mantiene constante. Como resultado se reduce la producción de subproductos.

En el caso del lactato en células animales se ha logrado una reducción significativa, pero nunca se ha agotado completamente sin modificar el crecimiento. Curiosamente, hemos observado que bajo ciertas condiciones de cultivo las células de los mamíferos son capaces de co-consumir una fuente de carbono junto con un ácido orgánico sin que el crecimiento se vea afectado.

El **capítulo 1** constituye una introducción a los bioprocesos generales basados en microorganismos y al “state of the art” tanto en ingeniería de bioprocesos como en biología de sistemas. Posteriormente, en el **capítulo 2** se establecen los objetivos de la tesis para centrar los capítulos de resultados en los desafíos declarados.

El **capítulo 3** se centra en la presentación de los diferentes metabolismos de la glucosa y el acetato en los cultivos de *Escherichia coli* (*E. coli*) M15, como productor de acetato, y de *E. coli* BL21, como no productor de acetato. Con el fin de profundizar en las razones de la producción de acetato, se ha realizado un análisis de la distribución del flujo intracelular de cada cepa mediante el análisis de equilibrio de flujo (FBA). El FBA demostró que, cuando se comparó *E. coli* M15 con *E. coli* BL21, la producción de acetato se produjo debido a un desequilibrio de carbono en el paso de la reacción entre la vía glicolítica y el Ciclo de los Ácidos Tricarboxílicos (TCA). Específicamente, en la reacción del acetil-CoA en el TCA. Como resultado se produce acetato para equilibrar el exceso de carbono en la glicolisis respecto de la velocidad del TCA. En el caso de *E. coli* BL21, esta es capaz de internalizar todo el acetil-CoA producido al presentar un flujo glicolítico menor y un flujo en el TCA mayor.

Además, utilizando estudios de cultivo en continuo, donde se comprueban varias disponibilidades de glucosa, se demuestra que *E. coli* BL21 es capaz de modificar el consumo de glucosa mientras que el crecimiento no es afectado. En consecuencia, la conversión de la glucosa en biomasa se es optimizado. Así, este metabolismo se vuelve muy interesante desde el punto de vista de los bioprocesos, debido a que la conversión de carbono podría ser optimizada para obtener más biomasa con la misma cantidad de sustrato.

El **capítulo 4** trata de la presentación de la relación entre el metabolismo de la glucosa y la producción de etanol en los cultivos de *S. cerevisiae*, como productor de etanol y de *P. pastoris*, como productor de bajo nivel de etanol. Para estudiar más a fondo las causas de la producción de etanol, se analiza la distribución del flujo intracelular de cada cepa mediante el método Flux Balance Analysis (FBA). El FBA demuestra que cuando se compara *S. cerevisiae* con *P. pastoris*, El etanol se produce a causa de un desequilibrio en el potencial redox citoplasmático causado por la diferencia entre el flujo de NADH procedente de la vía glicolítica y la capacidad de las lanzadoras mitocondriales para regenerarlo. Como resultado, el etanol y el glicerol se producen para equilibrar el NADH citoplasmático. En el caso de *P. pastoris*, el flujo limitado de NADH procedente de la vía glicolítica casi se regenera completamente mediante las lanzaderas mitocondriales y solo se requiere una pequeña formación de etanol. Hay que tener en cuenta que *S. cerevisiae* tiene un alto flujo a través de la vía glicolítica que no puede ser regenerado por medio de las lanzaderas mitocondriales, en consecuencia, la producción de etanol y glicerol es necesaria para equilibrar el NADH citoplasmático. Además, en un estudio en *S. cerevisiae* basado en comprender la relación entre el consumo de glucosa y su disponibilidad en el medio de cultivo, se ha observado una disminución del flujo de carbono procedente de la vía glicolítica que, como consecuencia, optimiza la formación de biomasa gracias a la reducción del etanol producido mientras que no se genera glicerol. Como se menciona con anterioridad, este metabolismo se vuelve muy interesante desde el punto de vista de los bioprocesos, debido a que el metabolismo del carbono se hizo más eficiente en lo que respecta a la producción de biomasa.

El **capítulo 5** se centra en la presentación de los metabolismos del lactato cuando se utiliza la glucosa como fuente de carbono en los cultivos de la línea humana HEK293 y del hibridoma murino KB26.5, dos líneas celulares muy utilizadas en la industria biotecnológica.

El lactato es el subproducto principal del metabolismo de la glucosa, llegando a representar hasta un 90% de la glucosa consumida. Con el fin de realizar un estudio más profundo de la conversión de la glucosa en lactato, se realiza un análisis de la distribución del flujo intracelular para las diferentes fases en ambas líneas celulares mediante la metodología FBA. Esta demuestra que el lactato se produce a causa de un desequilibrio en el potencial redox citoplasmático causado por la diferencia entre el flujo de NADH procedente de la vía glicolítica y el flujo de NADH regenerado a partir de las lanzaderas mitocondriales. A continuación, la reducción de la conversión de glucosa en lactato se toma como objetivo basándonos en dos frentes: un cambio en la fuente de carbono o llevar a cabo modificaciones genéticas.

Se observa que cuando HEK293 crece utilizando fructosa en lugar de glucosa, no hay generación de lactato, aunque se obtiene una reducción en el crecimiento. Por otro lado, al suplementar la fructosa con un ácido orgánico como el propio lactato no se obtiene reducción del crecimiento y se evita la generación de lactato. Por lo tanto, se consigue la eliminación total del lactato mientras que el crecimiento no se ve afectado.

En relación con el hibridoma KB26.5, el consumo de otra fuente de carbono no se consigue puesto que esta solo puede crecer utilizando la glucosa como fuente de carbono. Sin embargo, es posible reducir la producción de lactato mediante modificaciones genéticas como, por ejemplo, la expresión de un gen anti-apoptótico, el gen BHRF1. Además de su efecto anti-apoptótico, la expresión de este gen provoca mejoras en el crecimiento y en la conversión de los sustratos en biomasa. Además, el uso del hibridoma KB26.5 que expresa BHRF1 en estrategias de bioproceso es un punto muy interesante ya que presenta una mejora en el crecimiento a la vez que una reducción en la producción de lactato.

En el **capítulo 6**, se desarrolla una hipótesis global sobre los rasgos metabólicos observados en bacterias, levaduras y células animales para establecer un "puente" entre los estudios de metabólico y la definición de bioprocesos. Respecto a la producción de acetato en bacterias, se hipotetiza que el desbalance observado de carbono entre glicólisis y TCA se debe buscar en la evolución bioquímica de los organismos anaerobios heterótrofos hacia un metabolismo aerobio heterótrofo, mucho más eficiente y por la coincidencia de ambos dentro de las bacterias, hecho que provoca frente a altas concentraciones de sustratos carbonados el desbalance entre TCA y glicolisis.

Respecto a la producción de etanol por levaduras y lactato en células animales, en ambos casos se propone que todos los desequilibrios metabólicos en el balance redox celular observados están relacionados con la formación del dominio Eukarya. A pesar de que varias teorías explican la formación del dominio Eukarya, en este trabajo se utiliza la endosimbiótica. Esta expone que la formación del primer microorganismo basado en mitocondrias está relacionada con la endosimbiosis de dos bacterias con diferentes consumos de carbono. El microorganismo resultante de la endosimbiosis, a causa de las características metabólicas de sus predecesores, contiene los dos metabolismos a la vez. En consecuencia, se observa un desequilibrio redox en el punto de unión entre ambos metabolismos.

En la levadura y las células animales, la formación del primero eucarionte (basada en el endosimbiosis de dos microorganismos, uno de los cual era el antecesor de la mitocondria) puede explicar tanto el metabolismo del etanol y el glicerol en la levadura como el metabolismo del lactato en las células animales. Cada uno de ellos es el resultado de la compartimentalización de las células y de la diferencia en el consumo de carbono de los dos predecesores. Teniendo en cuenta esto, se puede explicar el desequilibrio citoplasmático de NADH causado por un elevado consumo de glucosa y una restricción a las lanzaderas mitocondriales cuando se producen etanol, glicerol y lactato.

Además, utilizando la teoría de la evolución, se puede afirmar que la continuidad de los seres vivos a lo largo del tiempo está relacionada con su interacción con el medio ambiente y su capacidad para cambiar las condiciones ambientales y adaptarse a ellas.

Por último, se propone la optimización de la biomasa en bioprocesos que consiste a cambiar la interacción entre el entorno y el microorganismo. Esta optimización se basa en la descripción del metabolismo del carbono de todos los microorganismos seleccionados. Por lo tanto, se utiliza para diseñar estrategias de bioproceso que tienen como principal objetivo aumentar la productividad volumétrica a través del aumento de la concentración de biomasa. En relación con el desarrollo y la optimización de bioprocesos, los fed-batch y las perfusiones generalmente se consideran opciones más atractivas para la industria que los procesos en batch. Sin embargo, la aplicación eficiente de estos procesos requiere la disponibilidad de sistemas de medida en línea fiables para la estimación de la densidad celular y la actividad metabólica de las células. Para lo cual, se desarrollan varias herramientas de control en línea basadas en la estimación de un perfil de biomasa a través del seguimiento variables fisiológicas.

En el **capítulo 7**, se describe el diseño de una estrategia de cultivo utilizando *E. coli* BL21 que tiene como objetivo aumentar la concentración de biomasa. En primer lugar, se realiza la descripción de un batch de referencia. En segundo lugar, para aumentar todavía más la biomasa obtenida, se desarrolla un medio fortificado a partir del medio de referencia. Como resultado, la biomasa se incrementa 2,48 veces, a pesar de que se llega a la máxima adición disponible de la fuente de carbono. Finalmente, para aumentar todavía más la concentración de biomasa, se desarrollan estrategias en fed-batch. El estudio analiza cinco algoritmos de alimentación que utilizando la conversión óptima de glucosa en biomasa determinada en el **capítulo 3** para calcular el perfil de alimentación óptimo.

El primero fed-batch utilizado como referencia se basa en un crecimiento exponencial teórico para calcular el perfil de alimentación. Como resultado, la concentración de biomasa aumenta en un 5,75 veces. Aun así, se observa una limitación del crecimiento a causa de la subestimación

del perfil de alimentación óptimo. El error en este perfil es causado por la diferencia entre el perfil experimental de biomasa y el teórico. Para resolver este problema, se desarrollan los siguientes tres perfiles de alimentación basados en la relación entre un parámetro fisiológico y el metabolismo del carbono para predecir la concentración de biomasa:

- Una relación entre la adición de base causada por compuestos que son productos o sustratos relacionados con el metabolismo del carbono.
- Una relación entre la Oxygen Uptake Rate (OUR) y el oxígeno consumido como aceptor de electrones en el metabolismo del carbono.
- Una relación entre la Carbon dioxide Evolution Rate (CER) y el dióxido de carbono producido por la oxidación de la fuente de carbono mediante el metabolismo del carbono.

En las primeras etapas del fed-batch, los tres perfiles de alimentación desarrollados siguen la concentración de biomasa, debido a los cambios imprevisibles en el metabolismo del carbono durante las fases mediana y tardía del fed-batch la concentración de biomasa es subestimada conjuntamente con la subestimación o sobrevaloración del perfil de alimentación. Este error se explica por el hecho que el perfil de alimentación requiere parámetros metabólicos por su cálculo y se supone que son constantes durante el transcurso del experimento. Sin embargo, tal como se observa, estos parámetros no son constantes durante el fed-batch.

Por lo tanto, para superar la incapacidad de predecir el comportamiento metabólico, se desarrolla un algoritmo de alimentación que no se basa en la estimación de la biomasa ni en el uso de un parámetro metabólico. Como resultado, la concentración de biomasa aumenta 5,37 veces, mientras que *E. coli* BL21 crece a su velocidad óptima.

Además, para probar este nuevo perfil de alimentación, se lleva a cabo un fed-batch con fase de inducción de una proteína recombinante modelo. La idea detrás de este procedimiento es observar si la variación inducida por la inconstancia del metabolismo del carbono durante la fase de inducción puede ser seguida por el nuevo algoritmo. Por lo tanto, se prueba la nueva metodología en las peores condiciones posibles: la producción de una proteína modelo - GFP recombinante - mediante inducción IPTG. Se realiza el fed-batch con fase de inducción y el perfil de alimentación está capaz de satisfacer las necesidades de carbono durante la fase de crecimiento y también de inducción sin limitar el crecimiento.

En el **capítulo 8** se describe la definición de una estrategia de cultivo que tiene como objetivo aumentar la concentración de biomasa de *S. cerevisiae*. En primer lugar, se realiza un de un batch de referencia. Para incrementar todavía más la biomasa obtenida, se desarrolla un medio

de fortificación basado en el medio del batch. Como resultado, la biomasa se incrementa 3,43 veces. Posteriormente, se desarrollan estrategias fed-batch para aumentar todavía más la concentración de biomasa. A causa de las conclusiones obtenidas en relación con los perfiles de alimentación desarrollados al **capítulo 7**, este estudio analiza un fed-batch que se basa en un crecimiento exponencial teórico para determinar si se pueden mantener los parámetros metabólicos durante la alimentación. Además, la conversión óptima de glucosa en biomasa determinada al **capítulo 4** se utiliza en el cálculo del perfil de alimentación.

Se observa que durante la fase fed-batch que los parámetros metabólicos cambian en función de las condiciones ambientales. Sobre esta base, el siguiente fed-batch que se realiza es el que no utiliza la estimación de la concentración de biomasa ni de los parámetros metabólicos. En cuanto al resto de perfiles de alimentación, se descartan por el hecho que no tiene sentido utilizar un perfil de alimentación que solo se pueda ajustar a las demandas de carbono en las primeras etapas de un fed-batch. A causa de la aparición de condiciones de inhibición del crecimiento en la última etapa de los dos fed-batch realizados, la estrategia de fortificación y la estrategia fed-batch consiguen la misma concentración de biomasa. Sin embargo, el uso de estrategias fed-batch reduce la conversión de carbono a etanol en un 50%, ya que los datos metabólicos del **capítulo 4** se utilizan para calcular el perfil de alimentación.

Además, se propone la inducción de una proteína modelo durante una estrategia fed-batch. Al contrario del que se lleva a cabo al **capítulo 7**, la proteína se produce mediante un marcador auxotrófico con *S. cerevisiae* expresando distintas auxotrofías en lugar de un antibiótico. A causa de una limitación de crecimiento observada en el *S. cerevisiae* auxotrófico en comparación con el wildtype, este trabajo se detiene. Pero, se propone una alternativa basada al expresar la GFP en un *S. cerevisiae* wildtype que es seleccionado por un antibiótico como marcador de selección; a pesar de que solo se llega a plantear la estrategia a seguir.

En el **capítulo 9**, se describe la definición de una estrategia de cultivo que tiene como objetivo aumentar la concentración de biomasa en cultivos de una célula animal murina, el hibridoma KB26.5-BHRF1. Para empezar, se realiza la descripción de un batch de referencia. Para aumentar todavía más la biomasa obtenida, se desarrollan estrategias fed-batch. En este estudio se analiza un fed-batch basado en un crecimiento exponencial teórico para determinar si se pueden mantener los parámetros metabólicos durante el periodo de alimentación. Como resultado, la biomasa aumenta 1,43 veces. Principalmente, se observan dos hechos durante la fase fed-batch: una inhibición del crecimiento que tiene lugar durante la fase fed-batch y la variación de los parámetros metabólicos en función de las condiciones ambientales. Sobre esta base, para aumentar todavía más la concentración de biomasa, la siguiente estrategia realizada es una

estrategia de perfusión que asegura condiciones ambientales constantes mientras los inhibidores del crecimiento se retiran del medio de cultivo. Como resultado, se evitan las condiciones de inhibición y se incrementa la concentración de biomasa 6,46 veces.

Se han hecho contribuciones sustanciales tanto en biología de sistemas como en ingeniería de bioprocesos. Aun así, esta tesis pretendía ser el punto de partida para entender mejor el metabolismo celular para aplicarlo en el desarrollo de bioprocesos. Finalmente, se ha incluido el **capítulo 10** con el objetivo de resumir las conclusiones generales de la tesis y el trabajo futuro que podría ser interesante llevar a cabo.

Resum

Totes les proteïnes d'alt valor afegit amb aplicacions tant diagnòstiques com terapèutiques es produeixen utilitzant plataformes d'expressió que es poden dividir en tres grups principals de microorganismes: bacteris, llevats i cèl·lules animals. La diferència entre ells recau en la capacitat cel·lular de realitzar modificacions post-traduccionals per produir proteïnes biològicament actives. Al voltant del 60%, inclosos anticossos monoclonals, vacunes víriques i vectors de teràpia gènica, es produeixen en cèl·lules de mamífers a causa de la seva capacitat de produir complexes modificacions post-traduccionals (PtM). Mentre que el 40 % restant es produeixen en bacteris o llevats en funció de les PtM requerides. Encara que l'ús cada plataforma d'expressió es defineix pel producte que s'expressa, tots comparteixen la mateixa característica, la productivitat volumètrica obtinguda quan la producció de proteïnes es trasllada a escala industrial.

Sobre aquesta base, aquest treball es centra en augmentar la productivitat volumètrica de cultius de bacteris, llevats i cèl·lules animals. Per dur-ho a terme, s'estudien diverses metodologies de cultiu en funció de la seva capacitat per afegir la font de carboni i els nutrients principals quan es requereix i per optimitzar la conversió de carboni cap a la formació de biomassa.

En aquest context, la tesi es divideix en dues seccions principals per abordar els dos camps principals que la indústria biotecnològica està dirigint gran part dels esforços actuals per tal d'augmentar la productivitat volumètrica dels bioprocessos: la biologia de sistemes i l'enginyeria dels bioprocessos. En altres paraules, començant per entendre el metabolisme cel·lular i després utilitzant aquest coneixement per desenvolupar nous sistemes de control i monitorització per millorar-ne el rendiment. A més, la comprensió del metabolisme permet detectar possibles modificacions genètiques per tal de millorar els microorganisme emprats.

Aprofundint en el treball, una de les limitacions més importants de bacteris, llevats i cèl·lules animals és el seu metabolisme ineficient, caracteritzat pel gran consum de quantitats de substrats i la producció concomitant de subproductes, com l'acetat en el cas dels bacteris, l'etanol en els llevats i el lactat en cultius de cèl·lules animals. La minimització de la producció subproductes és un tema d'alt interès i s'ha abordat des d'una infinitat d'enfocaments diferents per poder augmentar la conversió de carboni a biomassa. S'ha aconseguit una reducció significativa de l'acumulació d'acetat i d'etanol, però mai s'ha evitat completament sense afectar

la taxa de creixement o mitjançant modificacions genètiques. Curiosament, hem observat que en determinades condicions de cultiu, els bacteris i els llevats són capaços de regular la captació de la font de carboni mentre la taxa de creixement específica de creixement es manté constant. Com a resultat, s'optimitza la conversió de carboni cap a la formació de biomassa.

En el cas del lactat, s'ha aconseguit una reducció significativa tot i que mai no s'ha esgotat del tot sense modificar el creixement. No obstant això, hem observat que en determinades condicions de cultiu, les cèl·lules de mamífers són capaces de co-consumir lactat una font de carboni sense produir lactat mentre el creixement no es veu afectat.

El **capítol 1** esta format per una introducció als bioprocessos en general basats en microorganismes i la descripció del *state of art* de l'enginyeria de bioprocessos i la biologia de sistemes. Després, en el **capítol 2** s'estableixen els objectius de la tesi per centrar els capítols de resultats en els reptes declarats.

El **capítol 3** se centra en la presentació del metabolisme de la glucosa i l'acetat en cultius d'*Escherichia coli* (*E. coli*) M15, com a productor d'acetat, i *E. coli* BL21, com a no productor d'acetat. Per tal de realitzar un estudi més profund de les raons darrere de la producció d'acetat, s'ha realitzat una anàlisi de la distribució del flux intracel·lular per a cada soca mitjançant la metodologia del Flux Balance Analysis (FBA). El FBA mostra que, quan es compara *E. coli* M15 amb *E. coli* BL21, la producció d'acetat es deu a l'aparició d'un desequilibri en el flux de carboni entre la via glicolítica i el cicle d'àcid tricarboxílics (TCA). Concretament, en la etapa de reacció que interioritza l'acetil-CoA al TCA. Com a resultat, l'acetat es produeix per equilibrar el fluxos d'acetil-CoA. En canvi, en el cas d'*E. coli* BL21, no es produeix acetat ja que tot l'acetil-CoA pot ser interioritzat al TCA. A més, també s'observa que el consum de glucosa d' *E. coli* BL21 es pot modificar sense que el creixement es vegi afectat i, llavors, la conversió de glucosa en biomassa s'optimitza. Per tant, aquest metabolisme esdevé molt interessant des d'un punt de vista del bioprocés, ja que la conversió de substrats es podria optimitzar per obtenir més biomassa amb la mateixa massa de substrat.

El **capítol 4** es centra en presentar la relació entre el metabolisme de la glucosa i la producció d'etanol i glicerol utilitzant dos llevats. *S. cerevisiae*, com a llevat productor d'etanol, i *P. pastoris*, com a llevat de baixa producció d'etanol. Per tal de realitzar un estudi més profund sobre la producció d'etanol i glicerol, s'analitza la distribució del flux intracel·lular de cada llevat mitjançant la metodologia FBA. El FBA mostra que, quan es compara *S. cerevisiae* amb *P. pastoris*, l'etanol es produeix a causa d'un desequilibri en el potencial redox citoplasmàtic causat per la diferència entre el flux de NADH procedent de la via glicolítica i la capacitat de les

llançadores mitocondrials per regenerar-lo. Com a resultat, etanol i glicerol es produeixen per regenerar el NADH citoplasmàtic. En el cas de *P. pastoris*, el flux limitat de NADH procedent de la via glicolítica gairebé es regenera completament mitjançant els llançadores mitocondrials i només es requereix una petita formació d'etanol. D'altra banda, *S. cerevisiae* presenta un flux elevat de NADH citoplasmàtic procedent de la via glicolítica que no potser regenerat mitjançant les llançadores mitocondrials, per la qual cosa es requereix la producció d'altres quantitats d'etanol i glicerol per equilibrar el NADH citoplasmàtic. A més, en un estudi en *S. cerevisiae* basat en comprendre la relació entre el consum de glucosa i la seva disponibilitat en el medi de cultiu, s'ha observat una disminució del flux de carboni procedent de la via glicolítica que com a conseqüència, s'optimitza la formació de biomassa gràcies a la reducció de l'etanol produït mentre no es genera glicerol. Tal com s'ha mencionat amb anterioritat, aquest metabolisme esdevé de gran interès des del punt de vista d'optimització de bioprocessos, ja que el la conversió de carboni a biomassa esdevé més eficient.

El **capítol 5** es centra en descriure el metabolisme del lactat en cultius de la línia cel·lular humana HEK293 i la murina de l'hibridoma KB26.5, dues línies cel·lulars animals àmpliament utilitzades a la indústria. Per tal de realitzar un estudi més profund de la conversió de glucosa en lactat, s'ha realitzat una anàlisi de la distribució dels fluxos intracel·lulars per a les dues línies cel·lulars mitjançant la metodologia FBA. Aquesta demostra que el lactat es produeix a causa d'un desequilibri en el potencial redox citoplasmàtic causat per la diferència entre el flux de NADH procedent de la via glicolítica i el flux de NADH regenerat a partir de les llançadores mitocondrials. A continuació, la reducció de la conversió de glucosa en lactat es pren com a objectiu basant-nos ens dos fronts: un canvi en la font de carboni o dur a terme modificacions genètiques. S'observa que quan els cultius de HEK293 creixen utilitzant fructosa en lloc de glucosa com a font de carboni, no hi ha generació de lactat, però s'observa una reducció en el creixement. D'altra banda, al suplementar la fructosa amb un àcid orgànic no s'obté reducció del creixement i s'evita la generació de lactat. Per tant, s'aconsegueix l'eliminació total del lactat mentre que el creixement no es veu afectat.

En relació amb el hibridoma KB26.5, el consum d'una altra font de carboni no s'aconsegueix ja que aquesta només pot créixer utilitzant la glucosa com a font de carboni. No obstant això, és possible reduir la producció de lactat mitjançant modificacions genètiques com per exemple, l'expressió d'un gen anti-apoptòtic, el gen BHRF1. L'expressió d'aquest gen provoca millores en el creixement i en la conversió de glucosa en biomassa. Ademés, l'ús de el hibridoma KB26.5 que expressa BHRF1 en estratègies de bioprocés és un tret molt interessant ja que presenten una millora en el creixement conjuntament amb una reducció en la producció de lactat.

En el **capítol 6**, es desenvolupa una hipòtesi global sobre els trets metabòlics observats en bacteris, llevats i cèl·lules animals per tal d'establir un "pont" entre els estudis de metabòlic i la definició de bioprocessos. Pel que respecta a la producció d'acetat en bacteris, es proposa que el desbalanç observat entre glicòlisis i TCA està relacionat amb l'evolució bioquímica dels organismes anaerobiosis als aerobis en bacteris primitius. Aquest bacteris que eren anaeròbics heteròtrofs van evolucionar a un metabolisme heteròtrof aeròbic per addició del TCA a la glicòlisis, per això la coexistència d'ambdós metabolismes en la mateixa cèl·lula provoca el desbalanç de carboni ja que les taxes d'utilització del carboni i generació d'energia son força diferents.

Respecte de la producció d'etanol en llevats i de lactat en cèl·lules animals, en aquest cas es proposa que tots els desequilibris metabòlics observats estan relacionats amb la formació del domini Eukarya. Tot i que diverses teories expliquen la formació del domini Eukarya, en aquest treball s'utilitza l'endosimbíotica. Aquesta exposa que la formació del primer microorganisme basat en mitocondris està relacionada amb l'endosimbiosis de dos bacteris amb diferent consums de carboni. El microorganisme resultant de l'endosimbiosis, a causa de les característiques metabòliques dels seus predecessors, expressa els dos metabolismes alhora. En conseqüència, s'ha d'observar un desequilibri del potencial redox i del carboni en el punt d'unió entre ambdós metabolismes.

La formació del primer eucariota (basada en l'endosimbiosis de un dos microorganismes, un dels qual era el antecessor de la mitocondria) pot explicar tant el metabolisme de l'etanol i el glicerol en el llevat com el metabolisme del lactat en les cèl·lules animals. Cadascun d'ells és el resultat de la compartimentalització de les cèl·lules i de la diferència en el consum de carboni dels dos predecessors. Tenint en compte això, es pot explicar el desequilibri citoplasmàtic de NADH causat per un elevat consum de glucosa i una restricció a les llançadores mitocondrials quan es produeixen etanol, glicerol i lactat. A més, utilitzant la teoria de l'evolució, es pot afirmar que la continuïtat dels éssers vius al llarg del temps està relacionada amb la seva interacció amb el medi ambient i la seva capacitat per canviar les condicions ambientals i adaptar-se a elles.

Per últim, es proposa l'optimització de la biomassa en bioprocessos que consisteix a canviar la interacció entre l'entorn i el microorganisme. Aquesta optimització es basa en la descripció del metabolisme del carboni de tots els microorganismes seleccionats. Per tant, s'utilitza per dissenyar estratègies de bioprocés que tenen com a principal objectiu augmentar la productivitat volumètrica a través de l'augment de la concentració de biomassa. En relació amb el desenvolupament i l'optimització de bioprocessos, els fed-batch i les perfusions generalment

es consideren opcions més atractives per a la indústria que els processos en batch. No obstant això, l'aplicació eficient d'aquests processos requereix la disponibilitat de sistemes de mesura en línia fiables per a l'estimació de la densitat cel·lular i l'activitat metabòlica de les cèl·lules. Per a això, es desenvolupen diverses eines de control en línia basades en l'estimació d'un perfil de biomassa a través del seguiment variables fisiològiques.

En el **capítol 7**, es descriu el disseny d'una estratègia de cultiu utilitzant *E. coli* BL21 que té com a objectiu augmentar la concentració de biomassa. En primer lloc, es realitza la descripció d'un batch de referència. En segon lloc, per augmentar encara més la biomassa obtinguda, es desenvolupa un medi fortificat a partir del medi de referència. Com a resultat, la biomassa s'incrementa 2,48 vegades, tot i que s'arriba l'addició de la font màxima de carboni disponible. Finalment, per augmentar encara més la concentració de biomassa, es desenvolupen estratègies en fed-batch. L'estudi analitza cinc algoritmes d'alimentació que utilitzant la conversió òptima de glucosa en biomassa determinada al **capítol 3** per tal de calcular el perfil d'alimentació òptim.

El primer fed-batch utilitzat com a referència es basa en un creixement exponencial teòric per calcular el perfil d'alimentació. Com a resultat, la concentració de biomassa augmenta 5,75 vegades. Tanmateix, s'observa una limitació del creixement a causa de la subestimació del perfil d'alimentació òptim. L'error en aquest perfil és causat per la diferència entre el perfil experimental de biomassa i el teòric. Per resoldre aquest problema, es desenvolupen els següents tres perfils d'alimentació basats en la relació entre un paràmetre fisiològic i el metabolisme del carboni per predir la concentració de biomassa:

- Una relació entre l'addició d'àlcali causada per compostos que són productes o substrats relacionats amb el metabolisme del carboni.
- Una relació entre la Oxygen Uptake Rate (OUR) i l'oxigen consumit com a acceptor d'electrons en el metabolisme del carboni.
- Una relació entre la Carbon dioxide Evolution Rate (CER) i el diòxid de carboni produït per l'oxidació de la font de carboni mitjançant el metabolisme del carboni.

En les primeres etapes del fed-batch, els tres perfils d'alimentació proposats segueixen la concentració de biomassa, degut als canvis imprevisibles en el metabolisme del carboni durant les fases mitjana i tardana del fed-batch la concentració de biomassa es subestimada conjuntament amb la subestimació o sobrevaloració del perfil d'alimentació. Aquest error s'explica pel fet que el perfil d'alimentació requereix paràmetres metabòlics pel seu càlcul i se suposa que són constants durant el transcurs de l'experiment. Tal com s'observa, aquests

paràmetres no són constants durant el fed-batch. Per tant, per superar la incapacitat de predir el comportament metabòlic, es desenvolupa un algorisme d'alimentació que no es basa en l'estimació de la biomassa ni en l'ús d'un paràmetre metabòlic. Com a resultat, la concentració de biomassa augmenta 5,37 vegades, mentre que *E. coli* BL21 creix a la velocitat òptima. A més, per provar aquest nou perfil d'alimentació, es duu a terme un fed-batch amb fase d'inducció d'una proteïna recombinant model. La idea darrere d'aquest procediment és observar si la variació induïda per la inconstància del metabolisme del carboni durant la fase d'inducció pot ser seguida pel nou algorisme. Per tant, es prova la nova metodologia en les pitjors condicions possibles: la producció d'una proteïna model - GFP recombinant- mitjançant inducció IPTG. Es realitza el fed-batch amb fase d'inducció i el perfil d'alimentació està capaç de satisfer les necessitats de carboni durant la fase de creixement i també d'inducció sense limitar-ne el creixement.

Al **capítol 8** es descriu la definició d'una estratègia de cultiu que té com a objectiu augmentar la concentració de biomassa de *S. cerevisiae*. En primer lloc, es realitza la descripció d'un batch de referència. Per tal d'incrementar encara més la biomassa obtinguda, es desenvolupa un medi de fortificació basat en el medi del batch. Com a resultat, la biomassa s'incrementa 3,43 vegades. Posteriorment, es desenvolupen estratègies fed-batch per augmentar encara més la concentració de biomassa. A causa de les conclusions obtingudes en relació amb els perfils d'alimentació desenvolupats al **capítol 7**, aquest estudi analitza un fed-batch que es basa en un creixement exponencial teòric per determinar si es poden mantenir els paràmetres metabòlics durant l'alimentació. A més, la conversió òptima de glucosa en biomassa determinada al **capítol 4** s'utilitza en el càlcul del perfil d'alimentació.

S'observa que durant la fase fed-batch que els paràmetres metabòlics canvien en funció de les condicions ambientals. Sobre aquesta base, el següent fed-batch que es realitza és el que no utilitza l'estimació de la concentració de biomassa ni dels paràmetres metabòlics. Pel que fa a la resta de perfils d'alimentació, es descarten pel fet que no té sentit utilitzar un perfil d'alimentació que només es pugui ajustar al requeriment de carboni en les primeres etapes d'un fed-batch. A causa de l'aparició de condicions d'inhibició del creixement en l'última etapa dels dos fed-batch realitzats, l'estratègia de fortificació i l'estratègia fed-batch aconseguixen la mateixa concentració de biomassa. No obstant això, l'ús d'estratègies fed-batch redueix la conversió de carboni cap a etanol en un 50 %, ja que les dades metabòliques del **capítol 4** s'utilitzen per calcular el perfil d'alimentació.

A més, es proposa la inducció d'una proteïna model durant una estratègia fed-batch. Al contrari del que es dur a terme en el **capítol 7**, la proteïna es produeix mitjançant un marcador auxotròfic amb *S. cerevisiae* expressant diferents auxotrofies en lloc d'un antibiòtic. A causa d'una limitació de creixement observada en el *S. cerevisiae* auxotròfic en comparació amb la soca wildtype, aquest treball s'atura. Però, es proposa una alternativa basada en expressar la GFP en un *S. cerevisiae* wildtype que és seleccionat mitjançant un antibiòtic com a marcador de selecció; tot i que només s'arriba a plantejar la estratègia a seguir.

En el **capítol 9**, es descriu la definició d'una estratègia de cultiu que té com a objectiu augmentar la concentració de biomassa en hibridoma KB26.5-BHRF1. En primer lloc, es realitza la descripció d'un batch de referència. Per tal d'augmentar encara més la biomassa obtinguda, es desenvolupen estratègies fed-batch. Aquest estudi analitza un fed-batch basat en un creixement exponencial teòric per determinar si es poden mantenir els paràmetres metabòlics durant el període d'alimentació. Com a resultat, la biomassa augmenta 1,43 vegades. Principalment, s'observen dos fets durant la fase fed-batch: una inhibició del creixement que té lloc durant la fase fed-batch i la variació dels paràmetres metabòlics en funció de les condicions ambientals. Sobre aquesta base, per augmentar encara més la concentració de biomassa, la següent estratègia realitzada és una estratègia de perfusió que assegura condicions ambientals constants mentre els inhibidors del creixement es retiren del medi de cultiu. Com a resultat, s'eviten les condicions d'inhibició i s'incrementa la concentració de biomassa 6,46 vegades.

S'han fet contribucions substancials tant en biologia de sistemes com en enginyeria de bioprocessos. Tanmateix, aquesta tesi pretenia ser i el punt de partida per entendre millor el metabolisme cel·lular per aplicar-lo encara més en el desenvolupament de bioprocessos. Finalment, s'ha inclòs el **capítol 10** amb l'objectiu de resumir les conclusions generals de la tesi i el treball futur que podria ser interessant dur a terme.

1 Overall introduction

1.1 Biotechnology and red biotechnology.

The etymology of the word biotechnology comes from the Greek βιοτεχνολογία, which derives from three words: bios (βίος)- life; technos (τεχνης)–technology and logos (λόγος)-thinking (Kafarski, 2012). The whole concept of biotechnology covers a large field of study, in a simple way, it is a broad area of technical activity and its development is dependent on interrelation between various disciplines of science, whose aim is to give services and products to society. In regard with the finality of the services and products, biotechnology could be distributed into several groups related to its framework application, as shown in **Figure 1-1**. (Arfin & Sonawane, 2019).

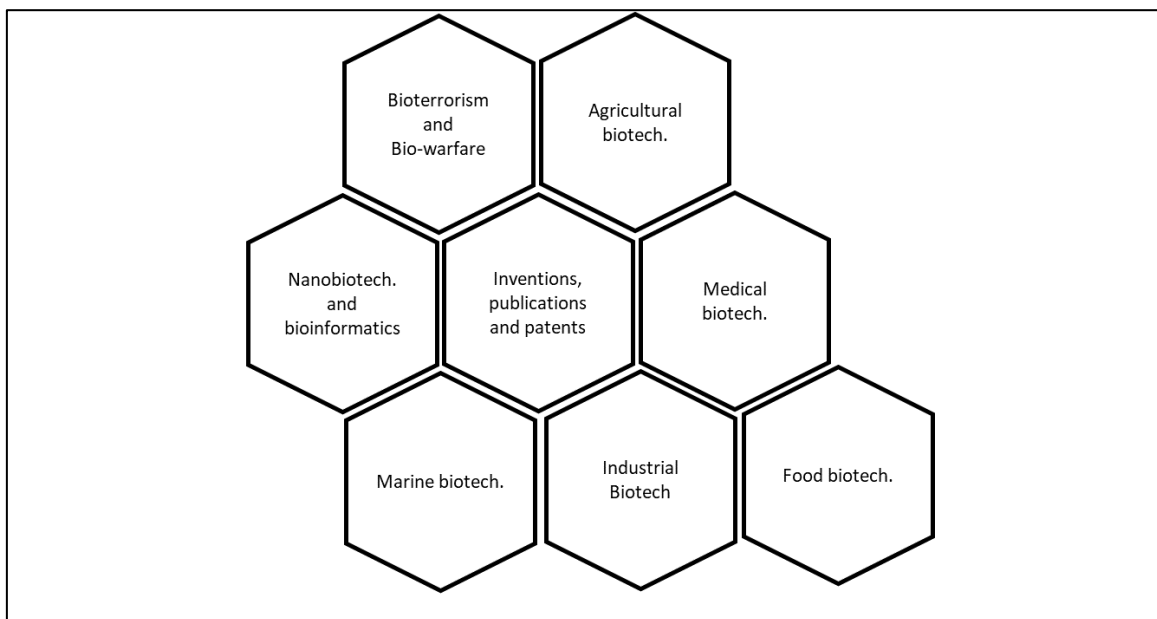


Figure 1-1 Applications areas in biotechnology (data from (Arfin & Sonawane, 2019)).

Thus, in order to develop a classification of the previous mentioned applications that leads to an easy identification, as well as clusters formation regarding its framework, a colour code was established as an alternative field classification (Kafarski, 2012), as shown in table 1.1.

Table 1-1 Definition of the colour code in relation to biotechnological applications framework.

Colour code	Biotechnological framework applications
Red	Medicine and human health
Green	Development of agriculture
White	Industrial biotechnology
Yellow	Nutritional biotechnology
Blue	Biotechnology applications based on marine environments
Violet	Law, ethics and philosophical issues related to the use biotechnology
Brown	Biotechnology applications based on dry and desert environments
Grey	Environmental safety
Gold	Bioinformatics and bio-hardware development
Black/Dark	Bioterrorism and biological weapons

This classification is grouped into 10 colours in order to divide the applications:

- Red biotechnology consists of all the applications that focus on health preservation, the production of vaccines and antibiotics, discovering new drugs, regenerative therapies, construction of artificial organs and new diagnostics (Kafarski, 2012).
- Green biotechnology consists of all the applications that relay on producing more fertile and resistant, plants that ensure the use of environmentally friendly fertilizers and bio-pesticides, and lastly its genetically modification if a wealthy aid is needed (Laursen, 2010).
- The white one consists of all the applications that are related to the use of a biocatalyst in industrial processes, for instance the production of biodegradable polymers, fuel starting from renewable resources and production of industrially relevant enzymes and microorganisms (S.Olempska-Beer et al., 2006)(Rehm, 2009) (Kamm et al., 2010).
- The yellow one groups all the applications that are based on the improvement of food properties to obtain the most nourishing one and fortified with health-promoting additives (Siró et al., 2008).
- The blue biotechnology is related to all the applications that are based on using a sea organism as an extract for Beauty and Health Products (H.-M. D. Wang et al., 2015) and

as an expression platform for producing recombinant proteins like biopharmaceuticals (Rosales-Mendoza, 2016) or biodiesel (Krohn et al., 2011).

- The violet one tackles all regulation and settlements coming from legal, ethical and philosophic issues within the use of biotechnology (Jameel, 2011).
- The brown biotechnology consists in all the applications that considers management of arid lands and deserts, for instance cultivation of desert crops; development of saline agriculture and aquaculture; and the rational use of water, wastewater and other water resources (DaSilva et al., 2002).
- And lastly, the newest colours: grey, gold and black/dark that are related to the applications within environmental biotechnology; bioinformatics and nanobiotechnologies; and bioterrorism and bio-warfare, respectively (Matyushenko et al., 2016).

This work will be revolving around the red biotechnology, and a brief summary of its main applications, summarized in **Figure 1-2**, is described in the list below:

- Gene profiling: applications related to the measurement of gene expression, for instance to monitor and investigate the gene expression that directs the complex cascade of molecular events leading to tumour development and progression (Mocellin et al., 2005).
- Gene therapy: those applications whose principal trait is to insert a gene into the body or part of it which has to be treated (Dunbar et al., 2018).
- Biopharmaceuticals: applications that are based on synthesizing drug molecules that have therapeutic effects in biological cell systems (Mehta, 2019).
- Skin grafting: all the applications related to treat non-healing wounds on skin (Kirsner, 1993).
- Pharmacogenomics: applications that study how genes affect a person's response to drugs (Evans & Relling, 2004).
- Inherited disease diagnosis: the diagnosis of a disease caused by one or more abnormalities in gene expression (Cooper & Schmidtke, 1992)
- Vaccine development: applications related to the production and innovation of vaccines against emerging and neglected infectious diseases (Possas C. et al., 2020).
- DNA fingerprinting: the use of methodologies that consist in the identification of an individual by looking at unique patterns in its DNA, to type bacterial strains and to

visualize and evaluate the amplification results from an electrophoretic separation (Skutkova et al., 2019).

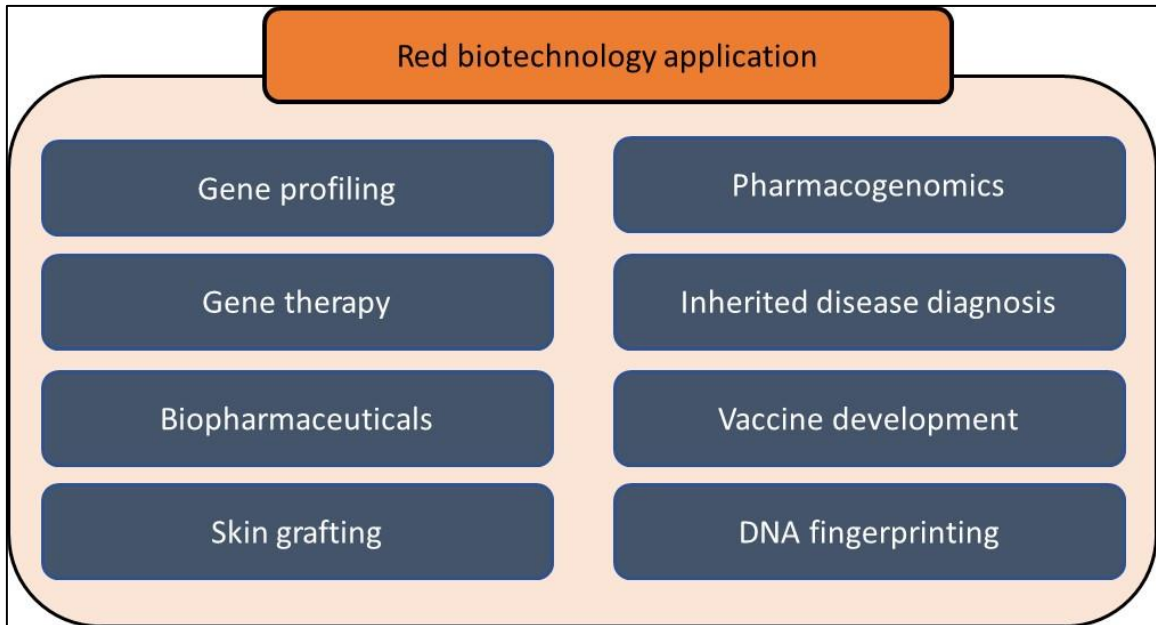


Figure 1-2 Applications of red biotechnology (data from (Arfin & Sonawane, 2019)).

Choosing U.S.A and Europe as a benchmark reference, as shown in **Figure 1-3**, most of the biopharmaceuticals that are related to the previously mentioned applications are defined as recombinant proteins,. In this case, recombinant proteins are mainly distributed in eight categories: recombinant clotting factors; recombinant thrombolytics, anticoagulants and other blood-related products; recombinant hormones; recombinant growth factors; recombinant cytokines; recombinant vaccines, monoclonal antibody–based products; and other recombinant products (Walsh, 2018).

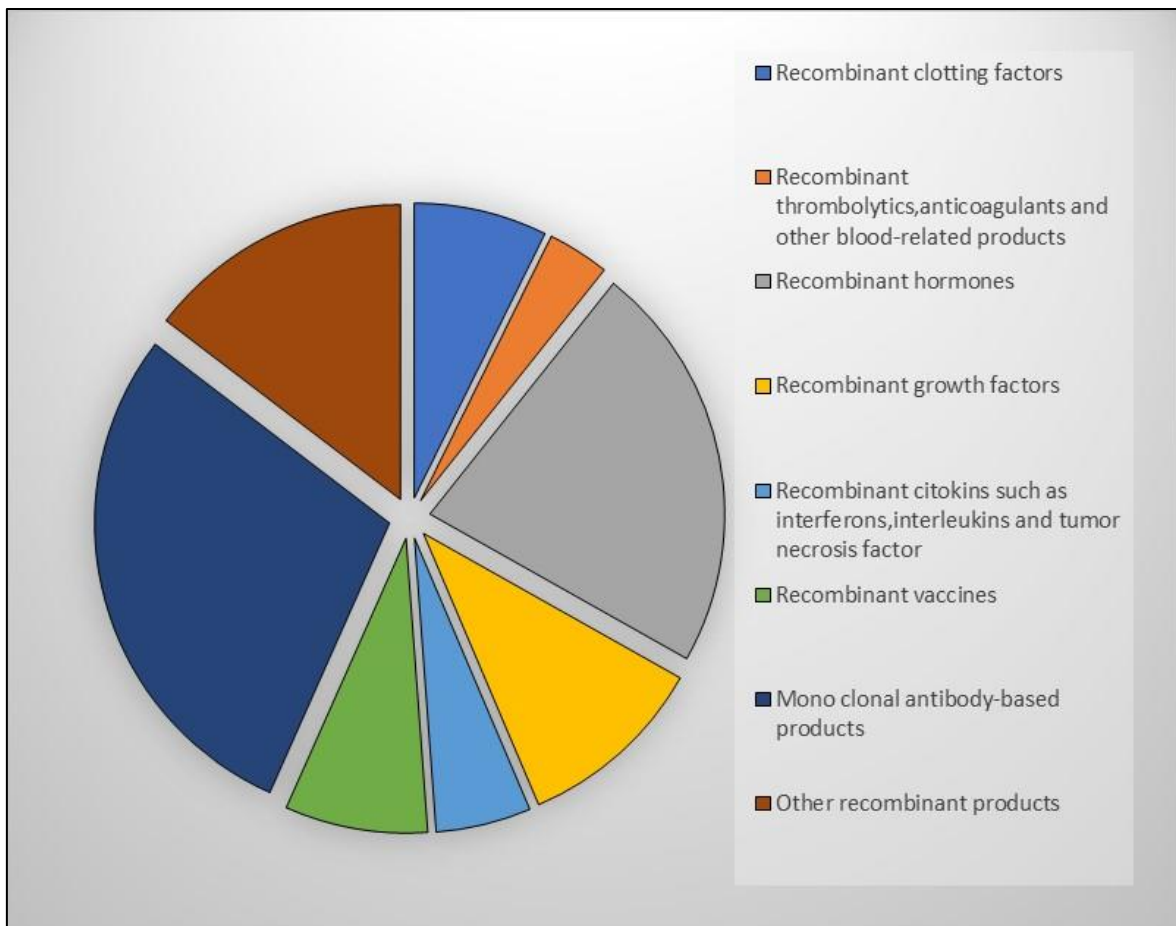


Figure 1-3. Distribution of the whole recombinant proteins produced in 2018 (data from (Walsh, 2018)).

As shown in

Table 1-2, these recombinant proteins are produced by bacteria, yeast or mammalian cells. Specifically, recombinant cytokines are solely produced by bacteria, while recombinant vaccines and blood-related products are produced by yeast and recombinant clotting factors and antibodies by animal cells. On the other side, recombinant hormones are produced either by bacteria or by yeast and recombinant growth factors and other recombinant products, such as fusion proteins or bone morphogenic proteins, are produced either by bacteria or by mammalian cells.

Table 1-2 Description of the mostly produced pharmaceutical products in 2018 regarding the expression platform used (data from (Walsh, 2018)).

Product category	Main expression platform used	Specific products
Recombinant cytokines	Bacteria	Interferons, interleukins and tumour necrosis factor
Recombinant vaccines	Yeast	Mainly against hepatitis B
Recombinant thrombolytics, anticoagulants and other blood-related products	Yeast	Tissue plasminogen activator and hirudin
Recombinant clotting factors	Mammalian cells	Chiefly factor VIII and others such as factor IX and VIIa
Mono clonal antibody-based products	Mammalian cells	Monoclonal anti-body, drug or cytokine conjugate
Recombinant Hormones	Bacteria and yeast	Insulin, human growth hormone, follicle-stimulating hormone and others such as metreleptin or teriparade
Recombinant growth factors	Bacteria and mammalian cells	Mainly Erythropoietin and colon-stimulating factors
Other recombinant products	Bacteria and mammalian cells	Bone morphogenic protein, recombinant enzymes and fusion proteins

The criteria to select the appropriate expression platform for producing a specific recombinant protein is decided on its biological properties (protein folding and post-translational modifications) as well as the features of each platform expression. For this purpose, pros and cons of each one are shown in **Table 1-3**, and a brief description is presented hereafter as well:

Bacteria is the most used expression platform for producing recombinant proteins that do not require a glycosylation pattern or a complex 3D structure. Moreover, regarding its intrinsic characteristics, *Escherichia coli* (*E. coli*) has the highest growth rate among the expression platforms, high cell density cultures are easily achieved and it exhibits ease of genetic manipulation and well-characterized genetics. To the contrary, *E. coli* is a non-secretor expression platform that presents problems in relation to the formation of inclusion bodies and problems related to post-translational modifications, for instance protein folding and glycosylation and phosphorylation patterns (Baneyx & Mujacic, 2004). Moreover, when the recombinant protein is being produced by *E. coli*, the growth rate decreases in some strategies owing to a metabolic burden caused by the mechanism related to the expression system (Hoffmann & Rinas, 2004).

On the other hand, yeast and mammalian cells are secretory expression platforms whose differences lie in the post-translational modifications and the growth rate. Whereas yeast has a

higher growth rate than animal cell lines, animal cell lines are able to perform glycosylation patterns over the recombinant protein that lead to a higher biological activity and no-response regarding its immunogenicity (Baghban et al., 2019).

Table 1-3 Pros and cons of the most used platform expression within red biotechnology.

	PROS	CONS
Bacteria	<ul style="list-style-type: none"> • Highest growth rate (duplication time 30 min - 1,5 h) • Ease genetic manipulation • Well-characterized genetics • The cheapest culture medium 	<ul style="list-style-type: none"> • Non-secretory platform • Non-post-translational modifications • Formation of inclusion bodies • Protease contamination from host proteins • Endotoxins accumulation
Yeast	<ul style="list-style-type: none"> • Moderate growth rate (duplication time around 2,5 h) • Secretory platform • Pathogen free production 	<ul style="list-style-type: none"> • Glycosylation patterns based on hypermannosylated glycans • Not proper for proteins with complex 3D structures • Low plasmid stability
Mammalian cells	<ul style="list-style-type: none"> • Secretory platform • Most suitable for performing glycosylation patterns that do not trigger immunogenicity • Proper protein's folding 	<ul style="list-style-type: none"> • Lowest growth rate (duplication time 18 - 24 h) • More expensive culture medium

As it has been mentioned up until now, most of the recombinant proteins related to red biotechnology are produced by three expression platforms: bacteria, yeast and animal cells. It is important to point out that within bacteria *E. coli* is the most used platform, while *Saccharomyces cerevisiae* (*S. cerevisiae*) is the preferred yeast and CHO, hybridoma and HEK293 are the mainly used mammalian cell platforms, as shown in **Figure 1-4**. Therefore, *E. coli*, *S. cerevisiae*, Hybridoma and HEK293 will be the core of the study that will be presented in this work

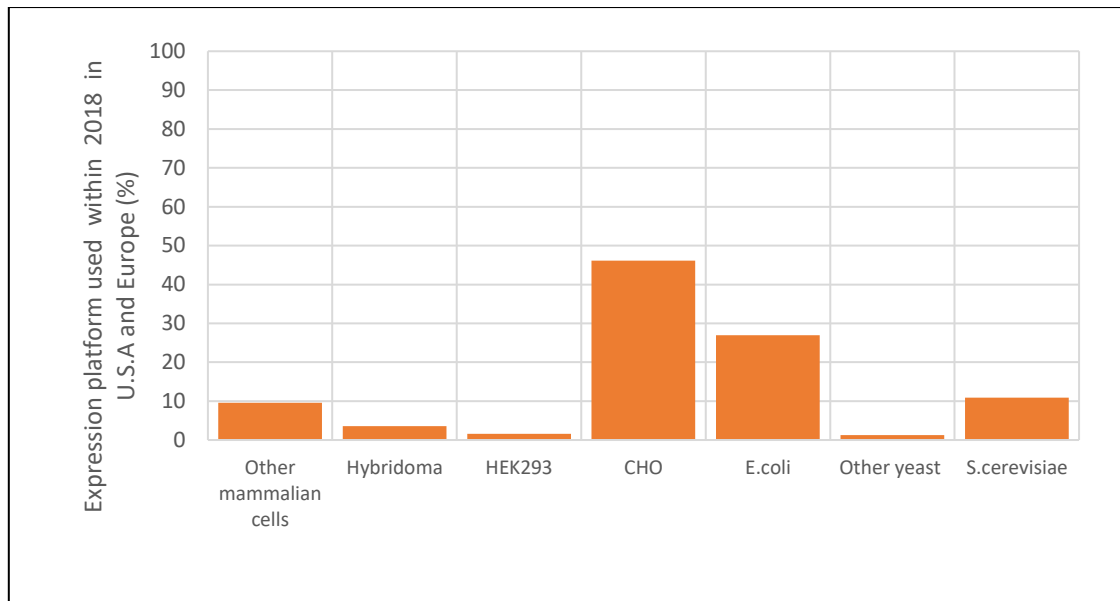


Figure 1-4 Expression platform used for producing red biotechnology products (data from (Walsh, 2018)).

For the selected expression platforms, this work will delve into the design of the corresponding bioprocess aiming to maximize their volumetric productivity. This maximization will enhance the cost-efficiency of the product in order to be more competitive within the market of red biotechnological products, whose main trait over the last years has been precisely a high competitiveness. (Gambardella et al., 2000) (Chen et al., 2018).

1.2 Bioprocess engineering and volumetric productivity

Bioprocess engineering is a wide field that tack several science fields such as chemistry, physics, biology, mathematics and others. It deals with the design and development of all processes involved in the manufacturing of products from biological material.

An outstanding feature in biotechnological processes is the volumetric productivity, which provide a deep view concerning how good the process in terms of product concentration over time is. Volumetric productivity (VP), as shown in Error! Reference source not found.**Error! Reference source not found.**, depends on the specific product production rate of the selected organism (q_p) as well as on the biomass concentration ($[X]$).

Equation 1-1 Volumetric productivity.

$$VP \left(\frac{g \text{ Product}}{Volume \cdot Time} \right) = q_p \left(\frac{g \text{ Product}}{g \text{ Biomass} \cdot Time} \right) \cdot [X] \left(\frac{g \text{ Biomass}}{Volume} \right)$$

Accordingly, the improvement of volumetric productivity is based on two approaches: the use of genetic engineering and/or metabolic engineering for enhancing the specific production rate, and the use of several engineering tools to raise the maximum available biomass concentration in a bioprocess.

Therefore, this work will be focused on improving volumetric productivity by enhancing biomass production, in order to achieve higher product titters. With this aim, the physiology and metabolism of each selected expression platform has to be taken into account, since a change in biomass production might be caused by a change in extracellular conditions (Duarte et al., 2014) or a metabolic restructuring related to a genetic modification (Noh et al., 2017).

1.3 Physiology and Metabolism

The study of physiology and metabolism describes how an organism or a cell interacts with the extracellular environment while growing at its optimal rate. To grow at the optimal rate, the previously three selected expression platforms have to metabolize a carbon source (normally glucose) in order to produce the precursors and energy required for the biomass synthesis. Specifically, in this study, the cell growth of each expression platform has been performed on aerobic conditions, being oxygen a key element in carbon source metabolism.

A metabolic overview in relation to how glucose is metabolized together with oxygen is shown in **Figure 1-5**. As depicted, initially glucose and oxygen go through the cell membrane and, once inside the organism, glucose goes into the central carbon metabolism where is oxidized to produce: ATP, electron carriers, precursors required for biomass synthesis, and carbon dioxide (CO₂). On the other hand, oxygen goes into the energy metabolism where is reduced to water by NADH. As a consequence of this reduction, ATP is generated. Then, ATP is consumed in reactions related to the biomass synthesis and to maintain the structural processes that are not related to biomass synthesis. Some of these reactions are those involved in the proton motive force, osmoregulation, the degradation of macromolecules and regulated shifts in metabolic pathways (van Bodegom, 2007) (Hoehler & Jørgensen, 2013) (Lever et al., 2015) .

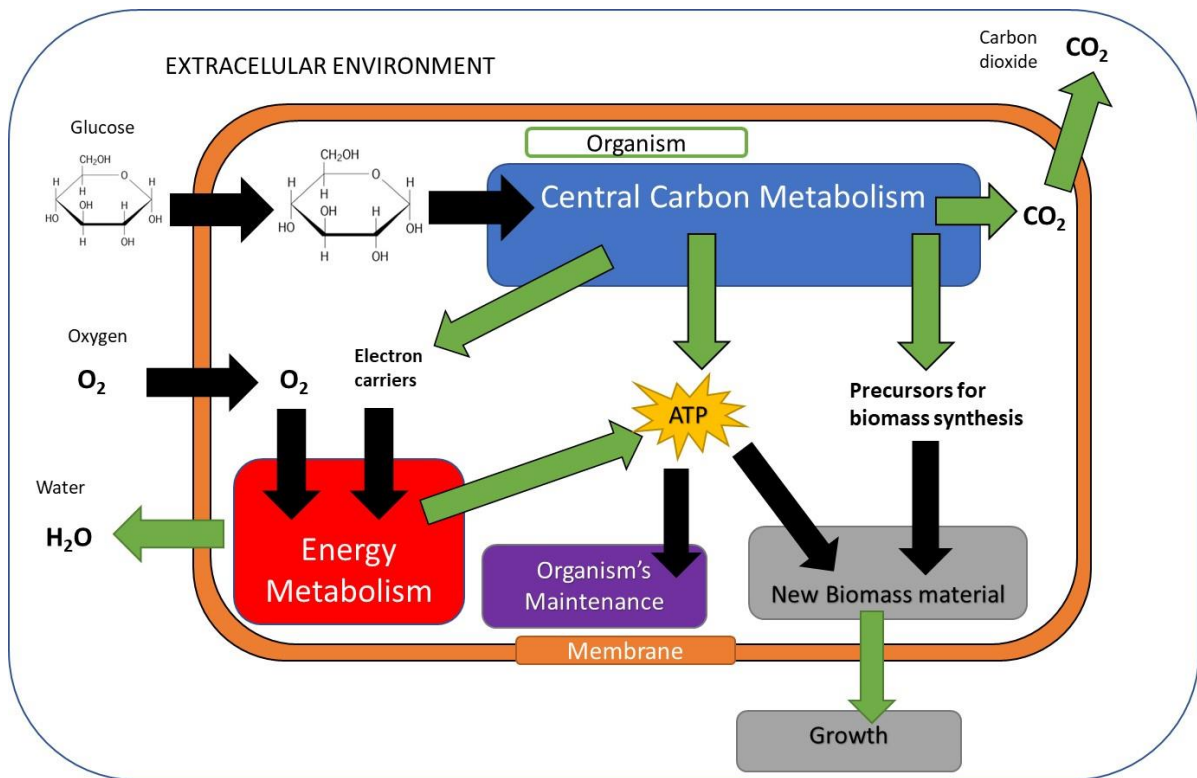


Figure 1-5 Metabolic overview of how glucose is metabolized inside the cell while growing in presence of oxygen at the optimal growth rate (black arrows indicates consumption while green arrows indicate production).

Regarding the metabolism overview presented up until now, a brief description of the central carbon and energy metabolisms will be presented hereafter. In chapter 4, 5, and 6 of the present work the description of both metabolisms will be presented in a more detailed way.

In the first place as shown in **Figure 1-6** Error! Reference source not found., the central carbon metabolism (CCM) tackles mainly three groups of reactions: glycolytic pathway (**Figure 1-7**), pentose phosphate pathway (PPP) (**Figure 1-8**), and Tricarboxylic acid cycle (TCA cycle) (**Figure 1-9**). As was mentioned before, glucose is metabolized in the CCM to produce ATP, electron carriers, precursors required for biomass synthesis, and carbon dioxide as a by-product of those reactions. All the precursors for the synthesis of biomass comes from at least one intermediate metabolite related to one of the groups previously mentioned.

The glycolytic pathway is described as a reaction mechanism that converts glucose to pyruvate (**Figure 1-7**), the PPP mainly might be described as a reaction mechanism required for converting glucose-6-phosphate to ribose-5-phosphate and erythrose-4-phosphate (**Figure 1-8**), and TCA

cycle (**Figure 1-9**) tackles a cyclical reaction mechanism required for the complete oxidation of pyruvate to CO_2 .

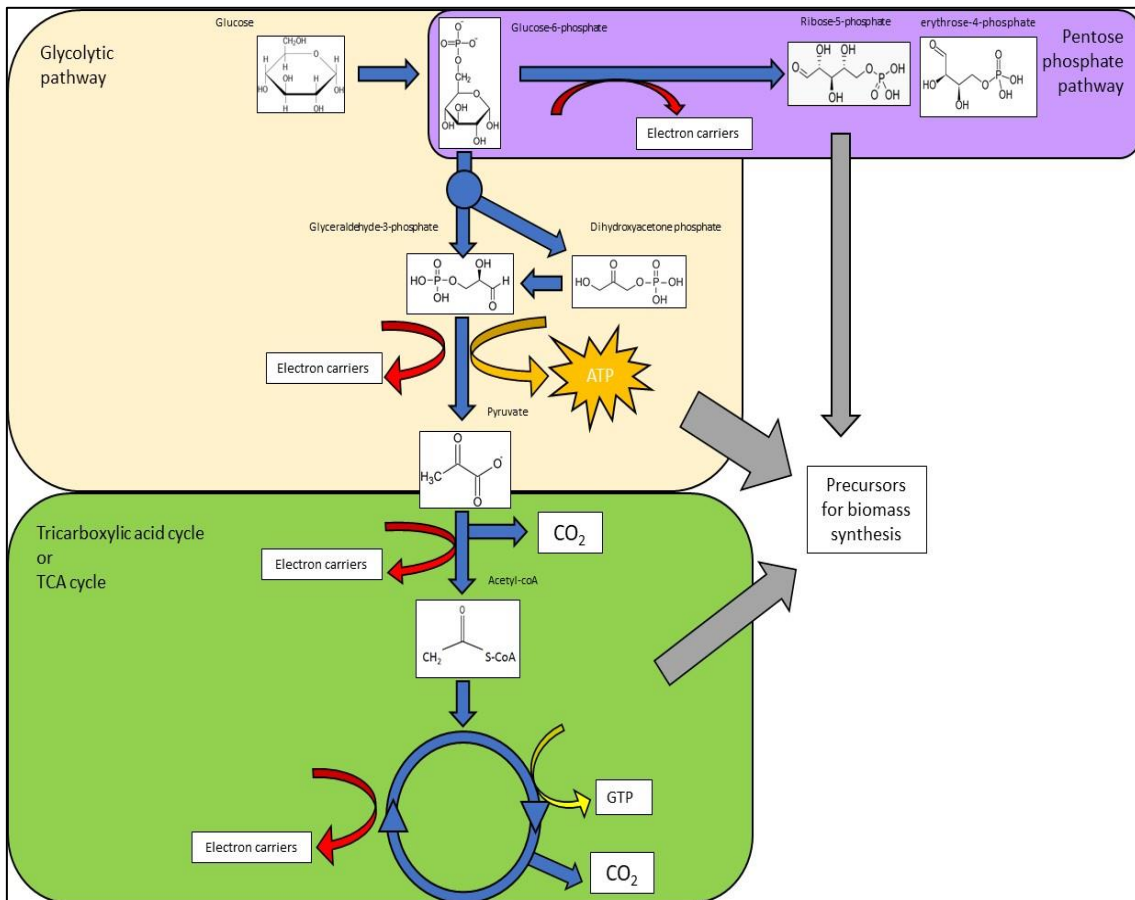


Figure 1-6. Briefly description of which are the main reactions groups within the central carbon metabolism. Blue arrow indicates the reactions where glucose is oxidized, red arrow indicates the reactions where electron carriers are produced, dark yellow one is related to the reaction of the ATP formation, light yellow one is related to the reaction of the GTP formation and the grey one is related to the formation of the precursors required for biomass synthesis.

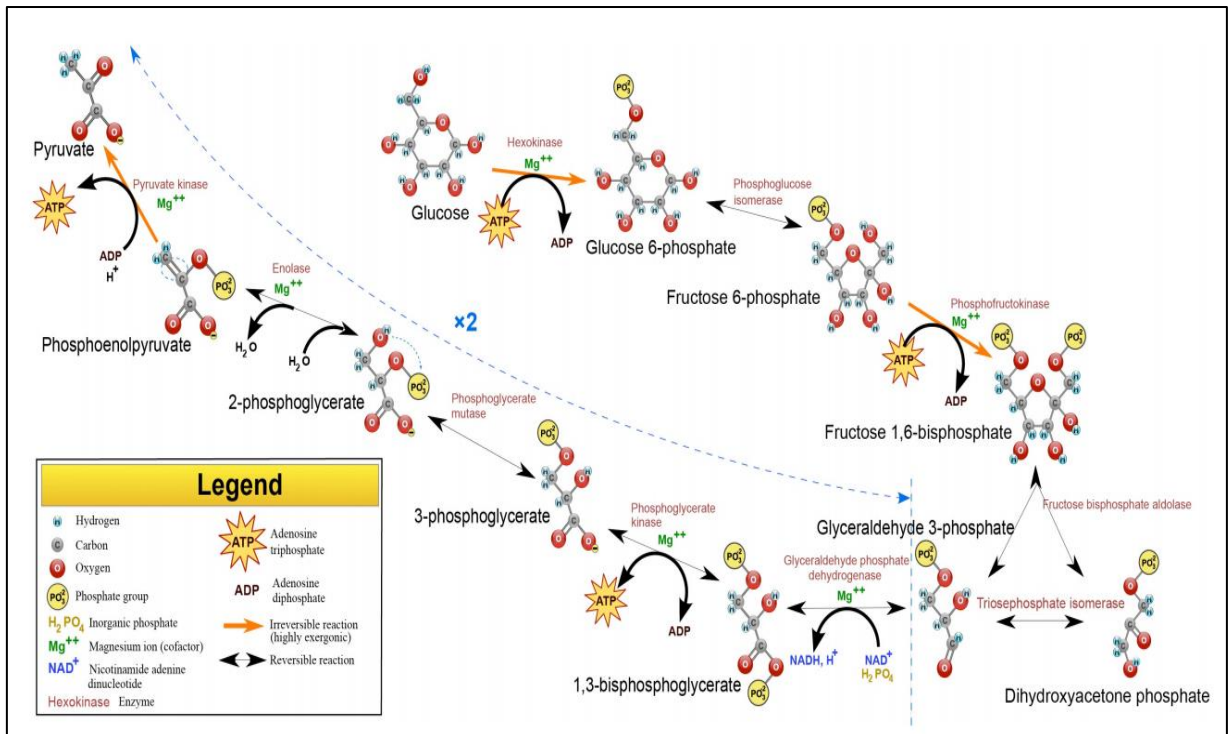


Figure 1-7. Scheme of all the reactions involved in the glycolytic pathway.

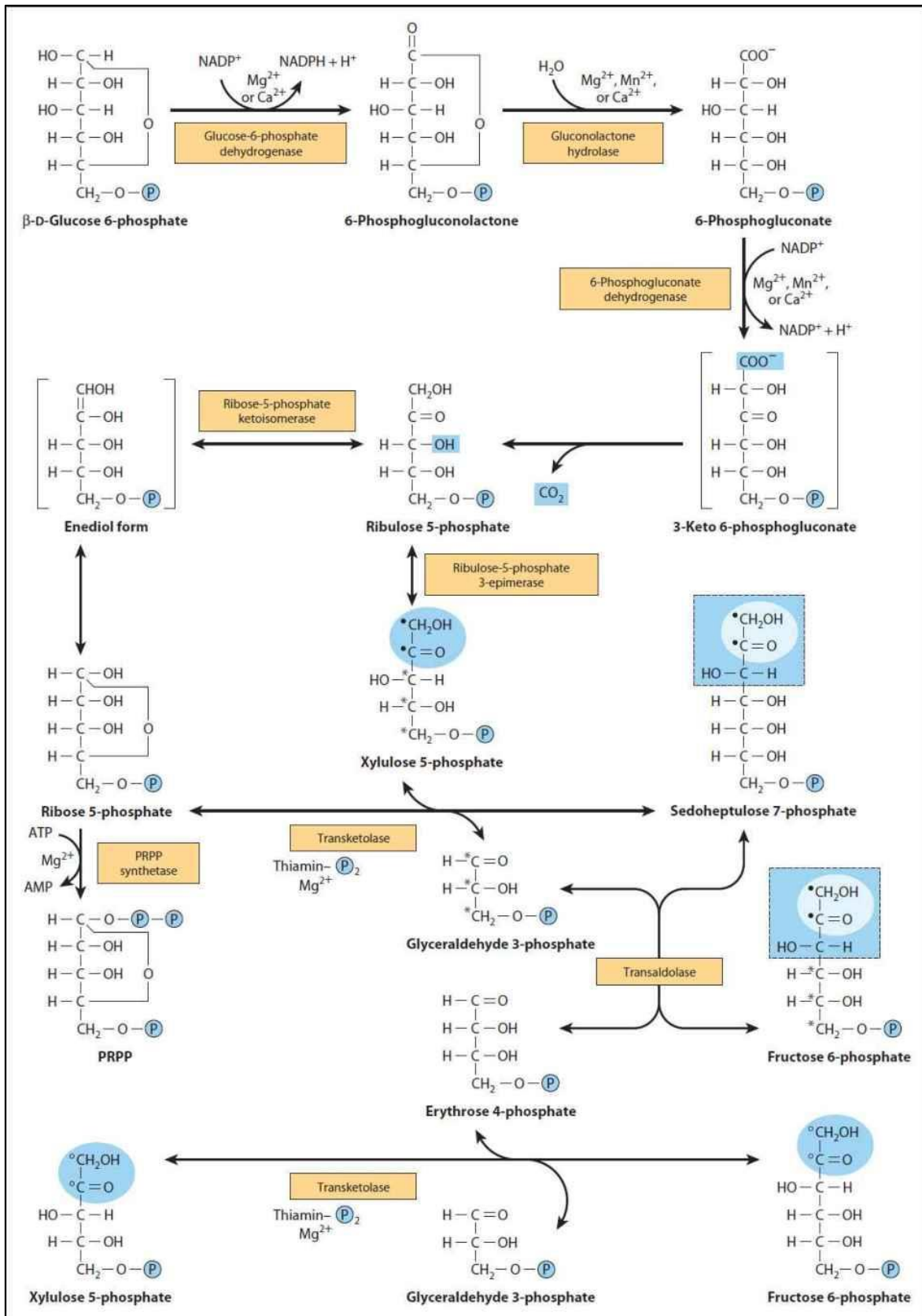


Figure 1-8. Scheme of all the reactions involved in the pentose phosphate pathway.

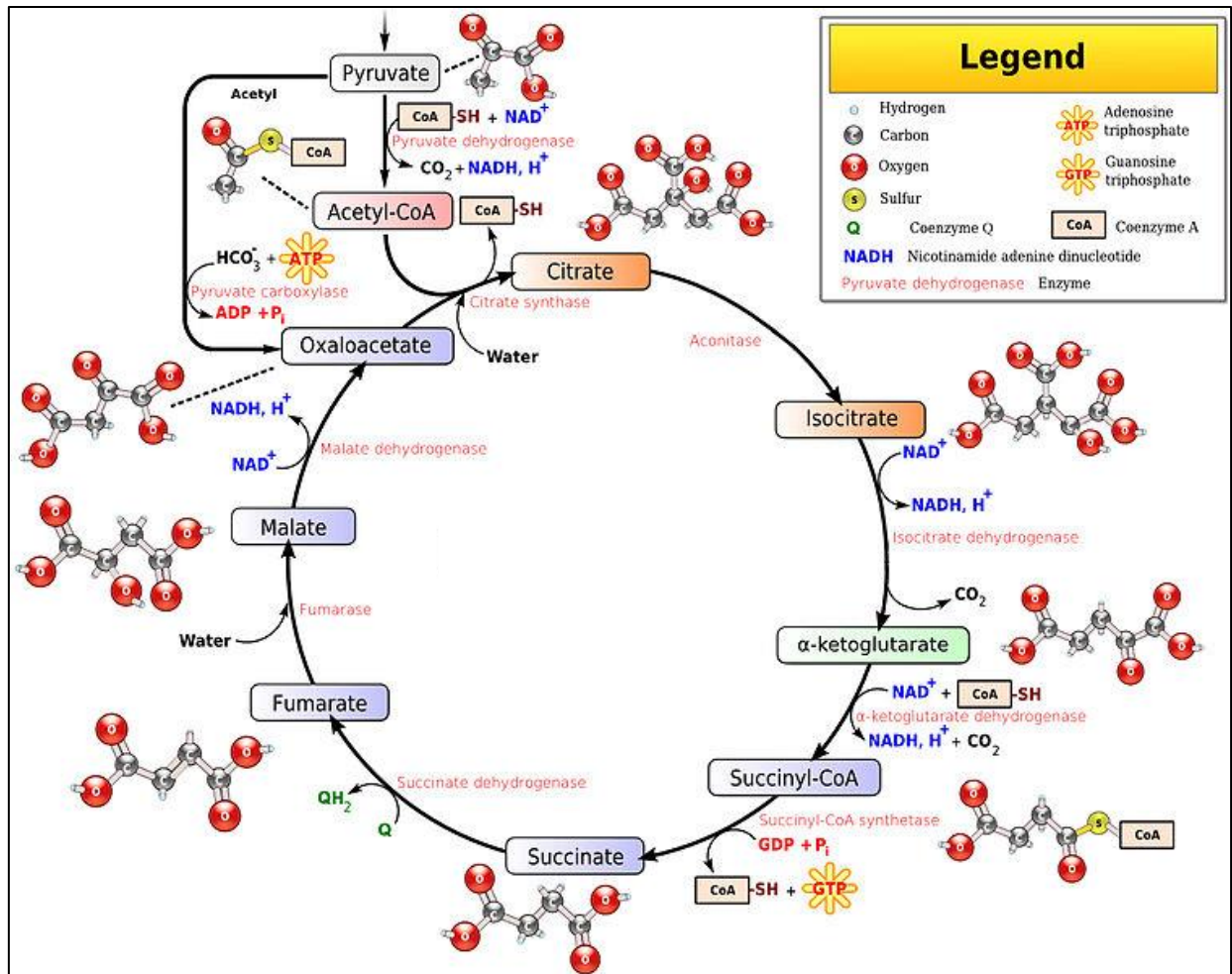


Figure 1-9. Scheme of all the reactions involved in the TCA cycle.

As is shown in the previous figures, first of all glucose is uptaken into the cell via PTS system which performs its phosphorylation to glucose-6-phosphate. The glucose-6-phosphate is then directed towards PPP via glucose-6-phosphate dehydrogenase and towards glycolytic pathway via phosphoglucose isomerase reaction. Next, the glucose-6-phosphate directed towards PPP is converted to ribose-5-phosphate and erythrose-4-phosphate, producing an essential electron carrier (NADPH) regarding biomass synthesis as well. On the other hand, part of glucose-6-phosphate that maintains within glycolytic pathway is converted to fructose-6-phosphate and then it is metabolized until undergoes a reversible aldol condensation to glyceraldehyde-3-phosphate and dihydroxyacetone phosphate. The continuation of this pathway is the interconversion of glyceraldehyde-3-phosphate and dihydroxyacetone phosphate, followed by a chain reaction that converts glyceraldehyde-3-phosphate to pyruvate producing ATP and electron carriers as well. Thereupon, pyruvate is directed towards TCA cycle where firstly is converted to acetyl-coA and thus, acetyl-coA reacts with oxaloacetate by means of a

condensation reaction in order to go in the TCA cycle. Once within TCA, acetyl-coA is oxidized until carbon dioxide resulting in the production of electron carriers (NADH, FADH₂) and GTP as well.

The mentioned mechanism is coordinated in this manner to produce the previously remarked molecules that will be explained down below.

- ATP (adenine triphosphate) is an organic compound that is able to act as a cofactor, which acts as a chemical high energy-bond molecule, and also as a biomass precursor required for the synthesis of DNA (deoxyribonucleic acid) and RNA (ribonucleic acid). On the other hand, GTP (guanosine triphosphate) is a nucleoside triphosphate just as ATP and is required as an energy source by specific GTP-dependent reactions (for instance the process for translocating proteins across the endoplasmic reticulum membrane (Connolly & Gilmore, 1993) or the formation of GTP-binding proteins which are related to signal transduction (Kahn, 2019)) and it is required for gluconeogenesis as well.
- Electron carriers, glycolytic pathway solely produces NADH (nicotinamide adenine dinucleotide reduced form) which is a cofactor performing as an electron transfer molecule that will be directed towards energy metabolism. PPP produces NADPH (nicotinamide adenine dinucleotide phosphate reduced form) which is a cofactor acting as a reducing agent required for the synthesis of lipids and nucleic acids. Finally, TCA cycle produce NADH and FADH₂ (flavin adenine dinucleotide) whose function is just the same as the NADH.
- Precursors required for biomass synthesis, those that come from glycolytic pathway mainly are dihydroxyacetone phosphate, glyceraldehyde-3-phosphate and ATP. The ones that come from PPP are ribulose-5-phosphate, erythrose-4-phosphate and NADPH, and from TCA cycle are mainly acetyl-coA, oxoglutarate and GTP. All of them are mostly directed towards the formation of amino acids (proteins) and lipids, except ribulose-5-phosphate that is directed towards nucleoside synthesis. It is important to point out that the precursors related to the amino acids formation differ between the three selected expression platforms, due to the fact that *E. coli* and yeast are able to produce them from the precursors related to the oxidization of glucose, whereas animal cells are not. As a result, animal cells must use amino acids as precursors, the so-called essential amino acids, which must be added to the media.
- Carbon dioxide, that is the fully oxidized carbon molecule derived from glucose.

Thus, the energy metabolism is required for the production of ATP, whose main function is to couple the energy of exergonic and endergonic processes, making energetically unfavourable biochemical reactions able to proceed. For example, regarding TCA cycle, where the nearly equilibrium reactions such as the conversion of fumarate to malate by fumarase proceed because is coupled to high exergonic reactions such as the formation of citrate by citrate synthase (Park et al., 2016)). It is important to realize that ATP is able to be formed by the Substrate Phosphorylation (SP) that takes place in glycolytic pathway or it can be formed by the Oxidative Phosphorylation (OP) via the energy metabolism. The efficiency of obtaining ATP from OP is higher than that from SP owing to the mechanism used to obtain it. The SP mechanism is based on the formation of ATP, which comes from the phosphorylation of ADP via a reaction catalysed by a kinase protein, for instance pyruvate kinase and phosphoglycerate kinase. Whereas, the OP mechanism is based on the phosphorylation of ADP via a reaction catalysed by ATP synthase (ATPs). Therefore, the difference in production between SP and OP is related to the flux rate through kinase and synthase, respectively. Regarding SP, the flux rate is directly linked to glycolytic pathway, while OP is related to a proton motive force.

For a further insight regarding how the OP is related to the proton motive force within the energy metabolism, a detailed description of it will be presented in conjunction with **Figure 1-10** hereafter.

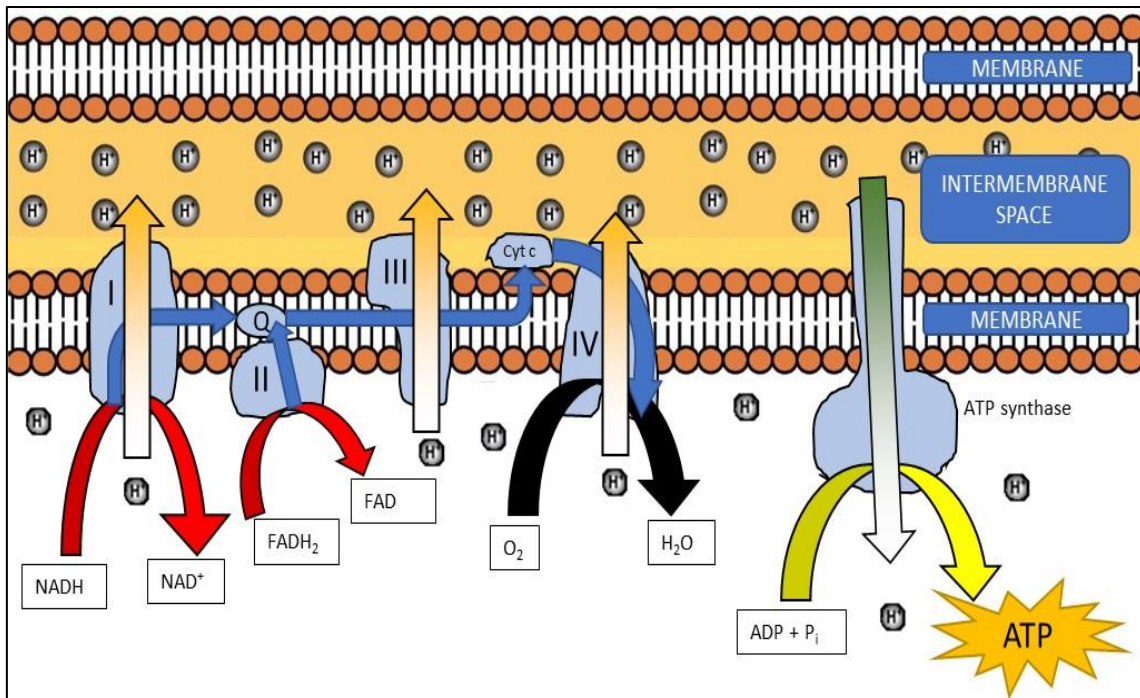


Figure 1-10. Description gradually of the oxidative phosphorylation. The colour code used is: red arrows represent the oxidation of NADH and FADH₂, black arrows represent the reduction of oxygen to water and the yellow ones represent the formation of ATP. Moreover, the arrows whose colour goes from white (low protons concentration) to orange (high protons concentration) represent the protons movement caused by an electron transport through the electron transport chain and arrows whose colour goes from dark green (high protons concentration) to white (low protons concentration) represent the protons movement caused by ATP synthase.

OP consists of two mechanisms: the electron transport chain and the protein ATP synthase, which are strictly related with each other regarding the formation of ATP. To have a functional OP, an intermembrane space is needed since this space is accountable for the formation of electrochemical gradient, based on a difference in proton concentration, which is required by the ATP synthetase in order to produce ATP.

As shown in **Figure 1-10**, the electron carriers (NADH and FADH₂) from the central carbon metabolism that are directed towards the energy metabolism are oxidized by the complex I and the complex II, respectively. Thereupon, a quinone (protein) is used as a mobile electron carrier from complex I and II to complex III. As a result, a proton motive force is created which promotes a proton movement through the complex I that goes from the inner side of the cell to the intermembrane space. Then, cytochrome c (protein, just as quinone) is used to transport electron from complex III to complex IV in order to reduce oxygen to water and, as a consequence, promoting the proton movement from the inner side of the cell to the intermembrane space trough complex III and IV. As a result of the proton motive force, a

difference in proton concentration between the inner side of the cell and the intermembrane space is achieved.

Finally, regarding the formation of ATP via OP by ATP synthase, ATP synthesis couples to an electrochemical gradient created by the difference in proton concentration between the intermembrane space and the inner side of the cell in order to phosphorylate ADP with a pyrophosphate. Therefore, the electrochemical gradient induced by the difference in proton concentration between the inner side of the cell and the intermembrane space owing the electron transport chain is used by ATP synthase to phosphorylate ADP to ATP.

Up until this point, the central carbon metabolism and the energy metabolism, related to the formation of precursors and ATP required for the synthesis of biomass, while growing on glucose-media at the optimal growth rate, have been described. However, there is a difference between the three selected expression platforms depending on where both metabolisms are carried out inside the cell. This difference lies in the fact that a bacteria is a prokaryotic cell while yeast and animal cell are eukaryotic cells. the central carbon metabolism and the energy metabolism regarding prokaryotic cells are located in cytoplasm and in the cytoplasmatic membrane, respectively. Meanwhile, regarding eukaryotic cells, the glycolytic pathway and PPP that take part in the central metabolism are located in cytoplasm, while TCA cycle is located inside the mitochondria and on the other hand, the energy metabolism solely takes place in the mitochondrial intermembrane space.

Despite the difference previously mentioned, the three expression platforms have a common behaviour towards the production of non-desired products that come from the central carbon metabolism while growing on glucose-media in aerobic conditions. As a result, they share a problem related to the incapacity of transforming all the available glucose into biomass, CO₂ and H₂O.

This problem has been widely stated in publications regarding the production of acetate in bacteria, ethanol in yeast, and lactate in animal cells. A metabolic study based on a further insight of the metabolic behaviour about why these products are produced will be developed in **chapter 3**, **chapter 4**, and **chapter 5**, respectively.

Several approaches trying to reduce or deplete the formation of these products have been the aim of many publications. In order to attain this objective, the publications revolve around two main topics:

1. The modification of the metabolic behaviour by introduction, knocking-down or knocking-out genes that are related to central carbon metabolism (Dittrich et al., 2005),
2. The decrease of the product formation by using engineering tools applied to the optimization of the bioprocess (De Mey et al., 2007).

Therefore, and taking into consideration how changes in metabolism affect biomass formation in the different expression platform, in order to achieve higher volumetric productivities this work will focused on the development of bioprocess engineering tools for bioprocess intensification.

On this basis, this work is structured in two blocks, the first one that is related to the study of the carbon and energy metabolism in each selected expression platform that tacks from **chapter 3** to **chapter 6** while the second one that tacks from **chapter 7** to **chapter 9** is based on the applications of the engineering tools.

1.4 Bioprocess design

A bioprocess can be defined as any process that involves cells or biological molecules, as raw materials or as integral components of the process itself, in order to obtain the desired products (Bailey, 1991). In general, as shown in **Figure 1-11** a bioprocess is divided in three specific processes: upstream, cell harvesting, and downstream (Clapp et al., 2018), which are described hereafter:

Upstream process includes operations such as culture or fermentation media preparation and cell expansion in a bioreactor. Regarding the preparation of media, it involves the selection of how the media compounds are sterilized (chemical, radiation, heat or filtration methodology) according to its chemical properties (for example, the thermolability of vitamins (Ryley & Kajda, 1994)) in order to perform the complete destruction or removal of undesired microorganisms. Thereupon, cell culture is defined as the process where cells are able to grow under controlled conditions until they are harvested.

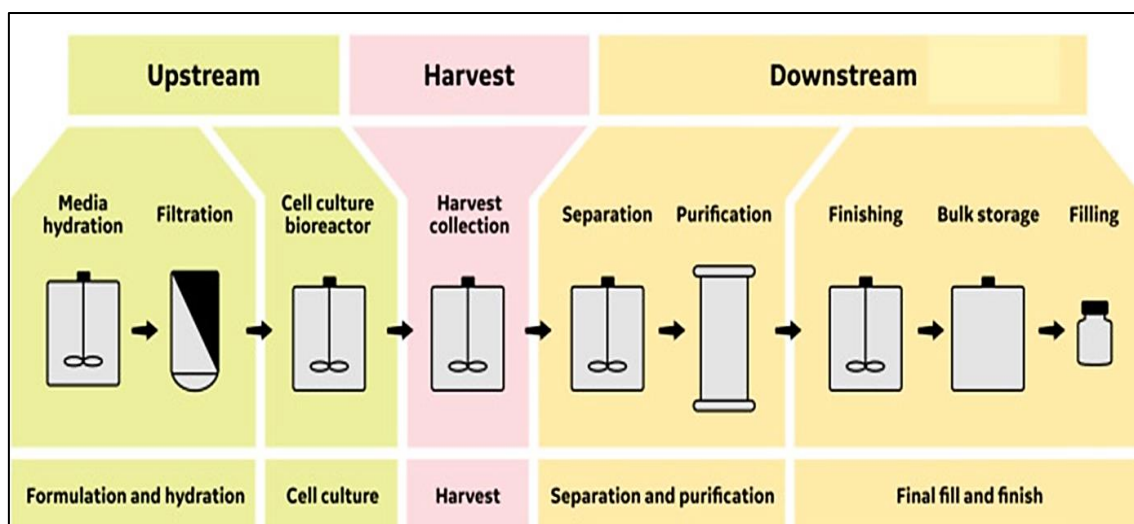


Figure 1-11. A simplified view of the several parts that take part in a bioprocess (graph from (Clapp et al., 2018)).

Several publications have been found that focus on the optimization of the upstream, downstream or both of them in order to increase volumetric productivity using different expression platforms. For instance, *E. coli* (Šiurkus et al., 2010) (von Stosch et al., 2016a) (von Stosch et al., 2016b), *S. cerevisiae* (Kumar et al., 2017) (Saranraj et al., 2017) and animal cells (Quiroga-Campano et al., 2018) (Lee et al., 2019).

As was mentioned before, the aim of this work is to increase the volumetric productivity by the increase of biomass concentration, which means the optimization of a key step of the upstream process. This task, as shown in **Figure 1-12**, includes various areas that tackle cell line development and engineering, cell clone selection, media definition, bioprocess development and scale up, reactor design, the control and monitor of the process and the corresponding analytics as well (Gronemeyer et al., 2014). Thereupon, a description regarding the applications associated to each area are presented hereafter.

Regarding the cell engineering area, it is based on the applications that are related to genetic modifications and alterations of host cells for enhancing the yield and quality of the expressed protein. For instance, the cassette optimization of the plasmid used for expressing the product in order to rise its production (Roldán, 2018) or the modification of specific genes that might restructure the metabolism in order to optimize the conversion of carbon source towards an specific product (Du et al., 2019).

The area related to medium consist on the applications that are based on looking for the maximum available concentration of the media compounds in order to produce the maximum

biomass concentration without inhibiting the growth rate (Landauer, 2014). Moreover, tackled in this area is found the optimization of the media regarding the change in its physicochemical properties (foam formation) owing to the interaction with the bioreactor operation conditions.

The definition of the mode of operation area tackles the applications that are based on proving several bioprocess strategies in order to increase the biomass or product production. The most used bioprocess strategies are batch, fed-batch, continuous and perfusion. A further description will be presented in the following section.

The area on top of the bioreactor design revolves around the applications that study the improvement of the containment system. For instance, the use of single-use reactors in order to surpass the limitations of the stainless steel regarding cleaning and sterilization procedures that brings several issues for process validation and reproducibility. These issues are solved by using single-use bioreactors, which are commercially supplied already sterile and validated for final usage (Lowry, 2018).

In regard with the process monitoring area, its objective is based on creating and improving monitoring tools based on proves that provide as much information of the process as possible, quickly and with high accuracy. As a result, the process can be more stable, reproducible, and efficient leading to the reproducibility of high-quality products (Biechele et al., 2015). Moreover, the definition of new monitoring tools will be useful for the improvement of bioprocess strategies such as fed-batch and perfusion because their success is strictly related to the monitoring tools capacity to provide accurate information with high cadence about the culture state

Finally, the analytics area is focused on the development of new physical or chemical measuring principles in order to fulfil the analytical requirements of the bioprocess regarding prove design, the detection and the quantification of products and media compounds as well. For instance the use of a fluorescent sensor in order to measure pH (X.-Y. Wang et al., 2016).

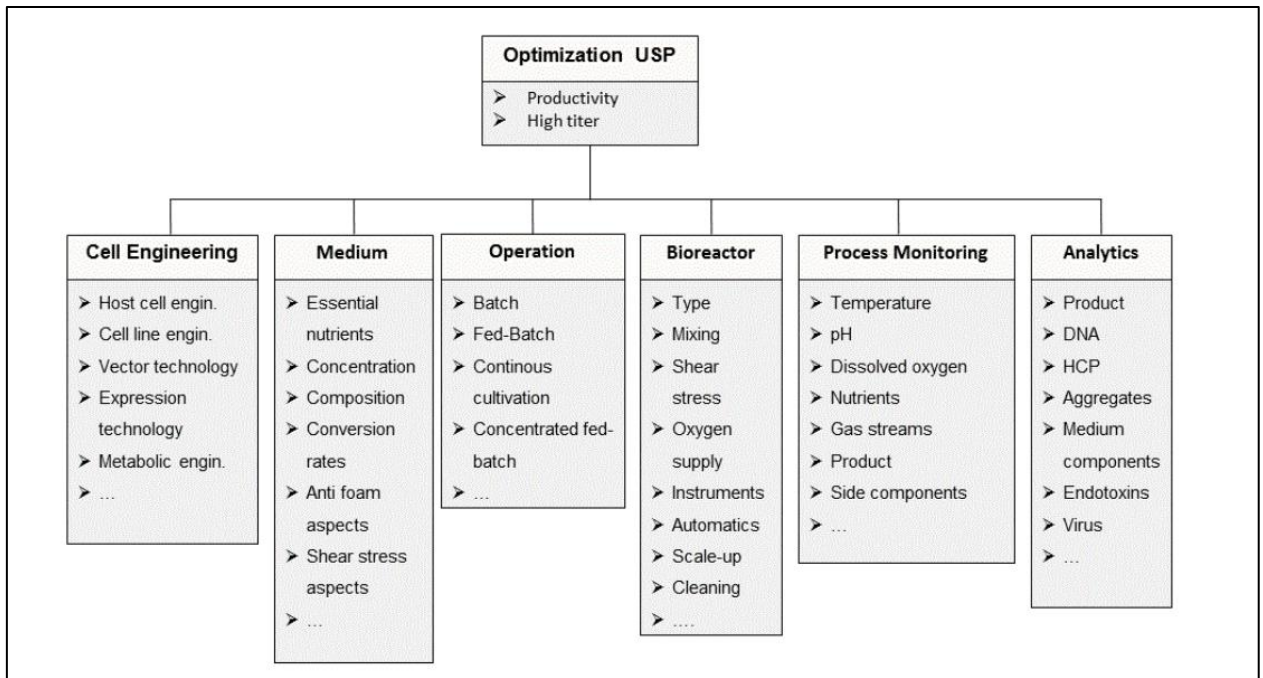


Figure 1-12. Detailed scheme of the different areas in USP optimization (graph from (Gronemeyer et al., 2014)).

Up until now the key issues related to the optimization of USP have been presented, although this work will be solely focused on increasing the volumetric productivity by means of the optimization of upstream process, in particular, the optimization of bioprocess strategies which is related to the areas previously described of medium, operation, bioreactor and process monitoring. It is important to point out that in order to provide innovations regarding this matter, this work will take the metabolic study of the used expression platform into consideration when the upstream optimization will be performed. The upstream optimization will be described for *E. coli*, *S. cerevisiae* and hybridoma cultures in **chapters 7, 8, and 9**, respectively.

1.4.1 Bioprocess strategies

The aim of bioprocess strategies is to increase biomass concentration by choosing the optimal culture media and culture operation strategy as well. This choice must be done based on a compromise between the scale of the process, the investment in both cost and time, and the final productivity desired (Kadic & Heindel, 2014).

Regarding media definition, one of the key elements within a bioprocess is the selection of the optimal culture media in order to produce the maximum biomass concentration in the minimum

time. Media not only have to contain all the nutrients and metabolites needed for cell growth and protein expression, but also have to provide with appropriate environmental conditions for cell expansion. Depending on the organisms cultured, culture media would contain glucose or other carbon sources, salts (as phosphor and nitrogen sources), vitamins, a mixture of amino acids, growth factors and other nutrients. Moreover, the definition of the media composition is related to studies about how variations in media composition affects growth rate, through inhibition or toxicity (Balaraman & Mathew, 2006).

Concerning culture operation strategies, the used ones in the biotechnological industry are batch, fed-batch, continuous, and perfusion (W-S. & W., 2012) whose main features are shown in **Figure 1-13** and described down below:

Batch:

The picked organism is cultured in a definite media until they stop growing. Nutrient limitation, low cell densities, low productivity and the high toxic accumulation by-products from the carbon metabolism are the disadvantages of this system.

Fed-batch:

A batch culture where a gradual addition of a fresh concentrated medium is added over time. This operation mode avoids the nutrient limitation, obtaining higher cell densities and product concentration. However, the accumulation of toxic metabolites in the culture media leads microorganism to stop growing.

Continuous:

Characterized for an inlet feeding medium continuously added into the bioreactor and an equal outlet product continuously extracted, keeping constant culture volume. Commonly used to perform metabolic studies, due to the possibility to obtain steady-state cell cultures, although not widely used by the industry due to the low productivities achieved.

Perfusion:

Continuous culture equipped with a cell retention system that permits removal of the growth-inhibitory by-products at the outlet stream while maintaining the cells in the bioreactor.

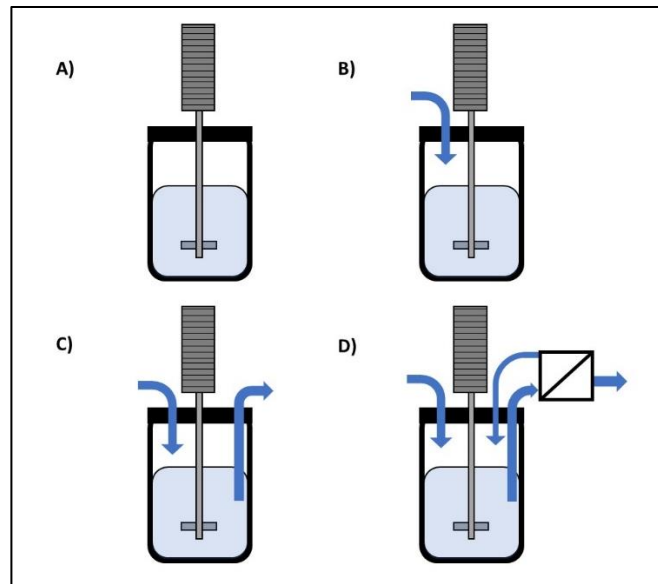


Figure 1-13. Scheme of the main culture operation strategies used in bioprocesses: (A) batch culture , B) Fed batch culture , C) Continuous culture and D) Perfusion culture).

Basically, the difference between bioprocess strategies lies in the maximum achieved biomass concentration, as shown in **Figure 1-14**, due to their different capacity to diminish or eliminate growth-inhibitor by-products such as acetate, ethanol or lactate that are produced by *E. coli*, *S. cerevisiae* and animal cells, respectively.

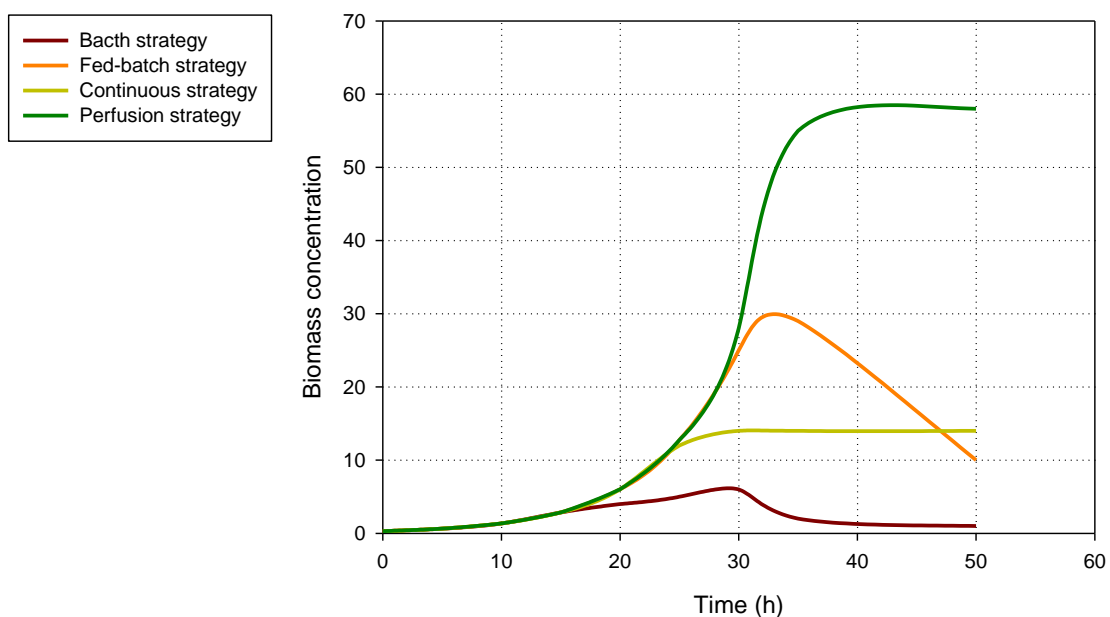


Figure 1-14. Theoretical overview of the biomass concentration that can be achieved in each bioprocess strategy (each strategy have an allocated colour: brown for the batch, dark yellow for the continuous, orange for the fed-batch and green for the perfusion).

Regarding the biomass achieved in each bioprocess strategy, the batch has the lesser biomass concentration because the initial glucose concentration is limited in order to avoid growth inhibition conditions and, as a result, the biomass that can be generated is limited by the initial amount of glucose. Therefore, in order to surpass this glucose amount limitation, a feeding flow of nutrients is required for achieving higher biomass concentrations while growth inhibition conditions are prevented. As a result, fed-batch strategies are designed. Moreover, the increase in biomass concentration leads to an increase of growth-inhibitor by-products in fed-batch strategies. Consequently, a limitation in the biomass concentration is achieved. Up to this point, there are two feasible solutions:

1. The use of continuous cultures, which have a low biomass concentration owing to cells leaving the bioprocess along with the continuously extracted media, although avoiding the by-product inhibition as well.
2. The use a perfusion strategy, that is a continuous culture coupled with a cell retention system that enables the cells to stay within the reactor. It is important the remark that the perfusion strategy is characterized by being a high productive process owing to high amounts of the interest product can be obtained due to the highest biomass concentrations can be achieved (Bonham-Carter & Shevitz, 2011).

Even if the best strategy to produce biomass is perfusion, it is the most complex strategy to perform regarding the bioreactor and downstream design. Specifically within animal cell cultures, in the last years perfusion has been the most used strategy owing to its volumetric productivity (Bielser et al., 2018) . On the other hand, fed-batch strategies are the preferred options within high cell density *E. coli* and *S. cerevisiae* bioprocesses (Riesenberg & Guthke, 1999).

Therefore, it might be stated that the biomass concentration is function of the bioprocess strategy used. On this basis, a further description of this relation by understanding how a bioreactor (the core of a bioprocess) is designed will be presented in the following section.

1.4.2 Bioreactor

As mentioned above, changing the culture operation strategy could drive to a maximization of volumetric productivity. However, if there is no possible change in culture operation strategy, a new approach based on understanding the characteristic equation of a bioreactor should be the aim.

First and foremost, a bioprocess is a combination of metabolic processes that involve stoichiometry, thermodynamics, microbial kinetics and physical processes such as mixing, power consumption, heat transport and mass transport. (Emal Qazizada, 2016)

For generating a mathematical algorithm that gives us information about the metabolic-physiologic and physical properties, the characteristic equation is needed. There are two different characteristic equations: the energy balance and the mass balance. (M.Doran, 2000)

The mass balance has a theoretical framework within the law of conservation of mass that establishes the next fact: “Mass is neither created nor destroyed in chemical reactions. In other words, the mass of any one element at the beginning of a reaction will equal the mass of that element at the end of the reaction. If we account for all reactants and products in a chemical reaction, the total mass will be the same at any point in time in any closed system” (Sterner et al., 2011).

Performing a mass balance in a bioreactor, a characteristic equation is created. This equation differs within culture strategies as shown in **Figure 1-15**.

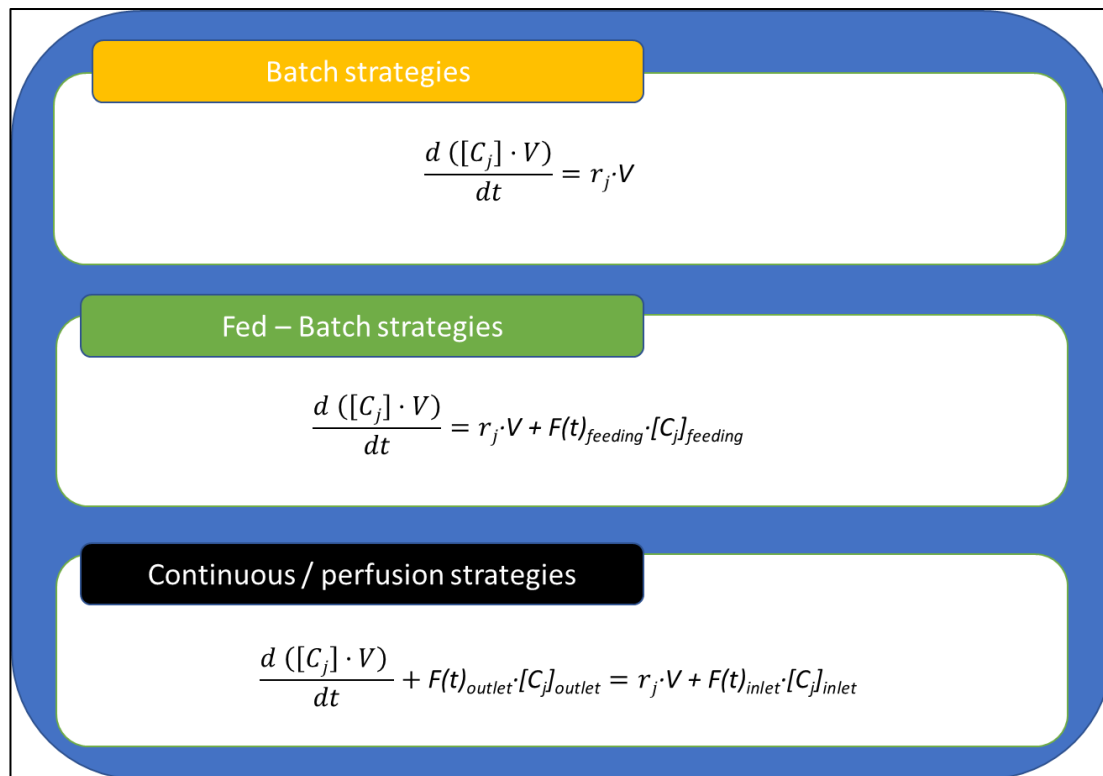


Figure 1-15. Characteristic equation of a compound j from all culture operation strategies.

More specifically, the characteristic equation informs about how whole the system (environment/bioreactor) interacts with the biocatalyst, for instance: the flow needed for growing at specific growth rate or the nutrient concentration of the inlet flow for achieving a biomass concentration in a continuous culture or the flow rate of feeding in fed batch cultures.

As a result, the operational values that define the bioprocess strategy are related to the metabolic data or, in other words, to the metabolic behaviour of the biocatalyst.

The metabolic data, already showed in a precedent section, will be studied using system biology tools that will be introduced and explained in the following section.

1.5 System biology and Omics

Although there is not yet a consensus about what is meant by “systems biology”, the clear goal of this field is to understand biological systems studying the structure and dynamics of cellular function, rather the characteristic of isolated parts of a cell; leading to the idea that the whole is greater than the sum of parts (Kitano, 2002) (Kitano, 2005).

The cycle of research in systems biology, which is shown in **Figure 1-16**, begins with the selection of the biological subject of study and the creation of a model representing the phenomenon that is studied. The model represents a computable set of assumptions and hypotheses that need to be tested or supported experimentally. Computational “*in silico*” experiments, such as simulation, on models reveal computational adequacy of the assumptions and hypotheses embedded in each model. Inadequate models would expose inconsistencies with established experimental facts, and thus need to be rejected or modified. Models that pass this test become subjects of a system analysis where a number of predictions may be made. Then, a set of predictions are selected for “*wet*” laboratory experiments. Successful experiments are those that eliminate inadequate models. Models that survive this cycle are deemed to be consistent with existing experimental evidence (Kitano, 2002).

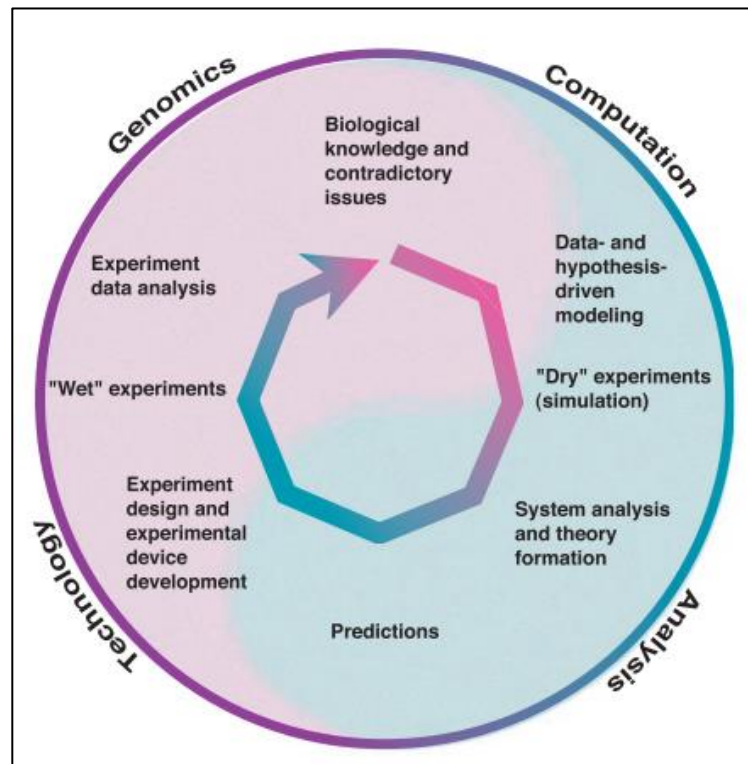


Figure 1-16. Hypothesis-driven research in Systems Biology (Kitano, 2002).

Nowadays, biologists tend to view cells as systems, rather than focusing their attention on individual cellular components. This change is owing to the emergence of high-throughput experimental technologies that generate a several sets of biological raw data; whose interrelation generates a multilayer system that give information about a cell as an interconnected system not as a “black box”, as shown in **Figure 1-17**.

The emergence of the “omics” branch of science that allows the characterization and quantification of biological molecules that translate into the structure, function and dynamics of an organism from a massive data sets has accelerated this process of recognizing a cell as an interconnected system (Bernhard Ø. Palsson, 2006). These new technologies allow to analyse and quantify the different biochemical constituents existing within the cell (Ram et al., 2012). On this basis, investigators are making progress in identifying, extracting and interpreting biological insights from omics data sets (Joyce & Palsson, 2006).

The most common used omics technologies that are used to generate these data sets are described down below:

- Genomics: covers the study of the genome sequence and the information contained therein. More than 300 genome-sequencing studies corresponding to different organisms have been published and hundreds are underway (Pagani et al., 2012). In this field, genome annotation defines the complement proteins and RNAs corresponding to the genome that are available for the cell (Joyce & Palsson, 2006).
- Transcriptomics: provides information about the identification and quantification of RNA transcripts, indicating the active compounds within the cell and giving crucial information regarding the expression state (Joyce & Palsson, 2006).
- Proteomics: Based on the identification and quantification of protein levels encoded by the genome (Cox & Mann, 2011). Proteomics is a particularly rich source of biological information because proteins are involved in almost all biological activities and they also have diverse properties, which collectively contribute greatly to our understanding of biological systems (Patterson & Aebersold, 2003)
- Metabolomics: Groups the identification and quantification of metabolome, that tackles the complete set of metabolites of the cell. The metabolome represents the output that results from the cellular integration of the transcriptome, proteome and the result of protein-DNA and protein-protein interactions. Therefore, provides not only a list of metabolite components but also a functional readout of the cellular state (Joyce & Palsson, 2006).
- Fluxomics: the total set of fluxes in the cell metabolic network. Flux analysis provides a true dynamic picture of the phenotype capturing the metabolome in its functional interactions with the environment and the genome (Cascante & Marin, 2008)

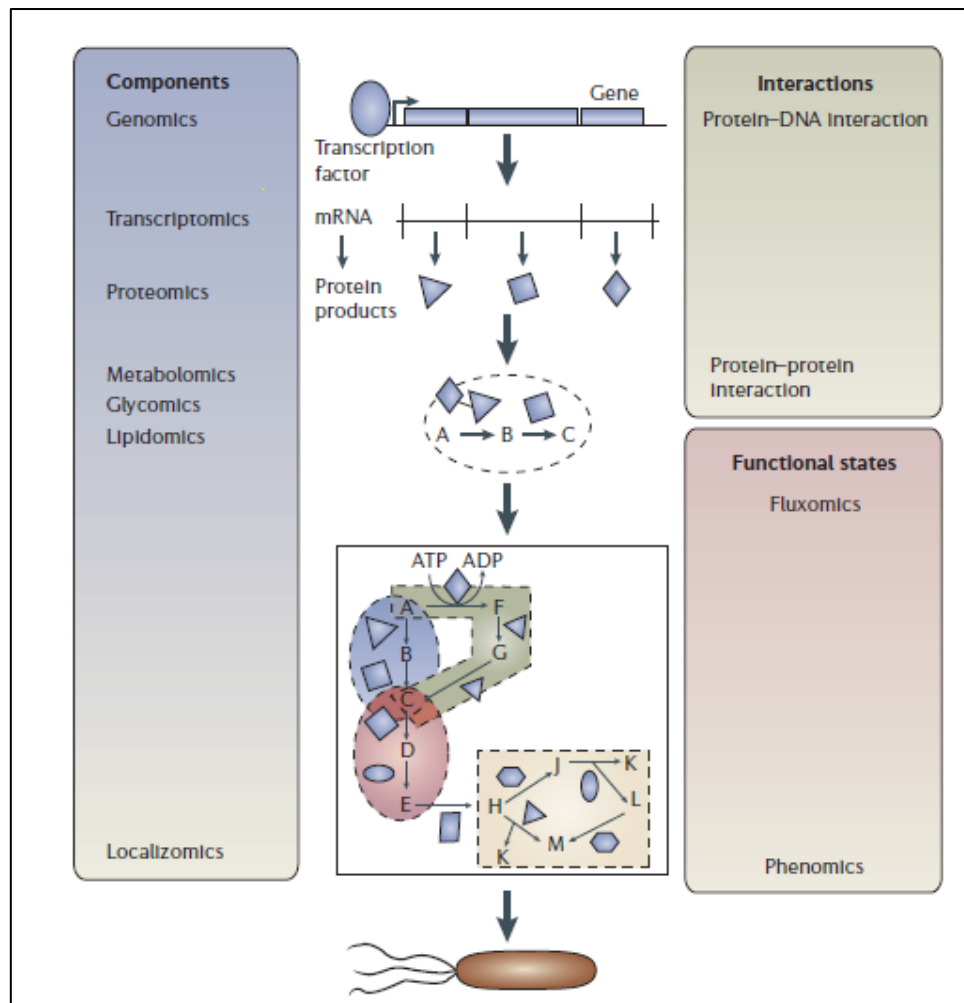


Figure 1-17. Interconnection between all OMICs.(graph from (Joyce & Palsson, 2006))

This work revolves around fluxomics in order to use metabolic models for understanding how the metabolism of the selected expression platforms behaves when growing on glucose-based media. Moreover, the behaviour described in the metabolic models will take part in the definition of the bioprocess strategy in order to enhance the volumetric productivity.

1.6 Genome-scale metabolic models as example of fluxomics

Genome-scale metabolic models have become a popular tool for systems biology, they have been used in many fields such as industrial biotechnology and others.(Zhang & Hua, 2016)

Genome-scale metabolic models are reconstructions of metabolic networks of many kinds of cells, including those of microorganisms, plants and mammals. For better understanding of the

metabolic networks, mathematical tools such as Flux Balance Analysis (FBA) have been developed.

As shown in **Figure 1-18**, FBA is based on the principle of conservation of mass in a network, which utilizes the stoichiometric matrix and a biologically relevant objective function to identify optimal reaction flux distributions and by far the most used for analysing the reaction's flux in a specific network. (Raman & Chandra, 2009)

FBA uses linear optimization, assuming there is no accumulation of metabolites, to determine the steady-state flux distribution by maximizing an objective function (Raman and Chandra, 2009) such as ATP maintenance or biomass production.

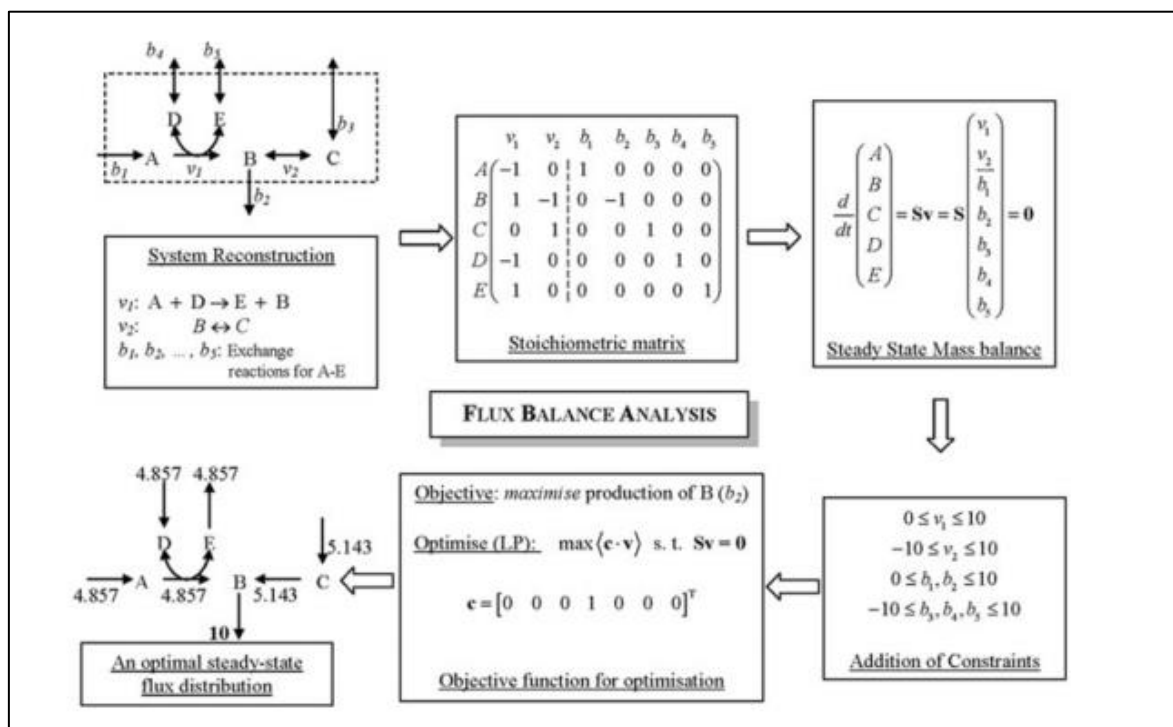


Figure 1-18. Outline of major steps in Flux Balance Analysis. (Raman & Chandra, 2009)

The variables used for FBA include the fluxes from metabolic reactions to transport; in addition to other model parameters such as reaction stoichiometry, biomass composition, ATP requirements, and the upper and lower bounds of individual fluxes, which define the boundaries of the reactions rate values in the model (Marín de Mas, 2015).

To sum up, the work presented establishes a link between metabolism studies and bioprocess optimization. In the first place, the core metabolism of the selected three expression platforms

(bacteria, yeast or animal cells) will be characterized using genome-scale metabolic models and flux balance techniques in bioreactor (**chapter 3 to chapter 6**). Thus, this knowledge will be applied in the optimization of operation culture strategies using the metabolic results in the definition of the key bioreactor parameters (**chapter 7 to chapter 9**). As a result, the volumetric productivity will be enhanced by the increase of biomass concentration.

1.7 References

- Arfin, T., & Sonawane, K. (2019). Integrating green chemistry and sustainable engineering. In *Ed .SHAHID -UL-ISLAM: Vol. Chap 18*.
- Baghban, R., Farajnia, S., Rajabibazl, M., Ghasemi, Y., Mafi, A. A., Hoseinpoor, R., Rahbarnia, L., & Aria, M. (2019). Yeast Expression Systems: Overview and Recent Advances. *Molecular Biotechnology*, 61(5), 365–384. <https://doi.org/10.1007/s12033-019-00164-8>
- Bailey, J. E. (1991). *20 Bioprocess Engineering* (pp. 425–462). [https://doi.org/10.1016/S0065-2377\(08\)60167-2](https://doi.org/10.1016/S0065-2377(08)60167-2)
- Balaraman, K., & Mathew, N. (2006). Optimization of media composition for the production of cyclosporin A by *Tolypocladium* species. *Indian Journal of Medical Research*, 123(4), 525–530.
- Baneyx, F., & Mujacic, M. (2004). Recombinant protein folding and misfolding in *Escherichia coli*. *Nature Biotechnology*, 22(11), 1399–1407. <https://doi.org/10.1038/nbt1029>
- Bernhard Ø. Palsson. (2006). *Systems Biology Properties of Reconstructed Networks*. <https://www.cambridge.org/gb/academic/subjects/life-sciences/genomics-bioinformatics-and-systems-biology/systems-biology-properties-reconstructed-networks?format=HB&isbn=9780521859035#contentsTabAnchor>
- Biechele, P., Busse, C., Solle, D., Scheper, T., & Reardon, K. (2015). Sensor systems for bioprocess monitoring. *Engineering in Life Sciences*, 15(5), 469–488. <https://doi.org/10.1002/elsc.201500014>
- Bielser, J. M., Wolf, M., Souquet, J., Broly, H., & Morbidelli, M. (2018). Perfusion mammalian cell culture for recombinant protein manufacturing – A critical review. *Biotechnology Advances*, 36(4), 1328–1340. <https://doi.org/10.1016/j.biotechadv.2018.04.011>
- Bonham-Carter, J., & Shevitz, J. (2011). A brief history of perfusion biomanufacturing. *BioProcess International*, 9(9), 24–31.
- Cascante, M., & Marin, S. (2008). *Metabolomics and fluxomics approaches*. 67–82.
- Chen, C., Wong, H. E., & Goudar, C. T. (2018). Upstream process intensification and continuous manufacturing. *Current Opinion in Chemical Engineering*, 22, 191–198. <https://doi.org/10.1016/j.coche.2018.10.006>
- Clapp, K. P., Castan, A., & Lindskog, E. K. (2018). Upstream Processing Equipment. In *Biopharmaceutical Processing* (pp. 457–476). Elsevier. <https://doi.org/10.1016/B978-0-08-100623-8.00024-4>
- Connolly, T., & Gilmore, R. (1993). GTP hydrolysis by complexes of the signal recognition particle and the signal recognition particle receptor. *Journal of Cell Biology*, 123(4), 799–807. <https://doi.org/10.1083/jcb.123.4.799>

- Cooper, D. N., & Schmidtke, J. (1992). Molecular Genetic Approaches to the Analysis and Diagnosis of Human Inherited Disease: An Overview. *Annals of Medicine*, 24(1), 29–42.
<https://doi.org/10.3109/07853899209164142>
- Cox, J., & Mann, M. (2011). Quantitative, High-Resolution Proteomics for Data-Driven Systems Biology. *Annual Review of Biochemistry*, 80(1), 273–299. <https://doi.org/10.1146/annurev-biochem-061308-093216>
- DaSilva, E. J., Baydoun, E., & Badran, A. (2002). Biotechnology and the developing world. *Electronic Journal of Biotechnology*, 5(1). <https://doi.org/10.2225/vol5-issue1-fulltext-1>
- De Mey, M., De Maeseneire, S., Soetaert, W., & Vandamme, E. (2007). Minimizing acetate formation in *E. coli* fermentations. *Journal of Industrial Microbiology and Biotechnology*, 34(11), 689–700.
<https://doi.org/10.1007/s10295-007-0244-2>
- Dittrich, C. R., Vadali, R. V., Bennett, G. N., & San, K. Y. (2005). Redistribution of metabolic fluxes in the central aerobic metabolic pathway of *E. coli* mutant strains with deletion of the *ackA-pta* and *poxB* pathways for the synthesis of isoamyl acetate. *Biotechnology Progress*, 21(2), 627–631.
<https://doi.org/10.1021/bp049730r>
- Du, L., Zhang, Z., Xu, Q., & Chen, N. (2019). Central metabolic pathway modification to improve L-tryptophan production in *Escherichia coli*. *Bioengineered*, 10(1), 59–70.
<https://doi.org/10.1080/21655979.2019.1592417>
- Duarte, T. M., Carinhas, N., Barreiro, L. C., Carrondo, M. J. T., Alves, P. M., & Teixeira, A. P. (2014). Metabolic responses of CHO cells to limitation of key amino acids. *Biotechnology and Bioengineering*, 111(10), 2095–2106. <https://doi.org/10.1002/bit.25266>
- Dunbar, C. E., High, K. A., Joung, J. K., Kohn, D. B., Ozawa, K., & Sadelain, M. (2018). *Gene therapy comes of age*. 4672(January). <https://doi.org/10.1126/science.aan4672>
- Emal Qazizada, M. (2016). Design of a batch stirred fermenter for ethanol production. *Procedia Engineering*, 149, 398–403.
- Evans, W. E., & Relling, M. V. (2004). Moving towards individualized medicine with pharmacogenomics. *Nature*, 429(6990), 464–468. <https://doi.org/10.1038/nature02626>
- Gambardella, A., Orsenigo, L., & Pammolli, F. (2000). Global Competitiveness in Pharmaceuticals : A European Perspective. *MPRA Paper*, 15965.
- Gronemeyer, P., Ditz, R., & Strube, J. (2014). *Trends in Upstream and Downstream Process Development for Antibody Manufacturing*. 188–212. <https://doi.org/10.3390/bioengineering1040188>
- Hoehler, T. M., & Jørgensen, B. B. (2013). Microbial life under extreme energy limitation. *Nature Reviews Microbiology*, 11(2), 83–94. <https://doi.org/10.1038/nrmicro2939>

- Hoffmann, F., & Rinas, U. (2004). *Stress Induced by Recombinant Protein Production in Escherichia coli* (pp. 73–92). <https://doi.org/10.1007/b93994>
- Jameel, S. (2011). Ethics in biotechnology and biosecurity. *Indian Journal of Medical Microbiology*, 29(4), 331. <https://doi.org/10.4103/0255-0857.90155>
- Joyce, A. R., & Palsson, B. (2006). The model organism as a system: Integrating “omics” data sets. *Nature Reviews Molecular Cell Biology*, 7(3), 198–210. <https://doi.org/10.1038/nrm1857>
- Kadic, E., & Heindel, T. J. (2014). *An Introduction to Bioreactor Hydrodynamics and Gas-Liquid Mass Transfer*.
- Kafarski, P. (2012). Rainbow code of biotechnology. *Chemik*, 66(8), 814–816.
- Kahn, R. A. (2019). Regulators of signal transduction: families of GTP-binding proteins. In *Developments In Cancer Chemotherapy vol.2*. (p. Chapter 4).
- Kamm, B., P.R., G., & Kamm, M. (2010). *Biorefineries – Industrial Processes and Products Review: status Quo and Future Directions*. <https://www.wiley.com/en-us/Biorefineries+Industrial+Processes+and+Products%3A+Status+Quo+and+Future+Directions-p-9783527329533>
- Kirsner, R. S. (1993). The Biology of Skin Grafts. *Archives of Dermatology*, 129(4), 481. <https://doi.org/10.1001/archderm.1993.01680250093014>
- Kitano, H. (2002). Systems biology: A brief overview. *Science*, 295(5560), 1662–1664. <https://doi.org/10.1126/science.1069492>
- Kitano, H. (2005). Computational systems biology. *Nature*, 420(November). <http://www.nature.com/nature/journal/v420/n6912/abs/nature01254.html>
- Krohn, B. J., McNeff, C. V., Yan, B., & Nowlan, D. (2011). Production of algae-based biodiesel using the continuous catalytic Mcgyan® process. *Bioresource Technology*, 102(1), 94–100. <https://doi.org/10.1016/j.biortech.2010.05.035>
- Kumar, R., Ghosh, A. K., & Pal, P. (2017). Fermentative energy conversion: Renewable carbon source to biofuels (ethanol) using *Saccharomyces cerevisiae* and downstream purification through solar driven membrane distillation and nanofiltration. *Energy Conversion and Management*, 150, 545–557. <https://doi.org/10.1016/j.enconman.2017.08.054>
- Landauer, K. (2014). *Designing Media for Animal Cell Culture: CHO Cells, the Industrial Standard* (pp. 89–103). https://doi.org/10.1007/978-1-62703-733-4_7
- Laursen, L. (2010). How green biotech turned white and blue. *Nature Biotechnology*, 28(5), 393–395. <https://doi.org/10.1038/nbt0510-393>

- Lee, S.-M., Plieskatt, J., Krishnan, S., Raina, M., Harishchandra, R., & King, C. R. (2019). Expression and purification optimization of an N-terminal Pfs230 transmission-blocking vaccine candidate. *Protein Expression and Purification*, 160, 56–65. <https://doi.org/10.1016/j.pep.2019.04.001>
- Lever, M. A., Rogers, K. L., Lloyd, K. G., Overmann, J., Schink, B., Thauer, R. K., Hoehler, T. M., & Jørgensen, B. B. (2015). Life under extreme energy limitation: a synthesis of laboratory- and field-based investigations. *FEMS Microbiology Reviews*, 39(5), 688–728. <https://doi.org/10.1093/femsre/fuv020>
- Lowry, A. (2018). *Single-Use Systems Advance Upstream Processing*.
- M.Doran, P. (2000). *Bioprocess Engineering Principles*.
- Marín de Mas, I. (2015). *Development and application of novel model-driven and data-driven approaches to study metabolism in the framework of systems medicine*. <http://diposit.ub.edu/dspace/handle/2445/65987>
- Matyushenko, I., Sviatukha, I., & Grigorova-Berenda, L. (2016). Modern Approaches to Classification of Biotechnology as a Part of NBIC-Technologies for Bioeconomy. *British Journal of Economics, Management & Trade*, 14(4), 1–14. <https://doi.org/10.9734/bjemt/2016/28151>
- Mehta, A. (2019). *Downstream Processing for Biopharmaceuticals Recovery*. <https://doi.org/10.1007/978-3-030-01881-8>
- Mocellin, S., Provenzano, M., Rossi, C. R., Pilati, P., Nitti, D., & Lise, M. (2005). DNA array-based gene profiling: From surgical specimen to the molecular portrait of cancer. *Annals of Surgery*, 241(1), 16–26. <https://doi.org/10.1097/01.sla.0000150157.83537.53>
- Noh, S. M., Park, J. H., Lim, M. S., Kim, J. W., & Lee, G. M. (2017). Reduction of ammonia and lactate through the coupling of glutamine synthetase selection and downregulation of lactate dehydrogenase-A in CHO cells. *Applied Microbiology and Biotechnology*, 101(3), 1035–1045. <https://doi.org/10.1007/s00253-016-7876-y>
- Pagani, I., Liolios, K., Jansson, J., Chen, I. M. A., Smirnova, T., Nosrat, B., Markowitz, V. M., & Kyrpides, N. C. (2012). The Genomes OnLine Database (GOLD) v.4: Status of genomic and metagenomic projects and their associated metadata. *Nucleic Acids Research*, 40(D1), 475–479. <https://doi.org/10.1093/nar/gkr1100>
- Park, J. O., Rubin, S. A., Xu, Y. F., Amador-Noguez, D., Fan, J., Shlomi, T., & Rabinowitz, J. D. (2016). Metabolite concentrations, fluxes and free energies imply efficient enzyme usage. *Nature Chemical Biology*, 12(7), 482–489. <https://doi.org/10.1038/nchembio.2077>
- Patterson, S. D., & Aebersold, R. H. (2003). Proteomics: The first decade and beyond. *Nature Genetics*, 33(3S), 311–323. <https://doi.org/10.1038/ng1106>

- Possas C. et al. (2020). Vaccines: Biotechnology Market, Coverage, and Regulatory Challenges for Achieving Sustainable Development Goals. In *Bioeconomy for Sustainable Development* (pp. 264–302). https://doi.org/https://doi.org/10.1007/978-981-13-9431-7_14
- Quiroga-Campano, A. L., Panoskaltsis, N., & Mantalaris, A. (2018). Energy-based culture medium design for biomanufacturing optimization: A case study in monoclonal antibody production by GS-NS0 cells. *Metabolic Engineering*, 47, 21–30. <https://doi.org/10.1016/j.ymben.2018.02.013>
- Ram, P. T., Mendelsohn, J., & Mills, G. B. (2012). Bioinformatics and systems biology. *Molecular Oncology*, 6(2), 147–154. <https://doi.org/10.1016/j.molonc.2012.01.008>
- Raman, K., & Chandra, N. (2009). Flux balance analysis of biological systems: Applications and challenges. *Briefings in Bioinformatics*, 10(4), 435–449. <https://doi.org/10.1093/bib/bbp011>
- Rehm, B. H. (2009). *Microbial production of biopolymers and polymer precursors: applications and perspectives*. [https://books.google.es/books?hl=es&lr=&id=Vu9kc0-uSJYC&oi=fnd&pg=PP1&dq=biopolymers+and+microorganisms&ots=8fNaLE2Qsm&sig=qIMpGIByRudsYYtquxsEMFC1nEY#v=onepage&q=biopolymers and microorganisms&f=false](https://books.google.es/books?hl=es&lr=&id=Vu9kc0-uSJYC&oi=fnd&pg=PP1&dq=biopolymers+and+microorganisms&ots=8fNaLE2Qsm&sig=qIMpGIByRudsYYtquxsEMFC1nEY#v=onepage&q=biopolymers+and+microorganisms&f=false)
- Riesenberger, D., & Guthke, R. (1999). High-cell-density cultivation of microorganisms. *Applied Microbiology and Biotechnology*, 51(4), 422–430. <https://doi.org/10.1007/s002530051412>
- Roldán, R. R. (2018). *Desarrollo de procesos de producción de proteínas terapéuticas: aumento de la productividad específica en células hek293*.
- Rosales-Mendoza, S. (2016). *Algae-Based Biopharmaceuticals*. Springer International Publishing. <https://doi.org/10.1007/978-3-319-32232-2>
- Ryley, J., & Kajda, P. (1994). Vitamins in thermal processing. *Food Chemistry*, 49(2), 119–129. [https://doi.org/10.1016/0308-8146\(94\)90148-1](https://doi.org/10.1016/0308-8146(94)90148-1)
- S.Olempska-Beer, Z., I.Merker, R., D.Ditto, M., & J.DiNovi, M. (2006). Food-processing enzymes from recombinant microorganisms—a review. *Regulatory Toxicology and Pharmacology, Volume 45*(2), 144–158. <https://www.sciencedirect.com/science/article/abs/pii/S0273230006000869?via%3Dihub>
- Saranraj, P., Sivasakthivelan, P., & Suganthi, K. (2017). *Baker 's Yeast : Historical Development , Genetic Characteristics , Biochemistry , Fermentation and Downstream Processing*. 6(7), 111–119.
- Siró, I., Kápolna, E., Kápolna, B., & Lugasi, A. (2008). Functional food. Product development, marketing and consumer acceptance—A review. *Appetite*, 51(3), 456–467. <https://doi.org/10.1016/j.appet.2008.05.060>
- Šiurkus, J., Panula-Perälä, J., Horn, U., Kraft, M., Rimšeliene, R., & Neubauer, P. (2010). Novel approach of high cell density recombinant bioprocess development: Optimisation and scale-up from

- microlitre to pilot scales while maintaining the fed-batch cultivation mode of *E. coli* cultures. *Microbial Cell Factories*, 9, 1–17. <https://doi.org/10.1186/1475-2859-9-35>
- Skutkova, H., Vitek, M., Bezdicek, M., Brhelova, E., & Lengerova, M. (2019). Advanced DNA fingerprint genotyping based on a model developed from real chip electrophoresis data. *Journal of Advanced Research*, 18, 9–18. <https://doi.org/10.1016/j.jare.2019.01.005>
- Sterner, R. W., Small, G. E., & Hood, J. M. (2011). The Conservation of Mass. *Nature Education Knowledge*. <https://www.nature.com/scitable/knowledge/library/the-conservation-of-mass-17395478/>
- van Bodegom, P. (2007). Microbial Maintenance: A Critical Review on Its Quantification. *Microbial Ecology*, 53(4), 513–523. <https://doi.org/10.1007/s00248-006-9049-5>
- von Stosch, M., Hamelink, J.-M., & Oliveira, R. (2016a). Toward intensifying design of experiments in upstream bioprocess development: An industrial *Escherichia coli* feasibility study. *Biotechnology Progress*, 32(5), 1343–1352. <https://doi.org/10.1002/btpr.2295>
- von Stosch, M., Hamelink, J. M., & Oliveira, R. (2016b). Hybrid modeling as a QbD/PAT tool in process development: an industrial *E. coli* case study. *Bioprocess and Biosystems Engineering*, 39(5), 773–784. <https://doi.org/10.1007/s00449-016-1557-1>
- W-S., H., & W., Z. (2012). *Cell culture bioprocess engineering*.
- Walsh, G. (2018). Biopharmaceutical benchmarks 2018. *Nature Publishing Group*, 36(12), 1136–1145. <https://doi.org/10.1038/nbt.4305>
- Wang, H.-M. D., Chen, C.-C., Huynh, P., & Chang, J.-S. (2015). Exploring the potential of using algae in cosmetics. *Bioresource Technology*, 184, 355–362. <https://doi.org/10.1016/j.biortech.2014.12.001>
- Wang, X.-Y., Huang, D.-W., Niu, C.-G., Guo, L.-J., Cui, J.-J., Hu, L.-Y., & Zeng, G.-M. (2016). An internal reference fluorescent pH sensor with two pH-sensitive fluorophores carrier. *Sensors and Actuators B: Chemical*, 234, 593–601. <https://doi.org/10.1016/j.snb.2016.05.036>
- Zhang, C., & Hua, Q. (2016). Applications of genome-scale metabolic models in biotechnology and systems medicine. *Frontiers in Physiology*, 6(JAN), 1–8. <https://doi.org/10.3389/fphys.2015.00413>

2. Objectives

The work presented in the thesis has been developed within the Cellular and Bioprocess Engineering Group of Universitat Autònoma de Barcelona. The main objective of the group is the development, optimization and scaling up of bioprocesses using bacteria, yeast and animal cells. In particular, this work is focused on the study and improvement of biopharmaceuticals production in *Escherichia coli* (*E. coli*), *Saccharomyces cerevisiae* (*S. cerevisiae*), HEK293 and a hybridoma animal cell lines. The first aim of the thesis is to study the metabolism of the entire microorganisms mentioned in bioreactor cultures, specifically regarding the carbon and energetic metabolism and the by-product production. This knowledge will be applied to design new control systems for the optimization of the feeding profiles in fed-batch and perfusion cultures, in order to obtain higher cell densities and productivities.

These two main objectives can be divided in the following sub-sections:

- To study the physiology of the glucose/acetate metabolism for two strains of *E. coli* using bioreactors. Specifically, *E. coli* M15 as an acetate producer and an *E. coli* BL21 as a non-acetate producer.
- To study the physiology of the glucose/ethanol metabolism for two yeast strains using bioreactors. Specifically, *S. cerevisiae* as an ethanol producer and *Pichia pastoris* (*P. pastoris*) as a low-ethanol producer.
- To study the physiology of several carbon sources/lactate metabolism for the human cell line HEK293 using bioreactors.
- To study the physiology of the glucose/lactate metabolism for two animal cell lines using bioreactors, specifically hybridoma KB26.5 and hybridoma KB26.5-BHRF1.
- To perform a deeper study of the glucose and acetate metabolic phenotypes observed in *E. coli* M15 and *E. coli* BL21 cultures by mean of Metabolic Flux Balance Analysis. To study and compare the flux of the main intracellular pathways through using the corresponding reduced genome-scale metabolic model.
- To perform a deeper study of the glucose and ethanol metabolic phenotypes observed in *S. cerevisiae* and *P. pastoris* cultures by mean of Metabolic Flux Balance Analysis. To study and compare the flux of the main intracellular pathways through using the corresponding reduced genome-scale metabolic model.
- To perform a deeper study of the glucose and lactate metabolic phenotypes observed in hybridoma KB26.5 and hybridoma KB26.5-BHRF1 cultures by mean of Metabolic Flux Balance Analysis. To study

and compare the flux of the main intracellular pathways through using the corresponding reduced genome-scale metabolic model.

- To perform a deeper study of the different carbon sources and lactate metabolic phenotypes observed in HEK293 cultures by mean of Metabolic Flux Balance Analysis. To study and compare the flux of the main intracellular pathways through using the corresponding reduced genome-scale metabolic model.
- To develop a global theory in order to explain the sub-product production in bacteria, yeast and animal cells, using the theories of biochemical evolution and endosymbiosis.
- To implement a new non-invasive monitoring tool based on the carbon exchange rate and the alkali buffer addition in bioreactors for the on-line estimation of biomass concentration in cultures of *E.coli* BL21 producing cells.
- Implementation of the previous new monitoring tool to optimize the nutrient feeding in fed-batch cultures of *E.coli* BL21 and its comparison with a theoretical exponential growth profile in respect of the final biomass concentration and the volumetric productivity of the process.
- To implement a new non-invasive monitoring tool based on the carbon dioxide response when glucose is nearly depleted in cultures of *E.coli* BL21 and *S. cerevisiae* producing cells.
- Implementation of the previous new monitoring tool to optimize the feeding in fed-batch cultures of *E. coli* BL21 and *S. cerevisiae* and its comparison with a theoretical exponential growth profile in respect of the final biomass concentration, and the volumetric productivity of the process.
- Implementation of the previous new monitoring tool to optimize the feeding in a fed-batch culture with and induction phase of *E. coli* BL21 expressing a model protein.
- To be able to monitor the entire microorganism cultures in bioreactor, despite the metabolic changes usually observed in bacteria, yeast and animal cells.
- To optimize the conversion of the carbon source to biomass in cultures of *E. coli* BL21, *S. cerevisiae* and hybridoma KB26.5-BHRF1, playing with the cell culture conditions.
- To reduce or removed entirely the lactate generation in mammalian cell cultures, playing with the cell culture conditions or using another techniques of genetic engineering tools.
- To reduce the ethanol generation in *S. cerevisiae* cultures, playing with the cell culture conditions.
- To establish a link between metabolism studies and bioprocess development, in order to increase the performance of mammalian cell-based production processes.

3. Physiology and metabolism of *Escherichia coli*

3.1 Nomenclature

DCW: dry cell weight ($\text{g}\cdot\text{L}^{-1}$)

OUR: Oxygen Uptake Rate ($\text{mM}\cdot\text{h}^{-1}$)

CER: Carbon Dioxide Evolution Rate ($\text{mM}\cdot\text{h}^{-1}$)

X_v : biomass concentration ($\text{gDCW}\cdot\text{L}^{-1}$)

q_m : specific consumption/production rate of metabolite m ($\text{mmol}\cdot\text{gDCW}^{-1}\cdot\text{h}^{-1}$)

$q_{s, \text{total}}$: total specific glucose consumption rate ($\text{mmol}\cdot\text{gDCW}^{-1}\cdot\text{h}^{-1}$)

$q_{s, \text{acetate}}$: specific glucose consumption rate directed towards acetate production ($\text{mmol}\cdot\text{gDCW}^{-1}\cdot\text{h}^{-1}$)

$q_{s, \text{maintenance}}$: specific glucose consumption rate directed towards cell maintenance ($\text{mmol}\cdot\text{gDCW}^{-1}\cdot\text{h}^{-1}$)

$q_{s, \text{biomass}}$: specific glucose consumption rate directed towards biomass formation ($\text{mmol}\cdot\text{gDCW}^{-1}\cdot\text{h}^{-1}$)

t: time (h)

F: gas volumetric flow ($\text{L}\cdot\text{min}^{-1}$)

V: bioreactor operational volume (L)

D: dilution rate in continuous culture strategy? (h^{-1})

C_j : concentration of metabolite j ($\text{g}\cdot\text{L}^{-1}$)

$C_{\text{outlet}, m}$: concentration of metabolite m in the outlet gas flow ($\text{g}\cdot\text{L}^{-1}$)

$C_{\text{inlet}, m}$: concentration of metabolite m in the inlet gas flow ($\text{g}\cdot\text{L}^{-1}$)

μ : specific growth rate (h^{-1})

μ_{max} : maximum specific growth rate (h^{-1})

K_s : affinity parameter of Monod equation ($\text{g}\cdot\text{L}^{-1}$)

$Y_{a/b}$: yield of compound A in relation to compound B ($\text{g}_a\cdot\text{g}_b^{-1}$)

TCA: tricarboxylic acid cycle

FBA: flux balance analysis

OP: oxidative phosphorylation

NADH: nicotinamide adenine dinucleotide reduced form

NAD: nicotinamide adenine dinucleotide oxidized form

ATP: adenosine triphosphate

PEP-OOA: phosphoenolpyruvate – Oxalacetate shunt

PTS: phosphotransferase system

3.2 Introduction

As mentioned in the overall introduction, the aim of the work presented revolves around increasing the biomass production, by means of performing high cell density cultures, in order to enhance the volumetric productivity. Specifically, in the chapter that is represented thereafter, the expression platform used as model is the bacteria *E. coli*.

Since 1970s, exploring the limitation of the high cell density cell cultures has been the aim for enhancing the volumetric productivity of the bioprocesses. On this basis, several studies have been based on improving cultivation conditions, using new engineering-based approaches in order to control the process, and implementing genetic modifications for the optimization of the *E. coli*'s physiology have been the main topics in bioprocess publications (Shiloah & Rinas, 2009) . Nevertheless, all the studies mentioned before are inherently related to the central carbon metabolism, since they try to “control” the organism by changing its interaction with the external conditions.

There is a trend in bioprocess publications regarding the enhancement of volumetric productivity that is focused on the comprehension of the central carbon metabolism by means of the use of system biology methodologies. In particular, using metabolic models to predict carbon flux distributions (Choi et al., 2019) . The one that will be studied in this section, the glucose metabolism in aerobic conditions when *E. coli* grows on glucose-based media.

There are several publications regarding how glucose is metabolized by *E. coli* which highlight the production of the inhibitory by-product acetate (Shiloah & Rinas, 2009) (Enjalbert et al., 2017). This metabolic behaviour is widely known as “bacterial Crabtree effect” and takes place when *E. coli* grows on excess of glucose-based media or other highly assimilable carbon sources in aerobically conditions (Doelte et al., 1982) (Rinas et al., 1989) (Luli & Strohl, 1990). Furthermore, it has been widely described that the acetate formation is related to two problematics: the influence in cell growth (El-Mansi, 2004) and in protein production (Brown et al., 1977) (Meyer et al., 1984) (Eiteman & Altman, 2006) . The acetate reduction in bacteria cultures makes one of the aims within scientific publications (Aristidou et al., 1995) (Farmer & Liao, 1997) (Eiteman & Altman, 2006) (Veeravalli et al., 2018).

Up until now, through genetic modifications and changing the interaction between *E. coli* and the culture media conditions, the acetate metabolism was modified. Contiero et al. concluded that depending on which gene involved in acetate metabolism was knocked-out, the acetate production was either reduced or increased (Contiero et al., 2000). Aristidou et al. observed a

reduction in the acetate production through the expression of an heterologous acetolactate synthase that promoted acetoin production (Aristidou et al., 1994). Moreover, other genetic modifications were proposed that affected the phosphotransferase system, the glycolytic pathways or the pyruvate “branch point” which resulted in the alteration of acetate production (Vemuri et al., 2007)(De Mey et al., 2007).

On the other hand, through the use of bioprocess strategies that are based on a feed-limiting fed-batch strategies (Riesenberger et al., 1991) (Ying Lin & Neubauer, 2000) or a growth rate-limited fed-batch strategies (S. Y. Lee, 1996) (Kim et al., 2004) acetate production was affected as well. However, neither genetic or bioprocess strategies were able to completely deplete the acetate production without affecting the growth rate.

In this chapter, the reduction of acetate production will be focused on understanding how *E. coli* interact with its environmental conditions. On this basis, and in regard with the latest advances in the high throughput data analysis described in **chapter 3**, the use of a genomic-scale metabolic model will be used in order to predict the metabolic fluxes distribution.

3.3 Results (I) – Analysis and modelling of *E. coli* M15 (K cell line): glucose/acetate metabolism in batch culture

3.3.1 Experiment in batch culture with the *E. coli* M15

The core of this section is to understand the metabolism of *E. coli* through the analysis and modelling of a specific experimental conditions and settings. The experimental setting was based on using a bioreactor as a containment culture system where each extracellular parameter can be controlled for ensuring an optimal growth rate (as shown in the section 3.9.4). The acetate producer strain used as a reference was the *E. coli* M15 and it was cultured in a bioreactor with minimal medium, whose initial glucose concentration was $20 \text{ g}\cdot\text{L}^{-1}$, as shown in the section 3.9.3.

As shown in the graph A) of the **Figure 3-1** and in Table 3-1, when *E. coli* M15 was cultured in glucose-based media, it had a specific growth rate of 0.65 h^{-1} and consumed $19 \text{ g}\cdot\text{L}^{-1}$ of glucose to achieve a maximum cell concentration of $6,11 \text{ gDCW}\cdot\text{L}^{-1}$ while $1,97 \text{ g}\cdot\text{L}^{-1}$ of acetate was produced. Moreover, and regarding how *E. coli* M15 allocates glucose, for each gram of consumed glucose $0,31 \text{ gDCW}$ of biomass was generated and $0,11 \text{ g}$ of acetic was produced. As

a result, it is often defined as a non-optimized carbon metabolism owing to a portion of glucose was converted to acetate instead of biomass, CO₂ and H₂O (Bernal et al., 2016).

Moreover, using the glucose and acetate profiles over time in relation with biomass trend, the specific rates were calculated (methodology calculation described in section 3.9.9). The specific consumption rate of glucose had a value of 10,9 (mmol·gDCW⁻¹·h⁻¹) that lead to an acetate specific production rate of 4,87 (mmol·gDCW⁻¹·h⁻¹) and also a biomass generation of 0,65 (gDCW·gDCW⁻¹·h⁻¹). The specific consumption rate of oxygen and the specific production carbon dioxide were calculated using the variables shown in **graph B of Figure 3-1**, carbon exchange rate (CER) and oxygen uptake rate (OUR). The specific production rate of carbon dioxide had a value of 16 mmol·gDCW⁻¹·h⁻¹ while the specific consumption rate of oxygen had a value of 16,5 mmol·gDCW⁻¹·h⁻¹.

It is important to point out that the ratio between OUR and CER, also known as respiratory quotient (RQ), had an expected value of 0,99, due to the fact that RQ gives information about a metabolic trait of *E. coli* growing on aerobic conditions. In general, when *E.coli* grows on glucose as a carbon source in aerobiosis, the RQ have a value of one (Saltveit, 2016). It is owing to the fact that *E. coli* is a non-compartmentalized organism, which leads to a specific correlation between the specific rate of carbon dioxide and oxygen. This correlation is based on the fact that all NADH from glucose oxidation is used to reduce oxygen via oxidative phosphorylation pathway (OP). Therefore, if there are not side reactions that might oxidize NADH instead of oxygen, then RQ is one. For instance, the lactate formation in anaerobic cultures or the generation of fermentative by-products in aerobic conditions, for example ethanol in yeast (De Deken, 1966) or lactate in animal cell (Potter et al., 2016).

Additionally, it has to be kept mind that the study about the by-product generation in aerobic conditions such ethanol produced by yeast and lactate produced by animal cell will be presented in chapter 3 and 4, respectively.

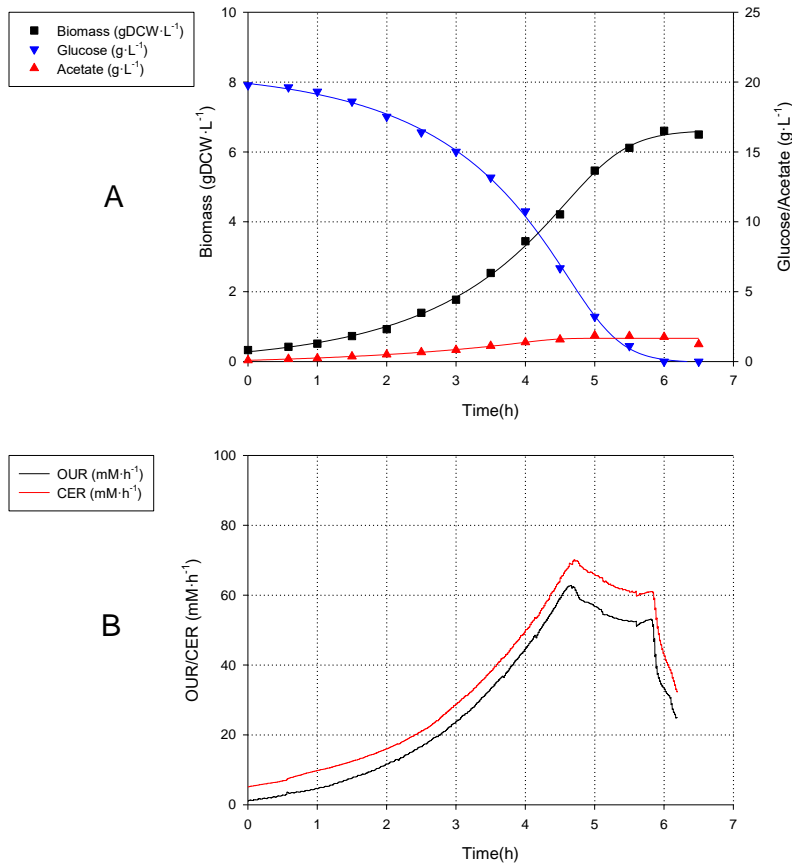


Figure 3-1 Profile of A) off-line variables such as biomass (■), glucose (▼), acetate (▲) and B) on-line variables such as C.E.R (—), O.U.R (—) *E. coli* M15 batch culture.

Table 3-1 Main characterization parameters for *E. coli* M15 in batch culture.

Achieved Biomass (gDCW·L ⁻¹)	6,11
Glucose Consumed (g·L ⁻¹)	19,70
Acetate produced (g·L ⁻¹)	1,90
$Y_{bio/gluc}$ (gDCW·g ⁻¹)	0,31
$Y_{ac/gluc}$ (g·g ⁻¹)	0,10
μ (h ⁻¹)	0,66
$q_{Glucose}$ (mmol · gDCW ⁻¹ ·h ⁻¹)	-10,90
$q_{Acetate}$ (mmol · gDCW ⁻¹ ·h ⁻¹)	4,86
q_{CO_2} (mmol · gDCW ⁻¹ ·h ⁻¹)	16
q_{O_2} (mmol · gDCW ⁻¹ ·h ⁻¹)	-16,5

As previously described, glucose is partially converted towards acetate instead of being fully transformed towards biomass. Therefore, in order to understand why acetate is produced when glucose is used as a carbon source, the intracellular fluxes that lead to acetate production within the glucose metabolism will be studied in the following section by means of using a genomic-scale metabolic model.

3.3.2 Study of *E. coli* M15 carbon metabolism by means of metabolic flux balance analysis

As it was mentioned before, a genomic-scale metabolic model will be used in order to describe how *E. coli* M15 transforms glucose to acetate and precursors for biomass synthesis, while getting the required energy for growing at optimal growth rate. The development and description of the model is explained in section 3.9.11.

For metabolic flux calculation, the model was constrained using the input-output fluxes of the corresponding metabolites that are shown in **Table 3-2**. As this data included the biomass formation, the objective function to maximize was the cytoplasmic hydrolysis of the ATP to ADP (maximum energy formation).. The optimization of the model was performed by means of the FBA protocol described in section 3.9.12.

Table 3-2 Specific rate limits used as drains for Flux Balance Analysis in *E. coli* M15 strain.

	q (mmol·gDCW ⁻¹ ·h ⁻¹)
Biomass	0,651 ± 0,048
Acetate	4,864 ± 0,344
Ammonium	-7,010 ± 0,496
Carbon Dioxide	29,773 ± 2,105
Glucose	-11,020 ± 0,779
Ethanol	0,000 ± 0,000
Oxygen	-28,391 ± 2,008

Once the intracellular fluxes were calculated and using the visualization software OMIX (Droste et al., 2013), **Figure 3-2** is generated. In this figure, the metabolic relation between glucose and acetate is displayed.

Firstly, 11 mmol·gDCW⁻¹·h⁻¹ of glucose were internalized from the media to cytoplasm and then, glucose was phosphorylated to glucose-6-phosphate via PTS. It has to be pointed out that the model considers the transport of glucose and its phosphorylation as a two independent reactions, although PTS is described as a specific bacteria mechanism that integrates either the glucose transport and its phosphorylation within the same reaction (Postma et al., 1993). The Glucose-6-phosphate flux whose value was 11 mmol·gDCW⁻¹·h⁻¹ was directed into two different routes: 90% was directed to the glycolytic pathway through conversion to fructose-6-phosphate via the phosphoglucose isomerase reaction and the remaining 10% to the oxidative branch of

the pentose-phosphate pathway, whose objective is the generation of all the precursor related to synthesis of DNA and RNA. Thereupon, the flux directed to glycolytic pathway ($14,61 \text{ mmol}\cdot\text{gDCW}^{-1}\cdot\text{h}^{-1}$) reacted until Acetyl-CoA where only 75% of the flux went into the Tricarboxylic Acid Cycle (TCA). As a result, the formation of $4,27 \text{ mmol}\cdot\text{gDCW}^{-1}\cdot\text{h}^{-1}$ of acetate was needed for balancing the Acetyl-CoA pool.

Regarding the biomass formation, the main precursors were generated from the next compounds: ribulose-5P (7,49 % of glucose carbon-mol uptake rate); dihydroxyacetone phosphate (0,45 % of glucose carbon-mol uptake rate); Acetyl-CoA (6,20 % of glucose carbon-mol uptake rate) and oxoglutarate (1,57 % of glucose carbon-mol uptake rate).

The following hypothesis is exposed to explain the acetate production in *E. coli* M15: The production of acetate is related to an unbalance in Acetyl-CoA reaction steps caused by a difference in the flux rate of the glycolytic pathway and the TCA cycle due to a limit rate in the TCA cycle.

The limitation of the TCA cycle might be related to two possibilities:

- High glucose consumption rates repress the expression of genes that are involved in TCA cycle and oxidative phosphorylation. Therefore, the generation of acetate is the consequence of balancing the acetyl-coA pool. On this basis, a mutant of *E. coli* was created with a deletion of the regulatory gene *arcA*, whose function is to regulate the expression of genes of aerobic function (Cotter & Gunsalus, 1992). As result, the deletion of *arcA* offered a partial reduction in the acetate production due to the increased capacities of TCA cycle and respiratory chain without affecting the specific growth rate. Moreover, Vemuri et al. 2006 combined the *arcA* deletion with the expression of an heterologous NADH oxidase and a non-acetate *E. coli* was obtained without affecting the specific growth rate (Vemuri et al., 2006).
- The maximum allowable flux through the anaplerotic reactions (PEP-OOA and glyoxylate shunts) might be a factor that determines the limitation in TCA cycle. Farmer et al. 1997, concluded that overexpressing PEP-OOA shunt and also deregulation glyoxylate shunt in *E. coli* lead to a metabolic state where acetate yield decreased four folds compared to the control strain without compromising the specific growth rate (Farmer & Liao, 1997).

In the final analysis, *E. coli* M15 strain produces acetate because the flux limitation in the TCA cycle might be provoked due to the combination of a high flux through glycolytic pathway and a

restriction in the flux through the anaplerotic reactions. A further description regarding the limitation of the TCA cycle will be presented in section 3.4.

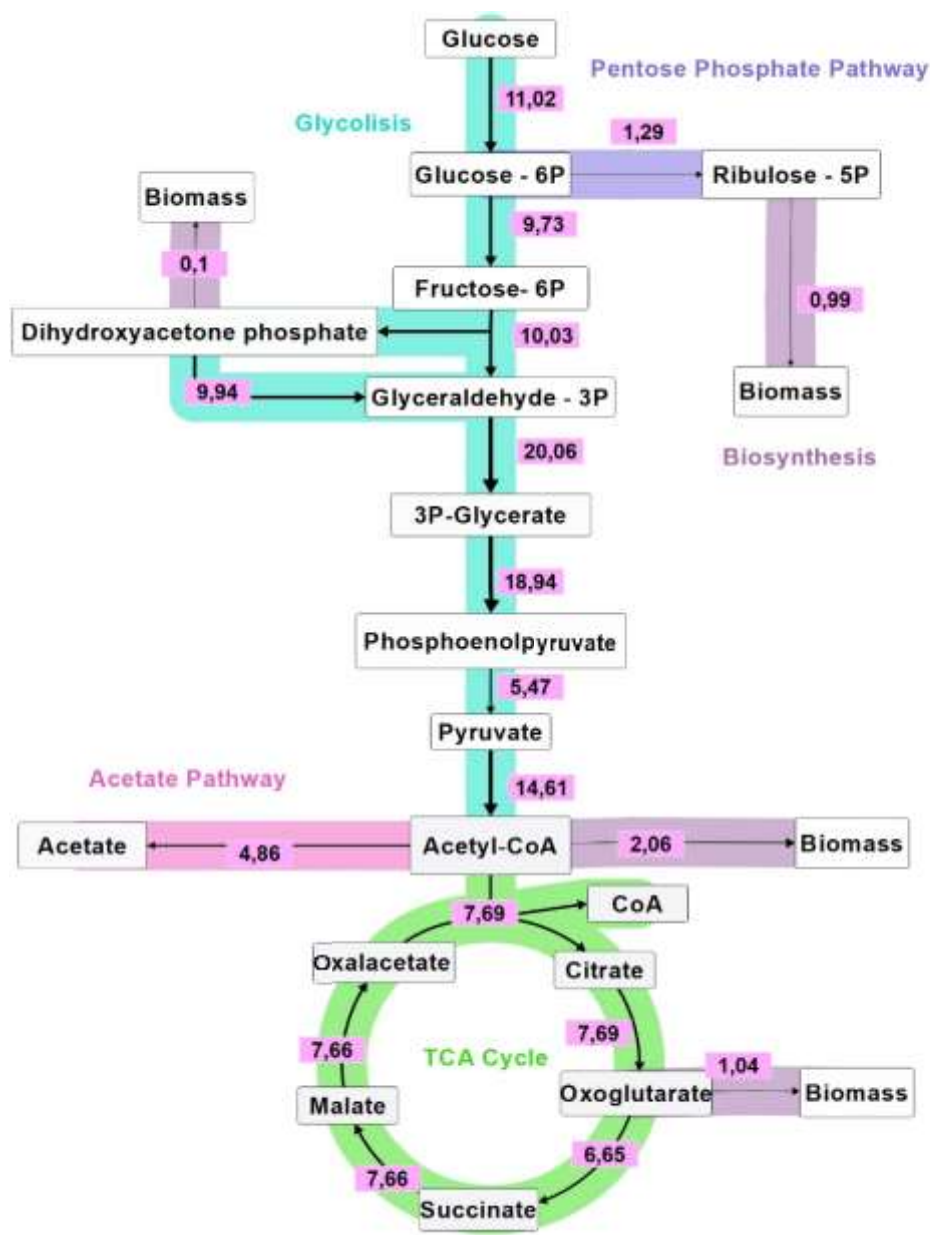


Figure 3-2 Scheme of the main metabolic fluxes calculated for *E. coli* M15 strain. Arrows indicate the direction of the flux and their width the magnitude of fluxes (the exact value is detailed close to the arrows). All the fluxes are expressed in mmol-gDCW⁻¹·h⁻¹.

Once the carbon metabolism is analysed and discussed, a study of the energy metabolism linked to the carbon metabolism will be presented in the following section. This study will be based on describing the proportion of the ATP produced and consumed regarding its provenance.

3.3.3 Study of *E. coli* M15 Energy metabolism by means of use of a metabolic model

In the previous section, a study of the central carbon metabolism was presented. It is important to realize that coupled with the carbon metabolism appears the energy metabolism. Therefore, to understand how the energy required for the synthesis of biomass precursors and cell maintenance is handled, the study of the energy metabolism will be described hereafter.

As shown in **graph A) of the Figure 3-3**, the proportion of the ATP produced mainly came from two sources (Farmer & Liao, 1997). The first source of ATP comes from ATP synthase, which is a protein involved in the oxidative phosphorylation (OP) (Jonckheere et al., 2012). The second source of ATP comes at the substrate level phosphorylation, which is a reaction that takes part of the glycolic pathway.

In aerobic conditions, OP is described as the main production resource of ATP due to the high efficiency in the phosphorylation of ADP by using transmembrane proton motion force (Anraku & Gennis, 1987). This proton motion is driven by an electron transport chain placed within cytoplasmic membrane whose intermediate involved in the first step is the Cofactor NADH (Stouthamer, 1973). For this reason, the ATP production by OP has a huge impact in ATP proportion because it couples all the NADH's flux from the glycolytic pathway and TCA cycle.

Regarding substrate level phosphorylation, the generation of ATP is based on the use of a specific group of proteins (pyruvate kinase, acetate kinase and phosphoglycerate kinase) that catalyse the transfer of phosphate groups from high-energy phosphate-donating molecules to specific substrates. In this case, from phosphoenolpyruvate to ADP (Reynard et al., 1961), from Acetyl-phosphate to ADP (Skarstedt & Silverstein, 1976) and from 1,3-bisphosphoglycerate to ADP (Bernstein & Hol, 1998).

On this basis, the difference in production regarding all the ATP sources was caused because OP had a higher incoming flux of the NADH from TCA cycle and glycolytic pathway than substrate level phosphorylation, which only depended on the flux from glycolytic pathway. The efficiency in the production of ATP from OP using ATP synthase along with a transmembrane proton

motion caused by the oxidation of NADH was higher than SP using kinase protein in order to transfer phosphate groups from high energy phosphate-donating molecules to ADP.

On the other side, **in graph B) of the Figure 3-3**, the proportion of ATP consumed showed an allocation of ATP mainly in cell maintenance, biomass generation and Phosphofructokinase reaction.

Cell maintenance tackles all the cellular process whose function is not related to formation of new cell material. Up to the present, there have been several attempts trying to describe which cellular process are involved, for instance the regulation of the proton motive force, the degradation of macromolecules, keeping the osmolarity conditions and regulated shifts in metabolic pathways (van Bodegom, 2007)(Hoehler & Jørgensen, 2013; Lever et al., 2015; van Bodegom, 2007). For keeping its performance 53 % of the ATP produced is required.

The energy requirements for synthesis of biomass precursors are defined by the biomass equation. As a result, the 30% of the ATP produced was dedicated for biomass generation. Finally, the last one of the main consuming ATP reactions (7%) was catalysed by the enzyme Phosphofructokinase whose metabolic function is the phosphorylation of fructose-6-phosphate.

Although, there are two points related to the energy metabolism of *E. coli* M15 growing on glucose-based media in aerobic conditions that has to be pointed out:

1. The 70% of the ATP produced came from the oxidative phosphorylation while the other 30 % came from glycolytic pathway.
2. In order to reach the optimal growth rate, the energetic requirements for cell maintenance (53%) were higher than the destined ones to new cellular material (30%).

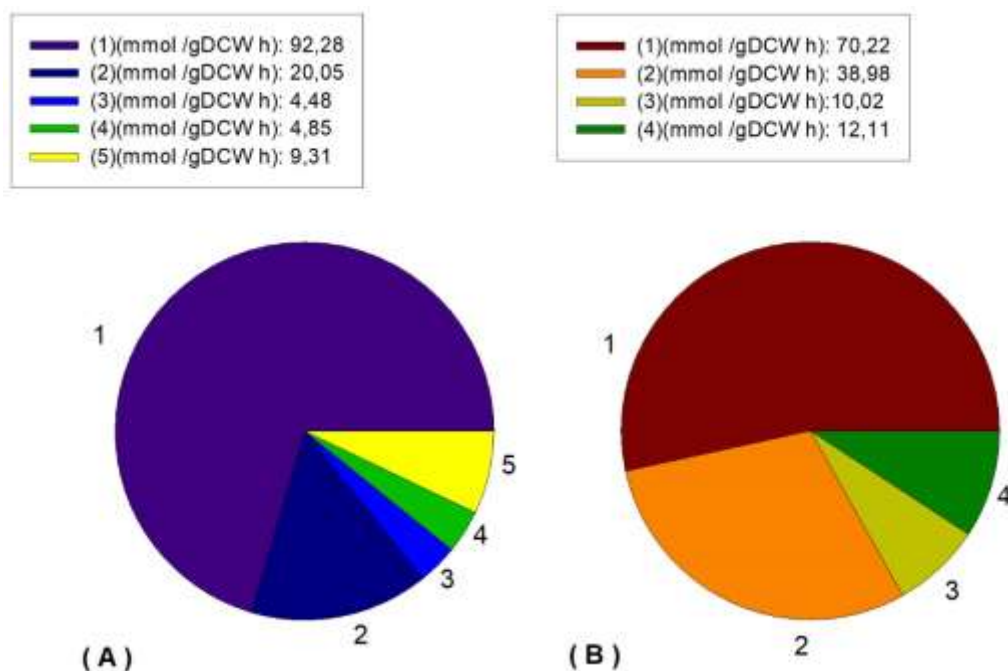


Figure 3-3 Proportions of ATP produced and consumed regarding its provenance in *E. coli* M15. In figure A, the ATP produced by *E. coli* is separated depending on its provenance (ATP synthase (1), Phosphoglycerate kinase (2), Pyruvate kinase (3), Acetate kinase (4) and other side reactions (5)). While in figure B, the ATP consumed by *E. coli* is separated depending on its provenance (Cell maintenance (1), Biomass formation (2), Phosphofructokinase (3) and other side reactions (4)).

In conclusion, after the analysis of the carbon and energy metabolism, the main metabolic issue of *E. coli* M15 has been found to be related to the uncoupling caused by the difference in flux through the glycolytic pathway and TCA cycle. As a consequence, the formation of acetate is required.

Up until now, the possible reasons for acetate production based on metabolic studies has been described, nevertheless another approach will be studied. This approach is based on understanding why a non-acetate producer *E. coli* do not produce acetate.

In the next section, a study of glucose metabolism in *E. coli* strain B as a non-acetate producer *E. coli* model will be presented to understand the acetate metabolism and thus, it will be compared with the producer strains.

3.4 Results (II) - Analysis and modelling of *E. coli* BL21 (B cell line): glucose/acetate metabolism in batch and continuous cultures

3.4.1 Experiment in batch culture with *E. coli* BL21

As it was mentioned before, a new approach for acetate production in *E. coli* M15 will be studied focusing on why there is no acetate production in a non-acetate producer *E. coli* strain by means of the study of the central carbon metabolism. The non- acetate producer strain that was used as a reference was a strain of the *E. coli* cell line B, the *E. coli* BL21. The experimental setting were based on using a bioreactor as containment culture system, where every extracellular parameter was controlled for ensuring an optimal growth rate (as is described in section 3.9.4).

E. coli BL21 was cultured in a minimal medium whose composition was the same that the one previously presented in *E. coli* M15 cultures.

As shown in **Figure 3-4** and in **Table 3-3**, when *E. coli* BL21 was cultured in glucose-based media, the specific growth rate had a value of $0,54 \text{ h}^{-1}$ and $17,60 \text{ g}\cdot\text{L}^{-1}$ of glucose was consumed in 7,5 h in order to achieve a maximum cell concentration of $6,28 \text{ gDCW}\cdot\text{L}^{-1}$ without producing acetate. Under those conditions, *E. coli* BL21 allocated the carbon source where for each gram of consumed glucose $0,34 \text{ gDCW}$ of biomass was generated.

Thus, the specific rate of biomass and glucose were calculated by using the methodology described in the section 3.9.9. The specific consumption rate of glucose had a value of $9,5 \text{ mmol}\cdot\text{gDCW}^{-1}\cdot\text{h}^{-1}$ that lead to a generation of $0,54 \text{ gDCW}\cdot\text{gDCW}^{-1}\cdot\text{h}^{-1}$ of biomass without producing acetate.

Moreover, the specific rates of oxygen consumption and carbon dioxide production were calculated by using Carbon Exchange Rate (CER) and Oxygen Uptake Rate (OUR), whose values are shown in **graph B) of Figure 3-4** in cooperation with the methodology described in section 3.9.8. As a result, the specific production rate of carbon dioxide had a value of $19 \text{ mmol}\cdot\text{gDCW}^{-1}\cdot\text{h}^{-1}$ and the specific consumption rate of oxygen had a value of $19,1 \text{ mmol}\cdot\text{gDCW}^{-1}\cdot\text{h}^{-1}$.

The ratio between both of them, also known as respiratory quotient, has a value of 0,99. RQ gives information about a principal trait of *E. coli* growing in glucose-based cultures. As was mentioned before in section 3.3.1, the value of RQ is one (Saltveit, 2016). *E. coli* BL21 and also *E. coli* M15 had an RQ nearly 1.

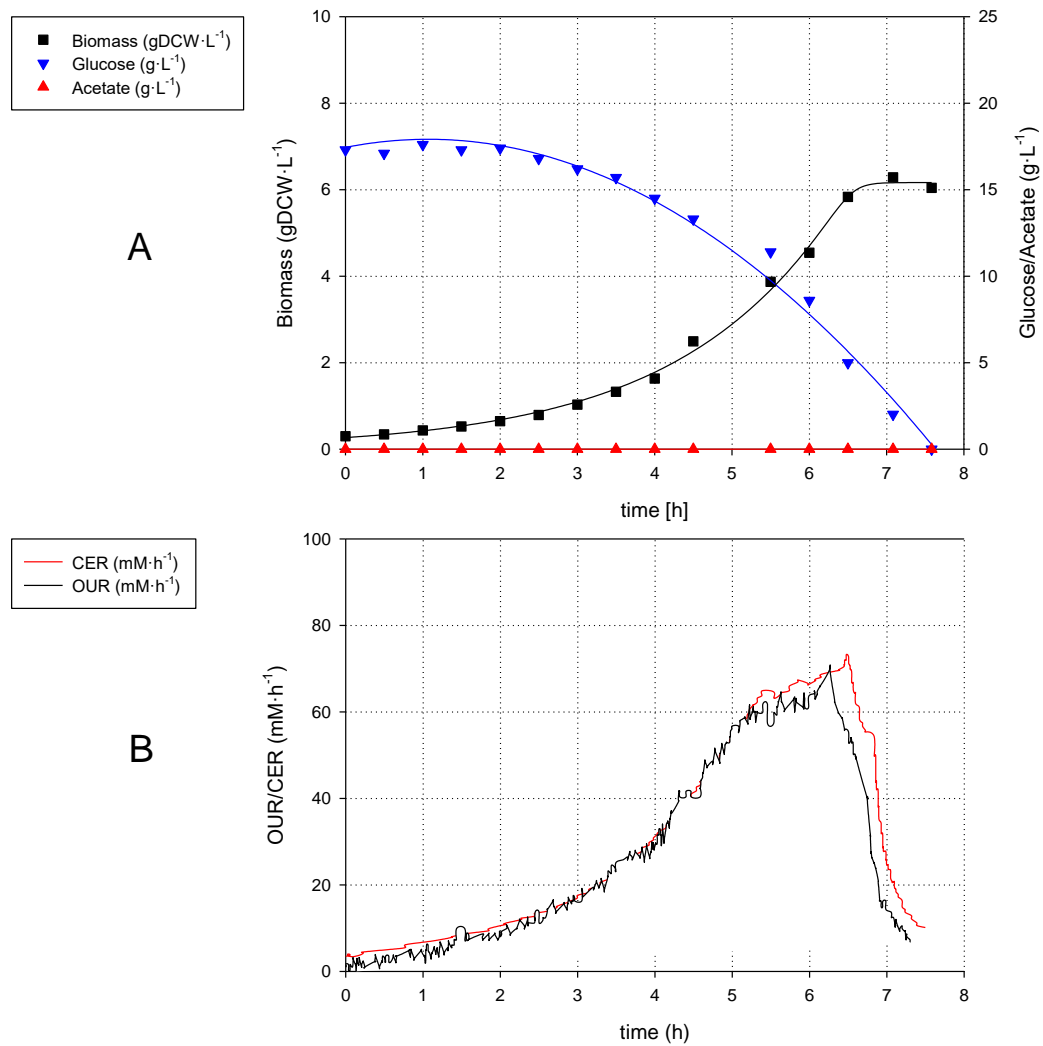


Figure 3-4 Profile of A) off-line variables such as biomass (■), glucose (▼), acetate (▲) and B) on-line variables such as C.E.R (—) and O.U.R (—) in pH-controlled batch culture.

Table 3-3 Main characterization parameters for *E. coli* BL21 in batch culture.

Biomass Achieved (gDCW·L ⁻¹)	6,28
Glucose Consumed (g·L ⁻¹)	17,60
Acetate produced (g·L ⁻¹)	0,00
$Y_{bio/gluc}$ (gDCW·g ⁻¹)	0,34
$Y_{ac/gluc}$ (g·g ⁻¹)	0,00
μ (h ⁻¹)	0,54
$q_{Glucose}$ (mmol · gDCW ⁻¹ ·h ⁻¹)	-9,50
$q_{Acetate}$ (mmol · gDCW ⁻¹ ·h ⁻¹)	0,00
q_{CO_2} (mmol · gDCW ⁻¹ ·h ⁻¹)	19
q_{O_2} (mmol · gDCW ⁻¹ ·h ⁻¹)	-19,1

For a better understanding of the reason behind why *E. coli* BL21 do not produce acetate, a study of the intracellular fluxes by means of the use of a genomic scale metabolic model will be presented in the following section.

3.4.2 Study of *E. coli* BL21 carbon metabolism by means of the use of a metabolic model

The genomic-scale metabolic model was used in order to analyse how *E. coli* BL21 transforms glucose to precursors for biomass synthesis without producing acetate, while getting the required energy for growing at optimal rate. The development and description of the model is found in section 3.9.11. It is important to remark that the model used in *E. coli* BL21 was the same that the one used in *E. coli* M15 modelling.

For metabolic flux calculation, the model was constrained using the input-output data of the corresponding metabolites that are shown in **Table 3-4**. As this data includes the biomass formation, the optimization of the model was performed by means of the FBA protocol described in 3.9.12, whose objective function to maximize was the cytoplasmatic hydrolysis of the ATP to ADP.

Table 3-4 Specific rate limits used as drains for a Flux Balance Analysis in *E. coli* BL21.

	q (mmol·gDCW ⁻¹ ·h ⁻¹)
Biomass	0,538 ± 0,038
Acetate	0,000 ± 0,000
Ammonium	-5,800 ± 0,410
Carbon Dioxide	34,675 ± 2,452
Glucose	-9,450 ± 0,668
Oxygen	-33,531 ± 2,371

Once the intracellular fluxes were calculated and using a visualization software named OMIX (Droste et al., 2013), **Figure 3-5** is presented. In this figure, the metabolic relation between glucose and acetate is displayed.

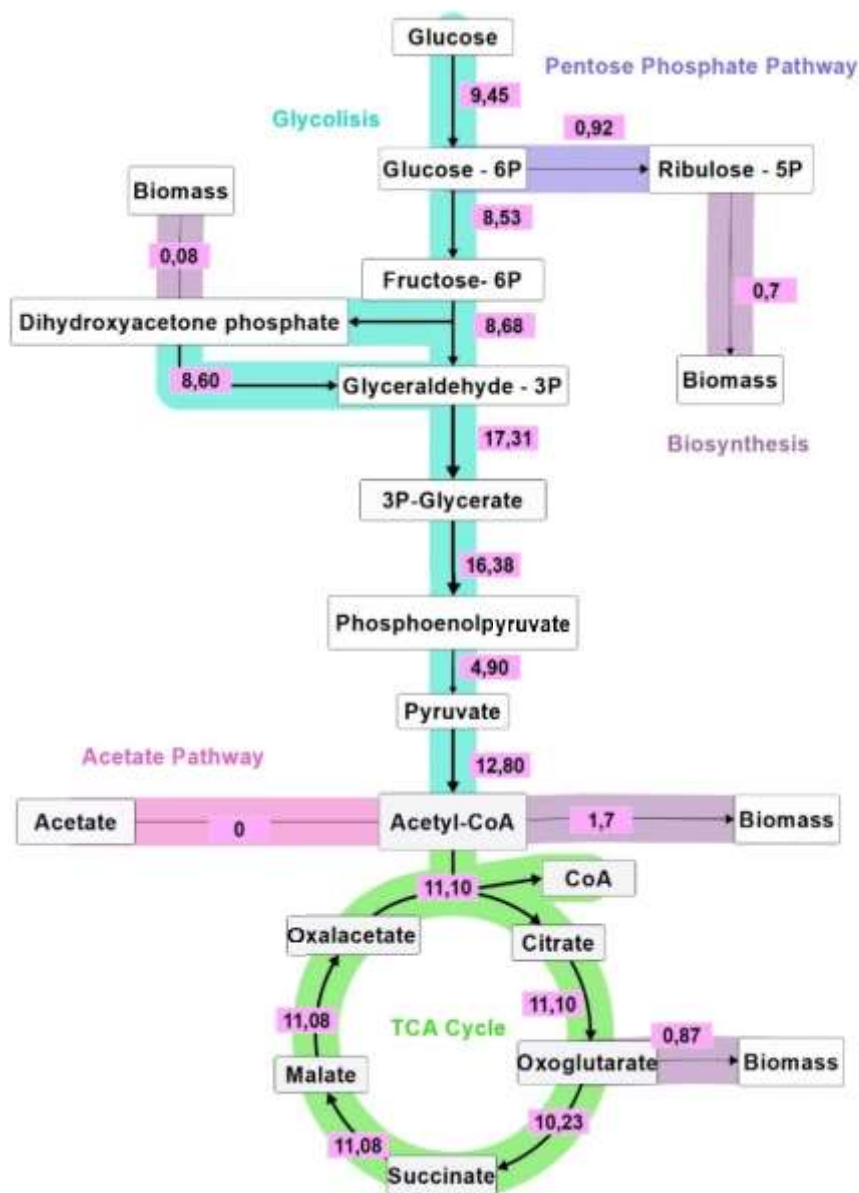


Figure 3-5 Scheme of the main metabolic fluxes calculated for *E. coli* BL21. Arrows indicate the direction of the flux and their width the magnitude of fluxes (the exact value is detailed close to the arrows). All the fluxes are expressed in $\text{mmol} \cdot \text{gDCW}^{-1} \cdot \text{h}^{-1}$.

Glucose, with a flux of $9,5 \text{ mmol} \cdot \text{gDCW}^{-1} \cdot \text{h}^{-1}$, is transported and phosphorylated via PTS system in order to get released into the cytoplasm as glucose-6-phosphate (the peculiarity of PTS system-carbohydrate phosphotransferase system has been described in section 3.3.2). The glucose-6-phosphate, whose flux was $9,5 \text{ mmol} \cdot \text{gDCW}^{-1} \cdot \text{h}^{-1}$, was directed into two different routes: 89% was directed to the glycolytic pathway through conversion to fructose-6-phosphate via the phosphoglucose isomerase reaction and 9,6 % $\text{mmol} \cdot \text{gDCW}^{-1} \cdot \text{h}^{-1}$ was directed to the oxidative branch of the pentose-phosphate pathway, whose objective is the generation of precursors for biomass synthesis. Thereupon, the flux directed to glycolytic pathway ($8,53 \text{ mmol} \cdot \text{gDCW}^{-1} \cdot \text{h}^{-1}$) reacts until Acetyl-CoA, where is fully converted to carbon dioxide and NADH

within the TCA cycle. As a result, the acetate production was not needed for balancing the Acetyl-CoA formation.

Regarding the biomass formation, the main precursors are generated from ribulose-5P (derivation of 6,14 % of glucose carbon-mol uptake rate); dihydroxyacetone (derivation of 0,42 % of glucose carbon-mol uptake rate); Acetyl-CoA (derivation of 6 % of glucose carbon-mol uptake rate) and oxoglutarate (derivation of 1,53 % of glucose carbon-mol uptake rate).

On this basis, the following hypothesis is exposed for explaining non-acetate production in *E. coli* BL21 regarding what has been previously described in section 3.3.2 (*E. coli* M15 metabolic study). *E. coli* BL21 do not produces acetate because the flux through the TCA cycle might be enhanced by anaplerotic reactions and also the decrease in the flux through the glycolic pathway could lead to a balance between the influx of TCA and outflux glycolysis. As a consequence, acetate might not be produced due to all flux through the glycolytic pathway might be able to be metabolized into TCA.

However, a decrease in the growth rate was observed coupled with the depletion in the acetate production. This difference might be based on a limitation in the formation of the biomass precursors due to a reduction in the flux through the glycolytic pathway. Moreover, a further description will presented in the comparison of both strains.

Once the carbon metabolism has been analysed, it is important to realize that coupled with carbon metabolism appears energy metabolism. Therefore, to understand how the energy required for the synthesis of the precursors destined to biomass generation and cell maintenance is handled, the study of the energy metabolism will be shown in the following section.

3.4.3 Study of *E. coli* BL21 energy metabolism by means of the use of a metabolic model

As shown in **graph A) of the Figure 3-6**, the proportion of the ATP production mainly comes from two places:

The first one come from ATP synthase which is involved in the oxidative phosphorylation system (OP). The 76 % of the ATP produced comes from OP because it couples all the NADH's flux from the glycolytic pathway and TCA cycle (the metabolic reason why OP has a huge impact was previously described in section 3.3.3 Study of *E. coli* M15 Energy metabolism by means of use of a metabolic model.

The second one, the 16% of the ATP produced comes from substrate level phosphorylation, which involves two reactions whose enzymes are pyruvate kinase and phosphoglycerate kinase, that are part of the glycolytic pathway. Their low proportion is due to the fact that both enzymes are couple directly to an intermediary reaction of the glycolytic pathway whose function is to transfer the phosphate group from high energy phosphate-donating molecules to specific substrates. As result, the ATP produced depends exclusively on the flux rate through the glycolytic pathway.

On the other hand, in the **graph B) of Figure 3-6**, the proportion of ATP consumed shows an allocation of ATP mainly in cell maintenance, biomass generation and in the phosphofructokinase reaction.

Cell maintenance tackles all the cellular process whose function is not related to formation of new cell material. For keeping its performance 64,2 % of the ATP produced is required.

The energy requirements for synthesis of biomass precursors are defined by the biomass equation, as a result the 22,9% of the ATP produced is consumed. Finally, the last one of the main consuming ATP reactions (6%) is catalysed by the enzyme Phosphofructokinase whose metabolic function is the phosphorylation of fructose-6-phosphate.

There are several points related to the energy metabolism of *E.coli* BL21 growing with glucose-based media in aerobic conditions that has to be pointed out:

1. The 76 % of the ATP produced comes from oxidative phosphorylation.
2. In order to grow at the optimal growth rate, the energetic requirement for cell maintenance (64,2%) was higher than the destined ones to new cellular material (22,9%).

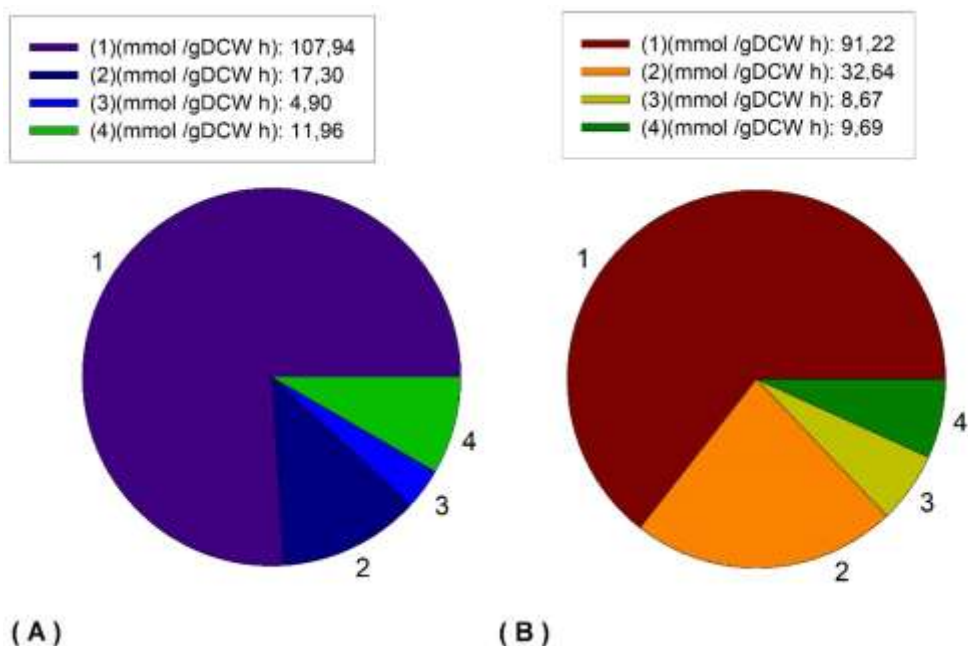


Figure 3-6 Proportions of ATP produced and consumed regarding its provenance in *E. coli* BL21. In figure A, the ATP produced by *E. coli* is separated depending on its provenance (ATP synthase (1), Phosphoglycerate kinase (2), Pyruvate kinase (3), Acetate kinase (4) and other side reactions (5)). While in figure B, the ATP consumed by *E. coli* is separated depending on its provenance (Cell maintenance (1), Biomass formation (2), Phosphofructokinase (3) and other side reactions (4)).

In the final analysis, regarding ATP handling, mainly the contribution in ATP produced is via oxidative phosphorylation and on the other hand, cell maintenance consumes more than a half of the ATP produced.

In addition, according to the data that have been shown up until now in reference to the acetate metabolism, it states that the acetate production might be based on the contribution of two metabolic functions: the repression of the TCA cycle and the contribution of anaplerotic reactions regarding TCA cycle. Thus, a global comparative view for both metabolisms will be shown hereunder in order to shed light on acetate production.

3.5 Results (III) - Metabolic Model Comparison between *E. coli* BL21 and *E. coli* M15: carbon metabolism.

Up until now, all the carbon metabolism referred to how *E. coli* BL21 and *E. coli* M15 consumes glucose and transforms it to biomass precursors with/without producing acetate has been

described independently. Although, the principal metabolic trait that is responsible for the acetate production in *E. coli* M15, also is responsible for the non-production in *E. coli* BL21.

To put in other way, the metabolic difference between both is related to how the Acetyl-CoA pool is managed. When the glycolytic flux is higher than the TCA cycle ones, acetate is produced for balancing the Acetyl-CoA pool. On the other hand, when both pathways admit the same carbon flux, acetate is not produced.

In order to begin with the study that will be presented hereafter, one assumption related to the metabolic model must be taken into consideration: the genome-scale metabolic model used was the same for both strains.

As shown in **Figure 3-7**, *E. coli* M15's fluxes regarding to *E. coli* BL21's fluxes have an increase of 16,6% through the glycolytic pathway and a decrease of 31% through the TCA cycle flux which leads to the production of acetate in order to balance the acetyl-coA pool.

As it was stated before in the section of *E. coli* M15, there are two hypotheses revolving around the limitation on the TCA cycle:

- High glycolytic pathway might repress the TCA cycle flux leading to the formation of acetate in *E. coli*. As a result, the metabolic difference between the *E. coli* BL21 and *E. coli* M15 might be caused by the decrease in the glycolytic pathway flux of the *E. coli* BL21 that might let the TCA accept all the carbon flux. As a result, there is not acetate production.
- The anaplerotic reactions linked to the TCA cycle (glyoxylate shunt and PEP-OOA reaction) are the responsible for its limitation. As a consequence, *E. coli* BL21 does not produce acetate, because the capacity for accepting carbon flux through the TCA cycle is enhanced by using the shunts more efficiently. In order to verify this hypothesis a carbon 13 experiment must be carried out as a future work, because If anaplerotic reactions are calculated using FBA protocol with non -labelled carbon source then, the correct shunt's value cannot be obtained because of they are parallel reaction steps (Wiechert et al., 2001).

Regarding this matter, a labelled glucose (C-13) experiment was carried out by Noronha et al 2000 using a *E. coli* B (*E. coli* BL21) and a *E. coli* K (*E. coli* M15) whose main objective was to shed light on the anaplerotic hypothesis. Its data concluded that *E. coli* B's glyoxylate shunt is active at 22% of the flux through the TCA cycle and is inactive in *E. coli* K. Moreover, in *E. coli* K the flux

of the PEP–OOA shunt is only third of the flux through the TCA cycle, while in *E. coli* B the flux through the shunt equals to the TCA (Noronha et al., 2000).

On the other hand, according to the hypothesis based how glycolytic pathway might repress TCA cycle, an experiment implementing new methodology to determine the shunt's fluxes of *E. coli* B and *E. coli* K were carried out by J.W. Lee et al. 2002. They concluded that as the growth rate in a glucose minimal medium increased, the cells increased the flux through glycolytic pathway and the TCA fluxes either levelled off or declined. Additionally, the pattern identified for the TCA fluxes corresponded to α -ketoglutarate dehydrogenase's induction-repression pattern, thereby suggesting that the induction-repression of the enzyme might result in significant flux changes (J. W. Lee et al., 2002).

Using the conclusions of the last two publications about the repression of the TCA and the anaplerotic reactions, it might be conclude that the non-acetate production in *E. coli* BL21 regarding the M15's acetate metabolism is related to the synergistic effect of two phenomena. A lower flux through glycolytic pathway that do not repress the TCA cycle and the more efficiently use of the shunts (glyoxylate shunt and PEP-oxaloacetate) to enhance its carbon capacity.

However, it has to be kept in mind that even though *E. coli* BL21 do not produces acetate, its growth rate ($0,54 \text{ h}^{-1}$) is lower than *E. coli* M15 ($0,66 \text{ h}^{-1}$). Therefore, it demonstrates that in order to reach the maximal available growth rate in *E. coli* the production of acetate is needed, owing to the requirements of a high flux in the biosynthesis reactions, as it succeed in *E. coli* M15 regarding *E. coli* BL21.

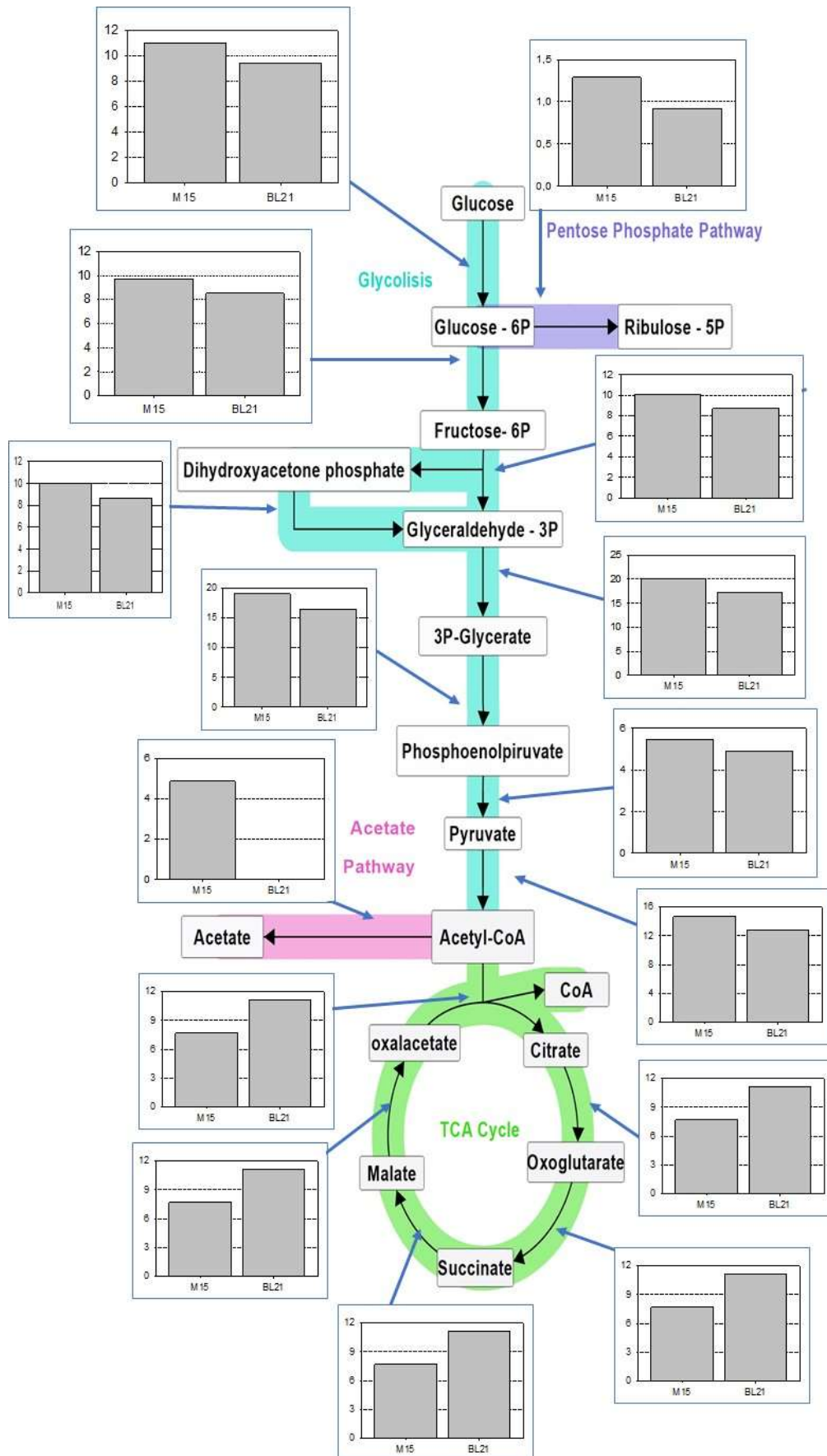


Figure 3-7 Comparison between intracellular fluxes of *E. coli* M15 (left side in the graph) and *E. coli* BL21(right side in the graph). All the fluxes are expressed in $\text{mmol-gDCW}^{-1}\cdot\text{h}^{-1}$.

Once in the carbon metabolism has been reached a feasible hypothesis for the acetate production in both *E. coli* strains, a global view of how this change in carbon metabolism affects the energy metabolism will be presented.

3.6 Results (IV) - Metabolic Model Comparison between *E. coli* BL21 and *E. coli* M15: energy metabolism

In order to begin with the study that will be presented hereafter, two assumptions related to the metabolic model must be taken into consideration, as the same genome-scale metabolic models was used for both strains:

- The relation that characterize the oxidative phosphorylation is the P/O value, which gives information about the ATP produced per oxygen atom reduced by the respiratory chain. It had a constant value of 2 in all the modelling done for both *E. coli* strains.
- The energy requirements used for biosynthesis are the same in all the modelling done for both *E. coli* strains.

Regarding to the ATP produced as shown in **Figure 3-8**, *E. coli* BL21 produce almost the same ATP than M15, 130,94 mmol·gDCW⁻¹·h⁻¹ and 142,22 mmol·gDCW⁻¹·h⁻¹, respectively. Even if the production is nearly the same, there are a few differences related to proportions in ATP produced and consumed (as shown in **Figure 3-9**) that have to be pointed out:

- The 76% of the ATP produced by *E. coli* BL21 comes from oxidative phosphorylation while in *E. coli* M15 only the 69% comes from it, because the TCA cycle in *E. coli* BL21 accepts more carbon flux than M15's ones.
- The ATP produced via glycolytic pathway in *E. coli* BL21 (15,6% / 22,2 mmol·gDCW⁻¹·h⁻¹) is less than in *E. coli* M15 (22,2% / 29,38 mmol·gDCW⁻¹·h⁻¹). This difference is due to the fact that *E. coli* M15 have a source of ATP production via acetate formation (4,85 mmol·gDCW⁻¹·h⁻¹) while *E. coli* BL21 do not have it and the flux through the glycolytic pathway is higher in *E. coli* M15 (11,02 mmol·gDCW⁻¹·h⁻¹) than in *E. coli* BL21 (9,45 mmol·gDCW⁻¹·h⁻¹).
- The most relevant matter regarding ATP consumption is related to cell maintenance, *E. coli* BL21 (91,75 mmol·gDCW⁻¹·h⁻¹) have a higher cell maintenance than *E. coli* M15 (70,12 mmol·gDCW⁻¹·h⁻¹) in spite of having a growth rate lower than *E. coli* M15. This

behaviour might indicate that for growing at optimal growth rate *E. coli* BL21 have more energy requirements than *E. coli* M15.

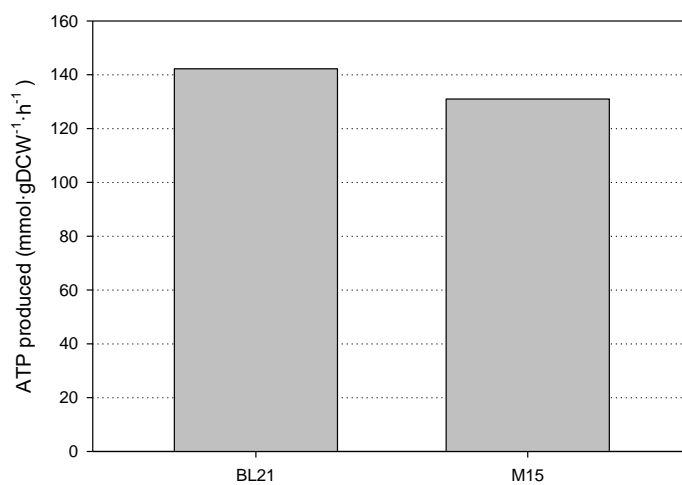


Figure 3-8. Total ATP produced by *E. coli* BL21 and *E. coli* M15.

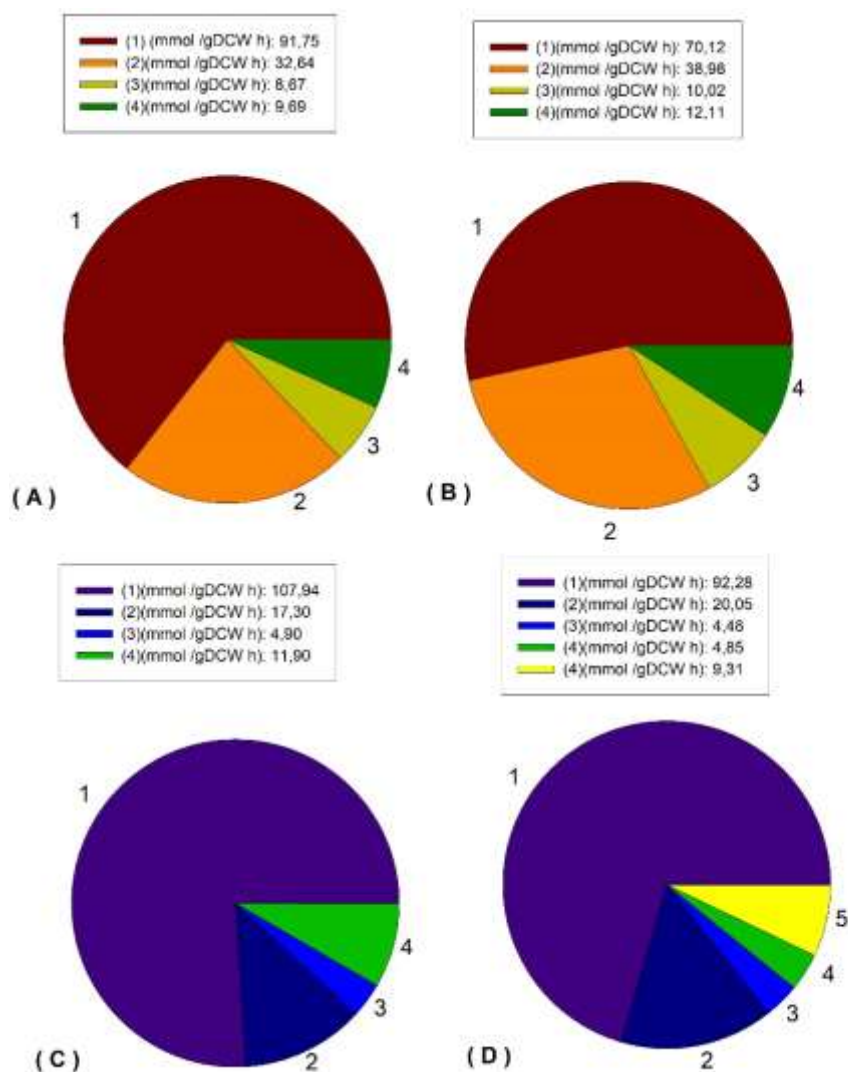


Figure 3-9 Comparison between ATP for *E. coli* BL21 (A and C) and *E. coli* M15 (B and D). . In figures C and D, the ATP produced by is separated depending on its provenance (ATP synthase (1), Phosphoglycerate kinase (2), Pyruvate kinase (3), Acetate kinase (4) and other side reactions (5)). While in figures A and B, the ATP consumed is separated depending on its provenance (Cell maintenance (1), Biomass formation (2), Phosphofructokinase (3) and other side reactions (4)).

To summarize, there are not big differences between ATP produced from *E. coli* BL21 and *E. coli* M15, nevertheless there are notorious changes in way it is handled. Oxidative phosphorylation is more active in *E. coli* BL21 than in *E. coli* M15, *E. coli* M15 generate more ATP via glycolytic pathway than *E. coli* BL21 and the cell maintenance of *E. coli* BL21 is higher than *E. coli* M15.

Up until now, a description about the carbon and energy metabolism from *E. coli* BL21 and *E. coli* M15 have been described and analysed. Therefore, in the next section, a study based on the following hypothesis which revolves around enhancing biomass glucose yield by means of the regulation of glycolytic pathway in *E. coli* BL21 will be presented hereunder.

- First of all, it must be considered that the principal carbon metabolic issue shown in *E. coli* is based on the capacity of the organism for balancing acetyl-coA in the cytoplasm. Roughly speaking, the capacity for balance the acetyl-coA is closely related to the difference between the flux rate through glycolic pathway and TCA cycle. When Glycolic flux is higher than TCA ones the production of acetate is required for balancing Acetyl-coA pool.

On this basis, the next hypothesis is presented: If there is a way to interact with the glycolytic pathway in order to decrease its flux through, then metabolism would be led to a more efficient carbon-biomass conversion. Following this hypothesis, two assumption in relation with how the glycolytic pathway can be interacted with might be done:

- The first assumption is based on identifying the main genes that regulates the glycolytic pathway and modifying its expression such as the deletion of the genes that lead to acetate formation (*ack*, *pta* and *poxB*). Regarding this genetic modification, the deletion of the mentioned genes provoked the depletion of acetate production as well as the secretion into the media of other sub-products like pyruvate or glutamate (Chang et al., 1999) (Tomar et al., 2003) (Dittrich et al., 2005) .
- The second assumption is based on reducing the glycolic pathway by means of constraining the rate of the glucose outer membrane transporter, though bioprocess-engineering strategies that limit the glucose consumption.

Therefore, due to the knowledge needed for conducting the first assumption and the difficulty for finding a combination of genes that its modification affects exclusively to acetate production, the second assumption is chosen as the main assumption. Thereupon, the second assumption that is based on the constriction of the glucose flux through the outer membrane will be presented hereafter.

In order to transport glucose from the media to cytoplasm, *E.coli* uses the amino-terminal hydrophobic domain of the transmembrane subunit (IIBC_{GIc}) protein, that is part of the bacterial phosphotransferase system (PTS) for binding and translocating glucose (Buhr & Erni, 1993). As a consequence, its reaction rate might follow a Michealis-Menten kinetics (Ainsworth, 1977). The Michealis-Menten kinetics states that there is a direct relation between the rate of glucose transport through the membrane via a protein and the extracellular glucose concentration (Ainsworth, 1977).

Regarding this kinetic special feature, a new approach based on a chemostat culture where several inlet glucose concentrations will be tested. As a result, the dependence between the extracellular glucose and glycolic pathway will be studied. To carry out this experiment a continuous culture has to be done to ensure a constant metabolic that will be representative considering the selected environmental conditions

3.7 Results (V) – Analysis and modelling of continuous cultures in *E. coli* BL21

As it was previously mentioned, in this section, the dependence between the extracellular glucose and glycolic pathway will be studied by carrying out a continuous culture where the inlet glucose concentration was changed and specific growth rate will be limited to $0,103 \text{ h}^{-1}$.

A metabolic flux analysis will be done for each stationary phase tested, regarding different glucose concentrations. . Moreover, steady state was assumed when the biomass concentration in the outlet (bioreactor) was constant, which occurred after at least three to five mean residence times had passed.

As shown in **Figure 3-10** the inlet glucose concentration was decreased from $44,5 \text{ g}\cdot\text{L}^{-1}$ to $15,1 \text{ g}\cdot\text{L}^{-1}$, consequently the outlet glucose concentration dropped from $11,85 \text{ g}\cdot\text{L}^{-1}$ to fully depletion in the first stationary state where the inlet glucose concentration dropped from $44,5 \text{ g}\cdot\text{L}^{-1}$ to $34,1 \text{ g}\cdot\text{L}^{-1}$. Moreover, it remained unchanged in the following stationary states, while dilution rate was kept constant ($0,103 \text{ h}^{-1}$). This decrease in the inlet glucose concentration leads the metabolism to a change, that is studied for understanding the tendencies of biomass, acetate, CER and OUR.

In relation with the biomass evolution regarding the glucose inlet concentration, there can be identified three “phases”:

- First phase (I and II in **Figure 3-10**), when glucose was dropped from $44,1 \text{ g}\cdot\text{L}^{-1}$ to $34,1 \text{ g}\cdot\text{L}^{-1}$, biomass increased from $5 \text{ gDCW}\cdot\text{L}^{-1}$ to $5,8 \text{ gDCW}\cdot\text{L}^{-1}$ and acetate was depleted from $1,25 \text{ g}\cdot\text{L}^{-1}$ to $0 \text{ g}\cdot\text{L}^{-1}$.
- Second phase (III, IV, V and VI in **Figure 3-10**), when glucose was dropped from $34,1 \text{ g}\cdot\text{L}^{-1}$ to $19,4 \text{ g}\cdot\text{L}^{-1}$ and biomass did not change ($5,8 \text{ gDCW}\cdot\text{L}^{-1}$).
- Third phase (VII in **Figure 3-10**), when the glucose was dropped to $15,1 \text{ g}\cdot\text{L}^{-1}$ and biomass also dropped from $5,8 \text{ gDCW}\cdot\text{L}^{-1}$ to $4,65 \text{ gDCW}\cdot\text{L}^{-1}$.

Moreover, as shown in **Table 3-7**, the yield of biomass-glucose increased from 0,028 to 0,055 while glucose concentration decreased from 44,1 g·L⁻¹ to 19,4 g·L⁻¹ and in the last stationary state where inlet glucose concentration dropped from 19,4 g·L⁻¹ to 15,1 g·L⁻¹, there was no change in biomass-glucose yield.

On the other hand, as shown in **Table 3-5**, the concentration of acetate reached 1,25 g·L⁻¹ when glucose inlet concentration is equal or higher to 44,5 g·L⁻¹ and when the glucose concentration was equal or lower than 34,1 g·L⁻¹ the acetate production was fully depleted. Regarding the acetate behaviour, it is important to emphasize that the acetate production in *E.coli* BL21 might be related to a uncoupling of the main carbon metabolic routes (TCA and glycolytic) which will be studied and discussed in the next section (section 3.7.1).

Moreover, as shown in **Figure 3-11**, the capacity of the organism for consuming oxygen (OUR) and producing carbon dioxide (CER) decreased from 85,2 mM·h⁻¹ and 75 mM·h⁻¹, when the glucose inlet concentration had a value of 44,1 g·L⁻¹ to 25,3 mM·h⁻¹ and 20 mM·h⁻¹, when glucose inlet concentration had a value of 15,1 g·L⁻¹, respectively. This behaviour is related to *E. coli* BL21 fluxes through of glycolytic and TCA pathways. An increase in those pathways will lead metabolism to increase the specific rate of carbon dioxide and oxygen in order to oxidize the glucose.

Furthermore, in relation with CER and OUR, also as shown in **Table 3-7**, the value of RQ is nearly maintained constant because the change in the available extracellular glucose do not unbalance the redox metabolism of the *E. coli* BL21. The Crabtree effect (Thierie & Penninckx, 2010) is found as an example of how an unbalanced redox metabolism might produce an RQ higher than one.

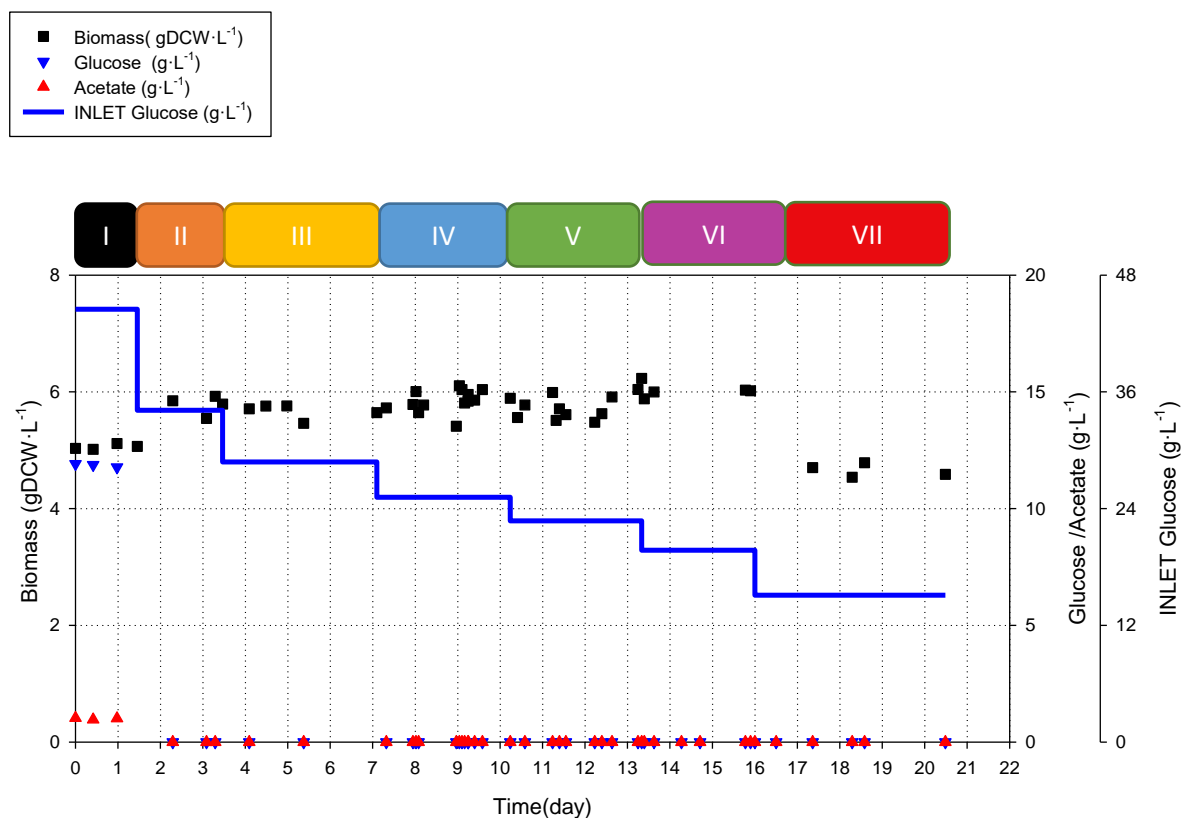


Figure 3-10 Profile of off-line variables such as Biomass (\blacksquare), INLET glucose (—), glucose (\blacktriangledown), acetate (\blacktriangle) for *E. coli* BL21 for the seven stationary state achieved from the continuous culture.

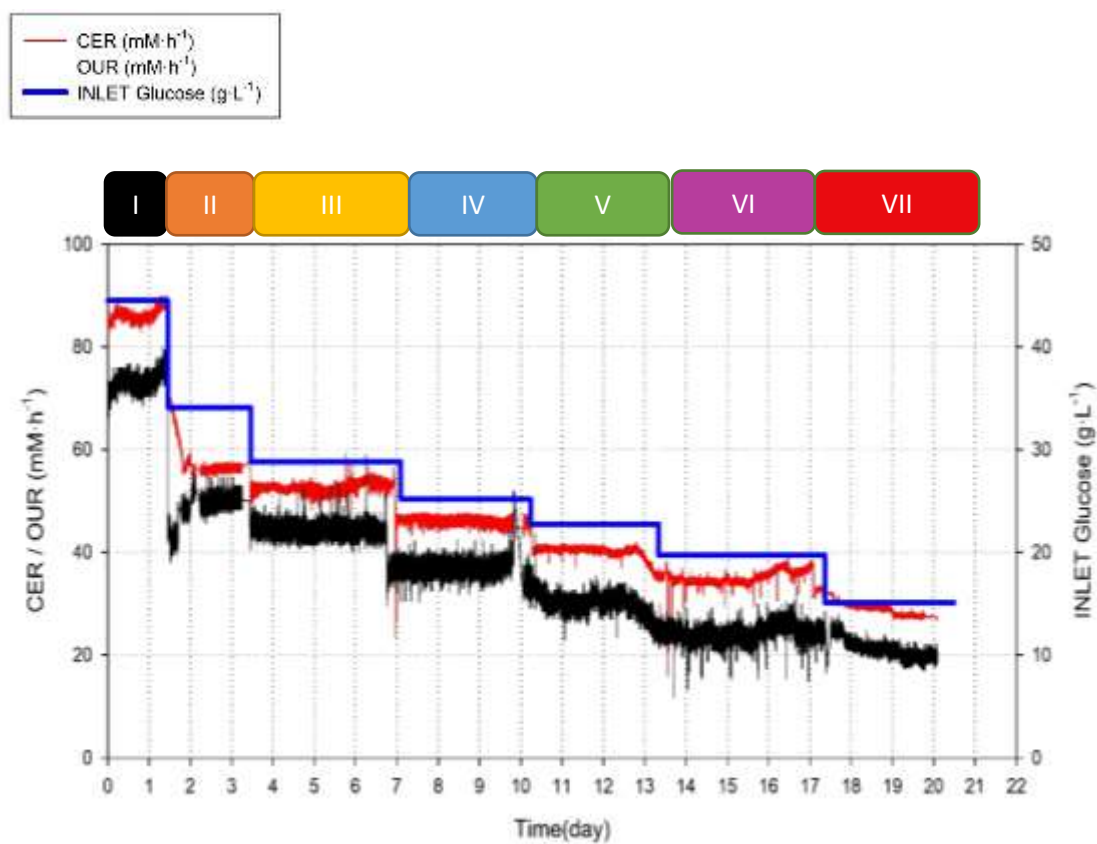


Figure 3-11 Profile of on-line variables such as OUR (—) and CER (—) and an off-line variable such as glucose inlet concentration (—) for *E. coli* BL21 continuous culture.

Up until now, the effect of the inlet glucose concentration on the physiologic state of the *E. coli* and its metabolism has been proved. Although, there is a particular trait that has to be deepened: The behaviour of biomass regarding each stationary state can be explained using the **Equation 3-1**. This equation states that the achieved biomass (X_v) in the stationary state is a function of the glucose available to be metabolized (A), its specific consumption rate ($q_{s,total}$) and the dilution rate (D). Moreover, two premises have to be pointed out:

1. the glucose specific consumption rate ($q_{s,total}$) is the sum of the glucose specific rate needed for biomass formation ($q_{s,biomass}$), acetate formation ($q_{s,acetate}$) and cell maintenance ($q_{s,maintenance}$).
2. The dilution rate can be excluded as a variable involved in the biomass behaviour, because it is constant in each stationary state.

The biomass achieved in the continuous culture depends on how the glucose availability affects the metabolism of *E. coli*, as show in the glucose mass balance (**Equation 3-1**). This effect might be related to two phenomena:

1. How glucose availability affects the kinetic parameters μ_{max} and K_s , due to the fact that the outlet glucose concentration ($[Gluc_{outlet}]$) follows a Monod equation (Kargi, 2009), as shown in **Equation 3-2**.
2. How the glucose availability affects the central carbon metabolism regarding the efficiency of converting glucose to biomass, which is related to glucose specific consumption rate ($q_{s,total}$).

Equation 3-1

$$Xv = D \cdot \frac{\{A = [Gluc_{inlet}] - [Gluc_{outlet}]\}}{\{q_{s,total} = q_{s,biomass} + q_{s,acetate} + q_{s,maintenance}\}}$$

Equation 3-2

$$[Gluc_{outlet}] = \frac{K_s \cdot D}{\mu_{max} - D}$$

Regarding the effect of glucose availability on the kinetic parameters, it might be done an assumption in regard with the biomass change exclusively at the first phase, because in the other phases, glucose was kept constant with a value of 0. Although, this assumption could be either

false or true due to the fact that the continuous culture was designed as a growth rate-limited one. Thus, for a further exploration of this assumption, a continuous culture where the dilution rate (D) is equal to the kinetic parameter μ_{max} could be required for reaching a feasible conclusion in order to prove that both μ_{max} and K_s might be affected by glucose availability.

Therefore, and in relation with what have been pointed out in regard with how glucose availability affects the kinetic parameters, the behaviour of the biomass in the continuous culture will be hypothesized according to how *E. coli* BL21 central carbon metabolism behaves when there is a change in glucose availability.

On this basis, it might be supposed that the variation of biomass is related to a limitation in the specific rate of glucose ($q_{s,biomass}$) that is directed towards biomass formation. This limitation can be the consequence of keeping an accurate cell maintenance rate ($q_{s,maintenance}$) and acetate formation rate ($q_{s,acetate}$).

As was mentioned previously, three phases regarding glucose inlet concentration were defined (the first one from 44,1 g·L⁻¹ to 34,1 g·L⁻¹, the second one from 34,1 g·L⁻¹ to 19,72 g·L⁻¹, and the last one from 19,72 g·L⁻¹ to 15,1 g·L⁻¹), thereafter a description of each one is detailed in the following list:

The first one will be considered a high glucose availability phase and is defined within 44,5 g·L⁻¹ to 34,1 g·L⁻¹. In this phase, the highest glucose uptake rate was achieved. This rate provoked an unbalance in metabolism leading it to acetate production (not observed in batch cultures), this particular metabolism has been studied previously in this work in relation with *E. coli* M15 metabolism in section 3.3.2. Regarding the biomass achieved, the value was determined by the total glucose availability and the total glucose specific rate. It might be supposed that the variation of biomass is related to a limitation in the specific rate of glucose ($q_{s,biomass}$) that is directed towards biomass formation. This limitation can be the consequence of keeping a certain cell maintenance rate ($q_{s,maintenance}$) and acetate formation rate ($q_{s,acetate}$) in order to maintain this metabolic state. Moreover, this phase might have the highest glucose oxidation due to the fact that the highest carbon dioxide and oxygen specific rates were achieved as shown in **Table 3-6**.

The second one will be considered a normal glucose availability phase and it is defined within 34,1 g·L⁻¹ to 19,72 g·L⁻¹. The change in biomass regarding phase 1 is due to the fact that the decrease in the glucose availability lead to the depletion of acetate and might induce the decrease of cell maintenance. As a result, this phase had a higher specific glucose rate directed towards biomass than phase one, therefore biomass was increased. On the other hand, for the rest of the phase, the constancy of biomass was due to the fact that the decrease in glucose

availability lead to a decrease in cell maintenance without reaching the minimum glucose specific rate directed towards biomass formation, as a result biomass was kept constant. Regarding the biomass achieved, the value was determined by the total glucose availability, which solely depended on the inlet glucose concentration and the total glucose specific rate to enable this metabolic state. As in phase one, the decrease in glucose availability lead to the decrease of carbon dioxide and oxygen specific rates. The decrease oxygen might imply a decrease of the energy requirements.

The last phase will be considered a constraining glucose availability phase and it is defined within $19,72 \text{ g}\cdot\text{L}^{-1}$ to $15,1 \text{ g}\cdot\text{L}^{-1}$. In this phase the drop in biomass concentration was caused by not having enough glucose directed towards biomass for keeping the previous one. Regarding the biomass achieved, the value was determined just as the previous phase. Moreover, the decrease in glucose availability lead to a minimum decrease of carbon dioxide and oxygen specific rates in comparison with the previous phase. Under those circumstances, a minim value for energy requirements might be achieved.

In the final analysis, the decrease in glucose availability caused by a decrease in the inlet glucose concentration lead the culture to a metabolic restructuration whose main traits were to produce acetate when the highest inlet glucose concentration was used and a shift in energy requirements for coping with the metabolic restructuration caused by glucose availability.

For a further insight, a genomic-scale metabolic model for each stationary state will be presented in the next section. However, the influence of the flux through the glycolytic pathway in the growth rate cannot be studied because of the limitations associated to the continuous strategy based on keeping the dilution rate constant.

Table 3-5 Used Values for specific rate calculations in *E. coli* BL21 continuous culture.

INLET Glucose ($\text{g}\cdot\text{L}^{-1}$)	Biomass ($\text{gDCW}\cdot\text{L}^{-1}$)	Glucose ($\text{g}\cdot\text{L}^{-1}$)	CER ($\text{mM}\cdot\text{h}^{-1}$)	OUR ($\text{mM}\cdot\text{h}^{-1}$)	Acetate($\text{g}\cdot\text{L}^{-1}$)
44,5	5,05	11,85	83,3	78,5	1,25
34,1	5,77	0	56,1	50,3	0
28,8	5,75	0	50,23	45,65	0
25,17	5,89	0	45,5	39,94	0
22,74	5,76	0	40,6	30,45	0
19,72	5,98	0	35,64	25,96	0
15,1	4,65	0	30,36	20,30	0

Table 3-6 Specifics rates in $\text{mmol} \cdot \text{gDCW}^{-1} \cdot \text{h}^{-1}$ used for Flux Balance Analysis in *E. coli* BL21 continuous culture.

INLET Glucose ($\text{g} \cdot \text{L}^{-1}$)	μ (h^{-1})	q_{Glucose}	q_{Acetate}	q_{O_2}	q_{CO_2}
44,50	0,11	-3,77	0,44	-17,34	17,56
34,10	0,11	-3,45	0,00	-16,29	16,51
28,80	0,11	-2,93	0,00	-13,14	13,36
25,17	0,11	-2,50	0,00	-10,56	10,78
22,74	0,11	-2,31	0,00	-9,39	9,61
19,72	0,11	-1,93	0,00	-7,23	7,45
15,10	0,11	-1,90	0,00	-6,50	6,72

Table 3-7 Yields and Respiratory quotient in *E. coli* BL21 continuous culture.

INLET Glucose ($\text{g} \cdot \text{L}^{-1}$)	$Y_{\text{Acetate/Glucose}}$ ($\text{g} \cdot \text{g}^{-1}$)	$Y_{\text{Biomass/Glucose}}$ ($\text{gDCW} \cdot \text{g}^{-1}$)	RQ
44,50	0,11	0,028	1,01
34,10	0,00	0,030	1,01
28,80	0,00	0,036	1,01
25,17	0,00	0,042	1,02
22,74	0,00	0,046	1,02
19,72	0,00	0,055	1,03
15,10	0,00	0,055	1,03

Up until now, the relation between inlet glucose concentration and the metabolic behaviour of *E. coli* BL21 shows a particular physiology where the change in glucose availability leads to a restructuration of the carbon metabolism. It is important to realize that this study only brings information from a philological view about how *E. coli* BL21 consumes glucose and oxygen and produces acetate, biomass and carbon dioxide.

The physiological point of view presented so far does not bring enough information about how *E. coli* BL21 changes its internal metabolic fluxes regarding changes in the glucose availability. As a result, for compiling all the results and presenting an accurate description of the metabolic behaviour shown in the continuous culture, the comparison between the metabolic models for each one of inlet glucose concentration stationary states will be presented in the following section.

3.7.1 Metabolic Model Comparison between each stationary states: carbon metabolism

Regarding the metabolic flux restructuring, in this section the metabolic fluxes are analysed using the same metabolic model for all the stationary states displayed in the continuous culture. The comparison between each one is shown in **Figure 3-12**. It has to be kept in mind that the obtained results follow two hypotheses due to the complexity of the metabolism and its adaptability to changes in environmental conditions:

- The first hypothesis states that the change in glucose concentration leads to a change in glucose availability.
- The second hypothesis states that the stoichiometric matrix will be the same for all the conditions tested.

In order to obtaining a representative and restricted metabolic model for each one of the conditions tested, the boundaries of the models were constrained using the input-output data of the corresponding metabolites that are shown in **Table 3-8** using the data extracted from **Figure 3-10**.

Table 3-8 Lower Specific rate limits values used as drains for a Flux Balance Analysis in *E. coli* BL21 in continuous culture.

	INLET Glucose Concentration (g·L ⁻¹); specific rates (mmol·gDCW ⁻¹ ·h ⁻¹)						
	44,5	34,1	28,8	25,17	22,74	19,72	15,1
Biomass	0,103 ± 0,000	0,103 ± 0,000	0,103 ± 0,000	0,103 ± 0,000	0,103 ± 0,000	0,103 ± 0,000	0,103 ± 0,000
Acetate	0,435 ± 0,031	0,000 ± 0,000	0,000 ± 0,000	0,000 ± 0,000	0,000 ± 0,000	0,000 ± 0,000	0,000 ± 0,000
Ammonium	-1,111 ± 0,079	-1,111 ± 0,079	-1,111 ± 0,079	-1,111 ± 0,079	-1,111 ± 0,079	-1,111 ± 0,079	-1,137 ± 0,080
Carbon Dioxide	17,562 ± 1,242	16,518 ± 1,168	13,368 ± 0,945	10,782 ± 0,762	9,612 ± 0,680	7,452 ± 0,527	6,724 ± 0,475
Glucose	-3,775 ± 0,267	-3,456 ± 0,244	-2,931 ± 0,207	-2,500 ± 0,177	-2,305 ± 0,163	-1,945 ± 0,138	-1,840 ± 0,130
Oxygen	-17,343 ± 1,226	-16,299 ± 1,153	-13,149 ± 0,930	-10,563 ± 0,747	-9,393 ± 0,664	-7,233 ± 0,511	-6,500 ± 0,460

Once the boundaries of the metabolic model had been fixed, all the calculation of the metabolic fluxes (the methodology is described in section 3.9.10) for each of the stationary states was done by means of the FBA protocol (The protocol is described in section 3.9.12).

While glucose was dropped from 44,5 g·L⁻¹ to 15,1 g·L⁻¹, there are different behaviours that have to be described and explained such as:

- The 2-fold decrease in the flux rate of glycolytic pathway from $3,77 \text{ mmol} \cdot \text{gDCW}^{-1} \cdot \text{h}^{-1}$ to $1,84 \text{ mmol} \cdot \text{gDCW}^{-1} \cdot \text{h}^{-1}$.
- The 2,6-fold decrease in the flux rate of tricarboxylic acids cycle from $5,62 \text{ mmol} \cdot \text{gDCW}^{-1} \cdot \text{h}^{-1}$ to $2,15 \text{ mmol} \cdot \text{gDCW}^{-1} \cdot \text{h}^{-1}$.
- The formation of an acetate flux only in the highest glucose concentration step whose value is $0,43 \text{ mmol} \cdot \text{gDCW}^{-1} \cdot \text{h}^{-1}$.
- The constant value of $0,18 \text{ mmol} \cdot \text{gDCW}^{-1} \cdot \text{h}^{-1}$ for pentose phosphate pathway flux related to biomass formation.

The 2-fold decrease in the glycolytic pathway indicates a relation between the glucose availability and the capacity of the cell for transporting glucose from the outer space to the cytoplasm. When the glucose concentration had the highest value of $44,5 \text{ g} \cdot \text{L}^{-1}$, the maximum value of $3,77 \text{ mmol} \cdot \text{gDCW}^{-1} \cdot \text{h}^{-1}$ for membrane transport and phosphorylation of glucose was achieved leading to the formation of an acetyl-coA flux of $6,38 \text{ mmol} \cdot \text{gDCW}^{-1} \cdot \text{h}^{-1}$. It is important to realize that the change in glucose concentration from $44,5 \text{ g} \cdot \text{L}^{-1}$ to $15,1 \text{ g} \cdot \text{L}^{-1}$ for each stationary state provokes a dropping in the fluxes above mentioned from $3,77 \text{ mmol} \cdot \text{gDCW}^{-1} \cdot \text{h}^{-1}$ to $1,84 \text{ mmol} \cdot \text{gDCW}^{-1} \cdot \text{h}^{-1}$ and from $6,38 \text{ mmol} \cdot \text{gDCW}^{-1} \cdot \text{h}^{-1}$ to $2,48 \text{ mmol} \cdot \text{gDCW}^{-1} \cdot \text{h}^{-1}$, respectively.

At the same time, the TCA flux drops accordingly to the change in glycolytic pathway, whose maximum value is $5,62 \text{ mmol} \cdot \text{gDCW}^{-1} \cdot \text{h}^{-1}$ and $2,15 \text{ mmol} \cdot \text{gDCW}^{-1} \cdot \text{h}^{-1}$ as the minimum.

Taking into account the behaviours of TCA and glycolytic pathway, an unusual fact appears, only when the highest glucose concentration was used, acetate was produced. The apparition of acetate is related to the fact that TCA reached his maximum flux. When TCA have reached its limit, an unbalance in Acetyl-coA is produced. Therefore, for overtaking this limit, Acetyl-coA was converted to acetate letting glucose be metabolized at the highest rate possible, which means that BL21 can also produce acetate when TCA and glycolysis are unbalanced, but the limits of operation are different of the observed in *E. coli* M15 strain.

As was mentioned in the section 3.5, *E. coli* BL21 have the capacity of enhancing TCA cycle flux by means of using the glyoxylate and PEP-OAA shunts. This experiment proved the existence of a maximum flux through the shunts that, when this maximum is achieved, *E. coli* BL21 will behave just as *E. coli* M15 regarding acetate metabolism.

For this reason, the acetate production in a non-acetate producer cell line is possible to obtain when the increase in glycolytic flux is not followed by an increase of the capacity for handling carbon flux in the TCA cycle. As a result, acetate is produced.

Regarding the biomass generation fluxes, which are mainly represented in PPP, its value does not change in each one of the stationary states. This constancy is related to the value of the growth rate. As shown in section 3.9.10, in the stationary state the growth rate is equal to the dilution rate. Given this information and taken into consideration that the dilution rate is fixed from the beginning of the experiment, the growth rate is fixed too.

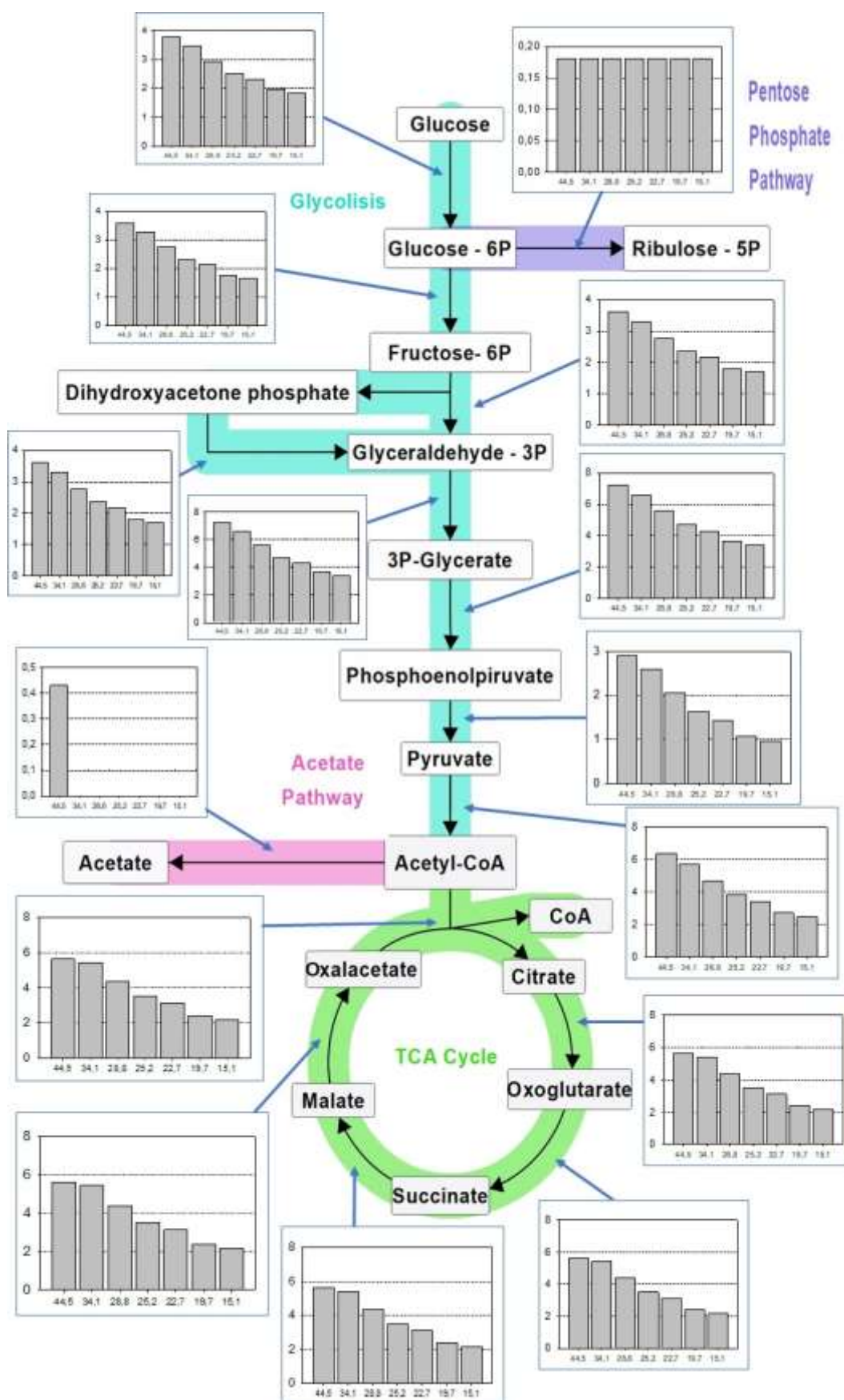


Figure 3-12 Scheme of the main metabolic fluxes calculated for *E. coli* BL21 where inlet glucose concentration is decreased from 44,5 $\text{g} \cdot \text{L}^{-1}$ to 15,1 $\text{g} \cdot \text{L}^{-1}$ (44,5 $\text{g} \cdot \text{L}^{-1}$, 34,1 $\text{g} \cdot \text{L}^{-1}$, 28,8 $\text{g} \cdot \text{L}^{-1}$, 25,2 $\text{g} \cdot \text{L}^{-1}$, 22,7 $\text{g} \cdot \text{L}^{-1}$, 19,7 $\text{g} \cdot \text{L}^{-1}$ and 15,1 $\text{g} \cdot \text{L}^{-1}$). Arrows indicate the direction of the flux. All the fluxes are expressed in $\text{mmol} \cdot \text{gDCW}^{-1} \cdot \text{h}^{-1}$.

In the final analysis, *E. coli* BL21 can adapt its flux through of glycolytic pathway and TCA cycle until a constraint is reached due to a limit in the shunt reactions (PEP-OAA and glyoxylate) directed towards TCA cycle. As a result, *E. coli* BL21 produce acetate in order to balance the acetyl-coA pool.

In order to further explore this adaptive metabolism where a change in glucose availability leads to a shift in the acetate metabolism or the enhancement of the biomass-glucose yield, a study of how *E. coli* BL21 handles ATP requirements will be presented.

3.7.2 Metabolic Model Comparison between each stationary states: energy metabolism

As has been shown in the section above, the central carbon metabolism is modified as long as there is a change in glucose availability. The main function of the central carbon metabolism is to produce precursors for biomass synthesis and high energetic molecules, such ATP or NADH, that will be used as a fuel. As a result, a variation in the central carbon metabolism might affect the energy metabolism.

On this basis, a study of the energy metabolism will be presented. This study will revolve around the comprehension of the change in the proportion of each reaction involved in consumption and generation of ATP in relation to changes in glucose availability.

E. coli BL21 can variate the ATP handle regarding the change in glucose availability until a minimum was achieved, as shown in **Figure 3-13**. As a result, the energy requirements for oxidizing glucose are lower as lower is the flux through the glycolytic pathway, due to a decrease in glucose availability, as was shown in the previous section.

As shown in **Figure 3-14**, the glucose availability has a huge impact in the distribution of the ATP consumption. It is important to realize that the reaction whose proportion in the ATP consumption is more dependent to glucose availability is the cell maintenance. *E. coli* BL21 might need to rise the cell maintenance for achieving the higher possible flux through the glycolytic pathway, **Figure 3-13** backs this hypothesis because the ATP handled rises too.

Otherwise, the proportion between each reaction involved in the generation of ATP does not change. The reason behind it is that all the reactions are affected equally by the increase in the flux through the central carbon metabolism owing to the change in glucose availability. The effect of decreasing glucose availability on the ATP generated solely provokes a decrease in the

total ATP generated, as show in **Figure 3-13**, because total ATP generated has to be the same than the handled one. In addition, the growth it is the same.

Therefore, in order to show a numerical view of the statements before mentioned, the following list is presented:

- The proportion of ATP produced from oxidative phosphorylation in relation with a change in the glucose availability only dropped from 78 % to 76,8 %, when disappears the acetate kinase contribution (**Enzyme number 4 of Figure 3-15**). Moreover, the change in glucose availability solely affected on total ATP produced, dropping from 72,2 $\text{mmol} \cdot \text{gDCW}^{-1} \cdot \text{h}^{-1}$ until 27,22 $\text{mmol} \cdot \text{gDCW}^{-1} \cdot \text{h}^{-1}$.
- The ATP produced via glycolytic drops as long as there might be a decrease in glucose availability from 56,21 $\text{mmol} \cdot \text{gDCW}^{-1} \cdot \text{h}^{-1}$ until 20,33 $\text{mmol} \cdot \text{gDCW}^{-1} \cdot \text{h}^{-1}$.
- The most relevant matter regarding ATP consumption is related to cell maintenance, dropping glucose availability leads to a decrease in the flux directed to cell maintenance from 61 $\text{mmol} \cdot \text{gDCW}^{-1} \cdot \text{h}^{-1}$ until 17,66 $\text{mmol} \cdot \text{gDCW}^{-1} \cdot \text{h}^{-1}$

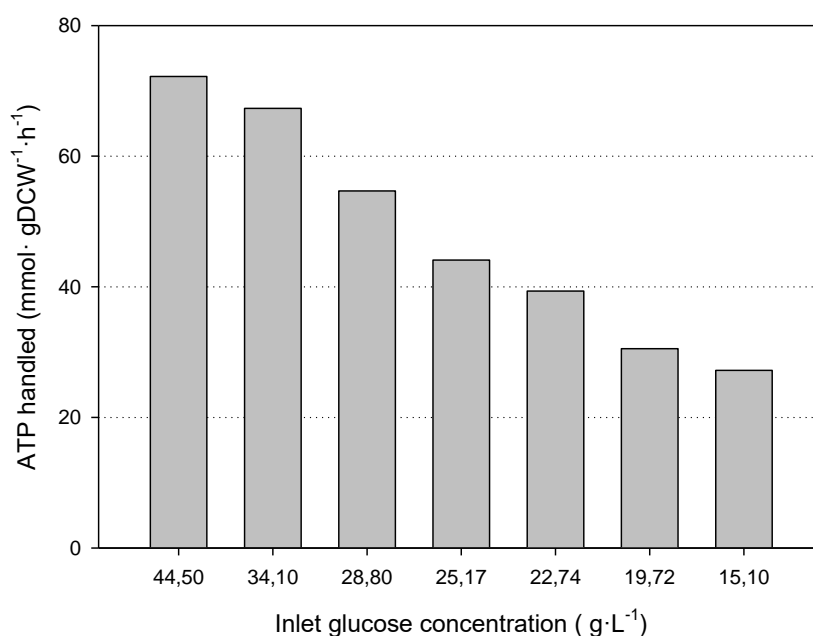


Figure 3-13 Variation of the ATP handled for each stationary state where different inlet glucose concentration was tested. All the fluxes are expressed in $\text{mmol} \cdot \text{gDCW}^{-1} \cdot \text{h}^{-1}$.

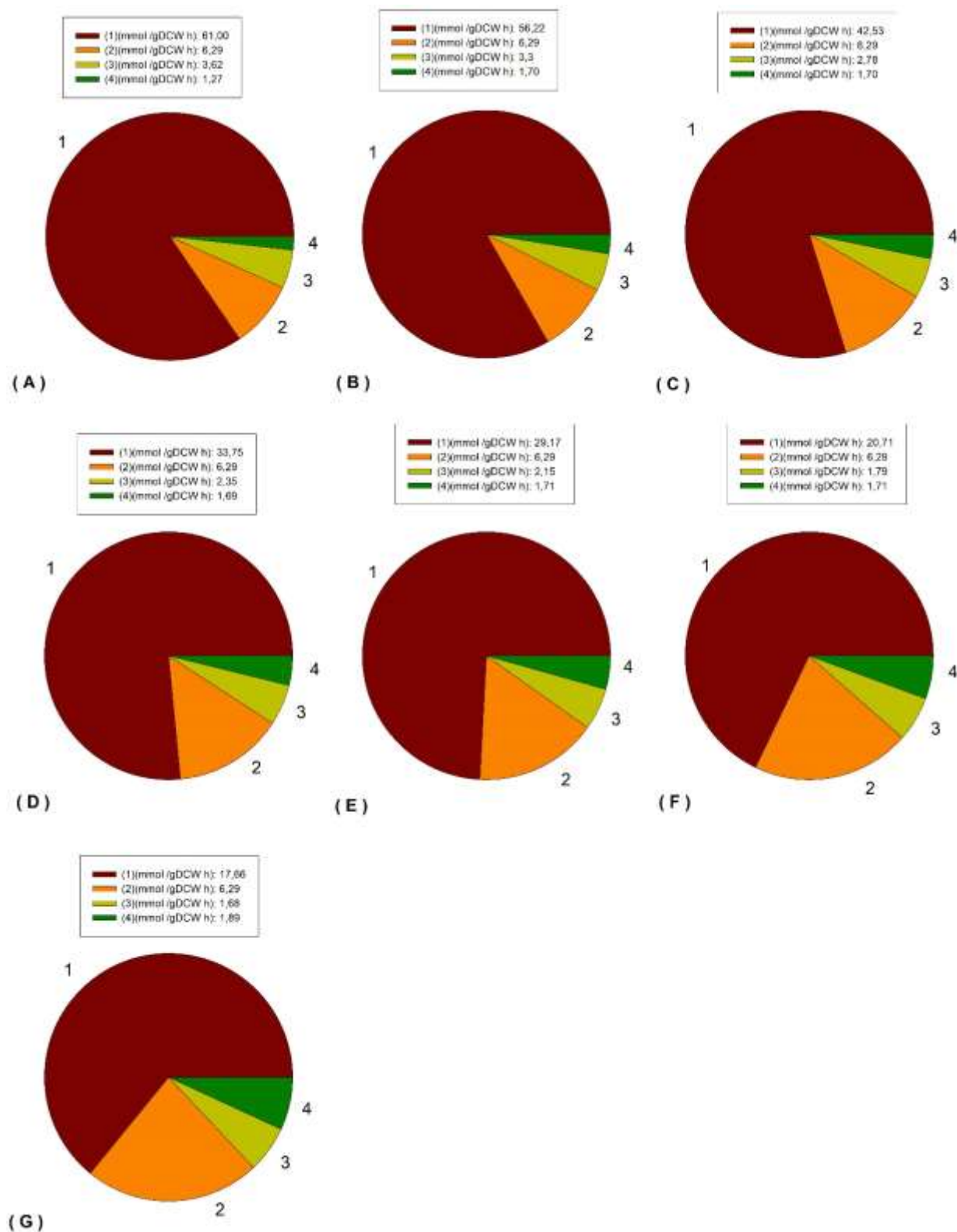


Figure 3-14 Proportions of ATP consumed regarding its provenance for each stationary state in *E. coli* BL21, where different inlet glucose concentration were used. All the fluxes are expressed in mmol-gDCW⁻¹·h⁻¹.

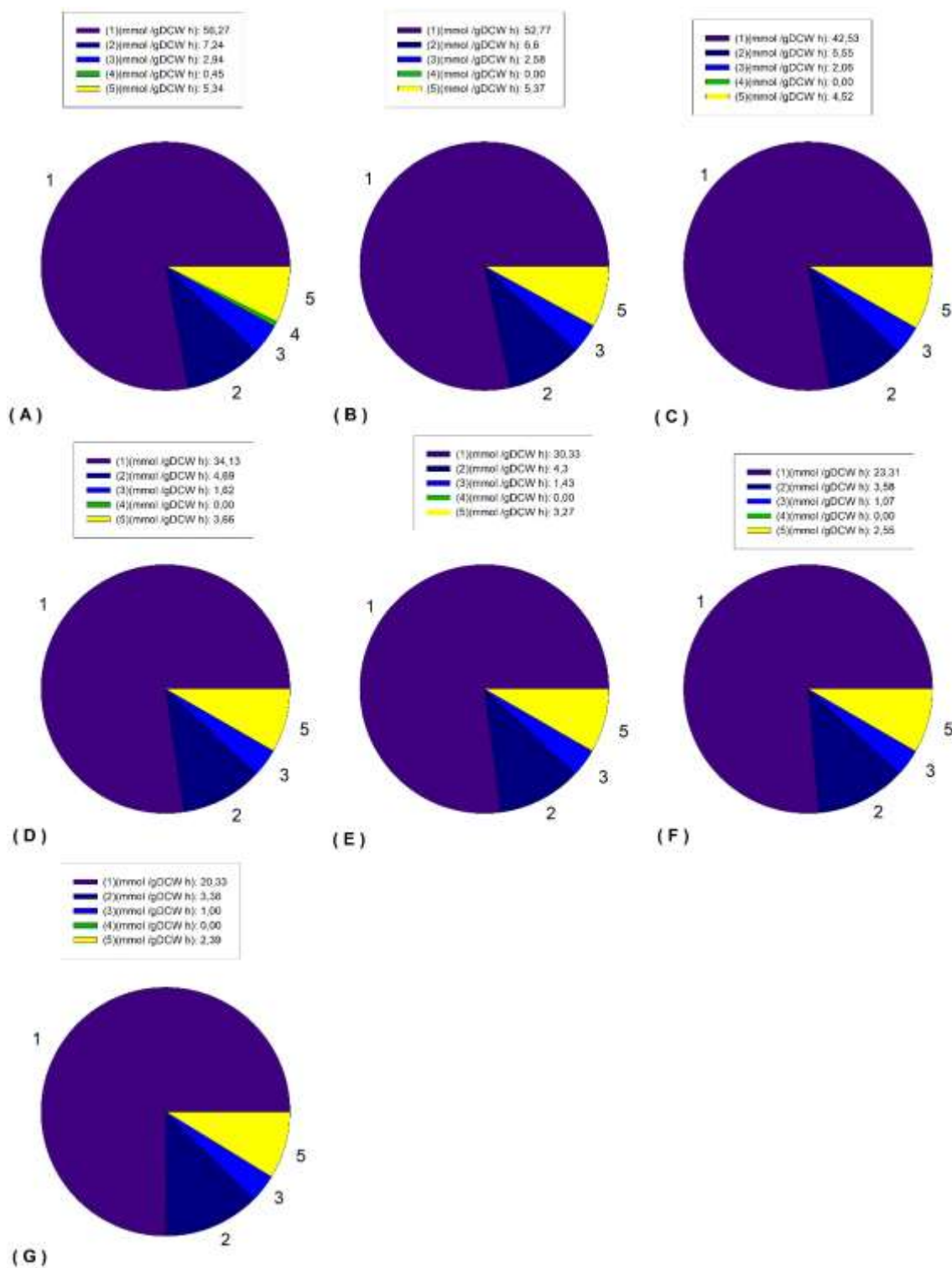


Figure 3-15 Proportions of ATP produced regarding its origin for each stationary state in *E. coli* BL21, where different inlet glucose concentration were used. All the fluxes are expressed in $\text{mmol-gDCW}^{-1}\cdot\text{h}^{-1}$.

3.8 Discussion and Conclusions

An extensive study of the metabolic flux distribution for the carbon and energy metabolic behaviours obtained in *E. coli* M15 and *E. coli* BL21 has been presented in this chapter. The conventional metabolic behaviour of *E. coli* M15 in batch cultures is characterized by glucose consumption while acetate is produced and secreted to the media, while *E. coli* BL21 do not produce acetate. Such metabolic behaviour has been studied since 1970, although in the last twenty years, thanks to the technological advances in relation with high-throughput data management within Systems Biology scope (Shah et al., 2007). Several hypotheses based on studying the genomic, proteomics and fluxomics to enlighten the reason behind acetate production has been published (Holms, 1996) (Shiloah & Rinas, 2009)(Basan et al., 2015)(Zeng & Yang, 2019).

The analysis of the metabolic fluxes using a reduced genomic-scale metabolic model performed suggests that this metabolism of acetate generation is related to an unbalance in acetyl-coA pool generated by a decoupling in the flux through glycolytic pathway and TCA cycle. The origin of decoupling can be hypothesized by high glycolytic pathway repress TCA's gene expression (J. W. Lee et al., 2002) and the oversize of flux carbon acceptance of the TCA by means of using the anaplerotic reactions as a "relief valve", glyoxylate and PEP-OOA shunts (Noronha et al., 2000) (Farmer & Liao, 1997). Moreover, the analysis of the proportion of metabolic fluxes of ATP in the energy metabolism suggests that Oxidative Phosphorylation Pathway is more active in *E. coli* BL21 than in *E. coli* M15. *E. coli* M15 generates more ATP via glycolytic pathway than *E. coli* BL21 and the cell maintenance of *E. coli* BL21 is higher than *E. coli* M15.

Once the study of the acetate production has led to an appropriate hypothesis, an extensive study in *E. coli* BL21 about how the flux through the glycolytic pathway is affected by means of changes in glucose availability has been presented in this chapter too. This study consists of a comparison between several metabolic models, previously used in the comparison between *E. coli* BL21 and *E. coli* M15, that describe the stationary states of a chemostat when several inlet glucose concentrations are tested keeping the dilution rate constant.

The comparison between the metabolic fluxes of the stationary states corroborates that an increase in the glucose availability leads *E. coli* BL21 to increase the flux through the glycolytic pathway and TCA cycle until a limit is reached. As a consequence, when TCA cannot metabolize all the acetyl-coA generated by the glycolytic pathway, acetate is produced. Although, it is

important to point out that due to the limitations of the continuous culture carried out, the study regarding how glucose availability affect the kinetic parameters was excluded. Therefore, this study will be an interesting work to develop.

Regarding the adaptability of the central carbon metabolism, *E. coli* BL21 might have at least two metabolic properties that affect the carbon influx capacity through the TCA cycle by means of: increasing the flux through glyoxylate and PEP-OAA shunts and not repressing TCA's gene expression as the flux through glycolytic pathway increases. Although, there is a limitation in one of the both or both metabolic function that leads to acetate production when the glucose availability is higher enough to uncouple the glycolytic pathway and TCA cycle. In order to find which one/both are responsible for the acetate production in *E. coli* BL21, ^{13}C and ^2H experiments might be carried out (J. W. Lee et al., 2002).

On the other hand, the analysis of the proportion of ATP consumed in the energy metabolism suggests that cell maintenance and ATP handled might have to rise for achieving a higher flux through the glycolytic pathway when there is an increase in glucose availability.

Finally, the results presented in this chapter, that were focused on the comprehension of carbon and energy metabolism *E. coli*, will be used to design engineering-based tools in order to monitor and control high-density cell cultures, for instance fed-batch cultures. In chapter 5, the definition of bioprocess strategies will be carry out taking into consideration the metabolic behaviour observed in the continuous culture. As it will be described in that chapter, the key aspect to design an optimal high cell density strategy is to use the optimal metabolic parameters that gives information about the conversion of glucose to biomass.

3.9 Materials and Methods

3.9.1 *E. coli* strains and cell maintenance

The *E. coli* strains that were used for the study of the acetate metabolism in batch cultures are described below:

- *E. coli* M15 (K-12 wild type derived) F⁻, Φ 80 Δ lacM15, thi, lac⁻, mtl⁻, recA⁺, KmR Villarejo, M.R. and Zabin, I. (1974) β -galactosidase from termination and deletion mutant strains. J. Bacteriol. 120, 466.
- *E. coli* BL21 (*E. coli* B) F⁻, ompT, gal, dcm, lon, hsdSB(rB⁻mB⁻), [malB⁺]K-12(λ S) Studier et al. (2009) J. Mol. Biol. 394(4), 653

The *E. coli* strain that was used for the study of glucose metabolism in a non-acetate producer *E. coli* in continuous cultures is the same *E. coli* BL21 strain used for batch cultures.

The pre-inoculum of both bacteria were cultured in 125 mL glass erlenmeyer with a working volume of 20 mL, incubated at 37°C (Steri-cult 2000 Incubator, Forma Scientific) using the media described in section 3.9.2 . Flasks were continuously agitated at 130 rpm on an orbital shaking platform (Stuart SSL110 Incubator, Forma Scientific). Moreover, both bacteria were maintained using petri dishes at 30°C with the media described in section 3.9.2.

3.9.2 Culture systems

For small scale or inoculum cultures have been performed in Erlenmeyer of different volumes (25, 50, 100 , 250 and 1000 ml) cultured at 37°C and 130 rpm using the media described in section 3.9.2. Moreover, the erlenmeyers were continuously agitated at 130 rpm on an orbital shaking platform (Shaker orbital Incubator, Sanyo).

The culture in petri plates was used as a starter solid culture support. Moreover, it was incubated at 37°C using an orbital incubator (Shaker orbital Incubator, Sanyo).

3.9.3 Media definition.

The media for cell maintenance and petri plates is described in

Table 3-9 and the ones used in all the cultures for both strains is described in **Table 3-10**.

Table 3-9 Composition LB and LB-Agar media.

Compound	Concentration (g·L ⁻¹)	
	LB	Agar-LB
Peptone	10	10
Yeast Extract	5	5
NaCL	10	10
Agar	0	12

Table 3-10 Composition of media used in batch and continuous cultures.

Compound	Concentration
Glucose H ₂ O	22 g/L
K ₂ HPO ₄	11,9 g/L
KH ₂ PO ₄	2,4 g/L
NaCl	1,8 g/L
MgSO ₄ 7H ₂ O	0,1 g/L
NH ₄ SO ₄	3 g/L
FeCl ₃ 6H ₂ O	0,01 g/L
Tiamina	0,03 g/L
AlCl ₃	0,023 mg/L
ZnSO ₄ 7H ₂ O	1,25 mg/L
CoCl ₂ 6H ₂ O	0,12 mg/L
CuSO ₄ 5H ₂ O	1,57 mg/L
H ₃ BO ₃	0,0072 mg/L
MnCl ₂ 4H ₂ O	1,02 mg/L
NiCl ₂ 6H ₂ O	0,0072 mg/L
Na ₂ MO ₄ 2H ₂ O	0,017 mg/L

3.9.4 Bioreactor cell culture

The stirred-tank bioreactor used in the present study was a commercial bioreactor (Biostat B, from Sartorius Stedim Biotech, Germany) with 2L-cylindrical jacketed vessel, equipped with probes and control systems for pH, D.O. (relative oxygen partial pressure) and temperature, stirred with two Rushton impellers.

The control systems of the before mentioned variables are described below:

- Dissolved oxygen concentration was monitored with a polarographic probe (Oxyferm, Hamilton), and maintained at 30% of saturation by means of an aeration flow using a sparger of 1 VVM together with a cascade control system based on a stirring control system and a gas mixing unit.
- Temperature was maintained at 37°C by switch between a heat exchanger when heat was needed and with a cooling water system when cold was needed.
- pH was measured with a standard electrode (EasyFerm Plus, Hamilton), and it was maintained at 7,02 if required a HCl 2M (Panreac) addition, and a subsequently addition of NaOH (300g·L⁻¹) (Panreac).

The working volume for the batch cultures was 2L, and for the continuous culture was 1,75L.

3.9.5 MFCS/win. Software for Data Acquisition, Monitoring and Control

BioPat® MFCS/win 3.0 (Sartorius Stedim Biotech, Germany) was used for monitoring and controlling all the physiological variables (pH, temperature, aeration and agitation) of the batch and continuous cultures. Moreover, the implementation of the OUR and CER calculation were carried using the algorithms presented in section 3.8.8.

3.9.6 Analytical methods

The sample volume for the analytics and biomass concentration was 1 mL. Cell mass was determined using a spectrophotometer at 600 nm by light scattering and by dry cell weight calculation using a general equation from an average *E. coli* (Lecina, 2007) according to

Equation 3-3

Equation 3-3

$$1 \text{ gDCW} \cdot \text{L}^{-1} = 0,27 \cdot \text{DO} + 0,019.$$

After cell counting, the remainder of each sample was centrifuged (6000 g for 5 min) and filtered with a filter of 0,45 µm of diameter to remove the cells, and the supernatant was frozen for further analysis.

The volumetric concentration of oxygen and carbon dioxide in the gas flow were analysed during the course of the experiment using a BlueinOne device from BlueSens gas sensor GmbH. Due to the use of this device, the determination of both the oxygen and carbon dioxide became in-line (Valero & López-Santín, 2017).

3.9.7 Metabolite determinations

Glucose concentrations were determined with an automated glucose and lactate analyser (biochemistry analyser 2700, YSI). Moreover, glucose, acetate concentrations were measured by HPLC as described in (Sanfeliu Sabater, 1995).

Oxygen and Carbon dioxide concentrations were determined with the analytical device BlueinOne Cell (BlueSens gas sensor GmbH) whose measuring principle is infrared IR for carbon dioxide and a galvanic cell for oxygen (Mueller & Schmale, 2004).

3.9.8 Oxygen uptake rate (OUR) and Carbon exchange rate (CER)

The deduction of both CER and OUR was carried out taking into consideration a mass balance from the gas phase and the liquid phase. It give information about the Oxygen Transfer Rate (OTR) or the Carbon dioxide Transfer Rate (CTR) , which are the rates that characterizes the transfer of oxygen and carbon dioxide from the gas phase to the liquid phase. AS observed in **Equation 3-4**, the OTR depend on the molar flow of oxygen while as observed in **Equation 3-5**, CTR depend on the molar flow of carbon dioxide

Equation 3-4

$$OTR \cdot V = F_{out,O_2} - F_{in,O_2}$$

Equation 3-5

$$CTR \cdot V = F_{out,CO_2} - F_{in,CO_2}$$

If it is considered that oxygen and carbon dioxide transfer is in a stationary state, then the OTR/CTR have the same value that the OUR /CER, respectively. As a result, a relation can described where the difference in the molar flow of oxygen and the carbon dioxide between the inlet and outlet gas flow is proportional to the OUR/CER as described in **Equation 3-6** and in **Equation 3-7**, respectively.

Equation 3-6

$$OUR \cdot V = F_{out,O_2} - F_{in,O_2}$$

Equation 3-7

$$CER \cdot V = F_{out,O_2} - F_{in,O_2}$$

Then, the ideal gas law (**Equation 3-8**) and **Equation 3-9** are used to convert the molar flow (F_j) to concentration expressed in % of volume. As a result, a direct relation between the OUR/CER and the difference in the oxygen or in the carbon dioxide concentration expressed in % of volume between the inlet volumetric gas flow ($Q_{T,inlet}$) and outlet volumetric gas flow ($Q_{T,outlet}$) is presented as described in

Equation 3-10 and in **Equation 3-11**, respectively.

Equation 3-8

$$P \cdot Q_j = F_j \cdot R \cdot T$$

Equation 3-9

$$Q_T \cdot \%_j = Q_j$$

Equation 3-10

$$OUR \cdot V = \frac{P}{RT} \cdot (Q_{T,inlet} \%_{O_{2,in}} - Q_{T,outlet} \%_{O_{2,out}})$$

Equation 3-11

$$CER \cdot V = \frac{P}{RT} \cdot (Q_{T,inlet} \%_{CO_{2,in}} - Q_{T,outlet} \%_{CO_{2,out}})$$

3.9.9 Specific rate calculations in batch cultures

The growth rate in batch cell culture is expressed by **Equation 3-12**. The specific growth rate (μ) was calculated in the exponential growth phase by linear regression of the natural logarithm of the concentration of biomass (X_v) as function of time (t), as presented in **Equation 3-13**

The consumption and production rate for glucose, acetate, oxygen and carbon dioxide are expressed by **Equation 3-14** for each metabolite (m). The specific consumption/production rate (q_m) was calculated integrating **Equation 3-12** and **Equation 3-14** together, obtaining the **Equation 3-15** for glucose and acetate. Although, the specific consumption/production rate (q_m) of oxygen and carbon dioxide was calculated using **Equation 3-14**

Linear regression tool of Microsoft Excel 2016 (Microsoft) was used for obtaining the specific growth rate (μ) and the specific consumption/production rate (q_m) of glucose and acetate.

Equation 3-12

$$\frac{dX_v}{dt} = r_X = \mu \cdot X_v$$

Equation 3-13

$$\ln(X_v) = \ln(X_{v,0}) + \mu \cdot (t - t_0)$$

Equation 3-14

$$\frac{dC_m}{dt} = r_m = q_m \cdot X_v$$

Equation 3-15

$$C_m = C_{m,0} + \frac{q_m \cdot X_0}{\mu \cdot e^{\mu \cdot t_0}} \cdot [e^{\mu \cdot t} - e^{\mu \cdot t_0}]$$

3.9.10 Specific rate calculations in continuous cultures

The growth rate in continuous cell culture is expressed by

Equation 3-16. The specific growth rate (μ) was calculated using the quotient of volumetric flow (F) and operational volume (V)

The consumption and production rate for glucose, acetate, oxygen and carbon dioxide are expressed by **Equation 3-17**.

Linear regression tool of Microsoft Excel 2016 (Microsoft) was used for obtaining the specific growth rate (μ) and the specific consumption/production rate (qc) of glucose and acetate.

Equation 3-16

$$\frac{F}{V} = \mu$$

Equation 3-17

$$q_m = \frac{F \cdot (C_{oulet,m} - C_{inlet,m})}{V \cdot X_v}$$

3.9.11 Reduced genome-scale metabolic model

In this study, we used a reduced genome scale metabolic model (ColiPruned) published by (Erdrich et al., 2015). This model is a free available in Systems Biology Markup Language (SBML) format at <http://www2.mpi-magdeburg.mpg.de/projects/cna/etcdownloads.html> (Erdrich et al., 2015).

The model was derived from the complete *E. coli* genome-scale metabolic model iAF1260 using a reduction algorithm (Erdrich et al., 2015). The generic genome-scale metabolic model was reconstructed as an updated genome-scale reconstruction of the metabolic network in *Escherichia coli* K-12 MG1655. (Feist et al., 2007). It is important to point out that the biomass equation of model iAF1260 uses the composition of the average wild type *E. coli* cell and for the ATP maintenance which account for non-metabolic processes was estimated using the hydrolysis of ATP (Feist et al., 2007).

The main differences between the *E. coli* genome iAF1260 and the reduced model using the reduction algorithm are shown in **Table 3-11**.

Table 3-11 main properties of the genome scale metabolic model iAF1260 and the reduced iAF1260 by means of the reduction algorithm described in (Erdrich et al., 2015) .

	iAF1260 model	Reduced iAF1260
reactions	2384	455
internal metabolites	1669	438
external metabolites	305	33
degrees of freedom	753	26

It might be noted that the reduced model can be used for both *E. coli* strains due to the fact that the biomass equation is an average one for a wild type *E. coli*.

Although, the reduced model was revised looking for errors in reversibility of reactions, main reaction directions and some software script incompatibilities between the sbml model and OptFlux program.

A list of all included metabolites and reactions in the model are detailed in **Appendix**. Reactions fluxes over the metabolic network are presented in $\text{mmols} \cdot \text{gDCW}^{-1} \cdot \text{h}^{-1}$.

3.9.12 Flux Balance Analysis protocol

3.9.12.1 Mathematical basis

FBA is mathematically based in Linear Programming formulation to calculate the values of all the fluxes over the reactions. For each metabolite included in the model, a mass balance has been carried out considering the consumption/ production rate. Mass balance must include transport rate across the external, mitochondrial membrane and periplasm space (if necessary). The specific consumption/production rate (q_j) for each metabolite is obtained from **Equation 3-18**, where $\alpha_{j,r}$ is the stoichiometric coefficient of metabolite j in the reaction r and f_r is the flux of reaction r .

Equation 3-18

$$q_j = \sum \alpha_{j,r} \cdot f_r$$

The set of equations are represented in matrix notation in **Equation 3-19**, where A is the stoichiometric matrix with $m \times r$ dimensions (as j rows as metabolites and as r columns as reactions). q is the vector of specific consumption or production rate for each metabolite (as j rows as metabolites) and f is the vector of fluxes (as r rows as reactions).

Equation 3-19

$$q_{(j,1)} = A_{(j,r)} \cdot f_{(r,1)}$$

The specific consumption/production rates (q_j) for each metabolite calculated above (see section 3.9.10 for more details) with data obtained during the fermentation correspond to the specific rate of the transport reactions in the external membrane of the cell. As explained above, external reactions were included in the model, therefore in **Equation 3-19** these reactions are included in stoichiometric matrix and in fluxes vector.

Considering pseudo steady state, where the concentration of a metabolite doesn't change over time inside the cell, and considering the conservation of mass law, the q vector term becomes zero, obtaining **Equation 3-20**.

Equation 3-20

$$A_{(j \times r)} \cdot f_{(r \times 1)} = 0$$

3.9.12.2 Flux calculation

Flux Balance Analysis (FBA) was performed for obtaining the flux value of all the reactions included in the reduced genome scale metabolic model. The general constraints contained in the model are the stoichiometric coefficients of each reaction, the reactions reversibility and the energy requirement for the biomass generation.

Nevertheless, as usual in FBA with genomic models, the system is underdetermined and there exist degrees of freedom. In this case, the system has 488 reactions fluxes, 471 balance equations, as a result the system have 47 degrees of freedom.

Therefore, to perform FBA is necessary to add external measured fluxes as additional constraints (**Table 3-12**). In this case it has been added 34 measured fluxes in total, but again it must to be account that some fluxes are linearly dependent each other. With measured fluxes, the system has 13 degrees of freedom, so it has a large space of possibility solutions. To find the optimal state, FBA uses the optimization of a certain objective function, in this case the cytoplasmic hydrolysis of ATP.

Flux Balance Analysis (FBA) was performed using freely available software OptFlux (Rocha et al., 2010).

Table 3-12 . Chosen metabolites as external measured fluxes in the reduced genomic scale metabolic model used.

External measured fluxes	
2-Oxoglutarate	Iron (II)
4-hydroxy-5-methyl-3,2H-furanone	Iron (III)
4-Hydroxy-benzyl-alcohol	lactate
5 -deoxyribose	L-Glutamate

Acetaldehyde	Magnesium
Acetate	Manganese
Ammonium	Molybdate
Calcium	Oxygen
Chloride	Phosphate
Cobalt	Potassium
Biomass	Proton
Carbon Dioxide	Pyruvate
Copper	Succinate
Ethanol	Sulphate
Formate	Water
Glucose	Zinc
Hydrogen	

3.9.13 Model visualization

Model visualization has been made using commercially available software Omix Visualization (Omix Visualization GmbH & Co. KG) as described in (Droste et al., 2013)

The representation of the principal metabolism has four groups which are detailed in the following list:

1. the glycolytic pathway, which is related to the catabolism of glucose to acetyl-coA (blue colour)
2. the pentose phosphate pathway, whose function is mainly the generation of biosynthesis precursors based on nitrogen bases (purple colour)
3. The acetate pathway, which leads to the generation of acetate (orange colour)
4. The TCA cycle, which is related to catabolism of acetyl-CoA to carbon dioxide and NADH (green colour).

3.9.14 Statistics

Duplicates for each culture conditions were performed, but only one of the repetitions is presented in the Results section. Since the runs have not performed in parallel (due to

equipment limitations), sampling time do not coincide and also other parameters may vary as the cell seeding density. Regarding the continuous culture only one experiment was carry out owing to in the stationary state three sample were taken. The sampling of the continuous culture was used as repetitions.

3.10 References

- Ainsworth, S. (1977). Michaelis-Menten Kinetics. In *Steady-State Enzyme Kinetics* (pp. 43–73). Macmillan Education UK. https://doi.org/10.1007/978-1-349-01959-5_3
- Anraku, Y., & Gennis, R. B. (1987). The aerobic respiratory chain of *Escherichia coli*. *Trends in Biochemical Sciences*, 12(C), 262–266. [https://doi.org/10.1016/0968-0004\(87\)90131-9](https://doi.org/10.1016/0968-0004(87)90131-9)
- Aristidou, A. A., San, K. -Y., & Bennett, G. N. (1994). Modification of central metabolic pathway in *Escherichia coli* to reduce acetate accumulation by heterologous expression of the *Bacillus subtilis* acetolactate synthase gene. *Biotechnology and Bioengineering*, 44(8), 944–951. <https://doi.org/10.1002/bit.260440810>
- Aristidou, A. A., San, K. -Yiu, & Bennett, G. N. (1995). Metabolic Engineering of *Escherichia coli* To Enhance Recombinant Protein Production through Acetate Reduction. *Biotechnology Progress*, 11(4), 475–478. <https://doi.org/10.1021/bp00034a019>
- Basan, M., Hui, S., Okano, H., Zhang, Z., Shen, Y., Williamson, J. R., & Hwa, T. (2015). Overflow metabolism in *Escherichia coli* results from efficient proteome allocation. *Nature*, 528(7580), 99–104. <https://doi.org/10.1038/nature15765>
- Bernal, V., Castaño-Cerezo, S., & Cánovas, M. (2016). Acetate metabolism regulation in *Escherichia coli*: carbon overflow, pathogenicity, and beyond. *Applied Microbiology and Biotechnology*, 100(21), 8985–9001. <https://doi.org/10.1007/s00253-016-7832-x>
- Bernstein, B. E., & Hol, W. G. J. (1998). Crystal Structures of Substrates and Products Bound to the Phosphoglycerate Kinase Active Site Reveal the Catalytic Mechanism †. *Biochemistry*, 37(13), 4429–4436. <https://doi.org/10.1021/bi9724117>
- Brown, T. D. K., Jones-Mortimer, M. C., & Kornberg, H. L. (1977). The enzymatic interconversion of acetate and acetylcoenzyme. *J. Gen. Microbiol.*, 102, 327–336. <https://doi.org/10.1007/BF02660110>
- Buhr, A., & Erni, B. (1993). Membrane topology of the glucose transporter of *Escherichia coli*. *Journal of Biological Chemistry*, 268(16), 11599–11603.
- Chang, D. E., Shin, S., Rhee, J. S., & Pan, J. G. (1999). Acetate metabolism in a pta mutant of *Escherichia coli* W3110: Importance of maintaining acetyl coenzyme A flux for growth and survival. *Journal of Bacteriology*, 181(21), 6656–6663. <https://doi.org/10.1002/jctb.698>
- Choi, K. R., Jang, W. D., Yang, D., Cho, J. S., Park, D., & Lee, S. Y. (2019). Systems Metabolic Engineering Strategies: Integrating Systems and Synthetic Biology with Metabolic Engineering. *Trends in Biotechnology*, 37(8), 817–837. <https://doi.org/10.1016/j.tibtech.2019.01.003>
- Contiero, J., Beatty, C., Kumari, S., DeSanti, C. L., Strohl, W. R., & Wolfe, A. (2000). Effects of mutations in acetate metabolism on high-cell-density growth of *Escherichia coli*. *Journal of Industrial Microbiology and Biotechnology*, 24(6), 421–430. <https://doi.org/10.1038/sj.jim.7000014>
- Cotter, P. A., & Gunsalus, R. P. (1992). Contribution of the *fnr* and *arcA* gene products in coordinate regulation of cytochrome o and d oxidase (*cyoABCDE* and *cydAB*) genes in *Escherichia coli*. *FEMS Microbiology Letters*, 91(1), 31–36. [https://doi.org/10.1016/0378-1097\(92\)90558-6](https://doi.org/10.1016/0378-1097(92)90558-6)
- De Deken, R. H. (1966). The Crabtree effect: a regulatory system in yeast. *Journal of General Microbiology*, 44(2), 149–156. <https://doi.org/10.1099/00221287-44-2-149>
- De Mey, M., De Maeseneire, S., Soetaert, W., & Vandamme, E. (2007). Minimizing acetate formation in *E. coli* fermentations. *Journal of Industrial Microbiology and Biotechnology*, 34(11), 689–700. <https://doi.org/10.1007/s10295-007-0244-2>
- Dittrich, C. R., Bennett, G. N., & San, K. Y. (2005). Characterization of the acetate-producing pathways in *Escherichia*

- coli. *Biotechnology Progress*, 21(4), 1062–1067. <https://doi.org/10.1021/bp050073s>
- Doelte, H. W., Ewings, K. N., & Hollywood, N. W. (1982). Regulation of Glucose Metabolism in Bacterial Systems. *Microbial Reactions*, 1–35.
- Droste, P., Nöh, K., & Wiechert, W. (2013). Omix - A visualization tool for metabolic networks with highest usability and customizability in focus. *Chemie-Ingenieur-Technik*, 85(6), 849–862. <https://doi.org/10.1002/cite.201200234>
- Eiteman, M. A., & Altman, E. (2006). Overcoming acetate in *Escherichia coli* recombinant protein fermentations. *Trends in Biotechnology*, 24(11), 530–536. <https://doi.org/10.1016/j.tibtech.2006.09.001>
- El-Mansi, M. (2004). Flux to acetate and lactate excretions in industrial fermentations: Physiological and biochemical implications. *Journal of Industrial Microbiology and Biotechnology*, 31(7), 295–300. <https://doi.org/10.1007/s10295-004-0149-2>
- Enjalbert, B., Millard, P., Dinclaux, M., Portais, J. C., & Létisse, F. (2017). Acetate fluxes in *Escherichia coli* are determined by the thermodynamic control of the Pta-AckA pathway. *Scientific Reports*, 7(February), 1–11. <https://doi.org/10.1038/srep42135>
- Erdrich, P., Steuer, R., & Klamt, S. (2015). An algorithm for the reduction of genome-scale metabolic network models to meaningful core models. *BMC Systems Biology*, 1–12. <https://doi.org/10.1186/s12918-015-0191-x>
- Farmer, W. R., & Liao, J. C. (1997). Reduction of aerobic acetate production by *Escherichia coli*. *Applied and Environmental Microbiology*, 63(8), 3205–3210.
- Feist, A. M., Henry, C. S., Reed, J. L., Krummenacker, M., Joyce, A. R., Karp, P. D., Broadbelt, L. J., Hatzimanikatis, V., & Palsson, B. (2007). A genome-scale metabolic reconstruction for *Escherichia coli* K-12 MG1655 that accounts for 1260 ORFs and thermodynamic information. *Molecular Systems Biology*, 3(121), 1–18. <https://doi.org/10.1038/msb4100155>
- Hoehler, T. M., & Jørgensen, B. B. (2013). Microbial life under extreme energy limitation. *Nature Reviews Microbiology*, 11(2), 83–94. <https://doi.org/10.1038/nrmicro2939>
- Holms, H. (1996). Flux analysis and control of the central metabolic pathways in *Escherichia coli*. *FEMS Microbiology Reviews*, 19(2), 85–116. [https://doi.org/10.1016/S0168-6445\(96\)00026-5](https://doi.org/10.1016/S0168-6445(96)00026-5)
- Jonckheere, A. I., Smeitink, J. A. M., & Rodenburg, R. J. T. (2012). Mitochondrial ATP synthase: Architecture, function and pathology. *Journal of Inherited Metabolic Disease*, 35(2), 211–225. <https://doi.org/10.1007/s10545-011-9382-9>
- Kargi, F. (2009). Re-interpretation of the logistic equation for batch microbial growth in relation to Monod kinetics. *Letters in Applied Microbiology*, 48(4), 398–401. <https://doi.org/10.1111/j.1472-765X.2008.02537.x>
- Kim, B. S., Lee, S. C., Lee, S. Y., Chang, Y. K., & Chang, H. N. (2004). High cell density fed-batch cultivation of *Escherichia coli* using exponential feeding combined with pH-stat. *Bioprocess and Biosystems Engineering*, 26(3), 147–150. <https://doi.org/10.1007/s00449-003-0347-8>
- Lecina, M. (2007). *Anàlisi d'alternatives per a un bioprocés de producció d'una vacuna animal*.
- Lee, J. W., Goel, A., Ataai, M. M., & Domach, M. M. (2002). Flux Regulation Patterns and Energy Audit of *E. coli* B/r and K-12. *Journal of Microbiology and Biotechnology*, 12(2), 258–267.
- Lee, S. Y. (1996). High cell-density culture of *Escherichia coli*. *Trends in Biotechnology*, 14(3), 98–105. [https://doi.org/10.1016/0167-7799\(96\)80930-9](https://doi.org/10.1016/0167-7799(96)80930-9)
- Lever, M. A., Rogers, K. L., Lloyd, K. G., Overmann, J., Schink, B., Thauer, R. K., Hoehler, T. M., & Jørgensen, B. B. (2015). Life under extreme energy limitation: a synthesis of laboratory- and field-based investigations. *FEMS Microbiology Reviews*, 39(5), 688–728. <https://doi.org/10.1093/femsre/fuv020>
- Luli, G. W., & Strohl, W. R. (1990). Comparison of growth, acetate production, and acetate inhibition of *Escherichia coli* strains in batch and fed-batch fermentations. *Applied and Environmental Microbiology*, 56(4), 1004–1011.
- Meyer, H.-P., Kuhn, H.-J., Brown, S. W., & Fiechter, A. (1984). Production of human leukocyte interferon by *Escherichia coli*. In *Proceedings of the Third European Congress on Biotechnology*, 1., 499–505.
- Mueller, H., & Schmale, U. (2004). Chap 3. Product description. In *BlueinOne Cell: operating manual* (pp. 6–9).

- Noronha, S. B., Yeh, H. J. C., Spande, T. F., & Shiloach, J. (2000). Investigation of the TCA cycle and the glyoxylate shunt in *Escherichia coli* BL21 and JM109 using ¹³C-NMR/MS. *Biotechnology and Bioengineering*, 68(3), 316–327. [https://doi.org/10.1002/\(SICI\)1097-0290\(20000505\)68:3<316::AID-BIT10>3.0.CO;2-2](https://doi.org/10.1002/(SICI)1097-0290(20000505)68:3<316::AID-BIT10>3.0.CO;2-2)
- Postma, P. W., Lengeler, J. W., & Jacobson, G. R. (1993). Phosphoenolpyruvate: Carbohydrate phosphotransferase systems of bacteria. *Microbiological Reviews*, 57(3), 543–594.
- Potter, M., Newport, E., & Morten, K. J. (2016). The Warburg effect: 80 years on. *Biochemical Society Transactions*, 44(5), 1499–1505. <https://doi.org/10.1042/BST20160094>
- Reynard, A., Hass, L. F., Jacobsen, D. D., & Boyer, P. (1961). The correlation of reaction kinetics and substrate binding with the mechanism of pyruvate kinase. *The Journal of Biological Chemistry*, 236.
- Riesenberger, D., Schulz, V., Knorre, W. A., Pohl, H. D., Korz, D., Sanders, E. A., Roß, A., & Deckwer, W. D. (1991). High cell density cultivation of *Escherichia coli* at controlled specific growth rate. *Journal of Biotechnology*, 20(1), 17–27. [https://doi.org/10.1016/0168-1656\(91\)90032-Q](https://doi.org/10.1016/0168-1656(91)90032-Q)
- Rinas, U., Kracke-Helm, H. A., & Schügerl, K. (1989). Glucose as a substrate in recombinant strain fermentation technology - By-product formation, degradation and intracellular accumulation of recombinant protein. *Applied Microbiology and Biotechnology*, 31(2), 163–167. <https://doi.org/10.1007/BF00262456>
- Rocha, I., Maia, P., Evangelista, P., Vilaça, P., Soares, S., P Pinto, J., Nielsen, J., R patil, K., C ferreira, E., & Rocha, Mi. (2010). *OptFlux: an open-source software platform for*.
- Saltveit, M. E. (2016). Respiratory metabolism. In *Postharvest Ripening Physiology of Crops* (Issue 1). Elsevier Inc. <https://doi.org/10.2307/1536588>
- Sanfeliu Sabater, A. (1995). *Producció d'anitcossos monoclonals mitjançant el cultiu invitro d'hibridomes en bioreactors: Anàlisi de la fisiologia i metabolisme cel·lulars*.
- Shah, A. R., Singhal, M., Klicker, K. R., Stephan, E. G., Wiley, H. S., & Waters, K. M. (2007). Enabling high-throughput data management for systems biology: The Bioinformatics Resource Manager. *Bioinformatics*, 23(7), 906–909. <https://doi.org/10.1093/bioinformatics/btm031>
- Shiloah, J., & Rinas, U. (2009). Chapter 18 Glucose and acetate metabolism in *E.coli* - SystemLevel analysis and Biotechnological Applicatoin in Protein Production Processes. In *Systems biology and biotechnology of Escherichia coli* (pp. 377–399). <https://doi.org/10.1007/978-1-4020-9394-4>
- Skarstedt, M. T., & Silverstein, E. (1976). *Escherichia coli* acetate kinase mechanism studied by net initial rate, equilibrium, and independent isotopic exchange kinetics. *Journal of Biological Chemistry*, 251(21), 6775–6783.
- Stouthamer, A. H. (1973). A theoretical study on the amount of ATP required for synthesis of microbial cell material. *Antonie van Leeuwenhoek*, 39(1), 545–565. <https://doi.org/10.1007/BF02578899>
- Thierie, J. G. E., & Penninckx, M. (2010). *Crabtree Effect. March*. <https://doi.org/10.1002/9780470054581.eib243>
- Tomar, A., Eiteman, M. A., & Altman, E. (2003). The effect of acetate pathway mutations on the production of pyruvate in *Escherichia coli*. *Applied Microbiology and Biotechnology*, 62(1), 76–82. <https://doi.org/10.1007/s00253-003-1234-6>
- Valero, F., & López-Santín, J. (2017). Online Analysis for Industrial Bioprocesses. In *Current Developments in Biotechnology and Bioengineering* (pp. 649–678). Elsevier. <https://doi.org/10.1016/B978-0-444-63663-8.00022-7>
- van Bodegom, P. (2007). Microbial Maintenance: A Critical Review on Its Quantification. *Microbial Ecology*, 53(4), 513–523. <https://doi.org/10.1007/s00248-006-9049-5>
- Veeravalli, K., Schindler, T., Dong, E., Yamada, M., Hamilton, R., & Laird, M. W. (2018). Strain engineering to reduce acetate accumulation during microaerobic growth conditions in *Escherichia coli*. *Biotechnology Progress*, 34(2), 303–314. <https://doi.org/10.1002/btpr.2592>
- Vemuri, G. ., Eiteman, M. ., & Altman, E. (2006). Increased recombinant protein production in *Escherichia coli* strains with overexpressed water-forming NADH oxidase and a deleted ArcA regulatory protein. *Biotechnology and Bioengineering*, 94(3), 538–542. <https://doi.org/10.1002/bit.20853>
- Vemuri, G. N., Eiteman, M. A., McEwen, J. E., Olsson, L., & Nielsen, J. (2007). Increasing NADH oxidation reduces overflow metabolism in *Saccharomyces cerevisiae*. *Proceedings of the National Academy of Sciences of the*

- United States of America, 104(7), 2402–2407. <https://doi.org/10.1073/pnas.0607469104>
- Wiechert, W., Möllney, M., Petersen, S., & De Graaf, A. A. (2001). A universal framework for ¹³C metabolic flux analysis. *Metabolic Engineering*, 3(3), 265–283. <https://doi.org/10.1006/mben.2001.0188>
- Ying Lin, H., & Neubauer, P. (2000). Influence of controlled glucose oscillations on a fed-batch process of recombinant *Escherichia coli*. *Journal of Biotechnology*, 79(1), 27–37. [https://doi.org/10.1016/S0168-1656\(00\)00217-0](https://doi.org/10.1016/S0168-1656(00)00217-0)
- Zeng, H., & Yang, A. (2019). Modelling overflow metabolism in *Escherichia coli* with flux balance analysis incorporating differential proteomic efficiencies of energy pathways. *BMC Systems Biology*, 13(1), 1–18. <https://doi.org/10.1186/s12918-018-0677-4>

4. Physiology and metabolism of *Saccharomyces cerevisiae*

4.1 Nomenclature

DCW: dry cell weight ($\text{g}\cdot\text{L}^{-1}$)

OUR: Oxygen Uptake Rate ($\text{mM}\cdot\text{h}^{-1}$)

CER: Carbon Dioxide Evolution Rate ($\text{mM}\cdot\text{h}^{-1}$)

X_v : biomass concentration ($\text{gDCW}\cdot\text{L}^{-1}$)

q_m : specific consumption/production rate of metabolite m ($\text{mmol}\cdot\text{gDCW}^{-1}\cdot\text{h}^{-1}$)

$q_{s, \text{total}}$: total specific glucose consumption rate ($\text{mmol}\cdot\text{gDCW}^{-1}\cdot\text{h}^{-1}$)

$q_{s, \text{ethanol}}$: specific glucose consumption rate directed towards ethanol production ($\text{mmol}\cdot\text{gDCW}^{-1}\cdot\text{h}^{-1}$)

$q_{s, \text{glycerol}}$: specific glucose consumption rate directed towards ethanol production ($\text{mmol}\cdot\text{gDCW}^{-1}\cdot\text{h}^{-1}$)

$q_{s, \text{maintenance}}$: specific glucose consumption rate directed towards cell maintenance ($\text{mmol}\cdot\text{gDCW}^{-1}\cdot\text{h}^{-1}$)

$q_{s, \text{biomass}}$: specific glucose consumption rate directed towards biomass formation ($\text{mmol}\cdot\text{gDCW}^{-1}\cdot\text{h}^{-1}$)

t: time (h)

F: volumetric flow rate (liquids) ($\text{L}\cdot\text{min}^{-1}$)

V: bioreactor operational volume (L)

D: dilution rate (h^{-1})

C_j : concentration of metabolite j ($\text{g}\cdot\text{L}^{-1}$)

$C_{\text{outlet}, m}$: concentration of metabolite m in the outlet flow either gas or liquid phase ($\text{g}\cdot\text{L}^{-1}$)

$C_{\text{inlet}, m}$: concentration of metabolite m in the inlet flow either gas or liquid phase ($\text{g}\cdot\text{L}^{-1}$)

μ : specific growth rate (h^{-1})

μ_{max} : maximum specific growth rate (h^{-1})

K_s : affinity parameter of Monod equation ($\text{g}\cdot\text{L}^{-1}$)

$Y_{a/b}$: yield of A regarding B ($\text{g}_a\cdot\text{g}_b^{-1}$)

TCA: tricarboxylic acid (metabolic pathway)

FBA: flux balance analysis

OP: oxidative phosphorylation (metabolic pathway)

NADH: nicotinamide adenine dinucleotide reduced form

NAD: nicotinamide adenine dinucleotide oxidized form

ATP: adenosine triphosphate

ADP: adenosine diphosphate

4.2 Introduction

As it was mentioned in the overall introduction (**chapter 1**), the aim of the work presented in this thesis revolves around increasing the biomass production in bioprocesses based on the use of microorganisms, by means of performing high cell density cultures, in order to enhance the volumetric productivity of the process. More specifically, in the chapter that is represented thereafter, the expression platform used as model is the yeast *Saccharomyces cerevisiae* (*S. cerevisiae*).

S. cerevisiae is one of the most studied eukaryotic expression platform due to the fact that it was the first transfected eukaryotic organism with a recombinant plasmid (Mendoza-Vega et al., 1994). Therefore, several studies whose aim has been the enhancement of the protein production have been continuously published as one of the main themes regarding yeast publication. These studies are mainly based on the two topics:

1. the enhancement of the protein production by means of the genetic modification
2. the enhancement of the protein production by changing the bioreactor physiological conditions in order to increase the biomass production.

Regarding the improvement of the protein production via changing the bioreactor physiological conditions, two clear approaches has been performed towards this objective. The enhancement of the biomass production via the design fed-batch culture strategies or via avoiding the generation of the principal non-desired by-products during the culture.

In order to improve the fed-batch strategies, a new biomass tracking algorithm has been develop using as a measured variable the cumulative oxygen consumption rate in order to perform the most fitted feeding profile depending on the in-line biomass concentration (Urnieszus et al., 2019). While, regarding the by-products elimination, a new technology was develop based on the use of vacuum technologies in order to avoid the growth rate inhibition due to high ethanol concentrations (Mota et al., 1984) (Kachrimanidou et al., 2020). As it will be presented in this work, all the biomass production strategies are inherently related to the central carbon metabolism owing to the feeding profiles are based on predicting the behaviour of the carbon metabolism.

Regarding the carbon metabolism, there are several publications regarding how glucose is metabolized by *S. cerevisiae* which highlight in the ethanol production, which is a growth inhibitory partially-oxidized by-product (Kubota et al., 2004). This metabolic behaviour, widely

well-known as Crabtree effect, takes place when *S. cerevisiae* grows on excess of glucose-based media, or other highly assimilable carbon sources (fructose), in aerobically conditions (De Deken, 1966) (Verduyn et al., 1990). Furthermore, it has been widely described that the ethanol formation is related to several problematics related to growth inhibition and to the modification of cell metabolism and macromolecular biosynthesis (Hu et al., 2007) (Stanley et al., 2010).

In order to reduce the production of ethanol, the most suited option that until now has been changing the way in which *S. cerevisiae* interacts with the culture media conditions, by means of fed-batch strategies. In order to fix a specific metabolic behaviour, these strategies are based on limiting the growth rate (Mendoza-Vega et al., 1994) or limiting the ratio between the oxygen consumption and the carbon dioxide produced (respiratory quotient) fed-batch strategies (Aiba et al., 1976).

On this basis, the aim of this chapter is to understand how *S. cerevisiae* interacts with its environmental conditions in order to reduce ethanol formation and increase the conversion of the carbon source to biomass. For this purpose, and also in regard with the latest advances in high throughput data methodologies that they were described in the introduction (**chapter 1**), a genomic-scale metabolic model will be used in order to perform a direct correlation between the metabolic flux distribution and the environmental conditions.

4.3 Results (I) - Analysis and modeling the carbon metabolism of *S. cerevisiae*: glucose /ethanol metabolism and Crabtree Effect in batch cultures

4.3.1 Experiment in batch culture with *S. cerevisiae*

The core of this section is to understand the metabolism of *S. cerevisiae* through the analysis and modelling of a controlled environment. In order to assure that the controlled conditions are obtained, a bioreactor was used as a containment culture system owing to all the physiological parameter were controlled to assure an optimal growth rate (as shown in section 4.9.5).

The ethanol producer reference strain was the *S. cerevisiae* *wildtype* and it was cultured in a bioreactor with a defined medium whose initial glucose concentration was $100 \text{ g}\cdot\text{L}^{-1}$ (as shown in the section 4.9.3 of Media definition.). As this experiment will be used to study the metabolism, and to ensure that there will be enough data points within the exponential, the glucose media concentration used was higher than the usual ones (a base media usually has $20 \text{ g}\cdot\text{L}^{-1}$).

As shown in the **graph A of the Figure 4-1** and in **Table 4-1**, when *S. cerevisiae* was cultured in glucose-based media, it had a specific growth rate of $0,405 \text{ h}^{-1}$ and consumed $100 \text{ g}\cdot\text{L}^{-1}$ of glucose in 9,5 h, achieving a maximum cell concentration of $5,35 \text{ gDCW}\cdot\text{L}^{-1}$ and producing mainly $36,48 \text{ g}\cdot\text{L}^{-1}$ of ethanol and $3,24 \text{ g}\cdot\text{L}^{-1}$ of glycerol. Moreover, and regarding how *S. cerevisiae* allocates glucose, for each gram of consumed glucose $0,05 \text{ gDCW}$ of biomass was generated, and $0,39 \text{ g}$ of ethanol and $0,03 \text{ g}$ of glycerol were produced. This is a widely known behaviour described as the Crabtree effect regarding ethanol production when glucose is used as a carbon source in aerobic conditions (De Deken, 1966).

Moreover, using the trend of glucose, ethanol and glycerol over time in relation with the biomass profile, the specific rates were calculated (methodology calculation is described in section 4.9.10). The specific consumption rate of glucose had a value of $35,36 \text{ (mmol}\cdot\text{gDCW}^{-1}\cdot\text{h}^{-1})$, that leads the production of ethanol and glycerol whose specific production rate were $56,4$ and $2,56 \text{ (mmol}\cdot\text{gDCW}^{-1}\cdot\text{h}^{-1})$ respectively, and also a biomass rate generation of $0,405 \text{ (gDCW}\cdot\text{gDCW}^{-1}\cdot\text{h}^{-1})$. On the other side, the specific consumption rate of oxygen and the specific production carbon dioxide were calculated using the variables of carbon exchange rate (CER) and oxygen uptake rate (OUR), shown in **graph B of Figure 4-1** (the OUR and CER calculations are described in section 4.9.9 Oxygen uptake rate (OUR) and Carbon exchange rate (CER)). The specific production rate of carbon dioxide had a value of $73,67 \text{ mmol}\cdot\text{gDCW}^{-1}\cdot\text{h}^{-1}$, while the specific consumption rate of oxygen had a value of $19,36 \text{ mmol}\cdot\text{gDCW}^{-1}\cdot\text{h}^{-1}$.

It is important to point out that the ratio between CER and OUR, also known as respiratory quotient (RQ), had an expected value higher than one (3,8). In general, when *S. cerevisiae* grows using glucose as a carbon source, it generates ethanol in aerobic conditions, and the RQ has a value higher than one (Hagman & Piškur, 2015). The ethanol production in aerobic conditions is characterized by an unbalance in the cytoplasmic redox potential that leads to a specific correlation between the specific rate of carbon dioxide and oxygen. As a result, the carbon source was wasted because it was not fully converted to biomass, CO₂ and H₂O.

Therefore, in order to understand the relation between the unbalance in cytoplasmic redox potential and ethanol production when glucose was used as a carbon source, the study of the intracellular fluxes distribution will be presented in the following section using a genomic- scale metabolic model.

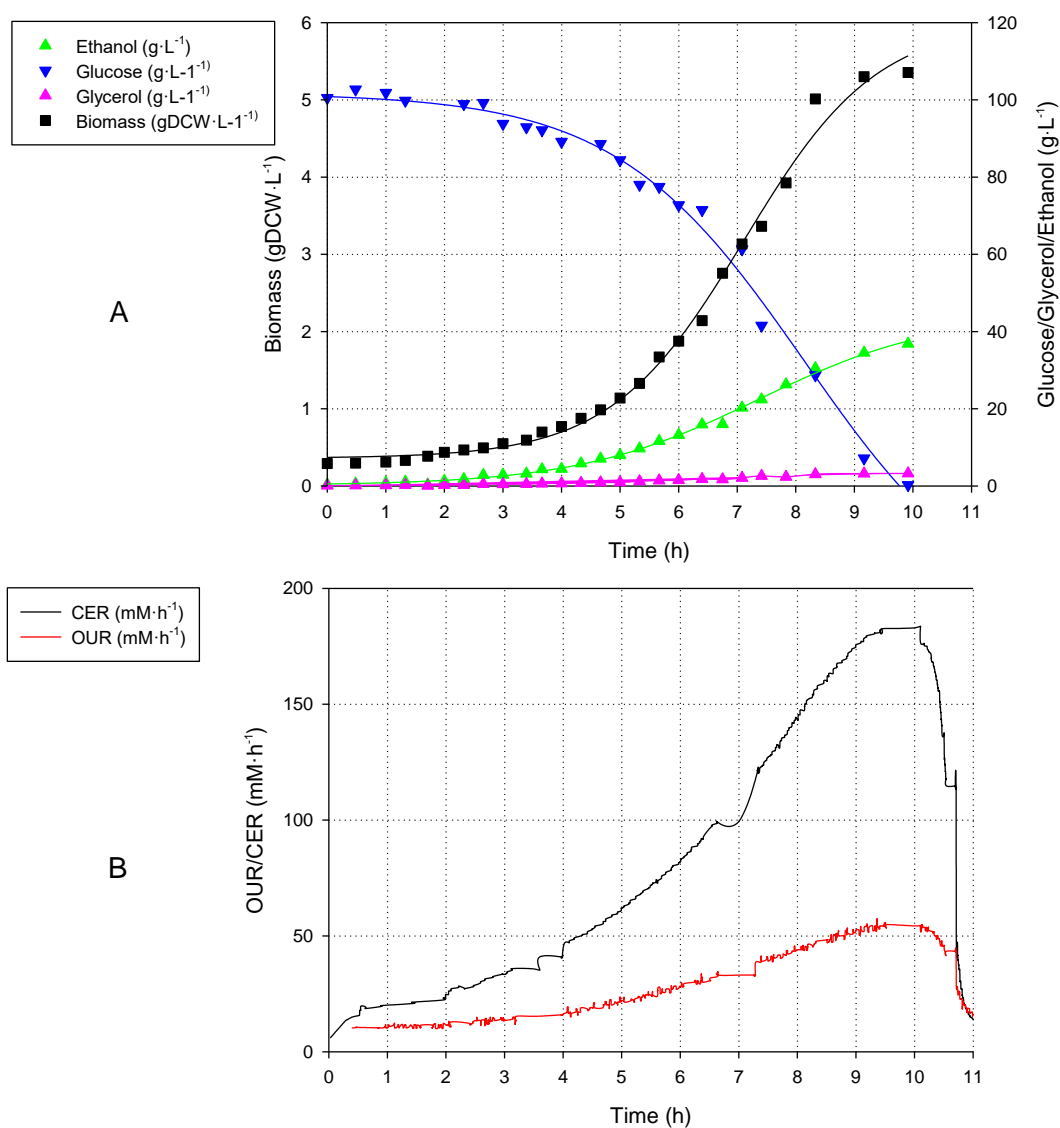


Figure 4-1 Profile of A) off-line variables such as Biomass (■), glucose (▼), ethanol (▲), glycerol(▲) and B) on-line variables such as C.E.R (—), O.U.R (—) for pH-controlled batch culture.

Table 4-1 Main metabolic parameters for *S. cerevisiae* in controlled culture.

Achieved Biomass (gDCW·L ⁻¹)	5,35
Ethanol production (g·L ⁻¹)	36,48
Glycerol production	3,24
Y bio/gluc(gDCW·g ⁻¹)	0,05
Y et/gluc (g·g ⁻¹)	0,39
Y glyc/gluc (g·g ⁻¹)	0,03
q _{glucose} (mmol · gDCW ⁻¹ ·h ⁻¹)	35,16
q _{ethanol} (mmol · gDCW ⁻¹ ·h ⁻¹)	56,4
q _{glycerol} (mmol · gDCW ⁻¹ ·h ⁻¹)	2,95

q_{O_2} (mmol · gDCW ⁻¹ ·h ⁻¹)	19,36
q_{CO_2} (mmol · gDCW ⁻¹ ·h ⁻¹)	73,67
μ (h ⁻¹)	0,405

4.3.2 Study of *S. cerevisiae* carbon metabolism by means of Flux Balance Analysis

As it was mentioned before, a genomic-scale metabolic model will be used in order to describe how *S. cerevisiae* transforms mainly glucose to ethanol and precursors for biomass synthesis, while getting the required energy for growing at optimal growth rate. It is important to remark that the model used was a reduction from the genomic-scale metabolic model. The description of used model is explained in section 4.9.12.

For metabolic flux calculation, the model was constrained using the specific rates of the corresponding measured metabolites that are shown in **Table 4-2**. This data included the biomass formation. As the model contains some degrees of freedom, the optimization was performed by means of the FBA protocol described in section 4.9.13, whose objective function is focused to maximize was the generation of ATP through the cytoplasmic hydrolysis of the ATP to ADP.

Table 4-2 Specific rates limits used as constraints for Flux Balance Analysis in *S. cerevisiae*.

	q (mmol · gDCW ⁻¹ ·h ⁻¹)
Oxygen	-18,000 ± 1,273
Ammonium	-2,260 ± 0,160
Glycerol	3,340 ± 0,236
Glucose	-33,891 ± 2,396
Ethanol	53,591 ± 3,789
Carbon Dioxide	73,388 ± 5,189
Biomass	0,404 ± 0,003

The intracellular fluxes were calculated and using the visualization software OMIX (Droste et al., 2013) is presented. In this figure, the metabolic relation between glucose and ethanol, as well as the core metabolism of *S. cerevisiae* is displayed.

Firstly, glucose is transported by facilitated diffusion through membrane into the cytoplasm (Lagunas, 1993)(Walker, 2009). In this case, the flux obtained is 33,89 mmol·gDCW⁻¹·h⁻¹. Then, it is phosphorylated in order to get released glucose-6-phosphate via two proteins (the iso-hexokinases encoded by HXK1 and HXK2 and a glucokinase encoded by GLK1) (Randez-Gil et al.,

1998). The generation of glucose-6-phosphate has a flux of $33,89 \text{ mmol-gDCW}^{-1}\cdot\text{h}^{-1}$, and it is directed into two different routes. 97,6% to the glycolytic pathway through conversion to fructose-6-phosphate via the phosphoglucose isomerase reaction and 2,4 % $\text{mmol-gDCW}^{-1}\cdot\text{h}^{-1}$ directed towards the formation of biosynthesis precursors, specifically, 57,5% towards the formation of plasmatic membrane compounds, such as glucans (Manners et al., 1973). The rest (42,5 %) is directed towards the formation of mainly nucleotides via the oxidative branch of the pentose-phosphate pathway. Thereupon, the 95 % of flux directed to glycolytic pathway ($33,09 \text{ mmol-gDCW}^{-1}\cdot\text{h}^{-1}$) reacts until glyceraldehyde-3 phosphate, owing to the formation of $3,74 \text{ mmol-gDCW}^{-1}\cdot\text{h}^{-1}$ of glycerol. Then, glyceraldehyde-3 phosphate is metabolized until pyruvate, where only the 15% of the produced pyruvate can be transported through the mitochondrial membrane, while the rest (85%) is decarboxylated to acetaldehyde via pyruvate decarboxylase and, then, is reduced to ethanol via alcohol dehydrogenase. The residual 1,4 % of pyruvate was converted to biomass precursors, mainly amino acids precursors or amino-donor molecules.

A key aspect of the *S. cerevisiae* metabolism, which is important to point out, is that either the production of ethanol or glycerol are related to the fact that not all the NADH generated via glycolytic pathway can be oxidized in the mitochondria via its introduction in the organelle using the malate-aspartate shuttle. Therefore, an unbalance metabolism related to NADH regeneration appears. Consequently, in order to balance the NADH, ethanol and glycerol were produced to reduce all the NADH generated in glycolysis due to the high glycolytic fluxes. Only 10 % of the NADH produced by glycolytic pathway can be oxidized via malate-aspartate shuttle, while the rest (90%) has to be principally oxidized via reduction of acetaldehyde to ethanol (Maconi et al., 1988) or the via reduction of dihydroxyacetone phosphate to glycerol 3-phosphate (Cronwright et al., 2002). It is important to remark that glycerol production was caused by an unbalance in the glycerol-3-phosphate provoked by the reduction of the dihydroxyacetone phosphate in order to balance the cytoplasmic NADH. As a result, in order to solve the unbalance of glycerol -3-phosphate, it was dephosphorylated via glycerol kinase producing glycerol.

On this basis, it can be stated that the main metabolic feature responsible for this metabolic behaviour (the production of fermentative by-products while growing on glucose-based media in aerobic conditions) might be related to an interaction between extracellular glucose and gene expression. This interaction tackles the repression or induction of determined genes or pathway depending on glucose extracellular conditions, for instance the repression of the respiratory metabolism or the over expression of glucose transports (Rolland et al., 2002). As a result, leading *S. cerevisiae* to a metabolic state where the majority of the NADH produced by glycolytic

pathway is oxidized via ethanol or glycerol pathway instead of being transported via shuttle-based mechanisms from the cytoplasm to the mitochondria. Therefore, producing ethanol and glycerol.

Regarding the biomass formation, the main precursors are generated from ribulose-5P (derivation of 1 % of glucose carbon-mol uptake rate); glucose-6-phosphate (derivation of 1,36 % of glucose carbon-mol uptake rate); pyruvate (derivation of 1,31 % of glucose carbon-mol uptake rate) and oxoglutarate (derivation of 1,02 % of glucose carbon-mol uptake rate).

4.3.3 Study of *S. cerevisiae* energy metabolism by means Flux Balance Analysis

This study was carried out using the data obtained in the previous section where the carbon metabolism was analysed. Moreover, an arrangement of the principal reactions in relation with the ATP metabolism were required in order to have a global view. The ATP production was separated in two groups: OP and substrate level phosphorylation. In this study the contribution of oxidative phosphorylation is related to ATP synthase, while to the substrate level phosphorylation is related to phosphoglycerate kinase, pyruvate kinase and Succinyl-CoA ligase.

While the ATP consumption was separated taking into account the following topics: cell maintenance, biomass formation, kinase reactions (catalysed by phosphofructokinase and hexokinase) and other side reactions.

As shown in **graph A) of the Figure 4-3**, the main proportion of the ATP produced comes from two sources (Farmer & Liao, 1997). The first source of ATP comes from ATP synthase, which is a protein involved in the oxidative phosphorylation in the mitochondria (OP) (Jonckheere et al., 2012). The second source of ATP comes at the substrate level phosphorylation, which is a reaction that takes part in glycolytic pathway in the cytoplasm.

Usually, in aerobic conditions and in compartmentalized cells (eukaryotic organisms), OP is described as the main source of ATP generation, based on the formation of an electrochemical proton gradient across the mitochondrial inner membrane. It is produced by an electron transport through the several proteins involved in OP mechanism, that is used by ATP synthase (complex V) to produce ATP via oxidative phosphorylation (Chaban et al., 2014). In the case of *S. cerevisiae*, the ATP produced by OP (32% of the total produced) has a lesser impact in ATP proportion than the substrate level phosphorylation (64% of the total produced) caused by the combination of a high flux through the glycolytic pathway and a low pyruvate transport to the mitochondria due to the ethanol production. Lastly, the rest of the ATP produced (4%) came from a mitochondrial ligase, (Succinyl-CoA ligase).

Regarding substrate level phosphorylation, the generation of ATP is based on the use of two specific group of proteins:

- The first one is related to the kinase group (pyruvate kinase and phosphoglycerate kinase), that catalyse the transfer of phosphate groups from high energy phosphate-donating molecules to specific substrates, specifically, from phosphoenolpyruvate to

ADP and from 1,3-bisphosphoglycerate to ADP (Hess & Sossinka, 1974)(Watson et al., 1982).

- The second one is based on a mitochondrial ligase, specifically Succinyl-CoA ligase.

On this basis, the difference in production regarding all the ATP sources was caused by a limitation regarding the transport of the NADH from the cytoplasm to the mitochondria, consequently, the total mitochondria NADH flux is lower than what would be expected. In contrast, all the ATP produced by glycolytic pathway is fully available, without restrictions. As a result, the substrate level phosphorylation, which only depends on the flux from glycolytic pathway, is 2-fold the ATP synthase rate, which was restricted by mainly the ethanol growth inhibition at high concentrations owing to the use of the NADH required for its formation, instead of being transported to the mitochondria.

On the other side, **in graph B) of the Figure 4-3**, the proportion of ATP consumption showed an allocation of ATP mainly in cell maintenance, biomass generation and in the reactions catalysed by phosphofructokinase and hexokinase proteins.

Cell maintenance tackles all the cellular process whose function is not related to formation of new cell material. Up to the present, there have been several attempts trying to describe which cellular process are involved, for instance the regulation of the proton motive force, the degradation of macromolecules, keeping the osmolarity conditions and regulated shifts in metabolic pathways (van Bodegom, 2007)(Hoehler & Jørgensen, 2013; Lever et al., 2015; van Bodegom, 2007). In the case presented, ATP required for cell maintenance was high, consuming 47 % of the total ATP produced.

Regarding the reactions catalysed by kinases, the 35 % of the total ATP produced was consumed by the phosphofructokinase (17%) and the hexokinase (18%), which is expected taking into consideration the rate flux through the glycolytic pathway in comparison with TCA cycle. In addition, it is important to point out that the above-mentioned kinases catalysed the phosphorylation using the ATP of fructose-6-phosphate and glucose, respectively.

Finally, the last of the main consuming ATP reactions is the biomass formation, whose ATP consumption was 12 % of the ATP produced, although it has to be taken into account that the energy requirements for synthesis of biomass precursors are defined by the biomass equation.

There are two points related to the energy metabolism of *S. cerevisiae* growing on glucose-based media in aerobic conditions that has to be pointed out:

1. Only the 33% of the ATP produced came from the oxidative phosphorylation while the other 67 % came from the kinase-based reaction related to the glycolytic pathway (glycolysis).
2. In order to reach the optimal growth rate, the energetic requirements for cell maintenance (47 %) were higher than the destined ones to new cellular material (12 %).

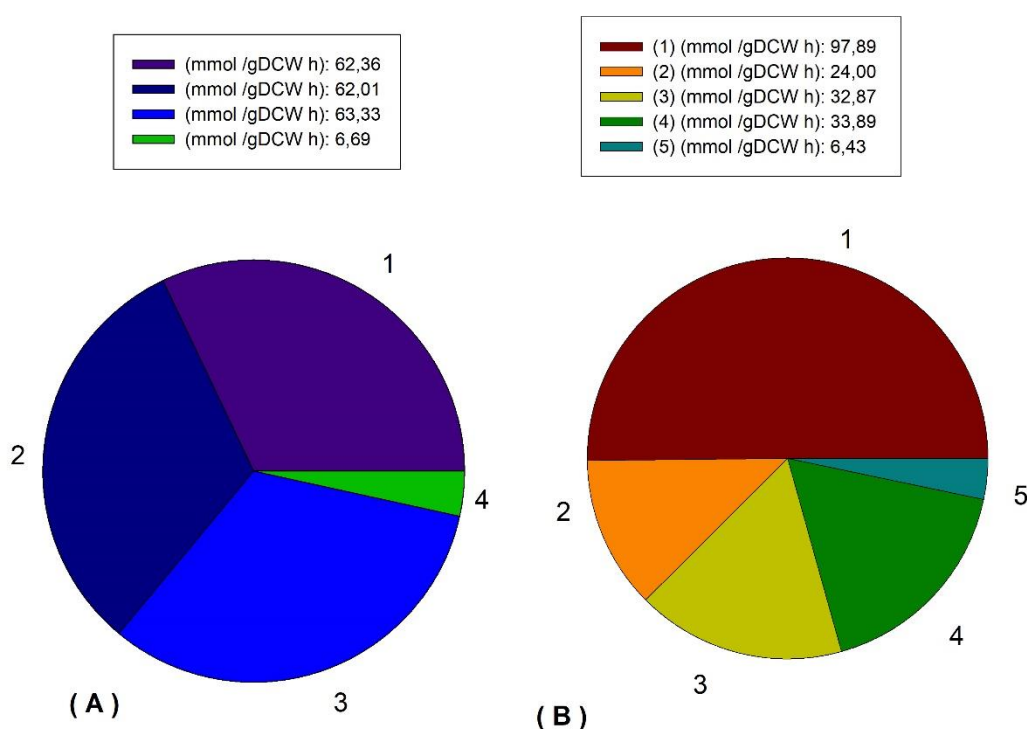


Figure 4-3 Distribution of ATP production and consumption in *S. cerevisiae*. In figure A, the ATP produced by *S. cerevisiae* is separated depending on its provenance (ATP synthase (1), Phosphoglycerate kinase (2), Pyruvate kinase (3), Succinyl-CoA ligase (4)). While in figure B, the ATP consumed is separated depending on its provenance (Cell maintenance (1), Biomass formation (2), Phosphofructokinase (3), Hexokinase (4) and other side reactions (5)).

To conclude, after the analysis of the carbon and energy metabolism, the main metabolic issue of *S. cerevisiae* has been found to be related to the unbalance in the cytoplasmic redox potential. The unbalance is caused by the restrictions in the regeneration of the reduced-form of cofactor NADH and that is responsible of the big amount of ethanol generated in growth in aerobic conditions. This restriction could be caused by an interaction between extracellular glucose and gene expression. This interaction tackles the repression or induction of determined genes or pathway depending on glucose extracellular conditions (Rolland et al., 2002). As a result, leading *S. cerevisiae* to a metabolic state where mainly the NADH produced by glycolytic pathway is oxidized via fermentative by-products pathways instead of being transported via shuttle-based

mechanisms from the cytoplasm to the mitochondria. These fermentative by-products take part in two oxidative pathways: the formation of ethanol using acetaldehyde dehydrogenase and the formation of glycerol using glycerol-3-phosphate dehydrogenase.

In this section, the possible reasons behind the production of ethanol and small amounts of glycerol in aerobic conditions in *S. cerevisiae* have been described based on physiologic and metabolic studies. In order to further enrich the metabolic discussion, a similar approach than presented will be used based on using a low-ethanol yeast producer, *Pichia pastoris*, in order to understand why it is described as a low-ethanol producer yeast. The metabolism of this type of organism could deepen the discussion of why ethanol is produced by *S. cerevisiae*. Therefore, in the next section, a study of glucose metabolism of *P. pastoris* as a low-ethanol producer yeast model will be presented.

4.4 Results (II) - Analysis and modeling the carbon metabolism of *Pichia pastoris*: glucose metabolism in aerobic batch cultures.

4.4.1 Experiment in batch culture with *P. pastoris*

As it was mentioned in the last section, a new approach to understand ethanol production in *S. cerevisiae* will be studied focusing on why there are other described yeasts referenced as “low-ethanol” producer or “negative-Crabtree”. These are characterized for being lower ethanol producers or even zero producers, in comparison to *S. cerevisiae* when they are cultured on glucose-based media. The study also will be performed by means of the study of the central carbon metabolism. The negative-Crabtree effect yeast that was used as a reference was *P. pastoris*, widely used as a negative-Crabtree yeast reference (Hagman et al., 2014) (Hagman & Piškur, 2015).

The experimental setting used were the same as the ones used in *S. cerevisiae* cultures (as described in section 4.9.5). However, *P. pastoris* was cultured in a different medium whose initial glucose concentration was 20 g·L⁻¹ and its media composition is described in section 4.9.3.

As shown in **Figure 4-4**, when *P. pastoris* was cultured in glucose-based media, the specific growth rate had a value of 0,276 h⁻¹ and 20 g·L⁻¹ of glucose was consumed in 13 h in order to achieve a maximum cell concentration of 3,43 gDCW·L⁻¹ and producing 1,78 g·L⁻¹ of ethanol. As shown in **Table 4-3**, under those conditions, *P. pastoris* allocated the carbon source where for

each gram of consumed glucose 0,09 gDCW of biomass was generated and 0,16 g of ethanol was produced.

Thus, the specific rate of biomass and glucose were calculated by using the methodology described in the section 4.9.10. The specific consumption rate of glucose had a value of 8,25 mmol·gDCW⁻¹·h⁻¹ that lead to a generation of 0,276 gDCW·gDCW⁻¹·h⁻¹ of biomass and the production of 2,25 mmol·gDCW⁻¹·h⁻¹ of ethanol.

Moreover, the specific rates of oxygen consumption and carbon dioxide production were calculated by using Carbon Exchange Rate (CER) and Oxygen Uptake Rate (OUR), whose values are shown in **graph B) of Figure 4-4** in cooperation with the methodology described in section 4.9.9. As a result, the specific production rate of carbon dioxide had a value of 37,68 mmol·gDCW⁻¹·h⁻¹ and the specific consumption rate of oxygen had a value of 35,36 mmol·gDCW⁻¹·h⁻¹.

The ratio between both of them, also known as respiratory quotient, has a value of 1,06. In contrast with the RQ value observed when *S. cerevisiae* was cultured using glucose, which was 3-fold higher. It could indicate that *P. pastoris* might internalize almost all the cytoplasmatic NADH produced by glycolytic pathway due to the way that both handle the balance of the cytoplasmic NADH.

The rate difference between the production and generation of cytoplasmic NADH is responsible for the ethanol production. Just as it was mentioned in the previous section, where an unbalance in the oxidation of the NADH due to the restriction of the respiratory metabolism or the transport of the electrons from the glycolytic pathway to the mitochondria provoked the ethanol production in *S. cerevisiae*.

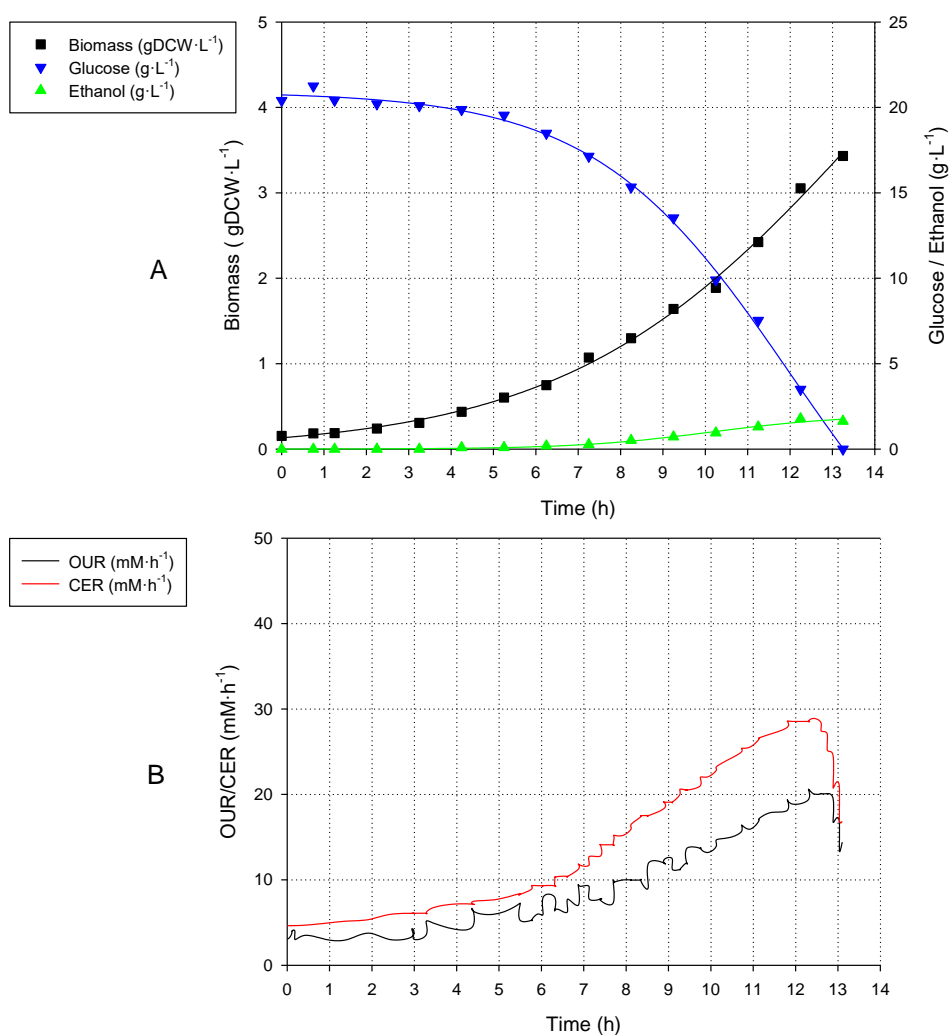


Figure 4-4 Profile of A) off-line variables such as Biomass (■), glucose (▼), ethanol (▲), and B) on-line variables such as C.E.R (—), O.U.R (—) for pH-controlled batch culture.

Table 4-3 Main parameters for *P. pastoris* in batch culture.

Biomass Achieved (gDCW·L ⁻¹)	3,43
Ethanol production (g·L ⁻¹)	1,78
$Y_{\text{bio/gluc}}$ (gDCW·g ⁻¹)	0,16
$Y_{\text{et/gluc}}$ (g·g ⁻¹)	0,09
q_{glucose} (mmol · gDCW ⁻¹ ·h ⁻¹)	8,25
q_{ethanol} (mmol · gDCW ⁻¹ ·h ⁻¹)	2,25
q_{glycerol} (mmol · gDCW ⁻¹ ·h ⁻¹)	0
q_{O_2} (mmol · gDCW ⁻¹ ·h ⁻¹)	35,36
q_{CO_2} (mmol · gDCW ⁻¹ ·h ⁻¹)	37,68
μ (h ⁻¹)	0,276

For a better understanding of the reason behind why *P. pastoris* produces less ethanol even though growing on glucose-based media than *S. cerevisiae*, a study of the intracellular fluxes by means of Flux Balance Analysis (FBA) will be presented in the following section.

4.4.2 Study of *P. pastoris* carbon metabolism by means of FBA

A genomic-scale metabolic model was used in order to analyse how *P. pastoris* cultured on glucose-based media transforms glucose to precursors for biomass synthesis while producing low concentrations of ethanol. The development and description of the model can be found in section 4.9.12. Moreover, it has to be mentioned that the model used was as the same one used in the study of the *S. cerevisiae* metabolism with a change in the biomass equation.

For metabolic flux calculation, the model was constrained using the input-output data of the corresponding metabolites that are shown in **Table 4-4**. As this data includes the biomass formation, the optimization of the model was performed by means of the FBA protocol described in 4.9.13, whose objective function to maximize was the cytoplasmic hydrolysis of the ATP to ADP.

Table 4-4 Specific rate limits used as a constraints for FBA in *P. pastoris*.

	q (mmol · gDCW ⁻¹ · h ⁻¹)
Oxygen	-35,402 ± 2,503
Ammonium	-1,536 ± 0,108
Glycerol	0,000 ± 0,000
Glucose	-8,480 ± 0,600
Ethanol	2,151 ± 0,152
Carbon Dioxide	37,864 ± 2,677
Biomass	0,274 ± 0,002

The intracellular fluxes are presented in **Figure 4-5**. In this figure, among others, the metabolic relation between glucose and ethanol is displayed.

Firstly, glucose is transported by facilitated diffusion through plasmatic membrane into the cytoplasm with a flux of 8,52 mmol·gDCW⁻¹·h⁻¹ (Lagunas, 1993) (Walker, 2009), and then is phosphorylated to glucose-6-phosphate via hexokinase-based reaction with a flux of 8,52 mmol·gDCW⁻¹·h⁻¹. The glucose-6-phosphate was directed into two different routes. 92,1% was

directed to the glycolytic pathway through conversion to fructose-6-phosphate, via the phosphoglucose isomerase reaction. 7,7 % $\text{mmol}\cdot\text{gDCW}^{-1}\cdot\text{h}^{-1}$ were directed towards the formation of biosynthesis precursors, specifically, 69 % towards the formation of plasmatic membrane compounds, such as glucans (Manners et al., 1973) and the rest, 31 %, towards the formation of mainly nucleotides via the oxidative branch of the pentose-phosphate pathway. Thereupon, the flux directed to glycolytic pathway ($7,85 \text{ mmol}\cdot\text{gDCW}^{-1}\cdot\text{h}^{-1}$) reacts until pyruvate, where the 77,1 % produced is transported from the cytoplasm to the mitochondrial through the mitochondrial membrane, while the 19,7 % is decarboxylated to acetaldehyde via pyruvate decarboxylase and, then is reduced to ethanol via alcohol dehydrogenase. The residual 3 % of pyruvate was converted to biomass precursors, mainly amino acids precursors or amino-donor molecules.

It is important to take into consideration that the production of a lower level concentration of ethanol and the absence of formation of glycerol are related to the fact that almost all the NADH generated via glycolytic pathway can be oxidized in mitochondria via malate-aspartate shuttle, although a slightly unbalance related to NADH appears. Consequently, in order to balance the NADH, ethanol is produced. Therefore, only 12 % of the NADH produced by glycolytic pathway is oxidized via reduction of acetaldehyde to ethanol (Maconi et al., 1988), while the rest (88 %) is principally oxidized in mitochondria, via malate-aspartate shuttle in order to transport the electron of the reduced form of NADH from cytoplasm to mitochondria.

This metabolic behaviour regarding the ethanol formation might be related to the flux of the glycolytic pathway. When the flux through the glycolytic pathway is low enough almost all the NADH produced can be transported to mitochondria via malate-aspartate shuttle, thus, only low amounts of ethanol might be produced. This is an expected behaviour because *P. pastoris* is described as a “respiratory” yeast whose main feature is a low or zero participation of both ethanol and glycerol pathways in the global carbon metabolism (Hagman & Piškur, 2015). In contrast with *S. cerevisiae*, *P. pastoris* only required low production of ethanol in comparison with the ethanol and glycerol required by *S. cerevisiae*. This trait might be caused by a restriction in the glucose transport that limits the uptake of glucose owing to *S. cerevisiae* glucose transporters enable a higher flux rate through the glycolytic pathways than *P. pastoris* (Mattanovich et al., 2009). As a consequence, the flux of NADH from the glycolytic pathway is lower and then, it can be almost fully oxidized via mitochondrial shuttle instead of via ethanol and glycerol production.

4.4.3 Study of *P. pastoris* energy metabolism by means of use of a metabolic model

As shown in **graph A) of the Figure 4-6**, the proportion of the ATP produced mainly came from two sources: OP and substrate level phosphorylation.

It is important to remember that as it was mentioned in the *S. cerevisiae* energy metabolism section (section 4.3.3), in aerobic conditions and in non-compartmentalized cells (just as *E. coli*), OP is described as the main production resource of ATP due to the high efficiency in the phosphorylation of ADP by using transmembrane proton motion force (Anraku & Gennis, 1987). However, in the case of *S. cerevisiae*, due to the restriction related to the NADH balance within the cytoplasm, the ATP production by OP (33% of the total produced) has less impact in ATP proportion as the substrate level phosphorylation (67% of the total produced). On the contrary, in this case, *P. pastoris* showed a contribution of the ATP synthetase that nearly reached more than 70% of the total ATP produced, the substrate level phosphorylation only presented a contribution of almost 21 % of the total produced and the last 7% was produced via mitochondrial succinyl-CoA ligase. This specific allocation, regarding the ATP contribution, is due to the combination of two metabolic features. The first one is related to the ATP flux obtained through the glycolytic pathway in comparison with the availability of the mitochondrial NADH, which contributes in the production of ATP via OP and the second one is related to a high electron transport capacity from the cytoplasm to mitochondria.

As it was previously mentioned, Regarding, the generation of ATP through substrate level phosphorylation is based on the use of two specific group of proteins: the kinase group and the mitochondrial ligase one (specifically Succinyl-CoA ligase). However, it is important to point out that in *P. pastoris* has not been reported specifically if this ligase is GTP or ATP dependent, therefore, it was considered ADP-dependent. Even if this consideration might prove to be wrong, it was described in several yeast the existence of a specific group of proteins which catalyse the phosphorylation of nucleotides via other higher-energy nucleotides called Nucleoside diphosphokinases (Parks & Aganwal, 1973). As a result, the assumption of considering succinyl-CoA ligase as an ADP-dependent one might be correct, due to Nucleoside diphosphokinases existence.

On this basis, the difference in production regarding all the ATP sources was caused because almost all electrons from NADH from the cytoplasm can be transported to the mitochondria. As a result, the expected flux in mitochondrial NADH might increase along with the ATP generation

via OP. While, all the ATP produced via substrate level phosphorylation is restricted by the low the flux through the glycolytic pathway. As a result, the ATP produced from the OP is 2-fold the ATP produced via substrate level phosphorylation.

On the other side, **in graph B) of the Figure 4-6** Error! Reference source not found., the proportion of ATP consumption showed an allocation of ATP mainly in cell maintenance, biomass generation and in the reactions catalysed by phosphofructokinase and hexokinase proteins.

As it has been explained in *S. cerevisiae* section, cell maintenance tackles all the cellular process whose function is not related to formation of new cell material. On this basis, in order to grant the optimal state for all the cellular process non-related to biomass synthesis, 82 % of the ATP produced was required.

Regarding the reactions catalysed by kinases, the 10,8 % of the total ATP produced was consumed equally either by the phosphofructokinase (5,2%) and the hexokinase (5,6%), which is expected taking into consideration the low value of flux through the glycolytic pathway.

Finally, the last one of the main consuming ATP reactions, the biomass formation whose ATP consumption was 4,6 % of the ATP produced, although it has to be taken into consideration that the energy requirements for synthesis of biomass precursors are defined by the biomass equation.

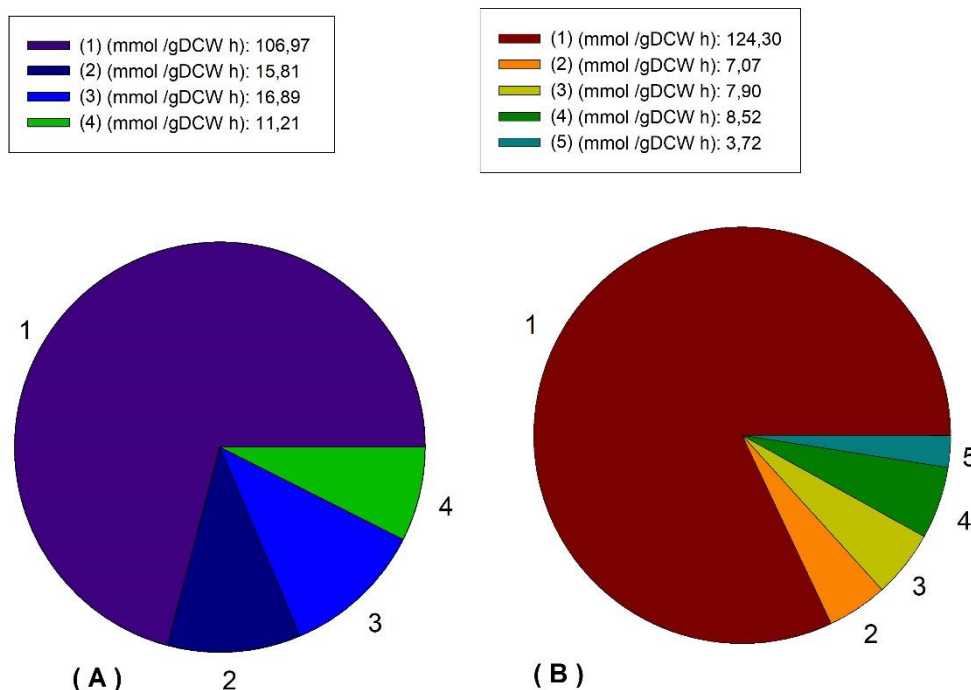


Figure 4-6 Distribution of ATP production and consumption in *P. pastoris*. In figure A, the ATP produced by *P. pastoris* is separated depending on its provenance (ATP synthase (1), Phosphoglycerate kinase (2), Pyruvate kinase (3), Succinyl-CoA ligase (4)). While in figure B, the ATP consumed is separated depending on its provenance (Cell maintenance (1), Biomass formation (2), Phosphofructokinase (3), Hexokinase (4) and other side reactions (5)).

In the final analysis, there are two points related to the energy metabolism of *P. pastoris* growing on glucose-based media in aerobic conditions that have to be pointed out:

1. The principal source of ATP was OP with a contribution of 71 % of the total ATP produced.
2. In order to reach the optimal growth rate, the energetic requirements for cell maintenance (82 %) were higher than the destined ones to new cellular material (4,6 %).

According to the data that have been shown up until now in reference to the ethanol metabolism, the ethanol production might be based on the contribution of two metabolic functions: the repression of the flux through the glycolytic pathway and the capacity to transport electrons from the cytoplasm to mitochondria. Moreover, both are related to how glucose interactions with the whole metabolism, promoting the repression or the induction of specific pathways. On this basis, a global comparative view for both metabolisms will be shown hereunder in order to shed light on ethanol production.

4.5 Results (III) - Metabolic comparison between *S. cerevisiae* and *P. pastoris* – carbon metabolism models.

Up until now, all the carbon metabolism referred to how *S. cerevisiae* and *P. pastoris* consumes glucose and, then, is converted to biomass precursors while producing different partially oxidized by-products such as ethanol and glycerol has been described independently. Although, the principal metabolic trait that is responsible for ethanol production in *S. cerevisiae*, also is present at a lower scale in *P. pastoris*.

To put in other way, the production of ethanol is related to the capacity of handling the balance of cytoplasmic NADH generated via glycolytic pathway in both *S. cerevisiae* and *P. pastoris*.

In order to begin with the study that will be presented hereafter, one assumption related to the metabolic model must be taken into consideration:

- The stoichiometric matrix is the same for both strains except its biomass equation. It has to be taken into consideration that each yeast has its own biomass equation, as described in section 4.9.12.

As shown in **Figure 4-7**, the comparison between *S. cerevisiae*'s fluxes and *P. pastoris*'s fluxes reveal interesting differences between them, the ones that are presented hereafter:

1. An increase of 3,96-fold of the flux through the glycolytic pathway.
2. An increase of 20-fold of the flux through the ethanol pathway.
3. The apparition of glycerol formation.
4. A decrease of nearly 50 % of the flux through the malate-aspartate shuttle.
5. A decrease of 37% of the flux through the TCA cycle flux.
6. A decrease of 35% of the flux through the pyruvate transport from the cytoplasm to mitochondria.

These differences might be explained taking into consideration the capacity for handling the balance of cytoplasmic NADH. This capacity is strictly related to mainly two aspects: the first one is related to the amount of the NADH produced via glycolytic pathway in the cytoplasm, and the second one, it is related to the metabolic mechanism on top of transporting the NADH electron from cytoplasm to mitochondria, therefore, performing the oxidation of the NADH to NAD^+ . The principal mechanism for the “electron transport” is based on the shuttle-based reaction mechanisms, such as the malate-aspartate shuttle, whose mechanism reaction

revolves around the reduction of oxaloacetate to malate in the cytoplasm and, then malate is transported via the antiport malate-oxoglutarate (Wills et al., 1984) (Easlon et al., 2008).

In the last years, several publications approaching the reason behind the ethanol production has been revolving around one topic, how glucose might have an effect on the gene expression that regulates the principal pathways behind cytosolic NADH. As a result, glucose might have dramatic effects on the regulation of carbon metabolism and on many other properties of yeast cells. These effects are based on glucose-repression or substrate-repression pathways which together are responsible for the downregulation of respiration, gluconeogenesis and the transport and catabolic capacity of sugars during growth on glucose (Rolland et al., 2002). Therefore, this work will be focusing on the downregulation of both the sugar transport and the respiration as a core building block in order to explain why the ethanol metabolism between *S. cerevisiae* and *P. pastoris* is so different.

First of all, the increase of 3,96-fold of the flux trough the glycolytic pathway in *S. cerevisiae* regarding to *P. pastoris* is related to a glucose-based regulation pathway on top of the overexpression of several glucose transports in order to maximize the glucose consumption. In *S. cerevisiae*, the glucose transport is controlled under the expression of the genes from the HXT-genes (HXT-gene family tackles 7 codifying genes from HXT1 to HXT7) (Rolland et al., 2002). These seven genes are responsible for the expression of seven glucose-transport proteins with different affinity for glucose. Moreover, all of them have its expression regulated via glucose-based regulation pathway, for instance, the repression under high glucose concentrations of the HXT2 and HXT4 genes which encode transporters with intermediate affinity via the Mig1 glucose-repression pathway (Ozcan & Johnston, 1995). In contrast, in *P. pastoris* only two of the seven HXT-gene are expressed, as a result the glucose consumption rate cannot be adapted to the availability of the external glucose. Moreover, the two expressed genes from the HXT family are the low-intermediate affinity for glucose (Prielhofer et al., 2015).

It has to take into consideration that coupled with the high affinity and the regulation pathway responsible for maximizing the consumption rate of glucose in *S. cerevisiae*, there is another factor as important as glucose consumption metabolic modulation, which is the capacity for changing the glycolytic fluxes depending on the glucose consumption rate. In *S. cerevisiae*, glucose causes a fast increase and transient overshoot in glycolytic intermediates. In addition, mutant studies have shown that increased levels of different metabolites trigger the induction of glycolytic genes (Boles et al., 1993). Therefore, the flux through the glycolytic pathway might be modulated in order to maximize the glucose consumption. On the other hand, in *P. pastoris*

it has been described that a change in the carbon source can produce a modulation in the expression of the glycolytic genes, for instance from glycerol to glucose (Prielhofer et al., 2015). Therefore, it would be hypothesized that a change in extracellular glucose concentration might have an effect on the *P. pastoris* glycolytic-gene expression, in a lower scale compared with *S. cerevisiae*. This assumption might be accepted if it is taken into consideration that *S. cerevisiae* carbon metabolism might be a high affinity glucose-conditions metabolism, while in *P. pastoris*, the carbon metabolism might be a low affinity one where glucose transport is limited.

It is important to point out that even if the increase in the glycolytic flux due to glucose-based gene regulation mechanisms, there is another metabolic feature that is also responsible for the 20-fold increase in the ethanol production regarding *S. cerevisiae* and *P. pastoris*. This is the regulation of the aerobic respiration under high glucose concentrations.

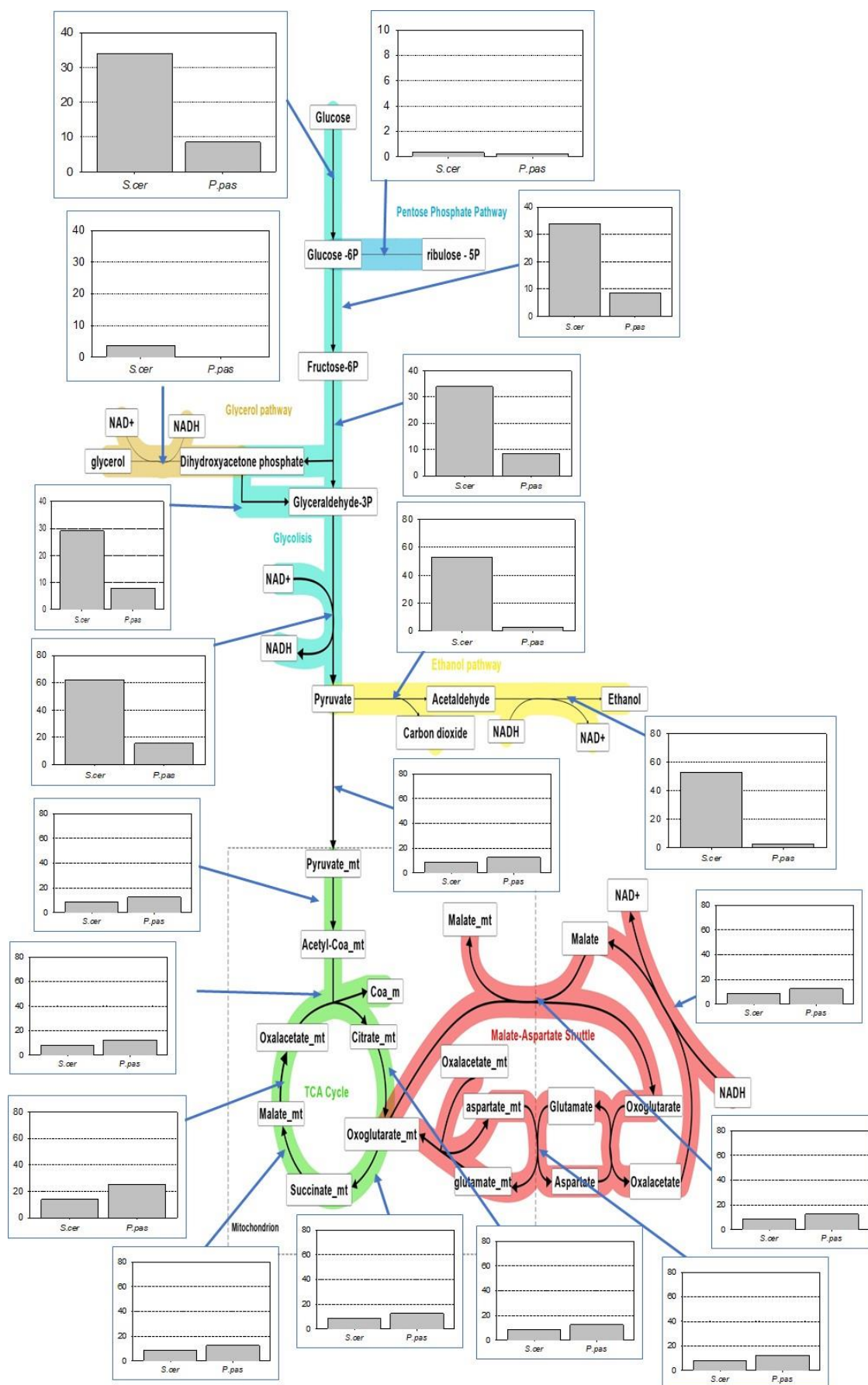
In *S. cerevisiae*, the respiration is repressed in excess of glucose conditions (Roberts & Hudson, 2006), thus respiration-associated functions such as oxidative phosphorylation, mitochondrial electron transport and ATP generation are induced upon glucose depletion (Dueñas-Sánchez et al., 2012). In contrast with *S. cerevisiae*, the aerobic metabolism of *P. pastoris* is not affected by high concentration of extracellular glucose. Moreover, it was also observed that the expression or repression of the gene involved in the aerobic respiratory was not affected when glucose was replaced by glycerol (Prielhofer et al., 2015).

Regarding the respiratory metabolism repression, it has to be mentioned that the bottom limit of the TCA has a lower flux values in *S. cerevisiae* compared with *P. pastoris*, owing to the repression of high glucose concentration. This trait might be related to the evolution of the yeasts, specifically, the apparition of *S. cerevisiae*. In this sense, a publication regarding the evolution of the yeast has stated that the origin of aerobic yeast (*P. pastoris*) is older than the aerobic-fermentative one (*S. cerevisiae*) (Hagman & Piškur, 2015). On this basis, it can be hypothesized that the upper limit in the TCA cycle, which is directly linked with the respiratory metabolism, has to be as maximum as the same value of the aerobic one in the case of aerobic-fermentative one, because one of the main differences between both is the aerobic metabolism repression. Therefore, a non-glucose repressed aerobic-fermentative yeast must have at least the same flux through the TCA than a glucose repressed one. Otherwise, when glucose is present, the repression of the TCA has to be lower than an aerobic yeast. Taking into consideration what has been described regarding the TCA cycle, the difference between the flux through the TCA cycle in *S. cerevisiae* and *P. pastoris* might be explained.

As a result, the interaction between the extracellular glucose conditions and the glucose transport, the glycolytic regulation and the interaction between glucose and aerobic metabolism, are present in a specific metabolism. This metabolism will present an overflow in the NADH production in the cytoplasm characterized also by a low transport of electron donor species from the cytoplasm to the mitochondria and, consequently, a high flux of partially-oxidized molecules, such as ethanol or glycerol. As the case of *S. cerevisiae*.

Although, it has to be kept in mind that a metabolism with these three specific traits might not be worse than one without them. This can be stated because if *S. cerevisiae* and *P. pastoris* are compared without taking into consideration how the glucose is converted to biomass or the value of carbon efficiency in regard with the metabolism, *S. cerevisiae* grows ($0,405\text{ h}^{-1}$) faster than *P. pastoris* ($0,276\text{ h}^{-1}$). Therefore, it could be stated that the ethanol production during aerobic conditions leads the metabolism to produce faster biomass building blocks (for instance, the increase in the ATP production rates due to the contribution of the fermentative pathway) and as a result, the biomass growth rate is increased.

Once in the carbon metabolism has been reached a feasible hypothesis for the ethanol and glycerol production, a global view of how this change in carbon metabolism affects the energy metabolism will be presented.

Figure 4-7 Comparison between FBA for *S. cerevisiae* and *P. pastoris*. All fluxes are expressed in $\text{mmol-gDCW}^{-1}\cdot\text{h}^{-1}$.

4.6 Results (IV) - Metabolic comparison between *S. cerevisiae* and *P. pastoris* – energy metabolism model

In order to compare the energy metabolism of *S. cerevisiae* and *P. pastoris* that will be presented hereafter, two assumptions related to the metabolic model must be taken into consideration:

- The relation that characterizes the oxidative phosphorylation, the P/O, has a constant value of 1,81 in both models.
- The energy requirements used for biosynthesis depended on the biomass equation, that is specific for each strain.

Regarding to the ATP produced, as shown in **Figure 4-8**, *S. cerevisiae* produce 24% more ATP than *P. pastoris*, 194,40 mmol·gDCW⁻¹·h⁻¹ and 151,73 mmol·gDCW⁻¹·h⁻¹ respectively. The increase in the ATP production might be related to the higher growth rate of *S. cerevisiae*. Moreover, there are several differences related to proportions in ATP produced and consumed (as shown in **Figure 4-9**) that have to be pointed out:

- The 81 % of the ATP produced by *S. cerevisiae* comes from the substrate level phosphorylation related to the glycolytic pathway, while in *P. pastoris* only the 21% comes from it. This difference is due to the fact that *S. cerevisiae* promotes the generation of high fluxes through glycolysis and the repression of the aerobic metabolism while growing on glucose, whereas *P. pastoris* do not. As a result, the ATP produced via aerobic metabolism based on TCA cycle shows the inverse ATP contribution, the 19 % of the ATP produced in *S. cerevisiae* comes from TCA, while in *P. pastoris* the ATP from TCA accounts around 79 % of the total ATP produced.
- The most relevant matter regarding ATP consumption is related to cell maintenance, *S. cerevisiae* have a lower cell maintenance than *P. pastoris* (97,84 compared with 124,3 mmol·gDCW⁻¹·h⁻¹) in spite of having a higher growth rate than *P. pastoris*. This behaviour might indicate that for growing at optimal growth rate *P. pastoris* have more energy requirements than *S. cerevisiae*. Other reason behind this discrepancy could be the value of the P/O ratio owing to both models uses the same ratio.

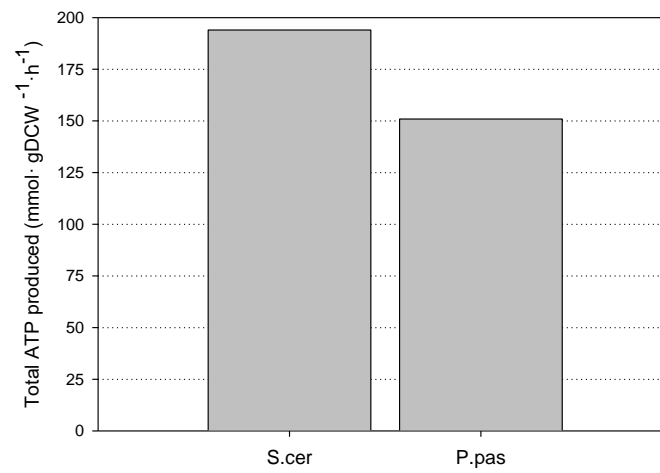


Figure 4-8. Total ATP produced by *S. cerevisiae* and *P. pastoris*

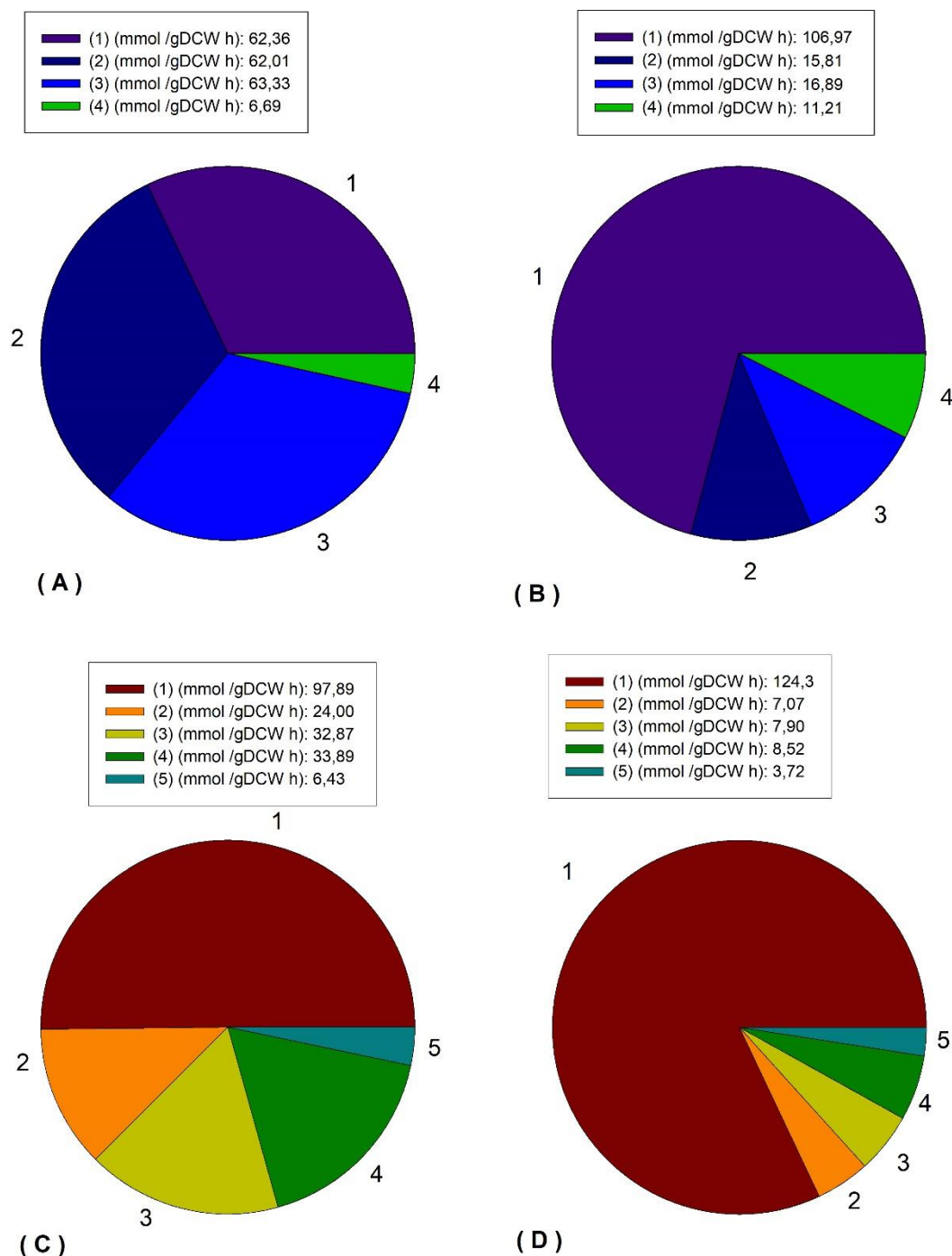


Figure 4-9 Comparison between ATP consumption and production for *S. cerevisiae* (graph A and C) and *P. pastoris* (graph B and D). In figures A and B, the ATP produced by *S. cerevisiae* and *P. pastoris* is separated depending on its provenance (ATP synthase (1), Phosphoglycerate kinase (2), Pyruvate kinase (3), Succinyl-CoA ligase (4)). While in figures C and D, the ATP consumed is separated depending on its provenance (Cell maintenance (1), Biomass formation (2), Phosphofructokinase (3), Hexokinase (4) and other side reactions (5)).

To summarize, there are big differences between ATP produced from *S. cerevisiae* and *P. pastoris* due to the difference in glycolytic fluxes. The contribution of the ATP from the oxidative phosphorylation is higher in *P. pastoris* than in *S. cerevisiae*. On the other hand, *S. cerevisiae* generate more ATP via glycolytic pathway than *P. pastoris*. Moreover, there is a peculiar trait

regarding cell maintenance, the higher energy requirements cannot be correlated to higher growth rates of *S. cerevisiae*.

Up until now, a description about the carbon and energy metabolism from *S. cerevisiae* and *P. pastoris* have been presented and analysed. Therefore, in the next section, a study based on the following hypothesis that revolves around enhancing biomass glucose yield by means of the regulation of glycolytic pathway in *S. cerevisiae* will be presented hereunder. The selection of *S. cerevisiae* over *P. pastoris* was because the ethanol production in *S. cerevisiae* is directly related to environmental conditions; therefore, it can be optimized without performing genetic modifications. Whereas, the carbon optimization regarding *P. pastoris* should be focused on genetic modifications due to a low interaction with the environment.

As it was mentioned before, the principal carbon metabolic issue shown in *S. cerevisiae* is based on the adaptation of metabolism under high glucose concentration via regulatory pathways whose objective is to maximize the glucose consumption rate and as a result, producing ethanol.

On this basis, the next hypothesis is presented: If there is a way to interact with the glycolytic pathway in order to decrease its flux through, the metabolism would be led to a more efficient carbon-biomass conversion, avoiding the ethanol generation. Following this hypothesis, two assumptions in relation with how the glycolytic pathway can be altered might be done:

- The first assumption is based on performing a genetic modification that will lead the metabolism to low glucose consumption rate and high use of the aerobic metabolism, while repressing the fermentative pathway. As a result, a non-ethanol *S. cerevisiae* might be generated. For instance, on this basis, a newly published approach has been released which focuses on undergoing a global rewiring of the entire metabolic network to abolish the partially oxidized products such as ethanol through rational engineering of pyruvate metabolism coupled with adaptive laboratory evolution (ALE). This global rewiring is based on the deletion of the pyruvate dehydrogenase (PDH) coupled with the expression of a bypass pathway whose function is to emulate the PDH one, using an ATP independent acetyl-CoA synthesis pathway. As a result, a non-ethanol *S. cerevisiae* was produced, although the growth rate was restricted in regard with the growth rate of *S. cerevisiae* growing in full aerobic conditions, therefore, in order to overcome this problem an ALE strategy was performed. In this study, it was found that a mutation at the RNA polymerase II mediator complex, the growth rate was the same as the wildtype one in full aerobic conditions (Dai et al., 2018).

- The second assumption is based on reducing the glycolic pathway by means of constraining the rate of the glucose outer membrane transporter via changing the extracellular glucose availability. As it was described before, the glucose transporters in *S. cerevisiae* are strongly regulated by the glucose concentration.

Therefore, due to the knowledge needed for conducting the first assumption and the difficulty for finding a combination of genes that its modification affects exclusively to acetate production, the second assumption is chosen as the main strategy. Thereupon, the second assumption that is based on the constriction of the glucose flux through the outer membrane will be presented hereafter.

In the following section in order to decrease the ethanol production in *S. cerevisiae*, a strategy where the modulation of the central carbon metabolism based on changing the extracellular glucose concentration will be presented. In order to do that a continuous strategy will be carry out owing to the batch strategies are not able to grant a constant metabolic state. The continuous culture is characterized by achieve a stationary state where all the physiological parameters remain constant, while in batch cultures all the physiological data change over time. Therefore, the continuous culture will grant a constant metabolic phase depending on the extracellular conditions.

4.7 Results (V) - Analysis and modelling of *S. cerevisiae* in continuous glucose-based media cultures.

In this section the dependence between the glucose availability in the extracellular space and core metabolism will be studied carrying out a continuous culture, where the feeding glucose concentration was changed from 18,10 g·L⁻¹ to 14,36 g·L⁻¹ in three steps. It is important to point out that all the feeding glucose steps were performed while the dilution rate was kept constant (0,098 h⁻¹) in order to get at least two stationary state for each day.

Regarding the definition of the stationary state, it was assumed when the biomass concentration reached a constant value, which occurred after at least three mean residence times.

As shown in **Figure 4-10** the evolution of the all the physiologic parameters related to glucose metabolism can be observed (biomass, glucose, ethanol, glycerol, CER, OUR). It is important to point out that the profile of biomass and ethanol concentrations are related to how the glucose concentration changes. The decrease in the glucose availability, which is the difference between the feeding glucose concentration and the outlet one, affected the metabolism in different ways as observed in the modification of the specific rate presented in **Table 4-6**. It is important to remark that even when the feeding glucose concentration was dropped, the outlet glucose concentration remained constant with a value of zero. The outlet glucose concentration reached a value of 0, due to the fact that the continuous culture was limiting the specific growth rate 4,25-fold. Moreover, if the variation in the glucose availability (difference between the inlet and outlet glucose concentration) along with both the biomass and ethanol profiles, an adapting metabolism based on reducing the ethanol production might be undergoing.

On this basis, two phases were defined depending on the interaction between the metabolism and the glucose availability:

- The first phase (blue box in **Figure 4-10**), that took place when the feeding glucose concentration changed from 18,10 g·L⁻¹ to 16,50 g·L⁻¹, where there was no change in the biomass concentration while, the ethanol production was reduced as a consequence of change in glucose feeding.
- The second phase (green box in **Figure 4-10**), that took place when the feeding glucose concentration changed from 16,50 g·L⁻¹ to 14,36 g·L⁻¹, where either the biomass and the ethanol concentration were reduced, as a consequence of the glucose feeding reduction.

It can be stated then that the metabolic redistribution owing to the drop in the glucose availability had, as a consequence, a metabolic redistribution regarding the first step, whereas in the second step there was an effect on substrate limitation, that affect either to the cell growth and metabolism.

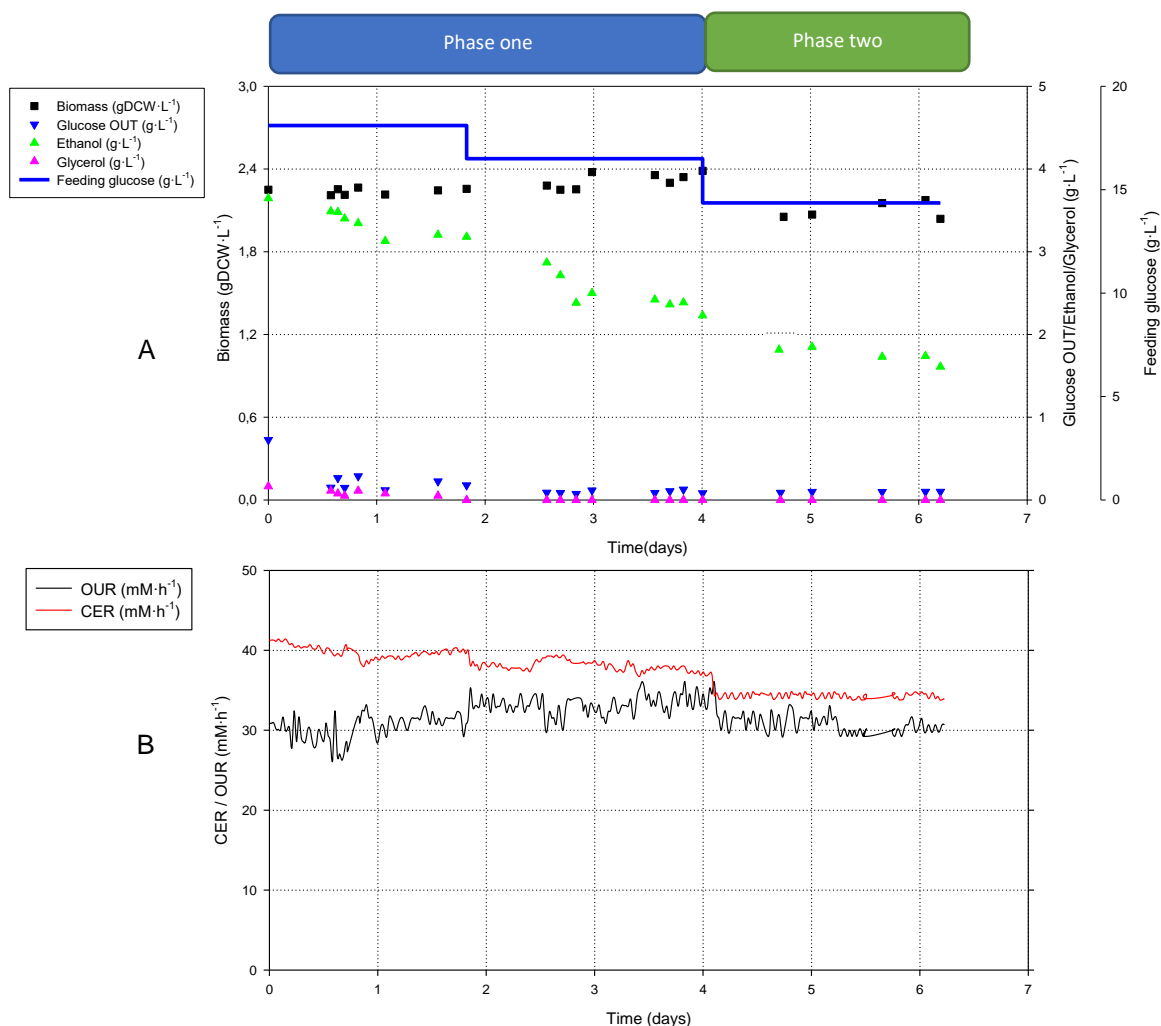


Figure 4-10 Profile of A) off-line variables such as biomass (■), glucose feeding (—), glucose OUT (▼), glycerol (▲), ethanol (▲) and B) on-line variables such as CER (—) and OUR (—).

Table 4-5. Stationary state values for the *S. cerevisiae* continuous culture.

	Continuous Culture Stationary States		
	1	2	3
Feeding Glucose (g·L ⁻¹)	18,1	16,5	14,36
Glucose OUT (g·L ⁻¹)	0,15	0,1	0,1
CER (mM·h ⁻¹)	38,5	38,00	34
OUR (mM·h ⁻¹)	31,3	33	30
Ethanol (g·L ⁻¹)	3,2	2,32	1,8

Glycerol (g·L ⁻¹)	0	0	0
Biomass (gDCW·L ⁻¹)	2,241	2,298	2,108
μ (h ⁻¹)	0,098	0,098	0,098

Table 4-6 Specifics rates in mmol·gDCW⁻¹·h⁻¹ used for Flux Balance Analysis in *S. cerevisiae* continuous culture.

Feeding Glucose (g·L ⁻¹)	q _{Glucose}	q _{Ethanol}	q _{CO2}	q _{O2}
18,10	4,33	2,95	17,04	14,06
16,50	3,87	2,14	16,48	14,33
14,36	3,66	1,81	15,94	14,12

Table 4-7 Yields and Respiratory quotient in *S. cerevisiae* continuous culture.

Glucose Feeding (g·L ⁻¹)	Y _{Ethanol/Glucose} (g·g ⁻¹)	Y _{Biomass/Glucose} (gDCW·g ⁻¹)	RQ
18,10	0,18	0,12	1,21
16,50	0,14	0,14	1,15
14,36	0,13	0,15	1,12

In order to explain the profiles on the biomass concentration, ethanol concentration, CER and OUR in relation with the decrease in the glucose availability, each variable will be studied and described individually hereafter.

Regarding the biomass concentration, there was no significant change in the biomass concentration when the feeding glucose concentration decreased from 18,10 g·L⁻¹ to 16,5 g·L⁻¹, while the biomass glucose yield increased 15% as shown in **Table 4-7**. Whereas, in the second steady-state, when the feeding glucose concentration dropped from 16,5 g·L⁻¹ to 14,36 g·L⁻¹, there was no significant change in biomass-glucose yield while biomass concentration decreased 28%.

On the other hand, as shown in

Table 4-5, there was a modification in the ethanol metabolism as function of glucose feeding. When the feeding glucose concentration change from $18,10 \text{ g}\cdot\text{L}^{-1}$ to $16,5 \text{ g}\cdot\text{L}^{-1}$, a 23% decrease in the yield ethanol-glucose was observed. In the last steady-state, there was no comparable change when the feeding glucose concentration change from $16,5 \text{ g}\cdot\text{L}^{-1}$ to $14,36 \text{ g}\cdot\text{L}^{-1}$. The reduction in the ethanol production might be related to either a repression of the glycolytic pathway or an induction of the TCA cycle. For a further insight, a metabolic flux analysis will be performed in the followings section (section 4.7.1) in order to understand the behaviour observed in respect to the ethanol production.

Coupled with the biomass and ethanol tendencies, and as shown in **Figure 4-10**, the variation in the CER and OUR achieved were related to metabolic redistribution caused by the glucose availability. As shown in **Table 4-6**, this metabolic adaptation was based on decreasing the specific carbon dioxide production rate, while leaving unaffected the specific oxygen uptake rate.

How the specific rate either of oxygen uptake and carbon dioxide generation behaved might be explained understanding the evolution of the RQ value. As shown in **Table 4-7**, the RQ value changed depending on the glucose availability. When the feeding glucose concentration decreased from $18,10 \text{ g}\cdot\text{L}^{-1}$ to $16,5 \text{ g}\cdot\text{L}^{-1}$, the RQ also decreased from 1,21 to 1,15. This decrease might be related to a modification in the flux through the glycolytic pathway due to a change in the glucose availability, which led the carbon metabolism to get adapted to a low glycolytic flux situation where ethanol metabolism was minimized. Consequently, the carbon dioxide linked to the first reaction step in the ethanol metabolism, which is the pyruvate decarboxylation, was reduced, and production of carbon dioxide diminishes. Furthermore, it can be observed that RQ had a lower value in regard with the capacity of adapting the flux through the glycolytic pathway. This limit was reached in the last steady state where the RQ presented almost no-change.

Up until now, the effect of the feeding glucose concentration on the physiologic state of the *S. cerevisiae* and its metabolism has been detailed. However, there is a behaviour that must be further described: the biomass profile.

In order to explain this behaviour, a mass balance equation (**Equation 4-1**) is used owing to it which relates the achieved biomass (X_v) in the stationary state with the glucose availability (described as the glucose available to be metabolized (A), which is the difference between the inlet and outlet concentration), its specific consumption rate ($q_{s,total}$) and the dilution rate (D).

In order to use this equation, the following three premises were stipulated:

1. The glucose specific consumption rate ($q_{s,total}$) is defined as: the sum of the glucose specific rate needed for biomass formation ($q_{s,biomass}$), the glucose specific rate needed for ethanol production ($q_{s,ethanol}$) and the glucose specific rate needed for cell maintenance ($q_{s,maintenance}$).
2. The specific glucose consumption directed towards the biomass only depends on the dilution rate.
3. The dilution rate is excluded from the biomass profile deduction because it is constant in each stationary state.

Equation 4-1

$$Xv = D \cdot \frac{\{A = [Gluc_{inlet}] - [Gluc_{outlet}]\}}{\{q_{s,total} = q_{s,biomass} + q_{s,ethanol} + q_{s,maintenance}\}}$$

Equation 4-2

$$[Gluc_{outlet}] = \frac{K_s \cdot D}{\mu_{max} - D}$$

As show in **Equation 4-1 and 4-2**, the biomass achieved in the continuous culture depends on two phenomena when there is a fixed decrease in the glucose availability: 1) how glucose metabolism, specifically the specific glucose uptake rate, is affected by the glucose availability and 2) how the glucose availability is affected by the Monod parameters (culture glucose limitation).

As shown in **Equation 4-2**, the Monod parameters μ_{max} and K_s defines the outlet glucose concentration. A change in these parameters might cause a restriction in the glucose availability higher than the related to the experimental approach, and as a consequence an unpredictable biomass behaviour. However, this assumption might not be applied in this case, because the outlet glucose concentration was kept constant with a value near $0,1 \text{ g} \cdot \text{L}^{-1}$. Therefore, there was no appreciable change in the Monod parameters between conditions tested. However, it is important to point out that this assumption could be either true or false due to the fact that the continuous culture was designed as a growth rate-limited conditions. In order to prove that both μ_{max} and K_s might be affected by glucose availability, a continuous culture where the dilution

rate (D) is equal to the kinetic parameter μ_{max} will be required for reaching a feasible conclusion.

On the other hand, as shown in **Equation 4-1**, in order to get the same biomass concentration when there is a decrease in the glucose availability (A) the only way would be decreasing the glucose specific consumption rate ($q_{s,total}$). Regarding the glucose metabolism, a decrease in the glucose specific rate could be directly related to a metabolic restructuring. On this basis, it could be stated that when glucose available is lower, the glucose consumption could be reduced by generating less by-products (ethanol), obtaining the same biomass.

Therefore, the behaviour of the biomass in the chemostat will be hypothesized according to how *S. cerevisiae* central carbon metabolism behaves when there is a change in glucose availability.

As mentioned previously, two phases regarding the biomass profile can be defined (the first one from 18,10 g·L⁻¹ to 16,5 g·L⁻¹ and the second one from 16,5 g·L⁻¹ to 14,36 g·L⁻¹), thereafter a description of each one is detailed:

The first phase (blue box in **Figure 4-10**) where glucose availability was decreased from 18,10 g·L⁻¹ to 16,5 g·L⁻¹ will be considered a phase where the metabolic features that prevails is the ethanol reduction due to a decrease in the glucose availability, while there was no significant change in the biomass concentration. In this phase, the decrease in the glucose uptake rate did not affect the biomass concentration because the ethanol production was reduced as well. As observed in the reduction of the ethanol concentration from 3,2 g·L⁻¹ to 2,3 g·L⁻¹. As result, the total glucose converted to biomass was the same. Moreover, coupled with this decrease in the glucose uptake rate, Both glucose and ethanol rates are linked by cytoplasmic NADH metabolism, being the ethanol production the main cytoplasmic reaction in order to get regenerate NADH, that cannot be fully regenerated via the mitochondrial shuttles (malate-aspartate shuttle).

Regarding the biomass behaviour, as show in **Equation 4-1**, its concentration was determined by the relationship between the glucose availability and the glucose specific rate. Even if there was no significant change in the biomass concentration achieved, the yield biomass-glucose increased 25%.

As shown in **Equation 4-3**, the biomass glucose yield depends solely on the specific growth rate and on the specific glucose rate. On this basis, the increase in the biomass glucose yield can only be a consequence of a decrease in the specific glucose rate (specific growth rate was constant along the experiment) ,as shown in **Equation 4-4**.

Equation 4-3

$$Y_{bio/gluc} = \frac{\mu}{q_s}$$

Equation 4-4

$$Y_{\frac{bio}{gluc}} \Big|_1 > Y_{\frac{bio}{gluc}} \Big|_2 ; q_s \Big|_1 < q_s \Big|_2 ; \mu \Big|_1 = \mu \Big|_2$$

Regarding how the specific glucose rate might be decreased, as shown in **Equation 4-5**, there are two possible ways:

1. Decreasing the part of the specific glucose rate that is directed towards the ethanol formation ($q_{s,ethanol}$), on other words, decreasing the ethanol specific production rate.
2. Decreasing the part of the specific glucose uptake rate that is directed towards cell maintenance ($q_{s,maintenance}$).

Equation 4-5

$$1 = \frac{q_{s,biomass}}{q_{s,total}} + \frac{q_{s,ethanol}}{q_{s,total}} + \frac{q_{s,maintenance}}{q_{s,total}}$$

As a result, when there is a drop in the specific rate of ethanol formation, less glucose is required for enabling the same biomass growth rate. However, it is important to point out that this theoretical approach considers that the only way to change the rate of glucose directed solely towards biomass($q_{s,biomass}$) is changing the specific growth rate. In other words, changing the dilution rate ($\mu=D$). Therefore, the increase in the yield biomass- glucose is directly related to decrease in the ethanol production.

The second phase (green box in **Figure 4-10**) where glucose availability was decreased from 18,10 g·L⁻¹ to 16,5 g·L⁻¹ is considered as a carbon limiting phase, obtained when the feeding glucose concentration dropped from 16,50 g·L⁻¹ to 14,36 g·L⁻¹. In this phase the decrease in biomass concentration was caused by not having enough glucose directed towards biomass in order to keep the same metabolic ratio between the different glucose contribution as shown in **Equation 4-5**. Moreover, the decrease in glucose availability lead to a decrease of carbon dioxide and oxygen specific rates in comparison with the previous one. Under those circumstances, a minim value for energy requirements might be achieved. This minimum requirement will be discussed in the following sections, more specifically in the study of the energy metabolism.

In the final analysis, the decrease in glucose availability caused by the decrease in the feeding glucose concentration lead the culture to a metabolic restructuration based on improving the conversion of glucose to biomass instead of ethanol production, until a limit were observed the feeding glucose concentration reached the value of 14,36 g·L⁻¹.

Up until now, the relation glucose availability and the metabolic behaviour of *S. cerevisiae* shows a particular physiology where the change in glucose availability leads to a restructuration of the carbon metabolism. It is important to highlight that the physiological view does not bring enough information about how *S. cerevisiae* changes its internal metabolic fluxes owing to changes in the glucose availability. As a result, in order to present an accurate description of the metabolic behaviour shown in the continuous culture, the comparison between the internal fluxes for each steady-state will be presented in the following section,

4.7.1 Metabolic comparison between steady states regarding the carbon metabolism

In this section, the metabolic fluxes are analysed for all the steady states displayed in the continuous culture. The fluxes comparison between each steady state is shown in **Figure 4-11**. It must be kept in mind that the obtained results follow three hypotheses due to the complexity of the metabolism and its adaptability to changes in glucose availability conditions:

- Change in feeding glucose concentration leads to a change in glucose availability.
- Glucose availability is described as the difference between the feeding glucose concentration and outlet glucose concentration.
- Genome scale metabolic model is the same for all the conditions tested, including the biomass equation.

In order to obtain a representative and restricted metabolic model for each one of the conditions tested, the boundaries of the models were constrained using the input-output data of the corresponding metabolites that are shown in **Table 4-8**, using the data extracted from the experiments shown in **Figure 4-10**.

Table 4-8 Specific rate limits values used as drains for a Flux Balance Analysis in *S. cerevisiae* in continuous culture for different feeding glucose concentrations

Feeding Glucose Concentration (g·L ⁻¹); specific rates (mmol·gDCW ⁻¹ ·h ⁻¹)		
18,10	16,50	14,36

Biomass	0,097 ± 0,006	0,097 ± 0,006	0,097 ± 0,006
Carbon Dioxide	17,400 ± 1,556	16,482 ± 1,166	15,942 ± 1,128
Ethanol	3,100 ± 0,141	2,120 ± 0,150	1,932 ± 0,127
Glucose	-4,305 ± 0,035	-3,960 ± 0,280	-3,760 ± 0,266
Oxygen	-14,690 ± 0,891	-14,332 ± 1,013	-14,121 ± 0,998

Once the boundaries of the metabolic model have been fixed, all the fluxes calculations (methodology described in section 4.9.11) for each of the steady states were done by means of the FBA protocol (described in section 4.9.13).

As shown in **Figure 4-10**, while the feeding glucose was dropped from 18,10 g·L⁻¹ to 14,36 g·L⁻¹, there are different behaviours that have to be described and explained owing a decrease in the glucose availability:

- The 15% decrease in the flux rate of glycolytic pathway from 4,33 mmol·gDCW⁻¹·h⁻¹ to 3,76 mmol·gDCW⁻¹·h⁻¹ when feeding glucose was dropped from 18,10 g·L⁻¹ to 16,50 g·L⁻¹.
- The maintenance of the flux rate through TCA in the all the feeding glucose concentration used.
- The 37% decrease in the flux through the ethanol metabolism from 2,95 to 1,88 mmol·gDCW⁻¹·h⁻¹ when feeding glucose was dropped from 18,10 g·L⁻¹ to 14,36 g·L⁻¹.
- The no significant variation in the intracellular metabolic flux distribution of the last glucose steady state when feeding glucose was dropped from 16,50 g·L⁻¹ to 14,36 g·L⁻¹.

The 15% decrease in the glycolytic pathway indicates a relation between the glucose availability and the capacity of the cell for transporting glucose from the outer space to the cytoplasm. This metabolic trait was mentioned before in the study of *S. cerevisiae* metabolism (section 4.3.2), where in *S. cerevisiae* a modulation of the glucose consumption rate depending on the availability of glucose was described. As a result, it is possible to decrease the glucose consumption rate without entering in a carbon limitation phase, just as is observed in the last steady state. This is an interesting fact because, up until now, it has been extensively described that the flux through the glycolytic pathway might be changed depending on the specific growth rate (Postma et al., 1989). In this case, it can be said that keeping the same dilution rate and changing the feeding glucose concentration, is possible to undergo a metabolic restructuration in order to decrease the flux through the glycolytic pathway.

On the other hand, coupled with the decrease in the glycolytic pathway, the decrease in the flux through the ethanol generation can be explained due to changes in the glycolytic pathway. In order to understand why ethanol is decreased, it is important to take into consideration why ethanol was produced. The production of ethanol is related to an unbalance of cytoplasmic NADH metabolism caused by an overflow in the glucose transport coupled with an aerobic metabolism repression (Vemuri et al., 2007). As a result, the formation of partially oxidized products, as ethanol, are required for balancing the cytoplasmic NADH. It is important to point out that even if there is a decrease in glucose availability until the carbon-limited phase was reached (phase II), the ethanol production might not be eluded. In order to fully deplete ethanol production, one of the most used method is to reduce the growth rate until a specific threshold where ethanol is not produced (Postma et al., 1989). It could be that this limit threshold can only be overcome through growth rate limitation and not through glucose availability. Therefore, in the present case of study, ethanol fully depletion was not possible, although a reduction of 37% in the ethanol specific rate was achieved.

Regarding the aerobic metabolism, specifically in the TCA fluxes, the drop in glycolytic pathway caused by the decrease in the glucose availability did not lead a modification in the flux through the TCA or in the flux through the mitochondrial shuttles on top of internalizing NADH from the glycolytic pathway. This behaviour might take place due to a minimum flux through the TCA that cannot be decreased. Therefore, the efficiency of transporting pyruvate from the cytoplasm to the mitochondria was not affected, as observed in **Figure 4-12**.

It is clear that *S. cerevisiae* can adapt its flux through of glycolytic pathway in order to minimize the ethanol production while the flux of pyruvate that was transported from the cytoplasm to the mitochondria remains constant. However, even if the flux of pyruvate transported to the mitochondria was not affected, the conversion of glucose to available pyruvate to be fully oxidized was increased by 9,2%.

It is important to highlight that the ethanol production cannot be depleted only by changing the glycolytic flux, due to a limit threshold for the ethanol production related to the dilution rate used. To explore this adaptive metabolism, where a change in glucose availability leads to a reduction in the ethanol generation and the enhancement of the biomass-glucose yield, a study of how *S. cerevisiae* handled ATP requirements will be presented hereafter.

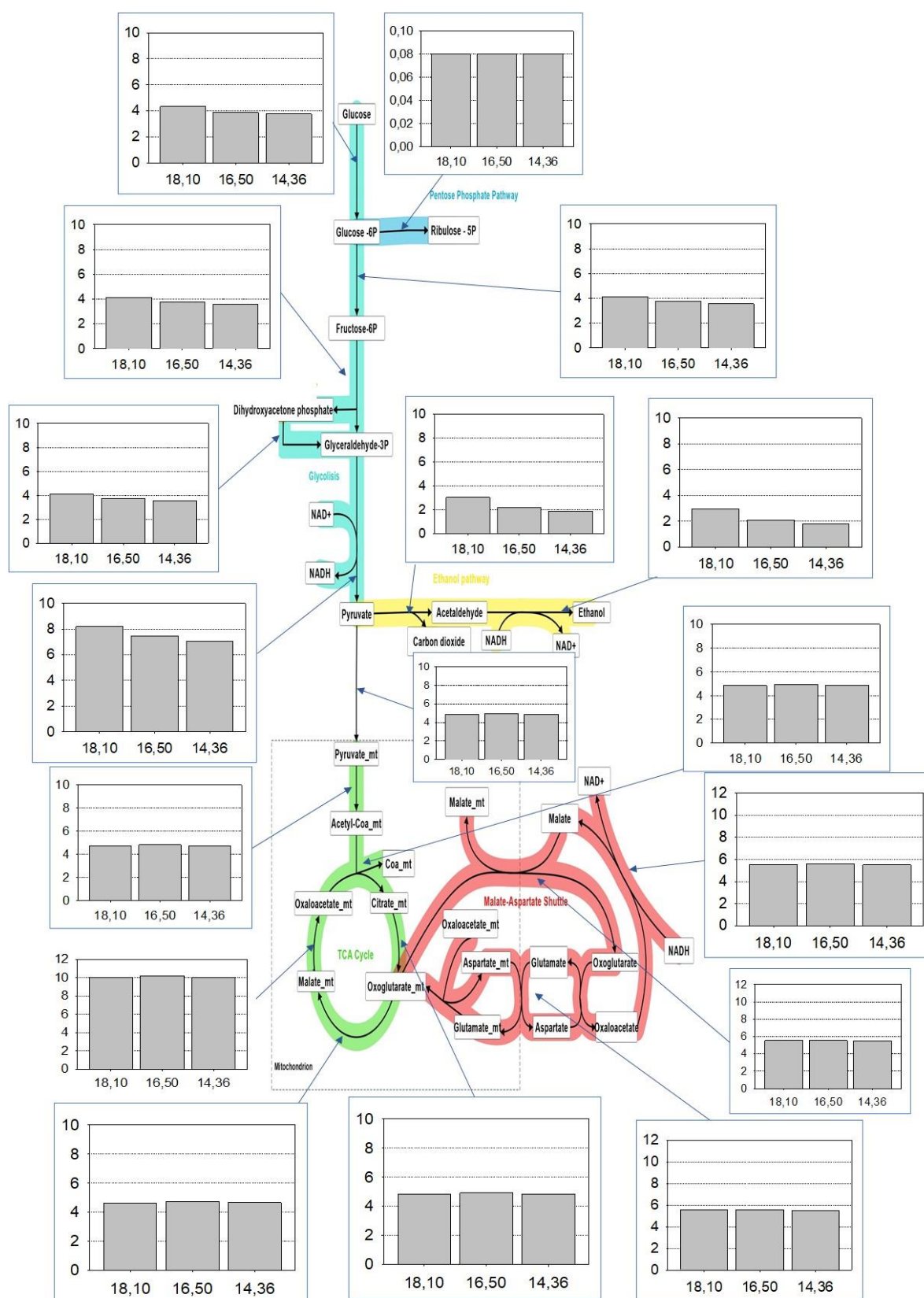


Figure 4-11. Metabolic flux distribution comparing several feeding glucose concentrations for *S. cerevisiae* continuous culture. Each graph indicates the flux through the selected reaction (Y-axis flux rate - mmol·gDCW⁻¹·h⁻¹- and x-axis feeding glucose concentrations -18,10 g·L⁻¹, 16,50 g·L⁻¹ and 14,36 g·L⁻¹-).

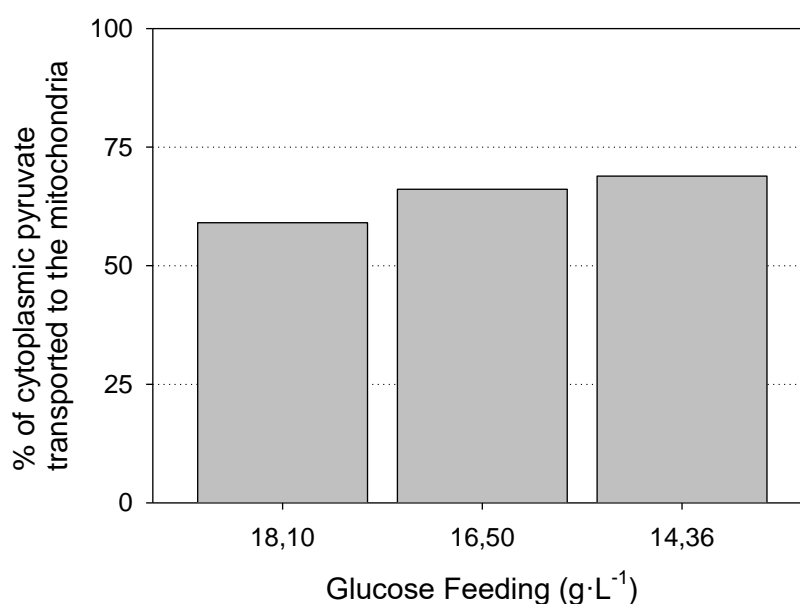


Figure 4-12 Percent of the cytoplasmic pyruvate that was transported to the mitochondria for each stationary state.

4.7.2 Energetic Metabolism Comparison between the different steady states - ATP distribution

As it has been shown in the previous section, the carbon metabolism can be modified if there is a change in the glucose availability. The main function of the carbon metabolism is to produce precursors for biomass synthesis and high energetic molecules such as ATP. As a result, it can be hypothesized that a variation in the carbon metabolism might influence the energy metabolism. Two assumptions related to the metabolic model must be taken into consideration:

- The relation that characterizes the oxidative phosphorylation, the P/O , has a constant value of 1,8 in all the modelling done for each steady state.
- The energy requirements used for biosynthesis are the same in all the models calculated for each steady state.

As shown in **Figure 4-13**, the total ATP handled was slightly affected by a change in the glucose availability. Moreover, as shown in **Figure 4-14** and **Figure 4-15**, the distribution in how the ATP was produced and consumed was almost not affected as well. With this data, it can be hypothesized that the energy requirements for undergoing the three steady states were slightly the same due to the reduction in the flux through the glycolytic pathway.

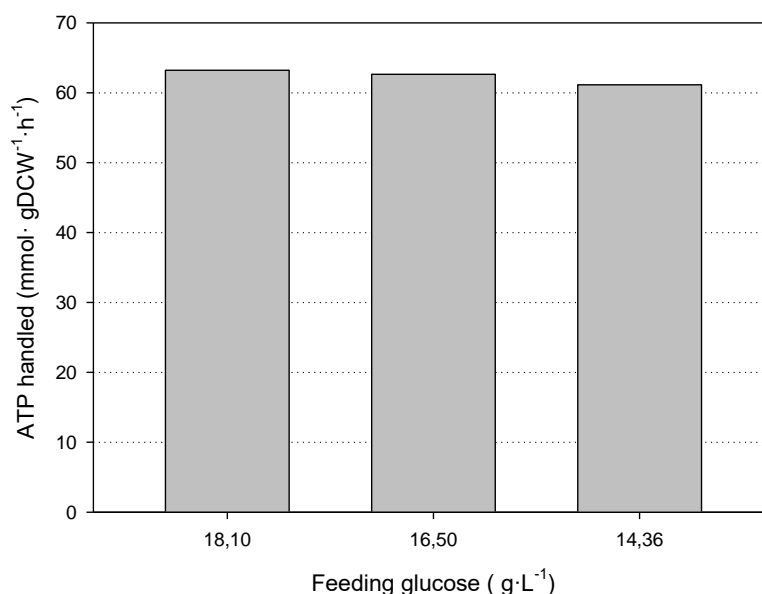


Figure 4-13 Variation of the ATP handled for each stationary state where different feeding glucose concentration were tested. All the fluxes are expressed in mmol·gDCW⁻¹·h⁻¹.

This trait might be related to two phenomena: what pathways were affected by the glucose availability and how and in which extend they were affected. It might be stated that the decrease in the glycolytic flux caused by the decrease in the glucose availability affected the same way all the reactions involved in the glycolytic pathway. However, only the flux through them was modified, not the ratio between the different reactions.

Moreover, when the non-variation of flux through the TCA during the three steady states coupled with the optimization in the use of carbon source directed towards the aerobic metabolism are take into consideration, another conclusion can be obtained. The energy requirements for undergoing all the cell processes granting a correct cell functionality did not change when the glucose availability dropped.

However, as shown in **Figure 4-14**, it can be stated that 75 % of the total ATP produced came from aerobic metabolism (oxidative phosphorylation) and 25 % from fermentative metabolism. Moreover, the slightly decrease in the total ATP handled was caused by the decrease in the flux through the glycolytic pathway. Regarding the consumption of ATP, as shown in **Figure 4-15**, more than 75 % of the total ATP produced was used for cell maintenance and kept constant through the different steady states. In order to put numbers in the statements mentioned before, the following points are presented:

- There was a slightly change in the total ATP handled when there was a decrease in the glucose availability.
- The proportion of ATP produced remained constant with the following proportion: 65 % of the ATP produced from ATP synthase, 12,5% from phosphoglycerate kinase, 12,7 % from pyruvate kinase and 10,0 % from Succinyl-CoA ligase. On this basis, it can be stated that 75 % of the ATP came from aerobic metabolism while 25% came from the fermentative one.
- The most relevant matter regarding ATP consumption is related to cell maintenance that consumed 75 % of the total ATP produced in all steady states.

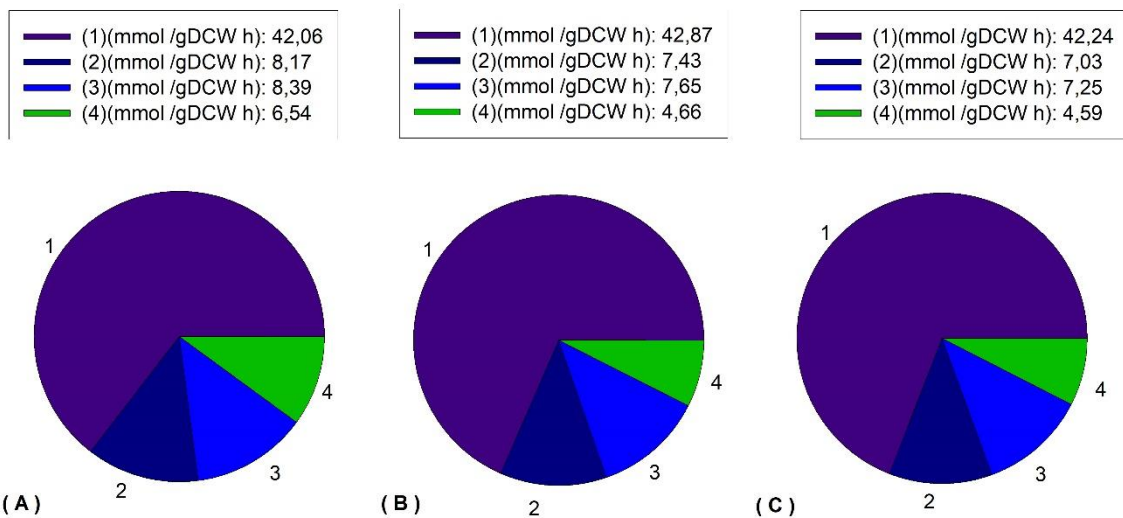


Figure 4-14 Distribution of ATP production depending on its provenance (ATP synthase (1), Phosphoglycerate kinase (2), Pyruvate kinase (3), Succinyl-CoA ligase (4)) for *S. cerevisiae* continuous cultures stationary states, where different feeding glucose concentration are used. Values were calculated using FBA. All the fluxes are expressed in mmol-gDCW⁻¹·h⁻¹. In figure A, the ATP produced by *P. pastoris* is presented when the feeding glucose was 18,1 g·L⁻¹; in figure B, when it was 16,5 g·L⁻¹ and in figure C, when it was 14,36 g·L⁻¹.

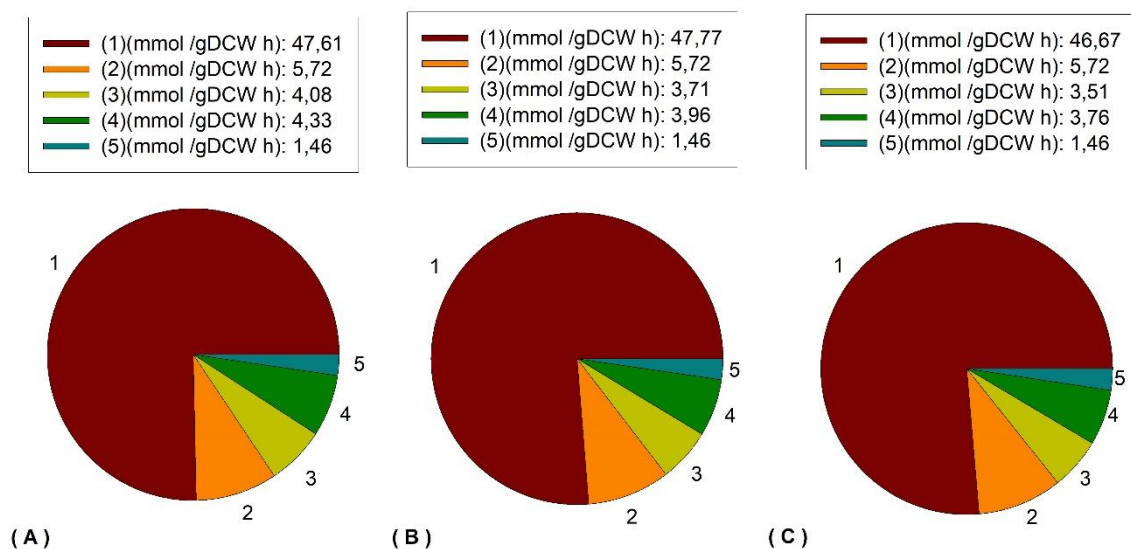


Figure 4-15 Distribution of ATP consumption depending on its provenance (cell maintenance (1), biomass formation (2), phosphofructokinase (3), hexokinase (4)) and other side reactions (5)) for *S. cerevisiae* continuous cultures stationary states, where different feeding glucose concentration are used. Values were calculated using FBA. All the fluxes are expressed in $\text{mmol} \cdot \text{gDCW}^{-1} \cdot \text{h}^{-1}$. In figure A, the ATP produced by *P. pastoris* is presented when the feeding glucose was $18,1 \text{ g} \cdot \text{L}^{-1}$; in figure B, when it was $16,5 \text{ g} \cdot \text{L}^{-1}$ and in figure C, when it was $14,36 \text{ g} \cdot \text{L}^{-1}$.

To summarize, the decrease in the glycolytic flux caused by the decrease in the glucose availability did not affect the energy metabolism. This independency is because the metabolic restructuration undergone by the drop in the feeding glucose concentration only affected the cytoplasmic reactions, specifically, the ethanol metabolism while remaining unaffected the main source of ATP, the aerobic metabolism. Moreover, the decrease in the substrate level phosphorylation due to the reduction of the glycolytic pathway was backed up by a slightly increase in transport of pyruvate to the mitochondria.

4.8 Discussion and conclusions

An extensive study of the metabolic flux distribution for the carbon and energy metabolic behaviours obtained in *S. cerevisiae* and *P. pastoris* has been presented in this chapter. The conventional metabolic behaviour of *S. cerevisiae* was characterized by a high glucose consumption, while partially-oxidized products (such as ethanol) were being produced and secreted to the media in an uncontrolled manner, leading the metabolism to an inefficient conversion from glucose to biomass. On the other hand, *P. pastoris* growing on glucose-based media was able to almost fully convert all the glucose to biomass, producing very low levels of ethanol.

The Crabtree Effect in yeast has been extensively studied, although in the last decade, thanks to the technological advances in relation with high-throughput data management within Systems Biology scope several hypotheses explaining this effect have been published (Shah et al., 2007). These hypotheses are based on studying the genomic, transcriptomics, proteomics and fluxomics in order to enlighten the reason behind the generation of partially-oxidized by-products in aerobic conditions (Dueñas-Sánchez et al., 2012) (Navarrete et al., 2014).

Regarding *S. cerevisiae*, the analysis of the metabolic fluxes carried out using a reduced genomic-scale metabolic model suggested that the ethanol production is related to an unbalance in the cytoplasmatic NADH pool generated by three pathways regulated by the glucose availability:

1. The overexpression of the glucose transporters under excess glucose conditions in order to maximize the glucose consumption rate.
2. The regulation of the flux through the glycolytic pathway in order to be able to obtain high glucose consumption rates.
3. The repression of the aerobic pathway under high external glucose concentrations in order to promote the regeneration of the NADH through the formation of partially-oxidized products instead of by the oxidative phosphorylation.

In contrast, in the case of *P. pastoris* almost no ethanol production was obtained owing to the cytoplasmic NADH pool was completely balanced with the mitochondrial shuttle mechanism. The mitochondrial shuttles were able to balance the cytoplasmic all the NADH because the NADH from the glycolytic pathway was limited, due to the low transport of extracellular glucose. The low transport of glucose was caused by: a glucose transporters with a low or intermediate affinity towards glucose, a low regulation of the glycolytic pathway in regard with the glucose

availability and a non-repression of the aerobic pathway related to the glucose availability. As a result, *P. pastoris* was almost a non-ethanol producer due to a limited flux through the glycolytic pathway.

Once the study of the ethanol production has led to an appropriate hypothesis, an extensive study about how glycolytic fluxes are affected by means of changes in glucose availability maintaining the specific growth rate has been presented for *S. cerevisiae*. This study consists in a comparison between several steady states in chemostat mode when several feeding glucose concentrations were tested keeping the dilution rate constant.

The comparison between the metabolic fluxes of the different steady states corroborated that a decrease in the glucose availability leaded the metabolism to a restructuration based on decreasing the flux through both the glycolytic and the ethanol pathways, keeping a constant flux through the TCA. Coupled with the change in the metabolic flux distribution, an improvement in the glucose conversion towards biomass was obtained when the glucose availability was decreased, owing to a decrease in the ethanol produced.

Regarding the ethanol metabolism, a decrease in the glucose availability was associated to a reduction in the ethanol produced, although, a lower limit rate appeared due to a metabolic threshold. This metabolic threshold set a minimum relation with a value revolving around 1,9 between the specific rates of glucose consumed and ethanol produced. However, it is important to keep in mind that an interesting metabolic restructuration lead the metabolism to enhance the glucose conversion towards biomass, although a fully ethanol depletion was not obtained.

Regarding the energy metabolism, the analysis of the ATP produced and consumed showed an interesting feature: the change in the glycolic flux did not affect the total ATP available and the distribution of ATP produced and consumed. This might be a peculiar trait of how the production of partially oxidized products due to a NADH cytoplasmic unbalance did not disturb the aerobic metabolism (the OP) and had a slightly impact in the ATP from the substrate level phosphorylation owing to a decrease in the flux through the glycolytic pathway.

Finally, the results presented in this chapter, that were focused on the comprehension of the carbon and energy metabolism of *S. cerevisiae*, will be used to design engineering-based tools in order to monitor and control high-density cell cultures in bioreactor. In the work that will be presented in **chapter 8**, the high-density cell cultures selected will be the fed-batch cultures, because one of the key aspects in its definition is the comprehension of the metabolism of the selected expression platform. Through its comprehension, a more suited feeding profile based

on the metabolic requirements will be designed in order to avoid one of the main issues in the yeast fed-batch cultures, the over-feeding that cause the ethanol production (growth inhibitor). An over-feeding in fed-batch cultures might occur when the feeding profile used is higher than the required one owing to a difference between the expected carbon metabolic behaviour and the real one (Schaepe et al., 2014).

In addition, the data from this chapter will be useful in the fed-batch strategies because the optimization described in relation with the conversion of glucose to biomass by reducing the ethanol production is a key parameter in the process definition. If it is taken into account that the goal of a fed-batch strategy is to generate biomass, the use of a non-expected metabolic parameter that will decrease the ethanol production while increasing the biomass concentration achieved will be a success. Therefore, the metabolic study described in this chapter will be taken into consideration in order to design a fed-batch strategy that might produce the maximum biomass concentration while the minimum amount of ethanol should be produced.

4.9 Materials and Methods

4.9.1 Yeast strains and maintenance

The yeast used in this work for the metabolic studies carried out in batch cultures were *S. cerevisiae* wildtype and *P. pastoris* X33 wild type. Moreover, *S. cerevisiae* wildtype was used for the study of glucose metabolism in continuous culture

The pre-inoculum of both yeast were cultured in 125 mL glass erlenmeyer with a working volume of 20 mL, incubated at 30°C (Steri-cult 2000 Incubator, Forma Scientific) using the media described in section 4.9.3 . Flasks were continuously agitated at 130 rpm on an orbital shaking platform (Stuart SSL110 Incubator, Forma Scientific). Moreover, both yeast were maintained using petri dishes at 30°C with the media described in section 4.9.3.

4.9.2 Culture systems

For small scale or inoculum cultures have been performed in glass erlenmeyer of different volumes (25, 50, 100, 250 and 1000 ml) cultured at 30°C and 130 rpm.

The cultures in petri plates was used as a starter solid culture support. Moreover, it was incubated at 30°C using an orbital incubator (Shaker orbital Incubator, Sanyo).

4.9.3 Media definition.

The media for petri plates is described in **Table 4-9**. While, the media used for batch cultures in *S. cerevisiae* is described in **Table 4-10**, on the other hand, the one used for continuous cultures is described in **Table 4-11** .

Regarding the media used in the batch culture of *P. pastoris*, it is described in the **Table 4-12**.

Table 4-9 Composition YPD and YPD-Agar media.

Compound	Concentration (g·L ⁻¹)	
	YPD	YPD-Agar
Peptone	20	20
Yeast Extract	10	10

Dextrose	20	20
Agar	0	20

Table 4-10 Composition of media used in batch cultures for *S. cerevisiae*.

Compound	Concentration
Glucosa·H ₂ O	110 g·L ⁻¹
(NH ₄) ₂ SO ₄	10 g·L ⁻¹
KH ₂ PO ₄	2 g·L ⁻¹
MgSO ₄ ·7H ₂ O	0,5 g·L ⁻¹
NaCl	0,1 g·L ⁻¹
CaCl ₂ ·2H ₂ O	0,26 g·L ⁻¹
Biotin	0,024 mg·L ⁻¹
Hemicalcium Acid Pantoteic Salt	4,8 mg·L ⁻¹
Folic Acid	0,024 mg·L ⁻¹
Inositol	24 mg·L ⁻¹
Niacine	4,8 mg·L ⁻¹
PABA	2,4 mg·L ⁻¹
Pyridoxine·HCl	4,8 mg·L ⁻¹
Riboflavin	2,4 mg·L ⁻¹
Thiamine·HCL	4,8 mg·L ⁻¹
H ₃ BO ₃	0,5 mg·L ⁻¹
CuSO ₄ ·5H ₂ O	0,04 mg·L ⁻¹
NaI	0,1 mg·L ⁻¹
FeCl ₃	0,2 mg·L ⁻¹
MgSO ₄	0,4 mg·L ⁻¹
Na ₂ MoO ₄ ·2H ₂ O	0,2 mg·L ⁻¹
ZnSO ₄	0,4 mg·L ⁻¹

Table 4-11 Composition of media used in continuous cultures for *S. cerevisiae*.

Compound	Concentration
Glucosa·H ₂ O	20 g·L ⁻¹
(NH ₄) ₂ SO ₄	5 g·L ⁻¹
KH ₂ PO ₄	1 g·L ⁻¹
MgSO ₄ ·7H ₂ O	0,5 g·L ⁻¹
NaCl	0,1 g·L ⁻¹

CaCl ₂ · 2H ₂ O	0,1 g·L ⁻¹
Biotin	0,002 mg·L ⁻¹
Hemicalcium Acid Pantoteic Salt	0,4 mg·L ⁻¹
Folic Acid	0,002 mg·L ⁻¹
Inositol	2 mg·L ⁻¹
Niacine	0,4 mg·L ⁻¹
PABA	0, 2 mg·L ⁻¹
Pyridoxyne-HCl	0,4 mg·L ⁻¹
Riboflavin	0, 2 mg·L ⁻¹
Thiamine-HCL	0,4 mg·L ⁻¹
H ₃ BO ₃	0,5 mg·L ⁻¹
CuSO ₄ ·5H ₂ O	0,04 mg·L ⁻¹
NaI	0,1 mg·L ⁻¹
FeCl ₃	0,2 mg·L ⁻¹
MgSO ₄	0,4 mg·L ⁻¹
Na ₂ MoO ₄ ·2H ₂ O	0,2 mg·L ⁻¹
ZnSO ₄	0,4 mg·L ⁻¹

Table 4-12 Composition of media used in *P. pastoris* batch culture.

Compound	Concentration
Glucose·H ₂ O	22 g·L ⁻¹
KH ₂ PO ₄	42,9 g·L ⁻¹
(NH ₄) ₂ SO ₄	5 g·L ⁻¹
CaSO ₄ ·2H ₂ O	1 g·L ⁻¹
K ₂ SO ₄	14,3 g·L ⁻¹
MgSO ₄ ·7H ₂ O	11,7 g·L ⁻¹
CuSO ₄ ·5H ₂ O	8 mg·L ⁻¹
NaI	0,32 mg·L ⁻¹
MnSO ₄ ·H ₂ O	12 mg·L ⁻¹
Na ₂ MoO ₄ ·2H ₂ O	0,8 mg·L ⁻¹
H ₃ BO ₃	0,08 mg·L ⁻¹
CaSO ₄ ·2H ₂ O	2 mg·L ⁻¹
CoCl ₂	2 mg·L ⁻¹
ZnCl ₂	28 mg·L ⁻¹
FeSO ₄ ·7	88 mg·L ⁻¹
Biotin	0,8 mg·L ⁻¹

4.9.4 Fermentation systems

The inoculum of both yeast were cultured in 1000 mL sterile glass erlenmeyer with a working volume of 200 mL, incubated at 30°C (Steri-cult 2000 Incubator, Forma Scientific) using the media described in section 4.9.3. Moreover, the erlenmeyers were continuously agitated at 130 rpm on an orbital shaking platform (Shaker orbital Incubator, Sanyo).

4.9.5 Bioreactor cell culture

The stirred-tank bioreactor used in the present study was a commercial bioreactor (Biostat B, from Sartorius Stedim Biotech, Germany) with 2L-cylindrical jacketed vessel, equipped with probes and control systems for pH, D.O. (relative oxygen partial pressure) and temperature, stirred with two Rushton impellers.

The control systems of the before mentioned variables, moreover, it has to be taken into consideration that culture conditions for batch yeast were the same and are described down below:

- Dissolved oxygen concentration was monitored with a polarographic probe (Oxyferm, Hamilton), and maintained at 30% of saturation by means of an aeration flow using a sparger of 0,5 VVM together with a cascade control system based on a stirring control system and a gas mixing unit.
- Temperature was maintained at 30°C by switch between a heat exchanger when heat was needed and with a cooling water system when cold was needed.
- pH was measured with a standard electrode (EasyFerm Plus, Hamilton), and it was maintained at 5,5 if required a HCl 2M (Panreac) addition, and a subsequently addition of NaOH (300g·L⁻¹) (Panreac).

The working volume for the batch cultures was 2L, and for the continuous culture was 2L as well.

4.9.6 MFCS/win. Software for Data Acquisition, Monitoring and Control

BioPat® MFCS/win 3.0 (Sartorius Stedim Biotech, Germany) was used for monitoring and controlling all the physiological variables (pH, temperature, aeration and agitation) of the batch and continuous cultures. Moreover, the implementation of the OUR and CER calculation were carried using the algorithms presented in **chapter 3** section 3.8.8.

4.9.7 Analytical methods

Cell mass was determined using a spectrophotometer at 550 nm by light scattering and by dry cell weight calculation using a general equation from an average *S. cerevisiae* (Lecina, 2007) according to **Equation 4-6**.

Equation 4-6

$$1 \text{ gDCW} \cdot \text{L}^{-1} = 0,19 \text{ DO}_{550} + 0,018$$

On the other hand, regarding *P. pastoris*, cell mass was determined using a spectrophotometer at 550 nm by light scattering and by dry cell weight calculation using a general equation from an average *P. pastoris* (Lecina, 2007) according to **Equation 4-7**.

Equation 4-7

$$1 \text{ gDCW} \cdot \text{L}^{-1} = 0,22 \cdot \text{DO}_{550}$$

After cell counting, the remainder of each sample was centrifuged (6000 g for 5 min) and filtered with a filter of 0,45 µm of diameter to remove the cells, and the supernatant was frozen for further analysis.

4.9.8 Metabolite measurements

Glucose concentrations were determined with an YSI 2700 automated glucose and lactate analyser (YSI, 2000). Moreover, glucose, ethanol and glycerol concentrations were measured by HPLC as described in (Sanfeliu Sabater, 1995)

Oxygen and Carbon dioxide concentrations were determined with the analytical device BlueinOne Cell (BlueSens gas sensor GmbH) whose measuring principle is infrared IR for carbon dioxide and a galvanic cell for oxygen (Mueller & Schmale, 2004).

4.9.9 Oxygen uptake rate (OUR) and Carbon exchange rate (CER)

All the description in relation with the calculation of OUR and CER are described in **chapter 3** section 3.8.8

4.9.10 Specific rate calculations in batch cultures

All the description in relation with the calculation of specific rates in batch cultures are described in **chapter 3** section 3.8.9

4.9.11 Specific rate calculations in continuous cultures

All the description in relation with the calculation of specific rates in continuous cultures are described in **chapter 3** section 3.8.10

4.9.12 Reduced genome-scale metabolic model

In this study, we used a reduced genome scale metabolic model published by (Jol et al., 2012). This model is free available from the supplementary data of the article mentioned before.

The model was derived from the complete *S. cerevisiae* genome-scale metabolic model iND 750 by means of isolating the core central carbon metabolism (Jol et al., 2012).

It is important to point out that the selected metabolic model was used for performing the flux balance analysis for *S. cerevisiae* and *P. pastoris*. Even though the core carbon metabolism was the same for both yeasts, each one had an independent biomass equation.

In the case of *S. cerevisiae*, the selected biomass equation was the one described in the publication Jol et al. 2012 (Jol et al., 2012). On the other hand, regarding *P. pastoris* metabolic model, the biomass equation used was from the publication Chung et. All, 2010 (Chung et al., 2010). Moreover, regarding the biomass incorporation in the model, the biomass compounds of both equation were the same, although the stoichiometric coefficients used were the ones selected from its own biomass equation.

Moreover, two internal metabolites were eliminated from the *P. pastoris* model owing to they were not used in the biomass equation,

Moreover, the main differences between the *S. cerevisiae* reduced model, the *P. pastoris* reduced one and the original one iND750 are shown in **Table 4-13**.

Table 4-13 main properties of the genome scale metabolic model iAF1260 and the reduced iAF1260 by means of the reduction algorithm described in (Erdreich et al., 2015) .

	iND750 model	Reduced model
Reactions	1149	230
Internal metabolites	943	206
External metabolites	116	14
Degrees of freedom	207	18

Moreover, the reduced model was revised looking for errors in reversibility of reactions, main reaction directions and some software script incompatibilities between the sbml model and OptFlux program (Rocha et al., 2010).

A list of all included metabolites and reactions in the model are detailed in **Appendix**. Reactions fluxes over the metabolic network are presented in $\text{mmols}\cdot\text{gDCW}^{-1}\cdot\text{h}^{-1}$.

4.9.13 Flux Balance Analysis protocol

4.9.13.1 Mathematical basis

The mathematical algorithms used to perform a FBA is described in **chapter 3** section 3.8.12.1

4.9.13.2 Flux calculation

Flux Balance Analysis (FBA) was performed for obtaining the flux value of all the reactions included in the reduced genome scale metabolic model. The general constraints contained in the model are the stoichiometric coefficients of each reaction, the reactions reversibility and the energy requirement for the biomass generation.

Nevertheless, as usual in FBA with genomic models, the system is underdetermined and there exist degrees of freedom. In this case, regarding the *S. cerevisiae* model, the system has 235 reactions fluxes, 220 balance equations, as a result the system have 18 degrees of freedom. While in the *P. pastoris* model, the system has 235 reactions fluxes, 219 balance equations, as a result the system have 20 degrees of freedom.

Therefore, to perform FBA is necessary to add external measured fluxes as additional constraints (**Table 4-14**). In this case it has been added 15 measured fluxes in total, but again it must to be account that some fluxes are linearly dependent each other. With these measured fluxes and regarding the FBA solution for *S. cerevisiae* and *P. pastoris*, the system has 5 and 7 degrees of freedom, respectively, therefore it has a large space of possibility solutions. To find the optimal state, FBA uses the optimization of a certain objective function, in this case the cytoplasmatic hydrolysis of ATP.

Flux Balance Analysis (FBA) was performed using freely available software OptFlux (SilicoLife) as described in (Rocha et al., 2010).

Table 4-14 . Chosen metabolites as external measured fluxes in the reduced genomic scale metabolic model used.

External measured fluxes
Acetate
Ammonium
Biomass
Carbon dioxide
Ethanol
Glucose
Glycerol
Inorganic phosphate
Oxygen
Proton
Pyruvate
Succinate
Sulphate
Water

4.9.14 Model visualization

Model visualization has been made using commercially available software Omix Visualization (Omix Visualization GmbH & Co. KG) as described in (Droste et al., 2013)

The representation of the principal metabolism has four groups which are detailed in the following list:

1. The glycolytic pathway, which is related to the catabolism of glucose to pyruvate (light blue colour)
2. The pentose phosphate pathway, whose function is mainly the generation of biosynthesis precursors based on nitrogen bases (dark blue colour)
3. The ethanol pathway, which leads to the generation of ethanol (light yellow colour)
4. The glycerol pathway, which leads to the generation of glycerol (dark yellow colour)
5. The TCA cycle, which is related to catabolism of acetyl-CoA to carbon dioxide and NADH (green colour).

6. The malate-aspartate shuttle, which is related to the electron transport from cytoplasm to mitochondria (red colour).

4.9.15 Statistics

Duplicates for each culture conditions were performed, but only one of the repetitions is presented in the Results section. Since the runs have not performed in parallel (due to equipment limitations), sampling time do not coincide and also other parameters may vary as the cell seeding density.

4.10 References

- Aiba, S., Nagai, S., & Nishizawa, Y. (1976). Fed batch culture of *Saccharomyces cerevisiae*: A perspective of computer control to enhance the productivity in baker's yeast cultivation. *Biotechnology and Bioengineering*, 18(7), 1001–1016. <https://doi.org/10.1002/bit.260180712>
- Anraku, Y., & Gennis, R. B. (1987). The aerobic respiratory chain of *Escherichia coli*. *Trends in Biochemical Sciences*, 12(C), 262–266. [https://doi.org/10.1016/0968-0004\(87\)90131-9](https://doi.org/10.1016/0968-0004(87)90131-9)
- Boles, E., Zimmermann, F. K., & Heinisch, J. (1993). Different signals control the activation of glycolysis in the yeast *Saccharomyces cerevisiae*. *Yeast*, 9(7), 761–770. <https://doi.org/10.1002/yea.320090710>
- Chaban, Y., Boekema, E. J., & Dudkina, N. V. (2014). Structures of mitochondrial oxidative phosphorylation supercomplexes and mechanisms for their stabilisation. *Biochimica et Biophysica Acta - Bioenergetics*, 1837(4), 418–426. <https://doi.org/10.1016/j.bbabi.2013.10.004>
- Chung, B. K. S., Selvarasu, S., Andrea, C., Ryu, J., Lee, H., Ahn, J., Lee, H., & Lee, D. Y. (2010). Genome-scale metabolic reconstruction and in silico analysis of methylotrophic yeast *Pichia pastoris* for strain improvement. *Microbial Cell Factories*, 9, 1–15. <https://doi.org/10.1186/1475-2859-9-50>
- Cronwright, G. R., Rohwer, J. M., & Prior, B. A. (2002). Metabolic Control Analysis of Glycerol Synthesis in *Saccharomyces cerevisiae*. *Applied and Environmental Microbiology*, 68(9), 4448–4456. <https://doi.org/10.1128/AEM.68.9.4448-4456.2002>
- Dai, Z., Huang, M., Chen, Y., Siewers, V., & Nielsen, J. (2018). Global rewiring of cellular metabolism renders *Saccharomyces cerevisiae* Crabtree negative. *Nature Communications*, 9(1), 3059. <https://doi.org/10.1038/s41467-018-05409-9>
- De Deken, R. H. (1966). The Crabtree effect: a regulatory system in yeast. *Journal of General Microbiology*, 44(2), 149–156. <https://doi.org/10.1099/00221287-44-2-149>
- Droste, P., Nöh, K., & Wiechert, W. (2013). Omix - A visualization tool for metabolic networks with highest usability and customizability in focus. *Chemie-Ingenieur-Technik*, 85(6), 849–862. <https://doi.org/10.1002/cite.201200234>
- Dueñas-Sánchez, R., Gutiérrez, G., Rincón, A. M., Codón, A. C., & Benítez, T. (2012). Transcriptional regulation of fermentative and respiratory metabolism in *Saccharomyces cerevisiae* industrial bakers' strains. *FEMS Yeast Research*, 12(6), 625–636. <https://doi.org/10.1111/j.1567-1364.2012.00813.x>
- Easlon, E., Tsang, F., Skinner, C., Wang, C., & Lin, S.-J. (2008). The malate-aspartate NADH shuttle components are novel metabolic longevity regulators required for calorie restriction-mediated life span extension in yeast. *Genes & Development*, 22(7), 931–944. <https://doi.org/10.1101/gad.1648308>
- Erdrich, P., Steuer, R., & Klamt, S. (2015). An algorithm for the reduction of genome-scale metabolic network models to meaningful core models. *BMC Systems Biology*, 1–12. <https://doi.org/10.1186/s12918-015-0191-x>
- Farmer, W. R., & Liao, J. C. (1997). Reduction of aerobic acetate production by *Escherichia coli*. *Applied and Environmental Microbiology*, 63(8), 3205–3210.
- Hagman, A., & Piškur, J. (2015). A Study on the Fundamental Mechanism and the Evolutionary Driving Forces behind Aerobic Fermentation in Yeast. *PLOS ONE*, 10(1), e0116942. <https://doi.org/10.1371/journal.pone.0116942>
- Hagman, A., Säll, T., & Piškur, J. (2014). Analysis of the yeast short-term Crabtree effect and its origin. *FEBS Journal*, 281(21), 4805–4814. <https://doi.org/10.1111/febs.13019>
- Hess, B., & Sossinka, J. (1974). Pyruvate kinase of yeast - Properties and crystals. *Die Naturwissenschaften*, 61(3), 122–124. <https://doi.org/10.1007/BF00606281>

- Hoehler, T. M., & Jørgensen, B. B. (2013). Microbial life under extreme energy limitation. *Nature Reviews Microbiology*, 11(2), 83–94. <https://doi.org/10.1038/nrmicro2939>
- Hu, X. H., Wang, M. H., Tan, T., Li, J. R., Yang, H., Leach, L., Zhang, R. M., & Luo, Z. W. (2007). Genetic dissection of ethanol tolerance in the budding yeast *Saccharomyces cerevisiae*. *Genetics*, 175(3), 1479–1487. <https://doi.org/10.1534/genetics.106.065292>
- Jol, S. J., Kümmel, A., Terzer, M., Stelling, J., & Heinemann, M. (2012). System-level insights into yeast metabolism by thermodynamic analysis of elementary flux modes. *PLoS Computational Biology*, 8(3), 1–9. <https://doi.org/10.1371/journal.pcbi.1002415>
- Jonckheere, A. I., Smeitink, J. A. M., & Rodenburg, R. J. T. (2012). Mitochondrial ATP synthase: Architecture, function and pathology. *Journal of Inherited Metabolic Disease*, 35(2), 211–225. <https://doi.org/10.1007/s10545-011-9382-9>
- Kachrimanidou, V., Vlysidis, A., Kopsahelis, N., & Kookos, I. K. (2020). Increasing the volumetric productivity of fermentative ethanol production using a fed-batch vacuform process. *Biomass Conversion and Biorefinery*. <https://doi.org/10.1007/s13399-020-00673-6>
- Kubota, S., Takeo, I., Kume, K., Kanai, M., Shitamukai, A., Mizunuma, M., Miyakawa, T., Shimoi, H., Iefuji, H., & Hirata, D. (2004). Effect of ethanol on cell growth of budding yeast: Genes that are important for cell growth in the presence of ethanol. *Bioscience, Biotechnology and Biochemistry*, 68(4), 968–972. <https://doi.org/10.1271/bbb.68.968>
- Lagunas, R. (1993). Sugar transport in *Saccharomyces cerevisiae*. *FEMS Microbiology Letters*, 104(3–4), 229–242. <https://doi.org/10.1111/j.1574-6968.1993.tb05869.x>
- Lecina, M. (2007). *Anàlisi d'alternatives per a un bioprocés de producció d'una vacuna animal*.
- Lever, M. A., Rogers, K. L., Lloyd, K. G., Overmann, J., Schink, B., Thauer, R. K., Hoehler, T. M., & Jørgensen, B. B. (2015). Life under extreme energy limitation: a synthesis of laboratory- and field-based investigations. *FEMS Microbiology Reviews*, 39(5), 688–728. <https://doi.org/10.1093/femsre/fuv020>
- Maconi, E., Griffini, A., Cavazzoni, V., & Aragazzini, F. (1988). Reduction of acetaldehyde to ethanol by some micro-organisms and its stereospecificity. *The Biochemical Journal*, 250(3), 929–932. <https://doi.org/10.1042/bj2500929>
- Manners, D. J., Masson, A. J., & Patterson, J. C. (1973). The structure of a β -(1 \rightarrow 3)-d-glucan from yeast cell walls. *Biochemical Journal*, 135(1), 19–30. <https://doi.org/10.1042/bj1350019>
- Mattanovich, D., Graf, A., Stadlmann, J., Dragosits, M., Redl, A., Maurer, M., Kleinheinz, M., Sauer, M., Altmann, F., & Gasser, B. (2009). Genome, secretome and glucose transport highlight unique features of the protein production host *Pichia pastoris*. *Microbial Cell Factories*, 8, 1–13. <https://doi.org/10.1186/1475-2859-8-29>
- Mendoza-Vega, O., Sabatié, J., & Brown, S. W. (1994). Industrial production of heterologous proteins by fed-batch cultures of the yeast *Saccharomyces cerevisiae*. *FEMS Microbiology Reviews*, 15(4), 369–410. [https://doi.org/10.1016/0168-6445\(94\)90070-1](https://doi.org/10.1016/0168-6445(94)90070-1)
- Mota, M., Strehano, P., & Goma, G. (1984). STUDIES ON CONJUGATE EFFECTS OF SUBSTRATE (GLUCOSE) AND PRODUCT (ETHANOL) ON CELL GROWTH KINETICS DURING FERMENTATION OF DIFFERENT YEAST STRAINS. *Journal of the Institute of Brewing*, 90(6), 359–362. <https://doi.org/10.1002/j.2050-0416.1984.tb04289.x>
- Mueller, H., & Schmale, U. (2004). Chap 3. Product description. In *BlueinOne Cell: operating manual* (pp. 6–9).
- Navarrete, C., Nielsen, J., & Siewers, V. (2014). Enhanced ethanol production and reduced glycerol formation in *fps1Δ* mutants of *Saccharomyces cerevisiae* engineered for improved redox balancing. *AMB Express*, 4(1), 86. <https://doi.org/10.1186/s13568-014-0086-z>

- Ozcan, S., & Johnston, M. (1995). Three different regulatory mechanisms enable yeast hexose transporter (HXT) genes to be induced by different levels of glucose. *Molecular and Cellular Biology*, 15(3), 1564–1572. <https://doi.org/10.1128/MCB.15.3.1564>
- Parks, R. E., & Aganwal, R. P. (1973). Nucleoside Diphosphokinases. *Enzymes*, 8(C), 307–333. [https://doi.org/10.1016/S1874-6047\(08\)60069-4](https://doi.org/10.1016/S1874-6047(08)60069-4)
- Postma, E., Verduyn, C., Scheffers, W. A., & Van Dijken, J. P. (1989). Enzymic analysis of the crabtree effect in glucose-limited chemostat cultures of *Saccharomyces cerevisiae*. *Applied and Environmental Microbiology*, 55(2), 468–477. <https://doi.org/10.1128/aem.55.2.468-477.1989>
- Prielhofer, R., Cartwright, S. P., Graf, A. B., Valli, M., Bill, R. M., Mattanovich, D., & Gasser, B. (2015). *Pichia pastoris* regulates its gene-specific response to different carbon sources at the transcriptional, rather than the translational, level. *BMC Genomics*, 16(1), 1–17. <https://doi.org/10.1186/s12864-015-1393-8>
- Randez-Gil, F., Herrero, P., Sanz, P., Prieto, J. A., & Moreno, F. (1998). Hexokinase PII has a double cytosolic-nuclear localisation in *Saccharomyces cerevisiae*. *FEBS Letters*, 425(3), 475–478. [https://doi.org/10.1016/S0014-5793\(98\)00289-0](https://doi.org/10.1016/S0014-5793(98)00289-0)
- Roberts, G. G., & Hudson, A. P. (2006). Transcriptome profiling of *Saccharomyces cerevisiae* during a transition from fermentative to glycerol-based respiratory growth reveals extensive metabolic and structural remodeling. *Molecular Genetics and Genomics*, 276(2), 170–186. <https://doi.org/10.1007/s00438-006-0133-9>
- Rocha, I., Maia, P., Evangelista, P., Vilaça, P., Soares, S., P Pinto, J., Nielsen, J., R patil, K., C ferreira, E., & Rocha, Mi. (2010). *OptFlux: an open-source software platform for*.
- Rolland, F., Winderickx, J., & Thevelein, J. M. (2002). Glucose-sensing and -signalling mechanisms in yeast. *FEMS Yeast Research*, 2(2), 183–201. [https://doi.org/10.1016/S1567-1356\(02\)00046-6](https://doi.org/10.1016/S1567-1356(02)00046-6)
- Sanfeliu Sabater, A. (1995). *Producció d'anitcossos monoclonals mitjançant el cultiu invitro d'hibridomes en bioreactors:Anàlisis de la fisiologia i metabolisme cel·lulars*.
- Schaepe, S., Kuprijanov, A., Simutis, R., & Lübbert, A. (2014). Avoiding overfeeding in high cell density fed-batch cultures of *E. coli* during the production of heterologous proteins. *Journal of Biotechnology*, 192, 146–153. <https://doi.org/10.1016/j.jbiotec.2014.09.002>
- Shah, A. R., Singhal, M., Klicker, K. R., Stephan, E. G., Wiley, H. S., & Waters, K. M. (2007). Enabling high-throughput data management for systems biology: The Bioinformatics Resource Manager. *Bioinformatics*, 23(7), 906–909. <https://doi.org/10.1093/bioinformatics/btm031>
- Stanley, D., Bandara, A., Fraser, S., Chambers, P. J., & Stanley, G. A. (2010). The ethanol stress response and ethanol tolerance of *Saccharomyces cerevisiae*. *Journal of Applied Microbiology*, 109(1), 13–24. <https://doi.org/10.1111/j.1365-2672.2009.04657.x>
- Urniezius, R., Survyla, A., Paulauskas, D., Bumelis, V. A., & Galvanauskas, V. (2019). Generic estimator of biomass concentration for *Escherichia coli* and *Saccharomyces cerevisiae* fed-batch cultures based on cumulative oxygen consumption rate. *Microbial Cell Factories*, 18(1), 1–17. <https://doi.org/10.1186/s12934-019-1241-7>
- van Bodegom, P. (2007). Microbial Maintenance: A Critical Review on Its Quantification. *Microbial Ecology*, 53(4), 513–523. <https://doi.org/10.1007/s00248-006-9049-5>
- Vemuri, G. N., Eiteman, M. A., McEwen, J. E., Olsson, L., & Nielsen, J. (2007). Increasing NADH oxidation reduces overflow metabolism in *Saccharomyces cerevisiae*. *Proceedings of the National Academy of Sciences of the United States of America*, 104(7), 2402–2407. <https://doi.org/10.1073/pnas.0607469104>
- Verduyn, C., Postma, E., Scheffers, W. A., & Van Dijken, J. P. (1990). Physiology of *Saccharomyces cerevisiae* in anaerobic glucose-limited chemostat cultures. *Journal of General Microbiology*, 136(3), 395–403. <https://doi.org/10.1099/00221287-136-3-395>

- Walker, G. M. (2009). Yeasts. In *In Desk Encyclopedia of Microbiology, 2nd ed.* Elsevier/Academic Press.
<https://rke.abertay.ac.uk/files/8488900/WalkerDeskEncyclopedia2009-Yeasts.pdf>
- Watson, H. C., Walker, N. P., Shaw, P. J., Bryant, T. N., Wendell, P. L., Fothergill, L. A., Perkins, R. E., Conroy, S. C., Dobson, M. J., & Tuite, M. F. (1982). Sequence and structure of yeast phosphoglycerate kinase. *The EMBO Journal*, 1(12), 1635–1640. <https://doi.org/10.1002/j.1460-2075.1982.tb01366.x>
- Wills, C., Benhaim, P., & Martin, T. (1984). Effects of mutants and inhibitors on mitochondrial transport systems in vivo in yeast. *Biochimica et Biophysica Acta (BBA) - Biomembranes*, 778(1), 57–66.
[https://doi.org/10.1016/0005-2736\(84\)90447-4](https://doi.org/10.1016/0005-2736(84)90447-4)
- YSI. (2000). *YSI 2700 - operational manual*.
<https://www.ysi.com/search?k=ysi+2700+biochemistry+analyzer>

5 Physiology and metabolism of animal cells

5.1 Nomenclature

mgDCW: dry cell weight ($\text{mg} \cdot \text{L}^{-1}$)

OUR: oxygen uptake rate ($\text{mM} \cdot \text{h}^{-1}$)

X_v : biomass concentration ($\text{gDCW} \cdot \text{L}^{-1}$)

q_m : specific rate of metabolite m ($\text{mmol} \cdot \text{gDCW}^{-1} \cdot \text{h}^{-1}$)

t: time (h)

C_j : concentration of metabolite j ($\text{g} \cdot \text{L}^{-1}$) (mM)

$C_{\text{outlet},m}$: concentration of metabolite m in the outlet flow ($\text{g} \cdot \text{L}^{-1}$)

$C_{\text{inlet},m}$: concentration of metabolite m in the inlet flow ($\text{g} \cdot \text{L}^{-1}$)

μ : specific growth rate (h^{-1})

$Y_{a/b}$: yield of A regarding B ($\text{g}_a \cdot \text{g}_b^{-1}$)

TCA: tricarboxylic acid

FBA: flux balance analysis

OP: Oxidative Phosphorylation

NADH: nicotinamide adenine dinucleotide reduced form

NAD⁺: nicotinamide adenine dinucleotide oxidized form

ATP: adenosine triphosphate

ADP: adenosine diphosphate

5.2 Introduction

One of the most used expression platforms responsible for the production of heterologous proteins whose pharmaceutical activity is based on a specific post-translational modification are the animal cell lines. One of the blockbuster products are the monoclonal antibodies, as it has been explained in the overall introduction. Over the last years its demand for monoclonal antibodies has severally increased, mainly for the new applications in therapy, but also for clinical diagnosis and highly specific purification processes (Walsh, 2018)(Grilo & Mantalaris, 2019).

As it was mentioned before, the capacity of mammalian cells to perform complex post-translational modifications to yield biologically active proteins has led them to be the preferred system for biopharmaceuticals production. About 70-80% of all biopharmaceuticals, including monoclonal antibodies, viral vaccines and gene therapy vectors are produced in mammalian cells; and among the top ten selling protein biopharmaceuticals in 2014, six are antibodies or antibody-derived proteins. Therefore, it is not surprising that monoclonal antibodies-based drugs production using mammalian cell-based systems in the 2016 reached almost the double of the 2010 value (Estes & Melville, 2013)(Walsh, 2018). In the last years, monoclonal antibodies industrial manufacturing has been based on mammalian cell lines such as CHO and hybridoma among others (Wurm, 2004)(Coco-Martin & Harmsen, 2008)(Estes & Melville, 2013).

Mammalian cell-based processes present an important limitation regarding apoptosis: the accumulation of metabolic by-products (i.e. lactate and ammonia) up to cytotoxic concentration as well as the depletion of essential nutrients, triggers the apoptosis (programmed cell death)(Arden & Betenbaugh, 2004). The prevention of apoptosis during the cell growth has a critical effect on final process productivity, as an increase of cell life-span results in an increase of product of interest synthesis and accumulation, since cells remain productive for a longer time even after the exponential cell growth phase (X. Zhang et al., 2018). Moreover, more robust cell lines less sensible to apoptosis allow the design of high cell density culture strategies based on keeping low nutrients concentration in narrower ranges(Casablanco, Gámez, et al., 2013).

In the last years, the strategies to generate stress-resistant cell lines preventing apoptosis have been focused on blocking the apoptotic transduction pathways (M. N. Henry et al., 2020). Although there are different pathways controlling the activation of signaling cascades of cell apoptosis activation, many of the apoptosis signals converge on the mitochondria, which stores numerous molecules that activate apoptosis (Arden & Betenbaugh, 2004). The most used

strategy to prevent apoptosis has been the overexpression of bcl-2 or bcl-xL genes, which inhibits the release of pro-apoptotic molecules from the mitochondria (Vives et al., 2003). This strategy has been successfully applied in different mammalian cell lines, as CHO or hybridoma, showing higher viabilities and improved robustness in cell culture (Fussenegger, Bailey, & Varner, 2000)(Mastrangelo, Hardwick, Zou, & Betenbaugh, 2000)(Tey, Singh, Piredda, Piacentini, & Al-Rubeai, 2000). Another approach has been the expression of different viral proteins has also been reported to have anti-apoptotic effects in hybridoma cell cultures, as ksbcl-2 from Kaposi's sarcoma-associated herpesvirus (Vives et al., 2003) and BHRF1 from Epstein-Barr virus (Juanola et al., 2009).

Additionally, anti-apoptotic genes have shown an effect on metabolism. However, this is not fully understood yet (Dorai et al., 2009)(Templeton et al., 2014). This is remarkable because cell-based processes present important limitations regarding the metabolism: deregulation substrates uptake (high consumption rates of mainly glucose and glutamine), linked to the secretion and accumulation of lactate and ammonia as by-products of the metabolism (Martínez-Monge et al., 2019)(Albiol et al., 2018).

The reduction of the secretion and accumulation of lactate remains a hot topic for biomanufacturing industry. Many different approaches have been explored to reduce or delay lactate generation in cell culture:

- Media design by substitution of glucose for alternative carbon sources like fructose or galactose (Altamirano, Illanes, Becerra, Cairó, & Gòdia, 2006)
- Different fed-batch strategies limiting glucose concentration (L. Zhang, Shen, & Zhang, 2004)(Casablanco, Gámez, et al., 2013)
- Several cell engineering approaches as the expression of pyruvate carboxylase (O. Henry & Durocher, 2011) or downregulation of lactate dehydrogenase (Chen, Liu, Xie, Sharp, & Wang, 2001).

In all the different scenarios described, a reduction of lactate accumulation up to a certain extend was observed, but never totally depleted. For a further analysis, the use of genomic-scale metabolic models have been a useful complement to obtain the representation of the carbon metabolic network (Martínez et al., 2013). As a result, how the lactate metabolism is affected by either genetic modifications or the media culture's modifications might be shed light on in order to develop strategies revolving around the conversion of glucose towards lactate.

5.3 Results (I) - Analysis of the physiological parameters for HEK293 and hybridoma KB26.5 when glucose is used as a carbon source.

The core of this section is to understand the carbon metabolism of two animal cell lines: a human cell line, the HEK293 and a murine cell line, the hybridoma KB26.5, through the analysis and modelling of a specific experimental conditions when glucose was used as a carbon source.

5.3.1 HEK293

First, the physiological behavior observed when glucose was used as carbon source will be described in regard with both cell lines. On this basis, the experimental settings defined in order to culture both cell lines were based on using a bioreactor as a containment culture system where every extracellular parameter can be controlled in order to ensure an optimal growth rate as shown in the section 5.8.4. In relation with the media used, both cell lines used its chemical defined media supplemented with 5% FBS where the main carbon source was glucose as shown in the section 5.8.2.

As observed in **Figure 5-1**, the first cell line to be analyzed was HEK293 growing on glucose.

As shown in the **graph A of Figure 5-1**, when it was cultured in a glucose-based media, the specific growth rate obtained was $0,028 \text{ h}^{-1}$ and it consumed $4,28 \text{ g}\cdot\text{L}^{-1}$ of glucose in order to achieve a cell concentration of $4,96\cdot 10^6 \text{ cell}\cdot\text{ml}^{-1}$ while $1,87 \text{ g}\cdot\text{L}^{-1}$ of lactate were produced. Moreover, as observed in **Table 5-1**, the carbon metabolism was not optimize to biomass production because for each gram of consumed glucose $0,43 \text{ g}$ of lactate was produced. Moreover, using the trend from glucose and lactate profiles over time in relation with the biomass, the specific rates were calculated. Where the specific consumption rate of glucose had a value of $650 \text{ (nmol}\cdot\text{mgDCW}^{-1}\cdot\text{h}^{-1})$, that lead to a lactate specific production rate of $950,25 \text{ nmol}\cdot\text{mgDCW}^{-1}\cdot\text{h}^{-1}$ while $0,042 \text{ mgDCW}\cdot\text{mgDCW}^{-1}\cdot\text{h}^{-1}$ were generated. On the other side, related to the oxidation of glucose, the specific consumption rate of oxygen had a value of $775,4 \text{ nmol}\cdot\text{mgDCW}^{-1}\cdot\text{h}^{-1}$ and it was calculated using the variable oxygen uptake rate (OUR) represented in **graph B of Figure 5-19**.

As a result, the carbon metabolism of HEK293 was characterized as a lactate producer where the 43 % of the consumed glucose was converted to lactate instead of biomass.

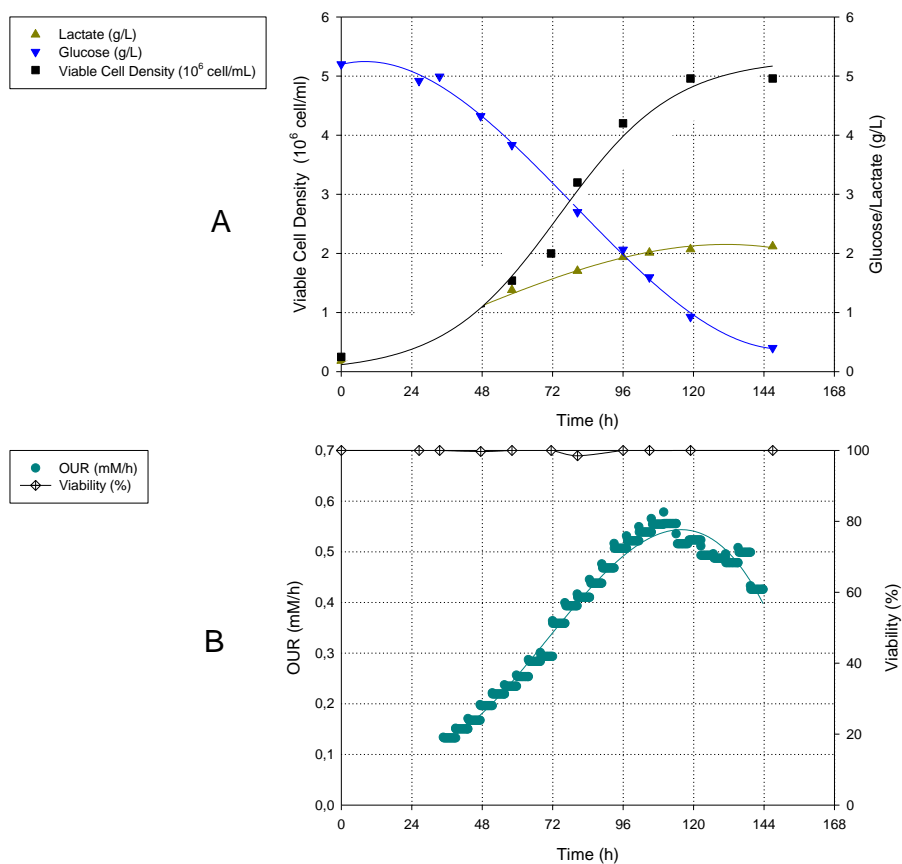


Figure 5-1 Profile of A) off-line variables such as Viable Cell Density (■), glucose (▼), lactate (▲) and B) an on-line variable such as O.U.R (●) and Viability (◇) for HEK293 batch culture using glucose as a carbon source.

Table 5-1 Main parameters for HEK293 batch culture using glucose as a carbon source.

Biomass achieved (10^6 cell/mL)	4,96
Glucose consumption (g/L)	4,28
Lactate production (g/L)	1,871
$Y_{\text{bio/gluc}}$ (10^6 cell/mL/g/L)	1,10
$Y_{\text{lac/gluc}}$ (g/g)	0,437
q_{glucose} ($\text{nmol} \cdot \text{mg}^{-1} \cdot \text{h}^{-1}$)	650,13
q_{lactate} ($\text{nmol} \cdot \text{mg}^{-1} \cdot \text{h}^{-1}$)	950,25
q_{O_2} ($\text{nmol} \cdot \text{mg}^{-1} \cdot \text{h}^{-1}$)	775,4
μ (h^{-1})	0,028

Therefore, the conversion of glucose to biomass was highly limited due to the lactate production. Once the HEK293 was studied, the description of the carbon metabolism of hybridoma KB26.5 will be analyzed in order to observe if both cell lines share the limitation in the conversion of glucose to biomass. Consequently, the physiological parameters of hybridoma KB26.5 growing on glucose are described below.

5.3.2 Hybridoma KB26.5

As shown in the **graph A of Figure 5-2**, when hybridoma KB 26.5 was cultured on glucose-based media, it had a specific growth rate of $0,033 \text{ h}^{-1}$ and consumed $2,97 \text{ g} \cdot \text{L}^{-1}$ of glucose in nearly 50 h, in order to achieve a maximum cell concentration of $2,2 \cdot 10^6 \text{ cell} \cdot \text{mL}^{-1}$ while producing $2,24 \text{ g} \cdot \text{L}^{-1}$ of lactate. Moreover, as presented in **Figure 5-2** in relation with how hybridoma KB 26.5 allocated glucose, 0,75 g of lactate was produced for each gram of consumed glucose. This was an inefficient carbon metabolism, where 75% of the carbon source was converted to lactate. Moreover, using the trend from both glucose and lactate profiles over time in relation with the biomass trend, their specific consumption and production rates were calculated (methodology calculation is described in section 5.8.7). The specific consumption rate of glucose had a value of $1200 \text{ nmol} \cdot \text{mgDCW}^{-1} \cdot \text{h}^{-1}$ that led to a lactate specific production rate of $2180 \text{ nmol} \cdot \text{mgDCW}^{-1} \cdot \text{h}^{-1}$ and a biomass generation of $0,033 \text{ mgDCW} \cdot \text{mgDCW}^{-1} \cdot \text{h}^{-1}$. On the other side, related to the oxidation of glucose, the specific consumption rate of oxygen had a value of $702 \text{ nmol} \cdot \text{mgDCW}^{-1} \cdot \text{h}^{-1}$ and it was calculated using the variable oxygen uptake rate (OUR) depicted in **graph B of Figure 5-2**, as described in section 5.8.6.

Another metabolic feature important was the fast decrease in the viability when glucose was almost depleted and non-growth conditions were achieved, as shown in **graph B of Figure 5-2**. There are several cell mechanisms responsible for its decrease, which can be grouped regarding the metabolic trigger of cell death. If its trigger is related to extreme environmental conditions, as physiological parameters like pH, temperature, osmotic pressure and others, necrosis is the cell mechanism responsible for cell death and the decrease in the viability. Whereas, when the physiological conditions are the optimal ones but a decrease in the viability occurs, apoptosis is the mechanism responsible for cell death.

Apoptosis is triggered when a growth-dependent media compound is depleted, such as glutamine or glucose (Fink & Cookson, 2005). Therefore, it can be hypothesized that based on the apoptosis mechanism was the cell mechanism responsible for the decrease in the viability when growth limiting conditions appeared owing to the depletion of a growth-dependent compound. Based on the data that have been analyzed up until now, it can be considered that

the hybridoma KB26.5 presented two metabolic issues: an inefficient carbon metabolism where only 25% of the carbon consumed was directed towards biomass synthesis and a highly sensible apoptosis response that is translated in a high cell death rate.

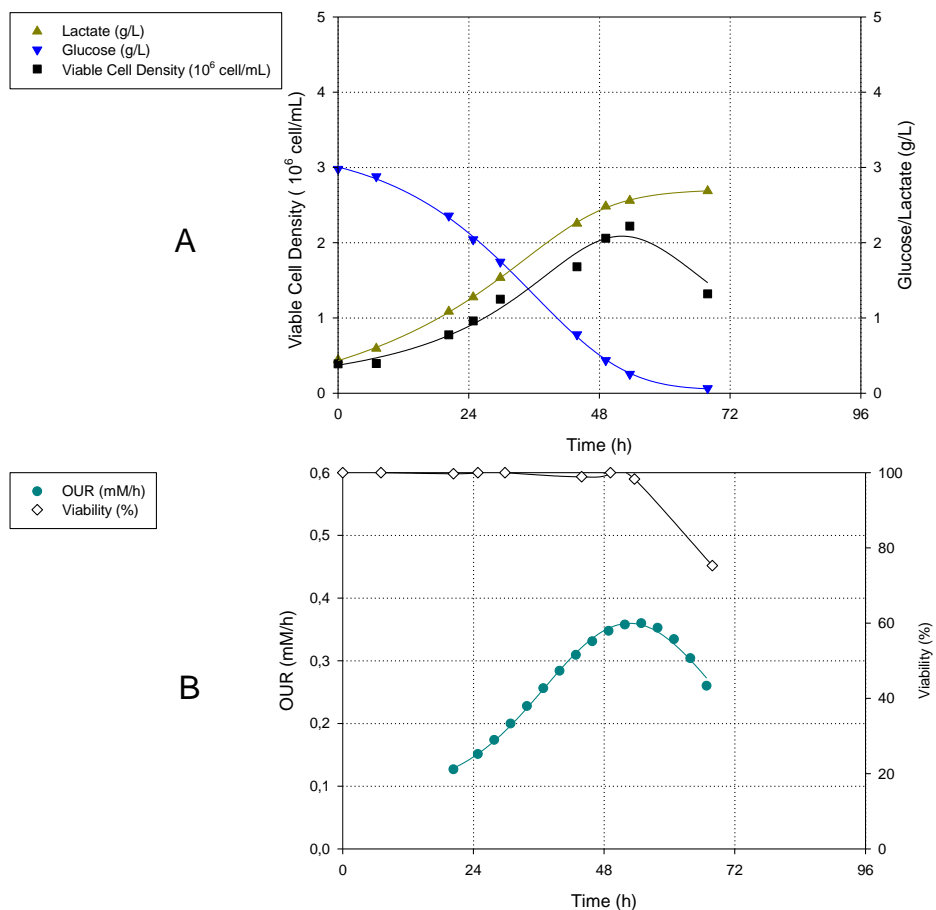


Figure 5-2 Profile of A) off-line variables such as Viable Cell Density (■), glucose (▼), lactate (▲) and B) the on-line variable OUR (●) and the off-line variable viability (◇) for hybridoma KB26.5 batch culture.

Table 5-2 Main characterization parameters for hybridoma KB26.5.

Biomass achieved ($10^6 \text{ cell} \cdot \text{mL}^{-1}$)	2,22
Glucose consumption ($\text{g} \cdot \text{L}^{-1}$)	2,97
Lactate production ($\text{g} \cdot \text{L}^{-1}$)	2,24
$Y_{\text{lac/gluc}}$ ($\text{g} \cdot \text{g}^{-1}$)	0,75
q_{glucose} ($\text{nmol} \cdot \text{mgDCW}^{-1} \cdot \text{h}^{-1}$)	1200
q_{lactate} ($\text{nmol} \cdot \text{mgDCW}^{-1} \cdot \text{h}^{-1}$)	2180
q_{O_2} ($\text{nmol} \cdot \text{mgDCW}^{-1} \cdot \text{h}^{-1}$)	702
μ (h^{-1})	0,033

Therefore, both cell line shared the same problem. An inefficient conversion of the carbon source to biomass owing to lactate production. Moreover, even if both cell lines shared the way that glucose is metabolized, the conversion of glucose to lactate in hybridoma KB26.5 was 32 % higher than the HEK293 one. This difference in the conversion of glucose to lactate should be explained if the consumption rate of glucose would have an effect on the lactate production. Because the highest lactate production was obtained with the cell line that had the highest glucose consumption rate. In this case, hybridoma KB26.5 should produce more lactate than HEK293 because the specific glucose consumption rate was higher.

On this basis and if it is taken into consideration that lactate is considered as a growth inhibitor (Marx, Mueller-Klieser, & Vaupel, 1988)(Hassell, Gleave, & Butler, 1991), it might be interesting to reduce the lactate production in order to increase the biomass produced and as a result, optimizing the carbon metabolism. However, before trying to solve the lactate problem it was important to comprehend it, so in the following section a metabolic model will be used in order to clarify and understand the lactate production and the difference in the lactate produced when both cell lines were cultured on glucose-based media. Therefore, in the following section, the carbon metabolism described will be the lactate production in HEK293 using a metabolic model.

5.4 Results (II) - Description of the HEK293 and hybridoma KB26.5 carbon metabolism by means of metabolic models

5.4.1 HEK293

5.4.1.1 Study of the HEK293 carbon metabolism by means of metabolic models

A genomic-scale metabolic model will be used in order to describe how HEK293 transformed glucose to lactate and precursors for biomass synthesis, while getting the required energy for growing at optimal growth rate. The development and description of the model is explained in section 5.8.4.

For metabolic flux calculation, the model was constrained using the input-output data of the corresponding metabolites that are shown in **Table 5-3**. This data included the biomass formation. The optimization of the model was performed by means of the FBA protocol

described in section 5.8.2, whose objective function to maximize was the cytoplasmatic hydrolysis of the ATP to ADP.

Table 5-3 Specific rates limits used as drains for the flux balance analysis methodology.

	q (nmol mgDCW ⁻¹ h ⁻¹)
L-Alanine	55,00 ± 1,65
L-Argininium	-24,00 ± -0,72
L-Asparagine	-20,00 ± -0,60
L-Aspartate	-22,03 ± -0,66
L-Cysteine	-3,82 ± -0,15
Glucose	-650,00 ± -19,50
L-Glutamine	-25,06 ± -0,50
L-Glutamate	-5,00 ± -0,20
L-Glycine	-0,50 ± -0,01
L-Histidine	-6,50 ± -0,32
L-Isoleucine	-29,30 ± -1,47
Lactate	950,00 ± 28,50
L-Leucine	-15,66 ± -0,63
L-Lysinium	-17,55 ± -0,18
L-Methionine	-4,39 ± -0,09
Ammonium	45,46 ± 0,91
Oxygen	-775,84 ± -7,76
L-Phenylalanine	-7,45 ± -0,07
L-Proline	-10,00 ± -0,40
L-Serine	-36,67 ± -0,73
L-Threonine	-8,97 ± -0,36
L-Tryptophan	-0,38 ± -0,02
L-Tyrosine	-4,58 ± -0,09
L-Valine	-26,00 ± -0,26
Biomass (10 ³)	28,70 ± 1,15

The intracellular fluxes were calculated using the visualization software OMIX (Droste, Nöh, & Wiechert, 2013), and then, **Figure 5-3** is presented. In this figure, the metabolic relation between glucose and lactate is displayed.

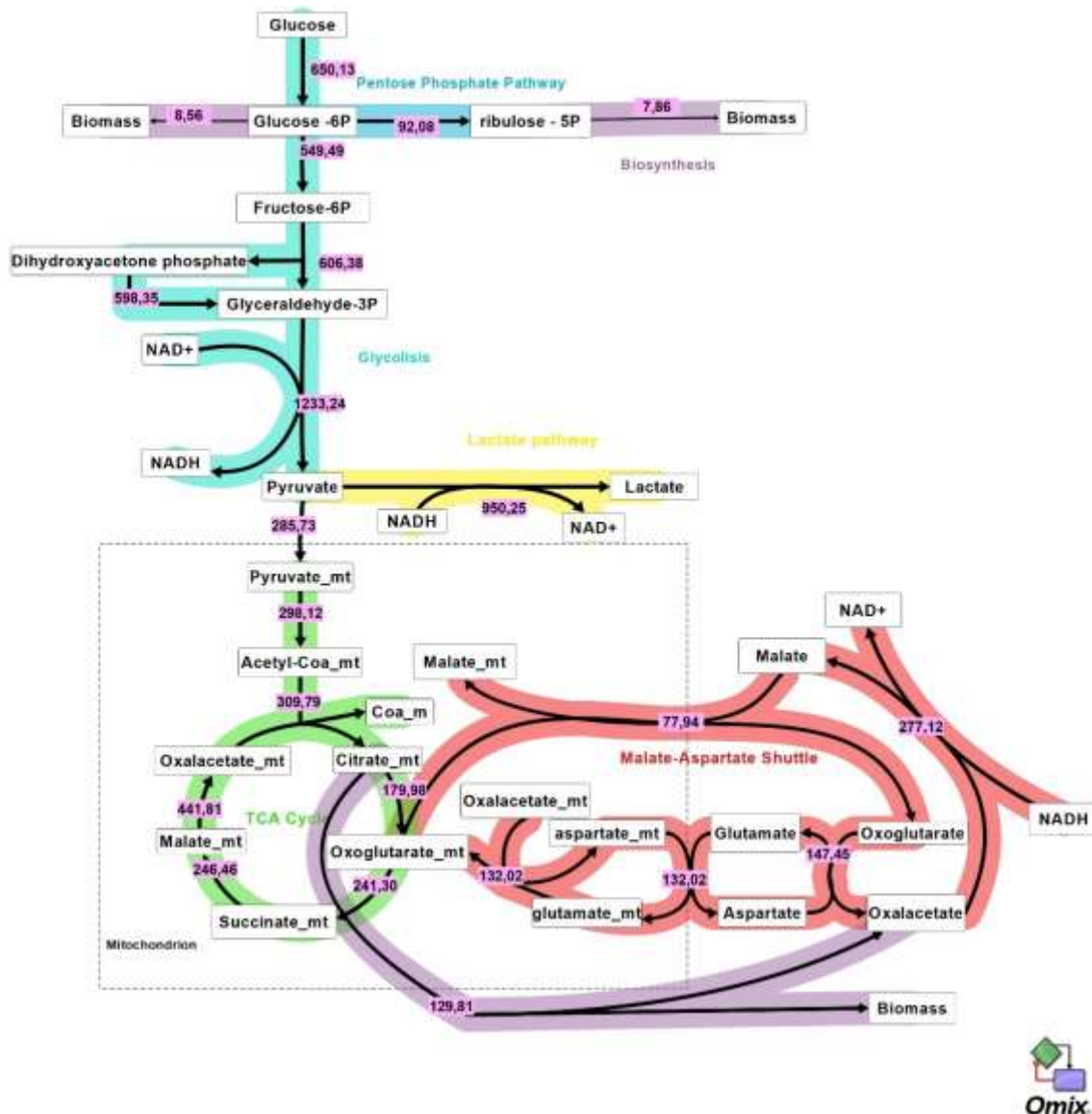


Figure 5-3 Scheme of the main metabolic fluxes calculated for HEK293 growing in Glucose Media. Arrows indicate the direction of the flux and their width the magnitude of fluxes (the exact value is detailed close to the arrows). All the fluxes are expressed in nmol-mgDCW⁻¹·h⁻¹.

Firstly, glucose was transported by facilitated diffusion through plasma membrane into the cytoplasm with a flux of 650,13 nmol-mgDCW⁻¹·h⁻¹, and then it was phosphorylated in order to get released glucose-6-phosphate via hexokinase-based reactions. The generation of glucose-6-phosphate has a flux of 650,13mmol-gDCW⁻¹·h⁻¹, and was directed into two different routes. 84,5% was directed to the glycolytic pathway through conversion to fructose-6-phosphate via the phosphoglucose isomerase reaction and 15,5 % was directed towards the formation of biosynthesis precursors, specifically, 8,5 % towards the formation of carbohydrate-related biomass compounds and plasmatic membrane compounds, and the rest (91,5 %) towards the formation of mainly nucleotides via the oxidative branch of the pentose-phosphate pathway.

Thereupon, the flux directed to glycolytic pathway ($549,49\text{nmol}\cdot\text{mgDCW}^{-1}\cdot\text{h}^{-1}$) reacts until glyceraldehyde-3 phosphate. Then, glyceraldehyde-3 phosphate reacts until pyruvate, where 20,9 % of the produced pyruvate can be transported through the mitochondrial membrane, while 77 % was reduced to lactate via lactate dehydrogenase.

The production of lactate was related to the fact that not all the NADH generated via glycolytic pathway can be oxidized in the mitochondria via its introduction to the organelle using the malate-aspartate shuttle, therefore an perturbation in the redox potential appeared caused by an unbalance related to cytoplasmic NADH. Consequently, in order to balance the NADH, lactate was produced. Therefore, only 22,4 % of the NADH produced by glycolytic pathway can be oxidized via malate-aspartate shuttle, while the 77 % of it has to be principally oxidized via reduction of pyruvate to lactate (73% of the glucose consumed).

On the other side, regarding the biomass formation, the main precursors are generated from ribulose-5P (derivation of 0,5 % of glucose carbon-mol uptake rate); glucose-6-phosphate (derivation of 1,33 % of glucose carbon-mol uptake rate); and citrate (derivation of 1,9 % of glucose carbon-mol uptake rate).

Therefore, the lactate production was related to an unbalance of cytoplasmic NADH from the glycolytic pathway due to a limitation in its regeneration. As a result, lactate was produced to reduce the cytoplasmic NADH that was unable to be regenerated via mitochondrial shuttle. Once the carbon metabolism has been analysed, it is important to realize that coupled with carbon metabolism appears energy metabolism. Therefore, to understand how the energy required for the synthesis of the precursors destined to biomass generation and cell maintenance was handled, the study of the energy metabolism will be shown in the following section.

5.4.1.2 Study of the HEK293 energy metabolism when glucose was used as a carbon source

In the previous section, a study of the central carbon metabolism was presented. It is important to realize that coupled with the carbon metabolism appears the energy metabolism. Therefore, to understand how the energy required for the synthesis of biomass precursors and cell maintenance is handled, the study of the energy metabolism will be described hereafter.

As shown in **graph A) of Figure 5-4**, and it was mentioned before, the proportion of the ATP produced mainly came from two sources: the first source of ATP comes from ATP synthase and

the second source of ATP comes at the substrate level phosphorylation, which is a reaction that takes part in glycolytic pathway in the cytoplasm. In aerobic conditions, and in compartmentalized cells (eukaryotic organisms), OP is described as the main source of ATP.

In the case of HEK293 growing on glucose, the ATP production by OP had more impact in ATP proportion than the substrate level phosphorylation due to the fact that only the 77 % of the NADH generated via glycolysis was oxidized by lactate dehydrogenase instead of being transported to the mitochondria via shuttle-based mechanism. Specifically, OP contributed in a 56,6 % of the total ATP produced while the contribution of the substrate level phosphorylation was 39,4%.

On the other side, **in graph B) of the Figure 5-4**, the proportion of ATP consumed showed an allocation of ATP mainly in cell maintenance, the reactions catalysed by phosphofructokinase and hexokinase proteins from the glycolytic and in the biomass generation pathway.

As previously mentioned, the cell maintenance tackles all the cellular process whose function is not related to formation of new cell material and in order to maintain its performance 64 % of the ATP produced was needed.

Regarding the reactions catalysed by kinases, nearly 22,19 % of the total ATP produced was mainly consumed by phosphofructokinase and hexokinase both from the glycolytic pathway. And finally, the last one of the main consuming ATP reactions is the biomass formation, whose ATP consumption was 13,77% of the ATP produced, although it has to be taken into consideration that the energy requirements for synthesis of biomass precursors are defined by the biomass equation.

Although, there are two points related to the energy metabolism that has to be pointed out:

1. The ATP produced from the oxidative phosphorylation had more contribution than the substrate level phosphorylation based on kinase-related reactions from to the glycolytic pathway.
2. In order to reach the optimal growth rate, the energetic requirements for cell maintenance (64 %) were higher than the required ones for the synthesis of new cellular material (13,77 %).

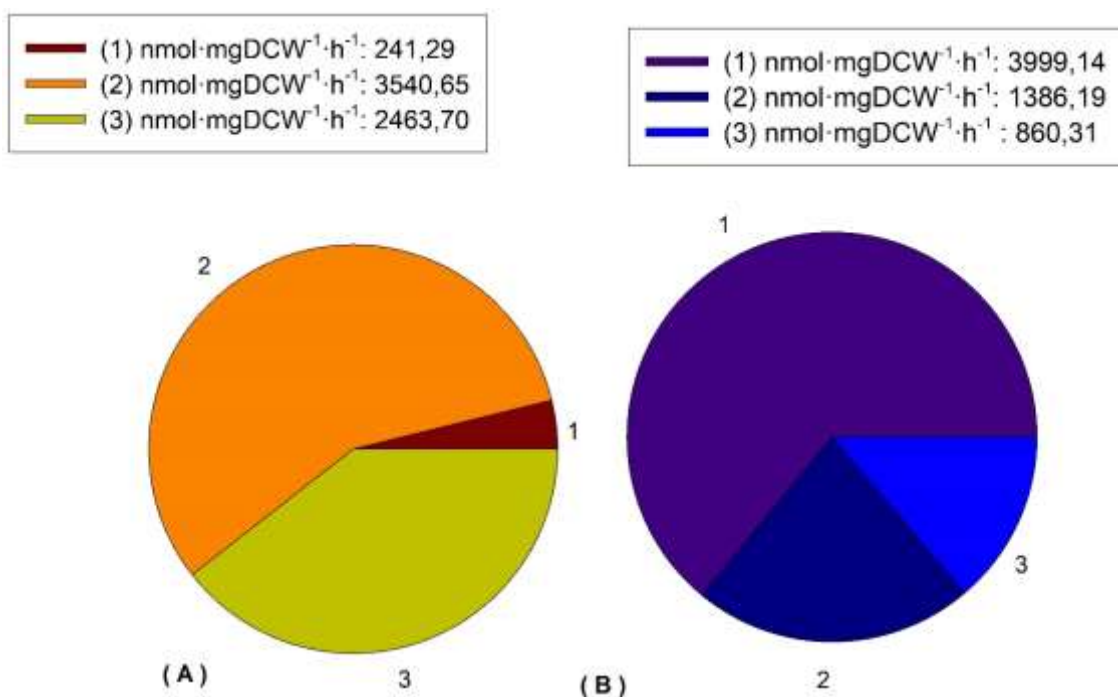


Figure 5-4 Distribution of ATP produced and consumed in HEK293 cultured on a culture's media where glucose was used as a carbon source. In figure A, the ATP produced is divided depending on its provenance (TCA cycle (1), Oxidative phosphorylation (2) and Glycolysis (3)). While in figure B, the ATP consumed is separated depending on its provenance (Cell maintenance (1), Glycolysis (2) and Biomass formation (3)).

To conclude, after the analysis of the carbon and energy metabolism, the main metabolic issue of HEK293 growing on glucose as a carbon source has been found to be related to an cytoplasmic NADH unbalance caused by the restrictions in its regeneration via mitochondrial shuttles. As a result, leading HEK293 to a metabolic state where mainly the NADH produced by glycolytic pathway was oxidized via lactate pathway instead of being transported via shuttle-based mechanisms from the cytoplasm to the mitochondria and then, oxidized via OP.

Once the HEK293 cultured on glucose has been analysed, a study of the hybridoma KB26.5 metabolic distribution will be carried out in the following section in order to describe the lactate metabolism. Moreover, it will be used to determine if the reason behind the lactate production is the same and if there is a relation between the conversion of glucose to lactate with the specific glucose consumption rate.

5.4.2 Hybridoma KB26.5

5.4.2.1 Study of hybridoma KB 26.5 carbon metabolism by means of using metabolic models

A genomic-scale metabolic model will be used in order to describe how hybridoma KB26.5 transforms glucose to lactate and precursors for biomass synthesis, while getting the required energy for growing at optimal growth rate. The development and description of the model is explained in section 5.8.8.

For metabolic flux calculation, the model was constrained using the input-output data of the corresponding metabolites that are shown in **Table 5-4**. This data included the biomass formation. The optimization of the model was performed by means of the FBA protocol described in section 5.8.9, whose objective function to maximize was the cytoplasmic hydrolysis of the ATP to ADP.

Table 5-4 Specific rate limits used as drains for a Flux Balance Analysis in hybridoma KB26.5 cell line (the fluxes are expressed in $\text{nmol} \cdot \text{mgDCW}^{-1} \cdot \text{h}^{-1}$).

	q ($\text{nmol} \cdot \text{mgDCW}^{-1} \cdot \text{h}^{-1}$)
$\mu (\cdot 10^3 \text{h}^{-1})$	35 ± 6
Glucose	$-933,44 \pm 134,56$
Lactate	$1435,5 \pm 348,74$
L-Alanine	$132,49 \pm 12,95$
L-Arginine	$-14,72 \pm 2,81$
L-Asparagine	$5,41 \pm 1,30$
L-Aspartic acid	$4,30 \pm 6,01$
L-Cysteine	$-5,02 \pm 2,11$
Glutamic acid	$7,85 \pm 0,26$
L-Glutamine	$-258,5 \pm 76,62$
L-Glycine	$-11,59 \pm 6,10$
L-Histidine	$-6,74 \pm 3,69$
L-Isoleucine	$-24,98 \pm 5,91$
L-Lactate	$1435,51 \pm 348,72$
L-Leucine	$-28,85 \pm 6,14$
L-Lysine	$-22,75 \pm 9,31$
L-Methionine	$-7,31 \pm 0,94$
Amonium	$156,13 \pm 11,06$
L-Phenylalanine	$-9,68 \pm 2,05$
L-Proline	$13,07 \pm 4,08$
L-Serine	$-15,14 \pm 6,18$
L-Threonine	$-16,88 \pm 3,21$
L-Tryptophan	$-2,58 \pm 3,29$
L-Tyrosine	$-8,34 \pm 1,83$
L-Valine	$-24,53 \pm 4,93$

The intracellular fluxes were calculated and presented using the visualization software OMIX (Droste et al., 2013) in **Figure 5-5**. In this figure, the metabolic relation between the main metabolites, and specially glucose and lactate is displayed.

Firstly, glucose is transported by facilitated diffusion through plasma membrane into the cytoplasm with a flux of $1027,80 \text{ nmol} \cdot \text{mgDCW}^{-1} \cdot \text{h}^{-1}$ (Plagemann & Richey, 1974), and then it is phosphorylated in order to get released glucose-6-phosphate via hexokinase-based reaction. The generation of glucose-6-phosphate has a flux of $1027,80 \text{ mmol} \cdot \text{gDCW}^{-1} \cdot \text{h}^{-1}$. Afterwards it was directed into two different routes the glycolytic pathway and the biomass formation. The 92,3% was directed to the glycolytic pathway through conversion to fructose-6-phosphate via the phosphoglucose isomerase reaction and 7,7 % was directed towards the formation of biosynthesis precursors. In the case of biomass formation, 66% towards the formation of carbohydrate-related biomass compounds and plasmatic membrane compounds, and the rest (34 %) towards the formation of mainly nucleotides via the oxidative branch of the pentose-phosphate pathway. Thereupon, the flux directed to glycolytic pathway ($1027,80 \text{ nmol} \cdot \text{mgDCW}^{-1} \cdot \text{h}^{-1}$) reacts until glyceraldehyde-3 phosphate. Then, glyceraldehyde-3 phosphate reacts until pyruvate, where only the 13,7% of the produced pyruvate can be transported through the mitochondrial membrane, while the rest (86,3%) is reduced to lactate via lactate dehydrogenase.

A key aspect of the hybridoma KB26.5 metabolism, as it has been discussed in 293HEK, is that the production of lactate was related to the fact that not all the NADH generated via glycolytic pathway could be oxidized in the mitochondria via its internalization through the malate-aspartate shuttle, therefore an unbalance related to NADH appeared. In order to grant a correct functionality of all the cellular processes a constant cytoplasmic redox potential was needed (Go & Jones, 2008). Its regulation is based on keeping a constant ratio between molecules a high redox activity, mainly the co-factors NAD and NADH (Xiao, Wang, Handy, & Loscalzo, 2018). On this basis, the lactate was produced to oxidize the accumulation of cytoplasmic NADH. As a result, only 10,1 % of the NADH produced by the glycolytic pathway can be oxidized via malate-aspartate shuttle, while the rest (89,9%) has to be principally oxidized via reduction of pyruvate to lactate (86,7% of the glucose consumed).

On this basis, it can be stated that the main metabolic trait responsible for this metabolic behaviour (the production of lactate while growing on glucose-based media in aerobic conditions) was related, also in this case, to an unbalance in the cytoplasmic NADH in order to

maintain a redox homeostasis. This unbalance was based on a rate difference between the flux through the glycolytic pathway and a limitation in the flux through the mitochondrial membrane shuttle responsible for the oxidation of the cytoplasmic NADH.

In the last decade, several studies pointed out the direct relation between the extracellular glucose concentration and the lactate production (Potter, Newport, & Morten, 2016a). On this basis, it could be stated that the lactate production might be related to the inability to regulate the flux through the glycolytic pathway when a high glucose flux through the plasma membrane is available. Therefore, the high flux through the glycolytic pathway was responsible for the high lactate generation and the waste of the carbon source.

Regarding the biomass formation, the main precursors are generated from ribulose-5P (derivation of 0,5 % of glucose carbon-mol uptake rate); glucose-6-phosphate (derivation of 1,33 % of glucose carbon-mol uptake rate); and citrate (derivation of 1,9 % of glucose carbon-mol uptake rate).

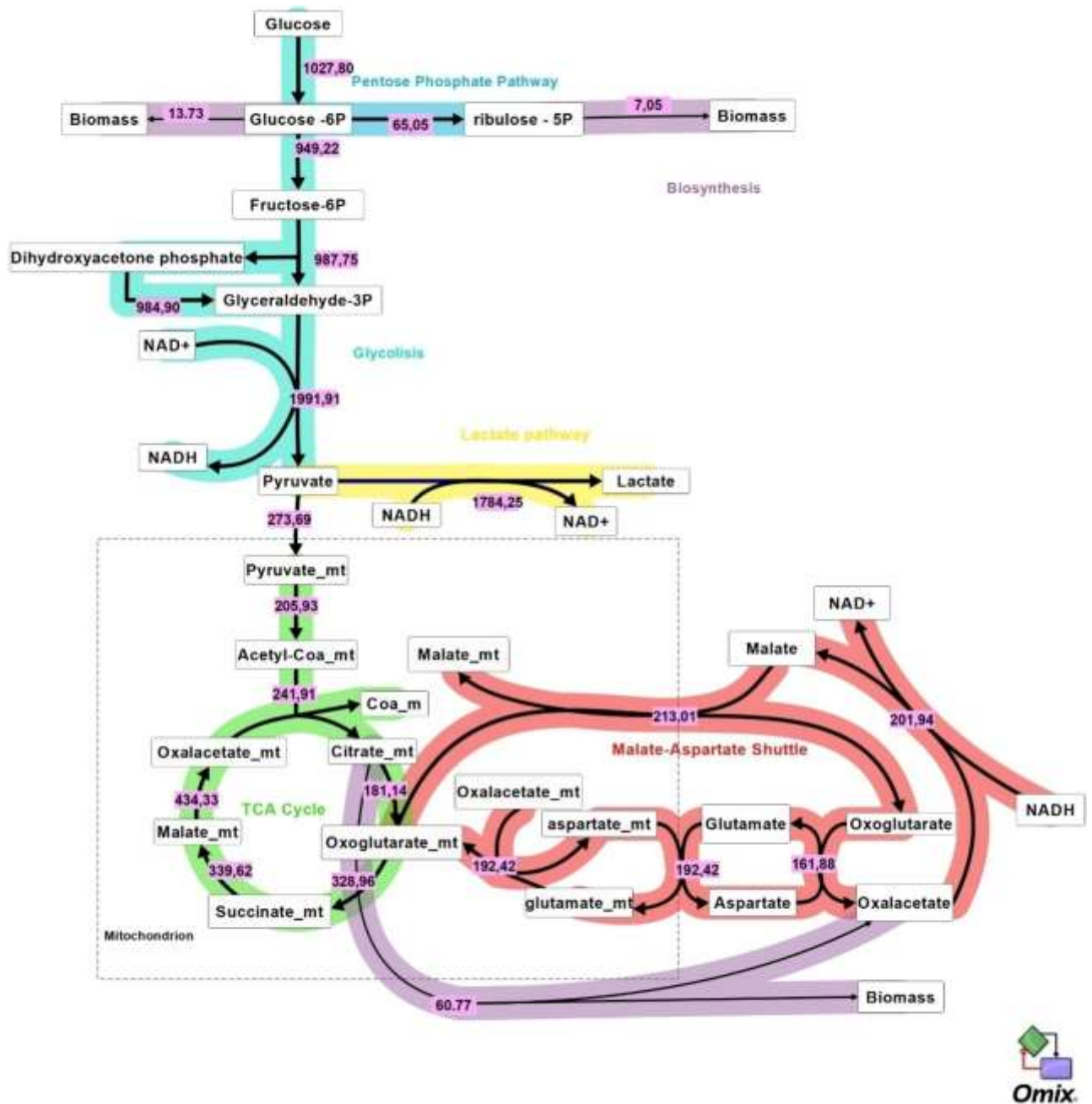


Figure 5-5 Scheme of the main metabolic fluxes calculated for hybridoma KB26.5. Arrows indicate the direction of the flux and their width the magnitude of fluxes (the exact value is detailed close to the arrows). All the fluxes are expressed in nmol·mg⁻¹·h⁻¹.

To understand how the energy required for the synthesis of the precursors destined to biomass generation and cell maintenance was handled, the study of the energy metabolism will be shown in the following section.

5.4.2.2 Study of hybridoma KB 26.5 energy metabolism by means of using metabolic models

As shown in **graph A) of Figure 5-6**, the proportion of the ATP produced mainly came from two sources (Kim, 1985)(Farmer & Liao, 1997): the first source of ATP comes from ATP synthase, which is a protein involved in the oxidative phosphorylation in the mitochondria (OP) (Alberts, Johnson, & Lewis, 2002). The second source of ATP comes at the substrate level phosphorylation, which is a reaction that takes part in glycolytic pathway in the cytoplasm.

In the case of hybridoma KB26.5, the ATP production by OP had the same impact in ATP proportion as the substrate level phosphorylation due to the fact that the almost all the NADH generated via glycolysis was reduced by the cytoplasmic pyruvate via lactate dehydrogenase instead of being transport to the mitochondria. As a result, only 10% of cytoplasmic NADH was transported to the mitochondria and oxidized via OP.

Regarding substrate level phosphorylation, the generation of ATP is based on the use of two specific groups of proteins:

- The first one is related to the kinase group (pyruvate kinase and phosphoglycerate kinase), that catalyse the transfer of phosphate groups from high energy phosphate-donating molecules to specific substrates, specifically, from phosphoenolpyruvate to ADP and from 1,3-bisphosphoglycerate to ADP
- The second one is based on a mitochondrial ligase, specifically succinyl-CoA ligase.

It is important to remark that the capacity of OP in order to produce ATP was limited due to the low transport of the NADH from the cytoplasm to the mitochondria and, as a consequence, the total mitochondria NADH flux is lower than what would be expected. On this basis, it might be hypothesized that a decrease in the lactate production could be related to an improvement of the cell growth based on the optimization of the glucose conversion to ATP.

On the other side, **in graph B) of the Figure 5-6**, the proportion of ATP consumed showed an allocation of ATP mainly in cell maintenance, biomass generation and in the reactions catalysed by phosphofructokinase and hexokinase proteins from the glycolytic pathway.

Cell maintenance tackles all the cellular process whose function is not related to formation of new cell material such as regulation of the proton motive force, the degradation of macromolecules or keeping the osmotic and chemiosmotic conditions. For keeping its performance 62 % of the ATP produced is required for maintenance of different cellular processes.

Regarding the reactions catalysed by kinases, nearly 25 % of the total ATP produced was mainly consumed by phosphofructokinase and hexokinase, both from the glycolytic pathway. In

addition, it is important to point out that the above-mentioned kinases catalysed the phosphorylation using ATP of fructose-6-phosphate and glucose, respectively.

Finally, the last one of the main consuming ATP reactions is the biomass formation, whose ATP consumption was 13 % of the ATP produced, although it has to be taken into consideration that the energy requirements for synthesis of biomass precursors are defined by the biomass equation.

Although, there are two points related to the energy metabolism of hybridoma KB26.5 growing on glucose-based media in aerobic conditions that has to be pointed out:

1. The ATP produced from the oxidative phosphorylation had the same contribution of the kinase-based reaction related to the glycolytic pathway, even if a high flux of lactate was limiting the transport of NADH cytoplasmic to the mitochondria.
2. In order to reach the optimal growth rate, the energetic requirements for cell maintenance (62 %) were higher than the required for the synthesis of new cellular material (13 %).

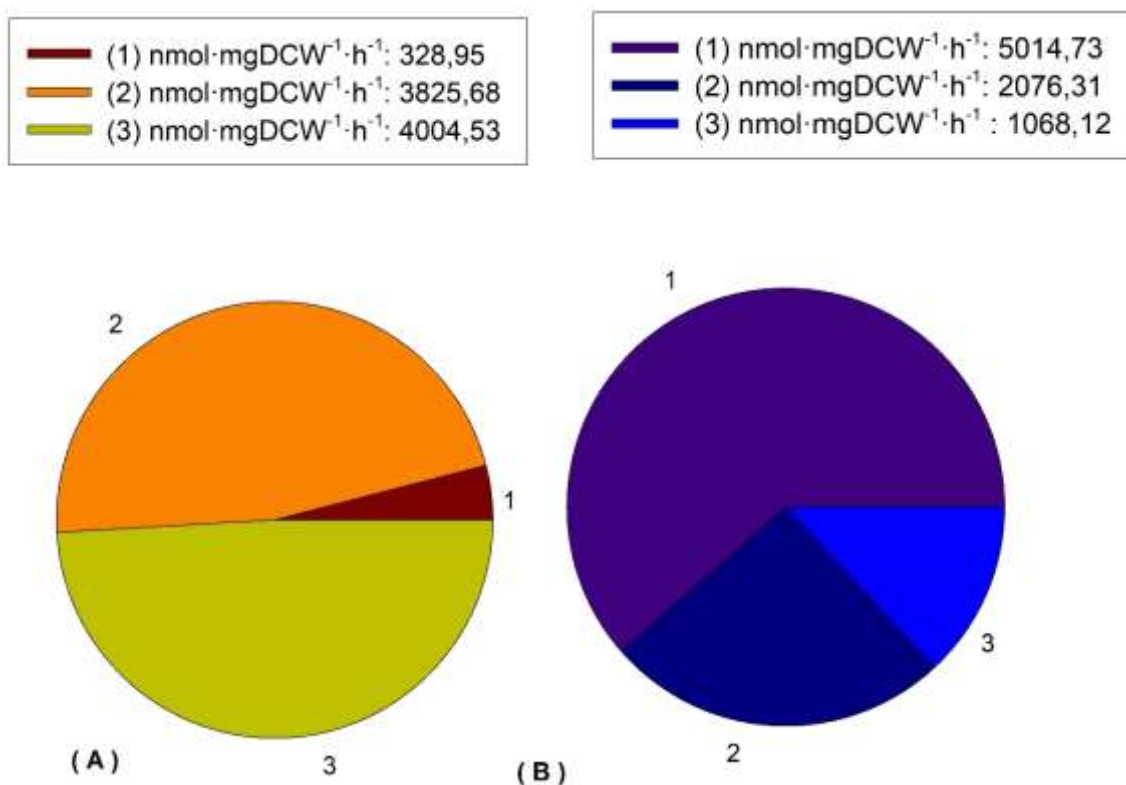


Figure 5-6 Distribution of ATP produced and consumed in hybridoma KB26.5. In figure A, the ATP produced is divided depending on its provenance (TCA cycle (1), Oxidative phosphorylation (2) and Glycolysis (3)). While in figure B, the ATP consumed is separated depending on its provenance (Cell maintenance (1), Glycolysis (2) and Biomass formation (3)).

To conclude, the main metabolic issue of hybridoma KB26.5 has been found to be related to an unbalance in the relation between NAD and NADH, provoked by a high flux through the glycolytic pathway and a low flux through the malate-aspartate shuttle on top of transporting the electron of NADH to the mitochondria via its oxidation. As a result, leading hybridoma KB26.5 to a metabolic state where mainly the NADH produced by glycolytic pathway was oxidized via lactate pathway instead of being oxidized by the malate-aspartate shuttle.

5.5 Results (III) - Reason behind the lactate production in HEK293 and hybridoma KB26.5 and its difference.

In the previous study, where the carbon metabolism of hybridoma KB26.5 and HEK293 was analysed, a metabolic trait was shared between them. The production of lactate was produced by a cytoplasmic unbalance regarding the redox potential. The unbalance was provoked by the incapacity to regenerate the cytoplasmic NADH generated by the glycolytic pathway via the mitochondrial shuttles. As a result, the only way to balance the excess of NADH was to reduce the pyruvate to lactate.

Moreover, it was also observed that the flux through the lactate production was strictly conditioned by the flux through the glycolytic pathway. On this basis, the difference in the lactate production regarding both cell lines is explained. Hybridoma KB26.5 had a higher glycolytic flux than HEK293 that required a higher lactate production in order to fulfil the balance of cytoplasmic NADH.

Up to this point, the reasons behind the lactate production were clarified. In the following sections, the reduction of lactate in order to improve the conversion of glucose to biomass will be studied.

5.6 Results (IV) - Reducing the lactate production in both cell lines

As it was described during all the analysis of the carbon metabolism in relation with the culture of HEK293 and hybridoma KB26.5, a carbon metabolism that converts more than 40 % of its main carbon source should be defined as an inefficient metabolism. Moreover, if it is taken into consideration that lactate is described as a growth inhibitory compound, its reduction should become an aim for the following sections.

Two ways to decrease the lactate production that are focused on solving the cytoplasmic NADH unbalance can be described. One way could be based on reducing the flux through the glycolytic pathway without genetic modifications. The other way could be using genetic modifications that will have an effect on the glycolytic pathway or on the mitochondrial shuttles.

If it is taken into consideration that when glucose was used as a carbon source a flux through the glycolytic pathway higher than the required one in order to avoid lactate production was observed, if its reduction without applying genetic modifications will be the target, one methodology should be decreasing the transport rate of extracellular glucose. The transport of glucose is a complex mechanism with multiple proteins on top of internalizing glucose (Holman, 2020). Consequently, its modification without adding inhibitors such as cytochalasin B (Ebstenen & Plagemann, 1972) or applying genetic modification might become quite difficult. However, due to the capacity of cells to grow on different kinds of sugar could be possible that one of these might present a low membrane transport. As it was described in Holman et al, the affinity of the major facilitators superfamily transporters (GLUT family) depends on the transported sugar. For example, GLUT1 has a higher affinity to transport glucose than to transport galactose (Holman, 2020).

Therefore, the next step will be focused on determining if HEK293 or hybridoma KB26.5 are able to grow on others carbon sources than glucose. As shown in **Table 5-5**, hybridoma KB26.5 was solely able to grow when the carbon source used was glucose (Casablancas, Xavier, & Sol, 2013). While, HEK293 is capable of growing on fructose and galactose instead of glucose (Reitzer & Wice, 1979). Consequently, in the following section, the study of how a change in carbon source might decrease the glycolytic pathway and have an effect on the lactate metabolism will be carried out using HEK293.

Table 5-5 . Growth results for the substitution of glucose for another carbon source in hybridoma KB26.5 and HEK293.

	Hybridoma KB26.5	HEK293
Glucose	+	+
Fructose	-	+
Galactose	-	+

5.6.1 Reducing the lactate production by means of changing the carbon source.

As it was previously mentioned, HEK293 can grow using several sugars; however, the growth on fructose presented an interesting fact. As shown **Figure 5-7**, a redistribution of the carbon metabolism was observed when the carbon source was replaced from glucose to fructose. This redistribution was based on a fully depletion of the lactate production. However, a reduction in the specific growth rate was also observed when glucose was replaced by fructose.

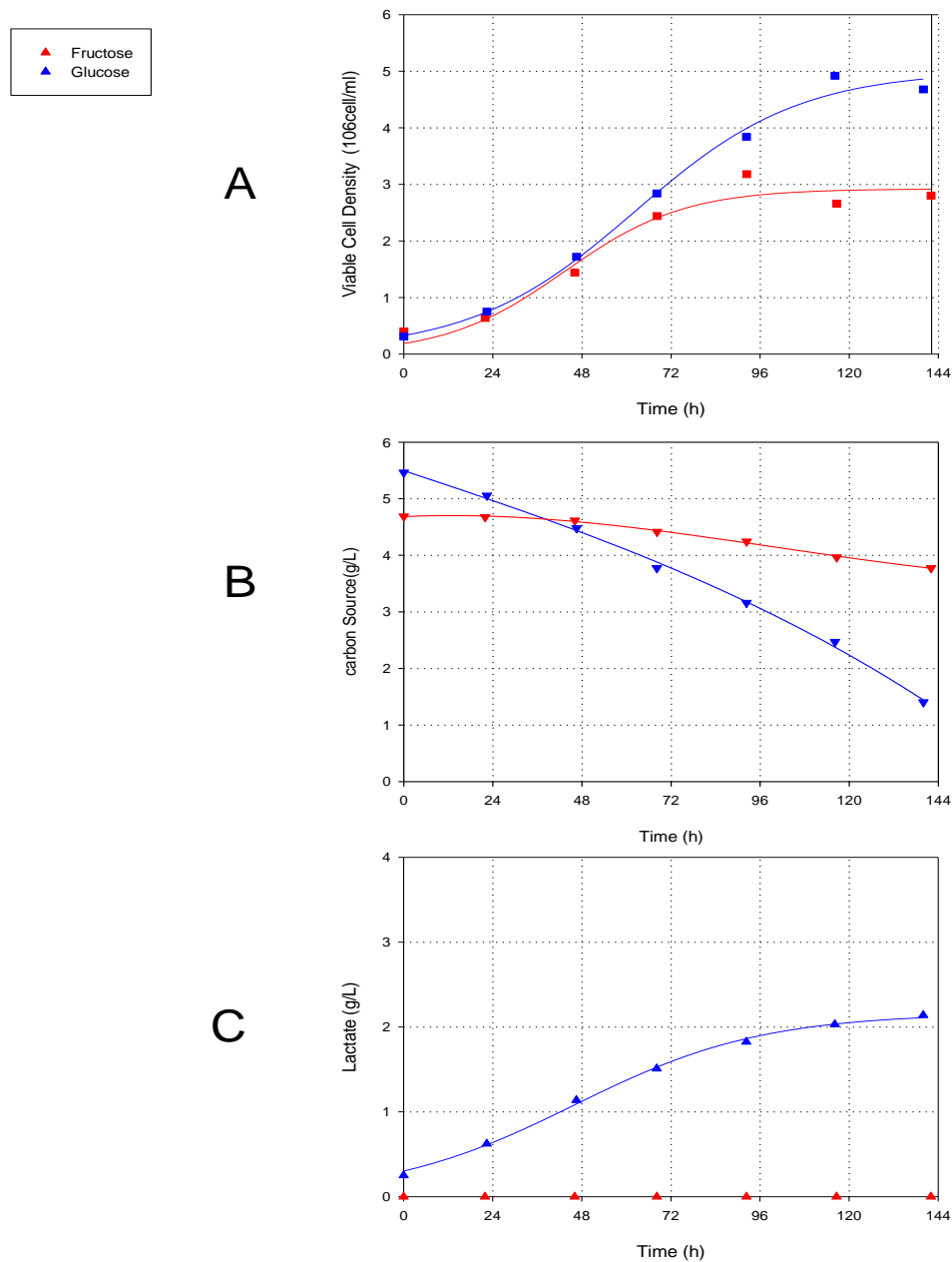


Figure 5-7 Erlenmeyer experiment where glucose and fructose were tested as a carbon source in HEK293 cell line. Each graph describes: A) Viable Cell Density, B) Main Carbon source (glucose or fructose), C) Lactate.

Therefore, in order to shed light on how a change in the carbon source from glucose to fructose provoked a metabolism adaptation of the carbon metabolism that eliminated the lactate produced, while the specific growth rate was reduced, a set of batch cultures will be carried out.

5.6.1.1 Using fructose as a carbon source

5.6.1.1.1 Experiment in batch culture

The experimental settings defined in order to culture the HEK293 were based on using a bioreactor as a containment culture system where every extracellular parameter can be controlled in order to ensure an optimal growth rate (as shown in the section 5.8.4). The media used was a chemical defined media supplemented with FBS in both cases which main carbon source was fructose (as shown in the section 5.8.2).

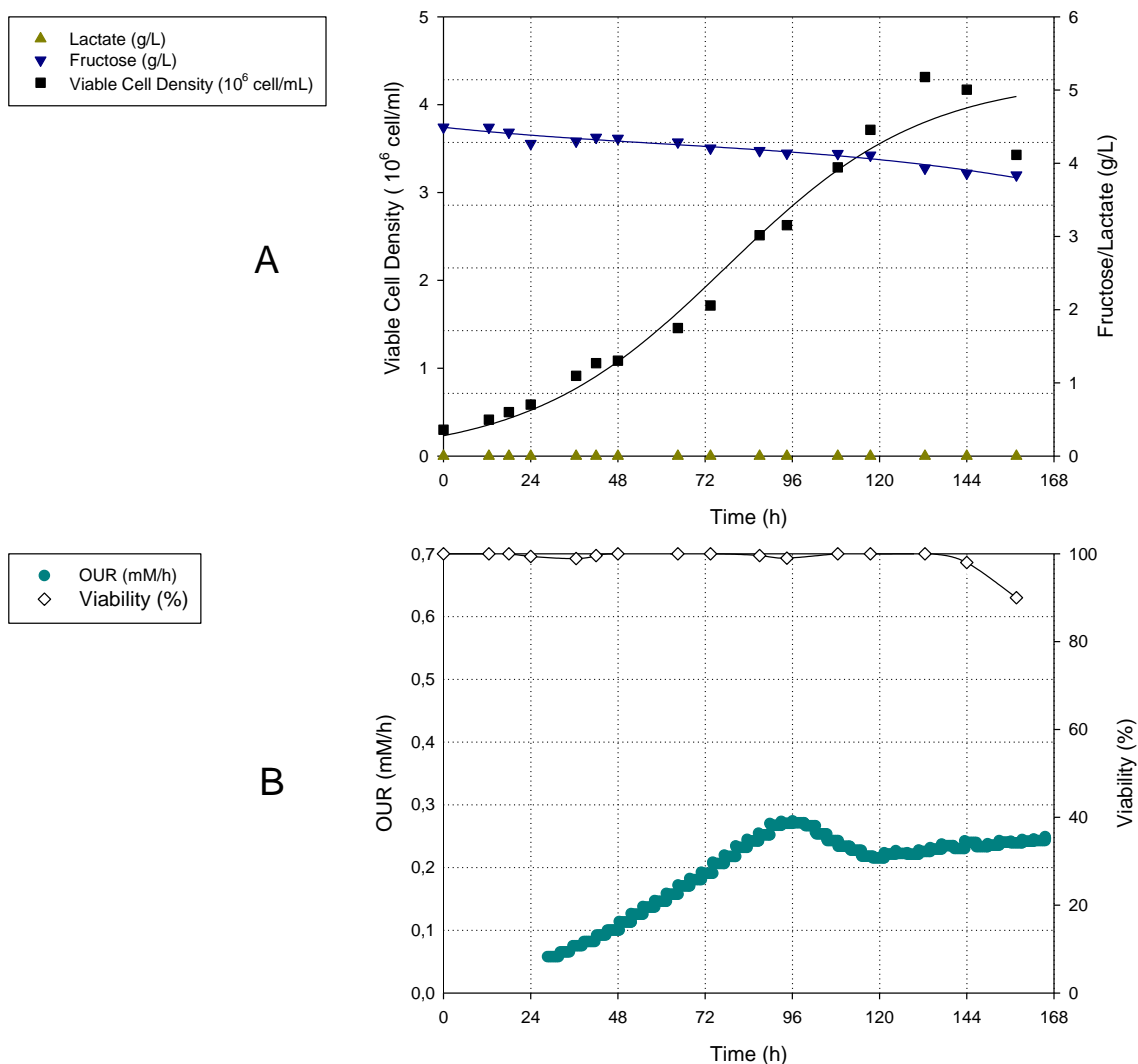


Figure 5-8 Profile of A) off-line variables such as Viable Cell Density (■), glucose (▼), lactate (▲) and B) the on-line variable such as OUR (●) and the off-line variable viability (◇) for HEK293 culture.

Table 5-6 Main parameters for HEK293 growing on Fructose culture.

Biomass achieved ($10^6 \text{ cell} \cdot \text{mL}^{-1}$)	4,02
Fructose consumption ($\text{g} \cdot \text{L}^{-1}$)	0,58
Lactate production ($\text{g} \cdot \text{L}^{-1}$)	0
$Y_{\text{bio/gluc}}$ ($10^6 \text{ cell} \cdot \text{mL}^{-1} \cdot \text{g}^{-1} \cdot \text{L}$)	4,845
$Y_{\text{lac/gluc}}$ ($\text{g} \cdot \text{g}^{-1}$)	0
q_{fructose} ($\text{nmol} \cdot \text{mg}^{-1} \cdot \text{h}^{-1}$)	79,50
q_{O_2} ($\text{nmol} \cdot \text{mg}^{-1} \cdot \text{h}^{-1}$)	262,3
μ (h^{-1})	0,024

As shown in the **graph A of Figure 5-8** and in **Table 5-6**, when HEK293 was cultured in a fructose-based media, it had a specific growth rate of $0,024 \text{ h}^{-1}$ and consumed $0,58 \text{ g} \cdot \text{L}^{-1}$ of fructose in order to achieve a maximum cell concentration of $4,02 \cdot 10^6 \text{ cell} \cdot \text{mL}^{-1}$ without producing lactate.

Moreover, regarding how the carbon source was allocated, it is important to remark that all the fructose was converted to biomass.

As it was previously commented, using the trend from both glucose and lactate profiles over time in relation with the biomass trend, the specific rates were calculated. The specific consumption rate of glucose had a value of $79,50 \text{ nmol} \cdot \text{mgDCW}^{-1} \cdot \text{h}^{-1}$ which led to the biomass generation of biomass $0,024 \text{ mgDCW} \cdot \text{mgDCW}^{-1} \cdot \text{h}^{-1}$. On the other side, related to the oxidation of fructose, the specific consumption rate of oxygen had a value of $262,3 \text{ nmol} \cdot \text{mgDCW}^{-1} \cdot \text{h}^{-1}$ and it was calculated using the variable oxygen uptake rate (OUR) represented in **graph B of Figure 5-8**.

As a result, the carbon metabolism of HEK293 was characterized as a non-lactate producer owing to all carbon source was converted to biomass instead of lactate.

Up to this point, it is important to highlight that the change in the carbon source from glucose to fructose provoked a metabolic restructuring of the carbon metabolism where the lactate production was completely depleted even if the specific growth rate was decreased by 15%

For a further analysis of the carbon network distribution, the modelling of the carbon and energy metabolism will be detailed hereafter in order to clarify the reasons behind this metabolic adaptation.

5.6.1.1.2 Study of the HEK293 carbon metabolism when fructose was used as a carbon source

A genomic-scale metabolic model will be used in order to describe how HEK293 transformed fructose to precursors for biomass synthesis, while getting enough energy in order to grow at the optimal growth rate. The development and description of the model is explained in section 5.8.8.1.

For metabolic flux calculation, the model was constrained using the input-output data of the corresponding metabolites that are shown in **Table 5-7**. This data included the biomass formation. The optimization of the model was performed by means of the FBA protocol described in section 5.8.9, whose objective function to maximize was the cytoplasmic hydrolysis of the ATP to ADP.

Table 5-7 Specific rate limits used as a drain for FBA in HEK293 using fructose as a carbon source.

	q (nmol mgDCW ⁻¹ h ⁻¹)
L-Alanine	17,33 ± 0,17
L-Argininium	-30,00 ± -0,30
L-Asparagine	-6,73 ± -0,27
L-Aspartate	-26,00 ± -0,52
L-Cysteine	-2,00 ± -0,02
Glucose	0,00 ± 0,00
L-Glutamine	-10,00 ± -0,20
L-Glutamate	-10,00 ± -0,10
L-Glycine	90,00 ± 0,90
L-Histidine	-20,00 ± -1,00
L-Isoleucine	-30,00 ± -0,60
Lactate	0,00 ± 0,00
L-Leucine	-13,15 ± -0,26
L-Lysinium	-17,22 ± -0,69
L-Methionine	-15,63 ± -0,16
Ammonium	29,79 ± 0,30
Oxygen	-262,39 ± -7,87
L-Phenylalanine	-6,25 ± -0,31
L-Proline	50,00 ± 2,50
L-Serine	-74,70 ± -1,49
L-Threonine	-7,54 ± -0,23
L-Tryptophan	-0,32 ± -0,12
L-Tyrosine	-3,85 ± -0,15
L-Valine	-30,00 ± -0,30
Biomass (10 ³)	24,10 ± 0,72

The intracellular fluxes were calculated and using the visualization software OMIX (Droste et al., 2013), and then, **Figure 5-9** is presented. In this figure, the distribution of the carbon metabolic network when fructose was used as a carbon source is displayed.

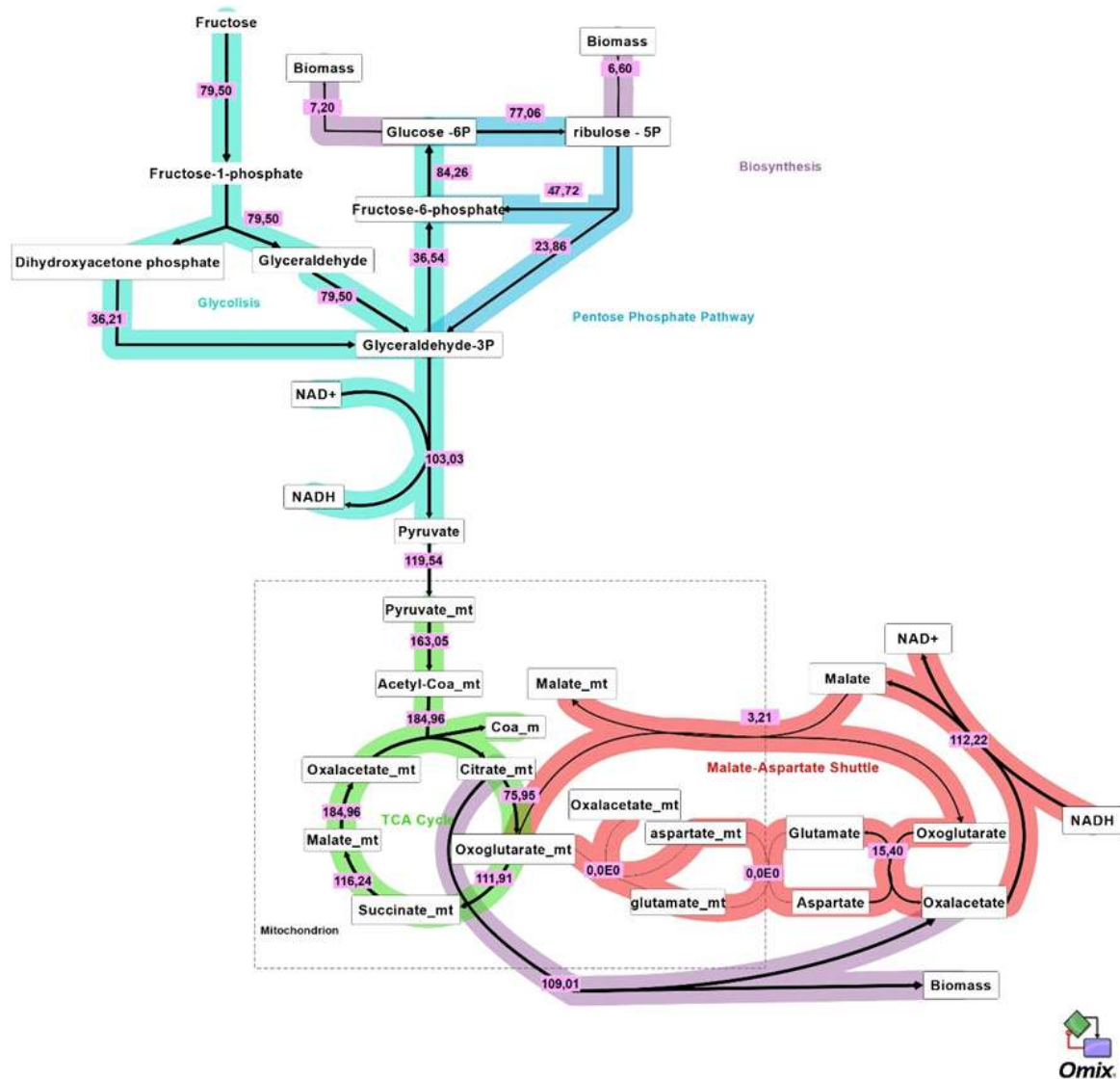


Figure 5-9 Scheme of the main metabolic fluxes calculated for HEK293 growing in Fructose Media. Arrows indicate the direction of the flux and their width the magnitude of fluxes (the exact value is detailed close to the arrows). All the fluxes are expressed in $\text{nmol} \cdot \text{mgDCW}^{-1} \cdot \text{h}^{-1}$.

Firstly, fructose was transported by facilitated diffusion through plasma membrane into the cytoplasm (Concha et al., 1997) (Nomura et al., 2015) with a flux of $79,50 \text{ nmol} \cdot \text{mgDCW}^{-1} \cdot \text{h}^{-1}$, and then it was phosphorylated in order to release fructose-1-phosphate via fructokinase-based reactions (Khitan & Kim, 2013). The generation of fructose-1-phosphate had a flux of $79,50 \text{ nmol} \cdot \text{mgDCW}^{-1} \cdot \text{h}^{-1}$, and then it was converted to glyceraldehyde and dihydroxyacetone phosphate. After that, the 45 % of the dihydroxyacetone phosphate flux was used by the protein responsible for the first step in the gluconeogenic pathway, the aldolic condensation of dihydroxyacetone phosphate and glyceraldehyde-3-phosphate catalysed by aldolase B. While the rest (45 %) was isomerized to glyceraldehyde-3-phosphate.

The generation of glyceraldehyde-3-phosphate has a flux of $139,54 \text{ mmol} \cdot \text{gDCW}^{-1} \cdot \text{h}^{-1}$, and was directed into two different routes:

The first route was related to the formation of biomass precursors, where a flux of $34,64 \text{ nmol} \cdot \text{mgDCW}^{-1} \cdot \text{h}^{-1}$ was directed towards the formation of biosynthesis precursors by means of a gluconeogenic step where glyceraldehyde-3-phosphate was converted to glucose-6-phosphate by means of an aldolic condensation, a dephosphorylation and, at the last step, an isomerization. Regarding the flux of glucose-6-phosphate flux, the 8,5 % of glucose-6-phosphate flux was directed towards the formation of carbohydrate-related biomass compounds and plasmatic membrane compounds, and the rest (91,5 %) towards the formation of mainly nucleotides via the oxidative branch of the pentose-phosphate pathway. It is important to highlight that the importance of the transketolase reaction of the pentose phosphate pathway owing to it had a huge impact in the formation of fructose-6-phosphate and glyceraldehyde-3-phosphate in the gluconeogenic pathway; for example, more than the 50 % of the fructose-6-phosphate generated was produced by a transketolase.

Regarding the second route, a flux of $103,03 \text{ nmol} \cdot \text{mgDCW}^{-1} \cdot \text{h}^{-1}$ was directed to the glycolytic pathway where it reacted until pyruvate, where 100 % of the produced pyruvate was transported through the mitochondrial membrane, without producing lactate. Regarding the lactate dehydrogenase responsible for the conversion of pyruvate to lactate, it could be state that low concentrations on glycolysis intermediates could repress the expression of lactate dehydrogenase or the expression of the gluconeogenic pathway could repress the lactate dehydrogenase, as a result, all the fructose was directed towards the obtaining of energy and biomass precursors.

Regarding the lactate metabolism, the substitution of the glucose by fructose as a carbon source provoked a redistribution of the carbon metabolism where the transport of the NADH generated from glycolysis was increased from 22,4 % to 100%. The main metabolic different between glucose and fructose were the coexistence of the gluconeogenic and the glycolytic pathways and the affinity of the protein on top of transporting via facilitated diffusion of fructose from the media to the cytoplasm. Regarding the transport of glucose to the cytoplasm, most of the proteins on top of transporting glucose have a higher affinity than the fructose one. As a consequence, a high flux of glucose to the cytoplasm can be obtained, while the fructose transporter had a low affinity, only limited amounts of fructose can be transported (Cura & Carruthers, 2012). This metabolic trait can be corroborated comparing the transported flux of glucose ($665 \text{ nmol} \cdot \text{mgDCW}^{-1} \cdot \text{h}^{-1}$) with the fructose one ($79,50 \text{ nmol} \cdot \text{mgDCW}^{-1} \cdot \text{h}^{-1}$), even if the extracellular concentration was the same.

In respect to the coexistence of the gluconeogenesis and glycolysis pathways, a relation between gluconeogenic and repression lactate dehydrogenase was not described in the bibliography, due to the fact that usually both metabolisms should not coexist. On this basis, the only reference of the coexistence of both metabolisms are the tumoral cells. The coexistence of both metabolism in tumoral cells provokes a chaotic regulation in the carbon metabolism not well understood, basically through the expression of three enzymes: the phosphoenol-pyruvate carboxykinase, the fructose-1,6-bisphosphatase, and the glucose-6-phosphatase (Wang & Dong, 2019). On this basis, it is hard to determine if the gluconeogenesis was affecting either the glycolytic pathway or the lactate metabolism because none of the mentioned enzymes were needed for the gluconeogenic pathway when fructose was used as a carbon source.

There was another important change in the carbon metabolism related to the decrease in the glycolytic pathway, the malate-aspartate shuttle was not used for transporting to the mitochondria the malate obtained by the oxidation of cytoplasmatic NADH. Otherwise, it was possible to transport the malate only with the mitochondrial antiport responsible for secreting to cytoplasm the citrate required for the biomass formation.

On the other side, regarding the biomass formation, the main precursors are generated from ribulose-5P (derivation of 0,5 % of glucose carbon-mol uptake rate); glucose-6-phosphate (derivation of 1,33 % of glucose carbon-mol uptake rate); and citrate (derivation of 1,9 % of glucose carbon-mol uptake rate).

Once the carbon metabolism has been analysed, it is important to realize that coupled with carbon metabolism appears energy metabolism. Therefore, to understand how the energy required for the synthesis of the precursors destined to biomass generation and cell maintenance was handled, the study of the energy metabolism will be shown in the following section.

5.6.1.1.3 Study of the HEK293 energy metabolism when fructose was used as a carbon source.

As shown in **graph A) of Figure 5-10**, and it was mentioned before, the proportion of the ATP produced mainly came from two sources: the first source of ATP comes from ATP synthase and

the second source of ATP comes at the substrate level phosphorylation, which is a reaction that takes part in glycolytic pathway in the cytoplasm. Furthermore, in aerobic conditions and in compartmentalized cells (eukaryotic organisms), OP is described as the main source of ATP.

In the case of HEK293 growing on fructose, the ATP production by OP had much more impact in ATP proportion than the substrate level phosphorylation because of the flux through the glycolytic pathway was reduced to the point of being minimum. This reduction was directly related to the low transport of fructose from the media to the cytoplasm. Specifically, OP contributed in an 81 % of the total ATP produced while the contribution of the substrate level phosphorylation was 12%.

On the other side, **in graph B) of the Figure 5-10**, the change in carbon source provoked a change in the allocation of ATP showed up until now, where the cell maintenance energetic requirements were more than 50 %. On the contrary, when fructose was used, the allocation of the ATP consumed changed where the formation of biomass and the cell maintenance tackled around the 85 % of the ATP produced and lastly, glycolysis.

As previously mentioned, the biomass formation required nearly the 42 % of the total ATP produced in order to grow at the optimal rate, while the cell maintenance that tackled all the cellular process whose function is not related to formation of new cell material required the 43 % of the ATP produced. The ATP consuming cellular process were the reactions catalysed by kinases, nearly 15% of the total ATP produced was mainly consumed by fructokinase, phosphofructokinase, both from the glycolytic pathway.

Therefore, there are two points related to the energy metabolism that has to be pointed out:

1. The ATP produced from the oxidative phosphorylation had much more contribution than the substrate level phosphorylation, 81 % in front of 12 %.
2. In order to reach the optimal growth rate, the energetic requirements for cell maintenance (43 %) was the same as the one required for the synthesis of new cellular material (42 %).

Regarding the data observed in this chapter, it can be stated that the cell maintenance could be directly related to at least the combination of the lactate production and the flux through the glycolytic pathway, due to the fact that higher the capacity of a carbon metabolism to produce lactate was, higher energetic requirements regarding the cell maintenance were required.

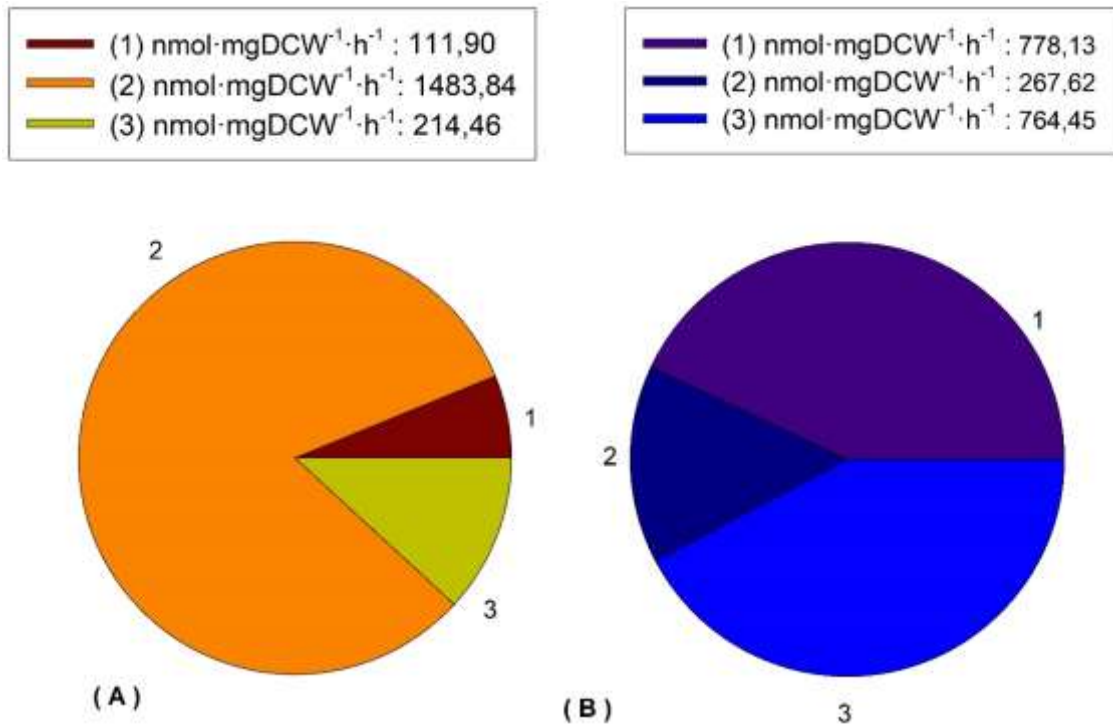


Figure 5-10 Distribution of ATP produced and consumed in HEK293 cultured on a culture's media where fructose was used as a carbon source. In figure A, the ATP produced is divided depending on its provenance (TCA cycle (1), Oxidative phosphorylation (2) and Glycolysis (3)). While in figure B, the ATP consumed is separated depending on its provenance (Cell maintenance (1), Glycolysis (2) and Biomass formation (3)).

To conclude, after the analysis of the carbon and energy metabolism, the main metabolic trait of HEK293 growing on fructose as a carbon source has been found to be related a low transport of fructose from the media to the cytoplasm and the coexistence and interaction between two invers pathways: the gluconeogenesis and the glycolysis. As a result, leading HEK293 to a metabolic state where all NADH produced by glycolytic pathway was transported via shuttle-based mechanisms from the cytoplasm to the mitochondria and then, oxidized via OP. Therefore, all the fructose was converted to biomass without producing any sub-products like lactate.

However, even if the lactate metabolism was completely reduced, the decrease in the growth rate was not acceptable. Therefore, an experiment based on rising the specific growth rate while fructose was used as a carbon source will be carried out in the following section.

In order to increase the specific growth rate of HEK293 growing on fructose, the following hypothesis regarding why the specific growth rate was reduced when glucose was replaced by fructose was exposed. Its reduction was caused by a low affinity between fructose and the transporter on top of its internalization (GLUT5) (Nomura et al., 2015)(Holman, 2020) that

provoked a low flux through the glycolytic pathway and as a result, it limited the fluxes towards the formation of biomass precursors. Therefore, the supplementation of another carbon source should be required in order to increase the flux through the glycolytic pathway and then, increasing the production of the biomass precursors.

Regarding the carbon supplementation, there is a particular trait observed in HEK293 where given certain conditions the co-consumption of glucose and lactate were observed (Martínez-Monge et al., 2019). On this basis, it can be stated that if fructose is supplemented via sodium lactate addition, a co-consumption might be possible. In order to verify the hypothesis, an experiment in shake-flask was carried out in as shown in **Figure 5-11**, where lactate was metabolized together with fructose resulting in a notorious recuperation of the specific growth rate at almost at the same level of glucose when fructose was supplemented with lactate.

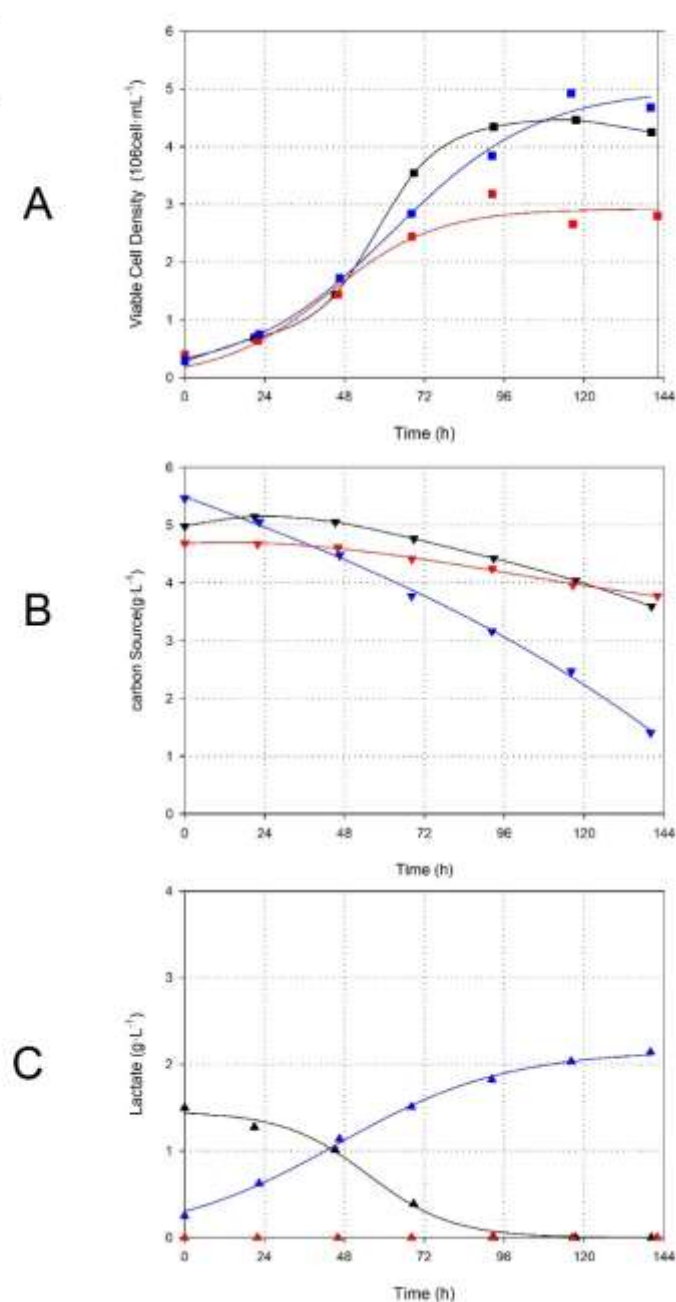


Figure 5-11. Profile comparison of viable cell density (A), the carbon source used (B) and lactate (C) for a shake-flask experiments where HEK293 was cultured on three carbon sources glucose, fructose and fructose supplemented with lactate.

Therefore, in order to shed light on how the supplementation of fructose with lactate provoked a metabolism adaptation of the carbon metabolism that increased the specific growth rate was observed, a batch culture will be carried hereafter.

5.6.1.2 *Using sodium lactate as carbon supplement when fructose was used as a carbon source.*

5.6.1.2.1 Experiment in batch culture

The experimental settings defined in order to culture the HEK293 were based on using a bioreactor as a containment culture system where every extracellular parameter can be controlled in order to ensure an optimal growth rate (as shown in the section 5.8.4). The media used was a chemical defined one supplemented with FBS in which the main carbon source was fructose (as shown in the section 5.8.2 and 5.8.2).

As shown in the **graph A** of **Figure 5-12** and in **Table 5-8**, when HEK293 was cultured in a fructose-based media supplemented with lactate, it had a specific growth rate of $0,028 \text{ h}^{-1}$ and consumed $0,4 \text{ g}\cdot\text{L}^{-1}$ of fructose in order to achieve a maximum cell concentration of $3\cdot 10^6 \text{ cell}\cdot\text{ml}^{-1}$ before lactate was fully consumed. Moreover, regarding how the carbon source was allocate, it is important to remark that all the fructose and lactated was converted to biomass.

As it was previously described, using the trend from both fructose and lactate profiles over time in relation with the biomass trend, the specific rates were calculated. The specific consumption rate of fructose had a value of $68 \text{ nmol}\cdot\text{mgDCW}^{-1}\cdot\text{h}^{-1}$ which lead to the biomass generation of biomass $0,028 \text{ mgDCW}\cdot\text{mgDCW}^{-1}\cdot\text{h}^{-1}$ while lactate was being consumed with a flux of $530,12 \text{ nmol}\cdot\text{mgDCW}^{-1}\cdot\text{h}^{-1}$. On the other side, related to the oxidation of fructose, the specific consumption rate of oxygen had a value of $1200,25 \text{ nmol}\cdot\text{mgDCW}^{-1}\cdot\text{h}^{-1}$ and it was calculated using the variable oxygen uptake rate (OUR) represented in **graph B** of **Figure 5-8**.

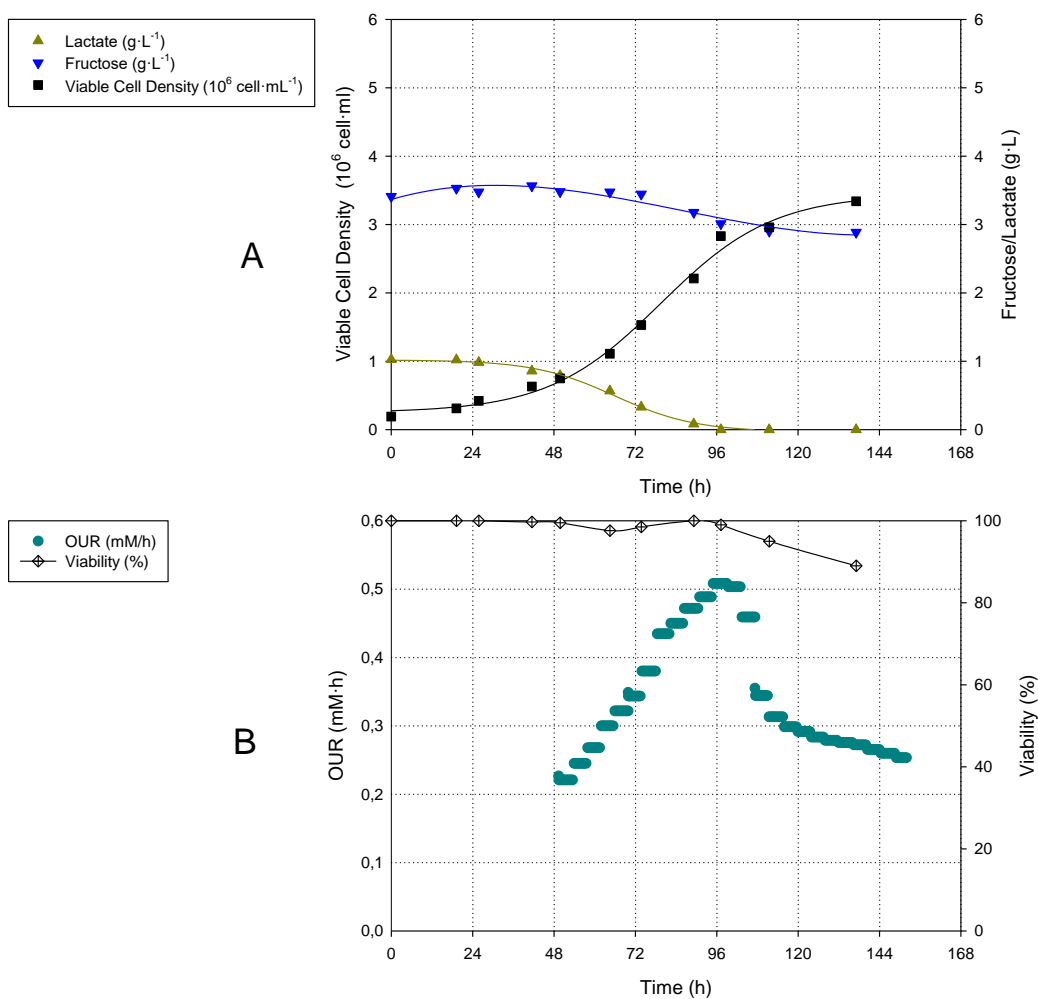


Figure 5-12 Profile of A) off-line variables such as viable cell density (■), fructose (▼), lactate (▲) and B) on-line variable such as OUR (●) and off-line variable such as viability (◇) for HEK293 culture when the carbon source used was fructose supplemented with sodium lactate.

Table 5-8 Main parameters for HEK293 growing on fructose supplemented with sodium lactate.

Biomass achieved ($10^6 \text{ cell} \cdot \text{mL}^{-1}$)	3,00
Fructose consumption ($\text{g} \cdot \text{L}^{-1}$)	0,4
Lactate consumption ($\text{g} \cdot \text{L}^{-1}$)	1,02
$Y_{\text{bio/fructose}}$ ($10^6 \text{ cell} \cdot \text{mL}^{-1} \cdot \text{g}^{-1} \cdot \text{L}$)	7,825
$Y_{\text{lac/fruc}}$ ($\text{g} \cdot \text{g}^{-1}$)	0
q_{fructose} ($\text{nmol} \cdot \text{mgDCW}^{-1} \cdot \text{h}^{-1}$)	68
q_{lactate} ($\text{nmol} \cdot \text{mgDCW}^{-1} \cdot \text{h}^{-1}$)	530,12
q_{O_2} ($\text{nmol} \cdot \text{mgDCW}^{-1} \cdot \text{h}^{-1}$)	1200,25
μ (h^{-1})	0,028

Up to this point, it is important to highlight that the supplementation of lactate to a fructose-based media provoked a metabolic restructuring of the carbon metabolism where the specific growth rate was increased by 15%. As a result, when glucose was replaced by fructose supplemented with lactate, the lactate production was avoided while the specific growth rate was unaffected. For a further analysis of the carbon network distribution, the modelling of the carbon and energy metabolism will be detailed hereafter in order to clarify the reasons behind this metabolic adaptation.

5.6.1.2.2 Study of HEK293 carbon metabolism when fructose was supplemented with lactate

A genomic-scale metabolic model will be used in order to describe how HEK293 transformed at the same time fructose and lactate to precursors for biomass synthesis, while getting enough energy in order to grow at the optimal growth rate. The development and description of the model is explained in section 5.8.8.1.

For metabolic flux calculation, the model was constrained using the input-output data of the corresponding metabolites that are shown in **Table 5-9**. This data included the biomass formation. The optimization of the model was performed by means of the FBA protocol described in section 5.8.9, whose objective function to maximize was the cytoplasmic hydrolysis of the ATP to ADP.

Table 5-9 Specific rate limits used as a drains for FBA in HEK293 using fructose supplemented with sodium lactate.

	q (nmol mgDCW ⁻¹ h ⁻¹)
L-Alanine	130,00 ± 6,50
L-Argininium	-30,00 ± -0,30
L-Asparagine	-19,82 ± -0,40
L-Aspartate	-22,00 ± -1,10
L-Cysteine	-2,00 ± -0,02
Glucose	0,00 ± 0,00
L-Glutamine	-10,00 ± -0,50
L-Glutamate	-10,00 ± -0,30
L-Glycine	0,69 ± 0,03
L-Histidine	-20,00 ± -0,60
L-Isoleucine	-13,23 ± -0,53
Lactate	-529,31 ± -5,29
L-Leucine	-15,28 ± -0,61

L-Lysinium	-20,01 ± -0,80
L-Methionine	-4,28 ± -0,21
Ammonium	-25,83 ± -0,26
Oxygen	-1100,00 ± -300,00
L-Phenylalanine	-7,27 ± -0,15
L-Proline	0,00 ± 0,00
L-Serine	-29,53 ± -0,59
L-Threonine	-8,76 ± -0,44
L-Tryptophan	-0,37 ± -0,01
L-Tyrosine	-4,47 ± -0,04
L-Valine	-24,51 ± -0,49
Biomass (10 ³)	28,00 ± 1,40

The intracellular fluxes were calculated and using the visualization software OMIX (Droste et al., 2013), and is presented in **Figure 5-13**. In this figure, the distribution of the carbon metabolic network when fructose supplemented with lactate were used as carbon sources is displayed.

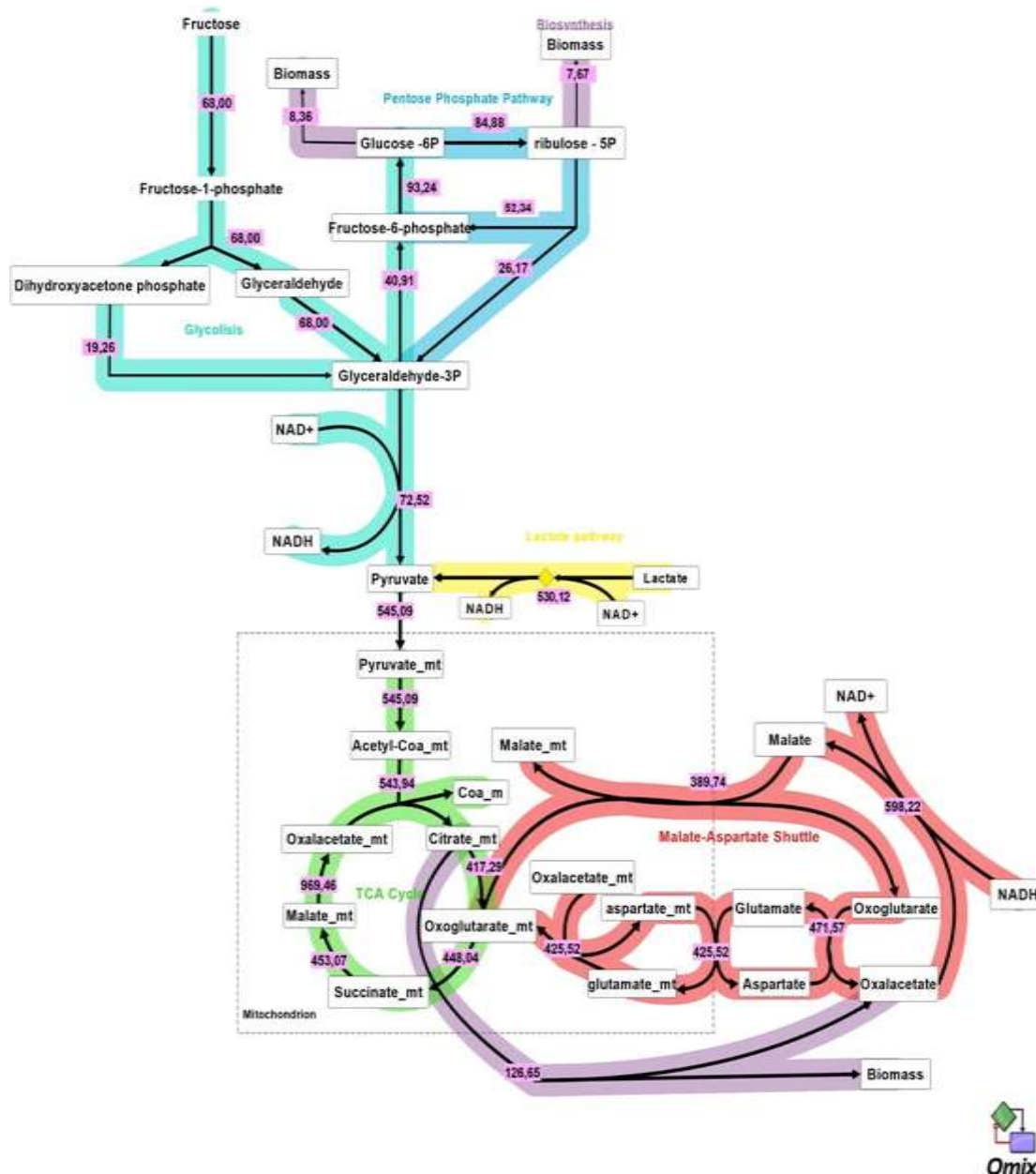


Figure 5-13 Scheme of the main metabolic fluxes calculated for HEK293 growing in Fructose + Lactate Media. Arrows indicate the direction of the flux and their width the magnitude of fluxes (the exact value is detailed close to the arrows). All the fluxes are expressed in $\text{nmol}\cdot\text{mgDCW}^{-1}\cdot\text{h}^{-1}$.

Firstly, fructose was transported by facilitated diffusion through plasma membrane into the cytoplasm with a flux of $68\text{nmol}\cdot\text{mgDCW}^{-1}\cdot\text{h}^{-1}$, and then it was phosphorylated in order to release fructose-1-phosphate via fructokinase-based reactions. The generation of fructose-1-phosphate had a flux of $68\text{nmol}\cdot\text{mgDCW}^{-1}\cdot\text{h}^{-1}$, and then it was converted to glyceraldehyde and dihydroxyacetone phosphate. After that, the 72 % of the dihydroxyacetone phosphate produced was used by the first step in the gluconeogenic pathway, the aldolic condensation of dihydroxyacetone phosphate and glyceraldehyde-3-phosphate catalysed by aldolase B. While the rest (28 %) was isomerized to glyceraldehyde-3-phosphate.

The generation of glyceraldehyde-3-phosphate has a total flux of $113,43 \text{ mmol} \cdot \text{gDCW}^{-1} \cdot \text{h}^{-1}$ which was directed into two different routes:

The first route was related to the formation of biomass precursors, where a flux of $40,91 \text{ nmol} \cdot \text{mgDCW}^{-1} \cdot \text{h}^{-1}$ was directed towards the formation of biosynthesis precursors by means of the gluconeogenic pathway where glyceraldehyde-3-phosphate was converted to glucose-6-phosphate via an aldolic condensation, a dephosphorylation and in the last step, an isomerization.

Regarding the flux of glucose-6-phosphate flux, the 8,9 % of glucose-6-phosphate flux was directed towards the formation of carbohydrate-related biomass compounds and plasmatic membrane compounds, and the rest (91,1 %) towards the formation of mainly nucleotides via the oxidative branch of the pentose-phosphate pathway. It is important to highlight that the importance of pentose phosphate pathway transketolase reactions, owing to it had a huge impact in the formation of fructose-6-phosphate and glyceraldehyde-3-phosphate in the gluconeogenic pathway, where the 56 % of the total fructose-6-phosphate was produced in this pathway.

Regarding the second route, a flux of $72,52 \text{ nmol} \cdot \text{mgDCW}^{-1} \cdot \text{h}^{-1}$ was directed to the glycolytic pathway where it reacted until pyruvate, where the total flux of pyruvate was increased from $72,52 \text{ nmol} \cdot \text{mgDCW}^{-1} \cdot \text{h}^{-1}$ to $545,09 \text{ nmol} \cdot \text{mgDCW}^{-1} \cdot \text{h}^{-1}$ owing the oxidation of lactate. All the pyruvate produced was transported through the mitochondrial membrane, without lactate being generated. Regarding the lactate dehydrogenase responsible for the conversion of pyruvate to lactate, it might be state that high lactate concentrations induced the conversion of lactate to pyruvate even if the glycolysis had a low impact on the carbon metabolism or a gluconeogenesis pathway was observed.

Regarding the lactate metabolism, the supplementation of fructose with lactate provoked a redistribution of the carbon metabolism where lactate was co-consumed with fructose. Moreover, the flux on top of transporting fructose through the plasmatic membrane was nearly unaffected by the sudden increase in the conversion of lactate to pyruvate. Therefore, it could be corroborating that fructose transporter was operating at the maximum possible rate, owing to the low affinity towards fructose (Cura & Carruthers, 2012). As a result, the fructose transport was not affected and the flux through it remained unaffected ($68 \text{ nmol} \cdot \text{mgDCW}^{-1} \cdot \text{h}^{-1}$) if it is compared with the flux obtain when HEK293 was growing on fructose ($79,5 \text{ nmol} \cdot \text{mgDCW}^{-1} \cdot \text{h}^{-1}$).

As it was described when HEK293 was cultured on fructose, it could be hard to determine if the gluconeogenesis was affecting either the glycolytic pathway or the lactate metabolism because none of the previously mentioned enzymes (the phosphoenol-pyruvate carboxykinase, the fructose-1,6-bisphosphatase, and the glucose-6-phosphatase (Wang & Dong, 2019)) were used in the gluconeogenic pathway when fructose was supplemented with lactate.

There was another important trait in the carbon metabolism related to the decrease in the glycolytic pathway, the activation of malate-aspartate shuttle. On the contrary of what happen when fructose was used as a carbon source, the cytoplasmic transport of the NADH generated via malate-aspartate shuttle was activated due to the oxidation of the supplemented lactate via lactate dehydrogenase. As a result, the shuttle increased its flux from 3 nmol·mgDCW⁻¹·h⁻¹ to 389,74 nmol·mgDCW⁻¹·h⁻¹ causing a high production of ATP from OP which will be described in the following sections.

On the other side, regarding the biomass formation, the main precursors are generated from ribulose-5P (derivation of 0,5 % of glucose carbon-mol uptake rate); glucose-6-phosphate (derivation of 1,33 % of glucose carbon-mol uptake rate); and citrate (derivation of 1,9 % of glucose carbon-mol uptake rate).

Once the carbon metabolism has been analysed, it is important to realize that coupled with carbon metabolism appears energy metabolism. Therefore, to understand how the energy required for the synthesis of the precursors destined to biomass generation and cell maintenance was handled, the study of the energy metabolism will be shown in the following section.

5.6.1.2.3 Study of HEK293 energy metabolism when fructose was supplemented with lactate

As shown in **graph A) of Figure 5-14**, and as it was mentioned before, the proportion of the ATP produced mainly came from two sources: the first source of ATP comes from ATP synthase and the second source of ATP comes at the substrate level phosphorylation, which is a reaction that takes part in glycolytic pathway in the cytoplasm. Furthermore, in aerobic conditions and in compartmentalized cells (eukaryotic organisms), OP is described as the main source of ATP.

In the case of HEK293 growing on fructose supplemented with lactate, the ATP production by OP had much more impact in ATP proportion than the substrate level phosphorylation because of the flux through the glycolytic pathway was reduced to the point of being minimum and also

the cytoplasmic NADH available to be transported to the mitochondria was increased due to the oxidation of lactate. As a result, the energy from the mitochondria was maximized owing to the cytoplasmic NADH solely can oxidized by the malate-aspartate shuttle when lactate was being consumed. Specifically, OP contributed in a 91 % of the total ATP produced while the contribution of the substrate level phosphorylation was 2 %.

On the other side, **in graph B) of the Figure 5-14**, it can be seen that the supplementation of lactate to fructose changed drastically the fructose allocation of ATP. The cell maintenance contribution increased from 42 % to 84,7% of the total ATP produced, the biomass formation decreased its contribution from 43% to 11,6 % and lastly, the glycolysis required only 3,7 % of the total ATP produced.

Therefore, there are two points related to the energy metabolism that has to be pointed out:

1. The ATP produced from the oxidative phosphorylation had much more contribution than the substrate level phosphorylation, 91 % in front of 2 %.
2. In order to reach the optimal growth rate, the energetic requirements for cell maintenance (84,7 %) was higher than the one required for the synthesis of new cellular material (11,6%).

In relation with the second point, if we take into consideration the last hypothesis presented in the previous section regarding the cell maintenance and the lactate metabolism, which stated that the cell maintenance was proportional to the capacity of the carbon source to produce lactate, more lactate produced – more cell maintenance was required.

With this new data, the hypothesis can be improved: the cell maintenance should not directly be related to only the lactate produced. It should be related to how the cytoplasmic pool of NADH is affected by the flux through the lactate metabolism without taking in account if the lactate was consumed or produced owing both behaviours are regulated by the same reaction.

.

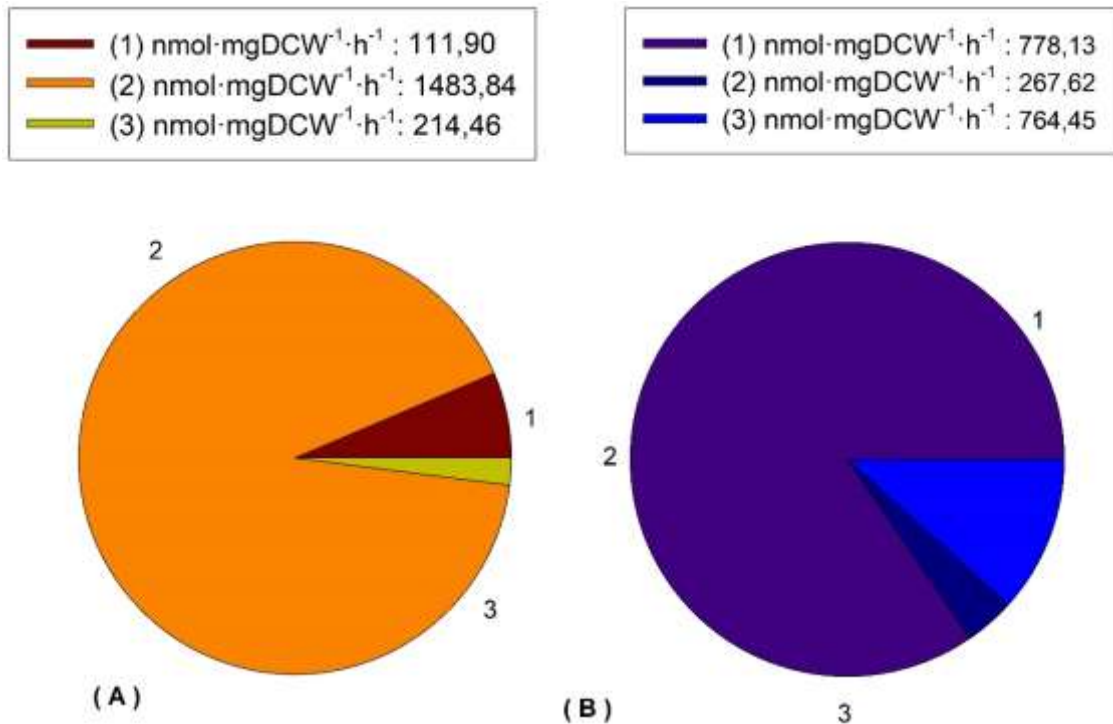


Figure 5-14. Distribution of ATP produced and consumed in HEK293 cultured on a culture's media where fructose was supplemented with sodium lactate. In figure A, the ATP produced is divided depending on its provenance (TCA cycle (1), Oxidative phosphorylation (2) and Glycolysis (3)). While in figure B, the ATP consumed is separated depending on its provenance (Cell maintenance (1), Glycolysis (2) and Biomass formation (3)).

To conclude, after the analysis of the carbon and energy metabolism, the metabolism of HEK293 growing on fructose supplemented with lactate has been found to be related to a low transport of fructose from the media to the cytoplasm along with a high lactate transport to the cytoplasm. Moreover, as it was described before when HEK293 was cultured on fructose, when fructose was supplemented with lactate the gluconeogenic pathway was also required in order to synthesis the biomass whose build-block was glucose-6-phosphate. However, if the distribution of the carbon metabolism was taken into consideration when HEK293 was cultured only in fructose-based media, the addition of lactate only provoked major modification on the mitochondria carbon and energy metabolism.

The flux through the TCA cycle and the OP were increased due to the fact the glycolytic or the gluconeogenic pathway were not affected by the consumption of lactate. The lactate consumption only increased the availability of cytoplasmic NADH and the cytoplasmic pyruvate and, as a result, the carbon flux of the mitochondria was enhanced while the glycolytic or the gluconeogenic pathway remained almost unaffected. Moreover, the mitochondrial metabolism being the one only affected by the lactate addition can also be observed if the change in the

allocation of ATP produced is taken into consideration, where the contribution of the OP changed from 42 to 91%. Regarding the ATP allocation, it was also observed that the consumption of lactate affected to the same extent the cell maintenance. An increase in the cell maintenance was observed from 43 % to 84,7% when fructose was supplemented with lactate.

Finally, the supplementation of lactate solved the growth issues related to growing HEK293 on fructose-based media where a decrease in the specific growth rate was observed. Therefore, when glucose was replaced by fructose supplemented with lactate, the specific growth rate was not affected while the lactate production was depleted. However, it could be interesting to present the metabolic changes provoked by replacing glucose for fructose or fructose supplemented with lactate in order to have a global overview of the carbon adaptation.

Therefore, in the following section a global comparison of how the metabolism is affected by a change in carbon source will be presented hereafter.

5.6.2 Metabolic comparison of HEK293 cultured on glucose, fructose and fructose supplemented with lactate.

Up until now, the entire carbon metabolism referred to how HEK293 under aerobic conditions consumed a carbon source and, then, it was converted to biomass precursors and, if it was required to by-products, has been described independently. Although, the principal difference between the carbon sources used (glucose, fructose and fructose supplemented with lactate) were related to how the glycolysis pathway, the lactate metabolism, the mitochondrial metabolism and the gluconeogenic pathway behaved in front of a change in the carbon sources.

For example, when glucose was used as a carbon source, the glycolytic pathway was maximized along with the lactate and lactate production, while the gluconeogenic pathway was not required and the mitochondrial metabolism was limited due to the use of the cytoplasmic NADH from the glycolysis by the lactate metabolism. On the contrary, when glucose was replaced with fructose, the glycolytic pathway was minimized along a full depletion of the lactate metabolism, while the gluconeogenic pathway was required for the synthesis of biomass and the mitochondrial metabolism was limited due to the low production of the cytoplasmic NADH from the glycolysis. And then, when fructose was supplemented with lactate, the glycolytic pathway and the gluconeogenic remained unaffected by the lactate addition while, on the other hand, the lactate metabolism was used as a cytoplasmic NADH donor where lactate was oxidized to

pyruvate and the mitochondrial metabolism was enhanced due to the production of the cytoplasmic NADH from the lactate metabolism.

In order to have a global overview of the described metabolic adaptations, a study will be presented hereafter.

5.6.2.1 Comparison between the carbon metabolism of HEK293 when glucose, fructose and fructose supplemented with lactate were used as a carbon source

In order to begin with the study, one assumption related to the metabolic model must be taken into consideration:

- The stoichiometric matrix was the same for all the conditions studied as well as its biomass equation.

The modifications of carbon metabolism will be detailed below in two figures regarding the glycolytic pathway (**Figure 5-15**) and reading the mitochondria metabolism (**Figure 5-16**).

When HEK293 was cultured on the selected carbons sources, interesting traits were revealed, which are presented hereafter:

1. The fructose mechanism based on the conversion of fructose to fructose-1-phosphate was unused when glucose was used as a carbon source, on the contrary, the glucose conversion to glucose-6-phosphate was unused when either fructose or fructose supplemented with lactate were used.
2. The flux through the fructose metabolism was not highly affected by the supplementation of lactate
3. The upper part of glycolysis was used as building-block pathway for the biomass synthesis when glucose was used as a carbon source, whereas the gluconeogenic pathway was required when glucose was replaced by either fructose or fructose supplemented with lactate.
4. Correlated with the third point, the glycolytic pathway from the glucose to glyceraldehyde-3-phosphate was fully repressed while from the glyceraldehyde-3-phosphate to pyruvate was affected by an 8-fold reduction.
5. While the lactate metabolism was depleted when glucose was replaced by fructose, when fructose was supplemented with lactate, the simultaneous consumption of both compounds was observed.

6. The lactate addition to a fructose-based media increased the flux through the TCA cycle by almost 4-fold if it is compared with results obtained when fructose was used as a carbon source and in 2-fold if it is compared with the glucose ones.
7. An almost fully inactivation of the malate-aspartate shuttle responsible for the internalization of the cytoplasmic NADH to the mitochondria was observed when glucose was replaced by fructose. However, when lactate was added as a carbon supplement in the fructose-based media, a completely and improved reactivation of the flux through it was observed. Mainly, because a high flux of pyruvate and NADH were released to the cytoplasm increasing the carbon and energy metabolism of the mitochondria when lactate was solely consumed.

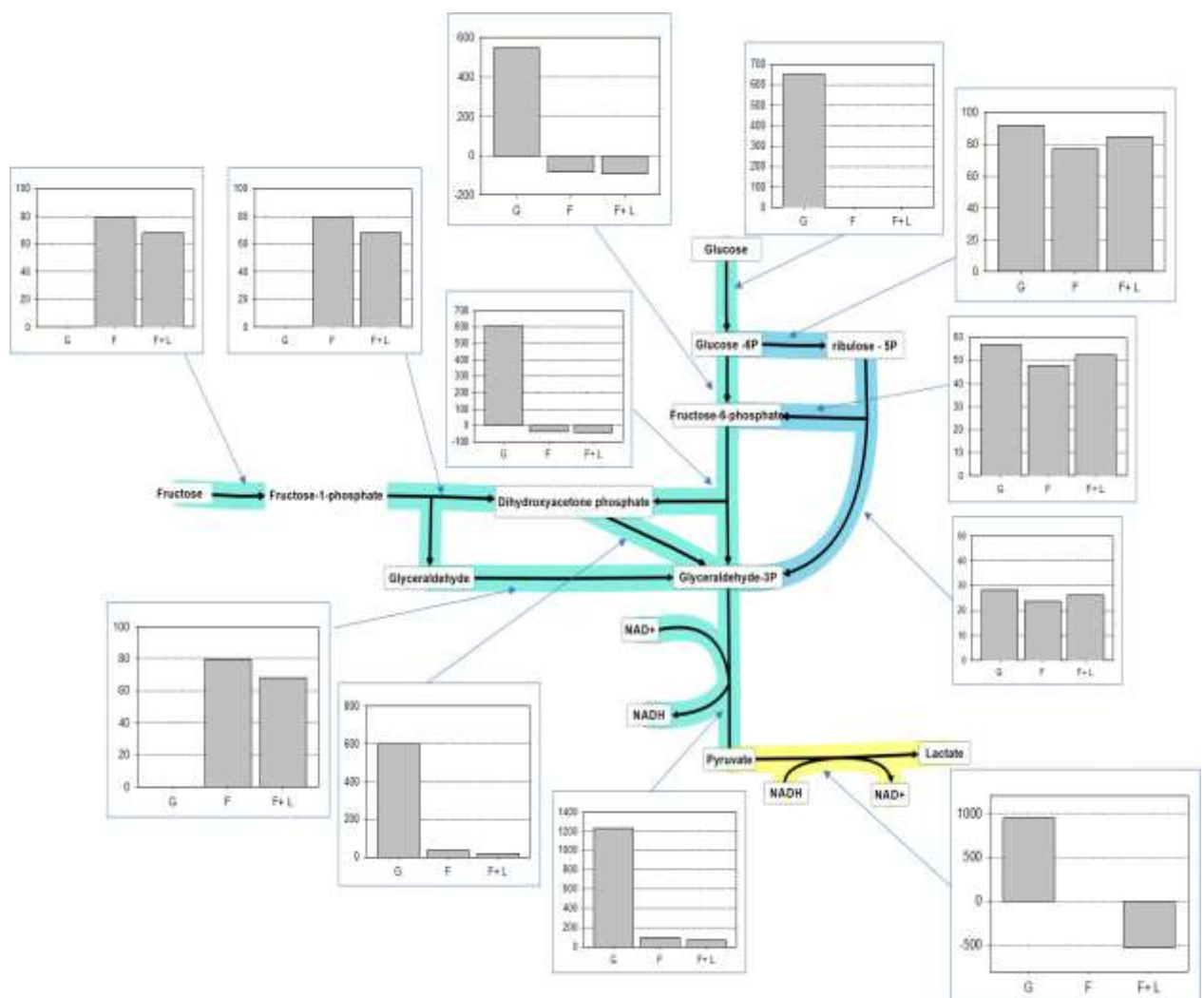


Figure 5-15 Metabolic comparison of the glycolytic pathway when HEK293 was cultured on glucose (G), fructose (F) and fructose supplemented with sodium lactate (F+L) as a carbon source. All the flux depicted are in nmol-mgDW⁻¹·h⁻¹.

As shown in **Figure 5-15**, the main difference between fructose and glucose in relation with the glycolytic pathway, which have repercussions over all the carbon metabolism, was the transport rate through the plasma membrane. The transporters responsible for moving across the plasmatic membrane (the GLUT family proteins) have a higher affinity to glucose than fructose.

It is described that the on GLUT family there several proteins capable of transporting glucose with different affinities, however only GLUT5 can internalize fructose from the cytoplasm with an acceptable rate even if it is described as a low affinity transporter (Concha et al., 1997)(Cura & Carruthers, 2012)(Nomura et al., 2015).

On the other side, the contribution in the gluconeogenesis of the PPP as an anaplerotic reaction has to be mentioned, owing to more the 50% of the required flux was contributed by the transketolase reactions.

During all this chapter, the lactate production has been described as a consequence of a high flux through the glycolytic pathway and consequently, a high cytoplasmic NADH generation that can not be fully oxidized via mitochondrial shuttles and has to be oxidized within the cytoplasm via lactate formation. As it can be observed, this statement can be corroborated due to the fact that when glucose was replaced by fructose, and as a result, the glycolytic flux was reduced by almost 8-fold, the lactate production was repressed. Furthermore, this metabolic trait was responsible for the production of lactate in two cell lines, HEK293 and hybridoma either KB26.5 or KB26.5-BHRF1. In relation with the decrease in the glycolytic pathway, a decrease in the cytoplasmic NADH was observed when glucose was replaced by fructose. However, when fructose was supplemented with lactate, a high increase in the cytoplasmic NADH proceed from the lactate oxidation was observed. It is important to keep in mind the capacity for reducing the NAD via glycolysis or lactate had a big impact in the mitochondrial metabolism.

Therefore, the glycolytic pathway was affected by the change of glucose to fructose, while it remained unaffected to the addition of lactate to the fructose. Moreover, the cytoplasmic NADH production was reduced when glucose was substituted by fructose and then, it was increased when fructose was supplemented with fructose. However, as shown in **Figure 5-16**, the decrease in the glycolytic pathway in relation with the use of fructose, was directly related to a decrease in the flux through the TCA cycle as well as the inactivation of the malate-aspartate shuttle. Even if the shuttle was inactivated, the oxidation of cytoplasmic NADH was still performed via a specific reaction from the malate-aspartate shuttle, the malate formation, when fructose was used as a carbon source where the internalization of malate from the cytoplasm to the

mitochondria was solely carried out by the antiport of citrate instead of via the malate-aspartate shuttle.

When fructose was supplemented with lactate a completely increase in the carbon influx to the mitochondria was observed, as shown in **Figure 5-16**, the pyruvate transported from the mitochondria reached a flux higher than the one obtained when glucose was used as a carbon source. An almost 2-fold decrease in the pyruvate was observed when glucose was substituted by fructose and thus, when lactate was added to fructose, the flux increased in almost 5-fold reaching a 2-fold increase in regard with the flux obtained when glucose was used as a carbon source. Moreover, the 5-fold increase was also paired with 5-fold increase and a fully activation of the malate-aspartate shuttle.

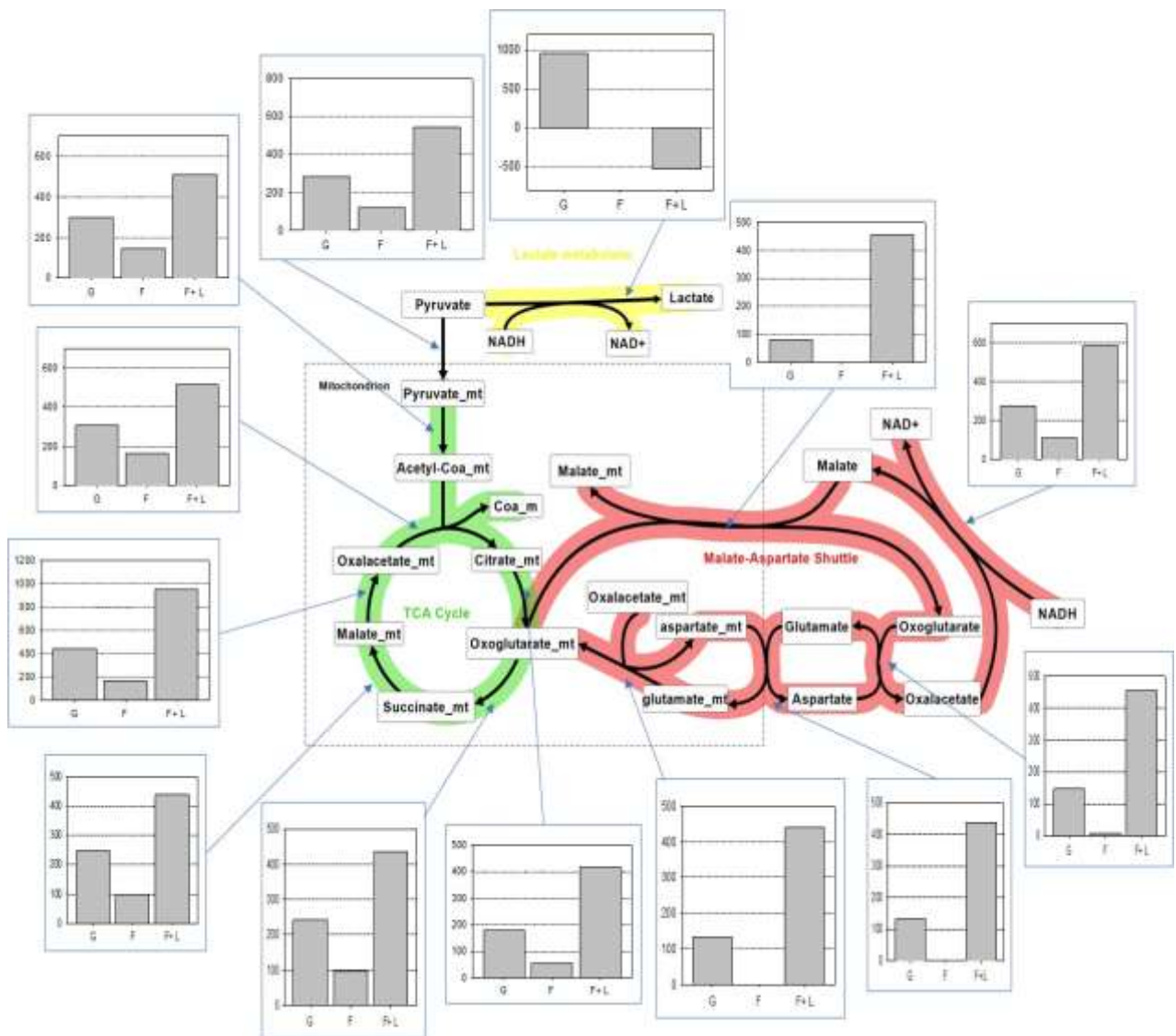


Figure 5-16 Metabolic comparison of the mitochondrial carbon metabolism when HEK293 was cultured on glucose (G), fructose (F) and fructose supplemented with sodium lactate (F+L) as a carbon source. All the flux depicted are in $\text{nmol-mgDW}^{-1}\cdot\text{h}^{-1}$.

Therefore, it could be state that lactate might be produced when the flux through the glycolytic pathway exceeds a certain value, as indicates the behaviour of the lactate metabolism when fructose was used instead of glucose. When the glycolytic flux is decreased, another issue appears which might be related to a carbon limitation or an energy limitation, the reduction of the growth rate. This reduction was overcome by the addition of lactate to the fructose-based media. Principally, the addition of lactate increased the pyruvate and cytoplasmic NADH availability and consequently increasing the carbon capacity of the mitochondria (both the TCA cycle and the malate-aspartate shuttle) until a level that were higher than the one obtained when glucose was used as a carbon source.

For a further description, the changes in the energy metabolism will be detailed and deepen in order to corroborate the conclusions presented in this section.

5.6.2.2 Metabolic model comparison between the energy metabolism of HEK293 when glucose, fructose and fructose supplemented with lactate were used as a carbon source

In order to begin with the study regarding how energy metabolism of HEK293 was affected by a change in the carbon source two assumptions related to the metabolic model must be taken into consideration:

- The relation that characterize the oxidative phosphorylation, the P/O, has a constant value of 4 in all the modelling done.
- The energy requirements used for biosynthesis depended on the stoichiometric value of the biomass equation.

Firstly, as shown in **Figure 5-17**, that the total ATP produce was based on three parameters: the availability of cytoplasmic NADH ,the lactate metabolism and the flux through the glycolytic pathway. When glucose was replaced by fructose, the lower level of ATP produced was achieved due to the lowest flux through glycolytic path and the lowest cytoplasmic NADH availability even if lactate was not produced. However, when fructose was supplement with lactate, even if the flux the through the glycolytic pathway until pyruvate formation was not increased, the oxidation of lactate to pyruvate increased the flux of pyruvate able to be transport to mitochondria while an increase in the cytoplasmic NADH was observed as well. Then, a carbon metabolism characterized by a low glycolysis pathway with the higher cytoplasmic availability in

regard with pyruvate and NADH was obtained along with an energy metabolism that produced more energy than the condition where glucose was used as a carbon source.

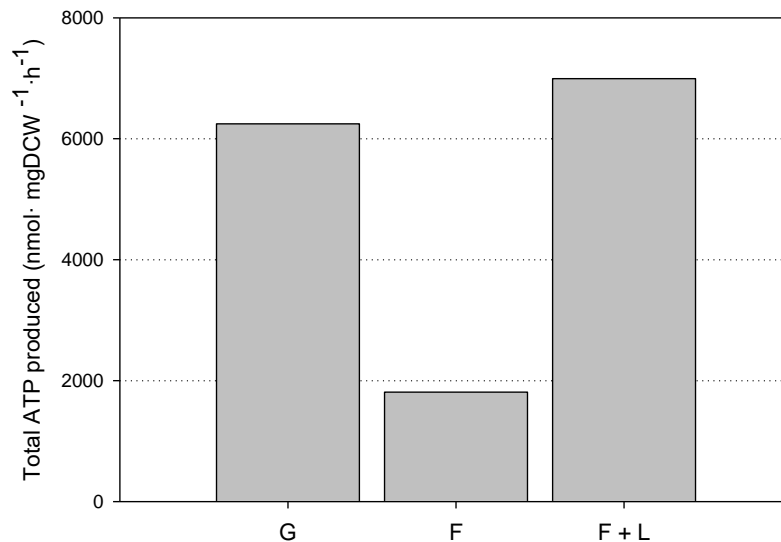


Figure 5-17. Comparison of the total ATP produced by HEK when glucose (G), fructose (F) and fructose supplemented with sodium lactate (F+L) were used as a carbon source.

As shown in **Figure 5-18**, when glucose was substituted by fructose the allocation of the ATP produced changed from a 56,9 % / 39,4 %, regarding the contribution of the OP and substrate level phosphorylation, to a 81% / 12% where the most part of the ATP produced came from OP. Moreover, there was a decrease of 21 % of the cell maintenance which it was already mentioned it might be related to the elimination of lactate production.

However, when lactate was added to the fructose-based media, the most OP oriented energy metabolism was obtained where more than 90 % of the total ATP came from the oxidative phosphorylation (OP). On the contrary, it was also the metabolic situation where the cell maintenance energy requirements were the highest (84%).

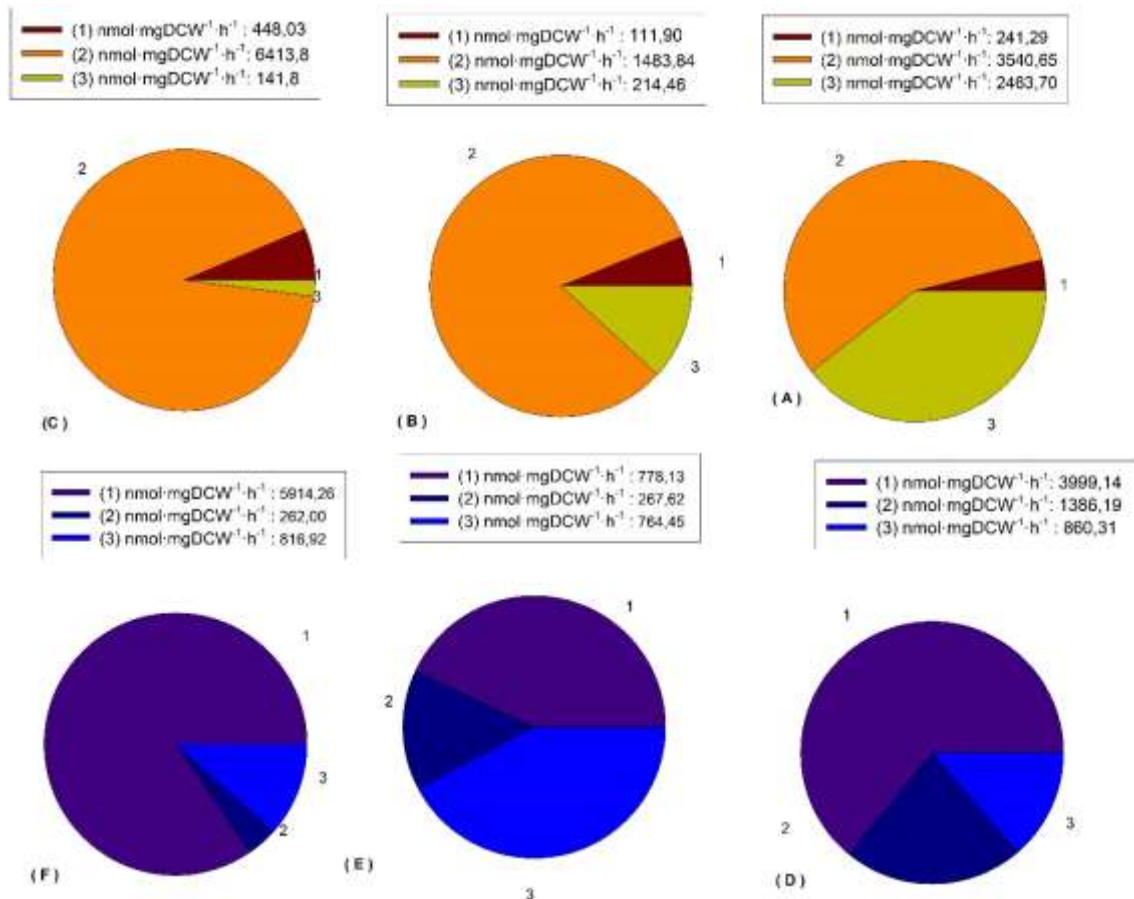


Figure 5-18 Comparison of the ATP produced and consumed by HEK cultured on different carbon sources. Figures: (A) distribution of ATP produced when glucose was used as a carbon source; (B) distribution of ATP produced when fructose was used as a carbon source; (C) distribution of ATP produced when fructose supplemented with sodium lactate was used as a carbon source; (D) distribution of ATP consumed when glucose was used as a carbon source; (E) distribution of ATP consumed when fructose was used as a carbon source; (F) distribution of ATP consumed when fructose supplemented with sodium lactate was used as a carbon source. The ATP produced was divided considering its provenance: 1) TCA cycle, 2) Oxidative phosphorylation and 3) Glycolysis. While the ATP consumed was divided in: 1) Maintenance, 2) Glycolysis and 3) Biomass synthesis.

Together with the distribution of the ATP and the total ATP produced, an update regarding the hypothesis between cell maintenance and carbon source can be presented.

Up until now, it was concluded that the cell maintenance was directly related to the relation between the flux through the glycolytic pathway and the lactate metabolism which, as it has been described, can be modified depending on which carbon sources was used. However, it should be express as the cell maintenance was directly related to the availability of cytoplasmic NADH to be transported to the mitochondria that was directly in touch with the flux through the glycolytic pathway and the lactate metabolism.

Therefore, when glucose was replaced by fructose, the redistribution in the energy metabolism was the consequence of adapting the carbon metabolism to a low cytoplasmic NADH availability

characterized by a low flux through the glycolytic pathway along with the presence of a gluconeogenic pathway in the upper part of the glycolysis. On the other hand, when fructose was supplemented with lactate, the redistribution in the energy metabolism was solely related to the improvement in the availability of pyruvate and NADH to be transported to the mitochondria owing to the cytoplasmic carbon metabolism until pyruvate remained almost unchanged.

Moreover, it can be concluded that the reduction in the specific growth rate caused by the replacement of glucose by fructose, might related to an energy limitation produced by the low capacity of fructose to be converted to ATP. On this basis, the addition of lactate was directly converted to ATP, as it can be observed in **Figure 5-17**, by means of the oxidative phosphorylation and then, the specific growth rate was increased.

Therefore, the lactate production in HEK293 cultures was avoided without having an effect on the specific growth rate because glucose was replaced by fructose supplemented with sodium lactate. However, hybridoma KB26.5 did not grown on other sugar; therefore, another way to decrease the lactate production will be studied. In this case, the study will be revolving around the expression of anti-apoptotic gene.

5.6.3 Reducing the lactate production by means of expressing an anti-apoptotic gene (BHRF1) using hybridoma KB26.5

As it was described at the beginning of the chapter, hybridoma KB26.5 was characterized by an inefficient carbon metabolism that converted the 75 % of the glucose consumed to lactate. The decrease of this proportion is the aim of this section, however the only way to interact the with the lactate metabolism is through genetic modification due to the incapacity of growing on others carbon sources instead of growing on glucose. A way to decrease the carbon metabolism was found in a previous study where its main objective was to solve a special problem of hybridoma KB26.5. This problem was based on a high apoptotic response when growth-limiting physiological conditions were achieved. In this study, an anti-apoptotic gene BHRF1 was transfected to hybridoma KB26.5, resulting in a new cell line called hybridoma KB26.5–BHRF1 (Juanola et al., 2009) . As a result, the overall metabolic behaviour of the hybridoma KB26.5 was modified due to the expression of the heterologous BHRF1 gene and the new cell line was conferred an resistance against apoptotic response. However, a collateral fact was observed, an optimization of the carbon metabolism via reducing the lactate generated that lead to an increase in the specific growth rate.

On this basis, in order to further explorer the genetic modification, the core of this section is to understand the changes in the carbon metabolism of Hybridoma KB 26.5–BHRF1 caused by the transfection of the anti-apoptotic gene (BHRF1), through the analysis and modelling of a specific experimental conditions and settings.

5.6.3.1 *Experiment in batch culture*

The experimental settings defined in order to culture the hybridoma KB 26.5–BHRF1 were based on using a bioreactor as a containment culture system. Moreover, every extracellular parameter can be controlled in order to ensure an optimal growth rate (as shown in the section 5.8.4) and the batch media used was a chemical defined media supplemented with FBS in both cases, which main carbon source was glucose (as shown in the section 5.8.2). Then, the carbon metabolism of hybridoma KB26.5–BHRF1 will be described and analyzed.

As shown in the **graph A of Figure 5-19**, when hybridoma KB 26.5–BHRF1 was cultured on a glucose-based media, it had a specific growth rate of $0,043 \text{ h}^{-1}$ and consumed $2,31 \text{ g}\cdot\text{L}^{-1}$ of glucose in order to achieve a maximum cell concentration of $3,8\cdot 10^6 \text{ cell}\cdot\text{ml}^{-1}$ while producing

1,23 g·L⁻¹ of lactate. Moreover, regarding how the carbon source was allocated, it is important to remark that for each gram of consumed glucose 0,53 g of lactate was produced as shown in **Table 5-10**.

As it was previously mentioned, using the trend from both glucose and lactate profiles over time in relation with the biomass trend, the specific consumption and production rates were calculated. The specific consumption rate of glucose had a value of 499 (nmol·mgDCW⁻¹·h⁻¹) that led to a lactate specific production rate of 689 (nmol·mgDCW⁻¹·h⁻¹) and a biomass generation of 0,043 (mgDCW·mgDCW⁻¹·h⁻¹). On the other side, related to the oxidation of glucose, the specific consumption rate of oxygen had a value of 690 nmol·mgDCW⁻¹·h⁻¹ and it was calculated using the variable oxygen uptake rate (OUR) represented in **graph B of Figure 5-19**.

As a result, the carbon metabolism of hybridoma KB26.5-BHRF1 was characterized as a moderate lactate producer owing 53 % of the carbon source was converted to lactate instead of biomass. However, it must take into consideration that the transfection of the BHRF1 gene decreased the conversion of glucose to lactate from 75% to 53%, as well as it can be observed an improvement of 30 % on the growth rate in comparison with hybridoma KB26.5.

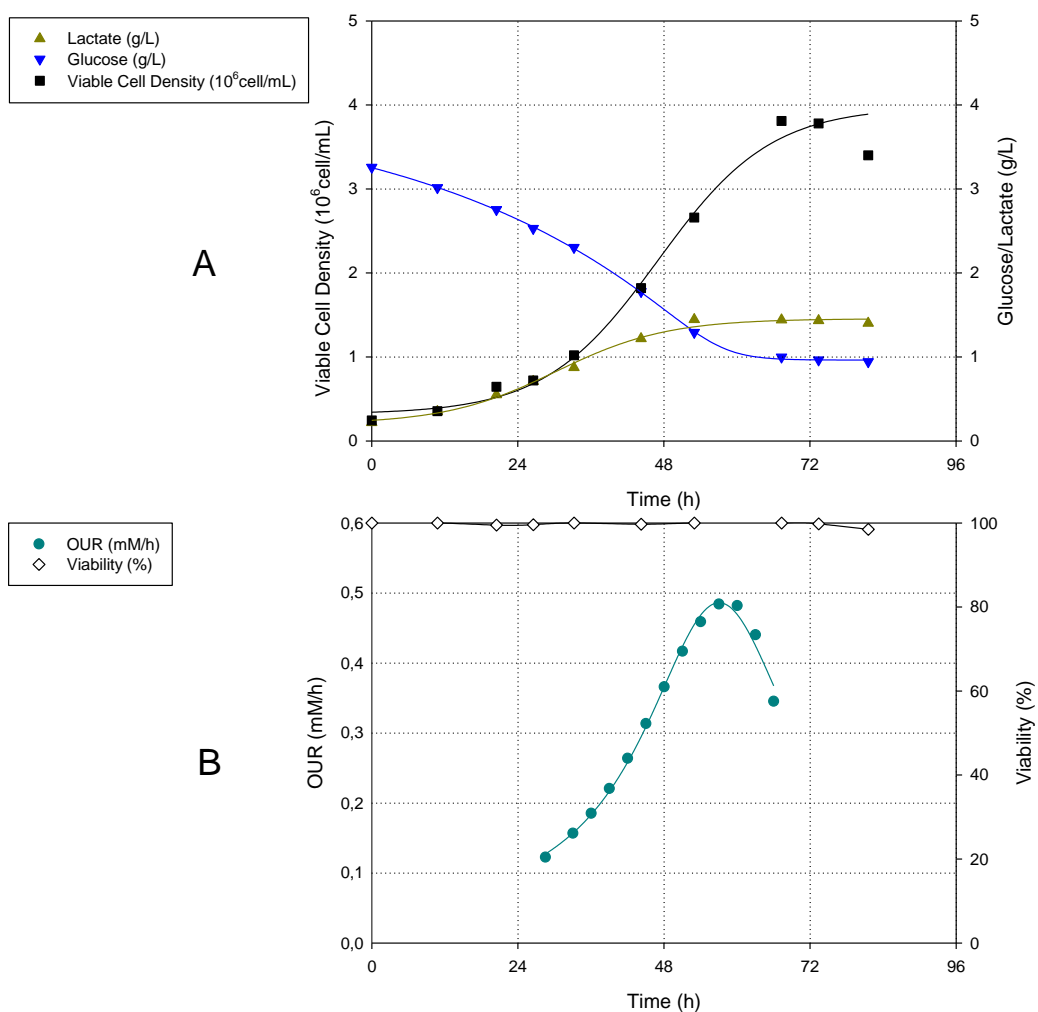


Figure 5-19 Profile of A) off-line variables such as Viable Cell Density (■), glucose (▼), lactate (▲) and B) on-line variable such as O.U.R (●) and off-line variable such as viability (◇) for hybridoma KB26.5-BHRF1 batch culture.

Table 5-10 Main characterization parameters for BHRF1 batch culture.

Biomass achieved ($10^6 \text{ cell} \cdot \text{mL}^{-1}$)	3,8
Glucose consumption ($\text{g} \cdot \text{L}^{-1}$)	2,31
Lactate production ($\text{g} \cdot \text{L}^{-1}$)	1,23
$Y_{\text{bio/gluc}}$ ($10^6 \text{ cell} \cdot \text{mL}^{-1} \cdot \text{g}^{-1} \cdot \text{L}$)	1,53
$Y_{\text{lac/gluc}}$ ($\text{g} \cdot \text{g}^{-1}$)	0,53
q_{glucose} ($\text{nmol} \cdot \text{mgDCW}^{-1} \cdot \text{h}^{-1}$)	499
q_{lactate} ($\text{nmol} \cdot \text{mgDCW}^{-1} \cdot \text{h}^{-1}$)	689
q_{O_2} ($\text{nmol} \cdot \text{mgDCW}^{-1} \cdot \text{h}^{-1}$)	690
μ (h^{-1})	0,043

Therefore, the transfection of the BHRF1 promoted the repression of the apoptosis response when non-growth conditions were reached, however another metabolic trait was observed. Together with the effect on the apoptosis mechanism, it had an effect on the carbon metabolism decreasing the conversion of glucose to lactate while improving the conversion of glucose to biomass. Consequently, the growth rate was enhanced.

For a further analysis, the modelling of the carbon and energy metabolism will be detailed hereafter in order to clarify the reasons behind the optimization of the carbon metabolism due to the expression of the BHRF1 gene.

5.6.3.2 Study of hybridoma KB 26.5–BHRF1 carbon metabolism by means of using metabolic models

A genomic-scale metabolic model will be used in order to describe how hybridoma KB26.5–BHRF1 transformed glucose to lactate and precursors for biomass synthesis, while getting the required energy for growing at optimal growth rate. The development and description of the model is explained in section 5.8.8.2.

For metabolic flux calculation, the model was constrained using the input-output data of the corresponding metabolites that are shown in **Table 5-4**. This data included the biomass formation. The optimization of the model was performed by means of the FBA protocol described in section 5.8.9, whose objective function to maximize was the cytoplasmic hydrolysis of the ATP to ADP.

Table 5-11 Specific rate limits used as drains for a Flux Balance Analysis in BHRF1 cell line ($\text{nmol} \cdot \text{mgDCW}^{-1} \cdot \text{h}^{-1}$).

Compound	Specific rate
$\mu (\cdot 10^3 \text{h}^{-1})$	47 ± 6
Glucose	$-542,20 \pm 177,45$
Lactate	$654,55 \pm 34,66$
Alanine	$48,30 \pm 4,15$
Arginine	$-15,51 \pm 8,82$
Asparagine	$3,05 \pm 0,68$
Aspartic acid	$0,48 \pm 0,80$
Cysteine	$-4,82 \pm 4,07$

Glutamic acid	0,84 ± 0,95
Glutamine	-179,66 ± 122,42
Glycine	-12,09 ± 6,78
Histidine	-5,36 ± 3,79
Isoleucine	-18,09 ± 16,35
Leucine	-24,59 ± 17,04
Lysine	-21,57 ± 17,48
Methionine	-6,51 ± 4,84
Ammonium	85,09 ± 15,90
Phenylalanine	-10,01 ± 8,84
Proline	1,99 ± 8,58
Serine	-13,91 ± 11,82
Threonine	-18,52 ± 18,50
Tryptophan	-1,07 ± 0,72
Tyrosine	-8,39 ± 7,97
Valine	-20,23 ± 18,01

The intracellular fluxes were calculated and using the visualization software OMIX (Droste et al., 2013), and are presented in **Figure 5-20**. In this figure, the metabolic relation between the different metabolites, mainly glucose and lactate is displayed.

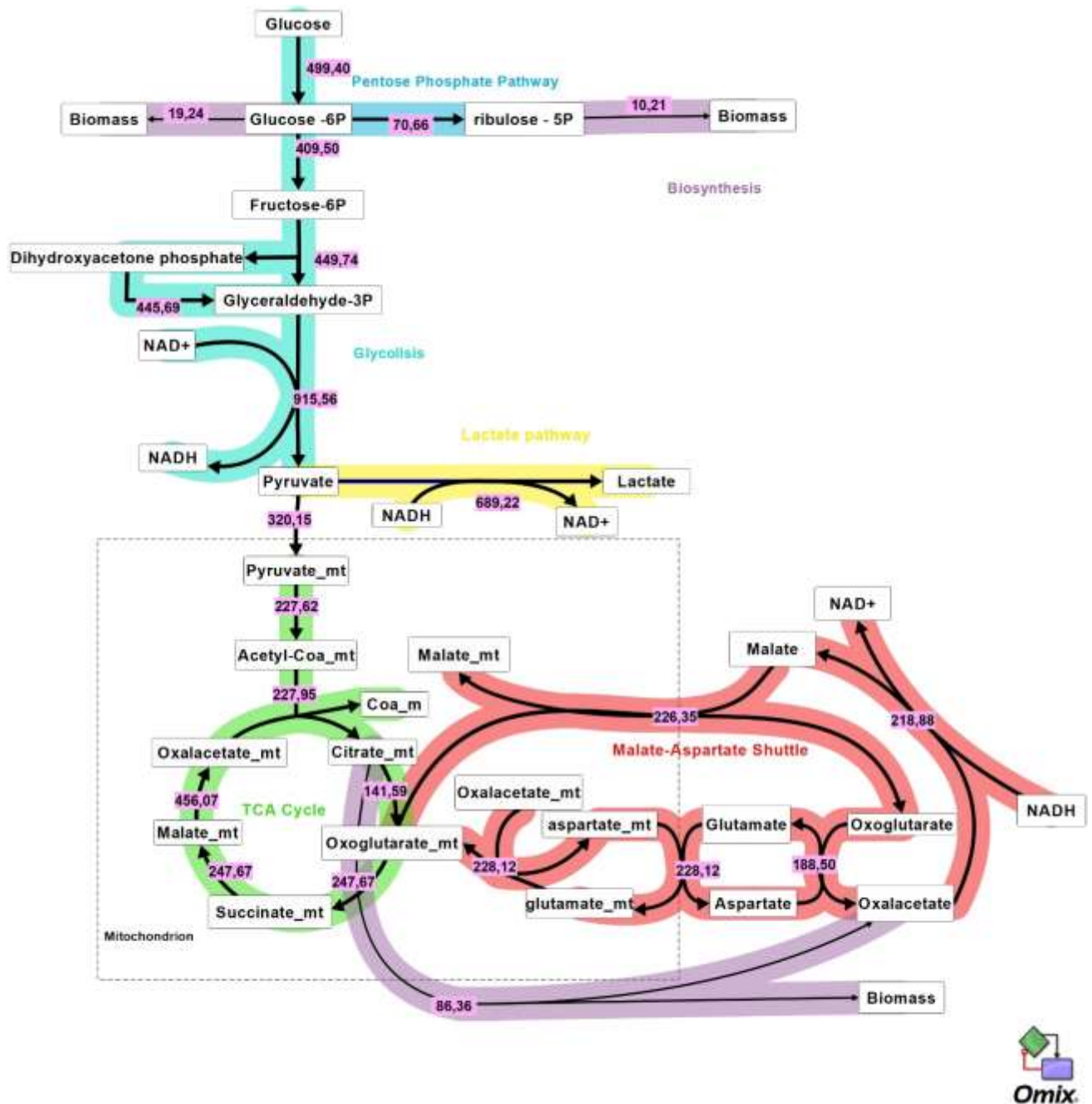


Figure 5-20 Scheme of the main metabolic fluxes calculated for BHRF1. Arrows indicate the direction of the flux and their width the magnitude of fluxes (the exact value is detailed close to the arrows). All the fluxes are expressed in $\text{nmol} \cdot \text{mgDCW}^{-1} \cdot \text{h}^{-1}$.

Firstly, glucose was transported by facilitated diffusion through plasma membrane into the cytoplasm (Plagemann & Richey, 1974), with a flux of $499,40 \text{ nmol} \cdot \text{mgDCW}^{-1} \cdot \text{h}^{-1}$ and then it is phosphorylated in order to get released glucose-6-phosphate via two proteins. The generation of glucose-6-phosphate has a flux of $499,40 \text{ mmol} \cdot \text{gDCW}^{-1} \cdot \text{h}^{-1}$. It was directed into two different routes: 82% was directed to the glycolytic pathway through conversion to fructose-6-phosphate via the phosphoglucose isomerase reaction and 18% was directed towards the formation of

biosynthesis precursors, specifically, 21,5% towards the formation of carbohydrate-related biomass compounds and plasmatic membrane compounds, and the rest (78,5 %) towards the formation of mainly nucleotides via the oxidative branch of the pentose-phosphate pathway. Thereupon, the flux directed to glycolytic pathway ($409,5\text{nmol}\cdot\text{mgDCW}^{-1}\cdot\text{h}^{-1}$) reacts until glyceraldehyde-3 phosphate. Then, glyceraldehyde-3 phosphate reacts until pyruvate, where 35% of the produced pyruvate can be transported through the mitochondrial membrane, while the rest (65%) was reduced to lactate via lactate dehydrogenase.

A key aspect of the hybridoma KB26.5–BHRF1 metabolism is that the production of lactate was related to the fact that not all the NADH generated via glycolytic pathway can be oxidized in the mitochondria via its internalization using the malate-aspartate shuttle, therefore an a perturbation in the cytoplasmic redox potential appeared caused by an unbalance in cytoplasmic NADH. Consequently, in order to balance the NADH, lactate was produced. Therefore, only 25 % of the NADH produced by glycolytic pathway can be oxidized via malate-aspartate shuttle, while the rest (75%) has to be principally oxidized via reduction of pyruvate to lactate (69% of the glucose consumed). However, the expression of the BHRF1 gene provoked an improvement in the glucose conversion to biomass owing to a 20% reduction of the lactate produced.

As it was mentioned before when hybridoma KB26.5 was described, it can be stated that the main metabolic trait responsible for the production of lactate while growing on glucose-based media in aerobic conditions was related to perturbations in the redox potential caused by an unbalance in the NADH cytoplasmic. This unbalance was caused by a rate difference between the flux through the glycolytic pathway and the flux through the mitochondrial membrane shuttle responsible for the oxidation of the NADH cytoplasmic. The relation between the expression of the gene BHRF1 and the modification caused by it will be described at section5.6.4.1.

Regarding the biomass formation, the main precursors are generated from ribulose-5P (derivation of 0,5 % of glucose carbon-mol uptake rate); glucose-6-phosphate (derivation of 1,33 % of glucose carbon-mol uptake rate); and citrate (derivation of 1,9 % of glucose carbon-mol uptake rate).

Once the carbon metabolism has been analysed, it is important to realize that coupled with carbon metabolism appears energy metabolism. Therefore, to understand how the energy required for the synthesis of the precursors destined to biomass generation and cell

maintenance was handled, the study of the energy metabolism will be shown in the following section.

5.6.3.3 Study of hybridoma KB 26.5 – BHRF1 energy metabolism by means of using metabolic models

As shown in **graph A) of the Figure 5-21**, the proportion of the ATP produced mainly came from two sources (Kim, 1985) (Farmer & Liao, 1997): the first source of ATP comes from ATP synthase and the second source of ATP comes at the substrate level phosphorylation, which is a reaction that takes part in glycolytic pathway in the cytoplasm.

In the case of hybridoma KB26.5–BHRF1, the ATP production by OP had more impact in ATP proportion as the substrate level phosphorylation due to the fact that the 25% of the NADH generated via glycolysis was transported to the mitochondria by means of shuttle-based mechanism instead of being oxidized by lactate dehydrogenase.

Regarding substrate level phosphorylation, the generation of ATP is based on the use of two specific group of proteins:

- The first one is related to the kinase group (pyruvate kinase and phosphoglycerate kinase), that catalyse the transfer of phosphate groups from high energy phosphate-donating molecules to specific substrates, specifically, from phosphoenolpyruvate to ADP and from 1,3-bisphosphoglycerate to ADP
- The second one is based on a mitochondrial ligase, specifically Succinyl-CoA ligase.

On the other side, in **graph B) of the Figure 5-21**, the proportion of ATP consumed showed an allocation of ATP mainly in cell maintenance, biomass generation and in the reactions catalysed by phosphofructokinase and hexokinase proteins from the glycolytic pathway.

As previously mentioned, the cell maintenance tackles all the cellular process whose function is not related to formation of new cell material and in order to maintain its performance 55 % of the ATP produced was needed.

Regarding the reactions catalysed by kinases, nearly 18 % of the total ATP produced was mainly consumed by phosphofructokinase and hexokinase both from the glycolytic pathway. Finally, the last one of the main consuming ATP reactions is the biomass formation, whose ATP consumption was 27 % of the ATP produced, although it has to be taken into consideration that

the energy requirements for synthesis of biomass precursors are defined by the biomass equation.

Although, there are two points related to the energy metabolism of hybridoma KB26.5 – BHRF1 growing on glucose-based media in aerobic conditions that has to be pointed out:

3. The ATP produced from the oxidative phosphorylation had more contribution than the kinase-based reaction from to the glycolytic pathway.
4. In order to reach the optimal growth rate, the energetic requirements for cell maintenance (55 %) were higher than the required ones for the synthesis of new cellular material (27 %).

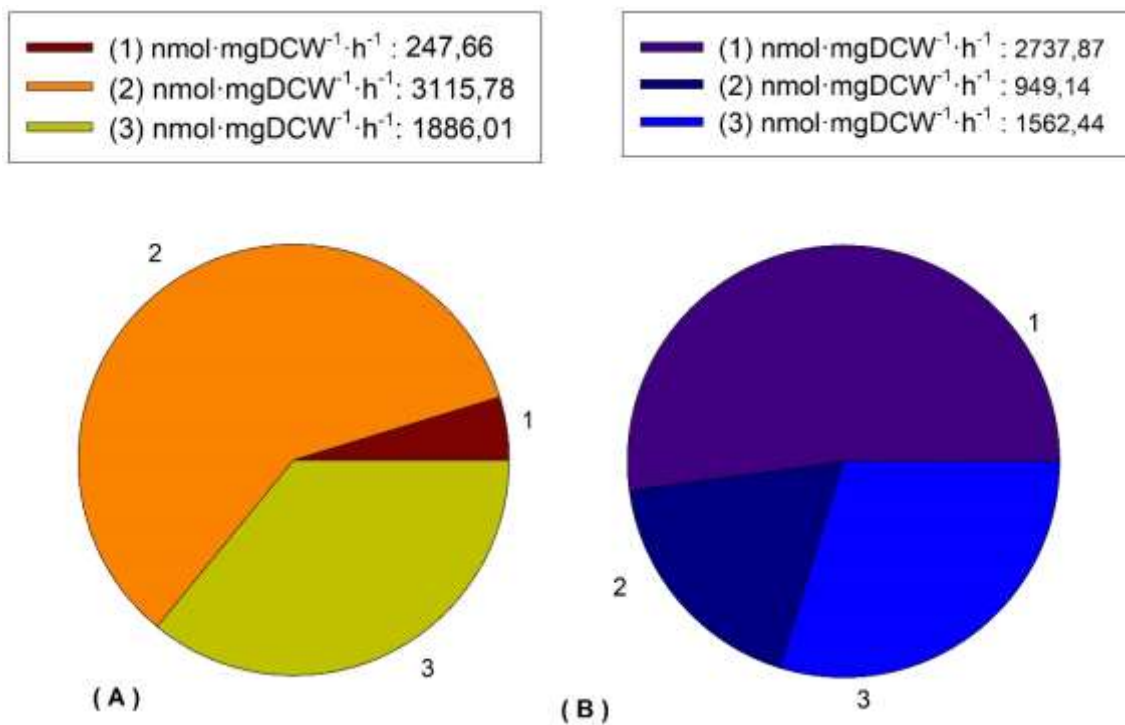


Figure 5-21 Distribution of ATP produced and consumed in hybridoma KB26.5-BHRF1. In figure A, the ATP produced is divided depending on its provenance (TCA cycle (1), Oxidative phosphorylation (2) and Glycolysis (3)). While in figure B, the ATP consumed is separated depending on its provenance (Cell maintenance (1), Glycolysis (2) and Biomass formation (3)).

To conclude, after the analysis of the carbon and energy metabolism, the main metabolic issue of hybridoma KB26.5–BHRF1 has been found to be related to an unbalance in NADH produced

flux caused by the restrictions in its regeneration of NADH owing to a high flux through the glycolytic pathway. As a result, leading hybridoma KB26.5-BHRF1 to a metabolic state where mainly the NADH produced by glycolytic pathway was oxidized via lactate pathway instead of being transported via shuttle-based mechanisms from the cytoplasm to the mitochondria and then, oxidized via OP. However, the transfection of the BHRF1 gene provoked a metabolic restructuring that optimized the carbon conversion towards biomass due to the reduction in the lactate generation. Moreover, not only the carbon conversion was optimized, the specific growth rate was increased as well.

Therefore, in order to present a global overview between the hybridoma KB26.5 and hybridoma KB26.5- BHRF1, a metabolic comparison where either the carbon metabolism or the energy one will be presented here after. On this basis, a more accurate hypothesis regarding the metabolic modification caused by the expression of the BHRF1 gene could be developed.

5.6.4 Metabolic model comparison between hybridoma KB26.5 and hybridoma KB26.5 – BHRF1

5.6.4.1 Metabolic model comparison between the carbon metabolism of hybridoma KB26.5 and KB26.5 – BHRF1.

Up until now, all the carbon metabolism referred to how hybridoma KB26.5 and *hybridoma KB26.5 – BHRF1* consumed glucose and, then, was converted to biomass precursors while producing lactate under aerobic conditions has been described independently. Although, the principal metabolic trait that is responsible for lactate production in hybridoma KB26.5, also was present in hybridoma KB26.5-BHRF1 because the main trait was related to the regulation of the cytoplasmic redox potential by handling the balance of cytoplasmic NADH generated via glycolytic pathway in both cell lines. However, it has to be remarked that the transfection of BHRF1 gene to hybridoma KB26.5 provoked a change in the carbon metabolism that decreased the conversion of glucose to lactate.

In order to begin with the study that will be presented hereafter, one assumption related to the metabolic model must be taken into consideration:

- The stoichiometric matrix was the same for both cell lines as well as its biomass equation.

As shown in **Figure 5-22**, the comparison between hybridoma KB26.5's fluxes and hybridoma KB26.5-BHRF1's ones revealed interesting traits, which are presented hereafter:

1. A decrease of 2 fold of the flux through the glycolytic pathway.
2. A 2,58 fold decrease of the flux through the lactate pathway.
3. There was no change in the flux through the malate-aspartate shuttle.

These differences might be explained taking into consideration the capacity to regulate the redox potential by means of handling the balance of cytoplasmic NADH. This capacity is strictly related to mainly two aspects: the first one is related to the amount of the NADH produced via glycolytic pathway in the cytoplasm, and the second one, it is related to the metabolic mechanism on top of transporting the electron from the NADH from cytoplasm to mitochondria, therefore, performing the oxidation of the NADH to NAD. The principal mechanism for the "electron transport" is based on the shuttle-based reaction mechanisms, such as the malate-aspartate shuttle, whose mechanism reaction revolves around the reduction of oxaloacetate to malate in the cytoplasm and, then malate is transported via the antiport malate-oxoglutarate (Matsuno, 1992).

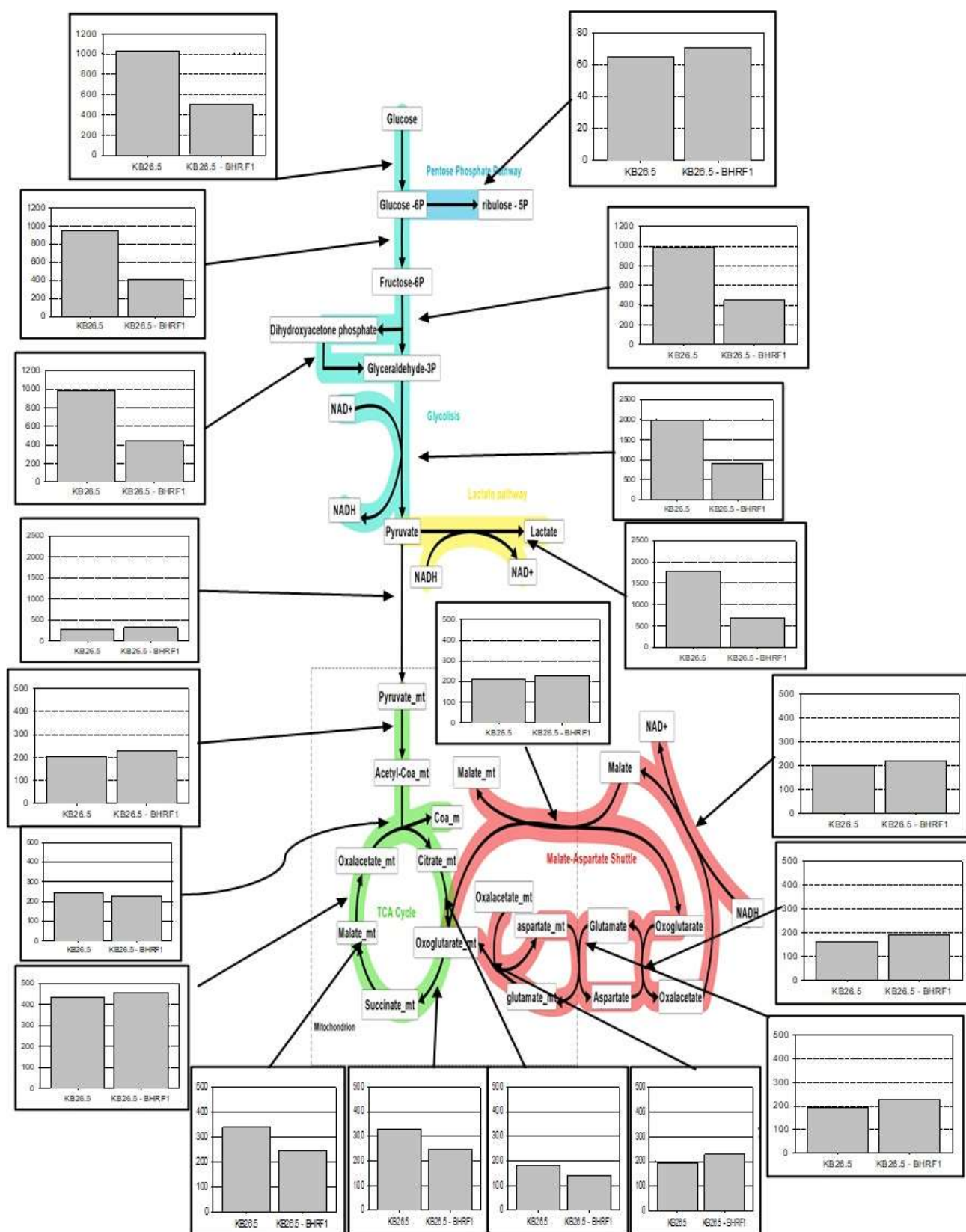


Figure 5-22. Metabolic comparison of the carbon metabolism between hybridoma KB26.5 (KB26.5) and hybridoma KB26.5-BHRF1 (KB26.5-BHRF1). All the flux depicted are in nmol-mgDW⁻¹·h⁻¹.

In the last years, several publications approaching the reason behind the lactate production has been revolving around different topics, from how the flux through the glycolytic pathway can be modified in order to transport the maximum flux of glucose to the cytoplasm (Potter, Newport, & Morten, 2016b) to how the mitochondrial metabolic state could affect the redox compartmentalization (Kietzmann, 2010). However, even if both theories disagree about which should be the initial trigger responsible for the lactate production, be a metabolic adaptation due to high extracellular glucose concentration or due to the mitochondria metabolic state. Both of them agree about that perturbation in the redox potential caused by an unbalance in the NADH cytoplasmic is the “key” condition in order to promote the lactate metabolism.

In order to explain why the transfection of the gene BHRF1 was related to the optimization of the carbon metabolism towards biomass formation by means of decreasing the lactate production, first what effect had BHRF1 on the cell metabolism should be explained. It is described that the expression of the gene BHRF1 as a homolog of BCL-2 (a pro-survivable protein) (Kvansakul et al., 2010) might be interacting with the physiology of the mitochondrial membrane owing to the BCL family is on top of regulating the permeabilization of the mitochondrial membrane when apoptotic conditions are triggered (Chipuk & Green, 2008).

A possible hypothesis on top of how the carbon metabolism was affected by the gene BHRF1, could be that the BHRF1 protein affected the metabolic state of the mitochondria altering its membrane physiology and as a result, interacting with the redox compartmentalization. This interaction was responsible for decreasing by 2-fold the glycolytic pathway and also by 2,58-fold the lactate pathway while optimizing the conversion of glucose to energy and biomass precursors.

However, there is an interesting fact regarding the oxidation of the mitochondrial NADH, even if there was a decrease in the lactate production, the oxidative phosphorylation was almost not affected if it is taken into consideration the effect on the glycolytic pathway. Therefore, it can be added that the expression of the BHRF1 gene provoked a metabolic modification of the glycolytic pathway focused on decreasing the lactate produced while the flux through the mitochondrial metabolism was almost or nearly unaffected .

Regarding the increase in the specific growth rate, it could be related to a slightly increase in the precursors from the mitochondria and also to an increase in the total ATP produced due to the modification of the mitochondrial energy metabolism by the expression of an anti-apoptotic gene, in this case the BHRF1 (Templeton et al., 2014). It is important to highlight that a modification in the mitochondrial energy metabolism might mean that the oxidative

phosphorylation might be improved changing the P/O ratio, as a result, more ATP than the expected might be produced. However, in the study presented, the modification of the P/O ratio was not taken into consideration.

Therefore, the expression of the anti-apoptotic gene BHRF1 modified the mitochondria metabolism and consequently, the relation between the redox potential of the cellular compartments changed, leading to a metabolic situation where the flux through the glycolytic pathway was reduced. The reduction in the glycolytic pathway provoked a decrease in the cytoplasmic NADH produced and as a result, the lactate metabolism was reduced. Finally, the carbon and energy metabolic modification promoted the synthesis of enough biomass precursors and energy which made possible a 30 % increase in the specific growth rate.

Lastly, once in the carbon metabolism has been reached a feasible hypothesis for the lactate production and the increase in the specific growth rate, a global view of how this change in carbon metabolism affects the energy metabolism will be presented.

5.6.4.2 Metabolic model comparison between the energy metabolism of Hybridoma KB26.5 and KB26.5 – BHRF1.

In order to begin with the study regarding the comparison between the energy metabolism of hybridoma KB26.5 and hybridoma KB26.5-BHRF1 that will be presented hereafter, two assumptions related to the metabolic model must be taken into consideration:

- The relation that characterizes the oxidative phosphorylation, the P/O, has a constant value of 2,5 in all the modelling done.
- The energy requirements used for biosynthesis depended on the biomass equation.

Regarding to the ATP produced, as shown in, hybridoma KB26.5 produce 55% more ATP than hybridoma KB26.5-BHRF1, $8153\text{nmol}\cdot\text{mgDCW}^{-1}\cdot\text{h}^{-1}$ and $5250\text{nmol}\cdot\text{mgDCW}^{-1}\cdot\text{h}^{-1}$ respectively. The increase in the ATP production might be related to grant a high lactate producer metabolism where high-energy requirements were needed in form of cell maintenance. On this basis, the decrease in cell maintenance calculated when the lactate production was reduced by the transfection of the BHRF1 gene might be expected.

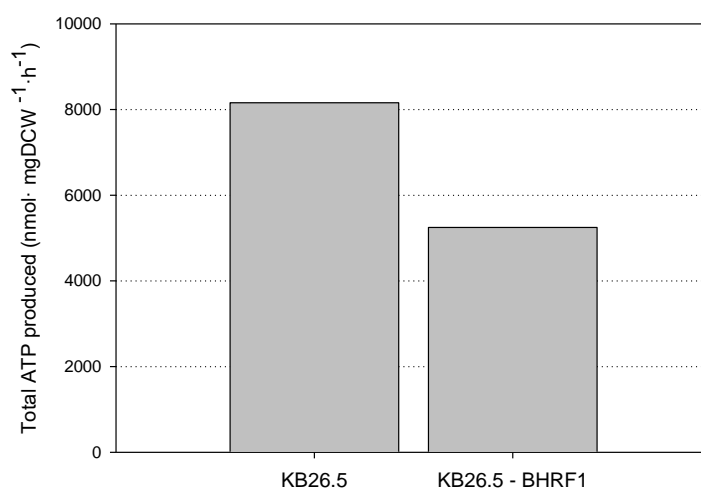


Figure 5-23. Comparison of the total ATP produced by hybridoma KB26.5 (KB26.5) and hybridoma KB26.5 – BHRF1 (KB26.5-BHRF1)

As shown in **Figure 5-24**, several differences regarding the allocation of the ATP were observed in relation with how the ATP produced and consumed was allocated taking into consideration how the transfection of the anti-apoptotic gene affected the carbon metabolism:

- The 49 % of the ATP produced by hybridoma KB26.5 comes from the substrate level phosphorylation related to the glycolytic pathway, while in hybridoma KB26.5–BHRF1 only the 35% comes from it. This difference was related because the flux through glycolysis was higher in hybridoma KB26.5 than in hybridoma KB26.5-BHRF1 and it is important to remember that the high lactate production in hybridoma KB26.5 limited the production of ATP from OP. As a result, the allocation of ATP produced via aerobic metabolism based on TCA cycle and OP increased from 46% of the total ATP produced to 56%, owing to the transfection of BHRF1 gene to the hybridoma KB26.5.
- The most relevant matter regarding ATP consumption is related to cell maintenance, hybridoma KB26.5 (5014,73 nmol·mgDCW⁻¹·h⁻¹) have higher cell maintenance than hybridoma KB26.5-BHRF1 (2737,87 nmol·mgDCW⁻¹·h⁻¹) even if the growth rate of hybridoma KB26.5 was lower than hybridoma KB26.5-BHRF1. As it was mentioned before, this behaviour might indicate that for growing at optimal growth rate hybridoma KB26.5 have more energy requirements than hybridoma KB26.5-BHRF1. Basically, one of the main reasons behind the cell maintenance decrease might be related to maintain a certain flux through carbon metabolism direct to produce high lactate fluxes.

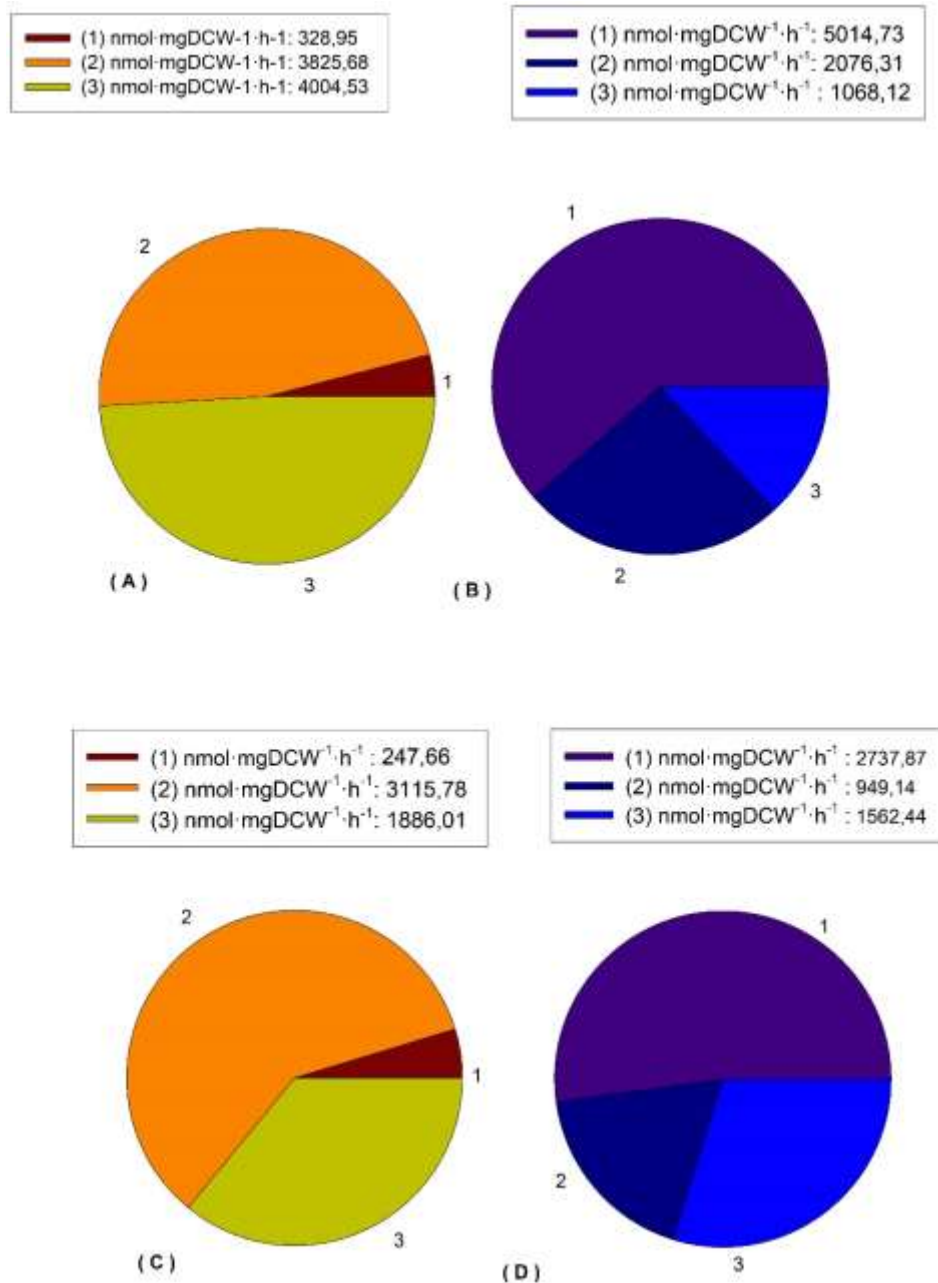


Figure 5-24. Comparison of the ATP produced and consumed of hybridoma KB26.5 and hybridoma KB26.5-BHRF1. (A) distribution of ATP produced by hybridoma KB26.5, (B) distribution of ATP consumed by hybridoma KB26.5, (C) distribution of ATP produced by hybridoma KB26.5-BHRF1 and (D) distribution of ATP consumed by hybridoma KB26.5-BHRF1. The ATP produced was divided considering its provenance: 1) TCA cycle, 2) Oxidative phosphorylation and 3) Glycolysis. While the ATP consumed was divided in: 1) Maintenance, 2) Glycolysis and 3) Biomass synthesis.

To summarize, there are big differences between ATP produced from hybridoma KB26.5 and hybridoma KB26.5-BHRF1 owing to the difference in their flux through the glycolytic pathway and the lactate metabolism. The contribution of the ATP from the oxidative phosphorylation is higher in hybridoma KB26.5-BHRF1 than in hybridoma KB26.5. Moreover, there is a peculiar trait regarding cell maintenance, the higher energy requirements cannot be correlated to higher

growth rates owing to hybridoma KB26.5–BHRF1 has the higher growth rate and the lower cell maintenance, although they might be related to the lactate production. The higher the lactate production was, the higher the cell maintenance was needed in order to grant the optimal specific growth rate.

5.7 Discussion and conclusions

An extensive study of the carbon metabolism focused on the conversion of the carbon source to lactate in three animal cell lines (hybridoma KB26.5, hybridoma KB26.5 -BHRF1 and HEK293) has been presented in this chapter. The conventional metabolic behaviour of all the cell lines studied was characterized by a high glucose consumption rate, while lactate was being produced and secreted to the media in an uncontrolled manner, leading the metabolism to an inefficient conversion from glucose to biomass. It has to be taken into consideration that the Warburg effect or the production of lactate in aerobic conditions in animal cells has been extensively studied (Potter et al., 2016a). However, the study presented was focused on the reduction of the lactate generated while the specific growth rate remained unaffected.

In order to do that a high producer animal cell line was selected as an initial point, in this case the hybridoma KB26.5. Hybridoma KB26.5 presented an accentuated production of lactate where the 75 % of the glucose consumed was converted to lactate along with a sensible apoptotic response when non-growth conditions were reached. Through the analysis of the metabolic fluxes carried out using a reduced genomic-scale metabolic model, it was suggested that the lactate production was related to a perturbation of the redox potential caused by an unbalance in the cytoplasmic NADH pool. The unbalance was caused by a difference between the fluxes through the glycolytic pathway and the one on top of its regeneration via mitochondrial shuttles.

A study regarding the apoptosis mechanism in hybridoma KB26.5 was found where excellent results were obtained when hybridoma KB26.5 was transfected with anti-apoptotic gene BHRF1. Basically, the transfection of the BHRF1 provoked a restructuration of the hybridoma KB26.5 carbon metabolism while gaining a resistance against the sensible apoptotic response that the hybridoma KB26.5 was characterized. This new cell line, the hybridoma KB26.5-BHRF1, was cultured and compared with the parental cell line, the hybridoma KB26.5, in order to understand the causes behind the different behaviour.

Hybridoma KB26.5-BHRF1 showed a reduced conversion of glucose to lactate while the specific growth rate was improved. The metabolic analysis concluded that the reduction in the lactate

produced revolved around a decrease in the flux through the glycolytic pathway that could be caused by the interaction between the BHRF1 gene and the mitochondrial metabolism that lead to the modification of the cellular redox compartmentalization. Moreover, the increase of the specific growth could be related to a slightly increase in the biomass precursors from the mitochondria and also to an increase in the total ATP produced due to the modification of the mitochondrial energy metabolism by the expression of an anti-apoptotic gene, in this case the BHRF1 (Templeton et al., 2014). It has to be pointed out that in the data from the energy metabolism regarding hybridoma KB26.5- BHRF1, an increase in the ATP was not observed due to the oxidative phosphorylation key parameter the ratio P/O had the same value as the one used with the hybridoma KB26.5. Therefore, the expression of the BHRF1 affected the energy metabolism, mainly the redox cofactor balance, which led to a metabolic condition where there were enough biomass precursors and energy for increasing the specific growth rate while the lactate production was reduced.

As it was expected when HEK293 was cultured on glucose, a high lactate producer metabolism was observed due to a high flux through the glycolytic pathway that provoked a high availability of cytoplasmic NADH. This cytoplasmic NADH was oxidized by pyruvate instead of being transport via malate-aspartate shuttle to the mitochondria. As a result, the metabolism of HEK293 growing on glucose was characterized by the conversion of 43 % of the consumed glucose to lactate and by an allocation in the energy metabolism where 39,4% came from glycolysis while 56,9% came from oxidative phosphorylation.

Then, when fructose was used as carbon source, a non-lactate producer metabolism was obtained due to a low flux through the glycolytic pathway that provoked a low availability of cytoplasmic NADH and a gluconeogenic pathway was required in order to synthesize the biomass precursor from the glucose-6-phosphate. All of the cytoplasmic NADH was oxidized by malate-aspartate shuttle and transported to the mitochondria. As a result, the metabolism of HEK293 growing on fructose was characterized by the fully conversion of fructose to biomass and by an allocation in the energy metabolism where the oxidative phosphorylation prevailed as the main ATP source (81% of the total ATP produced). However, a reduction in the growth rate was observed due to a rate limitation in production of biomass precursors related to either the carbon or the energy metabolism.

In order to increase the specific growth rate, fructose was supplemented with sodium lactate and as a result, the specific rate was recovered while fructose was consumed simultaneously with lactate. The addition of lactate only increased the mitochondrial metabolism because all

the lactate consumption was oxidized to NADH and pyruvate. Both compounds were internalized to the mitochondria where they were converted into biomass precursors and energy. As a result, this was almost a fully aerobic metabolism where almost all the energy produced by the cell was generated by the oxidative phosphorylation. However, one trait was observed, the cell maintenance was directly related to the cytoplasmic NADH production, the higher the cytoplasmic NADH handling, higher the cell maintenance was.

To conclude, an extensive study regarding how a specific carbon sources is metabolized in order to produce energy, biomass precursors and sub-products was described. Moreover, taking into consideration that lactate was the “star” sub-product when animal cells are cultured, several methodologies were carried out in order to reduce partially or completely the lactate production. These methodologies tackled different approaches: from a change in the extracellular conditions to a genetic modification based on an anti-apoptotic gene.

Finally, the results presented in this chapter, that were focused on the comprehension of the carbon and energy metabolism of animal cells lines, will be used to design engineering-based tools in order to monitor and control high-density cell cultures. In this work, the high-density cell cultures selected will be the fed-batch and perfusion cultures, because one of the key aspects in its definition is understanding the metabolism of the selected expression platform. Through its comprehension, a more suited feeding profile based on the metabolic requirements will be designed in order to avoid one of the main issues the over-feeding. The over-feeding should occur when a difference between the expected carbon metabolic behaviour and the real one takes place (Schaepe, Kuprijanov, Simutis, & Lübbert, 2014). Therefore, the metabolic study described in this chapter will be taken into consideration in order to design a fed-batch and perfusion strategy, as it will be presented in **chapter 9**.

5.8 Materials and Methods

5.8.1 Cell lines and cell maintenance

The cell lines used in this work were HEK293SF-3F6 cell line expressing a GFP; and two hybridoma cell lines: hybridoma KB 26.5 and hybridoma KB26.5-BHRF1 which was a cell line generated by means of transfecting the hybridoma KB26.5 with an anti-apoptotic gene BHRF1, the generation of this cell line was described in a previously work (Juanola Journé, 2007) .

All cell lines were cultured in 125 mL polycarbonate shake flasks (Corning Inc.) with a working volume of 12 mL, incubated in a 5% CO₂ air mixture and in a humidified atmosphere at 37°C (Steri-cult 2000 Incubator, Forma Scientific). Flasks were continuously agitated at 130 rpm on an orbital shaking platform (Stuart SSL110 Incubator, Forma Scientific). Cultures were seeded every 2 or 3 days using a viable cell density of $25 \cdot 10^5 \text{ cells} \cdot \text{mL}^{-1}$.

5.8.2 Cell media

The basal medium used for all experiments with HEK293 cells were a costumed-made SFMTransFx-293 (HyClone, Thermo Scientific), supplemented with the selected carbon source, supplemented with 4 mM glutamine (Gibco, Life Technologies, NY, USA) and 5 % (v/v) FBS (Sigma Aldrich, MO, USA). Regarding the cell maintenance of HEK293 cells, it was carried out using the basal media where the carbon source used was glucose at $4,5 \text{ g} \cdot \text{L}^{-1}$.

The basal medium used for all experiments and cell maintenance of both hybridoma cell line was DMEM (Gibco, Life Technologies), supplemented with 6 mM of glutamine (Gibco, Life Technologies), $3,7 \text{ g} \cdot \text{L}^{-1}$ sodium hydrogen carbonate, 50 ppm Antifoam C Emulsion (Sigma Aldrich) and $2 \text{ g} \cdot \text{L}^{-1}$ Kolliphor® P 188 (Sigma Aldrich).

Regarding all the conditions carried out in this study, in the following list are detailed:

- Comparison between hybridoma KB26.5 and hybridoma KB26.5 - BHRF1, the media used was the basal one.
- Comparison between several carbon sources with HEK293 cell line, the media used was the basal one supplemented with $4,5 \text{ g} \cdot \text{L}^{-1}$ of glucose in the glucose-related experiments, $4,5 \text{ g} \cdot \text{L}^{-1}$ of fructose in the fructose-related experiments and $4,5 \text{ g} \cdot \text{L}^{-1}$ of fructose supplemented with $1,68 \text{ g} \cdot \text{L}^{-1}$ of sodium lactate.

5.8.3 Shake-flasks culturing platform

For shake-flasks experiments, HEK293 and hybridoma cell lines were inoculated at the desired cell density in 250-mL polycarbonate shake flask (Corning Inc.) with 50-mL of working volume and cultured under the same conditions those described for the cell maintenance. Sampling volume was about 1000 μ L.

5.8.4 Bioreactor cell culture

The stirred-tank bioreactor used in the HEK293 study of several carbon source was a commercial bioreactor (BiostatDCU2, from Sartorius Stedim Biotech, Germany) with 2L-cylindrical vessel, equipped with probes and control systems for pH, D.O. (relative oxygen partial pressure) and temperature, stirred with two marine impellers and the working volume the working volume for the batch cultures was 1L.

The control systems of the before mentioned variables, moreover, it has to be taken into consideration that culture conditions depended on the experiment, they are described down below:

- For el conditions carried out, the dissolved oxygen concentration was monitored with a polarographic probe (Oxyferm, Hamilton), and maintained at 30% of saturation by means of an aeration flow using a sparger of 0,175 VVM together with a cascade control system based on a stirring control system and a gas mixing unit.
- For el conditions carried out, the temperature was maintained at 37°C by only with a heating blanket owing to cooling was not required.
- For el conditions carried out, the pH was measured with a standard electrode (EasyFerm Plus, Hamilton), and it was maintained at 7,1 with the two solution an acid solution of hydrochloric acid 0,5M (Panreac), and an alkali solution of 0,5 M of sodium hydroxide (Panreac).

On the other side, the stirred-tank bioreactor used in all the hybridoma experiments was a commercial bioreactor (BiostatMD, from Sartorius Stedim Biotech, Germany) with 2L-cylindrical jacketed vessel, equipped with probes and control systems for pH, D.O. (relative oxygen partial pressure) and temperature, stirred with two marine impellers. In addition, the working volume the working volume for the batch cultures was 1L.

The control systems of the before mentioned variables, moreover, it has to be taken into consideration that culture conditions were the same and are described down below:

- Dissolved oxygen concentration was monitored with a polarographic probe (Oxyferm, Hamilton), and maintained at 30% of saturation by means of an aeration flow using a sparger of 0,125 VVM together with a cascade control system based on a stirring control system and a gas mixing unit.
- Temperature was maintained at 37°C by switch between a heat exchanger when heat was needed and with a cooling system when cold was needed.
- pH was measured with a standard electrode (EasyFerm Plus, Hamilton), and the pH control was defined depending the experimental settings. if it was required two solution would be added: an acid solution of HCl 0,5M (Panreac), and an alkali solution of 0,5 M of NaOH (Panreac). Regarding the definition of the set-points, they are described in the list below:
 - Comparison between hybridoma KB26.5 and hybridoma KB26.5 - BHRF1, the was controlled with 7,1 as a set-point.

5.8.5 Metabolite determination

Sample was previously centrifuged at 3000 g for 3 min (Spectrafuge) and the supernatant was filtered using a 0.22 µm filter (Merck Millipore) to remove the cells and cell debris. Glucose and lactate concentration were determined using an automatic enzymatic glucose and lactate analyzer (YSI, Yellow Springs Instruments, 2700 Select).

All the metabolite determination carried out in this chapter in regard with its protocols and methodology has been already described in **section 8 of chapter 5**, except from the amino acids concentrations were determined by HPLC using post-column derivation method in a PEEK manufactured column with cation-exchange resin (Ultropac, polystyrene/divinylbenzene sulfonate) 5 µm, 200x4 mm (BiochromLTd.). Derivatized amino acids were detected colorimetrically at 570 and 440 nm wavelengths.

5.8.6 Oxygen uptake rate (OUR)

Determination of the oxygen uptake rate (OUR) was necessary to calculate the specific oxygen consumption rate (q_{O_2}) to be used on the further flux analysis. OUR was measured in the bioreactor applying the dynamic method. In short, D.O. (dissolved oxygen, % of relative oxygen concentration in the liquid phase in respect to the air saturation in equilibrium) is initially increased over 60% of air saturation. Afterwards, air supply is stopped and a N_2 flow (0,075 vvm) is introduced into the bioreactor headspace in order to obtain an oxygen-free gas phase and to avoid any oxygen transport back to the culture medium. O.U.R. calculation was performed from the decreasing profile between 56 and 29% of air saturation because of cells consumption. The N_2 inlet into the headspace drives oxygen desorption from the liquid phase that has been previously determined and considered in the mass balance equation through the desorption constant, K_{des} . To convert D.O. into absolute oxygen concentration (C_{O_2}), the oxygen solubility was considered constant during the culture and equal to 0.194 mmol/L (Miller, Blanch, & Wilke, 1988)(Ramirez & Mutharasan, 1990)(Higareda, Possani, & Ramírez, 1997). As shown in **Equation 5-1**, the dissolved oxygen concentration decreases due to both the respiratory activity of cells (first factor) and to the oxygen desorption from the liquid phase to the gas phase of the bioreactor (second factor). When D.O. drops below 29%, N_2 gas inflow is stopped and dissolved oxygen control resumed. The specific methodology used in this work is detailed somewhere else (Lecina et al., 2006) and the O.U.R. measurements were conducted with a lapse time of 12 hours.

Equation 5-1

$$OUR = \frac{(C_{O_2}(t_0) - C_{O_2}(t_f))}{t_f - t_0} + \frac{\left(\int_{t_0}^{t_f} (-K_{des} C_{O_2}(t)) dt \right)}{t_f - t_0}$$

Moreover, the oxygen specific consumption rate (q_{O_2}) can be obtained through the slope resulting from the direct representation of O.U.R. values versus the concentration of viable cells, as presented in **Equation 5-2**.

Equation 5-2

$$\frac{dO_2}{dt} = OUR = q_{O_2} \cdot X$$

5.8.7 Specific rate calculations

The specific rates either consumption or production used in this chapter in regard with its calculation and methodology have been already described in **section 8.2 of chapter 5**.

5.8.8 Reduced genome-scale metabolic model

In this study, each cell line had their own reduced genome-scale metabolic model. Hereafter, both of them will be described.

5.8.8.1 HEK293 cell line

The HEK293 metabolic model was derived from the last reconstruction published for the *Homo sapiens* RECON2.2 (Swainston et al., 2016). The RECON2.2 consists in the most complete and best annotated consensus of human metabolic reconstruction available from the Biocompare database (Li et al., 2010).

The model contains 5324 metabolites and 7785 reactions, and this implies that cells have access to all functionality encoded by the genome, which is not realistic from the point of view of the cell culture. The metabolic model was reduced following the protocol performed by Quek (L.-E. Quek et al., 2014) for adaptation of the RECON2.0 (Thiele et al., 2013) model for HEK293 cells. A few additional adaptations and constraint modifications were performed to further adapt this model to our experimental conditions. Namely, to allow fructose to be metabolised and gluconeogenesis when lactate alone was consumed. It must be stressed that the mitochondrial lactate metabolic capacities were already present in the initial model and only directional constraints were modified. The resulting model used for the metabolic flux calculation, that contains 322 reactions and 302 metabolites, is detailed in **Appendix**. Reaction fluxes over the metabolic network are presented in $\text{nmols}\cdot\text{mgDCW}^{-1}\cdot\text{h}^{-1}$, except for the biomass reaction that is represented in $\text{mg}\cdot\text{gDW}^{-1}\cdot\text{h}^{-1}$. Moreover, the reactions involved in the fructose metabolism were the ones most used by the human cell lines (Khitan & Kim, 2013).

5.8.8.2 Hybridoma KB26.5 and hybridoma KB26.5 -BHRF1

The metabolic model used in this study for both cell lines was derived from the reduced model obtained from a generic *Mus musculus* genome-scale metabolic model (L. E. Quek & Nielsen,

2008). The reduced model was first developed by L.-E. Quek, Dietmair, Krömer, & Nielsen, 2010 and afterwards used by Martínez et al., 2013; and is freely available in Systems Biology Markup Language (SBML) format in the supplementary files of the second publication. The resulting model used for the metabolic flux calculation, that contains 362 reactions and 359 metabolites, is detailed in **Appendix**. Reactions fluxes over the metabolic network are presented in $\text{nmols}\cdot\text{mgDCW}^{-1}\cdot\text{h}^{-1}$, except for the biomass reaction that is represented in $\text{mg}\cdot\text{gDCW}^{-1}\cdot\text{h}^{-1}$.

5.8.9 Flux Balance Analysis protocol

The description of all protocols used in this chapter in regard with its all the modelling done have been already described in **section 10.2 of chapter 5**.

5.8.10 Model visualization

Model visualization has been made using commercially available software Omix Visualization (Omix Visualization GmbH & Co. KG) as described in (Droste et al., 2013)

The representation of the principal metabolism has four groups which are detailed in the following list:

1. The glycolytic pathway, which is related to the catabolism of glucose to pyruvate (light blue colour)
2. The pentose phosphate pathway, whose function is mainly the generation of biosynthesis precursors based on nitrogen bases (dark blue colour)
3. The lactate pathway, which leads to the generation of ethanol (light yellow colour)
4. The TCA cycle, which is related to catabolism of acetyl-CoA to carbon dioxide and NADH (green colour).
5. The malate-aspartate shuttle, which is related to the electron transport from cytoplasm to mitochondria (red colour).
6. The biomass formation, which is related to reactions that take part in the synthesis of biomass precursors (purple colour).

5.8.11 Statistics

Duplicates for each culture conditions were performed, but only one of the repetitions is presented in the Results section. Since the runs have not performed in parallel (due to equipment limitations), sampling time do not coincide and also other parameters may vary as the cell seeding density.

5.9 References

- Alberts, B., Johnson, A., & Lewis, J. (2002). The Mitochondrion. In *Molecular Biology of the Cell*.
- Albiol, J., Solà, C., Liste-Calleja, L., Cairó, J. J., Martínez-Monge, I., Lecina, M., & Miret, J. (2018). Metabolic flux balance analysis during lactate and glucose concomitant consumption in HEK293 cell cultures. *Biotechnology and Bioengineering*, 116(2), 388–404. <https://doi.org/10.1002/bit.26858>
- Altamirano, C., Illanes, A., Becerra, S., Cairó, J. J., & Gòdia, F. (2006). Considerations on the lactate consumption by CHO cells in the presence of galactose. *Journal of Biotechnology*, 125(4), 547–556. <https://doi.org/10.1016/j.jbiotec.2006.03.023>
- Arden, N., & Betenbaugh, M. J. (2004). Life and death in mammalian cell culture: strategies for apoptosis inhibition. *Trends in Biotechnology*, 22(4), 174–180. <https://doi.org/10.1016/j.tibtech.2004.02.004>
- Casablanco, A., Gámez, X., Lecina, M., Solà, C., Cairó, J. J., & Gòdia, F. (2013). Comparison of control strategies for fed-batch culture of hybridoma cells based on on-line monitoring of oxygen uptake rate, optical cell density and glucose concentration. *Journal of Chemical Technology & Biotechnology*, 88(9), 1680–1689. <https://doi.org/10.1002/jctb.4019>

- Casablanco, A., Xavier, G., & Sol, C. (2013). *Comparison of control strategies for fed-batch culture of hybridoma cells based on on-line monitoring of oxygen uptake rate, optical cell and Francesc G odia*. (February), 1680–1689. <https://doi.org/10.1002/jctb.4019>
- Chen, K., Liu, Q., Xie, L., Sharp, P. A., & Wang, D. I. C. (2001). Engineering of a mammalian cell line for reduction of lactate formation and high monoclonal antibody production. *Biotechnology & Bioengineering*, 72(1), 55–61. [https://doi.org/10.1002/1097-0290\(20010105\)72:1<55::AID-BIT8>3.0.CO;2-4](https://doi.org/10.1002/1097-0290(20010105)72:1<55::AID-BIT8>3.0.CO;2-4)
- Chipuk, J. E., & Green, D. R. (2008). How do BCL-2 proteins induce mitochondrial outer membrane permeabilization? *Trends in Cell Biology*, 18(4), 157–164. <https://doi.org/10.1016/j.tcb.2008.01.007>
- Coco-Martin, J., & Harmsen, M. (2008). *A review of therapeutic protein expression by mammalian cells*.
- Concha, I. I., Velásquez, F. V., Martínez, J. M., Angulo, C., Droppelmann, A., Reyes, A. M., ... Golde, D. W. (1997). Human erythrocytes express GLUT5 and transport fructose. *Blood*, 89(11), 4190–4195. <https://doi.org/10.1182/blood.v89.11.4190>
- Cura, A. J., & Carruthers, A. (2012). Role of monosaccharide transport proteins in carbohydrate assimilation, distribution, metabolism, and homeostasis. *Comprehensive Physiology*, 2(2), 863–914. <https://doi.org/10.1002/cphy.c110024>
- Dorai, H., Yun, S. K., Ellis, D., Kinney, C. A., Lin, C., Jan, D., ... Betenbaugh, M. J. (2009). Expression of anti-apoptosis genes alters lactate metabolism of Chinese Hamster ovary cells in culture. *Biotechnology and Bioengineering*, 103(3), 592–608. <https://doi.org/10.1002/bit.22269>
- Droste, P., Nöh, K., & Wiechert, W. (2013). Omix - A visualization tool for metabolic networks with highest usability and customizability in focus. *Chemie-Ingenieur-Technik*, 85(6), 849–862. <https://doi.org/10.1002/cite.201200234>
- Ebstensen, R. D., & Plagemann, P. G. (1972). Cytochalasin B: inhibition of glucose and glucosamine transport. *Proceedings of the National Academy of Sciences of the United States of America*, 69(6), 1430–1434. <https://doi.org/10.1073/pnas.69.6.1430>
- Estes, S., & Melville, M. (2013). *Mammalian Cell Line Developments in Speed and Efficiency*. https://doi.org/10.1007/10_2013_260
- Farmer, W. R., & Liao, J. C. (1997). Reduction of aerobic acetate production by Escherichia coli. *Applied and Environmental Microbiology*, 63(8), 3205–3210.
- Fink, S. L., & Cookson, B. T. (2005). Apoptosis, Pyroptosis, and Necrosis: Mechanistic Description of Dead and Dying Eukaryotic Cells. *Infection and Immunity*, 73(4), 1907–1916. <https://doi.org/10.1128/IAI.73.4.1907-1916.2005>
- Fussenegger, M., Bailey, J. E., & Varner, J. (2000). A mathematical model of caspase function in apoptosis. *Nature Biotechnology*, 18(7), 768–774. <https://doi.org/10.1038/77589>
- Go, Y.-M., & Jones, D. P. (2008). Redox compartmentalization in eukaryotic cells. *Biochimica et Biophysica Acta (BBA) - General Subjects*, 1780(11), 1273–1290. <https://doi.org/10.1016/j.bbagen.2008.01.011>
- Grilo, A. L., & Mantalaris, A. (2019). The Increasingly Human and Profitable Monoclonal Antibody Market. *Trends in Biotechnology*, 37(1), 9–16. <https://doi.org/10.1016/j.tibtech.2018.05.014>
- Hassell, T., Gleave, S., & Butler, M. (1991). Growth inhibition in animal cell culture. *Applied Biochemistry and Biotechnology*, 30(1), 29–41. <https://doi.org/10.1007/BF02922022>
- Henry, M. N., MacDonald, M. A., Orellana, C. A., Gray, P. P., Gillard, M., Baker, K., ... Martínez, V. S. (2020). Attenuating apoptosis in Chinese hamster ovary cells for improved biopharmaceutical production. *Biotechnology and Bioengineering*, 117(4), 1187–1203. <https://doi.org/10.1002/bit.27269>
- Henry, O., & Durocher, Y. (2011). Enhanced glycoprotein production in HEK-293 cells expressing pyruvate carboxylase. *Metabolic Engineering*, 13(5), 499–507. <https://doi.org/10.1016/j.ymben.2011.05.004>
- Higareda, A. E., Possani, L. D., & Ramírez, O. T. (1997). The use of culture redox potential and oxygen uptake rate for assessing glucose and glutamine depletion in hybridoma cultures. *Biotechnology and Bioengineering*, 56(5), 555–563. [https://doi.org/10.1002/\(SICI\)1097-0290\(19971205\)56:5<555::AID-BIT9>3.0.CO;2-H](https://doi.org/10.1002/(SICI)1097-0290(19971205)56:5<555::AID-BIT9>3.0.CO;2-H)
- Holman, G. D. (2020). Structure, function and regulation of mammalian glucose transporters of the SLC2 family. *Pflügers Archiv European Journal of Physiology*, 472(9), 1155–1175. <https://doi.org/10.1007/s00424-020-02411-3>

- Juanola Journé, S. (2007). *ESTRATÈGIES GENÈTIQUES PER A LA INHIBICIÓ DE L'APOPTOSI EN CULTIUS IN VITRO D'HIBRIDOMES*.
- Juanola, S., Vives, J., Milián, E., Prats, E., Cairó, J. J., & Gòdia, F. (2009). Expression of BHRF1 improves survival of murine hybridoma cultures in batch and continuous modes. *Applied Microbiology and Biotechnology*, 83(1), 43–57. <https://doi.org/10.1007/s00253-008-1820-8>
- Khitan, Z., & Kim, D. H. (2013). Fructose: A key factor in the development of metabolic syndrome and hypertension. *Journal of Nutrition and Metabolism*, 2013. <https://doi.org/10.1155/2013/682673>
- Kietzmann, T. (2010). Intracellular redox compartments: Mechanisms and significances. *Antioxidants and Redox Signaling*, 13(4), 395–398. <https://doi.org/10.1089/ars.2009.3001>
- Kim, H. D. (1985). *ATP Metabolism in Mammalian Red Blood Cells*. https://doi.org/10.1007/978-3-642-70610-3_24
- Kvansakul, M., Wei, A. H., Fletcher, J. I., Willis, S. N., Chen, L., Roberts, A. W., ... Colman, P. M. (2010). Structural basis for apoptosis inhibition by Epstein-Barr virus bhrf1. *PLoS Pathogens*, 6(12), 1–11. <https://doi.org/10.1371/journal.ppat.1001236>
- Lecina, M., Soley, A., Gràcia, J., Espunya, E., Lázaro, B., Cairó, J. J., & Gòdia, F. (2006). Application of on-line OUR measurements to detect actions points to improve baculovirus-insect cell cultures in bioreactors. *Journal of Biotechnology*, 125(3), 385–394. <https://doi.org/10.1016/j.jbiotec.2006.03.014>
- Li, C., Donizelli, M., Rodriguez, N., Dharuri, H., Endler, L., Chelliah, V., ... Laibe, C. (2010). BioModels Database: An enhanced, curated and annotated resource for published quantitative kinetic models. *BMC Systems Biology*, 4(1), 92. <https://doi.org/10.1186/1752-0509-4-92>
- Martínez-Monge, I., Albiol, J., Lecina, M., Liste-Calleja, L., Miret, J., Solà, C., & Cairó, J. J. (2019). Metabolic flux balance analysis during lactate and glucose concomitant consumption in HEK293 cell cultures. *Biotechnology and Bioengineering*, 116(2), 388–404. <https://doi.org/10.1002/bit.26858>
- Martínez, V. S., Dietmair, S., Quek, L.-E., Hodson, M. P., Gray, P., & Nielsen, L. K. (2013). Flux balance analysis of CHO cells before and after a metabolic switch from lactate production to consumption. *Biotechnology and Bioengineering*, 110(2), 660–666. <https://doi.org/10.1002/bit.24728>
- Marx, E., Mueller-Klieser, W., & Vaupel, P. (1988). Lactate-induced inhibition of tumor cell proliferation. *International Journal of Radiation Oncology*Biophysics*, 14(5), 947–955. [https://doi.org/10.1016/0360-3016\(88\)90017-X](https://doi.org/10.1016/0360-3016(88)90017-X)
- Mastrangelo, A. J., Hardwick, J. M., Zou, S., & Betenbaugh, M. J. (2000). Part II. Overexpression of bcl-2 family members enhances survival of mammalian cells in response to various culture insults. *Biotechnology and Bioengineering*, 67(5), 555–564. [https://doi.org/10.1002/\(SICI\)1097-0290\(20000305\)67:5<555::AID-BIT6>3.0.CO;2-T](https://doi.org/10.1002/(SICI)1097-0290(20000305)67:5<555::AID-BIT6>3.0.CO;2-T)
- Matsuno, T. (1992). Oxidation of cytosolic NADH by the malate-aspartate shuttle in HOH13 human hepatoma cells. *International Journal of Biochemistry*, 24(2), 313–315. [https://doi.org/10.1016/0020-711X\(92\)90263-Z](https://doi.org/10.1016/0020-711X(92)90263-Z)
- Miller, W. M., Blanch, H. W., & Wilke, C. R. (1988). A kinetic analysis of hybridoma growth and metabolism in batch and continuous suspension culture: Effect of nutrient concentration, dilution rate, and pH. *Biotechnology and Bioengineering*, 32(8), 947–965. <https://doi.org/10.1002/bit.260320803>
- Nomura, N., Verdon, G., Kang, H. J., Shimamura, T., Nomura, Y., Sonoda, Y., ... Drew, D. (2015). Structure and mechanism of the mammalian fructose transporter GLUT5. *Nature*, 526(7573), 397–401. <https://doi.org/10.1038/nature14909>
- Plagemann, P. G. W., & Richey, D. P. (1974). Transport of nucleosides, nucleic acid bases, choline and glucose by animal cells in culture. *Biochimica et Biophysica Acta (BBA) - Reviews on Biomembranes*, 344(3–4), 263–305. [https://doi.org/10.1016/0304-4157\(74\)90010-0](https://doi.org/10.1016/0304-4157(74)90010-0)
- Potter, M., Newport, E., & Morten, K. J. (2016a). The Warburg effect: 80 years on. *Biochemical Society Transactions*, 44(5), 1499–1505. <https://doi.org/10.1042/BST20160094>
- Potter, M., Newport, E., & Morten, K. J. (2016b). The Warburg effect: 80 years on. *Biochemical Society Transactions*, 44(5), 1499–1505. <https://doi.org/10.1042/BST20160094>
- Quek, L.-E., Dietmair, S., Hanscho, M., Martínez, V. S., Borth, N., & Nielsen, L. K. (2014). Reducing Recon 2 for steady-state flux analysis of HEK cell culture. *Journal of Biotechnology*, 184, 172–178. <https://doi.org/10.1016/j.jbiotec.2014.05.021>

- Quek, L.-E., Dietmair, S., Krömer, J. O., & Nielsen, L. K. (2010). Metabolic flux analysis in mammalian cell culture. *Metabolic Engineering*, 12(2), 161–171. <https://doi.org/10.1016/j.ymben.2009.09.002>
- Quek, L. E., & Nielsen, L. K. (2008). *On the reconstruction of the Mus musculus genome-scale metabolic network model*.
- Ramirez, O. T., & Mutharasan, R. (1990). Cell cycle- and growth phase-dependent variations in size distribution, antibody productivity, and oxygen demand in hybridoma cultures. *Biotechnology and Bioengineering*, 36(8), 839–848. <https://doi.org/10.1002/bit.260360814>
- Reitzer, J., & Wice, M. (1979). *Evidence That Glutamine, Not Sugar, Is the Major Energy Source for Cultured HeLa Cells*. 254(8).
- Schaepe, S., Kuprijanov, A., Simutis, R., & Lübbert, A. (2014). Avoiding overfeeding in high cell density fed-batch cultures of E. coli during the production of heterologous proteins. *Journal of Biotechnology*, 192, 146–153. <https://doi.org/10.1016/j.jbiotec.2014.09.002>
- Swainston, N., Smallbone, K., Hefzi, H., Dobson, P. D., Brewer, J., Hanscho, M., ... Mendes, P. (2016). Recon 2.2: from reconstruction to model of human metabolism. *Metabolomics*, 12(7). <https://doi.org/10.1007/s11306-016-1051-4>
- Templeton, N., Lewis, A., Dorai, H., Qian, E. A., Campbell, M. P., Smith, K. D., ... Young, J. D. (2014). The impact of anti-apoptotic gene Bcl-2Δ expression on CHO central metabolism. *Metabolic Engineering*, 25, 92–102. <https://doi.org/10.1016/j.ymben.2014.06.010>
- Tey, B. T., Singh, R. P., Piredda, L., Piacentini, M., & Al-Rubeai, M. (2000). Influence of Bcl-2 on cell death during the cultivation of a Chinese hamster ovary cell line expressing a chimeric antibody. *Biotechnology and Bioengineering*, 68(1), 31–43. [https://doi.org/10.1002/\(SICI\)1097-0290\(20000405\)68:1<31::AID-BIT4>3.0.CO;2-L](https://doi.org/10.1002/(SICI)1097-0290(20000405)68:1<31::AID-BIT4>3.0.CO;2-L)
- Thiele, I., Swainston, N., Fleming, R. M. T., Hoppe, A., Sahoo, S., Aurich, M. K., ... Palsson, B. Ø. (2013). A community-driven global reconstruction of human metabolism. *Nature Biotechnology*, 31(5), 419–425. <https://doi.org/10.1038/nbt.2488>
- Vives, J., Juanola, S., Cairo, J. J., Prats, E., Cornudella, L., & Godia, F. (2003). Protective Effect of Viral Homologues of bcl-2 on Hybridoma Cells under Apoptosis-Inducing Conditions. *Biotechnology Progress*, 19(1), 84–89. <https://doi.org/10.1021/bp0255715>
- Walsh, G. (2018). Biopharmaceutical benchmarks 2018. *Nature Publishing Group*, 36(12), 1136–1145. <https://doi.org/10.1038/nbt.4305>
- Wang, Z., & Dong, C. (2019). Gluconeogenesis in Cancer: Function and Regulation of PEPCK, FBPase, and G6Pase. *Trends in Cancer*, 5(1), 30–45. <https://doi.org/10.1016/j.trecan.2018.11.003>
- Wurm, F. M. (2004). Production of recombinant protein therapeutics in cultivated mammalian cells. *Nature Biotechnology*, 22(11), 1393–1398. <https://doi.org/10.1038/nbt1026>
- Xiao, W., Wang, R.-S., Handy, D. E., & Loscalzo, J. (2018). NAD(H) and NADP(H) Redox Couples and Cellular Energy Metabolism. *Antioxidants & Redox Signaling*, 28(3), 251–272. <https://doi.org/10.1089/ars.2017.7216>
- Zhang, L., Shen, H., & Zhang, Y. (2004). Fed-batch culture of hybridoma cells in serum-free medium using an optimized feeding strategy. *Journal of Chemical Technology & Biotechnology*, 79(2), 171–181. <https://doi.org/10.1002/jctb.940>
- Zhang, X., Han, L., Zong, H., Ding, K., Yuan, Y., Bai, J., ... Zhu, J. (2018). Enhanced production of anti-PD1 antibody in CHO cells through transient co-transfection with anti-apoptotic genes Bcl-xL and Mcl-1. *Bioprocess and Biosystems Engineering*, 41(5), 633–640. <https://doi.org/10.1007/s00449-018-1898-z>

6. From metabolomics to bioprocess definition

6.1. The “shared” metabolism

In the previous chapters, the metabolic interaction between different living cells, belonging to the group of microorganisms most used in biotechnology, and their environment has been described, analysed and several conclusions were reached. In this chapter, a general overview taking all the conclusions will be carry out in order to find out a common explanation for all the metabolic traits observed.

To begin with, it is currently well recognized that a living cell is an exceedingly complex system containing a diverse multiplicity of structural components, which are nonetheless extremely well integrated to produce a chemically and biologically efficient unit. Moreover, it would seem reasonable that the large amount of subcellular structural features responsible for its functionality might be correlated with a specific degree of metabolic differentiation (Moses & Lonberg-Holm, 1966). As a result, several metabolic traits might be obtained depending on how the cell structure was modified to grant a specific degree of metabolic differentiation.

On this basis, living organisms can be divided into three basic domains: Bacteria, Archaea and Eukarya. However, two groups can defined taking into account the nucleus compartmentalization: the prokaryotic and the eukaryotic (Van Der Gulik et al., 2017). The prokaryotic cells are known as the simplest and oldest unicellular organisms that grouped the Bacteria and Archaea domains. On the other side, the eukaryotic cells that included the Eukarya domain were described as a highly specific and complex unicellular or multicellular organism (Sapp, 2005).

In this work, the metabolic analysis in aerobic conditions of bacteria, yeast and animal cells has been carried out to understand how the glucose is converted to biomass and why a fraction of this glucose might be transformed to sub-products. On this basis, it was concluded that in all the selected expression platforms when glucose was metabolized, a sub-product was generated in order to solve an unbalance in relation with carbon (bacteria) or potential redox (yeast, animal cells) that was provoked by the uncoupling of two pathways. As shown in **chapter 3**, in the case of bacteria, acetate was produced in order to solve a carbon unbalance, while as shown in **chapter 4** and **chapter 5**, in the case of yeast and animal cell, a by-product was produced in order to fulfil the cytoplasmic redox balance. In the case of yeast, ethanol was produced, while lactate

was produced in animal cells. We believe that this carbon uncoupling or redox unbalance is an evidence of the biochemistry and physiological evolution of the organism over the years.

In the following section, the biochemistry and cellular evolution will be taken into account in order to hypothesize how from an evolutionary point of view might be possible to explain all the specific metabolic features of bacteria, yeast and animal cells observed in this work. Therefore, the cause behind both the carbon unbalance and the redox unbalance will be explained considering both the evolution theory and the endosymbiotic theory.

6.2. The metabolic and physiologic story

As it is widely described, Charles Darwin proposed an evolution theory revolving around natural selection on the book *On the origin of species* whose main assumption was “*Organisms produce more offspring that are able to survive in their environment. Those that are better physically equipped to survive, grow to maturity, and reproduce. On the other hand, those that are lacking in such fitness either do not reach an age when they can reproduce or produce fewer offspring than their counterparts. Natural selection is sometimes summed up as “survival of the fittest” because the “fittest” organisms—those most suited to their environment—are the ones that reproduce most successfully, and are most likely to pass on their traits to the next generation*” (Darwin, 1859) .

If this assumption is more detailed and compared with how all the living beings are “generated” by means of integrating the new publications regarding the biological evolution (Kutschera & Niklas, 2004), this assumption can be altered as: the expansion phase of any living being is directly limited by the effect that its expansion has on the environment and *vice versa*. Moreover, the relation between the living being mutagenic capacity and the advantages that these mutations might provoked in order to overcome disadvantageous environments are the other “key” on top of the expansion of any living being. For example, how from a reductive atmosphere where only the non-oxygen related organism might survived, a fully oxidative atmosphere was achieved where mainly the oxygen-related organism survived.

Therefore, if how the environment affects the selection of a specific metabolism is added to fact that a selected metabolism should integrate the metabolism of its predecessors, a statement can be formulated in regard with the optimization of the carbon metabolism. The capacity to

regulate the glucose metabolism might be used as natural selection parameters that promoted the adaptation to a changing environment where only the most fitted survived. Moreover, regarding the fitness, there are two possibilities that have to be taken into consideration: the one where a living being can survive in adverse conditions and the one where a living being can grow at higher growth rates while the environment is not changing.

Consequently, the biochemical evolution on top of generating all the living beings will be explained through the application of the following premise: Natural selection is the most important force that shapes the course of phenotypic evolution (Kutschera & Niklas, 2004) .

In order to perform the biochemical evolution a starting point is required. The “zero” point in this work will be establish at the LUCA’s metabolism. As shown in **Figure 6-1**, LUCA is described as the Last Universal Common Ancestral whose apparition is dated before the bifurcation point that lead to the apparition of prokaryotic domain (the Eubacteria and the Archaea) (Tuller et al., 2010).

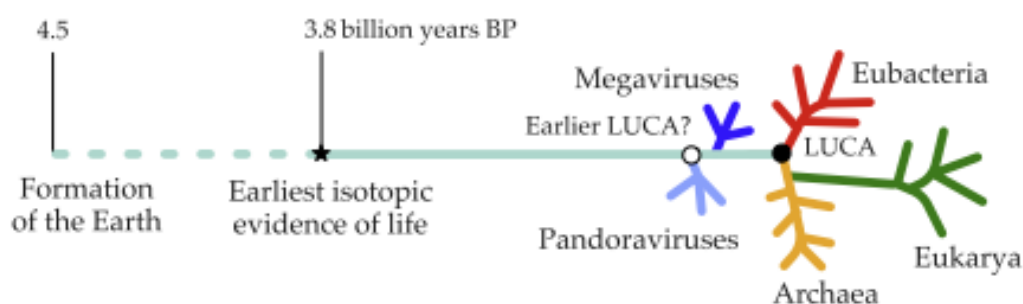


Figure 6-1 Time line where the LUCA organism should appear (from Cornish-Bowden et al (Cornish-Bowden & Cárdenas, 2017)).

When the bifurcation took place, the earth was at the Archean eon, which was characterized by an anoxic atmosphere (Nisbet & Fowler, 2011) . Due to this atmosphere, , as shown in **Table 6-1**, several metabolism prevailed within the Archean eon based on obtaining energy from light or chemical compounds and the carbon building blocks where anabolized from carbon dioxide or organic compounds without the presence of oxygen.

Table 6-1. Overall description of the metabolisms that prevailed in the Archaea eon.

Energy source	Carbon source	Main essential compounds	
		electron donor	electron acceptor
phototroph (energy from light)	Autotroph (carbon from carbon dioxide)	Reduced form of sulphur and iron such as sulfhydic acid or iron-based compounds.	Carbon dioxide
	Heterotroph (carbon from organic compound)	Reduced carbon form carbon-based compounds such as methane	Carbon dioxide
Chemolithotroph (energy from inorganic compounds)	Heterotroph (carbon from organic compound)	Inorganic matter	Oxidized form of sulphur or iron (So ₄ or FeO)
Chemoorganotroph (energy from organic compounds)		Organic matter	Oxidized form of sulphur or iron (So ₄ or FeO)

All the described metabolisms prevailed until a limiting concentration of reduced forms of sulphur were achieved. Then, the reduced oxygen from water via photolysis was used as a new energy source by photoautotroph organisms. From this moment, the accumulation of oxygen in the atmosphere started. This accumulation provoked a severe problematic: the alteration of the balance of oxidants and reductants available for energy metabolism, based on sulphur or iron (Nealson, 1997). After this point, as shown in **Table 6-2**, the organisms that prevailed were the ones whose metabolism was not based on sulphur and iron.

Table 6-2 Overall description of the metabolisms that prevailed when an oxidative atmosphere was present.

Energy source	Carbon source	Main essential compounds	
		electron donor	electron acceptor
phototroph (energy from light)	Autotroph (carbon from carbon dioxide)	water	carbon dioxide
	Heterotroph (carbon from organic compound)	reduced carbon form carbon-based compounds such as methane	carbon dioxide
Chemolithotroph (energy from inorganic compounds)	Heterotroph (carbon from organic compound)	inorganic matter	oxygen
Chemoorganotroph (energy from organic compounds)		organic matter	oxygen

After the atmosphere oxygenation. In order to survive to this new environment rich in oxygen, it might be stated that an anaerobic microorganism should have internalized a new metabolism based on the usage of oxygen as the electron acceptor through Horizontal Gene Transfer (HGT). The HGT enabled a prokaryote to move genetic material from other prokaryote without relying

on vertical gene transfer from its predecessor. On this basis, the use of oxygen as an electron acceptor might be taken from a restructuration of the electron chain used by a photosynthetic microorganism that undergone the photolysis of water in order to obtain electrons and, as a consequence, oxygen was produced as a by-product. Therefore, an aerobic prokaryote appeared that expressed an anaerobic metabolism along with an aerobic metabolism based on an electron chain that used oxygen as the electron acceptor. This organism should be the predecessor of *E. coli* because as shown in **Figure 6-2**, *E. coli* M15 suffered a carbon unbalance in the acetyl-CoA step where the anaerobic metabolism (glycolysis pathway) was connected to the aerobic one (TCA) that should be related to the coupling of both metabolism when the first aerobic prokaryote appeared through HGT.

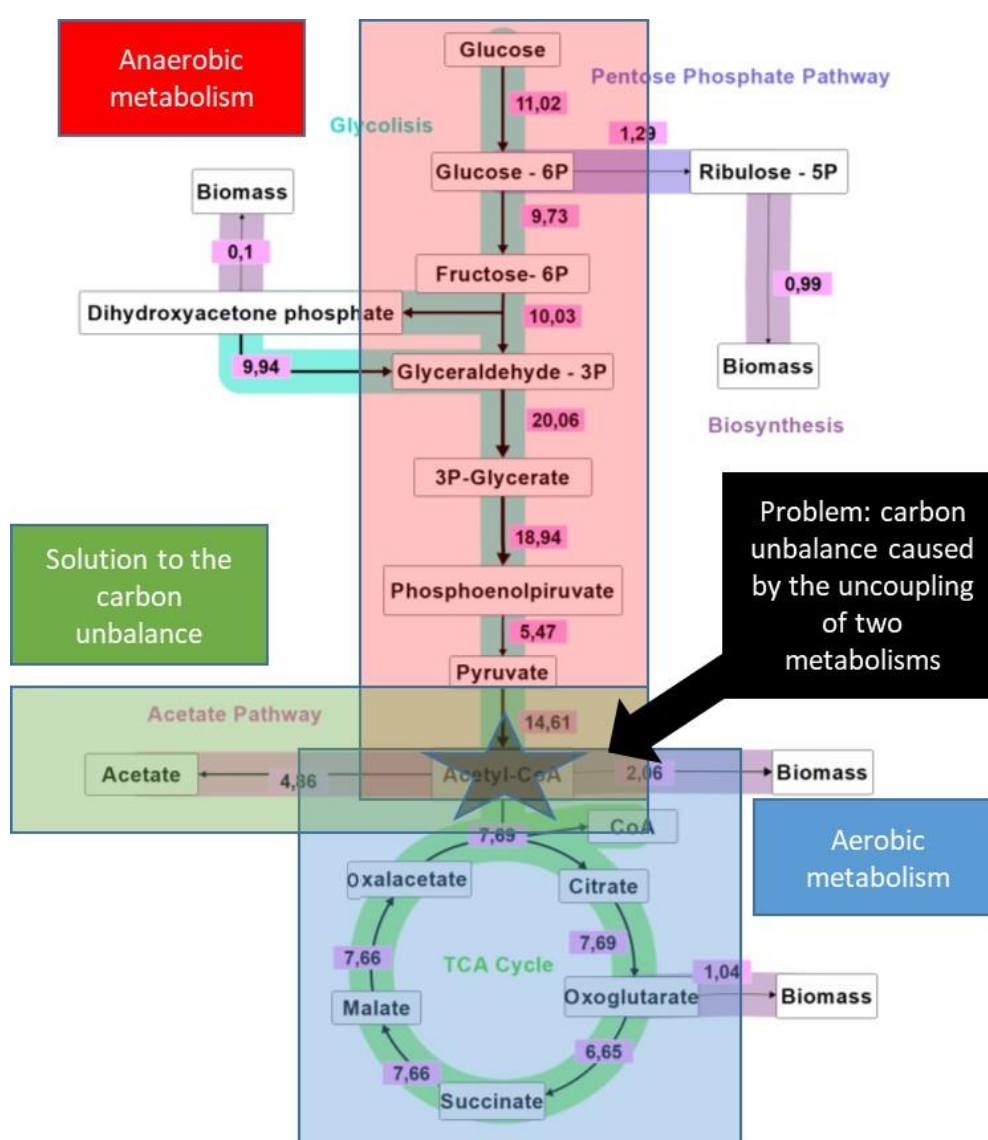


Figure 6-2 Carbon unbalance observed in *E. coli* M15 produced by the coupling of two metabolism (in blue - aerobic metabolism, in red - anaerobic metabolism, in black- the problem and in green – the solution to the observed problem).

Then, hundreds millions of years were required for the Eukarya domain to appear during an oxygenic atmosphere. Using the endosymbiotic theory, the Eukarya domain appeared due to the endosymbiosis based on an anaerobic prokaryote host that internalized an aerobic prokaryote (Martin et al., 2015). On this basis, it might be explained the metabolic behaviour of the eukaryotes *S. cerevisiae* and hybridoma KB26.5; due to both shared the same cause. As shown in **Figure 6-3** and **Figure 6-4**, a chemical compartmentalization that promoted an unbalance in the cytoplasmic redox potential, specifically, in the NADH balance, due to a limitation in the flux through the mitochondrial shuttles on top of its regeneration. The chemical compartmentalization should be related to symbiosis of two microorganisms that required different energy and carbon requirements (the mitochondria-based predecessor and the anaerobic host).

Considering the results obtained in relation with the metabolism of *E. coli*, *S. cerevisiae*, hybridoma KB26.5 as one of the studied animal cell lines, the postulate that explains all the results from an evolutionary point of view is the second one.

However, all the microorganisms shared the same solution, the generation of a determined by-product that solved the characteristic metabolic unbalances. As shown in **Figure 6-2**, *E. coli* M15 produces acetate in order to solve the Acetyl-coA carbon unbalance. While as shown in **Figure 6-3** and **Figure 6-4**, *S. cerevisiae* and hybridoma KB26.5, produced a carbon reduced molecule that was derived in both cases from pyruvate in order to balance the cytoplasmic redox potential. In the case of *S. cerevisiae*, ethanol was produced, while in hybridoma KB26.5, lactate was produced.

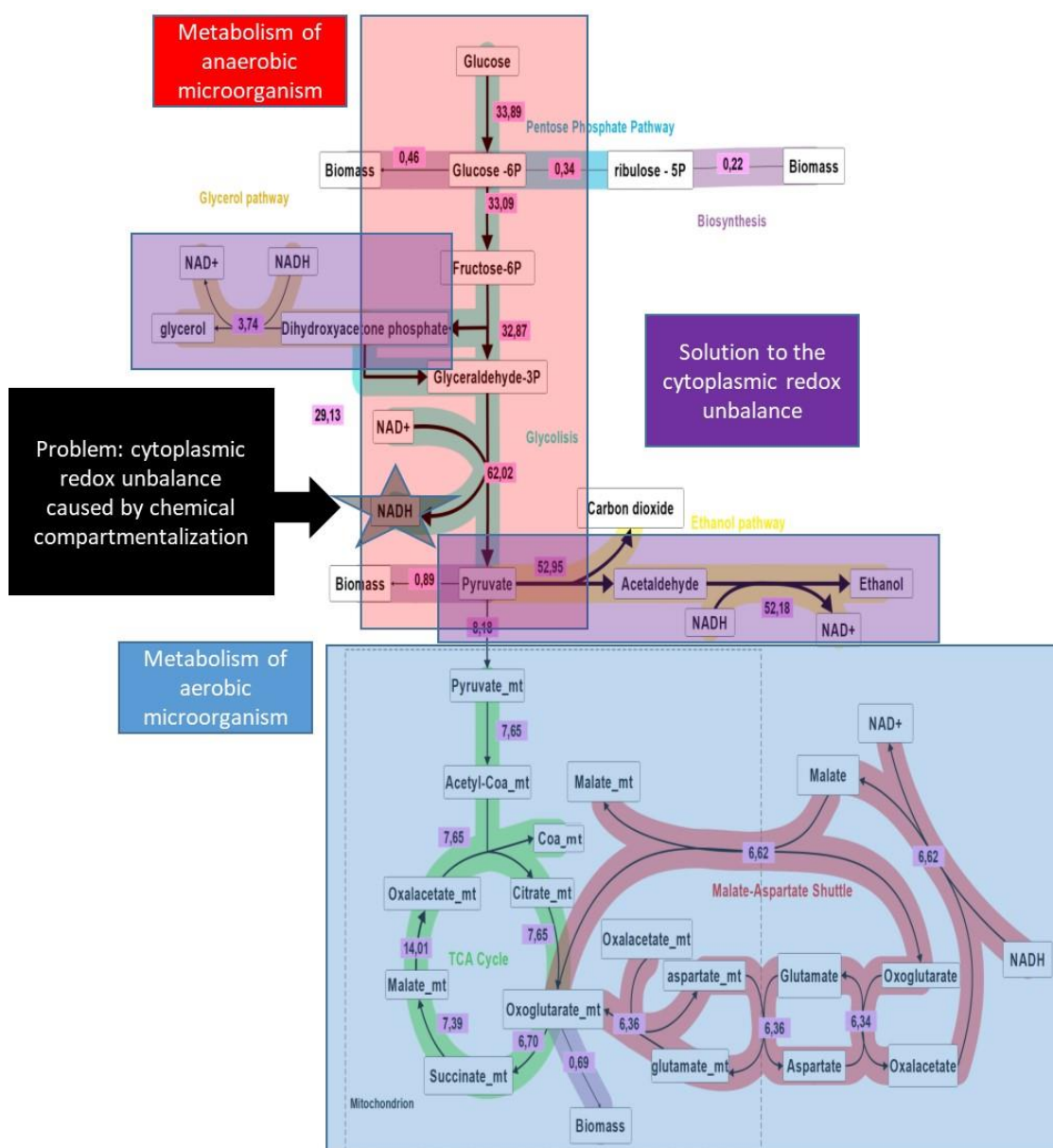


Figure 6-3 Cytoplasmic redox unbalance observed in *S. cerevisiae* produced by the symbiosis of two microorganism (in blue – the metabolism of the aerobic microorganism, in red - the metabolism of the anaerobic microorganism, in black – the problem and in purple – the solution to the observed problem)

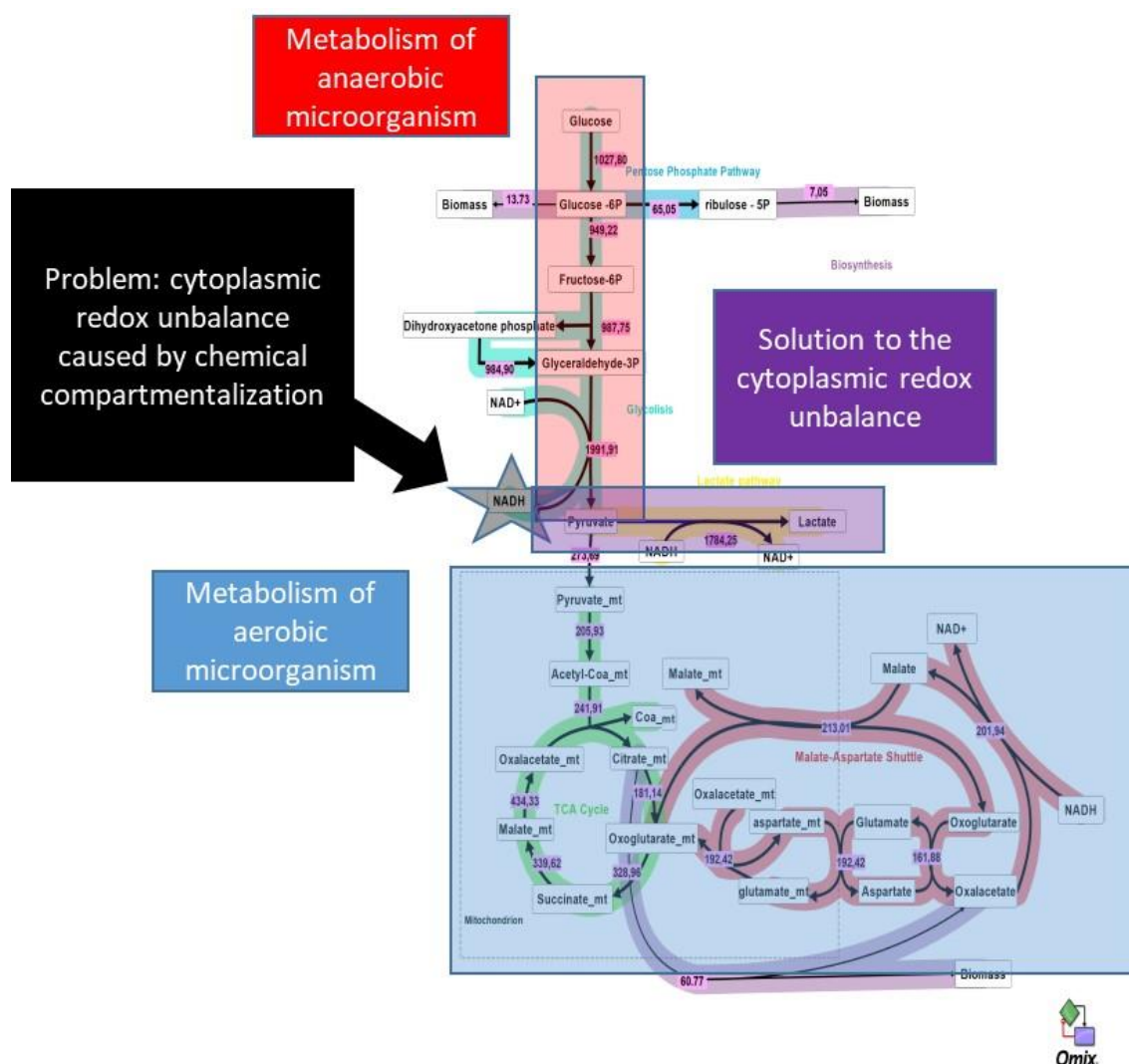


Figure 6-4 Cytoplasmic redox unbalance observed in hybridoma KB26.5 produced by the symbiosis of two microorganism (in blue – the metabolism of the aerobic microorganism , in red - the metabolism of the anaerobic microorganism , in black – the problem and in purple – the solution to the observed problem)

Taking into account that all the studied eukaryotes solved the redox potential by reducing the metabolite involved in reaction step that connects the cytoplasm to the mitochondria, the eukaryote as an endosymbiotic organism might be reaffirmed. The metabolic uncoupling provoked by the endosymbiosis of two microorganism that operated at different carbon rate provoked a cytoplasmic concentration of pyruvate higher enough to be used as the main electron acceptor in compartmentalized microorganisms. In addition, regarding the metabolism of *S. cerevisiae*, it should explain why the major reduced metabolite was the pyruvate instead of dihydroxyacetone phosphate. As it was observed, dihydroxyacetone phosphate can also be used as an electron acceptor producing glycerol along with ethanol, when the production of ethanol is not enough to regenerate all the NADH from glycolysis.

Therefore, the metabolic traits observed in this study regarding the unicellular microorganisms *E. coli* M15, as a prokaryote, and *S. cerevisiae* and hybridoma KB26.5, as a eukaryote, shared a common cause: the expression of two metabolism, in the case of prokaryote, or the symbiosis of two microorganisms, in the case of eukaryote, with different carbon and energy requirements. This difference provoked the observed unbalances that were solved producing acetate (in the case of *E. coli* M15) or ethanol and lactate (in the case of *S. cerevisiae* and hybridoma KB26.5, respectively).

On this basis, the biochemical evolution has been linked to how organisms modify the environment and how natural selection force the continuity or elimination of specific metabolisms depending on its adaptation to modifications in the environmental conditions. Moreover, the result obtained in the metabolic study presented in this thesis can be explained by the biochemical evolution. However, a new association based on the symbiosis of several unicellular microorganisms appeared in order to evolve in the life beings that are present in the actual age, the multicellular organisms. Those organisms are characterized by cell differentiation and specialization, as a result, group of cells might be specialized in order to undergone a particular function essential for the whole organism. It can be state that this function is related to keep a constant cell environmental in relation with their physiological conditions in order to maximize the cell efficiency in terms of carbon and energy requirements.

Considering the results from **chapter 3, 4 and 5** regarding the adaptation of the carbon metabolism to the environment and the fact that multicellular organisms might evolve in a way that should grant a specific cellular environmental condition within the organism, new statements in relation with the by-product generation should be done:

- The sub-product generation is directly related to the environmental conditions, specifically, the media composition if there are no genetic modifications.
- The sub-product generation can be regulated by means of changing the environmental conditions, however a limitation exists that is related to its genetic background, specifically to a metabolic threshold.

At this point, one of the mentioned statement can contribute in the definition of a bioprocess. The regulation of the product generation via the modification of the environmental conditions regarding the media composition, because one of the goals in the definition of bioprocess strategy is to increase the biomass production. In this case, optimizing the conversion of the carbon source to biomass via reducing the production of undesired products (for instance acetate, ethanol or lactate).

6.3. Stepping to bioprocess definition

As it was previously mentioned in **chapter 1**, the goal of all bioprocess is to improve the productivity of a specific product. It can be improved via genetic modification (Román Roldán, 2018) or via optimizing the biomass production (Monge, 2018). Optimizing the biomass production is related to both reaching higher biomass concentration and improving the conversion of the carbon source to biomass.

Reaching higher biomass concentration is often limited by how the carbon source is converted to biomass. On this basis, there are several ways to increase the biomass concentration for example, using several bioprocess strategies that are based on adding nutrients until a growth inhibition or a physical limitation appears (for instance, mass or energy transfer limitation or reaching a bioreactor's maximum working volume). However, the bioprocess strategies are based on mathematical algorithms that are focused on estimating how the carbon metabolism will behave in order to add the exact amount of the limiting compound, usually glucose. Then, the problem arises when the data that should be used might be not the fittest one. As it was presented in this chapter and in the previous metabolic ones (**chapter 3, 4 and 5**), the environment conditions affects the carbon metabolism as a result, the data used might be observed as the correct one instead of as the optimal one.

Therefore, all the bioprocess definition that will be carried out in the following chapters (chapter **7, 8 and 9**) will be designed focusing on reaching the maximum biomass cell density by means of optimizing the carbon conversion towards biomass through the modification of the culture media composition. On this basis, the definition of the more suited bioprocess strategies will be based on integrating the interaction between the cell metabolism and the culture's media (environmental conditions) and the metabolic data presented in **chapter 3, 4 and 5** depending on the expression platform used.

6.4. References

- Cornish-Bowden, A., & Cárdenas, M. L. (2017). Life before LUCA. *Journal of Theoretical Biology*, 434, 68–74.
<https://doi.org/10.1016/j.jtbi.2017.05.023>
- Darwin, C. (1859). *Origin of the species*.
- Kutschera, U., & Niklas, K. J. (2004). The modern theory of biological evolution: An expanded synthesis. *Naturwissenschaften*, 91(6), 255–276. <https://doi.org/10.1007/s00114-004-0515-y>
- Martin, W. F., Garg, S., & Zimorski, V. (2015). Endosymbiotic theories for eukaryote origin. *Philosophical Transactions of the Royal Society B: Biological Sciences*, 370(1678). <https://doi.org/10.1098/rstb.2014.0330>
- Monge, I. M. (2018). Development of tools for monitoring and controlling cell cultures through metabolic analysis. *Thesis, October*, 1–280.
- Moses, V., & Lonberg-Holm, K. K. (1966). The study of metabolic compartmentalization. *Journal of Theoretical Biology*, 10(2), 336–355. [https://doi.org/10.1016/0022-5193\(66\)90131-7](https://doi.org/10.1016/0022-5193(66)90131-7)
- Nealson, K. H. (1997). SEDIMENT BACTERIA: Who's There, What Are They Doing, and What's New? *Annual Review of Earth and Planetary Sciences*, 25(1), 403–434. <https://doi.org/10.1146/annurev.earth.25.1.403>
- Nisbet, E., & Fowler, C. M. R. (2011). The evolution of the atmosphere in the Archaean and early Proterozoic. *Chinese Science Bulletin*, 56(1), 4–13. <https://doi.org/10.1007/s11434-010-4199-8>
- Román Roldán, R. (2018). *Desarrollo de procesos de producción de proteínas bioterapéuticas: Aumento de la productividad específica en células HEK293*.
https://ddd.uab.cat/pub/tesis/2018/hdl_10803_650828/rrr1de1.pdf
- Sapp, J. (2005). The Prokaryote-Eukaryote Dichotomy: Meanings and Mythology. *Microbiology and Molecular Biology Reviews*, 69(2), 292–305. <https://doi.org/10.1128/mubr.69.2.292-305.2005>
- Tuller, T., Birin, H., Gophna, U., Kupiec, M., & Ruppín, E. (2010). Reconstructing ancestral gene content by coevolution. *Genome Research*, 20(1), 122–132. <https://doi.org/10.1101/gr.096115.109>
- Van Der Gulik, P. T. S., Hoff, W. D., & Speijer, D. (2017). In defence of the three-domains of life paradigm. *BMC Evolutionary Biology*, 17(1), 1–5. <https://doi.org/10.1186/s12862-017-1059-z>

7. *Escherichia coli* bioprocess definition

7.1 Nomenclature

gDCW: Dry cell weight amount in grams

$Y_{\text{eth/glc}}$: Yield between acetate produced and glucose consumed ($\text{gDCW} \cdot \text{g}_{\text{glucose}}^{-1}$)

$Y_{\text{x/glc}}$: Yield between biomass produced and glucose consumed ($\text{gDCW} \cdot \text{g}^{-1}$)

$Y_{\text{eth/x}}$: Yield between acetate produced and biomass produced ($\text{g} \cdot \text{gDCW}^{-1}$)

OUR: Oxygen uptake rate ($\text{mM} \cdot \text{h}^{-1}$)

CER: Carbon exchange rate ($\text{mM} \cdot \text{h}^{-1}$)

FDB: Abbreviation for Fed-Batch Strategy

q_{glucose} : Specific glucose consumption rate ($\text{mmol} \cdot \text{gDCW}^{-1} \cdot \text{h}^{-1}$)

$X(t_0)$: Biomass concentration at time zero (initial time)

$V(t_0)$: Volume of bioreactor at time zero (initial time)

$C_{\text{glucose, feeding}}$: Glucose concentration of the feeding solution used in the fed-batch strategies ($\text{g} \cdot \text{L}^{-1}$)

$F(t)$: Feed addition flow rate in fed-batch strategy ($\text{mL} \cdot \text{min}^{-1}$)

t : Time (h)

μ : Specific growth rate (h^{-1})

RQ: Respiratory Quotient

7.2 Introduction

In order to produce products by means of the use of organisms as a biocatalyst, several bioprocesses have been developed until now. Even though, the first ever produced wine and beer was by brewing – fermentation in ancient Egypt and Mesopotamia several millennia BC (Corran, 1975), they actually did not know that the core of their process was an organism. Therefore, the first time that the knowledge regarding the production of organic compounds such as alcohols and organic acids through fermentation is relatively recent and the first reports in the literature only appeared in the second half of the 19th century (Vasic-Racki, 2006). For instance, vinegar was produced by bacteria at 1823 or L-aspartic acid by *E. coli* at 1958 (Vasic-Racki, 2006). In relation with the production of products by organism this chapter is focus on the use of *E. coli* as a biocatalyst.

Therefore, regarding *E. coli*, it has to be kept in mind that in the last decades the most used application was to produce recombinant proteins, due to the fact that it is considered as the most well-established cell factory that has become a popular expression platform (Rosano & Ceccarelli, 2014). For this reason, and as it was mentioned in **Chapter 1**, there are several molecular tools and protocols for the high-level production of heterologous proteins, such as a vast catalogue of expression plasmids, a great number of engineered strains (Mahmoud Al-Hejin et al., 2019). Even though the understanding and developing of new genetic tools, mainly from the molecular biology field, can be a way to increase the protein production in order to obtain high titers (Lee et al., 2020). This chapter will be focused on studying several culture strategies in order to improve the biomass production and, consequently, the volumetric productivity, as stated in the introduction chapter (Chapter 3).

As it was mentioned above, the first fermentation is dated from 19th century, where most of the fermentations were based on batch strategy, whose main trait is to use a media whose substrate concentrations are increased until substrate inhibition appears. As a result, fed-batch strategies were designed in order to develop a culture strategy which might be able to control the concentration of the substrate and nutrients in a suitable ranges (Minihane & Brown, 1986).

Since 1976 there have been several approaches regarding the feeding optimization in fed-batch: the first was an approach based on a pre-determined exponential mathematical estimation of the biomass profile during the substrate fed-batch addition (Kishimoto et al., 1976). However, some issues appeared regarding the metabolism changes during the fermentation, leading the exponential feeding to a bad biomass estimation as it cannot detect those changes. Therefore,

the second approach was based on looking for a way to base the feeding on the overall activity of the culture and be able to control the feeding according to that.

In this context, the implementation of monitoring and control systems has been gaining relevance in the last decades. In this context, most of the monitoring devices can be classified regarding its monitoring techniques, specifically, by the nature of the measurement method (Zhao et al., 2015) or the sampling (Gálvez Sánchez, 2011)(Lourenço et al., 2012), as explained down below.

Regarding the nature of the measurement, two classifications can be done: the direct measurements, which are based on that the variable that is measured directly with a probe or analysis, whereas the indirect measurements are based on a calculation or estimation, through the measurement of another related variable.

On the other hand, the monitoring techniques also can be classified by the nature of the sampling: the off-line measurements whose main trait is that the measurement of the sample is performed *a posteriori*, normally in external laboratories. While in contrast, real-time measurement whose main feature is that the measurement of the sample is performed in situ.

Therefore, several strategies have been developed based on different monitored variables: the fed-batch based on controlling the feeding using the pH (Nishio et al., 1977) or the dissolved oxygen (Yano et al., 1978), which are based on online direct measurements. On the other one, it can be found others based on indirect variables such as the respiratory quotient (Wang et al., 1977).

However, it has to be kept in mind that all these strategies are designed to be able to detect to the non-predictive changes in the culture metabolism, in order to perform the more suitable addition. In the recent years, due to the improvement in the analytical devices regarding systems biology, there has been a new approach for performing fed-batch strategies whose main trait is the integration of all the data that systems biology might offer. For instance, the definition of the fed-batch parameters for a culture of *Corynebacterium glutamicum* through the comprehension and analyzation of its metabolism. The data obtained in relation with the carbon metabolism was used in the definition of fed-batch strategies in order to build an algorithm which could predict and anticipate the changes in metabolism during the fed-batch phase (Iwatani et al., 2008).

Thereupon, the following chapter will design a whole set of culture strategies for *E. coli* BL21 from batch to fed-batch, taking into consideration the metabolic data obtained in **chapter 3** in

order to optimize the biomass production and the volumetric productivity of the bioprocesses based on this bacterium.

7.3 Batch strategies

7.3.1 Batch

As has been previously described in the study of *E. coli*'s metabolism (**chapter 3**), specifically in regard with *E. coli* BL21 metabolism, glucose can be fully converted to biomass without producing acetate (at least at concentrations that not unbalanced glycolysis and TCA). Therefore, *E. coli* BL21 will be used as a reference strain for the design of bioprocess strategies, whose aim is to improve the volumetric productivity by means of enhancing the biomass generation.

First of all, *E. coli* BL21 was cultured in a 2L bioreactor where the environmental conditions were controlled in order to get the optimal growth rate and glucose was used as a media's main carbon source (the environmental conditions and the control variables related to it are described in section 7.7.8. The media composition is described in section 7.6.4.

As shown in **Figure 7-2-A** as well as in **Table 7-1**, *E. coli* BL21 cultured in batch strategy had a growth rate of $0,54 \text{ h}^{-1}$ and $6,2 \text{ gDCW} \cdot \text{L}^{-1}$ of biomass was produced consuming $18 \text{ g} \cdot \text{L}^{-1}$ of glucose without producing acetate. This characteristic feature regarding the conversion of glucose to biomass was previously explained in **chapter 3**. Furthermore, the biomass-glucose yield led the culture to produce $0,31 \text{ gDCW}$ of biomass for each gram of glucose consumed.

On the other hand, it is important to observe an interesting fact related to a correlation between biomass and other variables. In this case, there are three variables that follow the biomass

tendency profile in the culture; consequently, they give information related to its growth state and biomass formation: the oxygen uptake rate (OUR), carbon exchange rate (CER) and, lastly, the volume of the alkali addition related to pH control, as shown in Figure 8-1-B. Furthermore, a briefly description of each one will be presented hereafter.

Regarding CER and OUR, both variables are calculated taking into consideration the difference between the inlet and out gas flow concentration (global mass balance method) as described in section 7.7.9. Both of them give information about the culture growth state by means of analysing the temporal variation of oxygen (OUR) and carbon dioxide (CER), due to the fact that growth state is directly linked to the carbon dioxide production and oxygen consumption..

As it was previously mentioned in **chapter 3**, the metabolism of glucose leads to the formation of mainly two compounds: reduced electron acceptors and oxidized carbon molecules. The oxidized molecules consist of biomolecules required for biomass synthesis (dihydroxyacetone phosphate, acetyl-CoA, glyceral-3-phosphate and others) and the most oxidized state of glucose is carbon dioxide. As shown in figure **Figure 7-1**, a direct relation could be described between CER, OUR, alkali buffer addition and biomass evolution, specifically, the growth rate. The specific rate of the molecules directed towards biomass generation (μ) can be measured using the biomass concentration and it is related to the growth state as well. Moreover, the information in regard with the specific rate of carbon dioxide (q_{CO_2}) can be obtained by following the profile of CER, while a specific rate of pH modification can be calculated through the evolution of alkali buffer addition.

On the other hand, it is important to keep in mind that the reduced electron acceptors produced by the carbon metabolism must be regenerated in order to balance the redox metabolism. This regeneration takes place in the energy metabolism and it is based on the reduction of oxygen to water. Furthermore, the specific rate of oxygen (q_{O_2}) can be measured following the OUR profile.

Therefore, the culture's growth rate and its growth state can be extrapolated and followed measuring the profile of CER and OUR due to the fact that CER, OUR and biomass growth rate are linked owing to their relation with the glucose oxidation.

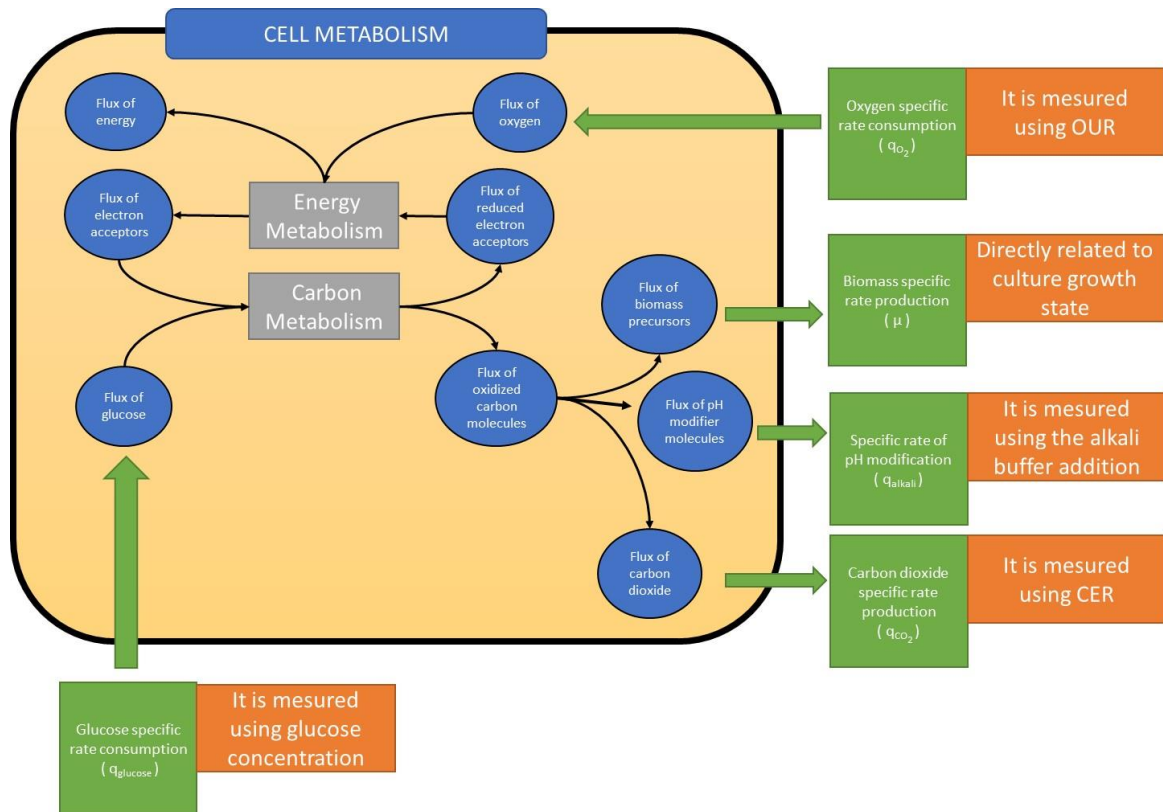


Figure 7-1 Main carbon specific rate relations of cell metabolism.

In addition, the alkali addition gives information in regard with the growth rate because there are several metabolites related to the carbon metabolism that can modify the pH while growing. For example the consumption of phosphate (Konings & Rosenberg, 1978) or the production of carbon dioxide via the formation carbonic acid ("The Kinetics of the Carbon Dioxide-Carbonic Acid Reaction," 1933). As a result, the biomass can be estimated if it takes into account how the alkali addition behaves to keep the pH constant.

For a further exploration regarding how to increase the biomass concentration by means of more nutrient feeding from the beginning of the culture and how the biomass can be related to OUR and CER as well pH profile (based on the previously batch culture carried out), the next experiment that will be presented is the fortified batch. In the following section the definition and characterization of it will be detailed.

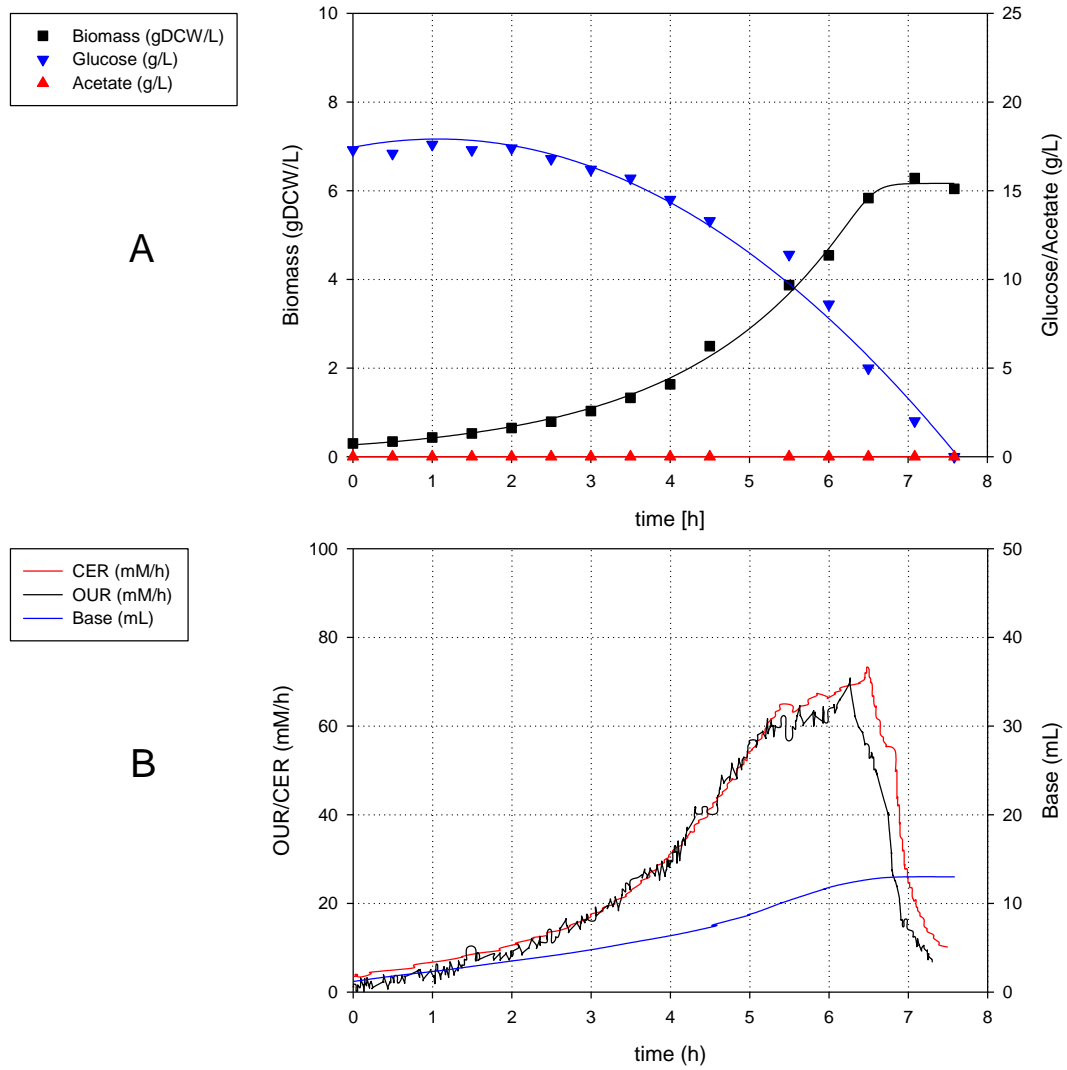


Figure 7-2 Profile of A) off-line variables such as Biomass (■), glucose (▼), acetate (▲) and B) on-line variables such as CER (—), OUR (—) and total alkali buffer addition (—) for *E. coli* BL21 batch culture.

Table 7-1 Main batch parameters for overall characterized culture strategies.

	Batch
Achieved Biomass (gDCW·L ⁻¹)	6,2
μ (h ⁻¹)	0,54
Acetate generation (g·L ⁻¹)	0
Glucose Consumption(g·L ⁻¹)	18
$Y_{x/s}$ (gDCW·g _{glucose} ⁻¹)	0,31

7.3.2 Fortified Batch

In order to increase the biomass concentration following the batch culture strategy and before going to more complicated strategies as fed-batch, there are several approaches that can be followed. In this section, the fortification of the batch will be studied.

It has to be taken into account that the batch fortification is based on rising the concentration of all the media compounds until they reach a growth-inhibitory concentration. Therefore, the first experiment that was carried out was the determination of the growth-inhibitory concentrations for the main nutrients of the culture media. First of all, the compounds of the media were split in 3 groups: the carbon source, the majority salts, and lastly, the microelements, as is described in **Table 7-2**.

Table 7-2. Distribution of the media compounds regarding its concentration and function.

Group	Compound
Carbon source	Glucose
Majority salts	Nitrogen-based and phosphor-based salts
Microelements	Vitamins and trace elements

Starting with glucose, a wide range of glucose concentrations were tested in shake flask. As shown in **Figure 7-3**, and detailed in **Table 7-3**. As it can be seen, the growth rate inhibition starts at glucose concentrations that are higher than 80 g·L⁻¹.

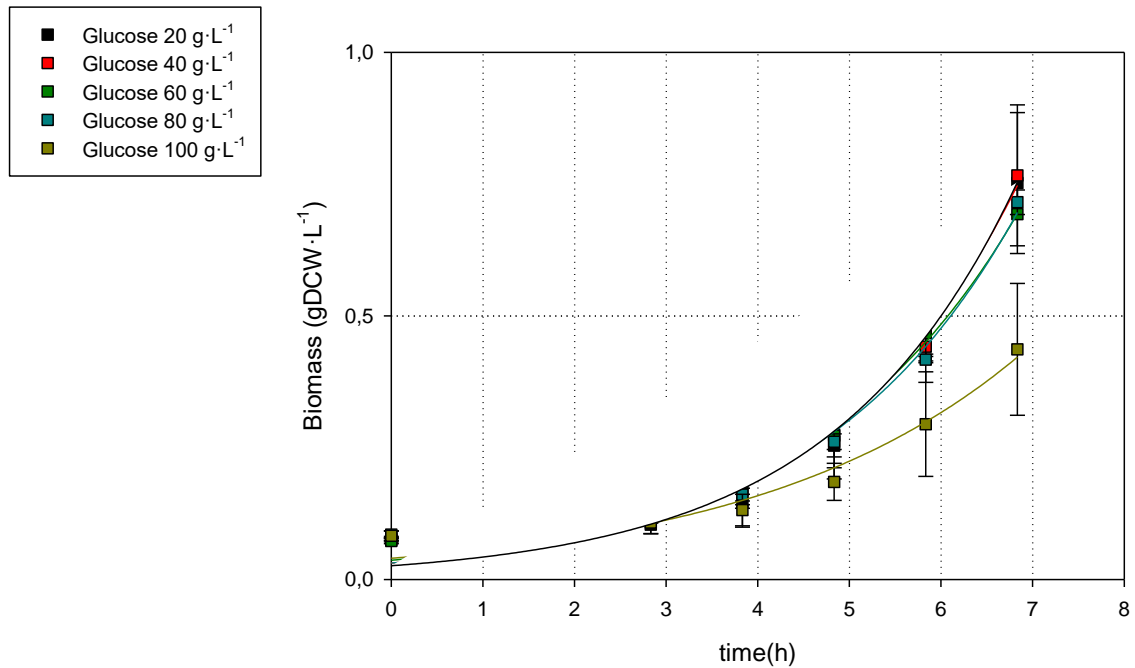


Figure 7-3 Profile for Biomass concentration ($\text{gDCW}\cdot\text{L}^{-1}$) where different glucose concentrations were tested.

Table 7-3 Growth rate comparison when several glucose media concentrations are tested.

Glucose concentration ($\text{g}\cdot\text{L}^{-1}$)	μ (h^{-1})
20	$0,450 \pm 0,027$
40	$0,450 \pm 0,001$
60	$0,452 \pm 0,022$
80	$0,453 \pm 0,022$
100	$0,356 \pm 0,020$

Once the glucose inhibition concentration has been determined, an experiment where the n-fold concentrations of the minority elements was carried out. It is important to emphasize that the glucose concentration used in this experiment was the one non inhibitory selected in the previous experiment, $80 \text{ g}\cdot\text{L}^{-1}$.

As shown in **Figure 7-4** and is corroborated in **Table 7-4** as well, the growth inhibitory concentration of microelements was found at concentrations higher than 2-fold.

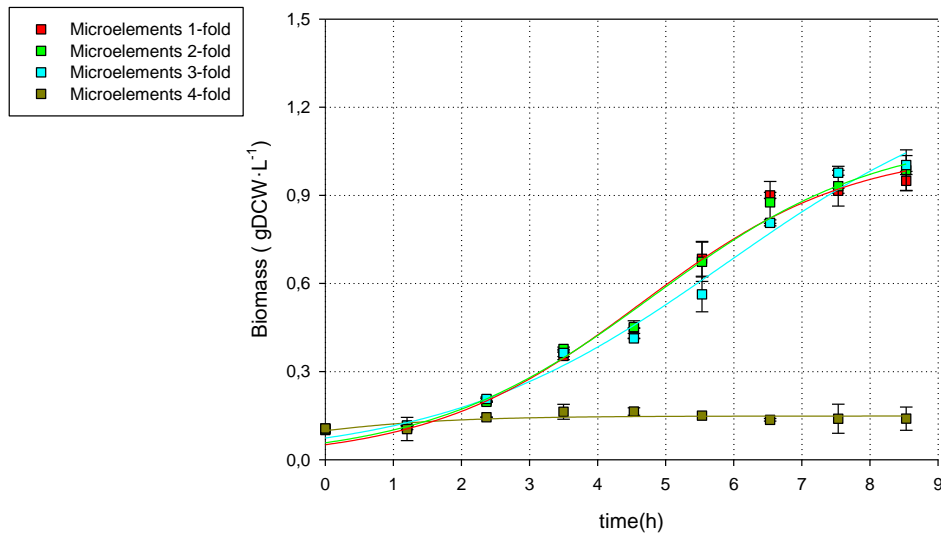


Figure 7-4 Profile of biomass concentration (gDCW·L⁻¹) where different trace elements concentrations were tested.

Table 7-4 Growth rate comparison when several trace elements media concentration.

Microelements (n-fold)	μ (h ⁻¹)
x1	0,43 ±0,002
x2	0,45 ±0,001
x3	0,35 ±0,001
x4	0,00±0,000

The next experiment was a fortified batch that was carried out where glucose concentration was set to 80 g·L⁻¹ and the microelements where concentrated 2-fold. In relation with the fortification of the majority salts, the nitrogen-based salts were not fortified because the amount added by the titter solution used by the pH control was ammonium hydroxide should avoid a nitrogen-based salts growth limitation. On the other side, the phosphate-based salts were not fortified because it main function was as a pH buffer. Consequently, its concentration was far from a phosphate-based growth inhibition.

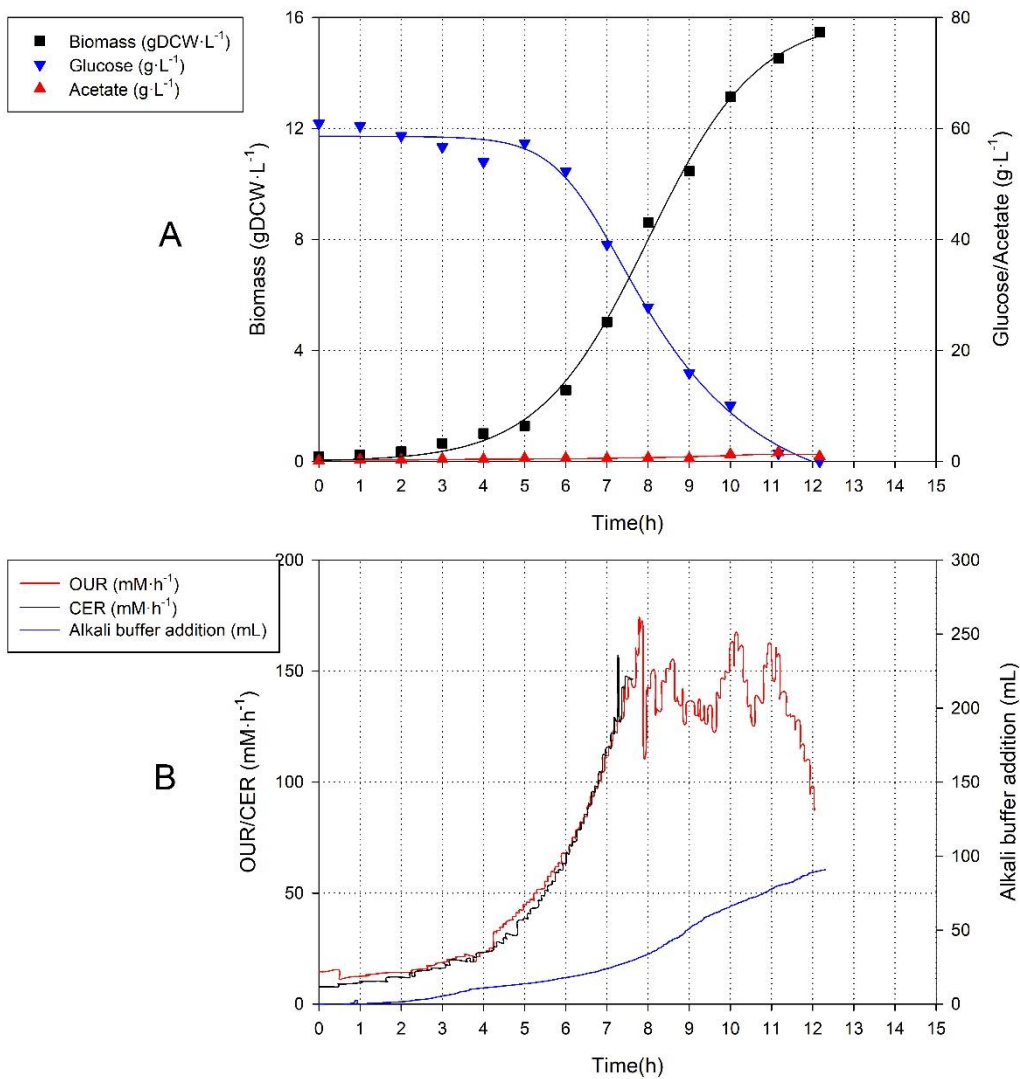


Figure 7-5 Profile of A) off-line variables such as Biomass (■), glucose (▼), acetate (▲) and B) on-line variables such as C.E.R (—), O.U.R (—) and total alkali buffer addition (—) for pH-controlled fortified batch culture.

As shown in **Figure 7-5**, 60 g·L⁻¹ of glucose were consumed in 12 h in order to produce 15,4 gDCW·L⁻¹ and 1,6 g·L⁻¹ of acetate. As a consequence, *E. coli* BL21 had a growth rate of 0,48 h⁻¹ and also a biomass-glucose yield of 0,22 gDCW·g⁻¹. Furthermore, it is important to describe why acetate was produced, as it was mentioned in **chapter 3** regarding the *E. coli* BL21 metabolism, acetate was produced due to high extracellular glucose concentrations, the flux through the glycolysis was higher than the one internalized by the TCA. Consequently, acetate was produced to balance the acetyl-coA.

On the other hand, as shown in **graph B of the Figure 7-5**, the oxygen uptake rate and the carbon exchange followed the growth tendency of the culture until they reached a maximum value of approximately 150 mM·h⁻¹. Moreover, the behaviour of the alkali addition was just as carbon

exchange rate (CER) and oxygen uptake rate (OUR) following the biomass profile. Even though it was followed by the variables shown in **graph B**, there is a slightly but important aspect regarding the relation between. OUR and CER are inherently linked to the growth tendency, where when a decrease of growth rate occurs a decrease of both variables will occur, because both variables are instantaneous variables. Whereas the alkali addition is an accumulative one. Therefore, a change in CER or OUR could bring information about a change in growth rate, while only the change in the slope of the alkali addition tendency is directly related to it.

To conclude with, the fortification of batch medium as shown in **Table 7-5**, led to an increase of the biomass produced from 6,2 gDCW·L⁻¹ to 15,4 gDCW·L⁻¹. Moreover, an 2,48-fold increase of biomass volumetric productivity was achieved, even though the specific growth rate was reduced by 12% and 1,6 g·L⁻¹ of acetate was produced.

Table 7-5 Main batch parameters for overall characterized culture strategies.

	Batch	Fortified Batch
Achieved Biomass (gDCW·L ⁻¹)	6,2	15,4
μ (h ⁻¹)	0,54	0,48
Acetate generation (g·L ⁻¹)	0	1,6
Glucose consumption (g·L ⁻¹)	18	60
Y _{X/s} (gDCW·g _{glucose} ⁻¹)	0,31	0,22

Up until now, the increase of the biomass production in order to increase the volumetric biomass productivity has been based on the fortification of the batch medium. In the following section a different approach will be described, based on using advanced culture techniques related to defining fed-batch culture strategies, where an increase in volumetric biomass productivity is expected at the same time that growth rate will not be reduced and acetate not to be produced.

7.4 Fed batch strategies

As it was previously described in the batch strategies, the increase of biomass production was accomplished by increasing the substrate concentration of batch media components. As a result, an increase of 24% of biomass volumetric productivity was achieved.

However, in order to increase even more the produced biomass, a different strategy based on fed-batch will be developed in this section. It is important to point out that a fed-batch is a bioprocess strategy that relays on knowing *a priori* the metabolic and physiologic condition of the organism that is going to be cultured. These requirements are needed because fed-batch strategies are inherently related to the specific rate of glucose consumed (main carbon source) and growth rate, as shown in section 7.7.12.

Moreover, the fed-batch strategies can be split into two groups taking into consideration how the feeding profile is calculated. The first one consists of the fed-batch strategies whose feeding profile is calculated using a theoretical preprogrammed biomass profile. Whereas, in the second group the feeding profile is calculated via on-line estimation of the experimental biomass by means of searching relations between measured variables (as OUR or CER) and the experimental biomass concentration.

Furthermore, there is a feature that has to be mentioned that is the initialization point of the fed-batch strategy. In this study, the starting point regarding the initialization was decided to be near the moment when the glucose concentration was almost zero in the batch. Therefore, the initialization moment of the fed-batch strategy is decided taking into consideration the glucose concentration profile, as a result, being manual and a worker-dependent one.

The first strategy that is going to be described is based on a preprogrammed exponential addition, whose main trait is that the growth of *E.coli* BL21 will be extrapolated directly from an biomass balance which the parameters of the exponential function will be set from data obtain from its batch phase, as shown in section 7.7.13. Moreover, the feeding profile will be based on contributing with the stoichiometric glucose required for growing at the optimal rate. To grant that glucose was defined as the stoichiometric compound in feeding media.

It is important to highlight that the parameter that will be used as the specific consumption rate of glucose in the calculation for the feeding addition will not be the one that the batch culture determines. As shown in **Figure 7-6**, the specific consumption rate of glucose calculated through the batch phase is not representative if it is compared with the data obtained in **chapter 4**, regarding the continuous culture, because there is a 5-fold decrease over the batch culture. This difference is because when *E. coli* BL21 is cultured in batch, it metabolizes all the possible glucose that can be metabolized by the bacteria, not the optimal. In fed-batch cultures, the

feeding profile used is the one that should grant the optimal conversion of glucose to biomass while growing at optimal rate. Therefore, the specific rate of consumption that will be used is the one obtained from the data of the continuous culture from the studies carried out in **chapter 3**, regarding *E. coli* BL21 glucose metabolism in continuous cultures.

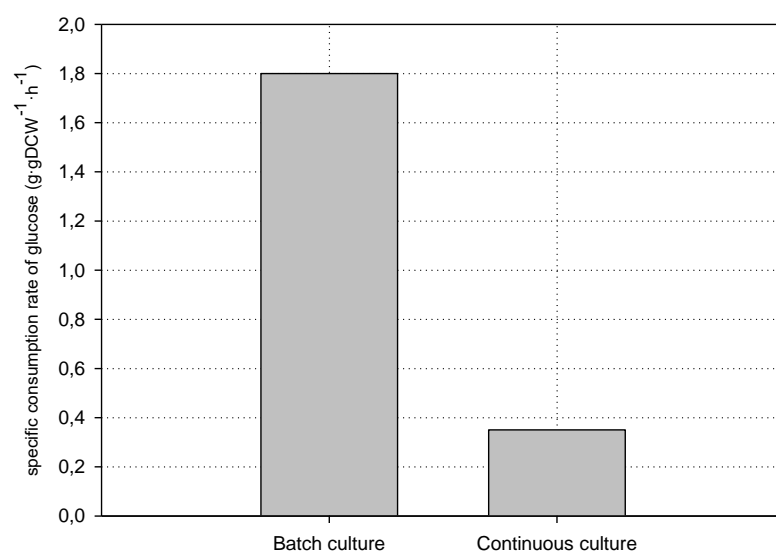


Figure 7-6. Comparison of the glucose specific consumption rate between the batch and continuous cultures.

7.4.1 Fed batch based on exponential feeding

In order to perform a fed-batch addition based on a preprogrammed exponential, several data was required. This data, as shown in **Equation 7-1** tackles mainly specific consumption rate of glucose ($q_{glucose}$), growth rate (μ) and glucose concentration in the feeding media ($C_{glucose,Feeding}$). Therefore, it is important to define the feeding media and the data required for the feeding algorithm. For this purpose, a detailed definition of both the feeding media and the algorithm mathematical are described in section 7.7.3 and section 7.7.13, respectively.

Equation 7-1

$$F(t) = \frac{-q_{glucose} \cdot X(t_0) \cdot V(t_0) \cdot \exp(\mu \cdot t)}{C_{glucose,Feeding}}$$

In the batch phase, the glucose conversion to biomass had a value of 0,31 gDCW·g⁻¹ with an obtained biomass concentration of 6,2 gDCW·L⁻¹ without producing acetate. In the exponential phase, the specific growth rate and the specific consumption rate of glucose had a value of 0,54 h⁻¹ and 1,80 g·gDCW⁻¹·h⁻¹, respectively. After the decrease in the OUR, in order to enable the culture's growth a fed-batch strategy based on a exponential feeding was carried out.

As shown in **Equation 7-1**, the fed-batch strategy requires setting some metabolic parameters to define the feeding profile. In this case, the feeding profile was based on parameters presented in **Table 7-6**. Regarding the specific glucose consumption rate, it has to be pointed out that it had a value of 0,35 g·gDCW⁻¹·h⁻¹ in order to grant an optimal conversion of glucose to biomass. Regarding the other specific growth rate, the feeding used the one calculated from the prior batch phase.

As shown in **Figure 7-7**, once the parameters had been fixed with the values that are shown in **Table 7-6**, the fed-batch phase was initiated when the batch OUR and CER dropped at 6 hours because as it was mentioned before, a decrease in the OUR and CER is related to a limitation in the growth rate.

As shown in **graph A of Figure 7-7** and **Table 7-6**, the achieved biomass in the fed-batch phase had a value of 35,7 gDCW·L⁻¹ that represented an increase of 5,83-fold in comparison with the previous batch. Moreover, the growth rate specific (0,51 h⁻¹) only differed from a - 5% in regard

with the estimated . This decrease might be caused by an under estimation of the feeding addition, which led the culture to a limited-growth state.

Regarding OUR and CER profiles obtained, shown in **graph B of Figure 7-7**, there are two important facts to be mentioned:

1. The feeding started when both OUR and CER values dropped. This is because they describe the “instantaneous” metabolism due to the fact that, as can be observed in the batch strategies section, when glucose concentration is near $0 \text{ g}\cdot\text{L}^{-1}$ a drop in both profiles occur.
2. Both CER and OUR followed the growth perfectly, although the OUR showed an error value which led to be discarded as a control tool for future strategies. This error occurred due to the fact that the aeration control used to maintain the culture’s dissolved oxygen in the liquid phase, mainly when high cell density was achieved, generated too much error in the OUR measurement. The main issue was related to the fact that OUR calculation used the oxygen concentration as a variable. On this basis, the aeration control was not able to maintain a correct gas mixing for granting a homogeneous oxygen concentration in the inlet gas flow. Consequently, the oxygen concentration in the inlet flow was not representative.

Moreover, as shown in **graph B of Figure 7-7**, there is another parameter that has been described previously in the batch section, which also follows the biomass evolution: the alkali buffer addition. It is related to biomass evolution due to the interaction between the acid produced in the metabolism and the bioreactor’s pH control by base addition in order to maintain the pH constant.

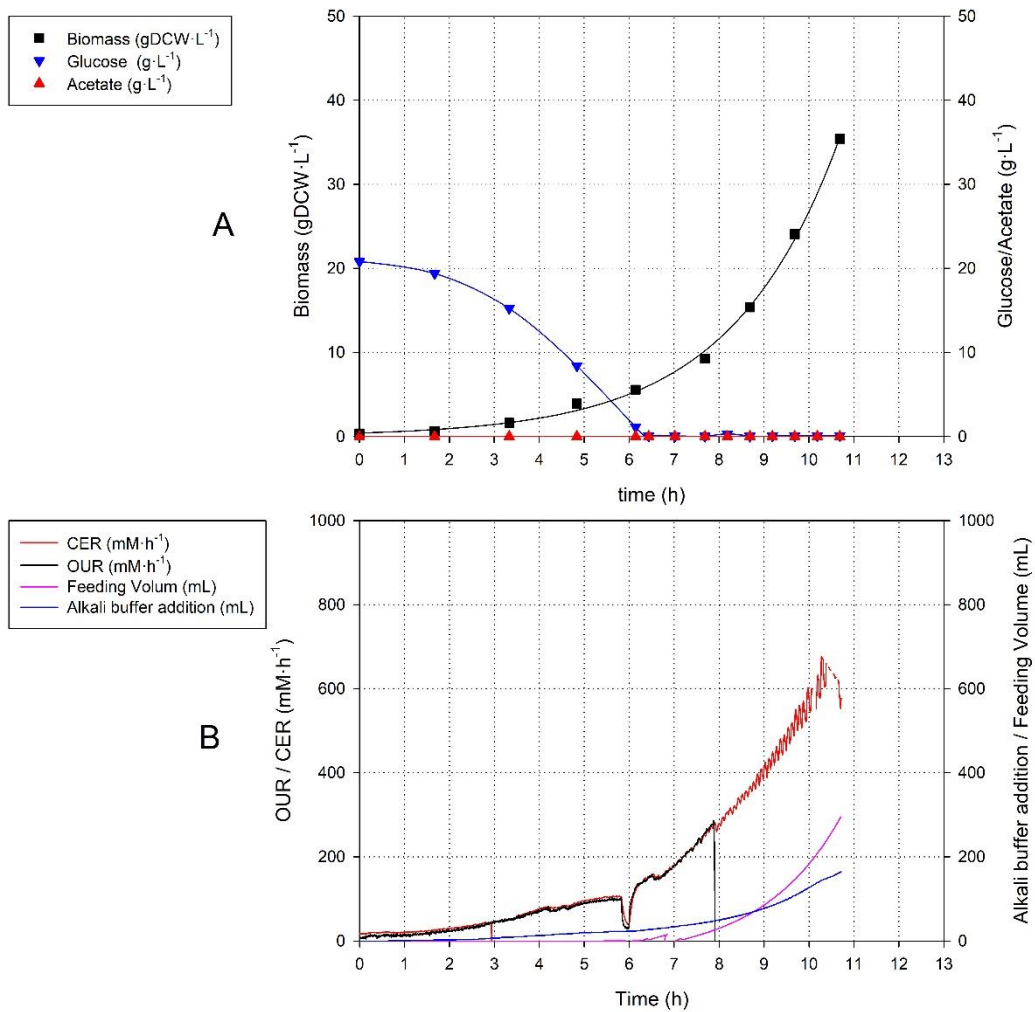


Figure 7-7 Profile of A) off-line variables such as Biomass (■), glucose (▼), acetate (▲) and B) on-line variables such as CER (—), OUR (—), feeding volume (—), and the alkali buffer addition (—) for *E. coli* BL21 fed-batch culture based on a preprogrammed exponential algorithm.

Table 7-6 Main fed batch parameters for overall Fed batch culture strategies.

	Fed batch feeding algorithm based on	
	Pre-programmed exponential	
Achieved biomass (gDCW·L ⁻¹)	35,7	
μ theoretical (h ⁻¹)	0,54	
μ experimental (h ⁻¹)	0,51	
q_{glucose} (g·gDCW ⁻¹ ·h ⁻¹)	0,35	
q_{CO_2} (g·gDCW ⁻¹ ·h ⁻¹)	x	
q_{base} (mL·gDCW ⁻¹ ·L)	x	
$Y_{x/s}$ (gDCW·g _{glucose} ⁻¹)	0,382	
Fedbatch time (h)	5	

To conclude, as shown in **Table 7-7**, the fed-batch strategy based on the exponential addition was a success taking into account the increase of the biomass achieved by almost 5,75-fold in comparison with reference batch culture. As a result, the volumetric productivity was increased by 5,75-fold as well.

Table 7-7 Main parameters for overall characterized culture strategies.

	Batch	Fortified Batch	FDB pre-programmed exponential
Achieved biomass (gDCW·L ⁻¹)	6,2	15,4	35,7
μ (h ⁻¹)	0,54	0,48	0,51
Acetate generation (g·L ⁻¹)	0	1,6	0
Y _{x/s} (gDCW·g _{glucose} ⁻¹)	0,31	0,25	0,382

The main issue obtained in this strategy was related to a decrease observed in the specific growth rate obtained provoked by an underfeeding. The underfeeding was caused by not using the correct parameters when the feeding profile was used. As a result, the specific growth rate was limited because the biomass estimated was lower than the experimental one.

Therefore, a tool to monitor biomass concentration in an online way is required in order to generate a feeding profile able to adapt to a change in the expected metabolic parameters. As it was mentioned before, three variables can be used to monitoring the biomass profile: CER, OUR and alkali buffer addition. However, only CER and alkali buffer addition might be used, because of OUR, became unstable in the middle of the fed-batch phase. As a result, it could provoke some errors in the biomass estimation, and consequently, not getting the optimal feeding for the cells.

This is why in the next sections, different fed-batch strategies are going to be designed looking for a way to estimate the biomass evolution in order to perform a “biomass-based” addition. Moreover, the “biomass-based” addition will be able to predict metabolic changes in advance and as a result, adapting the feeding profile to the culture requirements in order to optimize the fermentation.

7.4.2 Fed-batch feeding based on CER evolution

As it was mentioned before, the idea of the following sections is to design a fed-batch strategy that is able to adapt feed addition in order to let the culture grow at the optimal rate.

Taking into account the description of two variables that can be used in order to predict biomass evolution; this section starts with the carbon exchange rate (CER), which has been demonstrated that can be used as a parameter to predict the biomass evolution.

As it is described in section 7.7.14, the relation able of predicting the biomass through CER is based on the specific carbon dioxide production rate (q_{CO_2}), owing to CER and biomass have a proportional relation as show in **Equation 7-2**.

Equation 7-2.

$$CER(t) = q_{CO_2} \cdot Biomass(t)$$

As it was described in the previous fed-batch strategy, the fed-batch was split into two phases: the batch phase, which is defined within the first 6 hours, and the fed-batch phase, which occurs after the batch phase until the end of the experiment.

As shown in **graph A of Figure 7-8** in regard with the batch phase, it had the same behaviour as the previous batch one performed because the media used was the same. The most relevant parameters that will be used for further calculations in relation with the feeding addition algorithm are the growth rate ($0,54 \text{ h}^{-1}$) and the specific carbon dioxide production rate ($36,6 \text{ mmol} \cdot \text{gDCW}^{-1} \cdot \text{h}^{-1}$).

Then, as shown in **Table 7-8**, the parameters above mentioned were used in order to calculate a feeding algorithm that can take into consideration the biomass evolution. Regarding these parameters, the specific production rate of carbon dioxide, which was used to calculate the biomass profile on-line, had a value was of $36,6 \text{ mmol} \cdot \text{gDCW}^{-1} \cdot \text{h}^{-1}$ obtained from the prior batch phase. While, as it was mentioned before, the specific consumption rate of glucose was the one obtained from the continuous cultures (**chapter 4**) due to it presented the optimal conversion of glucose to biomass and it had a value of $0,35 \text{ g} \cdot \text{gDCW}^{-1} \cdot \text{h}^{-1}$.

Thus, the fed-batch phase was carried out as shown in **graph A of Figure 7-8**, where the initialization point was decided following the same criteria of the preprogramed exponential fed-batch strategy and the biomass concentration achieved had a value of $29,3 \text{ gDCW} \cdot \text{L}^{-1}$. The

maximum growth rate was $0,49 \text{ h}^{-1}$, which only differed from a 5% from the estimated one, and lastly, regarding glucose concentration, there was an accumulation of glucose due to a several problems of the CER-based algorithm in relation with how the algorithm interacts with unusual situations.

Taking into account that as shown in **Table 7-9** the biomass achieved is 5% lower over the preprogramed exponential strategy due to the fact that in order this strategy to succeed the culture has to keep its central carbon metabolic state constant. When there is a change in the biomass growth rate related to a shift in environmental conditions owing to the feeding addition, the same biomass might decrease or increase its CER. As a result, this metabolic restructuration can affect the algorithm because the algorithm might do a wrong biomass prediction, as observed in the last 3 hours of the **graph C of Figure 7-8**. Therefore, it is important to perform a rigorous description of all the changes of biomass-glucose-CER interactions.

As shown in **graph C of Figure 7-8**, in the first 2 hours of fed-batch the culture had a CER representative that estimated the biomass correctly. Although, there was a glucose accumulation phase which might be caused by an oversize of the feeding strategy set-up due to the use of a non-representative parameter when setting up the feeding profile. This parameter should be the metabolic ones because the other parameter (glucose concentration in the feeding solution) do not depend on a metabolic behaviour. Regarding the metabolic parameters, if either the specific consumption rate of glucose or the specific growth rate were oversized, the feeding profile will add more volume than the required one.

Therefore, the accumulation of the feeding might lead the culture to an instable state where there was not any constant metabolic state as shown **graph C of Figure 7-8** at 8 hours, where from that point CER did not estimate the biomass correctly. This metabolic inconstancy, that led to a wrong estimation of biomass added to the sensibility of the CER-biomass algorithm, provoked a burden to the culture that at the end fulfilled with a lower biomass concentration than pre-programmed exponential algorithm.

Moreover, regarding the monitoring and control of the strategy based on CER, it is important to point out an issue related to how the mathematical algorithm works when the culture enters in a limited condition, where the same biomass concentration dropped the specific rate of carbon dioxide production. This issue is related to a phenomenon described in **chapter 4** and is based on an inherent relation between the glucose limitation conditions and metabolic restructuration. This phenomena can be seen in the last two hours of the fed-batch phase presented in **Figure 7-8**, where an increase in the biomass concentration was not directly

correlated to an linear increase in the carbon dioxide produced (CER), due to there was not a specific correlation between. Therefore, the core hypothesis of the algorithm which is based on a lineal relation between biomass concentration and CER was not been fulfilled, and as a consequence, the estimated biomass concentration was not correct in the last three hours as shown in **graph C of Figure 7-8** . Furthermore, this error between the estimation and the experimental provokes a continuous decrease in the feeding addition owing to the following premise: the decrease in the biomass estimation provokes a decrease in the feeding addition, and consequently, a loop is set off where the feeding addition decreases. This loop is triggered because there is always the same biomass concentration and less feeding addition, and consequently, less CER is achieved with the same biomass.

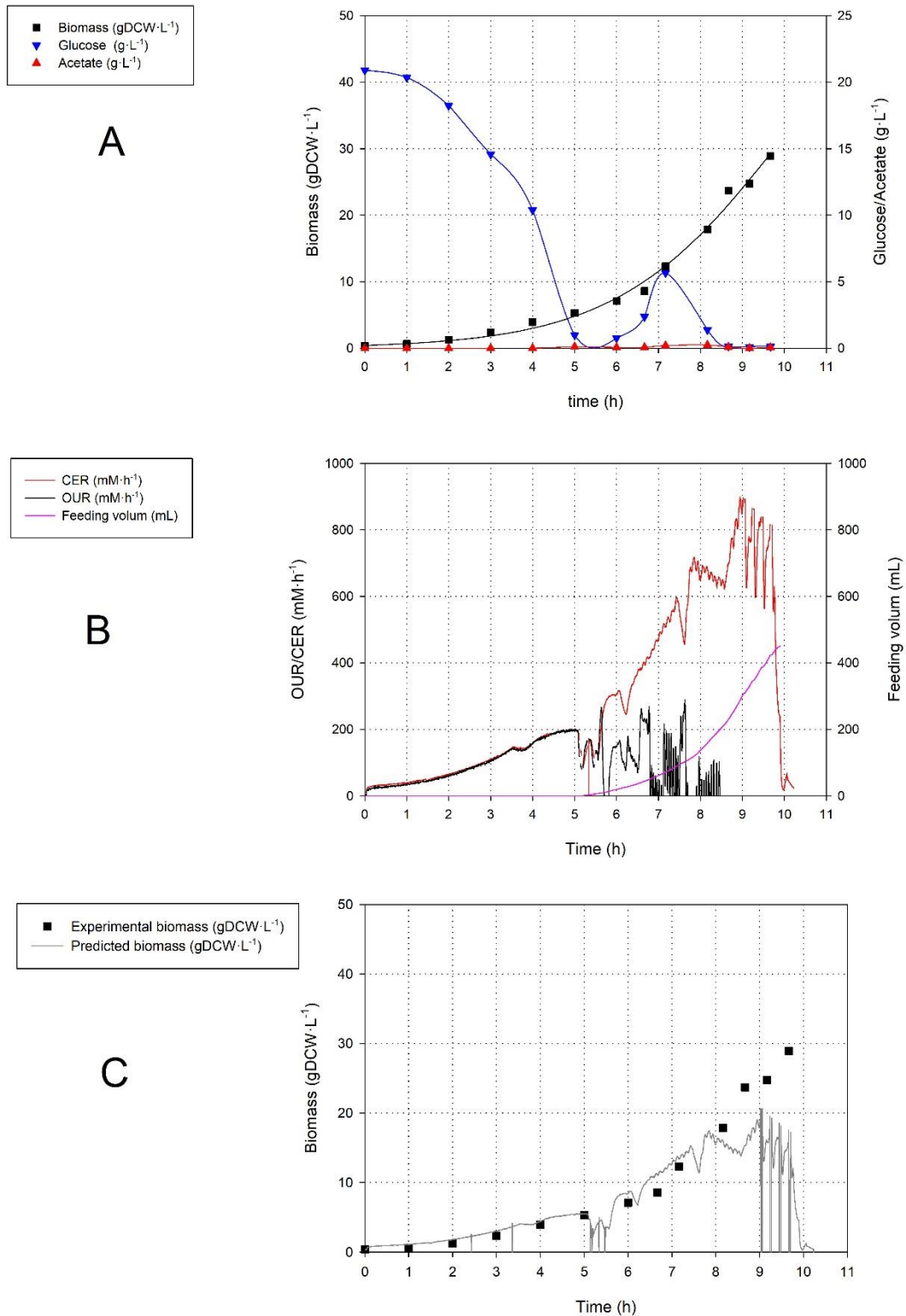


Figure 7-8 Profile of A) off-line variables such as Biomass (■), glucose (▼), acetate (▲), B) on-line variables such as C.E.R (—), O.U.R (—) and feeding volume(—) for pH-controlled fed-batch culture using CER algorithm for feeding, and on C) the comparison between the biomass calculated by the CER-based mathematical algorithm and the biomass experimental points.

Table 7-8 Main parameters for overall Fed-batch culture strategies

	Fed batch feeding algorithm based on	
	Preprogramed exponential	CER
Achieved biomass ($\text{gDCW}\cdot\text{L}^{-1}$)	35,7	29,3
μ theoric (h^{-1})	0,54	0,54
μ experimental (h^{-1})	0,51	0,49
q_{glucose} ($\text{g}\cdot\text{gDCW}^{-1}\cdot\text{h}^{-1}$)	0,35	0,35
q_{CO_2} ($\text{mM}\cdot\text{gDCW}^{-1}\cdot\text{L}\cdot\text{h}^{-1}$)	X	36,6
q_{base} ($\text{mL}\cdot\text{gDCW}^{-1}\cdot\text{L}\cdot\text{h}^{-1}$)	X	X
$Y_{x/s}$ ($\text{gDCW}\cdot\text{gglucose}^{-1}$)	0,382	0,27

As shown in **Table 7-9**, the fed-batch strategy presented in this section led to obtain the same biomass productivity regarding the non-biomass based algorithm, although less final biomass was achieved and the growth was inhibited due to a growth-limiting feeding profile in the last hours of the fed-batch phase. It is important to point out that, as shown in **graph C of Figure 7-8**, when the metabolic state was stable over time, the CER-based algorithm was able to predict correctly the biomass profile.

Table 7-9 Main parameters for overall characterized culture strategies

	Batch	Fortified Batch	FDB- preprogramed exponential	FDB - CER control
Achieved Biomass ($\text{gDCW}\cdot\text{L}^{-1}$)	6,2	15,4	35,7	29,3
μ experimental (h^{-1})	0,54	0,48	0,51	0,49
Acetate generation ($\text{g}\cdot\text{L}^{-1}$)	0	1,6	0	0
$Y_{x/s}$ ($\text{gDCW}\cdot\text{gglucose}^{-1}$)	0,31	0,256	0,382	0,27

Therefore, the next fed-batch strategy that is going to be designed in the following section will be addressed to use and perform an algorithm that also predicts the biomass evolution, although this core parameter should be more stable, less sensitive, and robust to biomass metabolic changes.

7.4.3 Fed-batch feeding based on alkali buffer addition

As it has been described up until now, an algorithm whose main feature is to predict the biomass concentration over time in order to perform an addition that is linked to biomass evolution was the goal of this chapter. The previous section, used CER in order to predict the biomass evolution, however, due to the promotion of growth-limiting conditions caused by the underestimation of the biomass, it was discarded. Therefore, it is necessary to look for a less sensitive and more robust parameter. On this basis, the selected parameter is the alkali buffer addition, because is an accumulative variable, not an instantaneous as just as CER.

As shown in section 7.7.15, the algorithm follows the hypothesis based on considering the total alkali buffer as a metabolite. As shown in **Equation 7-3**, a specific production rate of alkali buffer can be calculated and, then used in order to predict the biomass concentration.

Equation 7-3.

$$\frac{d(\text{Alkali buffer})}{dt} = q_{\text{alkali}} \cdot \text{Biomass}(t)$$

However, it has to be taken into consideration that the algorithm also needs the metabolic parameters which will be defined using the data from the batch phase (such as the specific growth rate) and from the continuous culture, the specific glucose consumption rate.

As shown in **graph A of the Figure 7-9**, the batch had the same behaviour than the previous batch phases performed, the growth rate ($0,56 \text{ h}^{-1}$) obtained in the batch phase was used as to calculate the feeding profile. In addition, as it was done in the previous fed-batch strategies, It is important to emphasise that the specific consumption rate of glucose ($0,35 \text{ g-gDCW}^{-1}\cdot\text{h}^{-1}$) used in the feeding profile calculations was the one obtained from the continuous culture data in order to obtain the optimal conversion of glucose to biomass.

Then, as shown in **Table 7-10**, the parameters above mentioned were used to calculate a feeding algorithm that take into consideration the biomass evolution. Regarding these parameters, it is important to stand out the specific production rate of alkali buffer, which value was of $1,9 \text{ ml-gDCW}^{-1}\cdot\text{L}\cdot\text{h}^{-1}$, because it is the core of the Alkali buffer-based algorithm in order to predict biomass profile and adjust the feeding profile to the culture demands.

Thus, the fed-batch phase was carried out as shown in **graph A of the Figure 7-9**, where the initialization point was decided following the same criteria of the previous fed-batch strategies and the biomass achieved had a value of $40,32 \text{ gDCW}\cdot\text{L}^{-1}$. The maximum growth rate was $0,52 \text{ h}^{-1}$, which only differed from a 7,3% in regard with the estimated one ($0,56 \text{ h}^{-1}$) and, lastly, regarding glucose concentration, there was an constant accumulation of glucose due to a wrong estimation of the parameters required for the feeding algorithm related to the metabolic state, which were calculated from the batch phase. As a result, an overfeeding occurred which led to a continuous accumulation of glucose until $32 \text{ g}\cdot\text{L}^{-1}$.

On the other hand, regarding the acetate production of $1,54 \text{ g}\cdot\text{L}^{-1}$ of acetate, it might start producing acetate in the last stages of the fed-batch culture, due to the constant changes in environmental conditions owing to the feeding addition. These changes might cause a metabolic restructuration that would have an impact on the specific glucose consumption rate and also the growth rate.

Moreover, regarding the alkali-based algorithm, when the specific production alkali rate is used in order to predict the biomass, as shown in **graph C of the Figure 7-9**, the biomass prediction is good enough to be used in the batch phase because of the relation between alkali addition and biomass is kept constant. On the contrary, when the fed-batch phase was started, the predicted biomass started to differ from the experimental one. This drift was caused by a change in the specific production rate of alkali buffer during the transition between batch ($1,9\text{ml}\cdot\text{gDCW}^{-1}\cdot\text{L}\cdot\text{h}^{-1}$) to fed-batch phase ($1,1\text{ml}\cdot\text{gDCW}^{-1}\cdot\text{L}\cdot\text{h}^{-1}$), as shown in **Figure 7-10**. Therefore, as it was not possible to predict the value's drift, the prediction of the biomass profile using the alkali buffer addition was wrong.

To conclude with, as shown in **Table 7-11**, the alkali buffer addition-based fed-batch strategy was a partially successful taking into account that this strategy led the biomass volumetric productivity to increase 1,1-fold regarding the reference fed-batch, although it led to a glucose accumulation of $30 \text{ g}\cdot\text{L}^{-1}$. Moreover, it is important to realize that even though the biomass algorithm predicted less biomass than the real one, as shown in **graph C of the Figure 7-9**, if the specific production rate of alkali buffer addition would be able to be remained constant during all the experiment, the drift in the biomass predict should be avoided. The fitness of this methodology can be corroborated during the batch phase owing to a perfect match between the predicted biomass and the experimental one.

Therefore, what the previous two strategies tested, to predict the biomass have shown is that there is a “major issue” related to the way of how the parameters that will be used for the

feeding algorithm are defined. Due to unpredictable changes in the metabolism from the batch phase to the fed-batch, a new way of performing the fed-batch strategy must be developed in order to improve this strategy. This improvement will have to tackle several assumptions: the feeding addition must not be relaying in previous data (from the batch phase), and at the end of the culture glucose concentration must be zero, while growing at the maximum rate. On this basis, and taking into consideration all the knowledge gain from now, in the following section a new strategy is proposed.

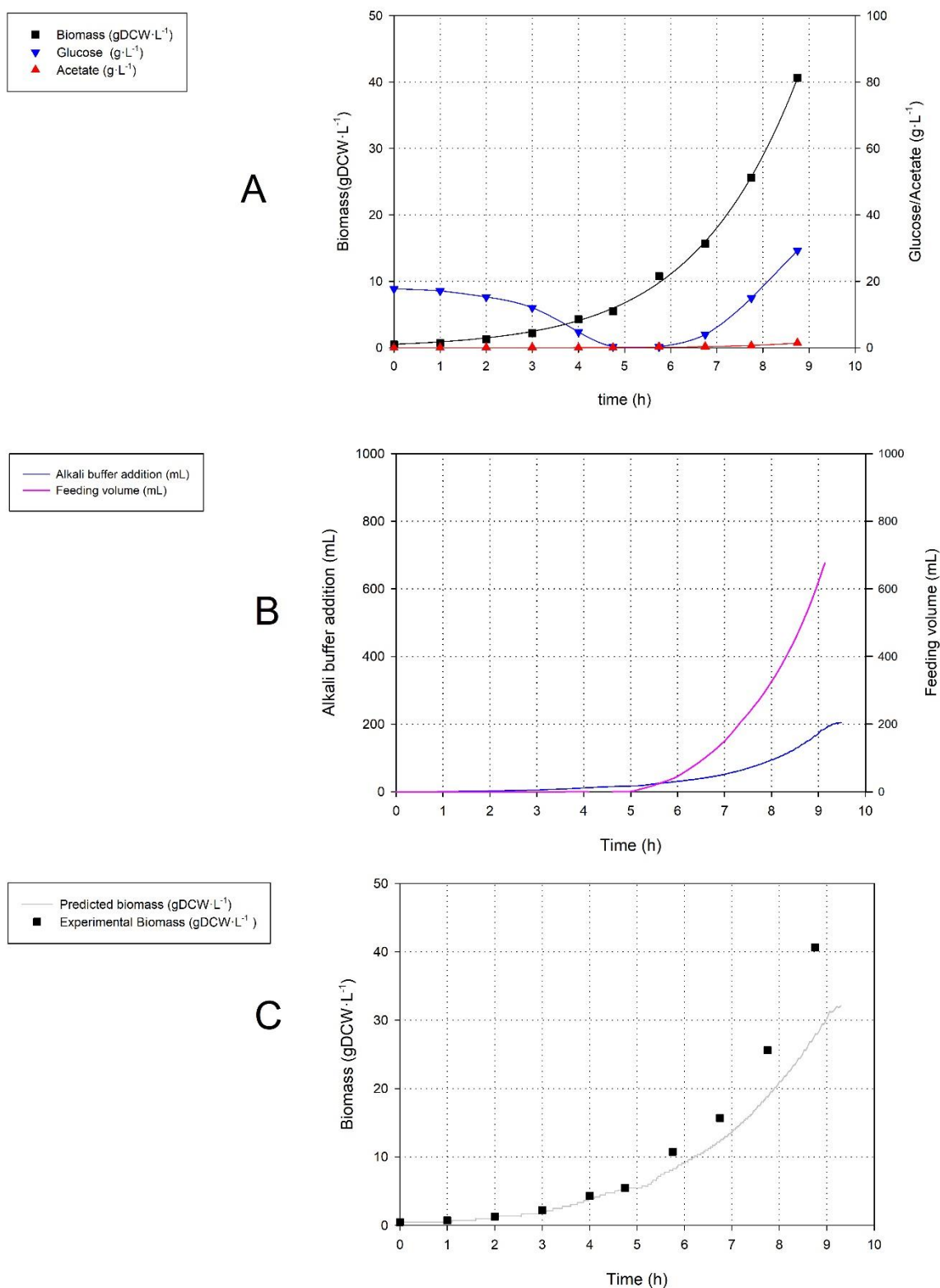


Figure 7-9 Profile of A) off-line variables such as Biomass (■), glucose (▼), acetate (▲), B) on-line variables such as alkali buffer addition (—) and feeding volume (—) for *E. coli* BL21 fed-batch culture using Base based algorithm for feeding and C) the comparison between the biomass calculated by the CER-based mathematical algorithm and the biomass experimental points.

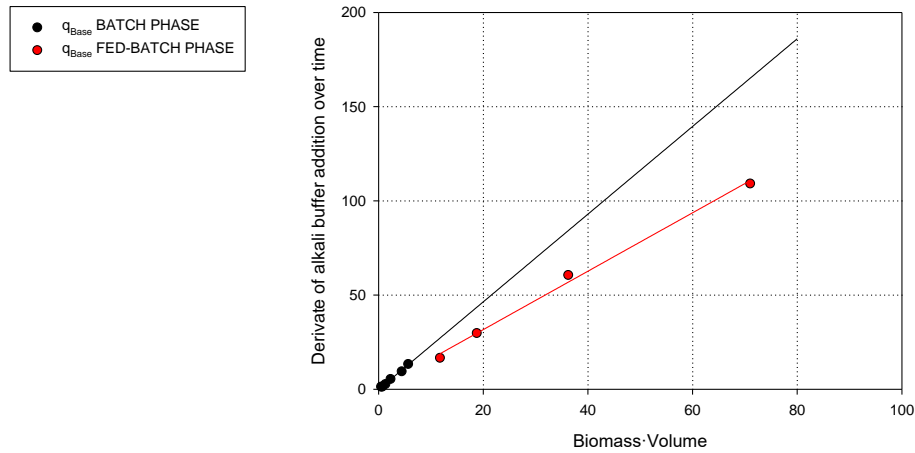


Figure 7-10 Slope comparison between batch phase (black) and fed-batch phase (red). It has to be taking into consideration that the parameter q_{alkali} is defined as the slope represented.

Table 7-10 Main parameters for all the fed-batch strategies

	Fed batch feeding algorithm based on		
	preprogramed exponential	CER	BASE
Achieved biomass ($\text{gDCW}\cdot\text{L}^{-1}$)	35,7	29,3	40,72
μ hypothetical (h^{-1})	0,54	0,54	0,56
μ experimental (h^{-1})	0,51	0,49	0,52
q_{glucose} ($\text{g}\cdot\text{gDCW}^{-1}\cdot\text{h}^{-1}$)	0,35	0,35	0,35
q_{CO_2} ($\text{mM}\cdot\text{gDCW}^{-1}\cdot\text{L}\cdot\text{h}^{-1}$)	x	36,6	X
q_{alkali} ($\text{mL}\cdot\text{gDCW}^{-1}\cdot\text{L}\cdot\text{h}^{-1}$)	x	x	0,54
$Y_{\text{x/s}}$ ($\text{gDCW}\cdot\text{g}_{\text{glucose}}^{-1}$)	0,382	0,27	0,267

Table 7-11 Comparison of the main features between all the designed strategies

	Batch	Fortified Batch	FDB- preprogramed exponential	FDB - CER control	FDB - pH control
Achieved biomass ($\text{gDCW}\cdot\text{L}^{-1}$)	6,2	15,4	35,7	29,3	40,72
μ (h^{-1})	0,54	0,48	0,51	0,49	0,52
Acetate generation ($\text{g}\cdot\text{L}^{-1}$)	0	1,6	0	0	1,54
$Y_{\text{x/s}}$ ($\text{gDCW}\cdot\text{g}_{\text{glucose}}^{-1}$)	0,31	0,256	0,382	0,27	0,267

7.4.4 Fed Batch feeding based on non-metabolism related parameter

In order to perform a strategy that not depend on previous data to design the feeding algorithm, a strategy based on how CER behaves when glucose is completely depleted from the culture media will be presented hereafter.

Frist of all, as show in the **graph A of Figure 7-2** in the section 7.3.1, when glucose was near depletion, an interesting behaviour occurs. At this moment, CER started to decrease, therefore, this drop might indicate the moment when *E. coli* needs nutrients in order to re-start its growth. On this basis, a pulse-addition system regulated by CER dropping will be designed and implemented in this section.

It is important to point out that this new method does not use any metabolic parameter, because the addition only depends on how CER behaves when a pulse of feeding media is added. The pulse regulation, the monitor of CER, and the interaction between both is explained in section 7.7.11.2. Therefore, the implementation of this methodology on a fed-batch is presented in **Figure 7-11**.

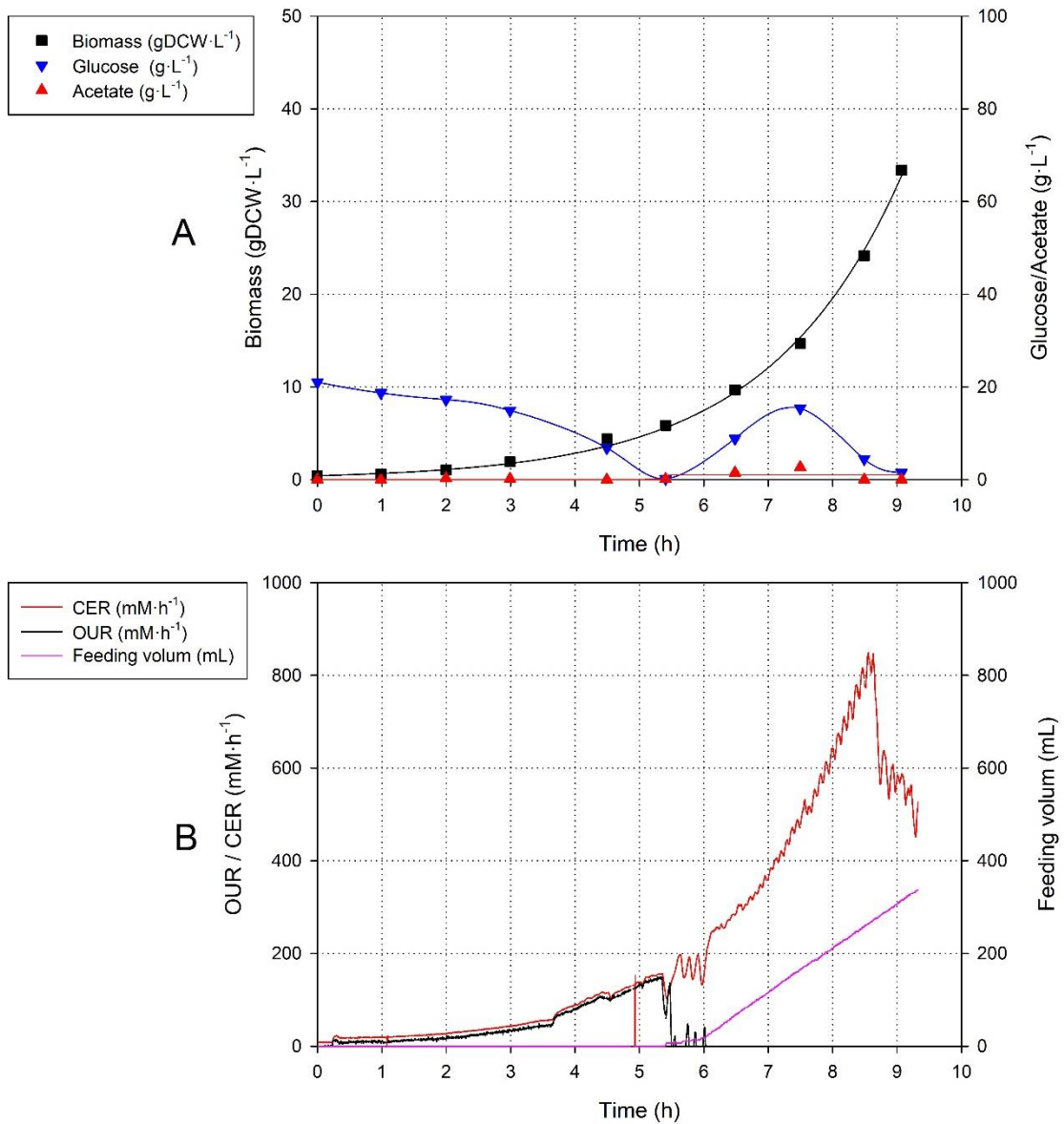


Figure 7-11 Profile of A) off-line variables such as biomass (■), glucose (▼), acetate (▲) and B) on-line variables such as CER (—), OUR (—) and feeding volume (—) for *E. coli* BL21 fed-batch culture using non-metabolic algorithm for feeding.

It is important to highlight that the one of the main difference between the fed-batch strategies described up until now and the new one is related to the moment of addition, this new strategy decides when the fed-batch phase must initiate taking into consideration the CER behaviour, otherwise in previous ones it was manually defined. As a result, this new algorithm initiated automatically the fed-batch phase when there was a significant drop in CER, as shown **graph A of Figure 7-11** at 5,5 hours. Moreover, this algorithm is devised as a 1 gram of glucose per pulse width.

Regarding the batch phase, the most relevant parameter that is described in this case is the growth rate, which had a value of $0,53 \text{ h}^{-1}$. Although, it is important to point out that knowing this parameter was not necessary in order to perform the feeding addition.

On the other hand, regarding the fed-batch phase, the addition was initiated automatically when there was a drop in the CER, as shown in shown **graph B of Figure 7-11**.

Then, the feeding solution was added in response to the culture requirements in order to grow at its optimal growth rate. As a result, this strategy led the culture to achieve $33,3 \text{ gDCW} \cdot \text{L}^{-1}$ with a slightly accumulation of glucose in early stages and from the middle stage it was consumed until the final glucose concentration was zero, as shown in **Table 7-12**.

Moreover, regarding how the algorithm works, this saw-like behaviour of CER that was present during all the fed-batch phase was because the addition of the feeding media only was solely carried out when the CER started to decrease, promoting the growth of the culture, therefore, increasing CER.

As shown in **Table 7-13**, there is not a “best” option in order to carry out a fed-batch culture because of the impossibility of obtaining high biomass volumetric productivities without either accumulating glucose or growing at a non-optimal growth rate. This limitation is mainly produced because of the inability of generating a mathematical model that would describe how the glucose metabolism changes along the culture when there is a change in the media conditions produced by the feeding media addition.

Although, taking into consideration all the pros and cons regarding the design of a fed-batch strategy and all the issues inherent to it, the best strategy would be the non-metabolic strategy, due to the fact that it does not require any batch parameters and its completely automated. Its addition system is utterly automatic promoting the optimal growth depending on the environmental conditions.

Table 7-12 Main parameters used for overall Fed batch culture strategies.

	Fed batch feeding algorithm based on			
	preprogrammed exponential	CER	BASE	non-metabolic
Achieved biomass ($\text{gDCW}\cdot\text{L}^{-1}$)	35,7	29,3	40,72	33,3
μ hypothetical (h^{-1})	0,54	0,54	0,56	x
μ experimental (h^{-1})	0,51	0,49	0,52	x
q_{glucose} ($\text{g}\cdot\text{gDCW}^{-1}\cdot\text{h}^{-1}$)	0,35	0,35	0,35	x
q_{CO_2} ($\text{mM}\cdot\text{gDCW}^{-1}\cdot\text{L}\cdot\text{h}^{-1}$)	x	36,6	x	x
q_{base} ($\text{mL}\cdot\text{gDCW}^{-1}\cdot\text{L}\cdot\text{h}^{-1}$)	x	x	1,9	x
$Y_{x/s}$ ($\text{gDCW}\cdot\text{g}_{\text{glucose}}^{-1}$)	0,382	0,27	0,278775	0,31

Table 7-13 Main parameters for overall characterized culture strategies

	Batch	Fortified Batch	FDB- preprogrammed exponential	FDB - CER control	FDB - pH control	FDB - non metabolic control
Achieved biomass ($\text{gDCW}\cdot\text{L}^{-1}$)	6,2	15,4	35,7	29,3	40,72	33,3
μ (h^{-1})	0,54	0,48	0,51	0,49	0,52	0,52
Acetate generation ($\text{g}\cdot\text{L}^{-1}$)	0	1,6	0	0	1,54	0
Glucose accumulation ($\text{g}\cdot\text{L}^{-1}$)	-	-	2,5	0	30	0
$Y_{x/s}$ ($\text{gDCW}\cdot\text{g}_{\text{glucose}}^{-1}$)	0,31	0,256	0,38	0,23	0,28	0,31

As it has been state, the non-metabolic strategy can follow the biomass by means of the demand related to the metabolic behaviour, moreover, it is a completely automated strategy that enables the optimal growth depending on the culture's conditions. For a further exploration and to include the protein production on the study, in the following section a fed-batch with an induction phase will be carried out. The induction was picked as a core in the following section because is widely known that the induction of recombinant proteins in *E.coli* produces a lot of metabolic stress due to the fact that a part of carbon flux is directed towards the formation of the protein instead of to biomass synthesis (Bhattacharya & Dubey, 1995)(Hoffmann & Rinas, 2004). Therefore, the induction will be used as proof of concept in order to observe if the variation induced by the inconstancy of the carbon metabolism during the induction phase, can be followed by the non-metabolic strategy.

7.5 Study of the induction phase of a recombinant protein

The objective of this section is to check if the non-metabolic algorithm for the feeding media addition is able to follow the metabolic behaviour of *E. coli* BL21 when an induction phase is being carried out during the fed-batch phase. However, it is important to highlight that all the feeding profile and initialization of the fed-batch phase will be carry out automatically without man-power, while the carbon requirements are supplied granting the optimal growth rate.

The model protein chosen for this study was a widely used fluorescent report protein known as GFP due to its facility to be analysed (Gerdes & Kaether, 1996). The reference strain that will be used in this section is an *E. coli* BL21 that express the model protein GFP. It has to be remarked that kanamycin was used as an antibiotic in order to assure the desired genetic background during the GFP production in the induction phase

. As described in section 7.7.2, this strain was transformed with a plasmid that consisted of:

- The Lac operon, as a strong inducible promoter.
- The model protein GFP.
- Kanamycin resistance, as a selective pressure.

The expression of GFP is under an inducible promoter whose expression is regulated by an operon Lac. In more detail, “wild type” operon lac is a genetic mechanism on top expressing three structural genes *lacZ*, *lacY* and *lacA* that are involved in the lactose metabolism (Zubay, 1972). Consequently, the operon lac should be induced when lactose is present in the media composition (Zubay, 1972). However, it was found a chemical compound that interacted with the operon lac as lactose did, moreover, when this new compound was used as an inductor, the induction response was higher. This chemical compound was Isopropyl-1-thiogalactopyranoside (IPTG) (Kilikian et al., 2000) .

The use of IPTG as an inductor has been widely used to express proteins owing to it is a strong promotor. However, a metabolic issue was observed depending on its concentration during the induction phase. High protein production induced by high concentration of IPTG provoked a metabolic burden in *E. coli* that might cause a growth inhibition (Koch, 1983).

On this basis, the first experiment that was carried out in this section was an erlenmeyer experiment based on describing the relation between the specific growth rate of *E. coli* BL21-GFP and the concentration of IPTG. In order to perform it, several concentration of IPTG from 0 to 500 μM were added at the beginning.

As shown in **Figure 7-12**, the concentration of IPTG affected the specific growth rate and the biomass achieved. The biomass achieved was affected by the IPTG concentration when it was higher than 150 μM . In addition, the specific growth rate was decreased by 26 % when the IPTG was 300 μM and by 35,5 % when it was 500 μM . Regarding the GFP production, as observed in **Figure 7-13**, when the IPTG concentration was higher than 150 μM a peak in the protein production was reached without compromising the specific growth rate and afterwards, the protein production was stabilized while the growth started to decrease.

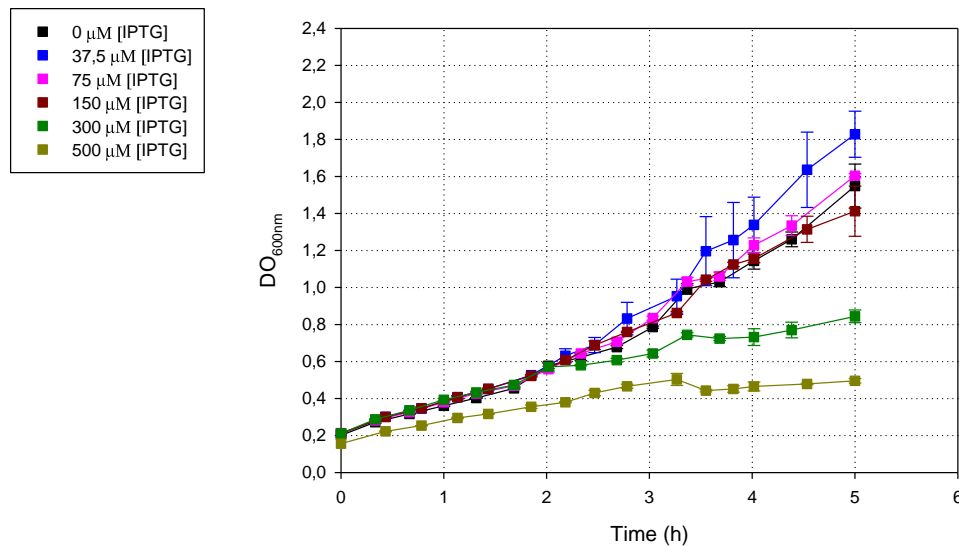


Figure 7-12 Effect of initial IPTG concentration on biomass profile when *E. coli* BL21-GFP was cultured using erlenmeyer.

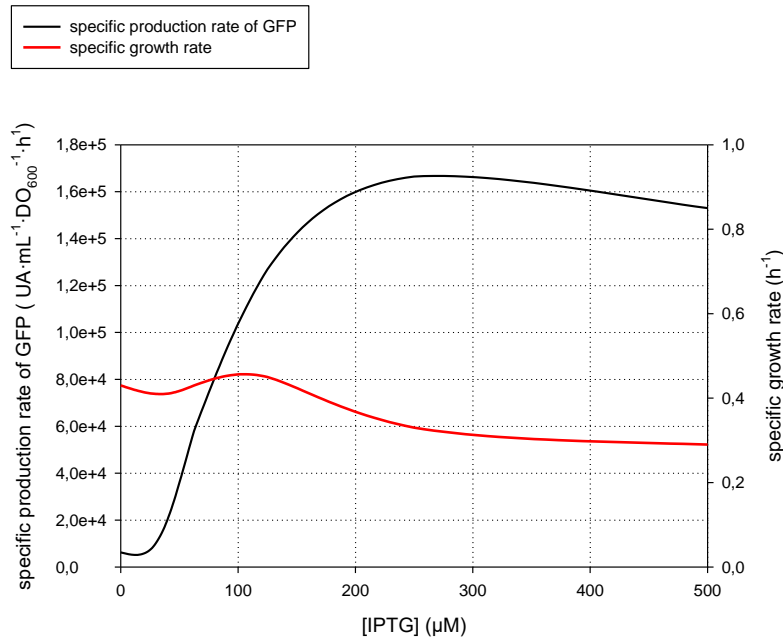


Figure 7-13 Effect of initial IPTG concentration on the specific rates of GFP production and growth.

However, in order to select the IPTG concentration a compromise between protein production and the growth is required. Therefore, the following study will be focused on describing the differences between GFP production in regard with two IPTG concentrations (150 μM and 500 μM) via batch experimentation.

7.5.1 Batch cultures

First, the definition of the induction methodology have to be determined focusing on two parameters: the induction time and the biomass concentration at the begging of the induction phase. The induction time is defined as the duration of the induction phase, and the biomass concentration is decided as the biomass that should achieve the culture before its induction. Usually, both parameters are dependent of each other because the biomass concentration set at the beginning of the induction phase is the one required for a specific induction time.

However, not always the growth is equal in each fermentation so both should be determined for each case of study.

In this case, the definition of the induction of model protein GFP expressed on *E. coli* BL21-GFP was based on setting the induction time to three hours and defining the biomass concentration

whose glucose concentration was higher enough to avoid a carbon limitation. On this basis, a batch reference of *E. coli* BL21 GFP was carried out in order to determine it. As shown in **graph A of Figure 7-14**, glucose was completely consumed in 6,5 hours to generate $6,1 \text{ gDCW}\cdot\text{L}^{-1}$ of biomass without producing acetate. Regarding the GFP, as shown in **graph B of Figure 7-14**, a basal expression was found with a peak value of $130 \text{ UA}\cdot\text{mL}^{-1}$, even though the culture was not induced. In order to have enough glucose during the induction time (3 hours), the biomass concentration selected was $2,4 \text{ gDCW}\cdot\text{L}^{-1}$.

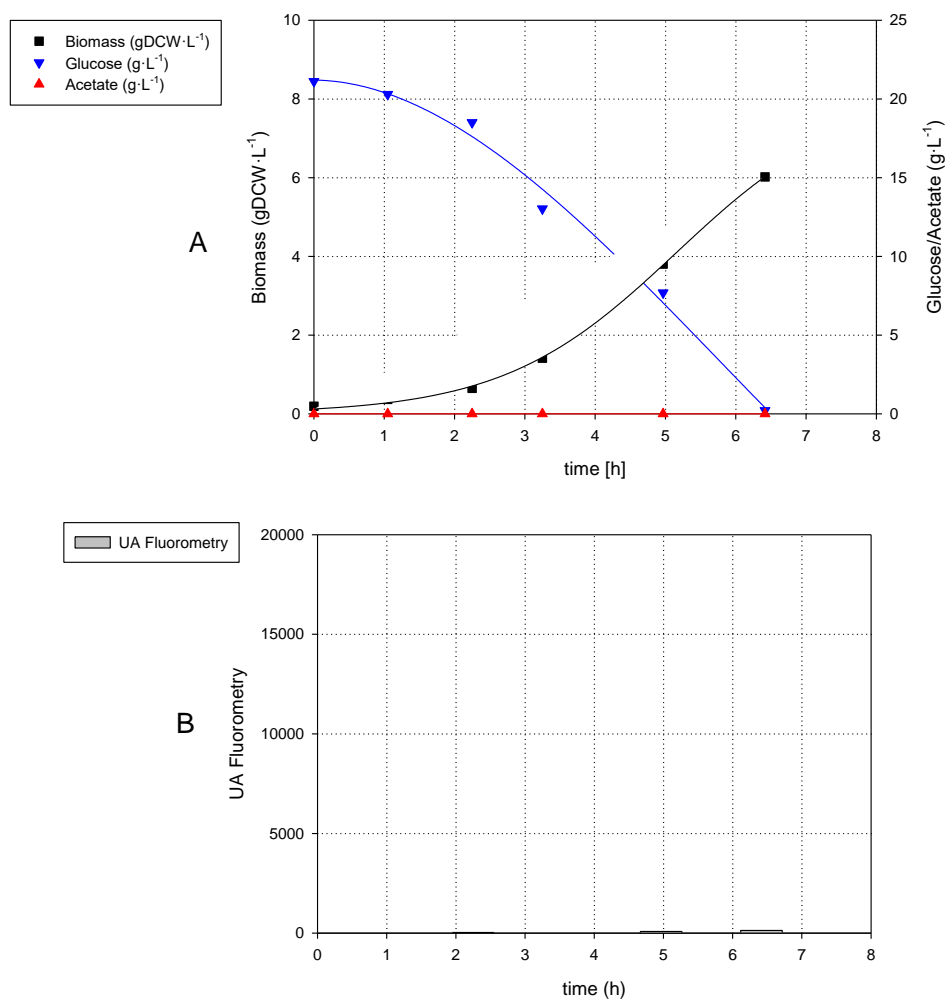


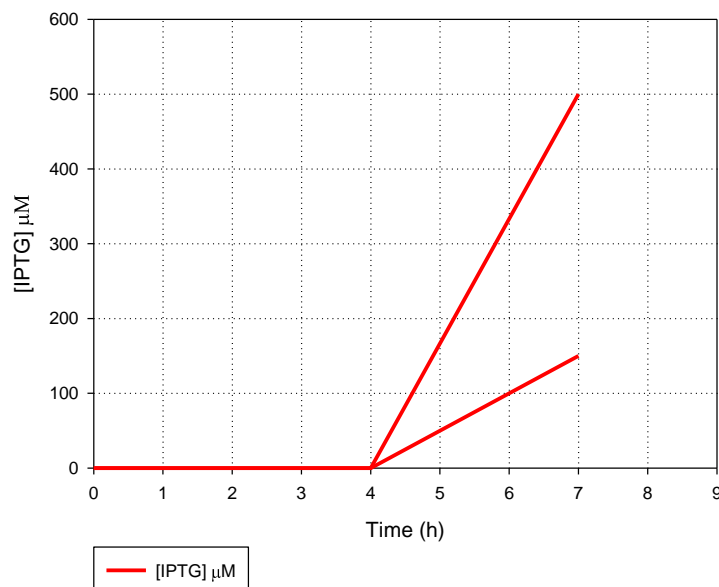
Figure 7-14 Profile of A) off-line variables such as Biomass (■), glucose (▼), acetate (▲) and B) the off-line variable fluorometric values for the *E. coli* BL21-GFP batch culture without induction phase.

Table 7-14. Main parameters for the *E. coli* BL21 GFP culture non-induced batch culture.

	Batch
Achieved biomass ($\text{gDCW}\cdot\text{L}^{-1}$)	6,0
μ (h^{-1})	0,54
Acetate generation ($\text{g}\cdot\text{L}^{-1}$)	0
$Y_{x/s}$ ($\text{gDCW}\cdot\text{g}_{\text{glucose}}^{-1}$)	0,30
Fluorometry ($\text{UA}\cdot\text{mL}^{-1}$)	180

Once the induction moment and the initial biomass concentration has been determined, the following step will be defining which IPTG's addition methodology will be used. There are several ways to perform it, although the used ones were the lineal methodology or the step methodology. In order to select the optimal, two sets of batch experiments were carried out where both methodologies were tested using the IPTG concentrations previously defined (150 μM and 500 μM). It has to be remembered that, as shown in **Figure 7-13**, these concentrations defined the optimal relation between specific production rate of GFP and the specific growth rate.

The first methodology tested was the lineal one. As shown in **Figure 7-15**, it is based on a linear addition, where the maximum IPTG concentration is reached at the end of the induction phase.

Figure 7-15 Evolution of IPTG in lineal addition method (500 and 150 μM IPTG)

Once the lineal addition was defined, a batch culture was carried out. As shown in **Figure 7-16**, the batch phase finished at 4,5 h and consumed 5 g·L⁻¹ of glucose in order to grant 3 hours of induction time. At this point, the addition of the IPTG started.

As a result, and as shown in **Table 7-15**, the addition of IPTG affected the cellular metabolism even if different concentrations were used. There was a decrease in growth rate in both cases, although the most affected was when the lineal induction with 500 μ M of IPTG was tested, decreasing it by 60%, from 0,54 h⁻¹ to 0,22 h⁻¹ and also a decrease in the final biomass concentration by 34 % compared with the reference batch. While, the addition of 150 μ M affected the growth rate by 53% from 0,54 h⁻¹ to 0,26 h⁻¹ and the maximum biomass achieved was reduced by 18%.

It is important to point out that even though the most metabolically effect was obtained at the 500 μ M addition, the 150 μ M condition was the most productive. As shown in **Figure 7-16**, the 150 μ M had a 10-fold enhancement in the production of GFP in comparison with the 500 μ M and as shown in **Table 7-15**, it had a higher yield of GFP produced per biomass.

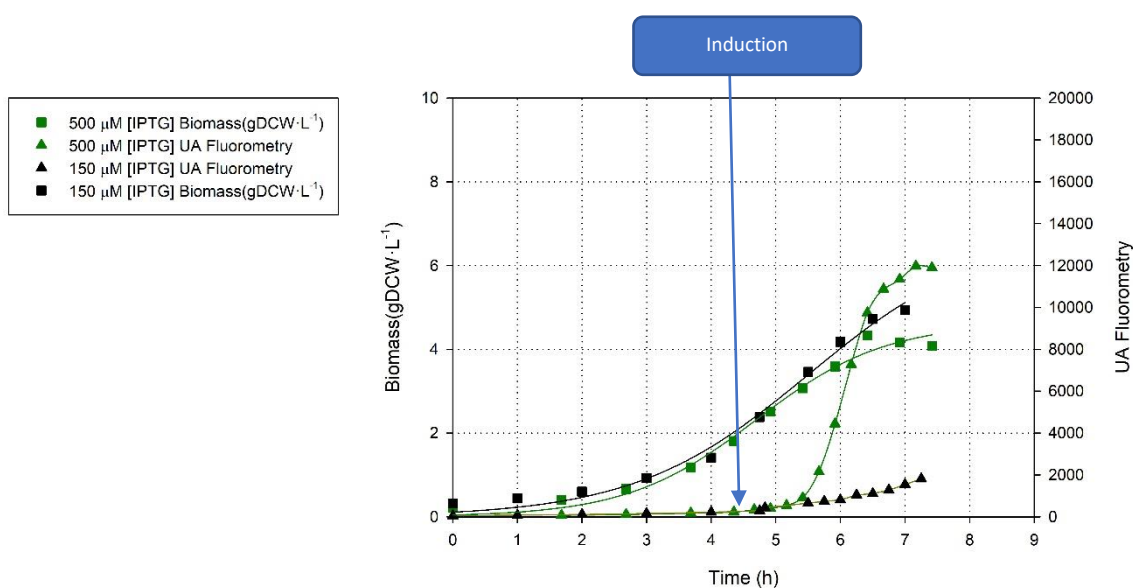


Figure 7-16 Comparison between biomass (■) and fluorometric values (▼) for two lineal addition induction IPTG method (150 μ M (green) and 500 μ M (black)) in *E.coli* BL21-GFP batch culture induced at 4,5 h.

Table 7-15 Main differential traits for lineal addition induction in *E.coli* BL21-GFP using IPTG in batch cultures.

Batch	500 μ M	150 μ M
-------	-------------	-------------

Achieved biomass (gDCW/L)	6	4,08	4,94
μ (h ⁻¹)	0,55	0,22	0,26
Fluorometry (UA·mL ⁻¹)	180	12000,00	1600,00
Y fluoro/bio (UA·mL ⁻¹ gDCW ⁻¹ ·L)	30	2941,18	323,89
Induction time (h)	x	3	3

Once the lineal addition of IPTG has been described, the next experiment will be the addition of IPTG via a step addition. In order to be able to compare both strategies, the pulse addition has to be carried out with the same bioreactor settings and parameters than the lineal procedure: the biomass concentration at the induction point has to be of 4 gDCW·L⁻¹, and the culture has to be induced during three hours.

As shown in **Figure 7-17**, the step addition is based on a single pulse addition at the start of the induction phase, where the maximum IPTG concentration is reached at the beginning. In addition, as it was described in lineal addition, two concentrations of IPTG were tested: 150 μ M and 500 μ M.

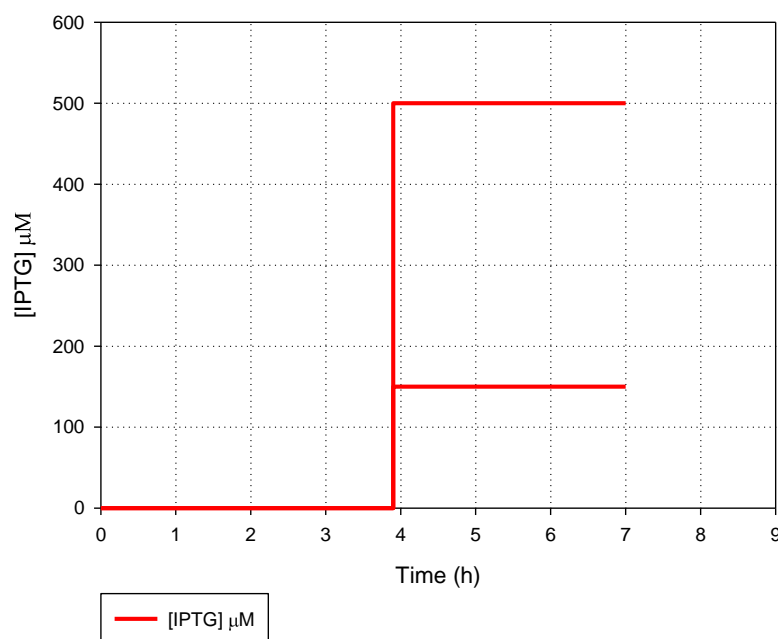


Figure 7-17 Evolution of IPTG batch concentration in a step addition method (500 and 150 μ M IPTG)

As shown in graph A of **Figure 7-18**, the batch phase lasted at 4 h from the beginning of the process in both experiments and nearly 7 g·L⁻¹ of glucose were consumed. At this point the

addition of the IPTG started. As a result, as shown in **Table 7-16**, the cellular metabolism was also affected.

As in the case of the lineal addition, there was a decrease in the growth rate in both conditions owing to the step addition. The most affected one was the condition with a single pulse that increased the IPTG in the reactor until 500 μM of IPTG. The induction had an effect on the growth rate decreasing it by almost 95 % from 0,54 h^{-1} to 0,04 h^{-1} and also decreasing the final biomass concentration by 51 % in comparison with reference batch. On the other hand, the addition of 150 μM affected the growth rate and the maximum biomass achieved as well, decreasing by 64 % from 0,54 to 0,20 and by 36 %, respectively. However, it is important to point out that even though the most metabolically affect was the 500 μM addition, the 150 μM addition had a higher yield GFP produced per biomass, as shown in **Table 7-16**. Specifically, the 150 μM addition had a 1,8-fold enhancement in the production of GFP regarding the 500 μM addition, as shown in **Figure 7-18**.

Additionally, there was an interesting fact in the a step addition when 500 μM was used that is related to how IPTG triggers the protein production. The effect of IPTG on the metabolism has been widely studied regarding the growth inhibition, although, the phenomena that will be described is related to how the protein production evolves after the induction. When the 500 μM induction was being carried out, there was a huge decrease in the protein production rate at 1 hour after the induction. It might be caused because of IPTG overstress the metabolism until it became an unbearable metabolic burden. Therefore, this burden would let the culture to make a change in the protein production in order to release the metabolic stress.

This behaviour might be described as a threshold in the protein production. When a protein production rate surpasses the upper threshold, a like-inhibition based response in relation with the protein production might be triggered. On this basis, as shown in **Figure 7-18**, the 500 μM addition had a higher production rate at early stages, producing 7000 $\text{UA}\cdot\text{mL}^{-1}$ until 1 hour after addition. in the two remaining hours, a significant decrease in protein production appeared owing to a metabolic burden caused by a high IPTG concentration, leading the culture to a low constant production phase, producing 3000 $\text{UA}\cdot\text{mL}^{-1}$. Interestingly, the 150 μM addition had a lower production rate at early stages, but due to the lower metabolic burden produced by the IPTG induction than the addition of 500 μM , the culture was able to keep a high protein production rate.

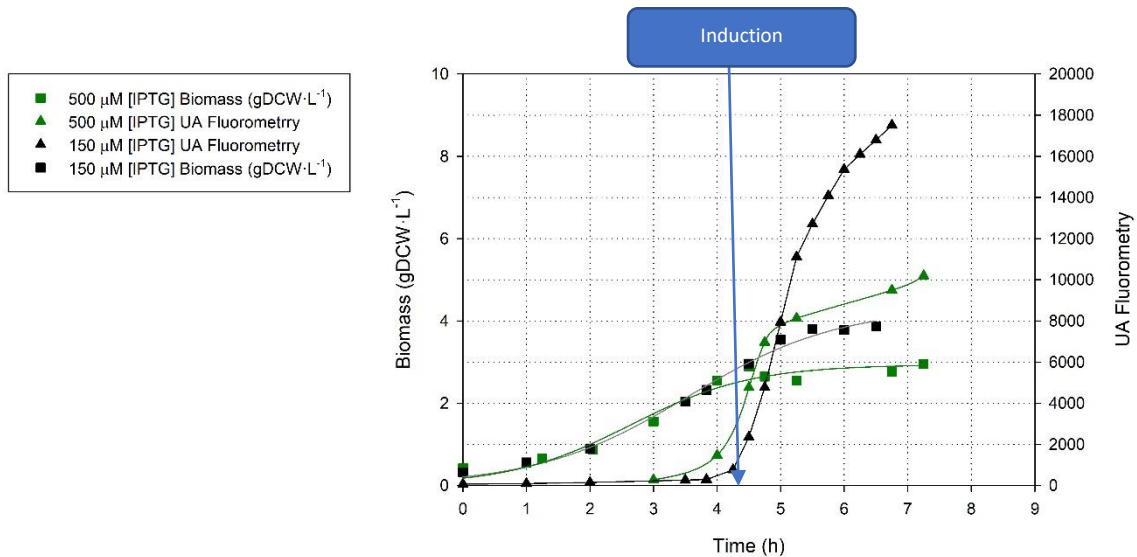


Figure 7-18 Comparison between biomass (\square) and fluorometric values (∇) for two step addition induction IPTG method in black 150 μM and in green 500 μM in *E. coli* BL21-GFP batch culture induced at 4h.

Table 7-16 Main traits for step method in *E. coli* BL21-GFP using IPTG in batch cultures.

	Batch	500 μM	150 μM
Achieved biomass ($\text{gDCW}\cdot\text{L}^{-1}$)	6	2,94	3,85
μ (h^{-1})	0,54	0,04	0,20
Fluorometry ($\text{UA}\cdot\text{mL}^{-1}$)	180	10200,00	18150,00
$Y_{\text{fluoro/bio}}$ ($\text{UA}\cdot\text{mL}^{-1}\cdot\text{gDCW}^{-1}\cdot\text{L}$)	30	3469,39	4714,29
Induction time (h)	x	3	3

Therefore, the protein production was affected by the IPTG concentration. However, a minimum concentration of 150 μM was required in order to obtain high specific production rate of GFP. As it was observed in the lineal addition of 150 μM , there was almost no protein production owing to the minimal concentration was achieved at the end of the phase. While, when the IPTG concentration was increased to 500 μM and the minimum concentration was reached earlier, the protein production was induced, as shown in **Figure 7-15**. Taking into account these results, it could be stated that reaching as fast as possible the desired IPTG concentration should be the best option. As observed in **Table 7-17**, it was confirmed when the pulse addition on top of increasing the reactor IPTG concentration to 150 μM or 500 μM instantaneously, produced a higher GFP production than the lineal addition. However, an interesting trait was observed in the early stages of the pulse addition, even if the 500 μM addition had the most productive phase of all the conditions tested at the first hour, then it started to effect the growth. It could be stated that

this GFP production had a metabolic burden that became impossible to sustain until the end. As a result, in remaining hours, GFP production was nearly inexistent, as observed in **Figure 7-18**. While, when the concentration was 150 μM , the GFP production produced a lower metabolic burden that enabled the continuous production of GFP, as a result, its production increased by 1,8-fold.

To conclude, as observed in **Table 7-17**, the most suitable addition was the step addition of 150 μM , due to it had the highest fluorometry obtained and the highest yield production fluorometry-biomass ratio.

Table 7-17 Overview of induction addition method

	Induction Addition Method			
	Step	Step	Lineal	Lineal
[IPTG] (μM)	500	150	500	150
Achived fluorometry ($\text{UA}\cdot\text{mL}^{-1}$)	10200,00	18150,00	12000,00	1600,00
μ induction (h^{-1})	0,04	0,20	0,22	0,26
$Y_{\text{fluoro/bio}}$ ($\text{UA}\cdot\text{mL}^{-1}\cdot\text{gDCW}^{-1}\cdot\text{L}$)	3469,39	4714,29	2941,18	323,89

Once the IPTG concentration as well as the induction strategy has been optimized, the next step will be to test the suitability of the non-metabolic fed-batch algorithm in front of a change in metabolism, which can be provoked by the induction. Therefore, an automatically fed-batch culture will be performed in the following section to check out its robustness in front of a step addition of IPTG of 150 μM .

7.5.2 Fed-batch induction strategy

In order to corroborate the robustness of the non-metabolic fed-batch algorithm, a fed-batch culture was carried out with a pulse induction of IPTG. It is important to point out that this culture strategy will have three phases: a batch phase, a fed-batch phase without induction, and then the induction phase. Moreover, the algorithm was tested in order to be able to start automatically the following steps: the start of the fed-batch feeding, the start of the induction phase and the feeding adaptation during the induction phase depending on the metabolic demands of the culture.

The non-metabolic strategy decided when the fed-batch phase must initiate taking into consideration the CER behaviour. As a result, this new algorithm initiated automatically the fed-batch phase when there was a significant drop in CER, as shown in **graph C of Figure 7-19** at 5,8 hours.

Regarding the batch phase, the most relevant parameter was the growth rate, which had a value of $0,51\text{h}^{-1}$ in order to have a parameter for comparing how fitted is the algorithm when a change in the metabolism take place.

Regarding the fed-batch phase, the addition was initiated automatically when there was a drop in the CER, as shown in **graph B of Figure 7-19**. Then, the feeding solution was added in response to the culture requirements in order to grow at its optimal growth rate. As a result, this strategy led the culture to achieve $15,5\text{ gDCW}\cdot\text{L}^{-1}$ accumulating $4\text{g}\cdot\text{L}^{-1}$ glucose, as shown in **Table 7-18**. This glucose accumulation was needed by the *E.coli* BL21-GFP in order to keep growing at the optimal rate, due to the nature of how the algorithm was defined, as mentioned in the section 7.4.4. It seems like there is a minim glucose concentration in order to enable the glucose consumption.

At this point the induction phase started. As shown in **graph A of Figure 7-19**, in the first hour of induction there was a slightly increase of biomass concentration from $15,5\text{ gDCW}\cdot\text{L}^{-1}$ to $20\text{ gDCW}\cdot\text{L}^{-1}$ while GFP was being produced. In the last two hours, the growth rate was almost inhibited.

As shown in **graph C of Figure 7-19**, the expression of the GFP had a stable expression until $70000\text{ UA}\cdot\text{mL}^{-1}$, afterwards, its production started to decrease. Consequently, the GFP productivity decreased nearly 3-fold from $32\ 000\text{ UA}\cdot\text{mL}^{-1}\cdot\text{h}^{-1}$ to $10\ 000\text{ UA}\cdot\text{mL}^{-1}\cdot\text{h}^{-1}$. The yield of biomass-glucose almost dropped until 0, specifically, from converting 1 gram of glucose to 0,3 grams of biomass to converting 1 gram of glucose to 0,02 grams of biomass, as shown the **Table 7-18**.

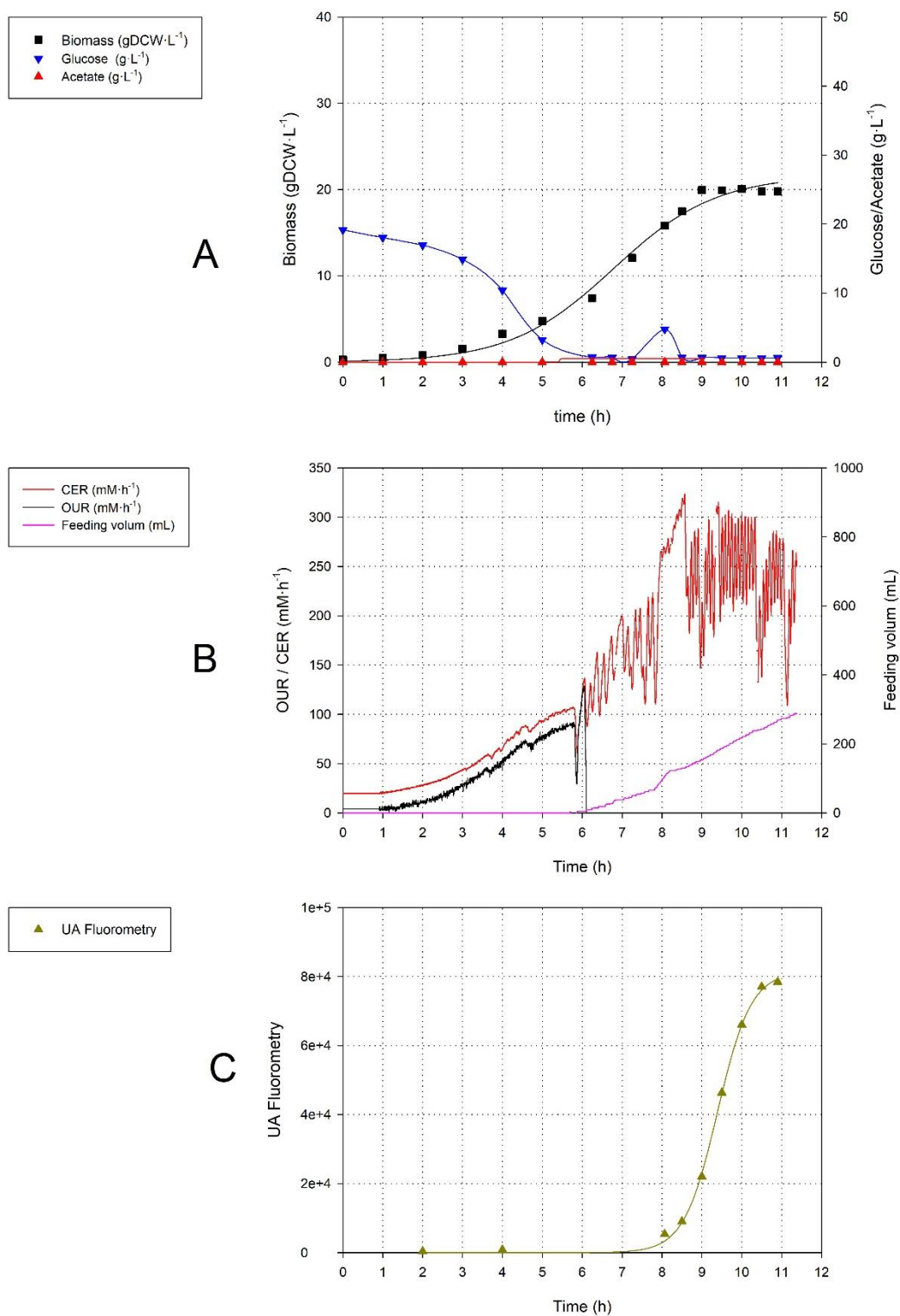


Figure 7-19 Profile of A) off-line variables such as biomass (■), glucose (▼), acetate (▲), B) on-line variables such as CER (—), OUR (—) and feeding volume (—) and C) fluorometric values (▲) for *E. coli* BL21-GFP fed-batch culture using the non-metabolic feeding profile for 2 h and induction with step method of 150 μ M [IPTG] at 8 h during 3 h.

Table 7-18 Main traits of *E.coli* BL21-GFP induced fed-batch.

Achieved batch biomass (gDCW·L ⁻¹)	6
Achieved Fed Batch biomass (gDCW·L ⁻¹)	15,5
Achieved induction biomass (gDCW·L ⁻¹)	20
μ batch (h ⁻¹)	0,50
μ fed-batch (h ⁻¹)	0,49
μ induction (h ⁻¹)	-
Fluorometry achieved (UA·mL ⁻¹)	80000
Fluorometry volumetric productivity (UA·mL ⁻¹ ·h ⁻¹)	36600
$Y_{GFP/s}$ (UA·mL ⁻¹ ·g _{glucose} ⁻¹) batch phase	4000
$Y_{x/s}$ (g _{DCW} · g _{glucose} ⁻¹) batch phase	0,30
$Y_{x/s}$ (g _{DCW} · g _{glucose} ⁻¹) Fed batch phase	0,29
$Y_{x/s}$ (g _{DCW} · g _{glucose} ⁻¹) induction phase	0,02

To conclude, the non-metabolic strategy was able to correct the addition when the induction by IPTG stopped the growth; as a result, there was no glucose accumulation. Furthermore, as shown in **Figure 7-20**, there is an increase of 6-fold between the fed-batch induction phase and the batch one.

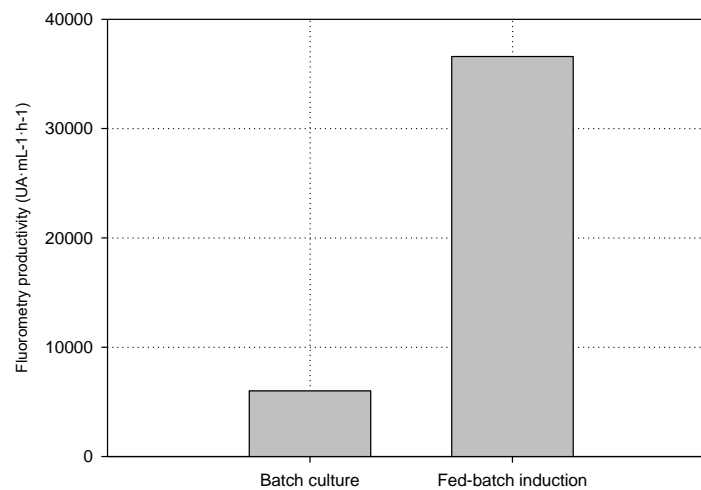


Figure 7-20. Comparison of the fluorometry productivity between the reference batch culture and the fed-batch induction (the induction concentration in both cases was the same, 150 μ M).

7.6 Discussion and conclusions

As stated at the beginning of the chapter, the final goal was to improve the biomass production, in order to enhance the biomass volumetric productivity. Therefore, several strategies were tested which mainly were tackled around changing the environmental conditions or modifying the feeding control system during the process.

The first thing done consisted in changing the environmental conditions. Regarding this, a new batch media was designed based on increasing the concentration of all the media components until a growth inhibition was reached. As a result, this new media was called fortified media and it increased the biomass productivity 2,48-fold between the fortified batch culture and the reference batch.

For a further biomass production, the next step was focus on using different fed-batch strategies, where the objective was to achieve the optimal growth rate. It is important to highlight two facts: the first one is that the studies performed in the metabolic chapter of *E. coli* BL21 were used in order to calculate the specific consumption rate of glucose used for designing fed-batch strategies during the fermentation. The second one was related with the fed-batch strategies, that they will be desirable performed at the optimal growth rate.

The first approach was based on a fed-batch strategy where the growth of the culture was estimated as an exponential function. As a result, the biomass productivity of the process increased 5,75-fold comparing the fed-batch with the previous batch, even though a slightly constant glucose accumulation was present. This glucose accumulation was hypothesized to be caused by a change in the culture growth rate during the experiment. Consequently, the feeding algorithm accumulated glucose due to the change in growth between the predicted behaviour and the experimental one.

In order to increase further the biomass productivity, a feeding algorithm, which took into consideration the biomass monitoring over the culture, was developed. This methodology was based on the estimation of the biomass by monitoring two physiological variables whose are inherently linked to biomass: the carbon exchange rate (CER) and the alkali buffer addition.

Regarding the fed-batch based on the CER, its application did not produce the expected results due to the biomass volumetric productivity was lower than the one obtained preprogramed exponential experiments, 4,75-fold vs 5,75-fold. However, it seems that this methodology limited the growth of the culture. As a result, there was not glucose accumulation at the end of

the culture. Even though the biomass estimation algorithm was able to predict the biomass evolution fairly enough until metabolic changes occurred. As it was mentioned above, this metabolic restructuring led the algorithm to provoke a growth-limiting situation. Therefore, it is not a good option regarding the process control, while could be a good option if it is used as a monitoring tool due to it gives indirect information regarding the metabolic state of the culture.

Otherwise, the fed-batch based on the estimation of biomass using alkali buffer addition got an increase of biomass productivity about 6,29-fold between the alkali buffer addition-fed batch and the batch media. In this case, even though the enhancement of biomass productivity, the algorithm oversized the addition of the media leading the culture to a high-pace constant accumulation of glucose.

Thus, gathering all the data from the carried-out fed-batch strategies in order to look for a solution regarding the optimization of the fed-batch cultures, a common issue of the fed-batch strategies appeared. This issue was related to the inability of *E. coli* BL21 to keep a constant metabolic state within the fed-batch phase. Therefore, it might be impossible to predict the metabolic parameters used by the feeding profiles, as a consequence, glucose was accumulated. To overcome this problem, a new fed-batch was developed which did not depend on the metabolic state of *E. coli* to calculate the feeding rate.

This strategy was successfully applied, and at the end of the culture there was no glucose accumulation and the biomass productivity were higher than the preprogramed fed-batch strategy, even if glucose was accumulated at early stages of the fed-batch phase. Specifically, the biomass productivity achieved was 5,37-fold over the batch media. Although, the difference in biomass concentration between the preprogramed strategy and the non-metabolic was not so different, it presented a lot of improvements:

1. A fully automated feeding strategy.
2. None parameters were required to calculate the feeding profile.
3. The optimal conversion of glucose to biomass was achieved without performing continuous cultures in order to look for the specific consumption rate of glucose related to the optimal conversion.

Thereupon this methodology was applied to an *E. coli* culture where the metabolic conditions were changing drastically during the culture. For this purpose, an *E. coli* BL21 expressing GFP when induced by IPTG was used.

At this point, the induction conditions were also optimized, and then a fed-batch using the non-metabolic algorithm was carried out, applying the controlling tool developed also after induction, where significant metabolic changes occurred. The optimal condition for the induction were defined as a single pulse of 150 μM of IPTG because this method acquired the highest yield of UA/ml per biomass ($4700 \text{ UA}\cdot\text{ml}^{-1}\cdot\text{gDCW}^{-1}\cdot\text{L}$).

The results obtained at the induction fed-batch stated that the algorithm fitted the *E. coli* BL21-GFP growth-related demands letting the culture firstly to grow and, thus, in the induction phase adapt the feeding without neither oversizing the glucose feeding nor limiting the protein production. In this case, the yield of the induced phase of the batch and fed-batch was a bit lower than the reference batch (near $4000 \text{ UA}\cdot\text{mL}\cdot\text{gDCW}^{-1}\cdot\text{L}$), while the overall fluorometric productivity increased 6-fold between the induced fed-batch and the reference induced batch. It can be stated that the glucose feeding was the necessary in order to completely reproduce the behaviour of the previously 150 μM pulse induction batch, which was used as a reference.

described in section 7.7.4. Flasks were continuously agitated at 130 rpm on an orbital shaking platform (Stuart SSL110 Incubator, Forma Scientific). Moreover, it was maintained using petri dishes at 37°C with the media described in section 7.7.4.

7.7.3 Culture systems

For small scale or inoculum cultures have been performed in Erlenmeyer of different volumes (25, 50, 100 , 250 and 1000 ml) cultured at 37°C and 130 rpm.

The culture in petri plates was used as a starter solid culture support. Moreover, it was incubated at 37°C using an orbital incubator (Shaker orbital Incubator, Sanyo).

7.7.4 Media definition.

The media composition used in the bioprocess section are described hereafter.

- Petri dishes: the media composition is described in **chapter 3** in section 3.8.3 using *E. coli* BL21 and *E. coli* BL21-GFP
- Pre-inoculum culture: the media composition is described in **chapter 3** in section 3.8.3 using *E. coli* BL21 and *E. coli* BL21-GFP
- Batch and Batch media in fed-batch strategies: the media composition is described in **chapter 3** in section 3.8.3 using *E. coli* BL21
- Fortified batch experiment: the media composition is described in **Table 7-20** using *E. coli* BL21
- Feeding addition in fed-batch strategy and the induction fed-batch strategy: the composition is described in **Table 7-21** using *E. coli* BL21 and *E. coli* BL21-GFP
- Batch media in the induction fed-batch strategies: the media composition is described in **Table 7-19** using *E. coli* BL21-GFP

Table 7-19 Composition of media used in batch phase of the induction fed-batch strategy.

Compound	Concentration
Glucose H ₂ O	22 g/L
K ₂ HPO ₄	11,9 g/L
KH ₂ PO ₄	2,4 g/L
NaCl	1,8 g/L
MgSO ₄ 7H ₂ O	0,1 g/L
NH ₄ SO ₄	3 g/L
FeCl ₃ 6H ₂ O	0,01 g/L
Thiamine	0,03 g/L
AlCl ₃	0,023 mg/L
ZnSO ₄ 7H ₂ O	1,25 mg/L
CoCl ₂ 6H ₂ O	0,12 mg/L
CuSO ₄ 5H ₂ O	1,57 mg/L
H ₃ BO ₃	0,0072 mg/L
MnCl ₂ 4H ₂ O	1,02 mg/L
NiCl ₂ 6H ₂ O	0,0072 mg/L
Na ₂ MO ₄ 2H ₂ O	0,017 mg/L
Kanamycin sulphate	2 mg/L

Table 7-20 Composition of media used in fortified batch culture strategy

Compound	Concentration
Glucose H ₂ O	80 g/L
K ₂ HPO ₄	11,9 g/L
KH ₂ PO ₄	2,4 g/L
NaCl	1,8 g/L
MgSO ₄ 7H ₂ O	0,2 g/L
NH ₄ SO ₄	3 g/L
FeCl ₃ 6H ₂ O	0,04 g/L
Thiamine	0,06 g/L
AlCl ₃	0,046 mg/L
ZnSO ₄ 7H ₂ O	2,5 mg/L
CoCl ₂ 6H ₂ O	0,24 mg/L
CuSO ₄ 5H ₂ O	3,14 mg/L
H ₃ BO ₃	0,0144 mg/L
MnCl ₂ 4H ₂ O	2,02 mg/L
NiCl ₂ 6H ₂ O	0,0144 mg/L
Na ₂ MO ₄ 2H ₂ O	0,034 mg/L

Table 7-21 Composition of media used as a feeding media in all the fed- batch culture strategy.

Compound	Concentration
Glucose H ₂ O	400 g/L
MgSO ₄ 7H ₂ O	9,56 g/L
FeCl ₃ 6H ₂ O	0,81 g/L
CaCl ₂ ·2H ₂ O	0,11 g/L
AlCl ₃	2,01 mg/L
ZnSO ₄ 7H ₂ O	109,38 mg/L
CoCl ₂ 6H ₂ O	10,5 mg/L
CuSO ₄ 5H ₂ O	137,38 mg/L
H ₃ BO ₃	0,63 mg/L
MnCl ₂ 4H ₂ O	88,37 mg/L
NiCl ₂ 6H ₂ O	0,63 mg/L
Na ₂ MO ₄ 2H ₂ O	1,48 mg/L

7.7.5 Biomass dry cell weight (DCW) determination

The biomass dry cell weight was determined as described in **chapter 3** section 3.8.6

7.7.6 Metabolite determination

The determination of Oxygen, carbon dioxide, glucose and acetate are described in **chapter 3** section 3.8.7

The determination of GFP was carried using a fluorimeter with an emission wavelength of 395 nm and an absorption one of 500nm. Due to the nature of the sample, the analysis of the GFP was directly from the culture sample without pre-treatment

7.7.7 IPTG

A solution of 86000 μ M of IPTG was used as the addition solution during the induction phase of the batch cultures and the fed-batch culture.

7.7.8 Bioreactor cell culture

The stirred-tank bioreactor used in the present study was a commercial bioreactor (Biostat B, from Sartorius Stedim Biotech, Germany) with 2L-cylindrical jacketed vessel, equipped with probes and control systems for pH, D.O. (relative oxygen partial pressure) and temperature, and a stirred with two Rushton impellers.

The control systems of the before mentioned variables are described below:

- Dissolved oxygen concentration was monitored with a polarographic probe (Oxyferm, Hamilton), and maintained at 30% of saturation by means of an aeration flow using a spargger flow of 1 VVM together with a cascade control system based on a stirring control system and a gas mixing unit.
- Temperature was maintained at 37°C by switch between a heat exchanger when heat was needed and with a cooling water system when cold was needed.
- pH was measured with a standard electrode (EasyFerm Plus, Hamilton), and it was maintained at 7,02 using a HCl 2M (Panreac) addition, and a subsequently addition of NH_4OH (15% v/v) (Panreac).

The working volume for the batch cultures was 2L, and for the fed-batch culture, the initial volume was 1L .

7.7.9 Oxygen uptake rate (OUR) and Carbon exchange rate (CER) abans de les recipes

The methodology to calculate OUR and CER is described in **chapter 3** section 3.8.8

7.7.10 Specific rate calculations in batch cultures

The methodology to calculate the specific rate in batch cultures is described in **chapter 3** section 3.8.9

7.7.11 MFCS/win. Software for Data Acquisition, Monitoring and Control

BioPat® MFCS/win 3.0 (Sartorius Stedim Biotech, Germany) was used for monitoring and controlling the cell culture. All the strategies that are described in this chapter are based on recipe from MFCSwin in order to get all the information needed for granting a correct running.

Briefly, the recipes that were designed interacts with the bioreactor sensors in order to get the data and convert it to feeding flow by means of the equation which are explained in **section 7.7.12**.

The different control recipes were programmed accordingly to the culture operations requirements (batch, fed-batch based on pre-programmed exponential, fed-batch based on CER, fed-batch based on alkali buffer, and fed-batch based on non-metabolic parameters). The control recipes were able to conduct the actions required automatically

7.7.11.1 Fed-batch strategy that is based on predicting the biomass concentration.

As shown in **Figure 7-22**, the recipe of the MFCSwin is based on a core flow function where several inputs are present. It is important to point that that this input can be the characteristics parameters of the flow function or the order to initialize it.

Basically, the parameters that the flow functions require for a fine operation are described in the following list and in the figure as well. Moreover, it is important to highlight that depending on the fed-batch strategies that will be performed, the parameter required might be different.

The parameters required for the pre-exponential phase are listed hereafter:

- specific growth rate (μ)
- specific consumption rate of glucose (q_{glucose})
- initial volume(V_0) at the initiation of the fed-batch phase
- initial biomass(X_0) at the initiation of the fed-batch phase

The parameters required for the CER-estimation are listed hereafter:

- specific growth rate (μ)
- specific consumption rate of glucose (q_{glucose})
- specific production rate of carbon dioxide(q_{CO_2})
- CER(t)
- volume ($V(t)$).

The parameters required for the pH-estimation are listed hereafter:

- specific growth rate (μ),
- specific consumption rate of glucose (q_{glucose}),
- specific production rate of alkali buffer(q_{alkali}), alkali buffer addition (t)
- volume ($V(t)$).

Once the input parameters are fixed, the other input is the order to start the culture process, in these processes the order is manual manage by the user. Once the flow function starts running, it gives values to the feeding flow continuously, as show **in the bottom graph of the Figure 7-22**.

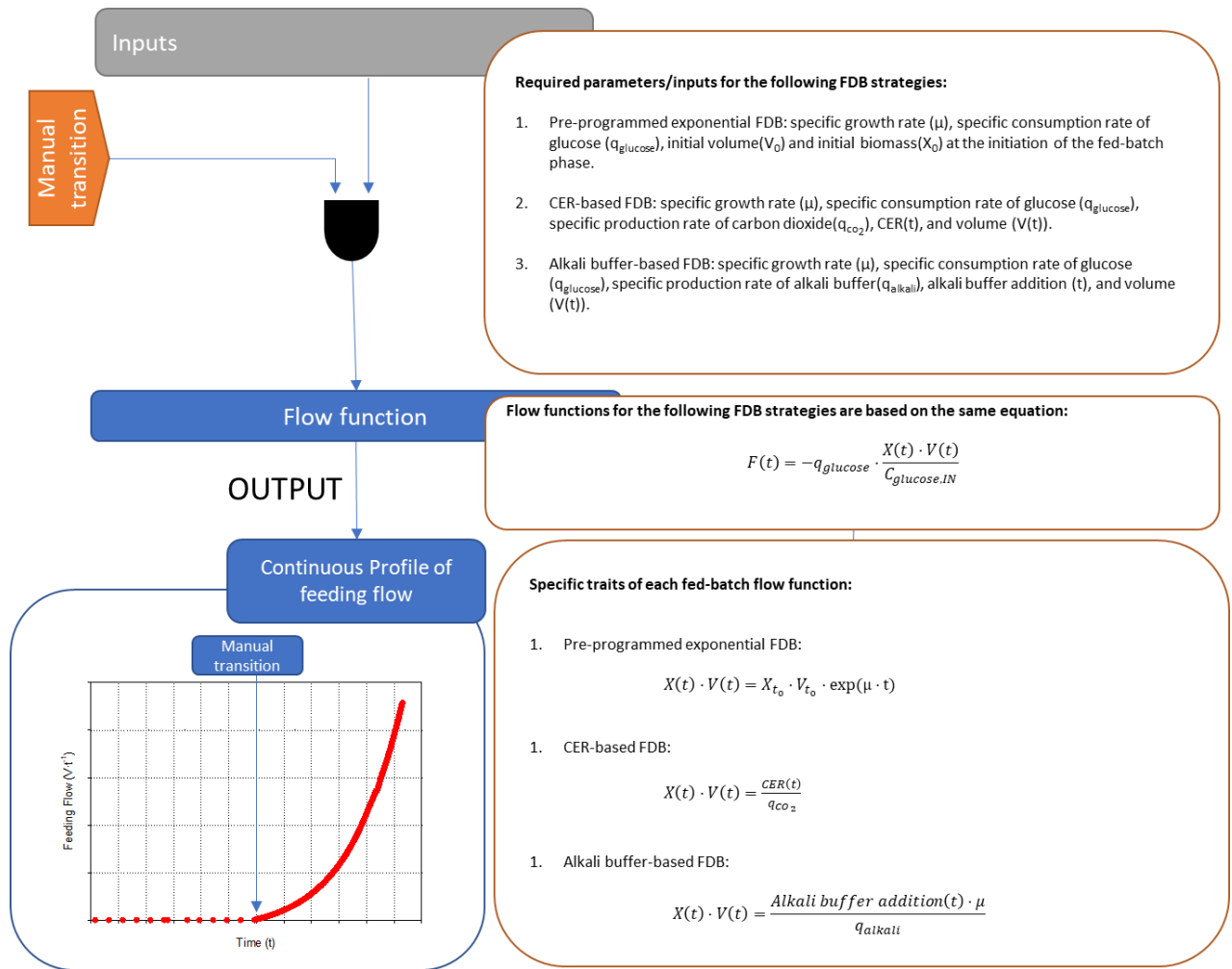


Figure 7-22. Flow diagram and description of the MFCSwin recipes whose objective is to calculate the feeding flow of the metabolic fed-batch cultures.

7.7.11.2 Non-metabolic Fed-batch strategy.

As shown in **Figure 7-23**, the recipe of the MFCSwin is based on a core flow function where several inputs are present. It is important to point out that this input only depends on one variable, not a parameter or a manual order.

Basically, the only variable required for a fine work of the flow function is the Carbon exchange rate (CER). Moreover, it is important to highlight that the decision in order to perform an addition is related to the difference regarding the CER evolution. When the CER evolution is greater than -0,5 the recipe does not do anything and it only stays within the loop without initializing any controller or actuator. Otherwise, if the CER evolution is less than -0,5, then, the activation of the pump for 10 s occurred. Once the pump turns off, the recipe goes to the first

step where the decision of how the evolution of the CER is undergoing, as a consequence, the loop of the recipe is closed until a decrease in CER occurs.

On this basis, it is important to point out that this recipe is only available for the non-metabolic fed-batch strategy.

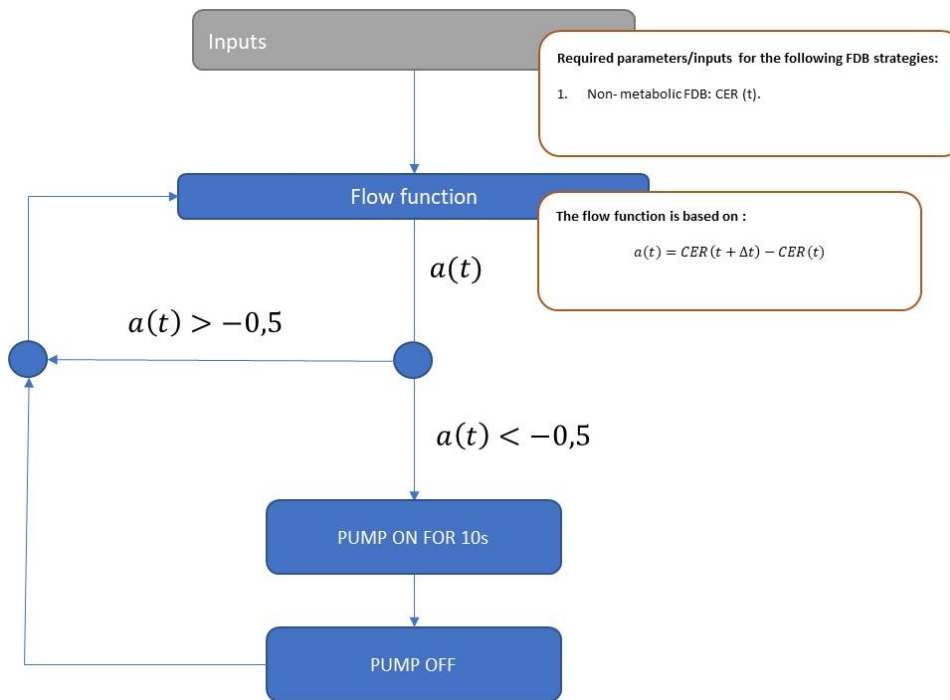


Figure 7-23 Flow diagram and description of the MFCSwin recipes whose objective is to calculate the feeding flow of the non-metabolic fed-batch strategy.

7.7.12 Fed-batch strategy

In order to carry out a fed-batch strategy, first of all a definition of the algorithm that will be used in order to describe how the feeding media is added must be defined. Although, it is important to point out that in this chapter two kinds of fed-batch algorithm have been described, the fed-batch whose biomass is estimated and the one whose is not estimated. The main difference between both strategies is that the strategy which is not related to biomass profile does not have a design equation. Otherwise, the design of the algorithm for the biomass-estimated fed-batch is based on **Equation 7-4**.

This equation is able to calculate the feeding flow ($F(t)$) by means of using the specific consumption rate of glucose ($q_{glucose}$), biomass (t), volume (t), and Feeding glucose concentration ($C_{glucose,Feeding}$)

Equation 7-4

$$F(t) = \frac{-q_{glucose} X(t) \cdot V(t)}{C_{glucose,Feeding}}$$

The calculation of biomass ($X(t)$) and volume ($V(t)$) will specify which strategy are you going to use regarding the estimation of biomass during the experiment. In the following

7.7.13 Biomass estimation by pre-programmed exponential

The pre-programmed exponential predicts the biomass by using the **Equation 7-5**. This equation only depends on time (t), and biomass concentration ($X(t_0)$) and volume ($V(t_0)$) at the beginning of the fed-batch phase. As a result, this equation does not predict the biomass concentration; otherwise, a theoretical growth profile is given.

Equation 7-5

$$X(t) \cdot V(t) = X(t_0) \cdot V(t_0) \cdot \exp(\mu \cdot t)$$

7.7.14 Biomass estimation by CER method

CER is the carbon exchange rate and it is related to biomass because carbon dioxide is produced when glucose is consumed by *E. coli* BL21 owing to carbon dioxide is the full oxidized from of glucose. Therefore, a mathematical equation converts CER to biomass.

This mathematical relation between CER and biomass concentration in culture is presented in **Equation 7-6**, where the specific production rate of carbon dioxide is defined as q_{CO_2} . It is important to emphasize that this equation is useful during all the experiment independently if it would be used at batch phase or fed-batch phase.

Equation 7-6

$$X(t) \cdot V(t) = \frac{CER(t)}{q_{CO_2}}$$

7.7.15 Biomass estimation by Alkali buffer addition method

An alkali buffer solution (NH₄OH 15 % v/v (Panreac)) was needed to neutralize the effect of carbon dioxide generation and the consumption of phosphate-based salts during the culture, keeping the pH at the desired set point. By means of the alkali buffer addition measurement, the biomass was estimated online in the culture, in order to add the exact feed media necessary to grant the maximum growth rate without accumulating glucose.

The mathematical relation between the alkali addition volume and biomass concentration in culture is presented in **Equation 7-7**, where the specific production rate of alkali buffer is defined as q_{alkali} . It is important to emphasize that this equation is useful during all the experiment independently if it would be used at batch phase or fed-batch phase.

Equation 7-7

$$X(t) \cdot V(t) = \frac{\text{Alkali buffer addition}(t) \cdot \mu}{q_{alkali}}$$

7.7.16 Statistics

Duplicates for each culture conditions were performed, but only one of the two duplicate experiment is presented in the Results section. Since the runs have not performed in parallel (due to equipment limitations), sampling time do not coincide, and other parameters may vary as the cell seeding density.

7.8 References

- Bhattacharya, S. K., & Dubey, A. K. (1995). Metabolic burden as reflected by maintenance coefficient of recombinant *Escherichia coli* overexpressing target gene. *Biotechnology Letters*, 17(11), 1155–1160. <https://doi.org/10.1007/BF00128377>
- Corran, H. S. (1975). A history of brewing. *David & Charles*.
- Gálvez Sánchez, J. (2011). *Desenvolupament i anàlisi d'un bioprocés per a l'obtenció de vectors adenovirals per a teràpia gènica*. [Universitat Autònoma de Barcelona.]. <https://ddd.uab.cat/record/70043?ln=ca>.
- Gerdes, H.-H., & Kaether, C. (1996). Green fluorescent protein: applications in cell biology. *FEBS Letters*, 389(1), 44–47. [https://doi.org/10.1016/0014-5793\(96\)00586-8](https://doi.org/10.1016/0014-5793(96)00586-8)
- Hoffmann, F., & Rinas, U. (2004). *Stress Induced by Recombinant Protein Production in Escherichia coli* (pp. 73–92). <https://doi.org/10.1007/b93994>
- Iwatani, S., Yamada, Y., & Usuda, Y. (2008). Metabolic flux analysis in biotechnology processes. *Biotechnology Letters*, 30(5), 791–799. <https://doi.org/10.1007/s10529-008-9633-5>
- Kilikian, B. V., Suárez, I. D., Liria, C. W., & Gombert, A. K. (2000). Process strategies to improve heterologous protein production in *Escherichia coli* under lactose or IPTG induction. *Process Biochemistry*, 35(9), 1019–1025. [https://doi.org/10.1016/S0032-9592\(00\)00137-0](https://doi.org/10.1016/S0032-9592(00)00137-0)
- Kishimoto, M., Yamane, T., & Yoshida, F. (1976). Sensitivity Analysis for Exponential Fed-batch Culture. *Journal of Fermentation Technology*, 54(12), 891–901.
- Koch, A. L. (1983). The protein burden of lac operon products. *Journal of Molecular Evolution*, 19(6), 455–462. <https://doi.org/10.1007/BF02102321>
- Konings, W. N., & Rosenberg, H. (1978). Phosphate transport in membrane vesicles from *Escherichia coli*. *Biochimica et Biophysica Acta (BBA) - Biomembranes*, 508(2), 370–378. [https://doi.org/10.1016/0005-2736\(78\)90339-5](https://doi.org/10.1016/0005-2736(78)90339-5)
- Lee, T.-Y., Min, W.-K., Kim, H. J., & Seo, J.-H. (2020). Improved production of 3-hydroxypropionic acid in engineered *Escherichia coli* by rebalancing heterologous and endogenous synthetic pathways. *Bioresource Technology*, 299, 122600. <https://doi.org/10.1016/j.biortech.2019.122600>
- Lourenço, N. D., Lopes, J. A., Almeida, C. F., Sarraguça, M. C., & Pinheiro, H. M. (2012). Bioreactor monitoring with spectroscopy and chemometrics: a review. *Analytical and Bioanalytical Chemistry*, 404(4), 1211–1237. <https://doi.org/10.1007/s00216-012-6073-9>
- Mahmoud Al-Hejin, A., Singh Bora, R., & Morsi M. Ahmed, M. (2019). Plasmids for Optimizing Expression of Recombinant Proteins in *E. coli*. *IntechOPEN*.
- Minihane, B. J., & Brown, D. E. (1986). Fed-batch culture technology. *Biotechnology Advances*, 4(2), 207–218. [https://doi.org/10.1016/0734-9750\(86\)90309-5](https://doi.org/10.1016/0734-9750(86)90309-5)
- Nishio, N., Tsuchiya, Y., Hayashi, M., & Nagai, S. (1977). A Fed-Batch Culture of Methanol-utilizing Bacteria with pH

- Stat: Studies on Methanol Metabolism (VI). *Journal of Fermentation Technology*, 55, 151-155.
- Rosano, G. L., & Ceccarelli, E. A. (2014). Recombinant protein expression in *Escherichia coli*: advances and challenges. *Frontiers in Microbiology*, 5. <https://doi.org/10.3389/fmicb.2014.00172>
- The kinetics of the carbon dioxide-carbonic acid reaction. (1933). *Philosophical Transactions of the Royal Society of London. Series A, Containing Papers of a Mathematical or Physical Character*, 232(707–720), 65–97. <https://doi.org/10.1098/rsta.1934.0003>
- Vasic-Racki, D. (2006). History of Industrial Biotransformations - Dreams and Realities. In *Industrial Biotransformations, Second Edition*. <https://doi.org/10.1002/9783527608188.ch1>
- Wang, H. Y., Cooney, C. L., & Wang, D. I. C. (1977). Computer-aided baker's yeast fermentations. *Biotechnology and Bioengineering*, 19(1), 69–86. <https://doi.org/10.1002/bit.260190107>
- Yano, T., Kobayashi, T., & Shimizu, S. (1978). Fed-batch culture of methanol-utilizing bacterium with DO-stat. *J Ferment Technol*, 56, 416–420.
- Zhao, L., Fu, H.-Y., Zhou, W., & Hu, W.-S. (2015). Advances in process monitoring tools for cell culture bioprocesses. *Engineering in Life Sciences*, 15(5), 459–468. <https://doi.org/10.1002/elsc.201500006>
- Zubay, G. (1972). The Mechanism of Activation of the Lac Operon. In *Metabolic Interconversion of Enzymes* (pp. 149–157). Springer Berlin Heidelberg. https://doi.org/10.1007/978-3-642-80698-8_11

8. *Saccharomyces cerevisiae* bioprocess definition

8.1 Nomenclature

gDCW: Dry cell weight amount in grams

$Y_{eth/glc}$: Yield between ethanol produced and glucose consumed ($gDCW \cdot g_{glucose}^{-1}$)

$Y_{gly/glc}$: Yield between glycerol produced and glucose consumed ($g \cdot g^{-1}$)

$Y_{x/glc}$: Yield between biomass produced and glucose consumed ($gDCW \cdot g^{-1}$)

$Y_{eth/x}$: Yield between ethanol produced and biomass produced ($g \cdot gDCW^{-1}$)

$Y_{gly/x}$: Yield between glycerol produced and biomass produced ($g \cdot gDCW^{-1}$)

OUR: Oxygen uptake rate ($mM \cdot h^{-1}$)

CER: Carbon exchange rate ($mM \cdot h^{-1}$)

YNB: Abbreviated named for the commercial media - Yeast Nitrogen Base

FDB: Abbreviation for Fed-Batch Strategy

$q_{glucose}$: Specific glucose consumption rate ($mmol \cdot gDCW^{-1} \cdot h^{-1}$)

$X(t_0)$: Biomass concentration at time zero (initial time)

$V(t_0)$: Volume of bioreactor at time zero (initial time)

$C_{glucose, feeding}$: Glucose concentration of the feeding solution used in the fed-batch strategies ($g \cdot L^{-1}$)

$F(t)$: Feed addition flow rate in fed-batch strategy ($mL \cdot min^{-1}$)

t: Time (h)

μ : Specific growth rate (h^{-1})

RQ: Respiratory Quotient

8.2 Introduction

Recombinant protein production emerged in the early 1980s, aiming at overcoming the limitations imposed by extraction of bioproducts from natural sources. Nowadays, recombinant proteins are considered a milestone for drug discovery and its current market size can verify its relevance, as it has been discussed in the general introduction of this work. Despite the fact that recombinant proteins are involved in other industries as the food, detergent, paper, chemical, and cosmeceutical, it has been reported that the largest market is held by pharmaceutical and biotechnology fields. In fact, one of the main driven forces for the continuous growth of recombinant protein market is the drug discovery conducted by the pharmaceutical and biotechnology companies (Kinch, 2015).

The development of drug discovery requires the expression of different proteins in different organisms. Among the most used expression platforms for recombinant protein production, the bacteria *Escherichia coli* is widely known as a preferential host, it has been discussed in previous chapters (**chapter 3**). Nevertheless, depending on the properties of the desired protein, utilization of bacteria might be not even possible. For example, when the recombinant protein requires post-translational modifications in order to be biologically active.

In order to overcome the bacteria limitation as expression systems, eukaryotic hosts such as yeasts (unicellular fungi), filamentous fungi, insects, plant and mammalian cell lines have been used (Ikonomou et al., 2003) (Wurm, 2004) (Plasson et al., 2009) (Ward, 2012). Among them, yeasts combine the simplicity of a unicellular organism, having lower nutritional demands when compared to insect and plant and mammalian cell lines, with the ability to realize most of the post-translational modifications required for a biologically active recombinant protein, and the capacity for secreting the recombinant protein to the media. Therefore, yeasts have been utilized for the production of various pharmaceutical proteins (Mattanovich et al., 2012) (Nielsen, 2013), as for example, the hormones insulin and glucagon, produced using *S. cerevisiae* as the expression platform (Nielsen, 2013).

Several publications regarding the bioprocess optimization whose focus was on the enhancement of volumetric productivity started to appear in order to increase the industrial use of the *S. cerevisiae* as an expression platform, basically, from two approaches. The first approach was based on its genetic modification, due to the vast synthetic biology tools developed thanks to its well-annotated genome, genetic tractability, and overall ease of use (Wagner & Alper,

2016), such as engineering the vesicle trafficking in order to improve the desired protein secretion and as a result, increasing its specific production rate (Hou et al., 2012). On the other hand, the second approach was based on bioprocess engineering field and the design of culture strategies, basically, related to the fed-batch strategies (Mendoza-Vega et al., 1994).

One of the main limitations when *S. cerevisiae* is cultured in a fed-batch conditions is the ethanol production, a widely known by-product that inhibits the growth (Valentinotti et al., 2003). The solutions to the ethanol problem tackled from the use of kinetic models in order to improve the carbon conversion towards biomass (Pham et al., 1998) to design feeding strategies based on mathematical models generated by monitoring physiological variables (Larsson et al., 1991) (Renard & Vande Wouwer, 2008) (Dewasme et al., 2010). However, in the last decade, the use of metabolic models started to appear in order to predict the whole carbon metabolism and, as a result, increasing the biomass production through the optimization of the carbon conversion towards biomass and product (Costenoble et al., 2007) (Hjersted & Henson, 2008).

Thereupon, the following chapter will be focused on design a whole set of culture strategies for *S. cerevisiae*, from batch to fed-batch, taking into consideration the metabolic data obtained from the flux analysis presented in **chapter 4** in order to optimize the volumetric productivity of the processes.

8.3 Results (I) - Batch strategies

8.3.1 Batch

As it has been previously described in **chapter 4**, *S. cerevisiae* metabolism can be optimized towards biomass formation instead of towards the production of non-desired products, such as ethanol when glucose is used as a carbon source. In this chapter, a *S. cerevisiae* *wildtype* will be used as a reference strain in order to design bioprocess strategies whose aim will be to improve the volumetric productivity by means of enhancing the biomass generation, while the specific growth rate will be kept at its optimal value.

To begin with, *S. cerevisiae* was cultured in a 2L batch bioreactor where the environmental conditions were controlled in order to get the optimal growth rate (the environmental conditions and the control variables are described in **section 8.7.8**). Moreover, glucose was set as the media's main carbon source and its composition is described in **section 8.7.4**.

As shown in **graph A from Figure 8-1** and in **Table 8-1**, when *S. cerevisiae* was cultured in bioreactor using a batch strategy, the specific growth rate had a value of $0,36 \text{ h}^{-1}$ and $1,60 \text{ gDCW}\cdot\text{L}^{-1}$ of biomass was produced altogether with two by-products: $5,92 \text{ g}\cdot\text{L}^{-1}$ of ethanol and $0,48 \text{ g}\cdot\text{L}^{-1}$ of glycerol. Related to the conversion of glucose to biomass, the biomass-glucose yield led the culture to produce $0,10 \text{ gDCW}$ of biomass for each gram of glucose consumed, while $0,37 \text{ g}$ of ethanol and $0,03 \text{ g}$ of glycerol were produced for each gram of glucose consumed. Moreover, a particular trait of *S. cerevisiae* was observed related to the relation between the CER and OUR during the experiment, widely known as named Respiratory Quotient (RQ).

As it was commented in the **chapter 4**, higher available glucose concentrations are directly related to higher ethanol productions and, as a result, a RQ value higher than one, owing to the oxidation of pyruvate to carbon dioxide and acetaldehyde by a cytoplasmic decarboxylation (Das et al., 1961). Consequently, an undesired metabolism took place where the carbon source was wasted due to the conversion of glucose to ethanol and glycerol instead of biomass.

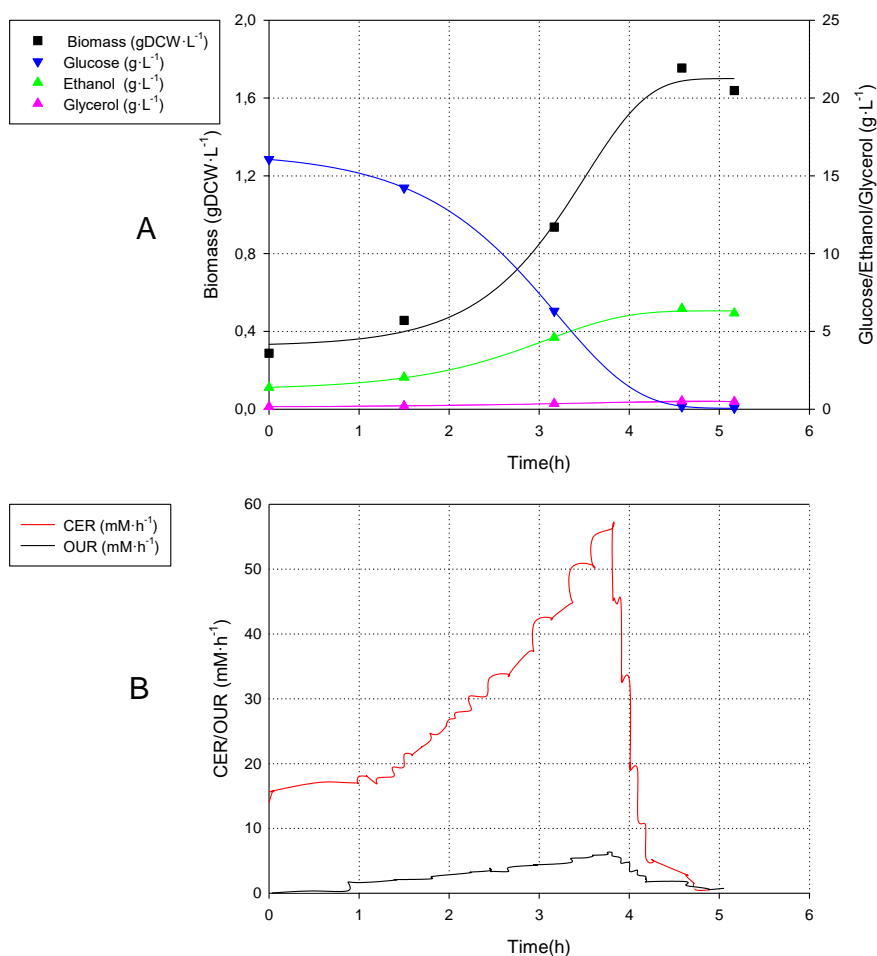


Figure 8-1 Profile of A) off-line variables such as Biomass (■), glucose (▼), ethanol (▲), and glycerol (▲) and B) on-line variables such as CER (—), OUR (—).

Table 8-1 Main batch parameters for overall characterized culture strategies.

Achieved biomass (gDCW·L ⁻¹)	1,60
μ (h ⁻¹)	0,36
Ethanol generation (g·L ⁻¹)	5,92
Glycerol generation (g·L ⁻¹)	0,48
$Y_{x/glu}$ (gDCW · g _{glucose} ⁻¹)	0,075
$Y_{et/glu}$ (g _{ethanol} · g _{glucose} ⁻¹)	0,37
$Y_{gly/glu}$ (g _{glycerol} · g _{glucose} ⁻¹)	0,03

To conclude, the batch strategy reached a biomass concentration of 1,60 gDCW·L⁻¹. The main problem arise then in the ethanol production, that account for 37% of the glucose consumed. After this point, in order to increase both the biomass concentration and the biomass productivity several approaches will be applied. Mainly, these approaches tackled the

fortification of the batch media composition and several fed-batch strategies. Therefore, in the following section, the approach that will be presented is the fortification of the batch media composition in order to increase the biomass concentration obtained through the concentration of the media composition.

8.3.2 Fortified Batch

The fortification of any batch culture is based on rising the concentration of some of the media compounds without reaching a growth-inhibitory concentration. The objective of that is to supply the enough nutrients to sustain growth and overcoming the carbon limitation in the batch cultures in order to obtain a higher biomass concentration. For that specific case, an Erlenmeyer experiment where the modification of the batch media was carried out. The criteria used to define the experimental settings were based on not modifying the ratios between glucose concentration, and trace elements and vitamins described in the base media. On the contrary, the relation between the glucose and either the concentration of phosphorus source or the other majority salts did not depend on the n-fold concentration, a fixed value was defined for them, a 2-fold and 1-fold respectively, as shown in **Table 8-2**. The relation was calculated based on its contribution towards biomass formation taking into consideration the *S. cerevisiae* biomass stoichiometric equation $\text{CH}_{1.613}\text{O}_{0.557}\text{N}_{0.158}$ described in (Villadsen et al., 2011) .

Table 8-2 Experimental settings for the batch media optimization experiment.

Group	Compound	1- fold reference concentration	n-fold concentration conditions					
			1-fold	5-fold	10-fold	20-fold	30-fold	40-fold
Carbon Source	Glucose	20 g·L ⁻¹	x1	x5	x10	x20	x30	x40
Majority salts	(NH ₄) ₂ SO ₄	5 g·L ⁻¹	x1	x2	x2	x2	x2	x2
	KH ₂ PO ₄	1 g·L ⁻¹	x1	x1	x1	x1	x1	x1
	MgSO ₄	0,5 g·L ⁻¹						
	NaCl	0,1 g·L ⁻¹						
	CaCl ₂	0,1 g·L ⁻¹						
Vitamins	Biotin	0,002 mg·L ⁻¹	x1	x5	x10	x20	x30	x40
	Calcium pantothenate	0,4 mg·L ⁻¹						
	Folic	0,002 mg·L ⁻¹						
	Inositol	2 mg·L ⁻¹						
	Niacin	0,4 mg·L ⁻¹						
	PABA	0,2 mg·L ⁻¹						
	Pyridoxine	0,4 mg·L ⁻¹						
	Riboflavin	0,2 mg·L ⁻¹						
Trace elements	Thiamine	0,4 mg·L ⁻¹	x1	x5	x10	x20	x30	x40
	H ₃ BO ₃	0,5 mg·L ⁻¹						
	CuSO ₄	0,04 mg·L ⁻¹						
	KI	0,1 mg·L ⁻¹						
	FeCl ₃	0,2 mg·L ⁻¹						
	MgSO ₄	0,4 mg·L ⁻¹						
	Na ₂ MoO ₄	0,2 mg·L ⁻¹						
	ZnSO ₄	0,4 mg·L ⁻¹						

As observed in **Figure 8-2**, when the media compounds were raised from 1-fold to 10-fold, the final biomass concentration increased almost 2,2-fold compared with the reference media (1-fold) . While, for concentrations higher than 10-fold, the biomass concentration obtained was 50% lower due to the reduction of the specific growth rate. Besides, when the concentration reached 30-fold and 40-fold, the culture did not grow.

In relation with the specific growth rate, as shown in **Figure 8-3**, there was a slightly increase until a peak was achieved at 0,299 h⁻¹ with the 5-fold concentration. When the n-fold was higher than 5, the growth inhibition started until a completely inhibition was achieved when the concentration was higher than 20-fold.

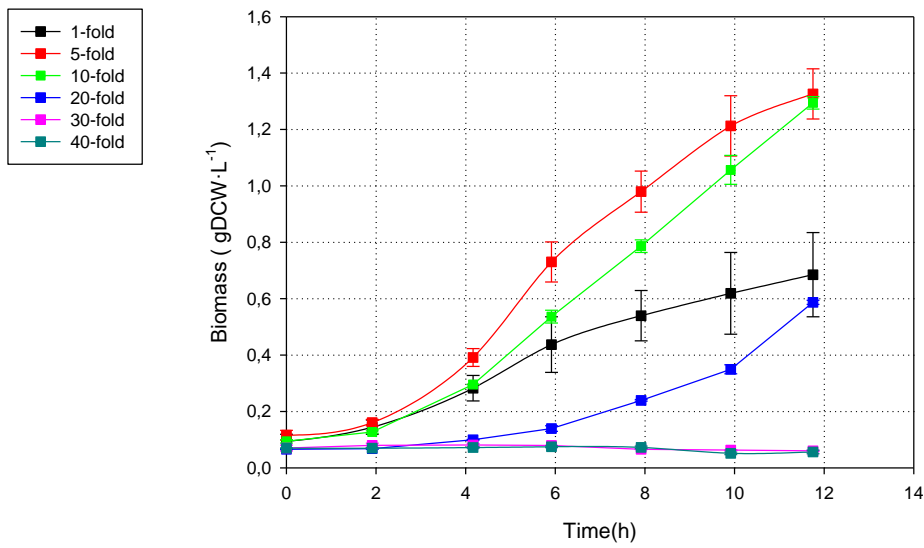


Figure 8-2 Growth comparison when several n -fold concentrations were tested in *S. cerevisiae* Erlenmeyer culture.

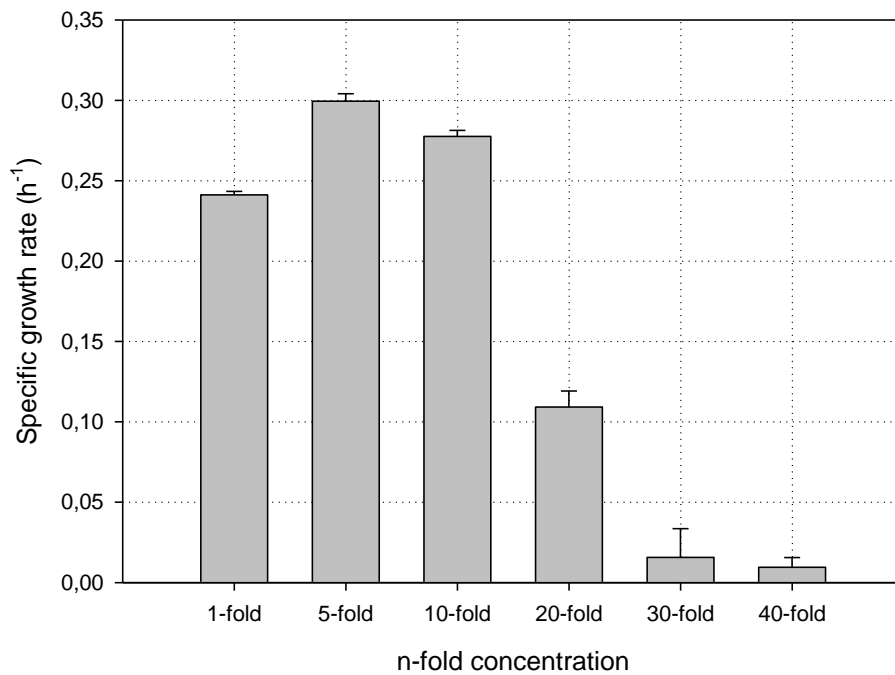


Figure 8-3. Comparison between the specific growth rate and the media concentration

Once the batch media composition was defined, a batch culture using this fortified media was carried out; using the 10-fold condition due the it was the condition where the specific growth rate was almost not affected by the n -fold concentration. After this point, this batch will be referred as the fortified batch.

As shown in **graph A of Figure 8-4** , 100 g·L⁻¹ of glucose were consumed in order to produce 5,5 gDCW·L⁻¹ of biomass , 36,86 g·L⁻¹ of ethanol and 3,24 g·L⁻¹ of glycerol, with a specific growth rate of 0,35 h⁻¹. On the other hand, as shown in **graph B of the Figure 8-4**, the oxygen uptake rate and the carbon exchange followed the growth tendency of the culture until they reached a maximum value of approximately 50 mM·h⁻¹ and 190 mM·h⁻¹, respectively. Therefore, it can be stated that the behaviour of the Carbon Evolution Rate (CER) and oxygen uptake rate (OUR) followed the tendency of growth curve.

It is important to describe why the partially oxidized by-products as ethanol and glycerol were produced. As it was mentioned in **chapter 4** (*S. cerevisiae* metabolism), both would be produced when a high glucose flux through the glycolytic pathway owing to high glucose concentrations uncouples the redox balance in cytoplasm. This unbalance was caused by a difference in the reduced form of the cofactor NAD fluxes generated by glycolytic pathway and consumed by the mitochondrial shuttles in order to be regenerated. Then, ethanol and glycerol were produced to counter the lack of cytoplasmic NAD⁺.

The fortification of batch medium, as shown in **Table 8-3** , promoted an increase of the biomass produced from 1,6 gDCW·L⁻¹ to 5,5 gDCW·L⁻¹ and as a result, a 3,43-fold increase of biomass productivity, without affecting either the specific growth rate or the yield between the by-products and glucose.

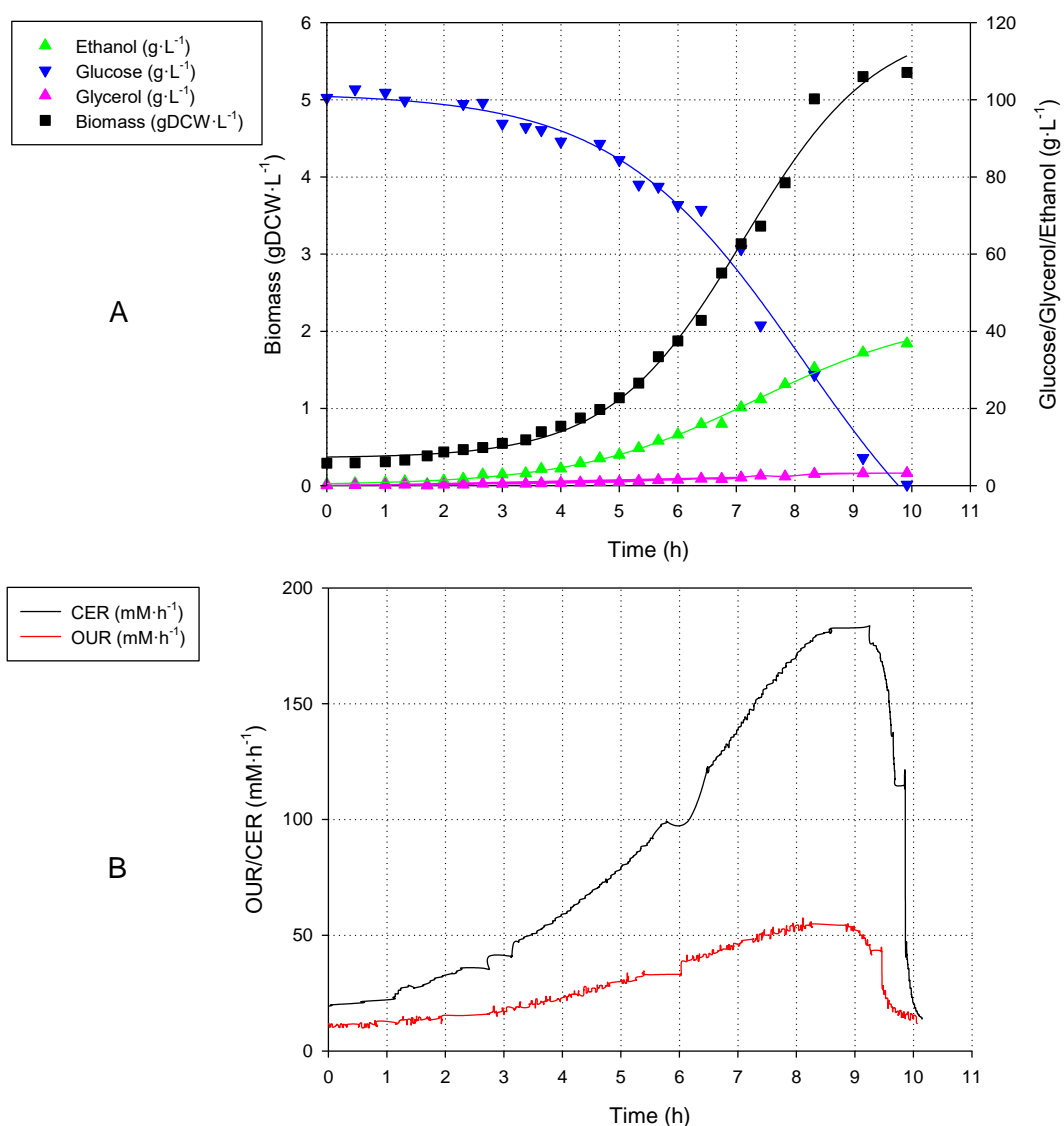


Figure 8-4. Profile of A) off-line variables such as Biomass (■), glucose (▲), ethanol (▲), and glycerol (▲) and B) on-line variables such as C.E.R (—), O.U.R (—).

Up until now, the increase of the biomass production in order to increase the volumetric productivity has been based on the fortification of the batch media. As a result, this fortification led to 3,43-fold increase of the biomass volumetric productivity, without having a significant effect on either the specific growth rate or the yield between by-products and glucose consumed.

Table 8-3 General overview of the parameters for the batch and the fortified batch experiments

	Batch	Fortified Batch
Achieved biomass ($\text{gDCW} \cdot \text{L}^{-1}$)	1,60	5,5
μ (h^{-1})	0,36	0,35
Ethanol generation ($\text{g} \cdot \text{L}^{-1}$)	5,92	36,86
Glycerol generation ($\text{g} \cdot \text{L}^{-1}$)	0,48	3,24
Glucose Consumption ($\text{g} \cdot \text{L}^{-1}$)	16,06	100
$Y_{x/\text{glu}}$ ($\text{gDCW} \cdot \text{g}_{\text{glucose}}^{-1}$)	0,075	0,06
$Y_{\text{eth}/\text{glu}}$ ($\text{g}_{\text{ethanol}} \cdot \text{g}_{\text{glucose}}^{-1}$)	0,37	0,36
$Y_{\text{gly}/\text{glu}}$ ($\text{g}_{\text{glycerol}} \cdot \text{g}_{\text{glucose}}^{-1}$)	0,03	0,03

In the following section a different approach will be deepened, the use of advanced culture technics related to defining fed-batch culture strategies to further increase the biomass concentration and to optimize the conversion of glucose to biomass. Consequently, the biomass productivity will be increased. It is important to remember that using the fortification methodology only the 63% of glucose consumed was converted to biomass even if the biomass concentration increased by 3,43-fold. The use of fed-batch strategies will improve the conversion of glucose to biomass through controlling the glucose availability because as it was mentioned in the study of the *S. cerevisiae* metabolism (**chapter 4**), the conversion of glucose to ethanol depended on the glucose availability.

8.4 Results (II) - Fed batch strategies

As it was previously described in the batch strategies, the increase of biomass production was accomplished in the fortified batch by increasing the concentration of batch media compounds. As a result, the biomass concentration was increased a 3,43-fold. However, in order to further increase the biomass produced a different strategy, based on a fed-batch culture, will be developed in this section. The development of fed-batch strategy solely focused on the bioprocess optimization and not in the media optimization, regarding batch culture media and feeding solution. A home-made minimum batch media and feeding solution tested for a fed-batch strategy was used as a reference (as described in section 8.7.4) in order to avoid ethanol generation and increasing the conversion of glucose to biomass.

It is important to remember that a fed-batch is a strategy that relays on knowing a priori the metabolic and physiologic condition of the organism that is going to be cultured. These requirements are needed because fed-batch strategies are inherently related to the specific rate of glucose consumed and to the growth rate, as shown in **section 8.7.10**.

This said, the fed-batch strategies could be split into two approaches taking into consideration how the feeding profile is calculated. The first one consists on the strategies whose feeding profile is calculated with a theoretical preprogrammed biomass profile. Whereas, in the second group the feeding profile is calculated via estimation of the experimental biomass by means of establishing relations between measured variables and the experimental biomass concentration.

The first strategy described is based on a preprogrammed exponential feeding addition, whose main traits are the specific growth rate of *S. cerevisiae* and the specific consumption rate of glucose, as described in **section 8.7.11** and in **section 8.7.10**. The specific growth rate will be extrapolated directly using a biomass balance from the data obtained in the priori batch phase. It is important to highlight that the parameter that was used as the specific consumption rate of glucose in the calculation for the feeding addition was not the one determined by the priori batch culture, as described in the next paragraph.

The decision regarding the change in the batch glucose specific rate was based on the results presented in the *S. cerevisiae* metabolism **chapter 4**, where a glucose-adapting metabolism was observed based on the regulation of the glucose specific consumption rate where an optimal value in the conversion of glucose towards biomass was found. Therefore, the specific consumption rate of glucose calculated through the priori batch phase was not representative if it is compared with the data obtained in **chapter 4**. As shown in **Figure 8-5**, a decrease of 6,25-fold decrease compared with the priori batch phase was observed. Therefore, the use of the continuous culture data will assure an optimal conversion of glucose to biomass.

Therefore, the specific rate of consumption that will be used is the one obtained from the data of the continuous culture from the studies carried out in **chapter 4**, regarding *S. cerevisiae* glucose metabolism in continuous cultures: $0,35 \text{ g} \cdot \text{gDCW}^{-1} \cdot \text{h}^{-1}$.

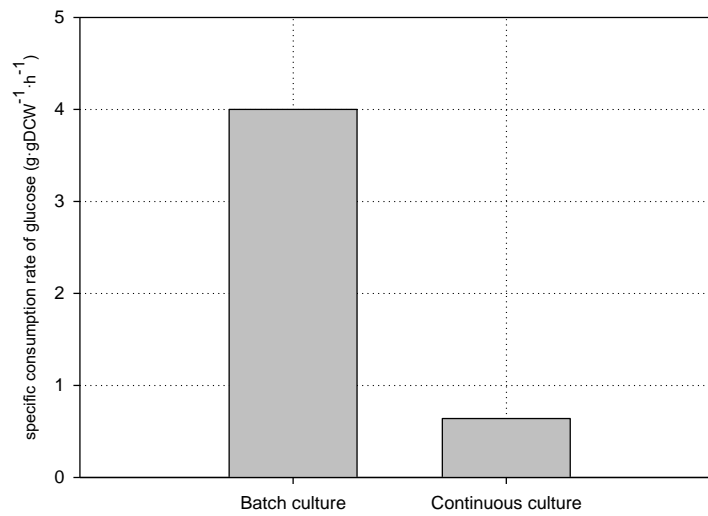


Figure 8-5. Comparison the specific consumption rate of glucose between the priori batch phase and continuous cultures.

On the other hand, there is a feature that must be remarked, as it was defined in the *E. coli* bioprocess chapter, the fed-batch initialization point was decided to be near the moment when CER or OUR dropped. As a result, the initialization moment of the fed-batch strategy was manually started.

8.4.1 Fed batch based on exponential feeding

In order to perform a fed-batch addition based on a preprogrammed exponential profile, several data were required, as shown in **Equation 8-1**: the specific consumption rate of glucose ($q_{glucose}$), the specific growth rate (μ) and the glucose concentration in the feeding solution ($C_{glucose,Feeding}$). A further definition of the mathematical algorithm and the feeding media composition are described in **section 8.7.12** and in **section 8.7.4**, respectively.

Equation 8-1

$$F(t) = \frac{-q_{glucose} \cdot X(t_0) \cdot V(t_0) \cdot \exp(\mu \cdot t)}{C_{glucose,Feeding}}$$

As shown in the following **graph A of Figure 8-6**, the fed-batch was split into two phases: the batch phase which was defined within the first 4,5 hours and the fed-batch phase, which occurred after the batch phase reached a glucose concentration near 0 g·L⁻¹ until the end of the experiment.

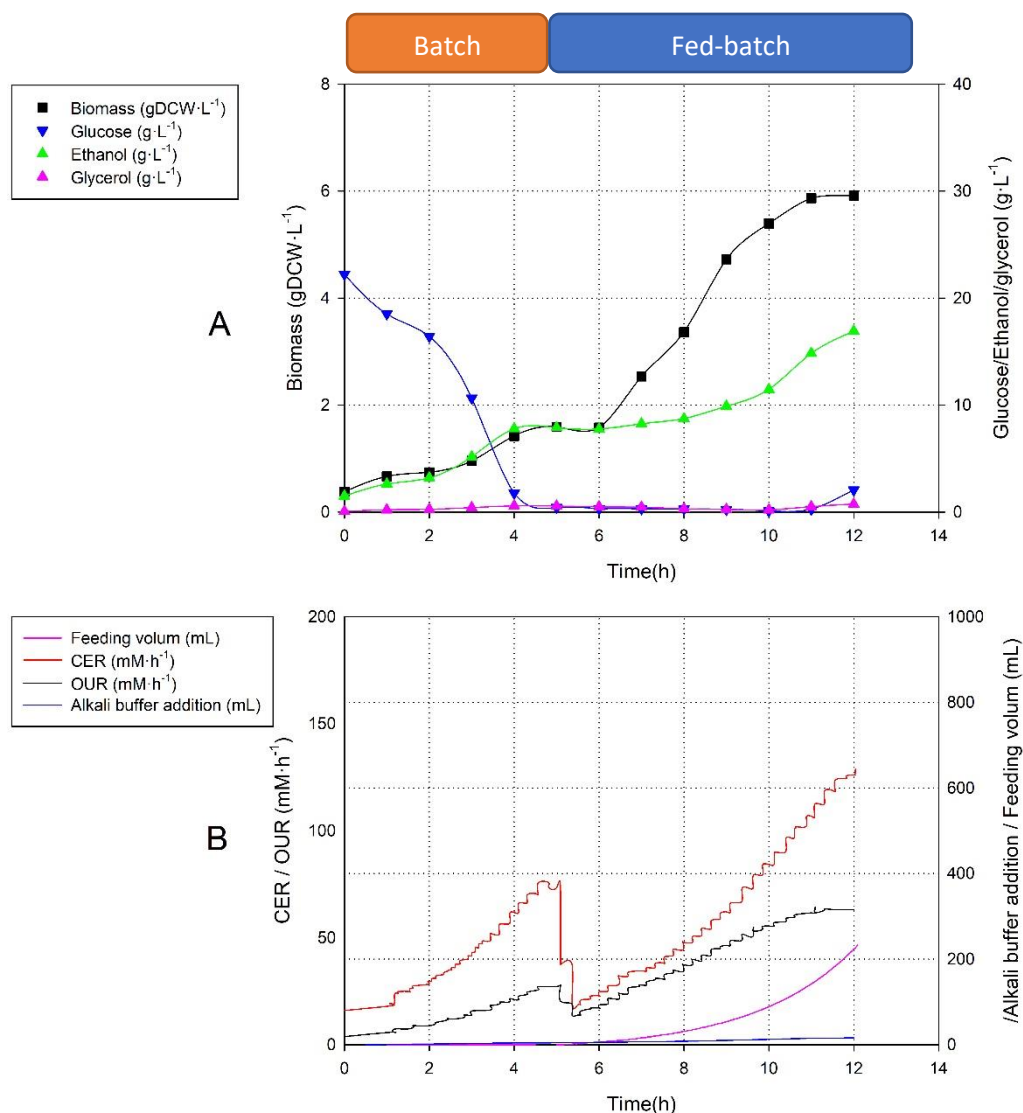


Figure 8-6. Profile of A) off-line variables such as Biomass (■), glucose (▼), ethanol (▲), glycerol (▲) and B) on-line variables such as OUR (—), CER (—), alkali buffer addition (—) and feeding volume (—) for the fed-batch culture based on a preprogrammed exponential feeding strategy.

Regarding the batch phase, 20 g·L⁻¹ of glucose were consumed in order to produce 1,6 gDCW·L⁻¹ of biomass, 6,46 g·L⁻¹ of ethanol and non-significant glycerol concentrations, with an specific growth rate of 0,35 h⁻¹. It is important to point out that for each gram of consumed glucose 0,12 gDCW of biomass and 0,30 g of ethanol were produced until glucose was fully depleted. At this point, the fed-batch strategy started. Regarding the definition of the fed-batch phase, the

feeding algorithm used the specific growth rate from the batch phase, while the specific glucose consumption rate used was the one from the continuous culture described in **chapter 4**, instead of the one obtained in the batch phase. The reason behind why the continuous culture's value was the one used instead of the batch one revolved around a conclusion reached in **chapter 4**. In that chapter, an optimal value in the specific glucose consumption rate in order to optimize the transformation of glucose to biomass was found. Even if the dilution rate of the continuous culture was not used in the feeding profile calculated, it was hypothesized that the specific consumption rate of glucose might be extrapolated to any dilution rates. Therefore, its use in the fed-batch cultures should be right.

On this basis, the specific glucose rate used in the fed-batch was one from the continuous culture ($0,35 \text{ g} \cdot \text{gDCW}^{-1} \cdot \text{h}^{-1}$) instead of the batch one ($1,80 \text{ g} \cdot \text{gDCW}^{-1} \cdot \text{h}^{-1}$) because the aim of the fed-batch strategy was to maximize the biomass production by means of optimizing the conversion of glucose to biomass. In this case, the carbon optimization was carried reducing the ethanol production by using the data from the continuous culture. A reduction of the ethanol production was described when the specific consumption rate of glucose was minimized due to the decrease of the flux through the glycolytic pathway.

As shown in **graph A of Figure 8-6**, the achieved biomass in the fed-batch phase had a value of $5,91 \text{ gDCW} \cdot \text{L}^{-1}$, the ethanol produced reached a concentration of $16,91 \text{ g} \cdot \text{L}^{-1}$ and also $0,74 \text{ g} \cdot \text{L}^{-1}$ of glycerol was produced. Moreover and it is shown in **Table 8-4**, there was a significant difference in the growth rate between the batch and the fed-batch phase. It appeared because the feeding rate was not the optimal one in order to carry out a fed-batch where the growth rate was not limited. As a result, it was underestimated.

Table 8-4 Main fed batch parameters for overall Fed batch culture strategies

Achieved biomass ($\text{gDCW} \cdot \text{L}^{-1}$)	5,91
Batch μ (h^{-1})	0,33
FDB μ (h^{-1})	0,26
q_{glucose} ($\text{g}_{\text{glucose}} \cdot \text{gDCW}^{-1} \cdot \text{h}^{-1}$)	0,35
Batch $Y_{x/\text{glc}}$ ($\text{gDCW} \cdot \text{g}_{\text{glucose}}^{-1}$)	0,10
FDB $Y_{x/\text{glc}}$ ($\text{gDCW} \cdot \text{g}_{\text{glucose}}^{-1}$)	0,13
Batch $Y_{\text{eth}/\text{glc}}$ ($\text{g}_{\text{ethanol}} \cdot \text{g}_{\text{glucose}}^{-1}$)	0,30
FDB $Y_{\text{eth}/\text{glc}}$ ($\text{g}_{\text{ethanol}} \cdot \text{g}_{\text{glucose}}^{-1}$)	0,20

It is important to remark that the use of the continuous culture glucose specific consumption rate was a correct decision owing to it produced an important decrease in the specific production rate of ethanol, as shown in **Figure 8-7**. As a result, the conversion of glucose towards biomass improved in a 30%, while its conversion towards ethanol was reduced by 50%, in regard with the data obtained from the batch phase even with the growth rate decrease of 21%.

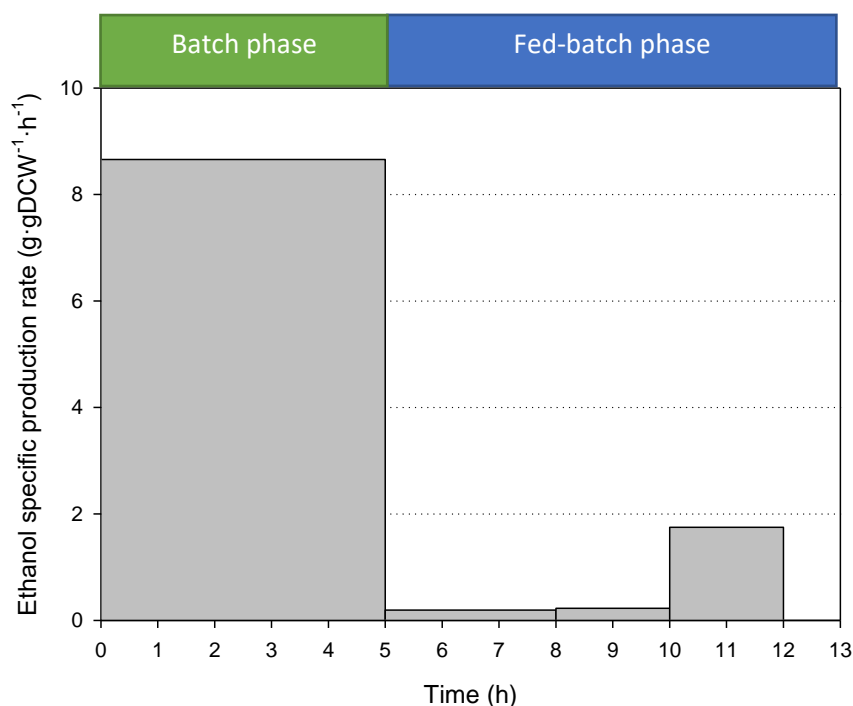


Figure 8-7 . Profile of ethanol's specific production rate during the batch and fed-batch phases.

On the other hand, as shown in **graph B of Figure 8-6**, the OUR and CER behaviours presented two important facts:

1. As can be observed in the batch phase, both the CER and OUR values dropped “instantaneously”, when the glucose concentration was near 0 g·L⁻¹. This drop in both profiles could be used as metabolic indicator which gives information about either the glucose metabolism or its near depletion. Furthermore, it is important to remember that this behaviour was also observed in *E. coli* bioprocess in **chapter 7**, therefore, it can be stated that both OUR and CER can be used as a variable that give instantaneous metabolic-related information about the state of the carbon metabolism when *S. cerevisiae* is used as a platform expression. Due to the fact that both CER and OUR are related to the glucose oxidation, a variation in their profile should be caused by a change in the carbon metabolism. Owing to CER gives information about the profile of the carbon dioxide produce when glucose is oxidized, while OUR provide information related to the electron acceptor, in this case oxygen, required for the glucose oxidation.

2. The second one is that the CER and OUR followed the growth perfectly during all the experiment, whereas in the *E. coli* strategies presented in **chapter 7** was not able to.

Moreover, regarding the physiological variables that can be used in order to predict the carbon metabolism apart from CER and OUR, there is also another parameter that had a relation with the biomass behaviour, as shown in **graph B of Figure 8-6**, the alkali buffer addition. The alkali buffer addition was directly related to the acidification of the media due to the reaction between the carbon dioxide produced in the decarboxylation of pyruvate and water (Pronk et al., 1996) (Butler, 1991). Even if the volume of the alkali addition buffer was low due to the use of high concentration titter ($300 \text{ g}\cdot\text{L}^{-1}$ of sodium hydroxide) coupled with the pH control, a relation between the biomass produced, growth state and the buffer added appeared. This relation was based on understanding the interaction between the carbon dioxide produced, as the unique product with an acid character in the metabolism, and the bioreactor's pH control, in order to maintain the pH at a constant value. Therefore, it can be used as a control variable in order to predict either the biomass concentration value and the growth state as well as CER and OUR and as a result, they can be grouped as biomass-related variables. The same conclusion was obtained regarding the biomass-related variables when *E. coli* was analysed in **chapter 8**. Therefore, it can be stated that these variables (CER, OUR and alkali buffer addition) can be used in both *E. coli* and *S. cerevisiae* cultures, although its use might be expanded to any kind of bacteria or yeast. Moreover, regarding the case of animal cells, it will be described in the following chapter.

To conclude, as shown in **Table 8-5**, the fed-batch strategy led the culture to increase the biomass achieved by 1,11-fold compared with the fortified batch culture. However, in the fed-batch strategy the conversion of glucose to biomass was increased by near 2-fold due to the 41% reduction in the transformation of glucose to ethanol. As a result, even if the specific growth rate was reduced in comparison with the fortified batch, the use of the preprogrammed exponential promoted an increase in the biomass concentration while a huge optimization of the carbon source was achieved.

Table 8-5 General overviews for the culture strategies carried out.

	Fortified Batch	FDB- preprogrammed exponential
Achieved biomass ($\text{gDCW}\cdot\text{L}^{-1}$)	5,30	5,91
$\mu \text{ (h}^{-1}\text{)}$	0,35	0,28
Ethanol generation ($\text{g}\cdot\text{L}^{-1}$)	36,86	16,91
Glycerol generation ($\text{g}\cdot\text{L}^{-1}$)	3,24	0,74

$Y_{x/s}$ ($\text{g}_{\text{DCW}} \cdot \text{g}_{\text{glucose}}^{-1}$)	0,06	0,13
$Y_{e/s}$ ($\text{g}_{\text{ethanol}} \cdot \text{g}_{\text{glucose}}^{-1}$)	0,36	0,21
$Y_{gly/s}$ ($\text{g}_{\text{glycerol}} \cdot \text{g}_{\text{glucose}}^{-1}$)	0,03	0,02

Even if the increase in either the biomass concentration was achieved, the specific growth rate in the fed-batch phase was not the optimal one (a 24% decrease compared with the fortified batch). The decrease in the growth rate was directly related to an underestimation of the feeding rate. This underestimation was caused by not using the optimal parameters when the preprogrammed exponential feeding was defined. It can be assumed that the parameter that underestimated the feeding rate might be the specific growth rate owing to it was not enough accurate. Regarding the specific consumption rate of glucose as the second parameter, as it was shown in **chapter 4**, taking into consideration that a reduction in the growth rate was not observed during the continuous culture, it could be considerate that the specific glucose consumption rate could be extrapolated to higher specific growth rate, such as this case. As a result, the inaccuracy in the specific growth rate calculated could provoked the growth-limiting feeding profile.

Therefore, there would be two ways to solve this accuracy problem:

- 1) A high-frequency biomass sampling in the batch phase in order to get a precise value.
- 2) Continuous methodologies based on monitoring biomass-related variables that will predict the biomass evolution.

For a high-frequency sampling, more than two workers should be required due to the nature of the sampling analysis, therefore, this approach should be discarded owing to the incapacity to apply the solution. Then, the approach that predicts the biomass during the course of the experiment by means of developing mathematical relations between the biomass concentration and biomass-related variables will be the one selected for solving the inaccuracy in the calculation of the specific growth. This will be based on a constant calculation of the biomass concentration during the course of the experiment.

After this point, the next step should be applying mathematical algorithms in order to develop a biomass-sensible feeding addition. In fact, this was also developed and tested in the previous *E. coli* bioprocess chapter (**Chapter 7**). Its conclusions regarding the fed-batch strategies must be applied and considered in order to avoid repeating or performing the same mistakes before carrying out the *S. cerevisiae* fed-batch strategies.

One of the things previously observed in *E.coli* fed-batch experiments controlled by biomass-related variables (as CER, OUR and alkali buffer addition) was the relation between them during the entire course of the experiment. However, their application as a feeding control variable shared a common issue: the disability of the feeding algorithm to adapt its response to an unpredicted change in the relation between the monitored variable and the biomass estimated. In order to solve this problem, a new methodology was developed, where the feeding algorithm was not based on metabolic parameters but rather on the capacity of predicting the glucose depletion in the process.

On this basis and as shown in **Figure 8-8**, the fed-batch strategy that will be used in this chapter will be directly the feeding algorithm based on non-metabolic parameters, due to the fact that the relations between biomass concentration and the biomass related variables (CER, OUR and alkali buffer) were not constant during the course of fed-batch.

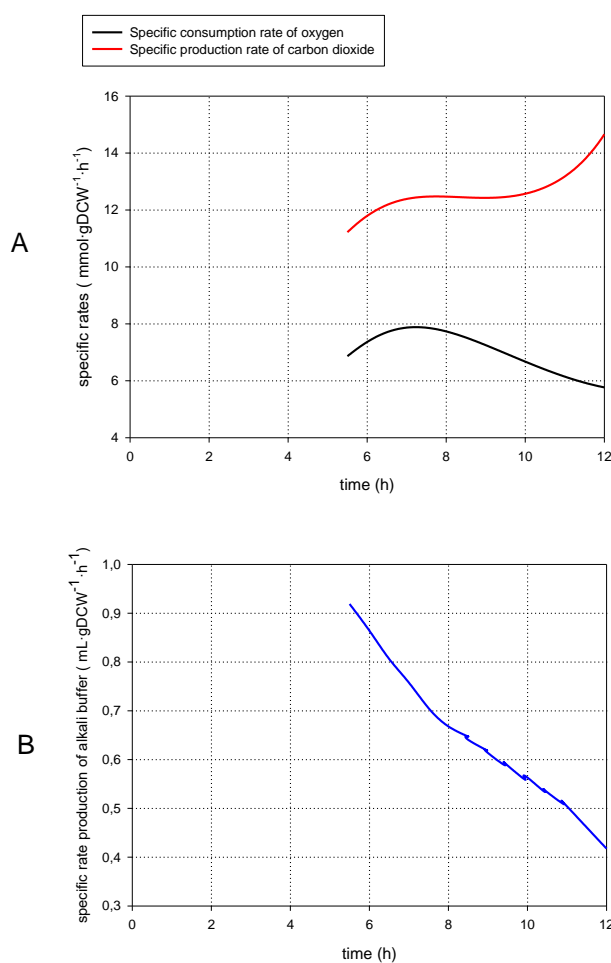


Figure 8-8. Specific rate profile for the biomass-related variables in the fed-batch phase (the specific consumption rate of oxygen shows the relation between OUR and biomass, the specific production rate of carbon dioxide shows the relation between OUR and biomass and the specific production rate of alkali buffer shows the relation between the alkali buffer added and the biomass).

However, as shown in **Figure 8-8**, the specific rate of oxygen, carbon dioxide and base that gave information about the relation between the biomass concentration and OUR, CER and the acidification rate of the media were not constant. This non-constancy in the relations can be explained thanks to the metabolic trait described in the *S. cerevisiae* metabolic chapter (**chapter 5**). In this chapter, the carbon metabolism showed the capacity of flux redistribution when the glucose availability was varied. However, it is important to keep in mind that even if the redistribution was caused by glucose concentration changing conditions, it cannot be assured that there will be other environmental conditions which might trigger this metabolic modification.

The obtained non-constant profiles of the relation between the biomass and biomass-related variables were consequence of a metabolic redistribution during the course of fed-batch phase. This restructuration was based on to the accumulation of feeding compounds that were not added at stoichiometry rate during the course of the fed-batch phase and, consequently, they could not be completely consumed. Therefore, they were accumulated in the media and affected the carbon metabolism.

On the other hand, and including the data obtained in the experiment presented just before, the discussion presented in the chapter of the *S. cerevisiae* metabolism (**chapter 5**) can be further debated.

The metabolic restructuration observed when the glucose availability was varied is not the only way to change the carbon metabolism. As it was shown in **Figure 8-9**, the first decrease in the specific production rate of ethanol was expected because the specific glucose rate used was selected for this purpose. However, what was not expected was a metabolic restructuration that took place in the last two hours (FDB (10-12h)) where an increase in the production of ethanol along with a growth inhibition were observed. The metabolic change could be explained based on an unknown compound added by feeding profile that triggered the inverse effect when its concentration reached a specific concentration due to its consumption rate was lower than the addition rate. Moreover, it is interesting to highlight that the increase in the duplication time started together with the increase in the production of ethanol. On this basis, it could be stated that a metabolic response caused by reaching a limit concentration of an unknown compound added by the feeding profile was responsible for both the growth rate inhibition and induction of the ethanol production.

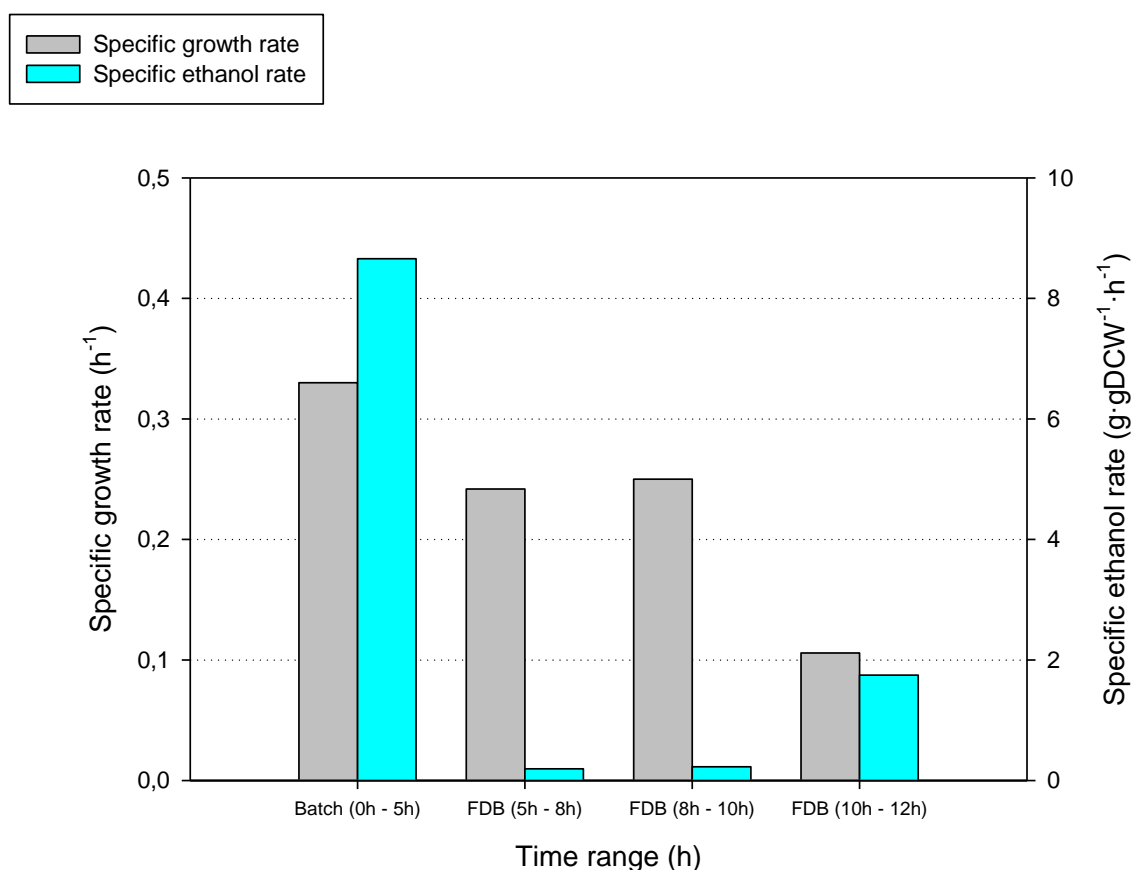


Figure 8-9. Evolution of the specific growth rate and the specific ethanol rate in the fed-batch culture for the preprogrammed exponential feeding strategy.

However, thanks to understanding of how the glucose affected the carbon metabolism an ethanol-low production metabolism was achieved in this experiment. As a result, the specific production rate of ethanol was reduced 95% when the environmental conditions were optimal, as it was showed in **Figure 8-7**. Moreover, due to the metabolic parameters behaviour observed during the batch phase, the following strategy to further increase the biomass concentration will be the non-metabolic strategy. Using this strategy that do not depend on any metabolic data or biomass concentration, the feeding profile will be able to adapt to the culture demands while the specific growth rate and the conversion of glucose to biomass will be at its optimal value.

The feeding profile will be dependent on the CER behaviour, specifically, to its response when a pulse of a defined amount of glucose is added and then, the CER response when it is consumed.

Therefore, in the following section, the non-metabolic fed-batch strategy will be carried out in order to improve the biomass productivity due to that *S. cerevisiae* metabolism is not constant during the entire fed-batch experiment.

8.4.2 Fed-batch feeding strategy based on a non-metabolic tool.

In order to perform a strategy that does not depend on actual data to design the feeding algorithm, a strategy based on how CER behaved when glucose was completely depleted from the culture media will be used hereafter.

This methodology has been already designed and tested in **chapter 7** and that the main core of it is the understanding of the relation between a pulse of defined glucose mass and CER. As it was showed previously in the **graph A of Figure 8-1**, when glucose concentration was near its depletion, the CER started to decrease because of not having enough glucose to maintain the carbon metabolism while growing at the optimal rate. On this basis, a pulse-addition system (1 gram of glucose) regulated by the CER response was implemented to provide the required nutrients for re-starting its growth. The regulation was based on the increase in the CER response when glucose was added, and then, the subsequent decrease when this amount of glucose was consumed. On this basis, a close loop between CER and the glucose pulse addition was carried out.

That way, this new method did not required any metabolic parameter, because the addition only depends on how CER behaved when a pulse of feeding media was added. The pulse regulation, the monitor of CER, and the interaction between both is detailed in **section 8.7.13**Error! Reference source not found..

The implementation of this methodology on a fed-batch is presented in **Figure 8-10** and as it is shown, the experiment should be split into two phases: the batch phase, which was defined within the first 4,5 hours, and the fed-batch phase, which occurred after the batch phase until the end of the experiment.

In that case, the moment when addition started was decided automatically, taking into consideration the CER behaviour. This is the first improvement that this methodology permits, because no manual decisions have to be made to decide the optimal moment to start the feeding. The new algorithm initiated automatically the fed-batch phase when a significant drop in CER occurred as a result of a glucose limiting conditions as shown **graph B of Figure 8-10** (4,5 hours).

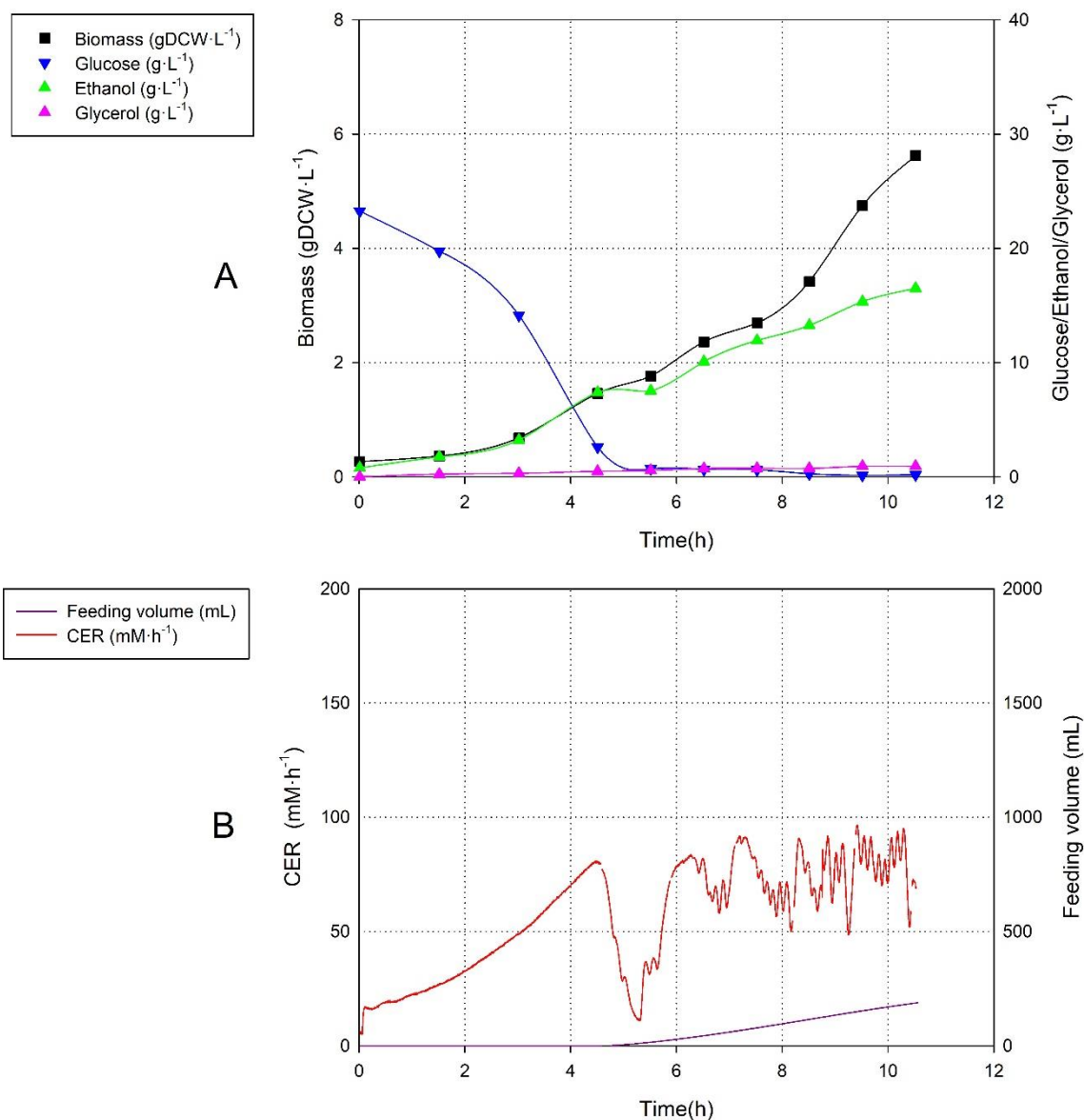


Figure 8-10 Profile of A) off-line variables such as Biomass (■), glucose (▼), ethanol (▲), glycerol (▲) and B) on-line variables such as CER (—) and feeding volume (—) for pH-controlled fed-batch culture using non-metabolic algorithm for feeding.

Regarding the batch phase, the most relevant parameter that is described in this case was the growth rate, which had a value of $0,34 \text{ h}^{-1}$. It is important to point out that the knowledge of this parameter together with the specific glucose rate is not necessary to perform the feeding addition. That would be the second improvement in regards the first strategy presented..

As shown in **graph B of Figure 8-10**, and led the culture to achieve a final cell concentration of $5,62 \text{ gDCW} \cdot \text{L}^{-1}$ without accumulating glucose. The feeding solution was added in response to the culture requirements, in order to grow at its optimal specific growth rate until a growth inhibition occurred, as it can be observed in **Figure 8-11**. It is important to highlight that the

feeding profile did not use any parameter for its calculation, it did not depend on the data of any other experiments such as the specific growth rate or the specific consumption rate of glucose.

This growth limitation was already observed in the previous fed-batch carried out based on... (section 8.4.1). Therefore, it can be concluded that there was at least one media compound that after reaching a specific concentration was responsible for the growth inhibition. This compound could be a growth-related one, for instance, formic acid, 2,3-butanediol and octanoic or decanoic acids which are described as growth-related inhibitors (Maiorella et al., 1983) (Viegas et al., 1989) or it could be one added with the feeding solution, such as the inhibitory effect of high concentrations of trace elements (cobalt, manganese or others) (Novozymes, 2017).

As it can be observed, there was a reduction in the final ethanol concentration due to the decrease in its specific production rate as it can be observed in **Figure 8-11**. This decrease was possible because the used addition methodology promoted a low-glucose environment and as it was described in **chapter 5**, *S. cerevisiae* adapts its carbon metabolism to the environmental conditions. As a result, the metabolism that prevailed was the optimal one depending on how the environmental conditions were changing during the course of the fed-batch phase. Therefore, with this strategy it was possible to let the culture grow at its optimal specific growth rate while the carbon metabolism was the optimal one in a low-glucose environment created by the 1g- glucose pulse used in fed-batch strategy. Moreover, it was possible to obtain an optimal carbon conversion towards biomass due to ethanol production was nearly depleted

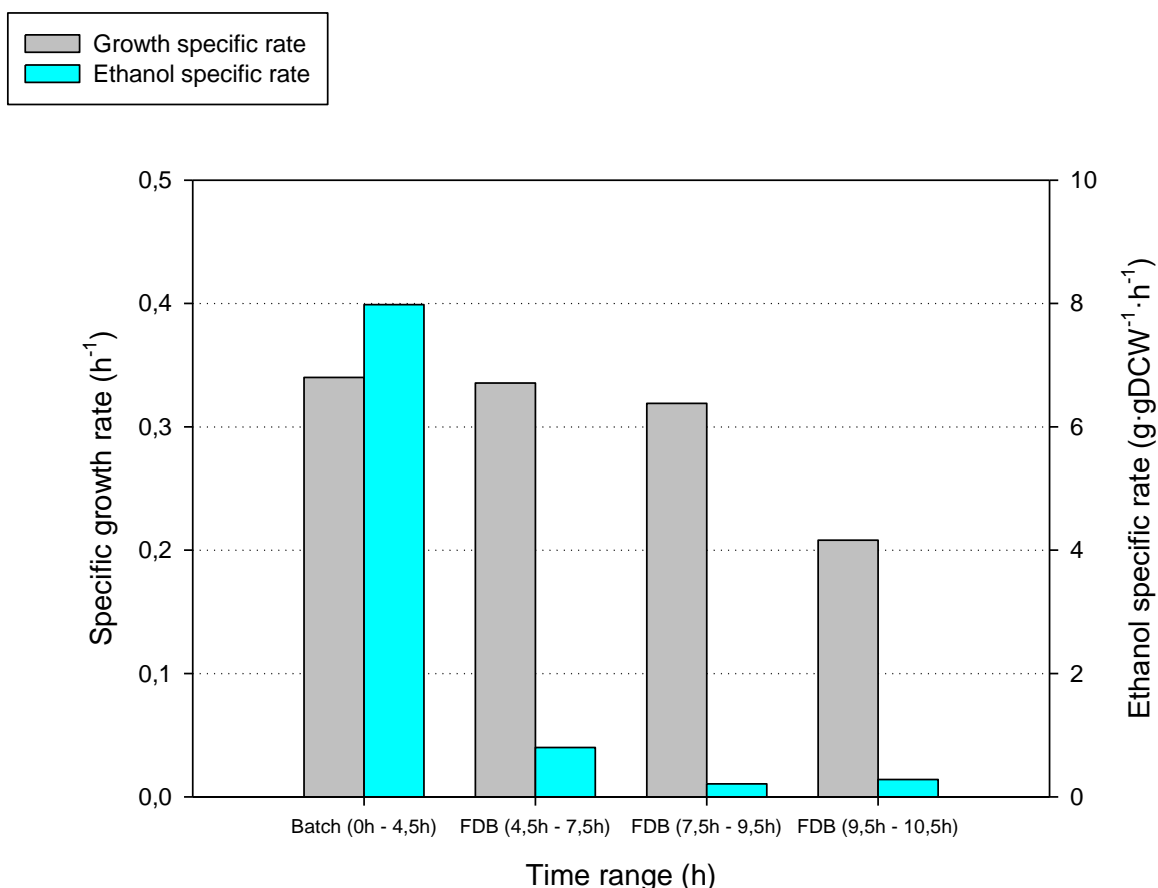


Figure 8-11 Evolution of the specific growth rate and the ethanol specific production rate in the non-metabolic fed-batch strategy.

It is important to highlight that this conditioned metabolic behaviour was already achieved in the previous section, regarding the preprogrammed exponential strategy. However, as shown in **Figure 8-12**, even if the decrease in the ethanol produced was a success, it was not possible to keep the optimal growth rate in the non-inhibition phase (5h-9h), as shown in **graph A of Figure 8-12**. In addition, as shown in **graph A of Figure 8-12**, it was possible to decrease the ethanol production at the same level as the exponential one during the entire course of the fed-batch phase (4,5h - 12h). Moreover, even if the same results as the exponential in relation with ethanol production and grant the optimal growth inhibition were observed, they were accomplished without relaying in the metabolic studies previously carried out (chapter 4). However, it must be remarked that the metabolic studies were necessary in order to understand why the carbon metabolism was changing depending on the environmental conditions

Therefore, the non-metabolic strategy is more fitted to be used as a feeding profile than the exponential one.

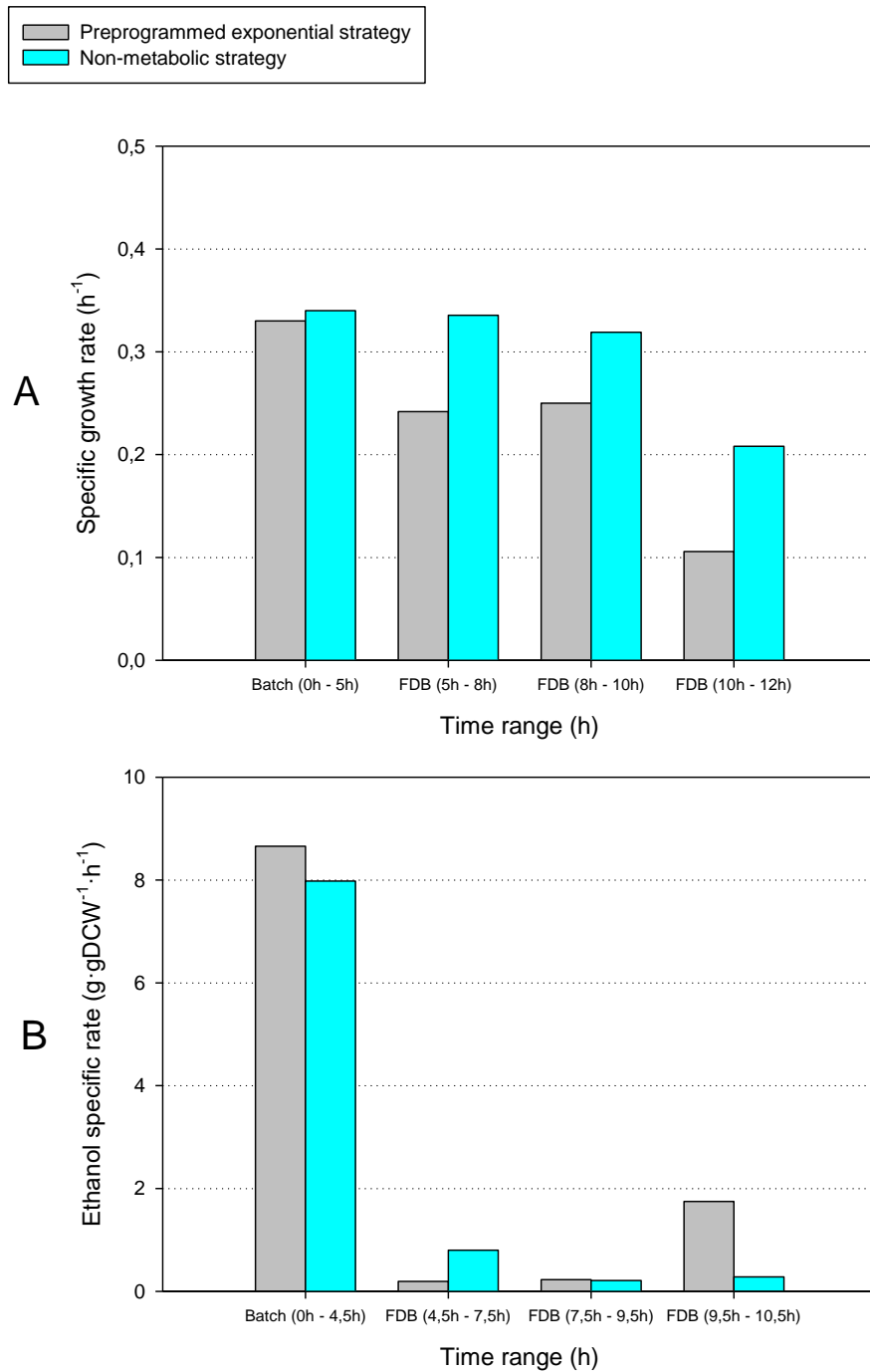


Figure 8-12. Comparison between the evolution of the specific growth rate and the ethanol specific production rate in the fed-batch culture when preprogrammed exponential and the non-metabolic strategies were carried out.

The difference between the two strategies mentioned above were related to the adaptability of the feeding algorithm to fulfil the metabolic requirements to get the optimal growth and, in addition, its capacity for predicting the culture's growth during the fed-batch phase.

As shown in **Figure 8-13**, the feeding flow profile generated by the preprogrammed exponential strategy differed a lot in regard with the non-metabolic strategy. The difference in the initial

steps was the responsible for the decrease in the growth rate when the preprogrammed exponential profile was used, while a higher flow in the non-metabolic one granted the optimal growth rate from the very beginning, taking into account the culture's carbon requirements. Moreover, the non-metabolic strategy was able to adapt the feeding flow to the growth inhibition conditions that appeared at the end of the experiment, while the preprogrammed strategy was not able to do it and consequently glucose was accumulated.

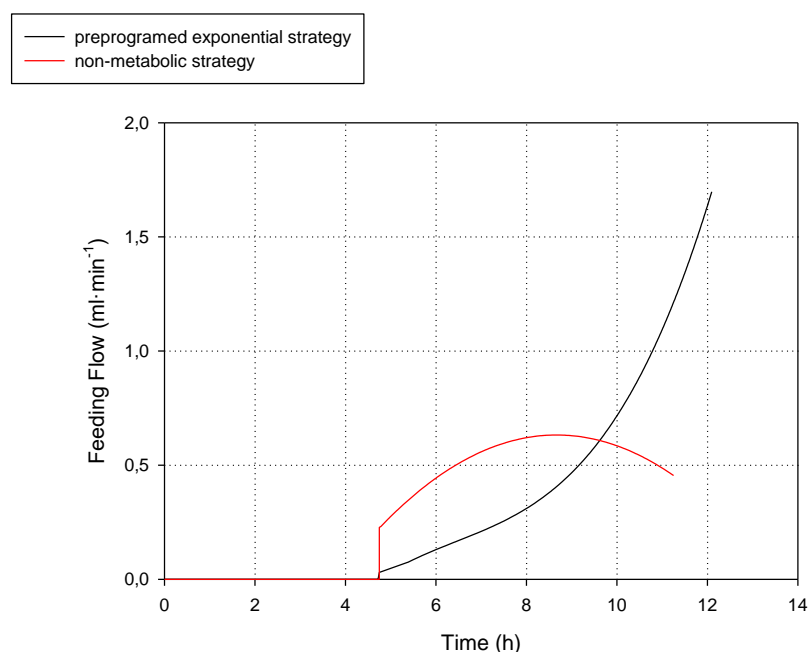


Figure 8-13. Comparison between the feeding flow profiles of the preprogrammed exponential strategy (black) and the non-metabolic one (red).

It can be stated that in the case of having an expression platform which carbon metabolism depended on the environmental conditions, such as the one that has been described in this chapter, the feeding profile should not be based on the preprogrammed exponential strategy, this should be based on the non-metabolic strategy used in this section.

To conclude with, and taking into consideration all the pros and cons regarding the design of a fed-batch strategy, the best strategy should be the non-metabolic strategy, due to the fact that it does not require any batch parameters or previous knowledge of the cell strain.

Even if the increase in the biomass productivity was only an 8% when the non-metabolic strategy was used instead of the preprogrammed exponential one, the non-requirements needed for performing this strategy should be the main reason behind why the non-metabolic strategy was better than the exponential preprogrammed one. Moreover, it was a fully automated strategy

without relying on any other calculations. Therefore, it was a friendly-implemented, non – worker dependent feeding strategy.

To sum up, as shown in **Table 8-6**, several strategies were developed and tested in order to increase the biomass productivity in *S. cerevisiae*-based processes. The media fortification promoted an increase in the biomass concentration of 3,43-fold in regard with the reference batch culture, although high concentrations of ethanol were produced due to the non-regulation of the carbon metabolism.

Table 8-6 General overview for all the data from the different strategies carried out in this chapter.

	Batch	Fortified Batch	FDB- preprogrammed exponential	FDB - non metabolic control
Achieved biomass (gDCW·L ⁻¹)	1,60	5,50	5,91	5,62
μ (h ⁻¹)	0,36	0,37	0,33	0,34
Ethanol generated (g·L ⁻¹)	5,92	36,86	16,91	16,49
Glycerol generated (g·L ⁻¹)	0,48	3,24	0,74	0,93
$Y_{x/glc}$ (gDCW·g _{glucose} ⁻¹)	0,10	0,06	0,13	0,12
$Y_{eth/x}$ (g _{ethanol} ·gDCW ⁻¹)	3,94	6,70	2,69	2,99
$Y_{gly/x}$ (g _{glycerol} ·gDCW ⁻¹)	0,4	0,6	0,12	0,16

In order to reach higher biomass productivities, while optimizing the conversion of glucose to biomass, two fed-batch strategies were tested. These strategies were based on two feeding profiles; one that was dependent on metabolic parameters, while the other on was independent to the metabolic parameters. The two strategies compared with the fortified batch results did not increase maximum the biomass concentration obtained as observed in **Table 8-6**.

However, there is a critical point in relation with designing feeding strategies, the necessity of performing previous experiments in order to determine and characterize how the carbon metabolism behaved for a certain strain. This issue is related to the design of the preprogrammed exponential feeding in order to find the optimal metabolic condition where glucose should be converted towards biomass while producing as less ethanol as possible. Whereas, the non-metabolic strategy was able to perform the same results without any previous experimental knowledge and full automated.

After this point and once the biomass productivity was increased, the next section would be focused on applying this feeding strategy to a producer expression platform. Therefore, the development of GFP producer *S. cerevisiae* and its bioprocess characterization will be described in the following section.

8.5 Results (III) - Study of the induction phase of a recombinant protein

As it was performed in the E.coli bioprocess chapter (**chapter 7**) , the objective of this section is to check if the non-metabolic algorithm for the feeding media addition described before is able to follow the metabolic behavior of *S. cerevisiae* when an induction phase is being carried out during a fed-batch strategy. The model protein chosen for this study was the fluorescent report protein known as GFP due to its facility to be analyzed (Gerdes & Kaether, 1996). The reference strain that will be used in this section is an *S. cerevisiae* that express the model protein GFP. In contrast of what was performed in the induction studies in regard with E. coli bioprocess, in this section the use of an antibiotic will be avoided.

As antibiotics will be not used, another way to grant the desired genetic background during the GFP production will be applied. The genetic background can be maintained using two types of selection pressure: using an antibiotic or using an auxotrophy. The difference between them lies in the protein that is expressed along with the model protein. In the case of an antibiotic, the protein confer resistance against the antibiotics attack. For instance, expressing a beta-lactamase in order to acquire resistance against ampicillin. While an auxotrophy, the protein confer the capacity to synthesis an essential metabolite. For example, expressing a beta-galactosidase in order to be able to grown consuming lactose as a unique carbon source.

In the case of this study, an auxotrophic *S. cerevisiae* (*S. cerevisiae INVCS1 - GFP*) was used as a reference strain. This strain was derived from a auxotrophic *S. cerevisiae INVCS1* (which was unable to synthesis the essential molecules histidine, tryptophan, leucine and uracil) that was transformed with a plasmid that conferred the expression of the model protein (GFP) along with the Imidazolglycerol-phosphate dehydratase (HIS3) which is involved in the histidine biosynthesis (Struhl, 1979).

As observed in section 8.7.3, this plasmid contained the HIS3 gene along with two inducible promoters, GAL1 and GAL10 in opposing orientation. The model protein (GFP) was under the

regulation of GAL10 while the other promoter was empty. Regarding the induction conditions, both promoters were repressed by the presence of glucose and induced by the galactose (Technologies, 2011). It has to be taken into consideration that the GFP did not have the signal peptide required for its secretion to the media; as a result, GFP was not be secreted. The decision of not using *S. cerevisiae* as a secretion platform in this study is because a non-secreted protein can be easily measured because is proportional to the biomass concentration.

Therefore, in the following section, the characterization of the auxotrophic *S. cerevisiae* *INCVs1-GFP* will be carried out using a batch strategy in order to be used as a reference in the induction fed-batch.

8.5.1 The auxotrophic GFP-producer *S. cerevisiae*.

S. cerevisiae *INCVs1-GFP* was cultured in a 2L bioreactor where the environmental conditions were controlled in order to get the optimal growth rate and the appropriate physiological parameters. Moreover, glucose was set as the media's main carbon source along with the addition of the three auxotrophies: tryptophan, leucine and uracil. Regarding the control variables used and the environmental conditions, they are described in **section 8.7.4** and in **section 8.7.8**, respectively.

In order to describe the core metabolism, a non-inductive culture where GFP was not expressed was carried out. However, even if the batch culture was not induced, a sample at the end of the experiment was induced by galactose.

As shown in **graph A from Figure 8-14** and in **Table 8-7**, when *S. cerevisiae* *INCVs1 - GFP* was cultured, it had a growth rate of $0,25 \text{ h}^{-1}$ and $0,88 \text{ gDCW}\cdot\text{L}^{-1}$ of biomass was produced together with $6,11 \text{ g}\cdot\text{L}^{-1}$ of ethanol and $0,44 \text{ g}\cdot\text{L}^{-1}$ of glycerol while $11,57 \text{ g}\cdot\text{L}^{-1}$ of glucose were consumed. Related to the profile of CER and OUR, as shown in **graph B from Figure 8-14**, a diauxic condition were observed at 5h from the beginning of the culture due to the decrease in the CER and OUR while glucose was not depleted. As a result, the variation of both profile was related to the limitation of other compound form the media instead of glucose. If it is taken into consideration that histidine was only produced though the expression of *HIS3*, a media compound instead of glucose became limiting owing to other metabolic routes were maximized in order to growth at the optimal rate for the given environmental conditions. For example, it could hypothesized that the unknown compound could be a vitamin owing to there are studies that showed a growth

adaptation when a vitamin was depleted from culture's media (H. Leonian & Greene Lilly, 1942) (Perli et al., 2020).

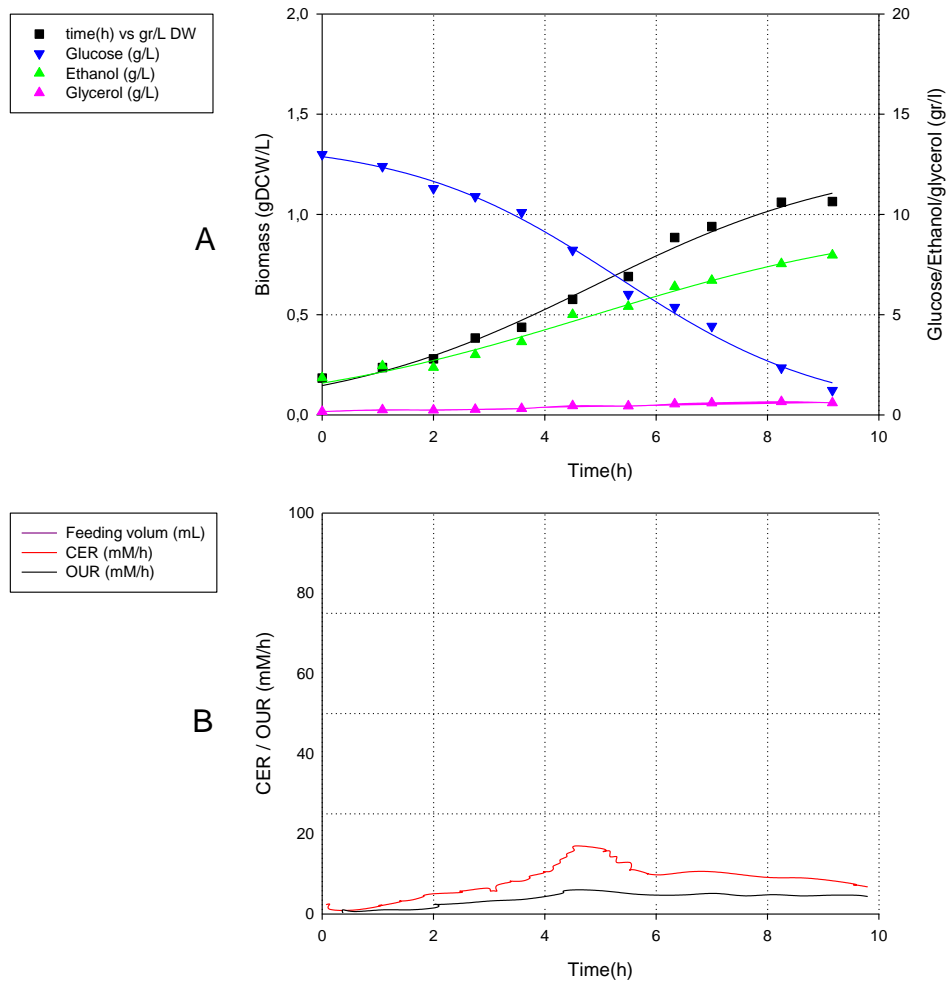


Figure 8-14 Profile of A) off-line variables such as Biomass (■), glucose (▼), ethanol (▲), and glycerol (▲) and B) on-line variables such as CER (—), OUR (—).

Table 8-7 Main parameters for the batch culture using the *S. cerevisiae* INCVs1 - GFP

μ (h ⁻¹)	0,25
Glucose consumption (g·L ⁻¹)	11,77
Ethanol generation (g·L ⁻¹)	6,11
Glycerol generation (g·L ⁻¹)	0,44
Biomass achieved (gDCW·L ⁻¹)	0,88
RQ	1,89

Regarding the sample extracted at the end of the experiment, as it was described in the plasmid definition, it was required a media change in order to eliminate all the glucose due to it is highly repressible by glucose. After that, a new media whose carbon source was lactose (the completed composition is described in section 8.7.4) was used to induce the GFP production in an erlenmeyer. In order to determine if the GFP was expressed, a fluorometric microscope was used to determine the fluorescence of GFP, while a contrast phase microscope was used to assure that the GFP was expressed within the cells. To conclude, as shown in **Figure 8-15**, the GFP was correctly produced.

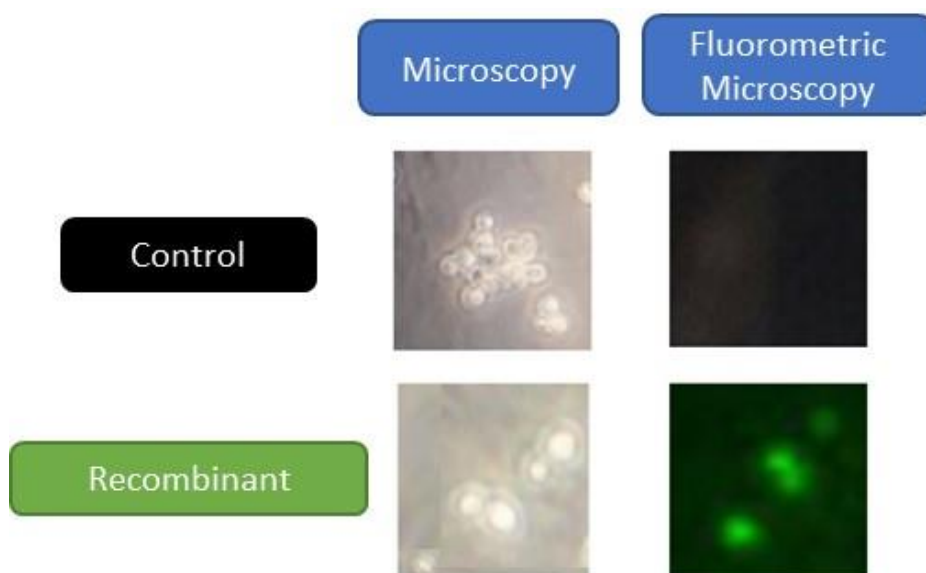


Figure 8-15 Results for the induction of the recombinant strain (INCVs1 – GFP) where the contrast phase Microscope and Fluorometric microscope were presented as a comparison between the control strain INCVs1 and recombinant strain INCVs1 – GFP in order to compare the GFP production when both strains were induced with Galactose.

However, a problematic was highlighted when *S. cerevisiae* INCVs1 – GFP was compared with *S. cerevisiae* wild type. As shown in **Table 8-8**, there is a difference of 30 % in the specific growth rate if *S. cerevisiae* INCVs1 – GFP is compared with the wild type one. Moreover, *S. cerevisiae* INCVs1 – GFP presented a non-optimized carbon metabolism where the conversion of glucose to ethanol was increased from $0,37 \text{ g}_{\text{ethanol}} \cdot \text{g}_{\text{glucose}}^{-1}$ to $0,52 \text{ g}_{\text{ethanol}} \cdot \text{g}_{\text{glucose}}^{-1}$.

This metabolic behaviour might indicate that the use of more than one auxotrophies in the reference strain might provoked a metabolic burden that concluded with a reduction in the specific growth rate along with the waste of the carbon source due to high ethanol production.

Table 8-8 Comparison between the physiological parameters of *S. cerevisiae* INCVs1 – GFP and *S. cerevisiae* Wild type

	<i>S. cerevisiae</i> INCVs1 - GFP	<i>S. cerevisiae</i> Wild type
μ (h ⁻¹)	0,25	0,36
$Y_{eth/gluc}$ (g _{ethanol} · g _{glucose} ⁻¹)	0,52	0,37
$Y_{gly/gluc}$ (g _{glycerol} · g _{glucose} ⁻¹)	0,04	0,03

In order to solve the “auxotrophic issue” presented in this section, two approaches will be described:

The first approach is based on the use a *S. cerevisiae* strain that had solely one auxotrophy. This strain should be transformed with a plasmid expressing the model protein along with the protein related to the auxotrophy. Moreover, the plasmid should integrate more than one copy of this protein. For example, using a *S. cerevisiae* auxotroph for histidine as a reference strain for producing GFP using a plasmid that integrate multiple copies of the HIS3 gene.

The second one is focused on using antibiotics as a selection marker instead of auxotrophies because the use of antibiotics should not have any interference with the carbon metabolism and the specific growth rate. For instance, transforming a *S. cerevisiae* wild type with a plasmid expressing the GFP along with the resistance to Zeozin.

The second approach was selected as a solution to the limiting-growth features of the *S. cerevisiae* INCVs1-GFP used in this work to express GFP. However, due to limitation in the time need to perform it, only the construction of the plasmid required for its realization was hypothesized.

The second approach was based on the use of *S. cerevisiae* wild type as a reference strain to produce GFP under the regulation of a plasmid that expressed the model protein along with a resistance against an antibiotic. In this case, the antibiotic that was proposed was blasticidin and the plasmid that confers its resistance is the same proposed in this section with a modification. The HIS3 gene should be replaced by the blasticidin resistance. As a result, an inducible GFP plasmid should be obtained whose genetic background will be assured by the blasticidin resistance.

8.6 Discussion and conclusions

As stated at the beginning of the chapter, the final goal was to improve the biomass production in bioprocesses based on *S. cerevisiae*, to enhance the biomass volumetric productivity. Therefore, several culture strategies were tested. These strategies were designed following two ideas: the change of the environmental conditions or the modification the feeding control system during the process.

The first approach done consisted in changing the environmental conditions by means of the optimization of the media's composition. Regarding this approach, a new batch media was designed, based on increasing the concentration of all media components until a growth inhibition was reached. As a result, this new media, called fortified media, increased the biomass productivity 1,51-fold in comparison with the reference batch.

For a further biomass production, the next step was focused on using different fed-batch strategies, where the objective was to further increase the biomass productivity. It is important to highlight two facts about the design of the fed-batch strategies:

- The first was that the studies performed in the metabolic chapter of *S. cerevisiae* were used in order to calculate the specific consumption rate of glucose in order to obtain the maxim conversion of glucose to biomass and
- The second one was related with the fed-batch strategies, that they will be desirable performed at the allowed maximum growth rate taking into consideration the environmental conditions.

The first approach was based on a fed-batch strategy where the culture's growth was estimated as an exponential function. As a result, the biomass productivity of the process increased 1,07-fold in comparison with the fortified batch carried out. It is important to remark that the use of the metabolic data obtain in **chapter 4** reduced the ethanol specific rate in a 56%, by means of optimizing the conversion of glucose towards biomass. Coupled with the metabolic distribution occurred between the transition of the batch phase to the fed-batch phase, another metabolic feature was observed, the incapability of the carbon metabolism to keep a steady metabolic phase during the course of the feeding addition. Consequently, glucose was accumulated and then ethanol was produced.

The incapability of predicting changes of the carbon metabolism depending on the environmental conditions observed lead to choose a feeding strategy where the feeding addition must take into consideration unexpected changes in the metabolic behavior. As it was described in the *E. coli* **chapter 8**, the non-metabolic strategy was selected owing to this strategy was not affected by a change in the metabolic behavior, although the results obtained were almost the same as the previous fed-batch strategy where the biomass reached values around $6 \text{ gDCW}\cdot\text{L}^{-1}$ in both cases. Even if there was not a high difference between both fed-batch strategies used, it is important to highlight that the non-metabolic strategy was able to carry out the optimal metabolic conditions during the course of the experiment without using any previous data. That is very important from a practical point of view, because no human actions are needed using the last strategy; for instance, determining automatically the starting point for feeding the culture when batch phase has been finished or adapting the media addition depending on the metabolism of the strain.

Once the optimal feeding strategy was selected, the next experimental goal was to carry out an induction experiment with the *S. cerevisiae* in order to evaluate how the feeding strategy might affect the protein production. For this purpose, a GFP producer *S. cerevisiae* was used as a reference. In this case, the *S. cerevisiae* *INCVs1-GFP*. Due to the growth limitation and the improvement of the production of ethanol owing to the auxotrophies expressed in *S. cerevisiae* *INCVs1-GFP*, the auxotrophic study was abandoned even if the GFP was correctly expressed. Then, another approaches were proposed. The elimination of the other auxotrophies expressed in *S. cerevisiae* *INCVs1-GFP* and as a result, only the auxotrophy regulated by the plasmid should be expressed. In this case, eliminating the auxotrophies for tryptophan, leucine and uracil while the histidine one will be expressed. The histidine auxotrophy will be used as a selection marker due to the plasmid should express the protein model along with the gene responsible for the histidine biosynthesis. On the other hand, the solution might be related to use antibiotics instead of auxotrophic markers. The use of antibiotics was selected as the solution to solve the growth issue of the expression platform used for producing GFP due to the limited capacity of this study in the molecular biology field.

On this basis, the expression of GFP using antibiotics was described using as a reference *S. cerevisiae* wild type and using the previously described plasmid with a modification. The change in the *HIS3* gene required for an auxotrophic marker with the resistance against blasticidin. Therefore, the expression of GFP should be carried out by a the induction of a *S. cerevisiae* wild type with galactose while blasticidin is used as a selection marker.

It is important to remark that even if the induction studies were not carried out, the increase of the biomass productivity by means of optimizing the carbon conversion towards biomass was achieved and increasing the biomass concentration. Moreover, it must not be forgotten that the fed-batch strategy used was able to bestow the optimal growth rate depending on the environmental conditions without previous data.

8.7 Materials and methods

8.7.1 *S. cerevisiae* Wildtype and cell maintenance

The strain used in the bioprocess optimization from the batch definition until the fed-batch characterization was *S. cerevisiae* wild type described in the **chapter 4**.

Cell line maintenance in petri dishes and inoculum were performed using the complex media YPD (whose composition is described in **section 8.7.4**).

8.7.2 *S. cerevisiae* INVCS1

S. cerevisiae INVCS1 is one of the most used *S. cerevisiae* strains for recombinant protein production when the selection marker used is an auxotrophic one. In this work, *S. cerevisiae* INVCS1 has solely been used in the induction section and presented 4 auxotrophies (uracil, histidine, leucine and tryptophan). It has the following genotype: *MATa his3D1 leu2 trp1-289 ura3-52 MAT his3D1 leu2 trp1-289 ura3-52*.

8.7.3 *S. cerevisiae* INVCS1 -GFP

In this work, *S. cerevisiae* INVCS1 -GFP has solely been used in the induction section and presented 3 auxotrophies (uracil, leucine and tryptophan). It has the following genotype: *MATa his3D1 leu2 trp1-289 ura3-52 MAT his3D1 leu2 trp1-289 ura3-52*.

The generation of the *S. cerevisiae* INVCS1 -GFP was carried out by means of the transformation of the *S. cerevisiae* INVCS1 used during all the experiments with the plasmid pESC_HIS_eGFP(GAL1) described at **section 8.7.3.1**. It is important to remark that the transformation of this strain was performed in another work.

8.7.3.1 Plasmid pESC_HIS_eGFP(GAL1)

The pESC_HIS_eGFP expression vector is a plasmid that used as a base vector a pESC Yeast Epitope Tagging Vector. This expression vector contains the GAL1 and GAL10 yeast promoters in opposing orientation and the auxotrophic marker gene (HIS3) as shown in **Figure 8-16**.

As shown in **Figure 8-17**, the eGFP gene (enhanced GFP) was introduced into the base vector under the control of the repressible promoter GAL1, moreover, regarding the GAL10 promoter, there was not a gene under its control, it was an empty space. Moreover, both promoters were induced by galactose and repressed by glucose.

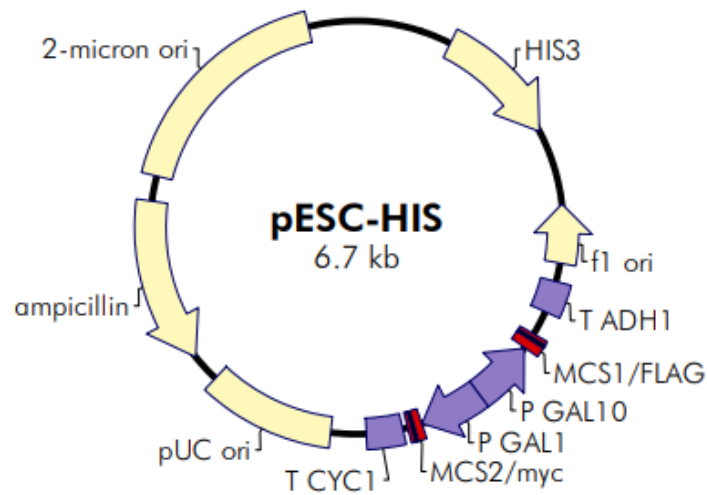


Figure 8-16 Map of pESC_HIS, adapted from Agilent (Technologies, 2011)

Thereupon, the media composition used in the induction section are described below.

- Solid culture *S. cerevisiae* INVCs1: the media composition is described in **chapter 4 section 4.9.3**
- Solid culture *S. cerevisiae* INVCs1 -GFP: the media composition is described in **chapter 4 section 4.9.3** supplemented with 2 mg·L⁻¹ of kanamycin sulphate.
- *S. cerevisiae* INVCs1 media: the media was prepared using the batch media composition described in **chapter 4 section 4.9.3**, and then, it was supplemented with a chemical defined mix (Drop out mix without histidine,(Aldrich, 2014)) whose final composition in the media is described in
-
-
- Table 8-12. For the final preparation, it was required the addition of 1,92 g of Drop out mix and 76 mg of histidine for each litre of the batch media prepared.
- *S. cerevisiae* INVCs1 -GFP media: the media composition is the same as the *S. cerevisiae* INVCs1 one without adding histidine and supplementing with 2 mg·L⁻¹ of kanamycin sulphate.

Table 8-9 Composition of media used in batch cultures strategy.

Compound	Concentration
Glucose H ₂ O	27,5 g/L
KH ₂ PO ₄	9 g/L
(NH ₄) ₂ SO ₄	17,23 g/L
MgSO ₄ 7H ₂ O	3,5 g/L
CaCl ₂ 2H ₂ O	5,12 mg·L ⁻¹
ZnSO ₄ 7H ₂ O	10,24 mg·L ⁻¹
MnCl ₂ 4H ₂ O	0,5 mg·L ⁻¹
CuSO ₄ 5H ₂ O	0,78 mg·L ⁻¹
CoCl ₂ 6H ₂ O	0,86 mg·L ⁻¹
FeSO ₄ 7H ₂ O	3,84 mg·L ⁻¹
Na ₂ MoO ₄ 2H ₂ O	0,56 mg·L ⁻¹
Folic acid	0,01 mg·L ⁻¹
Biotin	0,6 mg·L ⁻¹
Calcium penthonate	13,2 mg·L ⁻¹
Nicotinc Acid	12 mg·L ⁻¹
Myo-Inositol	300 mg·L ⁻¹

Thiamine HCl	12 mg·L ⁻¹
Pyridoxal-HCl	12 mg·L ⁻¹
Aplha-aminobenzoic acid(GABA)	2,4 mg·L ⁻¹

Table 8-10 Composition of media used in fortified batch culture strategy

Compound	Concentration
Glucose	100 g/L
(NH ₄) ₂ SO ₄	10 g/L
KH ₂ PO ₄	1 g/L
MgSO ₄	0,5 g/L
NaCl	0,1 g/L
CaCl ₂	0,1 g/L
Biotine	0,01 mg/L
Calcium penthonate	2 mg/L
Folic acid	0,01 mg/L
Myo-Inositol	10 mg/L
Nicotinic acid	2 mg/L
Pyridoxal-HCl	2 mg/L
Thiamine-HCl	2 mg/L
Aplha-aminobenzoic acid(GABA)	2,4 mg·L ⁻¹
H ₃ BO ₃	2,5 mg/L
CuSO ₄	0,2 mg/L
KI	0,5 mg/L

FeCl ₃	1 mg/L
MgSO ₄	2 mg/L
Na ₂ MoO ₄	1 mg/L
ZnSO ₄	2 mg/L

Table 8-11 Composition of media used as a feeding solution in all the fed- batch culture strategy.

Compound	Concentration
Glucose H ₂ O	275 g·L ⁻¹
KH ₂ PO ₄	4,5 g·L ⁻¹
Na ₂ SO ₄	0,14 g·L ⁻¹
K ₂ SO ₄	1,75 g·L ⁻¹
MgSO ₄ 7H ₂ O	2,56 g·L ⁻¹
CaCl ₂ 2H ₂ O	25,6 mg·L ⁻¹
ZnSO ₄ 7H ₂ O	0,3 mg·L ⁻¹
MnCl ₂ 4H ₂ O	6,6 mg·L ⁻¹
CuSO ₄ 5H ₂ O	6 mg·L ⁻¹
CoCl ₂ 6H ₂ O	150 mg·L ⁻¹
FeSO ₄ 7H ₂ O	6 mg·L ⁻¹
Na ₂ MoO ₄ 2H ₂ O	6 mg·L ⁻¹
Biotin	1,2 mg·L ⁻¹
Calcium penthonate	51,2 mg·L ⁻¹

Nicotinc Acid	2,5 mg·L ⁻¹
Myo-Inositol	3,9 mg·L ⁻¹
Thiamine HCl	4,3 mg·L ⁻¹
Pyridoxal-HCl	19,2 mg·L ⁻¹
Aplha-aminobenzoic acid(GABA)	2,8 mg·L ⁻¹

Table 8-12 Final media's composition when the required amount of commercial DROP-OUT media supplements were used.

Compound	Concentration
Adenine	18 mg·L ⁻¹
p-Aminobenzoic acid	8 mg·L ⁻¹
Leucine	380 mg·L ⁻¹
Alanine	76 mg·L ⁻¹
Arginine	76 mg·L ⁻¹
Asparagine	76 mg·L ⁻¹
Aspartic acid	76 mg·L ⁻¹
Cysteine	76 mg·L ⁻¹
Glutamic acid	76 mg·L ⁻¹
Glutamine	76 mg·L ⁻¹
Glycine	76 mg·L ⁻¹
myo-Inositol	76 mg·L ⁻¹
Isoleucine	76 mg·L ⁻¹
Lysine	76 mg·L ⁻¹
Methionine	76 mg·L ⁻¹
Phenylalanine	76 mg·L ⁻¹
Proline	76 mg·L ⁻¹
Serine	76 mg·L ⁻¹
Threonine	76 mg·L ⁻¹
Tryptophan	76 mg·L ⁻¹
Tyrosine	76 mg·L ⁻¹
Uracil	76 mg·L ⁻¹
Valine	76 mg·L ⁻¹

8.7.5 Biomass dry cell weight (DCW) determination

The biomass dry cell weight of both *S. cerevisiae* was determined as described in **chapter 4** section 4.9.7

8.7.6 Metabolite determination

All the metabolite determination carried out in this chapter in regard with its protocols and methodology is described in section 4.9.8 of **chapter 4**.

8.7.7 Culture systems

For small scale or inoculum cultures have been performed in a Erlenmeyer of different volumes (25, 50, 100 , 250 and 1000 ml) cultured at 30°C and 130 rpm.

The culture in petri plates was used as a starter solid culture support. Moreover, it was incubated at 30°C using an orbital incubator (Shaker orbital Incubator, Sanyo).

8.7.8 Bioreactor cell culture

The stirred-tank bioreactor used in the present study was a commercial bioreactor (Biostat B, from Sartorius Stedim Biotech, Germany) with 2L-cylindrical jacketed vessel, equipped with probes and control systems for pH, D.O. (relative oxygen partial pressure) and temperature, and a stirred with two Rushton impellers.

The control systems of the before mentioned variables are described below:

- Dissolved oxygen concentration was monitored with a polarographic probe (Oxyferm, Hamilton), and maintained at 30% of saturation by means of an aeration flow using a spargger flow of 0,15 VVM together with a cascade control system based on a stirring control system and a gas mixing unit.
- Temperature was maintained at 30°C by switch between a heat exchanger when heat was needed and with a cooling water system when cold was needed.

- pH was measured with a standard electrode (EasyFerm Plus, Hamilton), and it was maintained at 5,5 using a HCl 2M (Panreac) addition, and a subsequently addition of NaOH (15% v/v) (Panreac).

The working volume for the batch cultures was 2L, and the initial volume for the fed-batch culture was 1L batch.

8.7.9 Oxygen uptake rate (OUR) and Carbon exchange rate (CER)

The methodology to calculate OUR and CER is described in **chapter 3** section 3.8.8

8.7.10 Specific rate calculations in batch cultures

The methodology to calculate the specific rate in batch cultures is described in **chapter 3** section 3.8.9

8.7.11 Fed-batch strategy

The methodology to calculate feeding profiles is described in **chapter 7** section 7.6.12

8.7.12 Fed-batch strategy based on biomass estimation by pre-programmed exponential

The calculation for the biomass estimation used for the preprogrammed exponential strategy been already described in **chapter 7** section 7.6.13. Moreover, its practical methodology is described in **chapter 7** section 7.6.11.1.

8.7.13 Non-metabolic fed-batch strategy

The methodology to carry out the non-metabolic fed-batch strategy is described in **chapter 7** section 7.6.11.2

8.7.14 MFCS/win. Software for Data Acquisition, Monitoring and Control

All the MFCS protocols and methodology in order to calculate feeding profile for fed-batch and perfusion strategies related to the use of the software MFCS are described in **chapter 7** section 7.6.11.

8.7.15 Statistics

Duplicates for each culture conditions were performed, but only one of the two duplicate experiment is presented in the Results section. Since the runs have not performed in parallel (due to equipment limitations), sampling time do not coincide, and also other parameters may vary as the cell seeding density.

8.8 References

- Aldrich, S. (2014). *Drop-out Media Supplements*.
- Butler, J. N. (1991). Chapter 2 - Solution without gas phase. In *Carbon dioxide equilibria and their applications* (pp. 21–23).
- Costenoble, R., MÃ¼ller, D., Barl, T., van Gulik, W. M., van Winden, W. A., Reuss, M., & Heijnen, J. J. (2007). 13 C-Labeled metabolic flux analysis of a fed-batch culture of elutriated *Saccharomyces cerevisiae*. *FEMS Yeast Research*, 7(4), 511–526. <https://doi.org/10.1111/j.1567-1364.2006.00199.x>
- Das, M., Koike, M., & Reed, L. (1961). On the role of thiamine pyrophosphate in oxidative decarboxylation of alpha-keto acids. *Proceedings of the National Academy of Sciences of the United States of America*, 47, 753–759. <https://doi.org/10.1073/pnas.47.6.753>
- Dewasme, L., Richelle, A., Dehottay, P., Georges, P., Remy, M., Bogaerts, P., & Vande Wouwer, A. (2010). Linear robust control of *S. cerevisiae* fed-batch cultures at different scales. *Biochemical Engineering Journal*, 53(1), 26–37. <https://doi.org/10.1016/j.bej.2009.10.001>
- Gerdes, H.-H., & Kaether, C. (1996). Green fluorescent protein: applications in cell biology. *FEBS Letters*, 389(1), 44–47. [https://doi.org/10.1016/0014-5793\(96\)00586-8](https://doi.org/10.1016/0014-5793(96)00586-8)
- H. Leonian, L., & Greene Lilly, V. (1942). The Effect of Vitamins on Ten Strains of *Saccharomyces cerevisiae*. *American Journal of Botany*, 29(6), 459–464. <https://www.cceol.com/search/article-detail?id=306593>
- Hjersted, J. L., & Henson, M. A. (2008). Optimization of Fed-Batch *Saccharomyces cerevisiae* Fermentation Using Dynamic Flux Balance Models. *Biotechnology Progress*, 22(5), 1239–1248. <https://doi.org/10.1021/bp060059v>
- Hou, J., Tyo, K., Liu, Z., Petranovic, D., & Nielsen, J. (2012). Engineering of vesicle trafficking improves heterologous protein secretion in *Saccharomyces cerevisiae*. *Metabolic Engineering*, 14(2), 120–127. <https://doi.org/10.1016/j.ymben.2012.01.002>
- Ikonomou, L., Schneider, Y.-J., & Agathos, S. N. (2003). Insect cell culture for industrial production of recombinant proteins. *Applied Microbiology and Biotechnology*, 62(1), 1–20. <https://doi.org/10.1007/s00253-003-1223-9>
- Kinch, M. S. (2015). An overview of FDA-approved biologics medicines. *Drug Discovery Today*, 20(4), 393–398. <https://doi.org/10.1016/j.drudis.2014.09.003>
- Larsson, C., Lidén, G., Niklasson, C., & Gustafsson, L. (1991). Calorimetric control of fed-batch cultures of *Saccharomyces cerevisiae*. *Bioprocess Engineering*, 7(4), 151–155. <https://doi.org/10.1007/BF00387410>
- Maiorella, B., Blanch, H. W., & Charles, R. (1983). By-Product Inhibition Effects on Ethanol Fermentation by *Saccharomyces cerevisiae*. *Biotechnology*, XXV, 103–121.
- Mattanovich, D., Branduardi, P., Dato, L., Gasser, B., Sauer, M., & Porro, D. (2012). *Recombinant Protein Production in Yeasts* (pp. 329–358). https://doi.org/10.1007/978-1-61779-433-9_17
- Mendoza-Vega, O., Sabatié, J., & Brown, S. W. (1994). Industrial production of heterologous proteins by fed-batch cultures of the yeast *Saccharomyces cerevisiae*. *FEMS Microbiology Reviews*, 15(4), 369–410. [https://doi.org/10.1016/0168-6445\(94\)90070-1](https://doi.org/10.1016/0168-6445(94)90070-1)
- Nielsen, J. (2013). Production of biopharmaceutical proteins by yeast. *Bioengineered*, 4(4), 207–211. <https://doi.org/10.4161/bioe.22856>
- Novozymes. (2017). *Yeast Micronutrient and Growth Factor Requirements* (pp. 2–5).

- Perli, T., Wronska, A. K., Ortiz-Merino, R. A., Pronk, J. T., & Daran, J. M. (2020). Vitamin requirements and biosynthesis in *Saccharomyces cerevisiae*. *Yeast*, 37(4), 283–304. <https://doi.org/10.1002/yea.3461>
- Pham, H. T. B., Larsson, G., & Enfors, S.-O. (1998). Growth and energy metabolism in aerobic fed-batch cultures of *Saccharomyces cerevisiae*: Simulation and model verification. *Biotechnology and Bioengineering*, 60(4), 474–482. [https://doi.org/10.1002/\(SICI\)1097-0290\(19981120\)60:4<474::AID-BIT9>3.0.CO;2-J](https://doi.org/10.1002/(SICI)1097-0290(19981120)60:4<474::AID-BIT9>3.0.CO;2-J)
- Plasson, C., Michel, R., Lienard, D., Saint-Jore-Dupas, C., Sourrouille, C., March, G. G. de, & Gomord, V. (2009). *Production of Recombinant Proteins in Suspension-Cultured Plant Cells* (pp. 145–161). https://doi.org/10.1007/978-1-59745-407-0_9
- Pronk, J., Yde steensma, H., & Van djiken, J. (1996). Pyruvate Metabolism in *Saccharomyces cerevisiae*. *Yeast*, 12(16), 1607–1633. [https://doi.org/10.1002/\(SICI\)1097-0061\(199612\)12:16<1607::AID-YEA70>3.0.CO;2-4](https://doi.org/10.1002/(SICI)1097-0061(199612)12:16<1607::AID-YEA70>3.0.CO;2-4)
- Renard, F., & Vande Wouwer, A. (2008). Robust adaptive control of yeast fed-batch cultures. *Computers & Chemical Engineering*, 32(6), 1238–1248. <https://doi.org/10.1016/j.compchemeng.2007.05.008>
- Struhl, K. (1979). *The Yeast his3 Gene*. Stanford university.
- Technologies, A. (2011). *Manual: pESC Yeast Epitope Tagging Vectors*. 217451, 1–21. <http://www.chem.agilent.com/Library/usermanuals/Public/217451.pdf%5Cnfile:///Users/Eser/Google Drive/Papers2/Articles/2011/Technologies/2011 Technologies.pdf%5Cnpapers2://publication/uuid/3BF4C99A-694B-407C-8DB8-04DCC0DF202B>
- Valentinotti, S., Srinivasan, B., Holmberg, U., Bonvin, D., Cannizzaro, C., Rhiel, M., & von Stockar, U. (2003). Optimal operation of fed-batch fermentations via adaptive control of overflow metabolite. *Control Engineering Practice*, 11(6), 665–674. [https://doi.org/10.1016/S0967-0661\(02\)00172-7](https://doi.org/10.1016/S0967-0661(02)00172-7)
- Viegas, C. A., Rosa, M. F., Correia, I. S., & Novais, J. M. (1989). Inhibition of yeast growth by octanoic and decanoic acids produced during ethanolic fermentation. *Applied and Environmental Microbiology*, 55(1), 21–28. <https://doi.org/10.1128/aem.55.1.21-28.1989>
- Villadsen, J., Nielsen, J., & Lidén, G. (2011). Chapter 3 - Elemental and Redox balance. In *Bioreaction Engineering Principles* (pp. 63–117).
- Wagner, J. M., & Alper, H. S. (2016). Synthetic biology and molecular genetics in non-conventional yeasts: Current tools and future advances. *Fungal Genetics and Biology*, 89, 126–136. <https://doi.org/10.1016/j.fgb.2015.12.001>
- Ward, O. P. (2012). Production of recombinant proteins by filamentous fungi. *Biotechnology Advances*, 30(5), 1119–1139. <https://doi.org/10.1016/j.biotechadv.2011.09.012>
- Wurm, F. M. (2004). Production of recombinant protein therapeutics in cultivated mammalian cells. *Nature Biotechnology*, 22(11), 1393–1398. <https://doi.org/10.1038/nbt1026>

9. Animal cell bioprocess definition

9.1 Nomenclature

mg DCW: Dry cell weight in milligram

$Y_{\text{lac/glc}}$: Yield between lactate produced and glucose consumed ($\text{gDCW}\cdot\text{g}^{-1}$)

$Y_{\text{biomass/glc}}$: Yield between biomass produced and glucose consumed ($\text{gDCW}\cdot\text{g}^{-1}$)

OUR: Oxygen uptake rate ($\text{mM}\cdot\text{h}^{-1}$)

FDB: Abbreviation for Fed- Batch strategy

DMEM: Dubdelco Modified Eagle's Media

q_{glucose} : Specific consumption rate of glucose ($\text{mmol}\cdot\text{gDCW}^{-1}\cdot\text{h}^{-1}$)

$X(t_0)$: Biomass concentration at time zero

$V(t_0)$: Volume of bioreactor at time zero

$C_{\text{glucose, feeding}}$: Glucose concentration of the addition solution used in the fed-batch strategies ($\text{mmol}\cdot\text{L}^{-1}$)

$C_{\text{glucose, in}}$: Metabolite m concentration in the perfusion's inlet flow ($\text{mmol}\cdot\text{L}^{-1}$)

$C_{\text{glucose, out}}$: Metabolite m concentration in the perfusion's outlet flow ($\text{mmol}\cdot\text{L}^{-1}$)

$F(t)$: Fed-batch addition Flow rate ($\text{mL}\cdot\text{min}^{-1}$)

$F_p(t)$: Perfusion flow rate ($\text{mL}\cdot\text{min}^{-1}$)

t: Time (h)

μ : Specific growth rate (h^{-1})

9.2 Introduction

As it has been described in the general introduction mammalian cells are well-established systems for the production of a wide range of proteins with both diagnostic and therapeutic applications (Dingermann, 2008) (De Jesus & Wurm, 2011). In particular, hybridoma cell line has been one of the most used mammal cell lines for biopharmaceutical production, specifically Mab proteins, due to the fact that they are derived from immunoglobulin producing tumour line, which have the innate machinery for antibody production (Coco-Martin & Harmsen, 2008).

The media commonly used in batch cell cultures contains high concentrations of nutrients required for cell growth, being glucose the main energy and carbon source; and glutamine, also carbon and nitrogen source (Paredes et al., 1998). However, the high glucose concentration in the culture leads to obtain both high glucose consumption and therefore, a high lactate secretion and accumulation as a non-desired by-product, as it has been concluded in the analysis of animal cell metabolism (**chapter 5**). In this previous chapter, the explanation of lactate generation was based on a flux deregulation between NADH generation in glycolysis and its reduction via mitochondria shuttles required for balancing the redox potential in the cytoplasm. Consequently, the pyruvate generated through glycolysis was converted to lactate to fulfil the NADH regeneration in the cytoplasm, which is eventually secreted to the culture medium.

The generation of lactate from glucose is a process far less efficient from an energy perspective to its oxidation in the Krebs cycle (Martínez et al., 2013) and, moreover, involves the accumulation of high concentrations of lactic acid which is significantly detrimental to the culture (Ozturk et al., 1992). To overcome the disadvantages of batch cultures, mainly the limitation in the biomass production, other alternative cell culture strategies, providing an environment closer to the physiological state of cells *in vivo*, have already been implemented, such as fed-batch (Huang et al., 2010)(Casablanco et al., 2013) or perfusion (Lecina et al., 2011). In any case, for an effectively implementation of these culture strategies it might be recommended to have at least on-line measurements of cell concentration and cellular activity and if it was possible the concentration of the key compounds of the culture base media.

However, there are not any rules or an extensive study that determine which strategies are the fittest for a specific cell line, which strategy should be done or which might be avoided. Up until now, one conclusion was obtained taking into consideration all the metabolic behaviour that have been analysed in the metabolic chapters of this work (**chapter 3, chapter 4 and chapter 5**):

the carbon metabolism is continuously adapting to the environmental conditions looking for the optimal flux metabolic distribution.

It is important to remark that this conclusion can be shared without considering the platform expression used when a bioprocess is being defined. Therefore, in the following section a full study of an animal cell line will be described starting from the batch culture to the more advanced technics while deciding which are the best strategies and which ones can be avoided or not. On this basis, the decisions that will be made are going to be based on the information obtained via the physiological analysis together with the description of the cell line used presented in **chapter 5**.

9.3 Results (I) - Batch culture

As it has been previously described in **chapter 5**, the metabolism of hybridoma KB26.5-BHRF1 can be optimized towards biomass formation instead of towards the production of lactate when glucose is used as a carbon source. In this chapter, hybridoma KB26.5-BHRF1 will be used as a reference cell line in order to design bioprocess strategies whose aim will be to improve the volumetric productivity by means of enhancing the biomass concentration, while the specific growth rate will be at its optimal value. During the study of the carbon metabolism carried out in chapter 7, changing the carbon source from glucose to fructose, it was accomplished the depletion of the lactate produced. The main reason was using fructose because its membrane transport from the media to the cytoplasm was lower than glucose; consequently, the flux through the glycolytic pathway was the needed in order to avoid lactate production. However, the change in the carbon source was only accepted by HEK293. On the contrary, growing hybridoma KB26.5 using others carbon source than glucose was unsuccessful. However, it was observed an optimization in the conversion of glucose to biomass when a heterologous anti-apoptotic gene (BHRF1) was expressed even if the complete depletion of the lactate production was not obtained. If a further optimization of the carbon source was required, it was hypothesized that the use of culture strategies to restrict the glucose transport via controlling the extracellular glucose concentration should be an option.

Therefore, the goal of this section will be the definition of culture strategies in order to accomplish a higher volumetric productivity by increasing the concentration of biomass obtained while the specific growth rate was unaffected. To begin with, hybridoma KB26.5-BHRF1 was cultured in a 2L bioreactor where the environmental conditions were controlled in order

to get the optimal growth rate as described in **section 9.7.5**. And glucose was set as the media's main carbon source as it is described in **section 9.7.2**.

As shown in **Figure 9-1**, when hybridoma KB26.5-BHRF1 was cultured using a batch strategy, the specific growth rate had a value of $0,046 \text{ h}^{-1}$ and a biomass concentration of $3,9 \cdot 10^6 \text{ cell} \cdot \text{mL}^{-1}$ was obtained together with $1,4 \text{ g} \cdot \text{L}^{-1}$ of lactate. Moreover, as shown in **Table 9-1**, The biomass-glucose yield led the culture to produce $1,56 \cdot 10^6 \text{ cell} \cdot \text{mL}^{-1}$ of biomass for each gram per liter of glucose consumed, while $0,56 \text{ g}$ of lactate were produced for each gram of glucose consumed

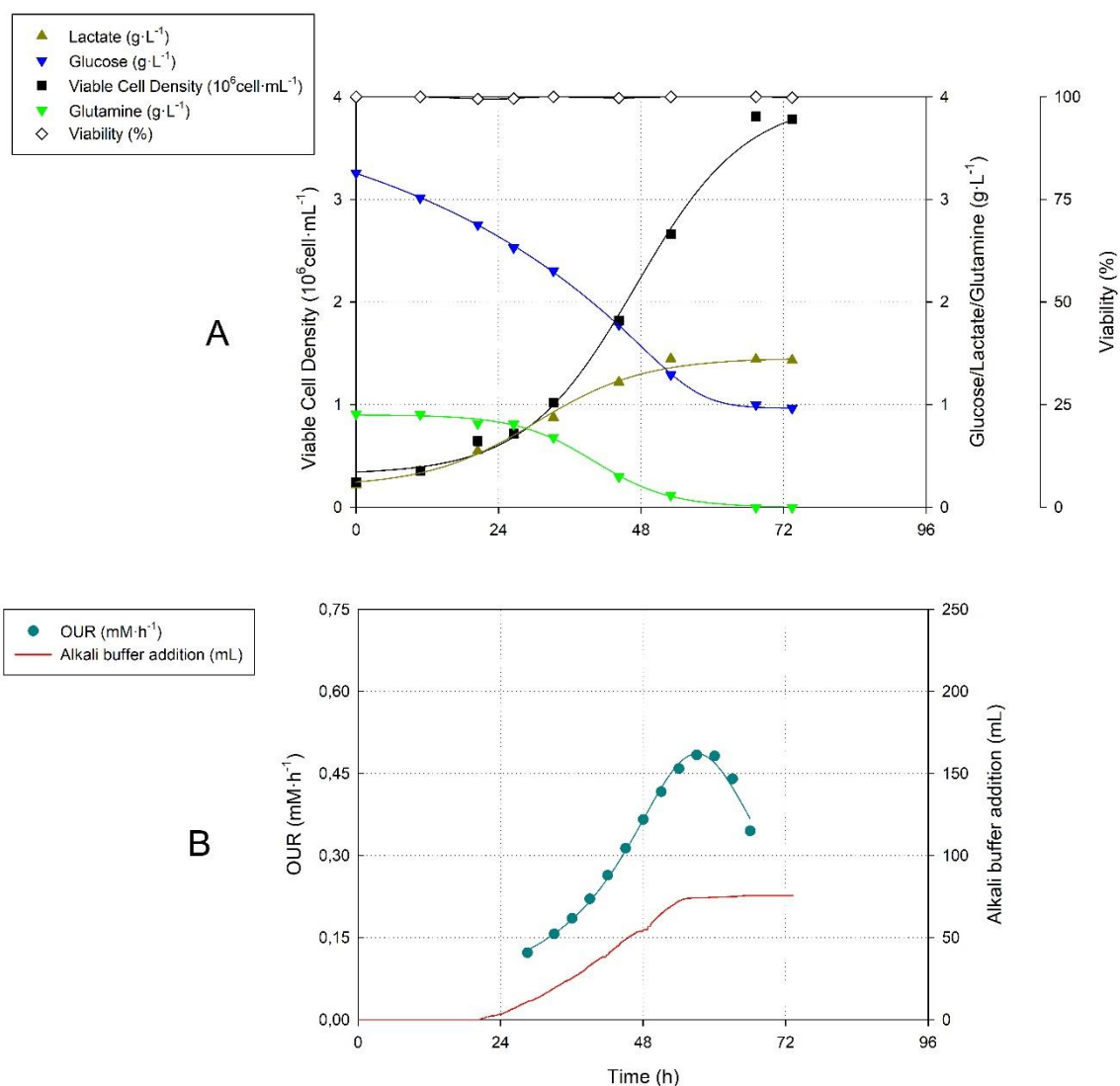


Figure 9-1 Profile of A) off-line variables: biomass (■), glucose (▼), glutamine (▼), lactate (▲) and viability (◇) while at graph B) on-line variables: OUR (●) and alkali buffer addition (—) for hybridoma KB26.5-BHRF1 batch culture.

Table 9-1 Main parameters for hybridoma KB26.5-BHRF1.

Achieved biomass ($10^6 \text{ cell} \cdot \text{mL}^{-1}$)	3,9
μ (h^{-1})	0,046
lactate generation ($\text{g} \cdot \text{L}^{-1}$)	1,4
glucose consumption ($\text{g} \cdot \text{L}^{-1}$)	2,5
$Y_{x/\text{glu}}$ ($10^6 \text{ cell} \cdot \text{mL}^{-1} \cdot \text{g}_{\text{glucose}}^{-1} \cdot \text{L}$)	1,56
$Y_{\text{Lactate}/\text{glu}}$ ($\text{g}_{\text{lactate}} \cdot \text{g}_{\text{glucose}}^{-1}$)	0,56

From the results, it is important to remark two traits: the first one was that the batch strategy reached a biomass concentration of $3,9 \cdot 10^6 \text{ cell} \cdot \text{mL}^{-1}$, and the second one was the lactate production, which accounted for 56 % of the glucose consumed. After this point, in order to increase the biomass productivity, several approaches might be analyzed.

Mainly, these approaches should tackle the fortification of the batch media composition and several culture strategies, for instance, fed-batch and perfusion strategies. Nevertheless, due to the high complexity of the media composition for animal cell cultures, the fortification of media might be challenging and hard time consuming, as it was described in all the publications in regard with the enhancement of the culture's media (De Alwis et al., 2007) (Xing et al., 2011) (Liste-Calleja et al., 2014) (Yao & Asayama, 2017). Therefore, the following section will be focused on developing culture strategies in order to surpass the biomass productivity accomplished in the batch culture by means of increasing the biomass concentration obtained.

9.4 Results (II) - Fed batch strategy

As it was previously described, when hybridoma KB26.5-BHRF1 was cultured on glucose-based media the biomass concentration achieved was $3,9 \cdot 10^6 \text{ cell} \cdot \text{mL}^{-1}$. In order to further increase the biomass produced, a fed-batch strategy will be developed in this section. The development of fed-batch strategy is often focused on the bioprocess optimization and not in the media optimization regarding the composition of the batch media and the feeding solution. However, in this case, the definition of the feeding solution was determined through experimentation. On the contrary, the batch media used in the fed-batch strategy was the one used before in the batch strategy, as it will be described in section 9.7.2.

9.4.1 Feeding media definition

The first experiment to be carried out in order to design a fed-batch strategy is the definition of the feeding solution composition. In order to define it, a shake-flask experiment was performed. The reference condition in this experiment was determined as the media composition before starting the fed-batch strategy - specifically when non-growth conditions were achieved. As observed in **Figure 9-2**, a batch culture was performed until the non-growth conditions were obtained and then, the media was filtrated. Consequently, the reference condition was obtained.

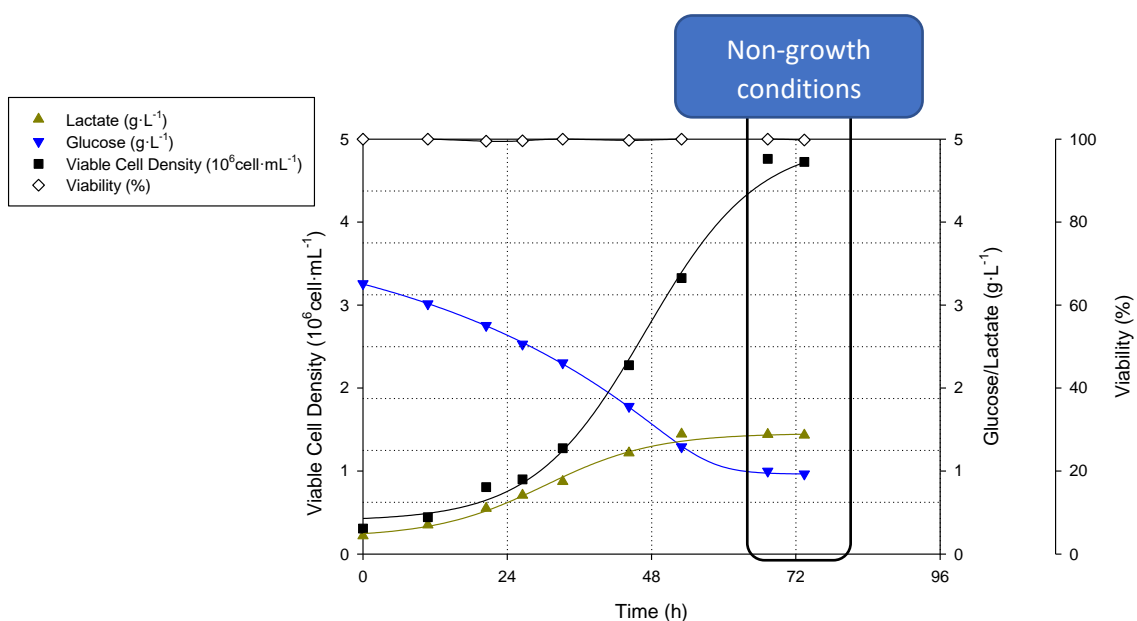


Figure 9-2. Reference media composition used for the definition of the feeding solution.

Concerning the feeding solution, two different compositions were added to the reference media. As observed in **Table 9-2**, the composition of both feeding solutions were based on two types of cell boost (Lifescience, 2015), supplemented with glutamine, glucose and FBS. In relation with the glutamine concentration, it was calculated using the relation between the glucose and glutamine specific rates predicted by the metabolic model described in **chapter 7**. This relation had a value of 1,6 mmol of glucose per mmol of glutamine

Table 9-2 Composition of the feeding solutions used to carry out the feeding media definition experiment.

Compound	Feeding solution 1	Feeding solution 2
FBS (Fetal bovine serum)	20%	20%
Glutamine	150 mM	150 mM
Glucose	45 g·L ⁻¹	45 g·L ⁻¹
Cellboost 5 (CB5)	15 g·L ⁻¹	-
Cellboost 6 (CB6)	-	15 g·L ⁻¹

As observed in **Figure 9-3**, when the reference media (RM) was supplemented with the feeding solutions, the growth was promoted. Otherwise in the reference condition, growth was not observed corroborating the non-growth conditions observed in the batch culture. Moreover, the biomass concentration and specific growth rate obtained when fresh media (FM) was used were higher than observed with the supplemented media (CB5 and CB6). The growth difference between the fresh media and the supplemented reference media, it could be stated that the difference observed should be related to:

- Lack of a compound in the feeding solution that only the fresh media brought, which promoted the growth.
- Possible presence of growth inhibitors compounds in the reference media. On this basis, there are several growth-related metabolites that might act as a growth inhibitors (Rønning et al., 1991)(Pereira et al., 2018).

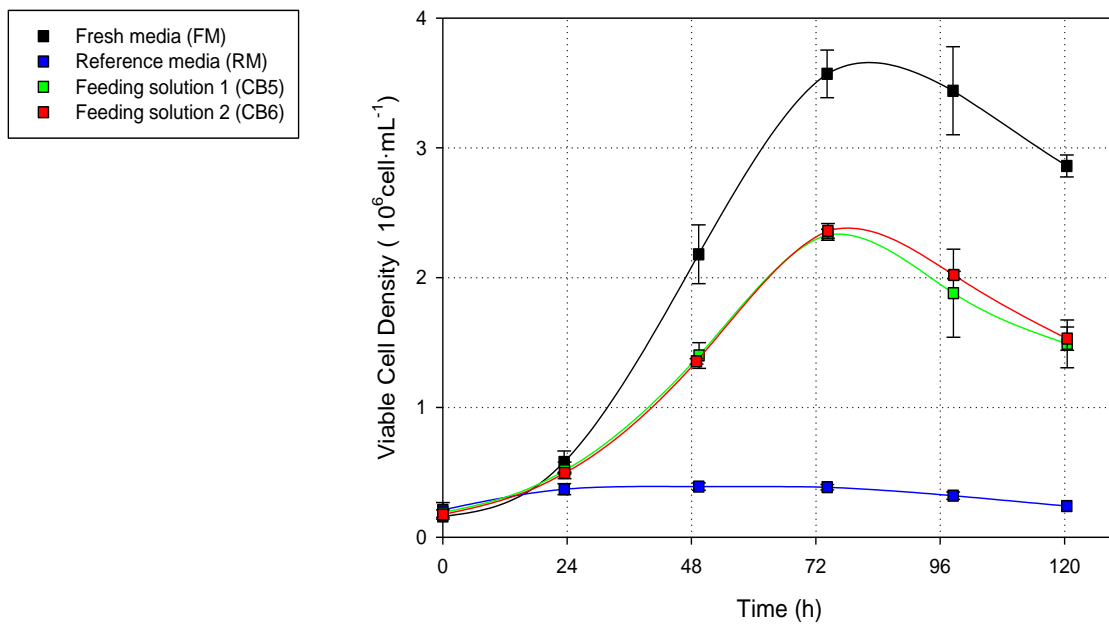


Figure 9-3 Growth comparison of hybridoma KB26.5-BHRF1 cultured on fresh media (FM), reference media (RM) and reference media supplemented with two feeding solutions (CB5 and CB6).

However, a feeding solution was found that promoted culture's growth when it was added to the reference media, even if the growth rate decreased in comparison with the fresh media. Because CB5 and CB6 did not show any growth difference between them, a feeding solution based on CB5 will be used as the feeding solution for the fed-batch strategy.

As it was described in the previous bioprocess chapters using other expression platforms (**chapter 7** and **8**), a fed-batch is a bioprocess strategy that relies on knowing a priori the metabolic and physiologic condition of the selected expression platform. These requirements were required owing to the definition of the feeding profile is related to the specific consumption rate of glucose and to the growth rate, as shown in **section 9.7.9**. On this basis, they can be split into two groups considering how the feeding profile is calculated. The first one consists of the fed-batch strategies whose feeding profile is calculated with a theoretical preprogrammed biomass profile. Whereas, in the second group the feeding profile is calculated via the estimation of the experimental biomass concentration by means of establishing relations between measured variables and the experimental biomass concentration.

Therefore, the first strategy that will be carried out is a fed-batch strategy based on a preprogrammed exponential feeding addition, whose key parameters are the specific growth rate and the specific consumption rate of glucose, as described in **section 9.7.7**. In relation with the specific rates used, they were extrapolated directly using a mass balance from the data

obtained in the priori batch phase. However, there is a feature that has to be remarked, the fed-batch initialization point. In this study, the starting point was decided to be near the moment when a drop in the OUR appeared because of it gives information about growth variations. Consequently, the initialization moment of the fed-batch strategy will be a work-dependent one based on the OUR profile and, as a result, it will be manually started.

9.4.2 Fed batch based on exponential feeding

In order to perform a fed-batch addition based on a preprogrammed exponential profile, several data were required. As shown in **Equation 9-1**, these data tackled the specific consumption rate of glucose ($q_{glucose}$), the specific growth rate (μ) and the glucose concentration in the feeding solution ($C_{glucose,Feeding}$). A further definition of the mathematical algorithm and the feeding media composition are described in **section 9.7.9** and in **section 9.7.2**, respectively.

Equation 9-1

$$F(t) = \frac{-q_{glucose} \cdot X(t_0) \cdot V(t_0) \cdot \exp(\mu \cdot t)}{C_{glucose,Feeding}}$$

As shown in the following **graph A of Figure 9-4**, the fed-batch was split into two phases: the batch phase which was defined within the first 59 hours and the fed-batch phase, which occurred after the batch phase reached a maximum value of OUR and then, it started to decrease until the end of the experiment. In this case, the use of the OUR as a control variable in order to decide the initialization of the feeding addition was based on the relation between the growth culture and the OUR. It was observed in the batch culture that the decrease in the OUR was directly related to the culture reaching the stationary phase, therefore the OUR showed online information about the culture's growth conditions.

Regarding fed-batch batch phase, 2,5 g·L⁻¹ of glucose were consumed to produce 3,75·10⁶ cell·mL⁻¹ of biomass, with an specific growth rate of 0,047h⁻¹ while 1,4 g·L⁻¹ of lactate was produced. It is important to point out that for each gram of consumed glucose 0,54 g of lactate was produced. The fed-batch strategy started at 59 h, when a decrease in the OUR was observed. The starting point was selected based on the information of the previously batch culture where the OUR decrease was directly related to reaching the culture growth limitation. Regarding the definition of the fed-batch phase, the feeding algorithm used the specific growth

rate and glucose consumption rate from the priori batch phase as key parameters as it was mentioned before.

As shown in **graph A of Figure 9-4**, the achieved biomass in the fed-batch phase had a value of $5,6 \cdot 10^6 \text{ cell} \cdot \text{mL}^{-1}$ and the lactate produced reached a concentration of $2,16 \text{ g} \cdot \text{L}^{-1}$. As shown in **Table 9-3**, there was a significant difference in the growth rate between the batch and the fed-batch phase. This difference appeared because the feeding rate was not the optimal one in order to carry out a fed-batch where the growth rate was not limited. Therefore, the feeding profile based on the key parameters of the prior batch did not perform a correct estimation of the cell requirements.



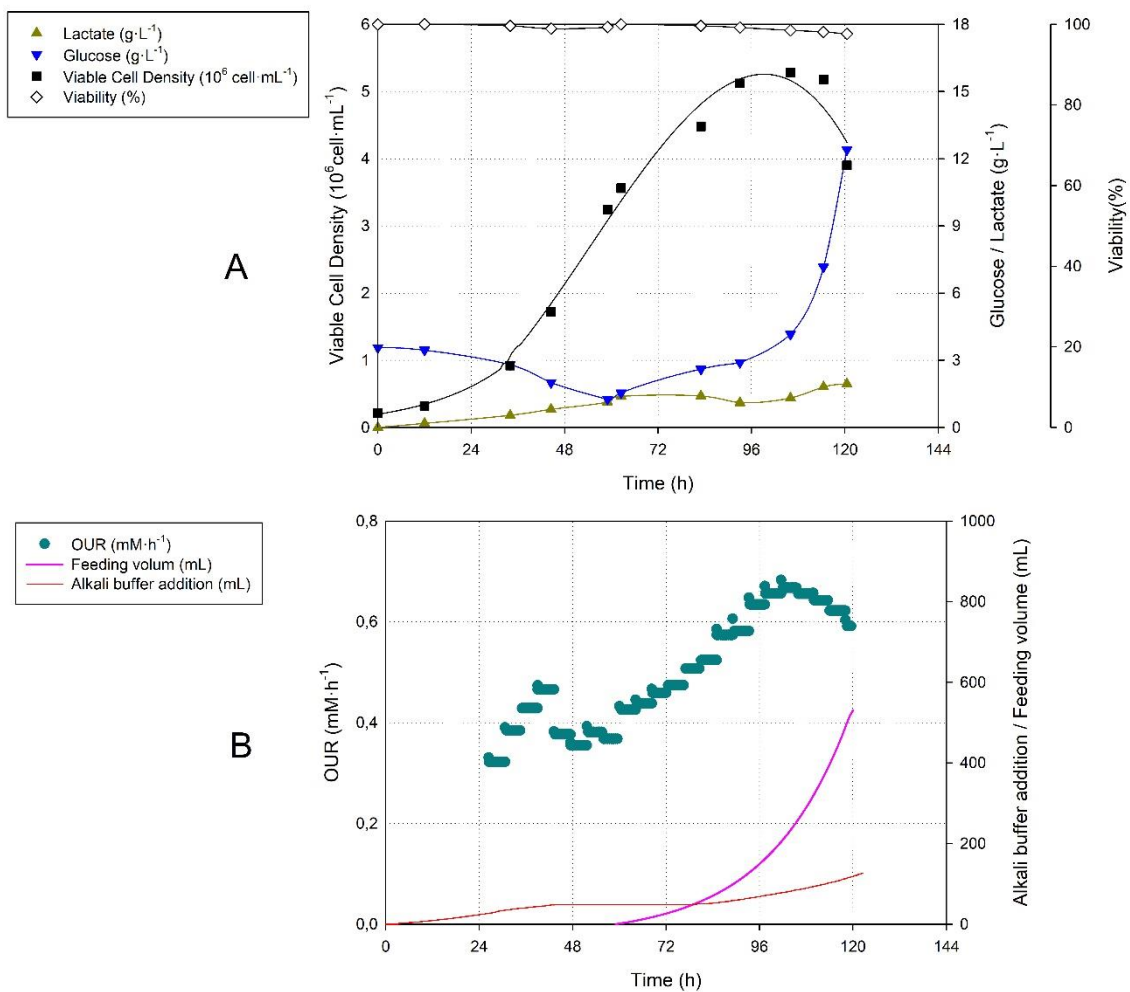


Figure 9-4 Profile of A) off-line variables such as Biomass (\blacksquare), glucose (\blacktriangledown), lactate (\blacktriangle) and viability (\diamond) and B) the on-line variables such as OUR (\bullet), volume of the feeding solution added (—) and the alkali buffer addition (—) for hybridoma KB26.5-BHRF1 fed batch culture where the feeding initiated at 59h.

Table 9-3 Main fed-batch parameters.

Achieved biomass ($10^6 \text{ cell} \cdot \text{mL}^{-1}$)	5,6
Batch μ (h^{-1})	0,047
FDB μ (h^{-1})	0,015
q_{glucose} ($\text{nmol} \cdot \text{mg}_{\text{DCW}}^{-1} \cdot \text{h}^{-1}$)	504
Batch $Y_{x/\text{glc}}$ ($10^6 \text{ cell} \cdot \text{g}_{\text{glucose}}^{-1}$)	1317,39
FDB $Y_{x/\text{glc}}$ ($10^6 \text{ cell} \cdot \text{g}_{\text{glucose}}^{-1}$)	795,91
Batch $Y_{\text{lac}/\text{glc}}$ ($\text{g}_{\text{lactate}} \cdot \text{g}_{\text{glucose}}^{-1}$)	0,54
FDB $Y_{\text{lac}/\text{glc}}$ ($\text{g}_{\text{lactate}} \cdot \text{g}_{\text{glucose}}^{-1}$)	0,10

On the other hand, as shown in **graph B of Figure 9-4**, the OUR behaviours presented two important facts:

1. A relation between the OUR and the biomass concentration was observed during all the experiment, although its value depended on the interaction between the carbon metabolism and the environmental conditions.
2. As described before, the OUR values dropped “instantaneously”, when the growth reached the stationary state. This drop in the OUR profiles could be used as metabolic indicator which gives information about a growth limitation due to non-growth conditions might be achieved. Furthermore, it is important to remember that this profile’s behaviour was also observed in both *E. coli* bioprocess in **chapter 7** and *S. cerevisiae* in **chapter 8**. It can be stated that the OUR, regarding the animal cell culture, can be used as a variable which give instantaneous metabolic-related information about the state of the carbon metabolism.

Therefore, the OUR profile can be used as a metabolic-related control variable for all the studied platform expression whose final electron acceptor is oxygen. On the other hand, the CER profile was not used in the animal cell culture due to the error associated to measure the carbon dioxide concentration in the out-let gas flow. There are several analytical methodologies to measure the carbon dioxide with the required accuracy to being used as a control variable, for instance a mass spectrometer (Haas et al., 2010) or an infra-red gas analyser (Bonarius et al., 1995). However, the one used in all the experiments presented in this work (BlueSense device, (Aehle, 2010)) did not have enough accuracy for carrying out the measures of the carbon dioxide produced by the animal cell. Considering the accuracy issues introduced, the OUR measurements were carried out using another methodology based on the oxygen balance in the liquid phase as described in **section 9.7.6**. On this basis, the analytic device used as well as the methodologies were different than the one used in both *E. coli* and *S. cerevisiae* chapters.

Regarding the physiological variables that can be used in order to predict the carbon metabolism just as the one described above (OUR), there also is another parameter, the alkali buffer addition, which had a relation with the biomass profile, as shown in **graph B of Figure 9-4**. The alkali buffer addition was directly related to the acidification of the media due to the lactate production and its secretion as lactic acid. Even if the volume of the alkali addition buffer was low owing to the use of high concentration titter coupled with the pH control, a relation between the biomass produced, growth state and the alkali buffer added appeared. This relation was based on understanding the interaction between the lactic acid secreted to the culture’s media and the bioreactor’s pH control, in order to maintain the pH at a constant value. Therefore, it might be used as a control variable in order to predict both the biomass value and the growth state as the OUR. As a result, both were grouped as biomass-related variables. Moreover, it has

to be remembered that the conclusion obtained up until now regarding the biomass-related variables, it was already analysed and described when *E. coli* and *S. cerevisiae* were selected as expression platforms in **chapter 7** and in **chapter 8**, respectively. Therefore, it can be stated that the information extracted from these variables (OUR and alkali buffer addition) can be used in all the expression platforms used (*E. coli*, *S. cerevisiae* and hybridoma KB26.5-BHRF1) to predict biomass value along with the growth state.

Table 9-4 hybridoma KB26.5-BHRF1 culture strategies Overview

	Batch	FDB- preprogrammed exponential
Achieved biomass ($10^6 \text{ cell} \cdot \text{mL}^{-1}$)	3,9	5,6
Overall μ (h^{-1})	0,046	0,034
Lactate generation ($\text{g} \cdot \text{L}^{-1}$)	1,4	2,1
$Y_{\text{bio/gluc}}$ ($10^6 \text{ cell} \cdot \text{g}_{\text{glucose}}^{-1}$)	1560	949,78
$Y_{\text{lactate/gluc}}$ ($\text{g}_{\text{lactate}} \cdot \text{g}_{\text{glucose}}^{-1}$)	0,54	0,36

In relation with the biomass production, even if the increase in either the biomass concentration, the specific growth rate in the fed-batch phase was not the optimal one (a 26% decrease compared with the batch). Usually, the decrease in the growth rate might directly related to an underestimation of the feeding rate, although recent publications pointed out a growth inhibition induced by growth-related compounds when several hybridoma cell lines were cultured (Rønning et al., 1991). However, an early carbon limitation was observed due to a possible underestimation of the feeding rate and then, a growth inhibition characterized by the post glucose accumulation during the fed-batch phase.

Regarding the carbon limitation, as observed in **Figure 9-5**, there was a slightly increase in acid buffer addition in the early stages of the fed-batch due to the presence of growth-limiting conditions in regard with the underestimation of the feeding rate. The acid addition could be motivated by the basification related to the lactate consumption.

It is widely studied that hybridoma can metabolize lactate when there is no other carbon source, although in this case due to the presence of glucose, it could not be determined if the lactate was simultaneously consumed with glucose. One other reason that might explain the acid addition would be the basification of the cultures media due to the pH of the feeding solution, however, it was previously set at the defined culture's pH.

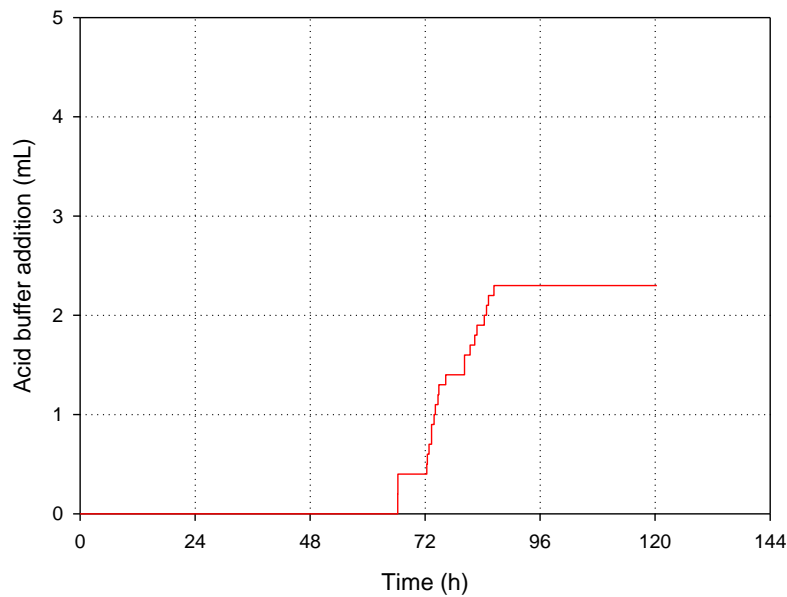


Figure 9-5 Profile of the acid buffer addition regarding the hybridoma KB26.5-BHRF1 fed-batch strategy based on the preprogrammed exponential feeding.

Therefore, the early phase where a carbon limitation was observed was characterized by the addition of acid titter due to the underestimation of the feeding profile. However, the following behaviour where glucose was accumulated cannot be explained by the underestimation of the feeding profile. On this basis, in order to explain the glucose profile, the presence and production of growth inhibitors was hypothesized. The glucose accumulation would be explained by a continuous inhibition of the growth rate during the FDB phase. As a result, the underestimated profile was converted to an overfeeding profile, which provoked the glucose accumulation and promoted a growth inhibition environment.

Therefore, it can be assumed that the parameters that underrated the feeding profile in the early stages were the selected values for both the specific growth rate and the specific glucose rate. Regarding the specific growth rate, the error associated to this value might be related to accuracy issue or not taking into consideration the possible presence of growth inhibitors. On the other hand, regarding the specific consumption rate of glucose, its value should have been obtained from a continuous cultures whose extracellular conditions emulated the initial point of the fed-batch strategy instead of from the prior batch phase. In previous publications, the hybridoma cell line presented a metabolic flexibility capable of adapting the carbon metabolism depending on the environmental conditions (Ray et al., 1989).

At this point, it is important to highlight that the capacity for adapting the carbon metabolism to the environmental conditions is a metabolic trait that the other expression platforms described and analysed in this work shared with animal cell cultures (in *E. coli* -**chapter 3**- and in *S. cerevisiae* - **chapter 4**). However, one trait was only observed in hybridoma KB26.5 –BHRF1 when it was cultured following a fed-batch strategy.

As mentioned before, there was a decrease in the growth rate, as it is depicted in **graph A of Figure 9-6**, which was already explained and whose cause was the combination of an early underestimated feeding problem combined with the production of growth inhibitors.

However, an interesting profile regarding the carbon metabolism was observed. The first decrease of the glucose specific rate occurred at 59-83h and it was expected due to the underestimation of the feeding profile. On this basis, the first interesting fact was the increase of almost 2-fold of the glucose specific rate in comparison with the obtained in the prior batch phase. This increase might be promoted by the high extracellular concentration of glucose combined with the capacity of adapting the glucose transport to the environment conditions (Ray et al., 1989). However, what was more interesting was the lactate behaviour, as observed in graph B of **Figure 9-6** . An early phase characterized by the consumption of lactate owing the low volume added of feeding solution was observed and then, due to the overfeeding, lactate was produced. In regard with the last phase of lactate production, there was a particular metabolic state where high rate of glucose were consumption with a low lactate production without growing. This metabolic restructuring could be hypothesized based on a redistribution of the carbon metabolism to maximize the production of a specific protein when the environmental conditions did not promote the growth. Several works reported that animal cell cultures are able to produce a specific protein when the growth rate is near zero (Altamirano et al., 2001). In this case, the protein that was produced was an immunoglobulin (IgG3), which was not analysed. Therefore, it was a hypothesis that could explain all the behaviours observed regarding the carbon metabolism during the fed-batch phase.

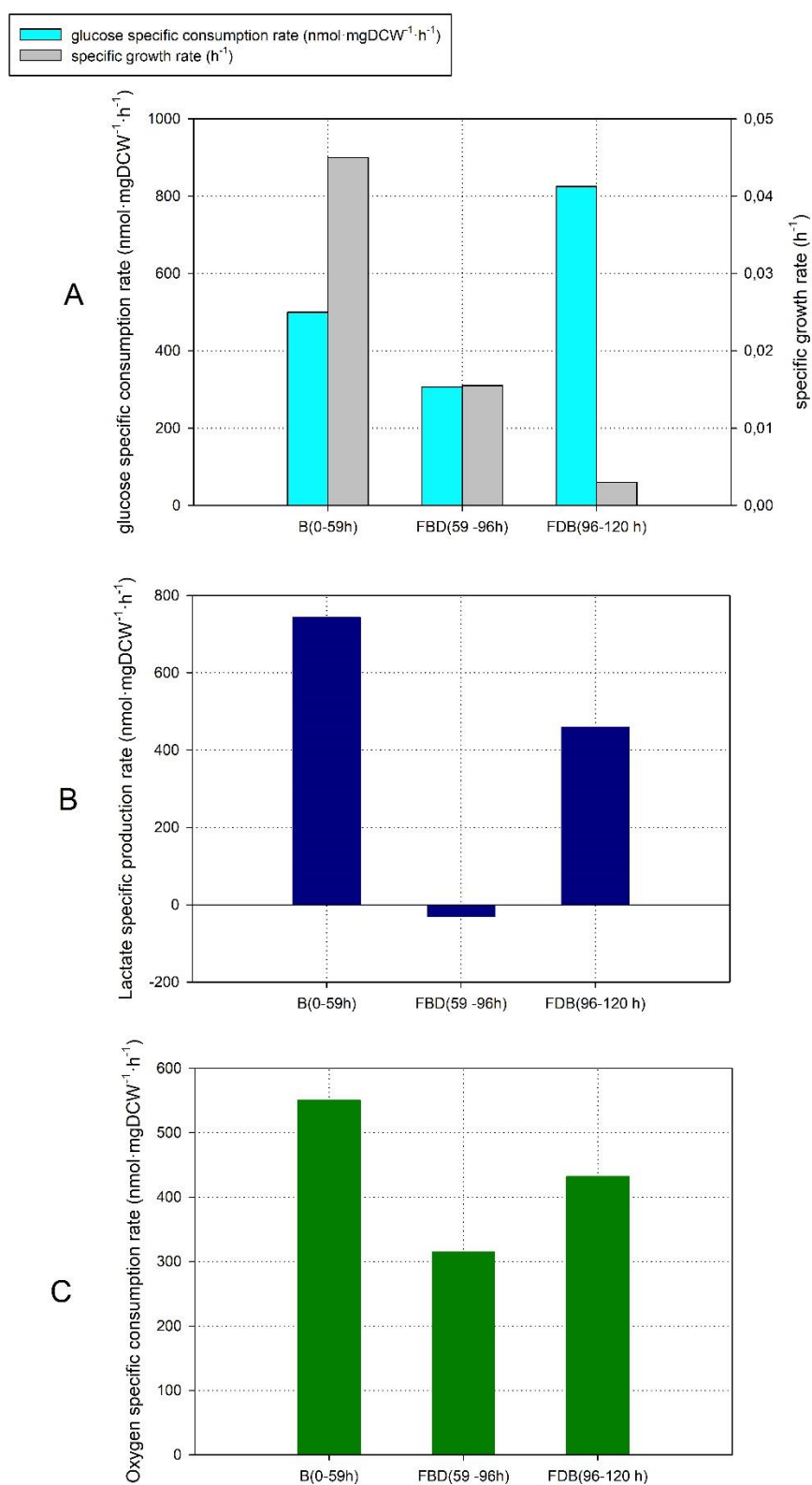


Figure 9-6 Profile of the main specific rates during three defined phases of the hybridoma KB26.5-BHRF1 fed-batch strategy: Batch phase –B(0-59h)–, early phase of fed-batch –FBD(59-90h)– and late FDB phase –(FDB(90-120h)–. In graph A, the specific growth rate along with the specific consumption rate of glucose are depicted, in graph B, the specific production rate of lactate and in graph C, the specific consumption rate of oxygen. All the specific rates are expressed in $\text{nmol} \cdot \text{mgDCW}^{-1} \cdot \text{h}^{-1}$

Once the entire behaviour of the fed-batch carried out was analysed and in order to improve the biomass production, the following step was based on the work performed in the previous bioprocess chapters. It was focused on applying mathematical algorithms in order to develop a biomass-sensible feeding addition. However, they have been already developed and tested in both the *E. coli* bioprocess chapter (**Chapter 7**) and the *S. cerevisiae* one (**chapter 8**) and a solid conclusion was obtained:

The most fitted feeding algorithm was the one that not depended on any prior metabolic parameters or any relation between the biomass value and a physiological value (for instance, the OUR/CER or the alkali buffer addition) due to the incapacity to predict unexpected changes during the course of the experiment. The feeding algorithm selected was the non-metabolic one, which presented the best results regarding performance and glucose-biomass conversion.

As shown in **graph A of Figure 9-6**, the metabolic parameters of hybridoma KB26.5-BHRF1 during the FDB phase did not remain constant as well as both relations between the biomass value and a physiological value such as the OUR/biomass (qO_2), as observed in **graph C of Figure 9-6**.

Therefore and taking into consideration the presence of growth inhibition conditions, the use of fed-batch strategies were discarded due to the fact that the main reason behind a fed-batch strategy is to postpone the growth inhibition phase related to a carbon limitation, not to the one related to growth inhibition due to growth related metabolites.

To conclude, the fed-batch strategy based on an preprogramed exponential feeding profile led the culture to increase the biomass concentration achieved by 1,43-fold compared with the batch culture, consequently, an increase in the biomass productivity. However, a growth inhibition related to growth inhibitors was observed. In order to surpass it, a different strategy will be used. The key feature of this strategy is that the culture's media will be kept at a constant concentration during all the experiment and as a result, the growth inhibitors will remain at non-inhibition concentrations. This strategy is widely known as perfusion.

Therefore, a perfusion strategy will be used in the following section in order to avoid the growth inhibition related to the accumulation of growth inhibitors molecules while growing at the optimal rate.

9.5 Results (III) - Perfusion strategies

In order to perform a strategy that should avoid the accumulation of growth inhibitors, a perfusion strategy was selected. One of the key aspect is the capacity for keeping a controlled environment along with the detoxification of toxic growth-related metabolites. The detoxification is based on a continuous exchange of medium that allows the maintenance of low concentrations of toxic metabolites while granting a continuous metabolic state. (Kretzmer, 2002). However, the overall advantage of perfusion cultures is the very small scale required compared with fed-batch/batch cultures due to the achievement of n-folds regarding the production titter. On this basis, several industrial perfusion processes have been described in the literature:

1. A spin filter perfusion hybridoma culture for antibody production whose volumetric productivity was approximately 10 times that of batch or fed-batch cultures (Deo et al., 1996).
2. A Coagulation factor VIII process using a continuous perfusion culture that increased a 30-fold the yield of factor VIII due to the fact that high cell densities were obtained (Boedecker et al., 1994).

There is an important trait in regard with the perfusion technologies, which is the selection of the cell retention device, due to the fact one of the main issues in the perfusion process definition is related to the effect that the cell retention system might have on the selected cell line culture. On this basis, the current retention systems were develop in order to decrease the effect that the separation process had on cell metabolism for instance, the cross-flow membrane filters, spin-filters, inclined settlers, continuous centrifuges and ultrasonic separators (Woodside et al., 1998).

In this work, a widely use cross-flow membrane filter known as hollow-fibers was selected as a cell retention system. However, two filtration methodologies in order to pump the culture media to the lumen of the fibers were described in the bibliography: the orthogonal method and the tangential method (Herterich et al., 2017). Both methods differed in the relative position between the culture's flow and the membrane. The best methodology described is the tangential one due to the fact that it minimized the filter clogging, which is one of the main issues regarding perfusion strategies (Zhang et al., 2020).

Regarding the tangential filtration methodologies, two approaches have been described: the alternative tangential flow filtration (ATF) and the tangential flow filtration (TFF). The main

difference between them was the shear stress in which the cell culture was submitted; it was higher in the TTF system than in the ATF one (Sierra, 2014). The reason behind this difference was that the TTF used a peristaltic pump in order to pump the culture in the lumen of the fibers while the ATF used a diaphragm pump to push and pull the culture's media in the fibres in an alternated way with a fixed interval of time. Therefore, the ATF system was selected for the perfusion strategy.

Once both the cell retention device and the filtration methodology were defined, the next step that was taken into consideration was the definition of the flow profile.

The general profile for a perfusion strategy is based on **Equation 9-2**. As it can be observed, the flow rate profile ($Fp(t)$) is directly related to the expected difference between the outlet and inlet glucose concentrations ($C_{glucose,out} - C_{glucose,in}$) and the biomass concentration ($X(t)$).

Equation 9-2

$$Fp(t) = \frac{-q_{glucose} \cdot X(t) \cdot V}{C_{glucose,out} - C_{glucose,in}}$$

The glucose difference between outlet and inlet was fixed owing to the glucose outlet concentration was defined as constant, whose value was the obtained in the prior batch phase (8,15 mM). Regarding the biomass, a mathematical algorithm to predict the biomass concentration evolution was required. On this basis, it is important to remember that the biomass prediction has been a “hot topic” in the studies presented in this thesis, mainly regarding bioprocess definition in all the expression platforms described: *E. coli* chapter (**chapter 7**), *S. cerevisiae* (**chapter 8**) and in this chapter a hybridoma KB26.5-BHRF1 as an example of an animal cell line.

There were two ways to predict a biomass profile: using a predefined profile characterized by metabolic parameters which were determined in the prior batch phase or using biomass-related variables in order to extrapolate the biomass concentration during the course of the experiment.

As it was concluded in the previous chapters, the worst possible outcome was obtained when the biomass profile was predicted using a defined profile (widely described and used as pre-programmed exponential) while using a biomass-related variables taking into account the sensor and the monitor capacity in animal cell culture might become the best option. In the animal cell cultures is not possible to carry the non-metabolic algorithm because the analytical device used for this methodology (BlueinOne, BlueSens gas sensor GmbH) is out of range and

accuracy issues are observed (Martínez-Monge et al., 2019). On this basis, the biomass-related variables that could be used in the perfusion strategy were OUR and the alkali buffer addition owing to both of them are related to the carbon metabolism (the metabolites: oxygen and lactate, respectively) and, as a consequence, to the biomass evolution. For this case, the OUR was used as a biomass –related variable in order to predict the biomass concentration owing to it was the easiest and simple methodology regarding the mathematical algorithm definition and possible unexpected perturbations.

Therefore, in order to overcome the growth inhibition observed in the fed-batch culture previously presented using hybridoma KB26.5-BHRF1, a perfusion strategy was carried out using the following features:

- Cell retention device: hollow-fiber as a type of cross-flow membrane filters.
- Filtration methodologies: ATF, alternative tangential flow filtration
- Biomass prediction: the OUR as a biomass-related variable.

9.5.1 Perfusion feeding based on OUR monitoring

Several data and information were required to perform a perfusion strategy based on OUR, which were split in two sections:

1. All the physiological information regarding the environmental conditions and all the media composition used (batch culture media and media feeding composition) which were described in **section 9.7.2** and **section 9.7.5**, respectively
2. The mathematical algorithms responsible for the perfusion feeding profile and the prediction of biomass concentration, both of them can be found at **section 9.7.10** and **section 9.5**.

Once all the information was set, the perfusion strategy was carried out. As shown in **Figure 9-7**, three phase are described: the batch phase, the first phase of the perfusion phase and the second phase.

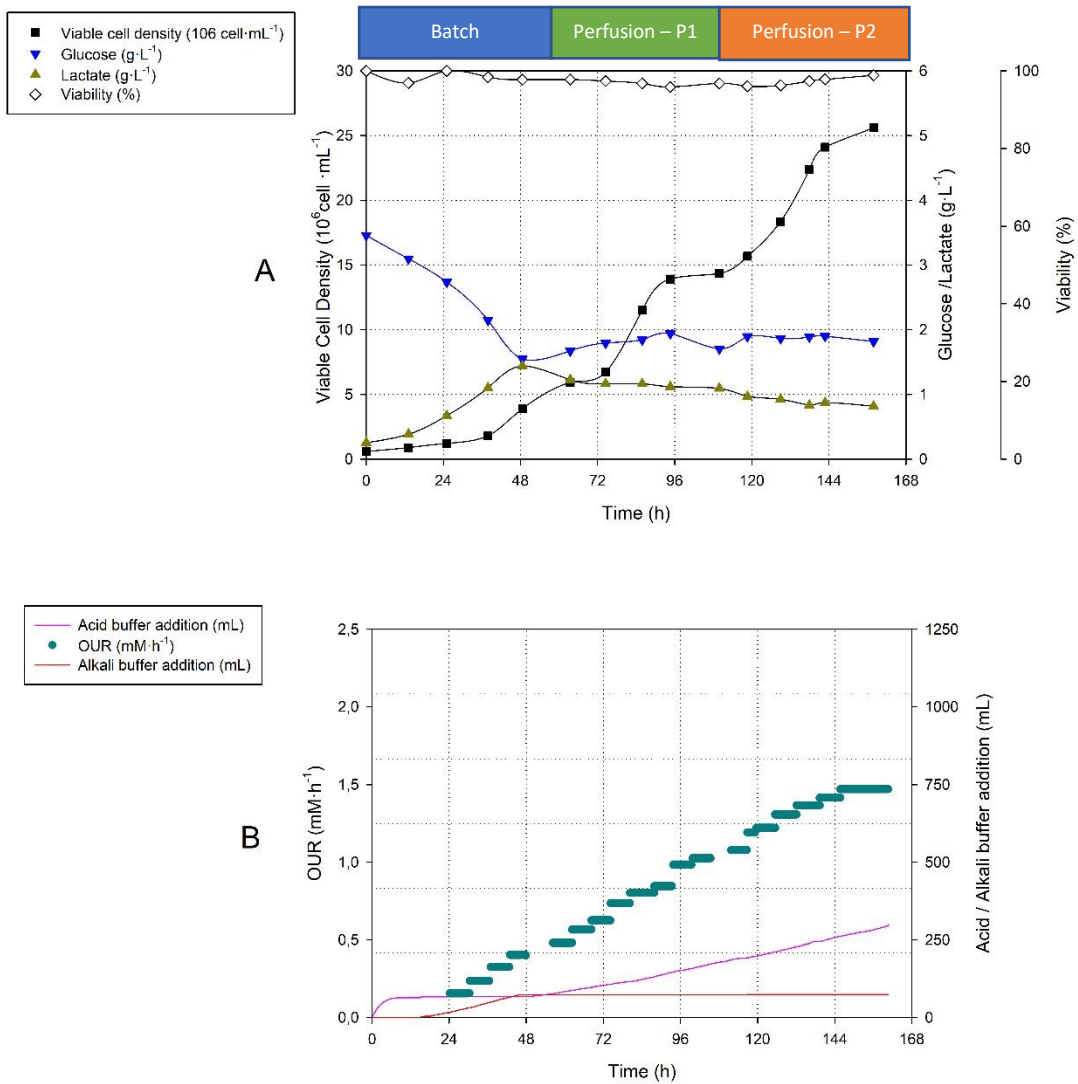


Figure 9-7 Profile of A) off-line variables such as Biomass (■), glucose (▼), lactate (▲) and viability (◇) and B) the on-line variables such as O.U.R (●), volume of the acid buffer addition (—) and the alkali buffer addition (—) for hybridoma KB26.5-BHRF1 perfusion culture where the feeding initiated at 59h.

The batch phase was used to get the metabolic information required for the algorithm on top of calculating the perfusion rate. This information tackled the specific growth rate and the glucose specific consumption rate. Regarding the initialization of the perfusion settings, it was selected using as a base data, the bath culture described in **section 9.3**. As it was previously presented in **Figure 9-1**, an inflexion point in the OUR was detected when the biomass concentration reached about $2.5\text{--}3 \cdot 10^6 \text{ cell} \cdot \text{mL}^{-1}$ owing to the apparition of growth limiting conditions. Therefore, in order to avoid the growth limiting conditions during the perfusion phase, the perfusion was initialized at $3 \cdot 10^6 \text{ cell} \cdot \text{mL}^{-1}$, when almost $1.8 \text{ g} \cdot \text{L}^{-1}$ of glucose was consumed while $1.06 \text{ g} \cdot \text{L}^{-1}$ of lactate was produced, as shown in **graph A of Figure 9-7**.

During the course of the perfusion strategy two phase were defined depending on the metabolic parameters used in the feeding algorithm. As shown in **Figure 9-9**, the growth rate (**graph A**) suffered a 33% reduction while the specific consumption rate of glucose (**graph B**) decreased a 42 % in the transition between the first perfusion phase (50-100h) and the prior batch culture (0-50h). Afterwards, the metabolic information used for the perfusion rate was updated with the new data obtained because the metabolic data used in the feeding algorithm had to be the most representative regarding the culture's metabolic state. However, as it can be observed in **Figure 9-9**, when the metabolic data was updated at the end of the first phase (50-100h) a reduction in the both growth and glucose rates was also obtained in the second phase (100-160h), 64% regarding the specific growth rate while 42% regarding the glucose consumption rate.

The continuous reduction of the metabolic parameters, specifically, the one related to the growth, can be explained with the promotion of the carbon limiting conditions and the accumulation of the growth inhibition compound observed in the fed-batch experiment even if its concentration was not known. In desirable conditions, It was supposed that the inhibitor concentration should be kept under an acceptable range if the metabolic data used by the perfusion rate was the culture's one. This supposition was based on the next statement: the specific production rate of the growth inhibition compound was several order magnitudes lower than either the glucose or the lactate specific rates; as a result, its concentration should have been near zero due to the dilution rate selected.

On this basis, the first change in the metabolic data (the transition between batch and the first phase of perfusion) should be predicted if two traits are taken into account and if the concentration of inhibitory compound was below limiting conditions:

1. A carbon limitation due to the underestimation of the metabolic parameters required for the perfusion rate calculation.
2. A carbon redistribution that took place taking into consideration the environmental conditions achieved (Ray et al., 1989).

The carbon limitation was the responsible for the first decrease of the growth rate and also it was responsible for a carbon redistribution, were a 30% reduction in the lactate production was achieved. As it was mentioned in the previously fed-batch section, the carbon redistribution is related to having a determined extracellular glucose concentration, lower than the one used at the batch culture. Therefore, the metabolic data required for the calculation of the perfusion rate was updated taking into consideration the new culture's metabolic requirements.

However, this first assumption regarding the inhibitory compound was wrong and as a result, the decrease in the updated metabolic information provoked accumulation of inhibitory compound instead of fulfilling the culture requirements at the optimal point. The feature responsible for the increasing in the inhibitor concentration was the decrease of the dilution rate provoked by the update in the perfusion rate, as it can be observed in **Figure 9-8**. As a result, in the next phase (100-160h) the concentration of the inhibitory compound increased undergoing a stronger growth inhibition, as observed in specific growth rate profile depicted in **graph A of Figure 9-9**.

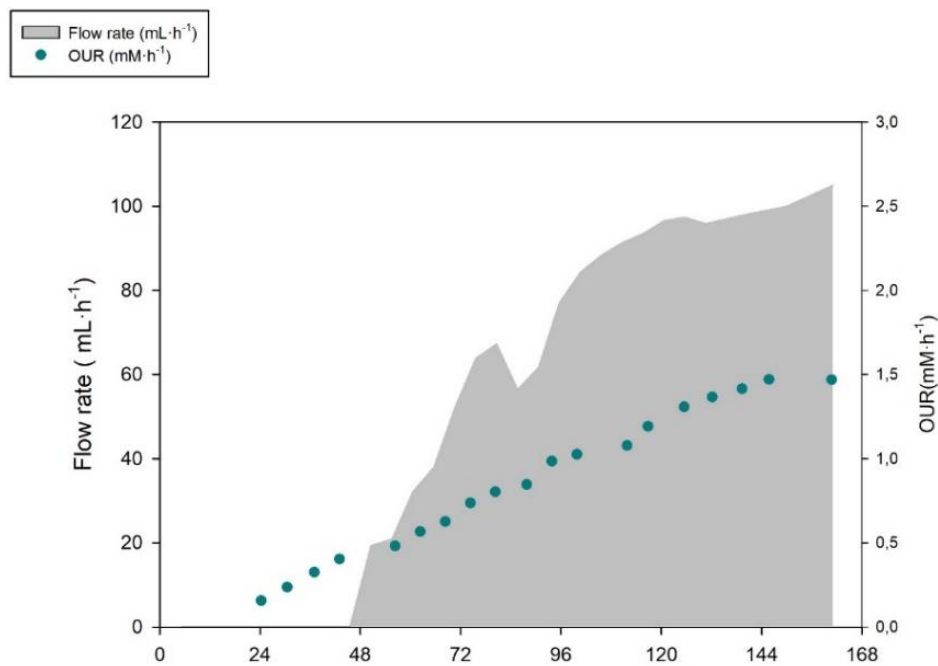


Figure 9-8. Profile of the perfusion rate along with OUR evolution during the course of the perfusion strategy.

Regarding the carbon metabolism, even if a growth inhibition was observed in the transitions between the first and the second phase as shown in **graph A of Figure 9-9**, the carbon metabolism was not modified. Only near 40% of the total carbon source was converted to lactate without depending on the growth rate. Therefore, it can be stated that the carbon distribution obtained in the first phase of the perfusion strategy was the most optimal one to convert glucose to biomass.

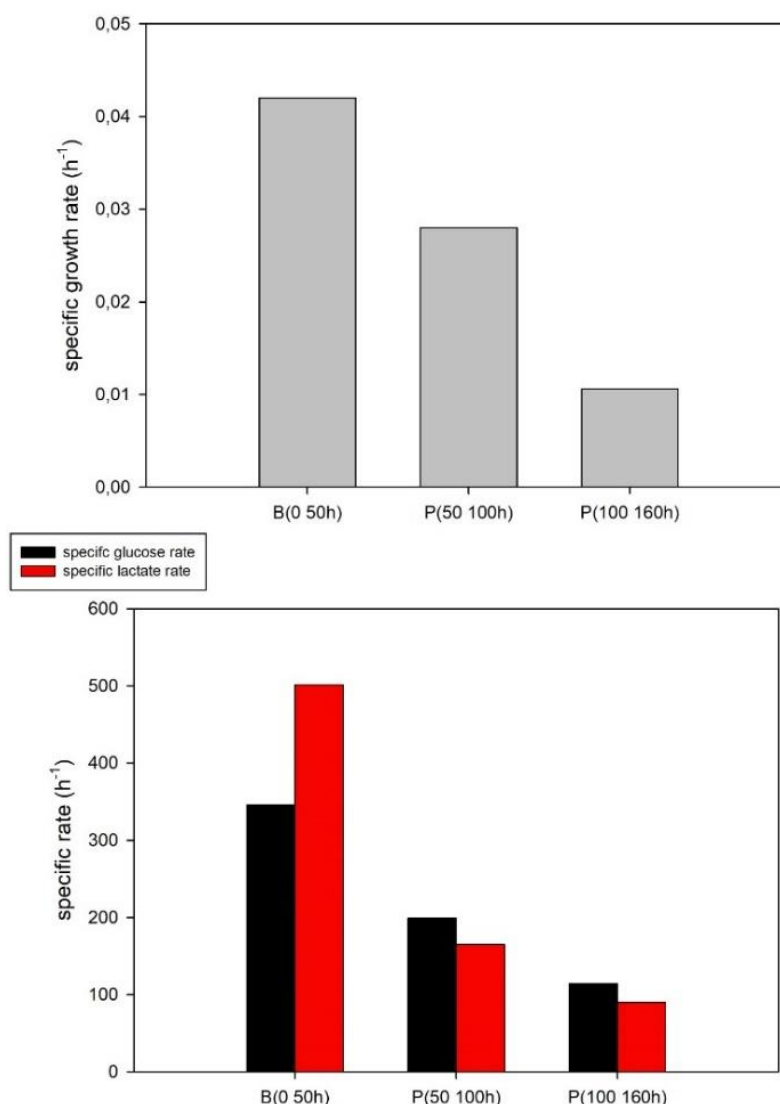


Figure 9-9 Profile of the main specific rates during three defined phases of hybridoma KB26.5-BHRF1 perfusion strategy: Batch phase –B(0-50h)-, first phase of perfusion strategy – P(50-100h)- and second phase of perfusion strategy –P(100-160h)-. In graph A, the specific growth rate is presented while in graph B, the specific production rate of lactate along with the specific consumption rate of glucose are depicted. All the specific rates are expressed in $\text{nmol} \cdot \text{mgDCW}^{-1} \cdot \text{h}^{-1}$

Regarding the use of OUR as a biomass related variable in order to predict the biomass evolution, as shown in **Figure 9-10**, there were two phases well defined: the batch phase and the perfusion where the OUR was able to predict correctly the biomass. However, it was possible due to the update in the specific consumption rate of glucose undergone by culture when the perfusion was activated. The specific consumption rate drop from $450 \text{ nmol} \cdot \text{mgDCW}^{-1} \cdot \text{h}^{-1}$ to $110 \text{ nmol} \cdot \text{mgDCW}^{-1} \cdot \text{h}^{-1}$ and then, it remained constant during all the course of the perfusion phase as it can be observed in **Figure 9-11**, where the linearity of the OUR and biomass was directly related to the value of the oxygen specific consumption rate. Moreover, the change in the

oxygen metabolism (in its specific consumption rate) appeared only in the first transition because it was solely on first transition that the carbon metabolism changed as well.

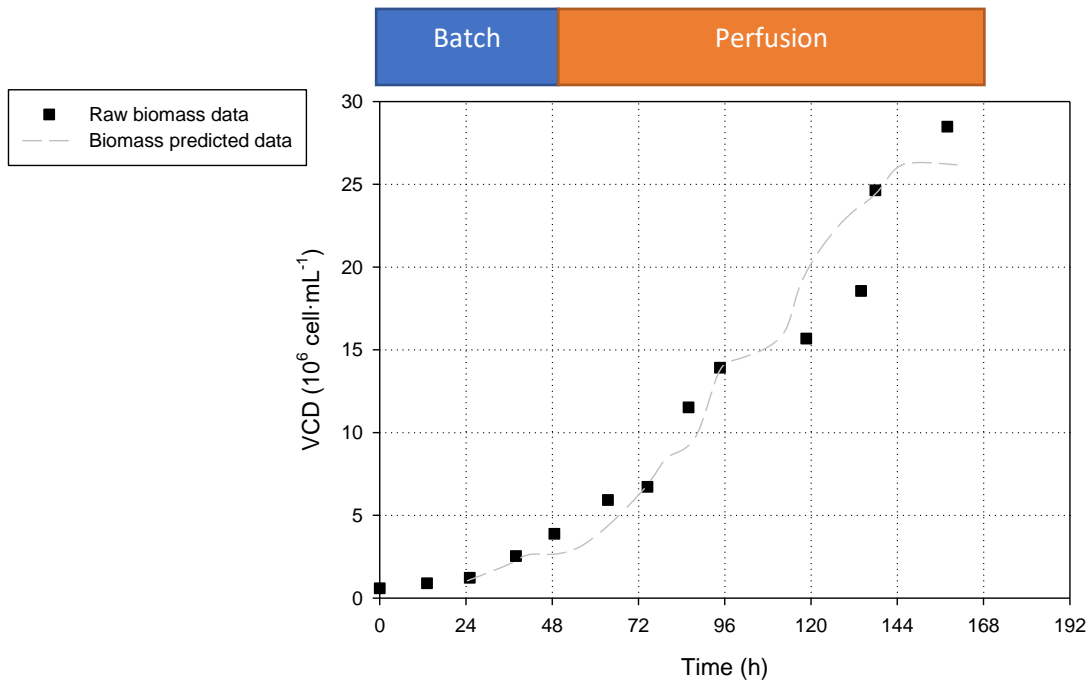


Figure 9-10 Comparison between the raw biomass data and the predicted one using the OUR as the core variable.

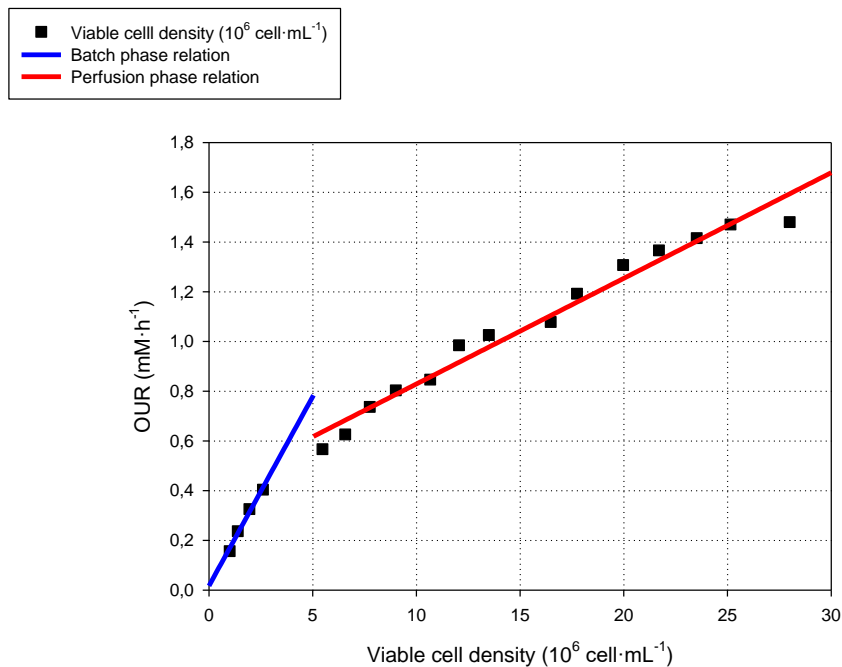


Figure 9-11 Relation between the OUR and viable cell density where the slope between them shows the value of the specific consumption rate of oxygen.

If the other biomass-related variables are analyzed, an unusual trait appeared in regard with the alkali addition. As it was mentioned in the previous fed-batch experiment, the alkali addition is directly related to neutralize the production of lactic acid during glucose consumption. However, if the **graph B of Figure 9-7** is analyzed, this behavior only took place in the batch phase, while in the perfusion phase only an acid addition was observed. The batch-behavior was the correct an expected, whereas the perfusion was provoked by the addition of an alkali feeding media. Therefore, the alkali buffer addition should be a possible monitoring variable in order to predict biomass if all the perturbations regarding the pH are corrected, mainly, the titrating of the feeding pH until the culture is achieved.

However, it cannot be forgotten that the perfusion strategy lead the culture to a high cell density situation. As shown in **Table 9-5**, the cell density increased from $3 \cdot 10^6 \text{ cell} \cdot \text{mL}^{-1}$ to $25 \cdot 10^6 \text{ cell} \cdot \text{mL}^{-1}$, in terms of biomass productivity, the perfusion was responsible for a 6,46-fold increase. Therefore, the perfusion strategy overcome the inhibition issue observed in the fed-batch strategy, leading the culture to increase the biomass productivity by a 6,46-fold in comparison with the batch culture.

Table 9-5 Overview of two main aspects for the hybridoma KB26.5-BHRF1 culture strategies.

	Batch	FDB- preprogramed exponential	Perfusion controlled by OUR
Achieved biomass ($10^6 \text{ cell} \cdot \text{mL}^{-1}$)	3,9	5,6	25,2

Once all the study of the biomass enhancement in animal cell lines has been described, it is important to detail several keys presented and not developed in this section that can be deepen in further works:

- The increase in the perfusion rate in order to keep the maximum growth rate while keeping at an almost depleted value the inhibitor concentration instead of looking for the optimal metabolic condition regarding the carbon conversion to biomass.
- The use of others biomass-related variable in order to perform another perfusion rate algorithm, in this case, the pH could be used as one, if several modifications would have been carried out.

Finally, in this study the protein production was directly related to the biomass concentration and as a result, more biomass achieved is translated to more protein production. However, for a further analysis, it might be favourable a metabolic study where the relation between the growth rate and the protein production was described. This study will bring interesting

information because the growth rate defined in a perfusions strategy can be modulated and fixed to a desired value.

9.6 Discussion and conclusions

As stated at the beginning of the chapter, the final goal was to improve the biomass production in a bioprocesses culturing hybridoma KB26.5-BHRF1, in order to enhance the biomass volumetric productivity. Several culture strategies were tested and designed following one idea: letting the culture reaching high cell density while the specific growth rate was at its optimal value.

A batch culture study was used as a reference point in order to design a fed-batch strategy to further increase the biomass productivity. The definition of the feeding solution was carried out via a shake-flask experiment testing two solutions based on a chemical defined supplement (Cell boost 5 and Cell boost 6). Even if there was no-growth difference between them regarding the shake-flask experiment, it was concluded that the feeding solution used for next fed-batch strategy was Cell boost 5. Once the feeding solution was determined, the fed-batch was carried out. The first approach was based on a fed-batch strategy where the culture's growth was estimated as an exponential function. As a result, the biomass concentration of the process increased 1,43-fold in comparison with the reference batch culture. However, two traits were observed:

- The first one was related to the use of metabolic data obtained in the prior batch phase instead of the data from a continuous culture. As it was expected, the metabolic data changed during the course of the experiment in an abruptly manner leading the feeding profile to be not representative to the culture growth requirements. As it was impossible to predict how the metabolism might behave, biomass-related variables were discarded for estimating the biomass evolution.
- The second one was related to the apparition of growth inhibition conditions.

Taking into consideration both issues, the most suited strategy was the perfusion owing to certain conditions might be granted:

- A constant metabolic state can be obtained and if was necessary an update of the metabolic data from the culture during the course of the experiment can be perform.

As a result, a constant metabolic state should be granted where the specific rate remained constant.

- The growth inhibition conditions observed in the previous fed-batch culture can be avoided if a correct dilution rate is used.

As a result, when the perfusion strategy was carried out, it presented a 6,46-fold increase in the biomass concentration, even if it was not fully optimized to convert glucose to biomass at the maximum specific growth rate. The optimization selected was based on improving the conversion of glucose to biomass while the specific growth rate was the optimal instead of the maximum. On this basis, a 30 % reduction in the lactate production was achieved while the specific growth rate was reduced by near 25 % owing to the profile of dilution rate was lower than the required one to avoid growth inhibition caused by the resultant concentration of the growth inhibitors.

Using OUR as a control variable in order to control the perfusion rate was succeed when constant update of the metabolic information is assured. On the other hand, the use of alkali buffer addition as a control variable should be possible if metabolism-related compounds carry out the media acidification. In this case, due to the pH perturbation provoked by the feeding media pH, the relation between biomass and pH controller was not representative. As a result, the alkali buffer addition feeding control should not be classified as a biomass-related variable. On the contrary, if the media pH is adjust to the culture physiological conditions, the use of alkali buffer addition as a biomass-related variable might be possible.

To conclude, it was possible to increase the biomass productivity because the biomass concentration was increased by 6,26-fold using a perfusion strategy, while the growth limiting conditions observed in fed-batch study was overcome. Moreover, due to the previously knowledge from the metabolic studies described in **chapter 5**, a metabolic redistribution was promoted leading the strategy to the most optimal carbon conversion situation even if the maximum growth rate was not achieved.

9.7 Materials and Method

9.7.1 Cell line

The hybridoma KB26.5-BHRF1 cell line used in this chapter in regard with its precedence and genetic background is described in **chapter 5 section 5.8.1**.

9.7.2 Culture Media definition.

The media composition used in the bioprocess section are described hereafter.

- Shake-flask culture: the media composition is described in **chapter 5 section 5.8.2**
- Batch experiments: the media composition is described in
- **Table 9-6** Composition of media used as a feeding media in the perfusion strategy.

Compound	Concentration
DMEM (D5671, merck)	Base media
FBS (Fetal bobine serum)	5%
Glutamine	6 mM
Antifoam (A5757, merck)	50 mg·L ⁻¹
Kolliphor (15759, merck)	100 mg·L ⁻¹

- Table 9-7
- Batch media in fed-batch strategies: the media composition is described in
- **Table 9-6** Composition of media used as a feeding media in the perfusion strategy.

Compound	Concentration
DMEM (D5671, merck)	Base media
FBS (Fetal bobine serum)	5%
Glutamine	6 mM
Antifoam (A5757, merck)	50 mg·L ⁻¹
Kolliphor (15759, merck)	100 mg·L ⁻¹

- Table 9-7
- Feeding addition in fed-batch strategy: the composition is described in **Table 9-6**
- Feeding media in the perfusion strategy: the composition is described in
- **Table 9-6** Composition of media used as a feeding media in the perfusion strategy.

Compound	Concentration
DMEM (D5671, merck)	Base media
FBS (Fetal bobine serum)	5%
Glutamine	6 mM
Antifoam (A5757, merck)	50 mg·L ⁻¹
Kolliphor (15759, merck)	100 mg·L ⁻¹

- Table 9-7

Table 9-6 Composition of media used as a feeding media in the perfusion strategy.

Compound	Concentration
DMEM (D5671, merck)	Base media
FBS (Fetal bobine serum)	5%
Glutamine	6 mM
Antifoam (A5757, merck)	50 mg·L ⁻¹
Kolliphor (15759, merck)	100 mg·L ⁻¹

Table 9-7 feeding composition of solution used in fed-batch strategy.

Compound	Concentration
FBS (Fetal bobine serum)	20%
Glutamine	150 mM
Glucose	45 g·L ⁻¹
Cellboost 5 (CB5)	15 g·L ⁻¹

9.7.3 Metabolite determination

All the metabolite determinations carried out in this chapter in regard with its protocols and methodology has been already described in **section 8 of chapter 5**.

9.7.4 Culture systems

For small scale or inocula cultures have been performed in an Erlenmeyer of different volumes (25, 50, 100, 250 and 1000 mL) at 37°C, 100 rpm and 5 % of CO₂.

9.7.5 Bioreactor cell culture

The stirred-tank bioreactor used in the present study was a commercial bioreactor (Biostat B, from Sartorius Stedim Biotech, Germany) with 2L-cylindrical jacketed vessel, equipped with probes and control systems for pH, D.O. (relative oxygen partial pressure) and temperature, and a stirred with two marine type impellers.

The control systems of the mentioned variables are described below:

- Dissolved oxygen concentration was monitored with a polarographic probe (Oxyferm, Hamilton), and maintained at 30% of saturation by means of an aeration flow using a spargger flow of 0,20 VVM together with a cascade control system. It was based on a stirring control system and a gas mixing unit while the carbon dioxide concentration was kept at 5% v/v for all the experiments carried out.
- Temperature was maintained at 37°C by switch between a heat exchanger when heat was needed and with a cooling water system when cold was needed.
- pH was measured with a standard electrode (EasyFerm Plus, Hamilton), and it was maintained at 7,02 using a HCl 0,5M (Panreac) addition, and a subsequently addition of NaOH (15% v/v) (Panreac).
-

The working volume for the batch cultures was 1L, and the initial volume for both the fed-batch and the perfusion culture was 1L.

9.7.5.1 Perfusion devices

As observed in **Figure 9-12**, the bioreactor was connected to an ATF system. The ATF system consisted of a hollow-fiber whose specification are described in **Table 9-8** and a diaphragm pump regulated by a pressure control that behaved as observed in **Figure 9-14**.

Table 9-8 Hollow-fiber specifications used in the perfusion experiment.

material	Polyethersulfone (PES)
Porus size	0,2 μm
Filter area	0,13 m^2
Reference (Repligen)	F2:RF02PES

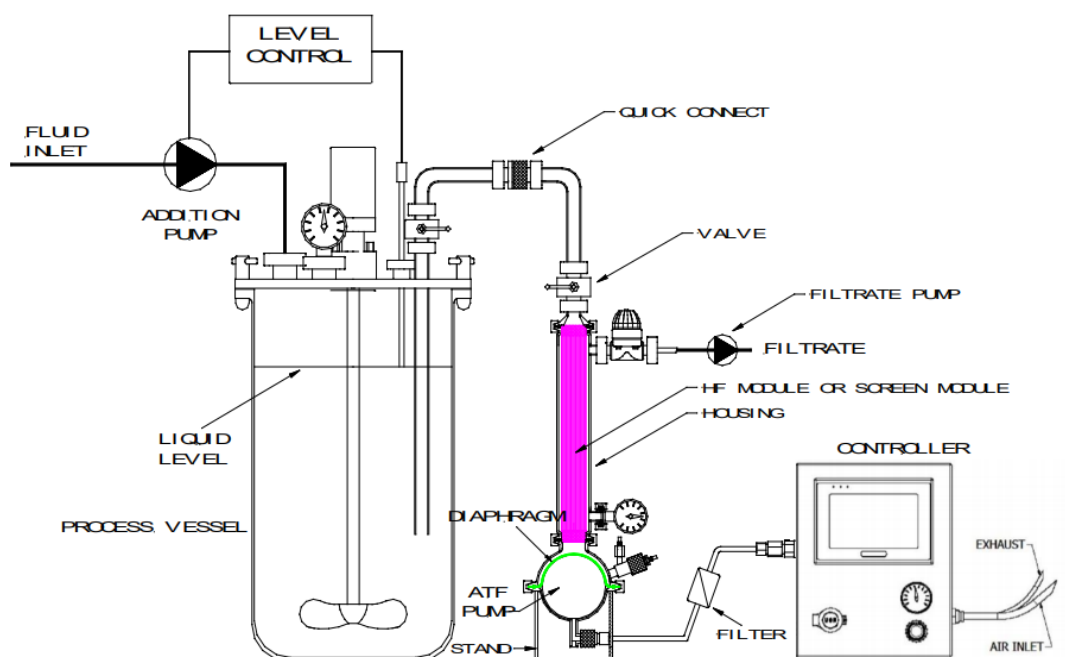


Figure 9-12. Connection between bioreactor and ATF system from (Pineda, 2018).

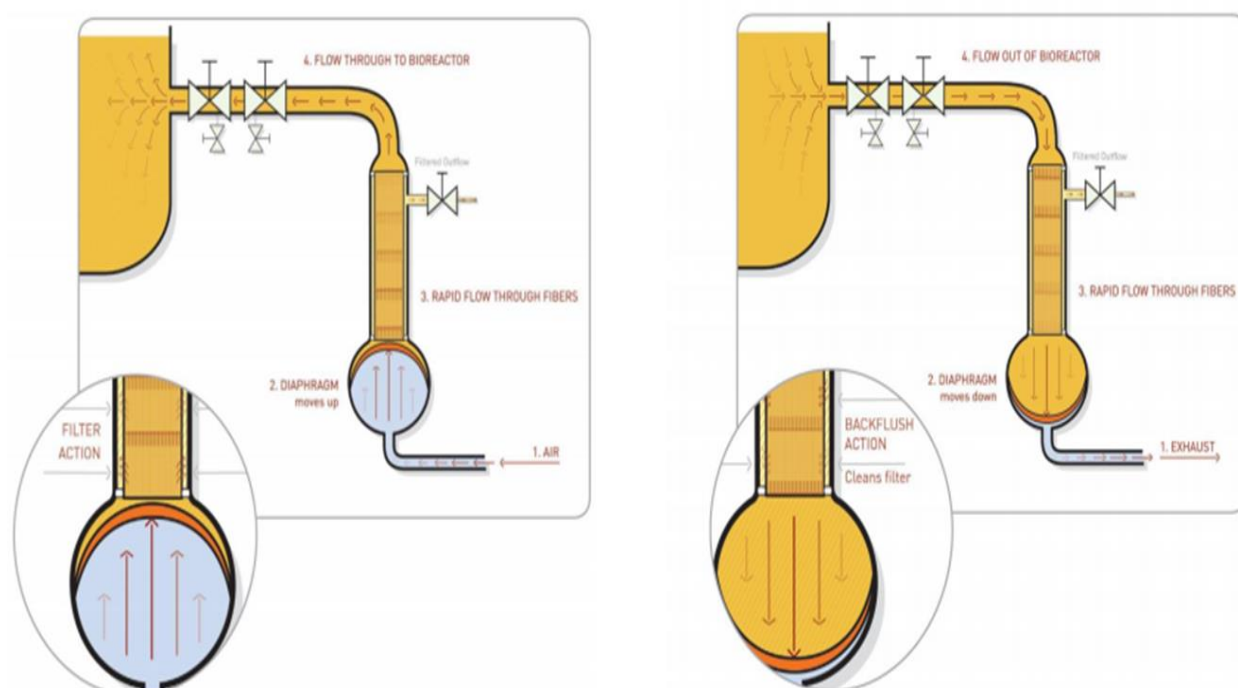


Figure 9-13. ATF pressure control system required for the diaphragm pump correct functionality from (Pineda, 2018).

9.7.6 Oxygen uptake rate (OUR)

The OUR used in this chapter in regard with its calculation and methodology have been already described in **chapter 5** section 5.8.6

9.7.7 Specific rate calculations in batch cultures

The methodology to calculate the specific rates in batch cultures is described in **chapter 3** section 3.8.9

9.7.8 Specific rate calculations in perfusion cultures

The growth rate in perfusion culture is expressed by **Equation 9-3**. The specific growth rate (μ) was calculated in the exponential growth phase by linear regression of the natural logarithm of the concentration of biomass (X) as function of time (t), as presented in **Equation 9-4**

The specific consumption/production rate (q_m) was calculated via numeric methods using **Equation 9-6** for glucose and lactate. The variables required for it were: the perfusion rate (Fp), the culture volume (V), the biomass concentration (X)), the metabolite concentration in the inlet flow ($C_{m,in}$) and in the outlet flow ($C_{m,out}$). Moreover, **Equation 9-7** was developed from resolving the differential term $\frac{\delta(C_{m,out} \cdot V)}{\delta t}$. On the other hand, the specific consumption rate (q_m) of oxygen was calculated using **Equation 9-5**.

Linear regression tool of Microsoft Excel 2016 (Microsoft) was used for obtaining the specific growth rate (μ) and the specific consumption/production rate (q_m) of glucose and lactate from **Equation 9-7**.

Equation 9-3

$$\frac{dX}{dt} = r_X = \mu \cdot X_v$$

Equation 9-4

$$\ln(X_v) = \ln(X_{v,0}) + \mu \cdot (t - t_0)$$

Equation 9-5

$$\frac{dC_m}{dt} = r_m = q_m \cdot X_v$$

Equation 9-6

$$Fp(t) \cdot (C_{m,out}(t) - C_{m,in}(t)) = q_m \cdot X(t) \cdot V - \frac{\delta(C_{m,out} \cdot V)}{\delta t}$$

Equation 9-7

$$\Delta (C_{m,out}(t) \cdot V) |_{(t - t_0)} = q_m \cdot \int_{t_0}^t (X(t) \cdot V) dt + \int_{t_0}^t (Fp(t) \cdot (C_{m,out}(t) - C_{m,in}(t))) dt$$

9.7.9 Fed-batch strategy

The methodology to calculate feeding profiles is described in **chapter 7** section 7.6.12

9.7.9.1 Biomass estimation by pre-programmed exponential

The calculation for the biomass estimation used for the preprogrammed exponential strategy been already described in **chapter 7** section 7.6.13. Moreover, its practical methodology is described in **chapter 7** section 7.6.11.1.

9.7.10 Perfusion strategy

In order to carry out a perfusion strategy, first a definition of the algorithm that will be used in order to describe how the feeding media is added must be defined. This algorithm is based on **Equation 9-8** and is able to calculate the feeding flow (F(t)) by means of using the specific

consumption rate of glucose ($q_{glucose}$), biomass ($X(t)$), volume (V), and the glucose concentration of both inlet and outlet flow ($C_{glucose,in}$) and ($C_{glucose,out}$), respectively.

Equation 9-8

$$F(t) = \frac{-q_{glucose} \cdot X(t) \cdot V}{C_{glucose,out} - C_{glucose,in}}$$

The calculation of biomass ($X(t)$) will specify which strategy are you going to use regarding the estimation of biomass during the experiment. In this case, the biomass estimation will be by using the OUR variable and the specific consumption rate of oxygen as shown in **Equation 9-9**.

Equation 9-9

$$X(t) = \frac{OUR(t)}{q_{oxygen}}$$

9.7.11 MFCS/win. Software for Data Acquisition, Monitoring and Control

BioPat® MFCS/win 3.0 (Sartorius Stedim Biotech, Germany) was used for monitoring and controlling the cell culture. All the strategies that are described in this chapter are based on recipe from MFCSwin in order to get all the information needed for granting a correct running.

Briefly, the recipes that were designed interacts with the bioreactor sensors in order to get the data and convert it to feeding flow by means of the equation which are explained in the section bellow.

The different control recipes were programmed accordingly to the culture operations requirements (batch, fed-batch based on pre-programmed exponential and perfusion based on OUR). The control recipes were able to conduct the actions required automatically.

9.7.11.1 Fed-batch strategy that is based on predicting the biomass concentration.

All the MFCS protocols and methodology in order to calculate feeding profile for fed-batch and perfusion strategies related to the use of the software MFCS are described in **chapter 7** section 7.6.11.

9.7.11.2 Perfusion strategy that is based on predicting the biomass concentration.

As shown in **Figure 9-14**, the recipe of the MFCSwin is based on a core flow function where several inputs are present. It is important to point that that this input can be the characteristics parameters of the flow function or the order to initialize it.

Basically, the parameters that the flow functions require for a fine operation are described in the following list and in the figure as well.

The parameters required for the OUR-estimation are listed hereafter:

- specific consumption rate of glucose (q_{glucose})
- specific production rate of carbon dioxide(q_{o_2})
- OUR(t)
- volume ($V(t)$).

Once the input parameters are fixed, the other input is the order to start the culture process, in these processes the order is manual manage by the user. Once the flow function starts running, it gives values to the feeding flow continuously, as show **in the bottom graph of the Figure 9-14**.

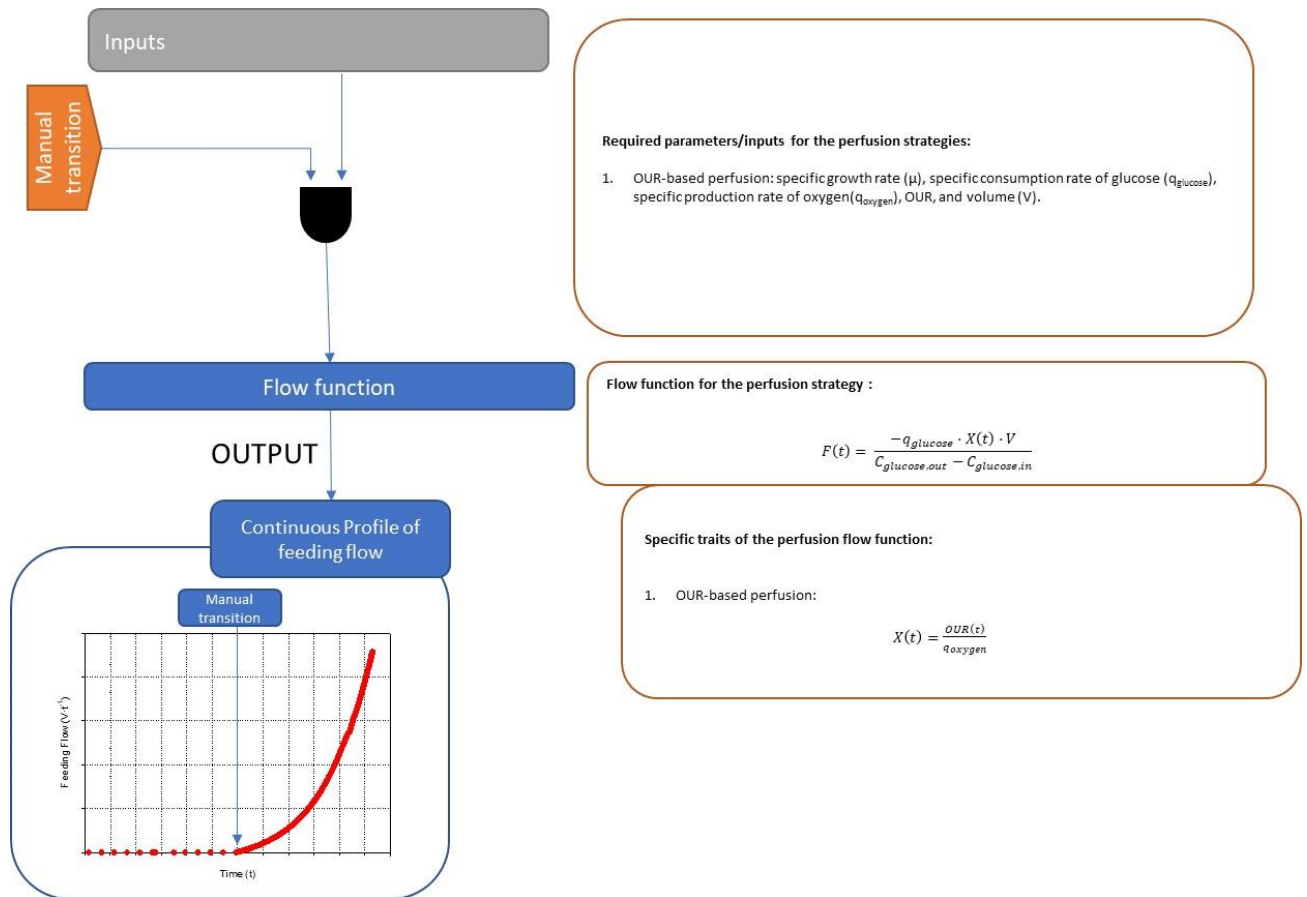


Figure 9-14 Flow diagram and description of the MFCSwin recipes whose objective is to calculate the feeding flow of the metabolic fed-batch cultures.

9.7.12 Statistics

Duplicates for each culture conditions were performed, but only one of the two duplicate experiment is presented in the Results section. Since the runs have not performed in parallel (due to equipment limitations), sampling time do not coincide, and other parameters may vary as the cell seeding density.

9.8 References

- Aehle, M. (2010). Application of BlueSens® Gas Analyzers in a Cell Culture Process. In *Report.1 - BlueSens* (pp. 22–28).
- Altamirano, C., Cairó, J. J., & Gòdia, F. (2001). Decoupling cell growth and product formation in Chinese hamster ovary cells through metabolic control. *Biotechnology and Bioengineering*, 76(4), 351–360. <https://doi.org/10.1002/bit.10096>
- Boedecker, B., Newcomb, R., Yuan, P., Braufman, A., & Kelsey, W. (1994). *Production of recombinant factor VIII from perfusion cultures*. (pp. 580–583).
- Bonarius, H. P. J., de Gooijer, C. D., Tramper, J., & Schmid, G. (1995). Determination of the respiration quotient in mammalian cell culture in bicarbonate buffered media. *Biotechnology and Bioengineering*, 45(6), 524–535. <https://doi.org/10.1002/bit.260450610>
- Casablancas, A., Gámez, X., Lecina, M., Solà, C., Cairó, J. J., & Gòdia, F. (2013). Comparison of control strategies for fed-batch culture of hybridoma cells based on on-line monitoring of oxygen uptake rate, optical cell density and glucose concentration. *Journal of Chemical Technology & Biotechnology*, 88(9), 1680–1689. <https://doi.org/10.1002/jctb.4019>
- Coco-Martin, J. M., & Harmsen, M. M. (2008). A review of therapeutic protein expression by mammalian cells. *BioProcess International*, 6(6), 28–33. http://www.bioprocessintl.com/wp-content/uploads/bpi-content/BPI_A_080606SUPAR04__78726a.pdf
- De Alwis, D. M., Dutton, R. L., Scharer, J., & Moo-Young, M. (2007). Statistical methods in media optimization for batch and fed-batch animal cell culture. *Bioprocess and Biosystems Engineering*, 30(2), 107–113. <https://doi.org/10.1007/s00449-006-0107-7>
- De Jesus, M., & Wurm, F. M. (2011). Manufacturing recombinant proteins in kg-ton quantities using animal cells in bioreactors. *European Journal of Pharmaceutics and Biopharmaceutics*, 78(2), 184–188. <https://doi.org/10.1016/j.ejpb.2011.01.005>
- Deo, Y. M., Mahadevan, M. D., & Fuchs, R. (1996). Practical Considerations in Operation and Scale-up of Spin-Filter Based Bioreactors for Monoclonal Antibody Production. *Biotechnology Progress*, 12(1), 57–64. <https://doi.org/10.1021/bp950079p>
- Dingermann, T. (2008). Recombinant therapeutic proteins: Production platforms and challenges. *Biotechnology Journal*, 3(1), 90–97. <https://doi.org/10.1002/biot.200700214>
- Haas, J., Tröbs, T., Clemens, C., Wunder, M., Rüger, M., & Schulz, T. W. (2010). Online Determination of Oxygen Uptake and Carbon Dioxide Production Rates in Mammalian Cell Culture Using Mass Spectrometry. In *Cells and Culture* (pp. 683–687). Springer Netherlands. https://doi.org/10.1007/978-90-481-3419-9_118
- Herterich, J. G., Xu, Q., Field, R. W., Vella, D., & Griffiths, I. M. (2017). Optimizing the operation of a direct-flow filtration device. *Journal of Engineering Mathematics*, 104(1), 195–211. <https://doi.org/10.1007/s10665-016-9879-1>
- Huang, Y.-M., Hu, W., Rustandi, E., Chang, K., Yusuf-Makagiansar, H., & Ryll, T. (2010). Maximizing productivity of CHO cell-based fed-batch culture using chemically defined media conditions and typical manufacturing equipment. *Biotechnology Progress*, 26(5), 1400–1410. <https://doi.org/10.1002/btpr.436>
- Kretzmer, G. (2002). Industrial processes with animal cells. *Applied Microbiology and Biotechnology*, 59(2–3), 135–142. <https://doi.org/10.1007/s00253-002-0991-y>
- Lecina, M., Tintó, A., Gálvez, J., Gòdia, F., & Cairó, J. (2011). Continuous perfusion culture of encapsulated hybridoma cells. *Journal of Chemical Technology & Biotechnology*, 86(12), 1555–1564. <https://doi.org/10.1002/jctb.2680>
- Lifescience, G. (2015). *Cell Boost™ Supplement* (p. 4). <https://gelifesciences.co.jp/catalog/pdf/29136822AACellBoost4.pdf>
- Liste-Calleja, L., Lecina, M., & Cairó, J. J. (2014). HEK293 cell culture media study towards bioprocess optimization: Animal derived component free and animal derived component containing platforms. *Journal of Bioscience and Bioengineering*, 117(4), 471–477. <https://doi.org/10.1016/j.jbiosc.2013.09.014>

- Martínez-Monge, I., Roman, R., Comas, P., Fontova, A., Lecina, M., Casablanco, A., & Cairó, J. J. (2019). New developments in online OUR monitoring and its application to animal cell cultures. *Applied Microbiology and Biotechnology*, 103(17), 6903–6917. <https://doi.org/10.1007/s00253-019-09989-4>
- Martínez, V. S., Dietmair, S., Quek, L.-E., Hodson, M. P., Gray, P., & Nielsen, L. K. (2013). Flux balance analysis of CHO cells before and after a metabolic switch from lactate production to consumption. *Biotechnology and Bioengineering*, 110(2), 660–666. <https://doi.org/10.1002/bit.24728>
- Ozturk, S. S., Riley, M. R., & Palsson, B. O. (1992). Effects of ammonia and lactate on hybridoma growth, metabolism, and antibody production. *Biotechnology and Bioengineering*, 39(4), 418–431. <https://doi.org/10.1002/bit.260390408>
- Paredes, C., Sanfeliu, A., Cardenas, F., & Cairo, J. J. (1998). *Estimation of the intracellular fluxes for a hybridoma cell line by material balances*. 0229(98), 187–198.
- Pereira, S., Kildegaard, H. F., & Andersen, M. R. (2018). Impact of CHO Metabolism on Cell Growth and Protein Production: An Overview of Toxic and Inhibiting Metabolites and Nutrients. *Biotechnology Journal*, 13(3), 1–13. <https://doi.org/10.1002/biot.201700499>
- Pineda, E. (2018). *Perfusion and Beyond The XCell™ ATF System Web ads*.
- Ray, N. G., Karkare, S. B., & Runstadler, P. W. (1989). Cultivation of hybridoma cells in continuous cultures: Kinetics of growth and product formation. *Biotechnology and Bioengineering*, 33(6), 724–730. <https://doi.org/10.1002/bit.260330610>
- Rønning, Ø. W., Scharthum, M., Winsnes, A., & Lindberg, G. (1991). Growth limitation in hybridoma cell cultures: The role of inhibitory or toxic metabolites. *Cytotechnology*, 7(1), 15–24. <https://doi.org/10.1007/BF00135634>
- Sierra, E. (2014). *CONTINUOUS MAMMALIAN CELL CULTURES CHARACTERIZATION AND OPTIMIZATION OF TWO PERFUSION SYSTEMS*.
- Woodside, S. M., Bowen, B. D., & Piret, J. M. (1998). Mammalian cell retention devices for stirred perfusion bioreactors. *Cytotechnology*, 28(1–3), 163–175. <https://doi.org/10.1023/a:1008050202561>
- Xing, Z., Kenty, B., Koyrakh, I., Borys, M., Pan, S.-H., & Li, Z. J. (2011). Optimizing amino acid composition of CHO cell culture media for a fusion protein production. *Process Biochemistry*, 46(7), 1423–1429. <https://doi.org/10.1016/j.procbio.2011.03.014>
- Yao, T., & Asayama, Y. (2017). Animal-cell culture media: History, characteristics, and current issues. *Reproductive Medicine and Biology*, 16(2), 99–117. <https://doi.org/10.1002/rmb2.12024>
- Zhang, Q., Fang, M., Li, J., & Cao, R. (2020). Development and optimization of perfusion process for mammalian cell culture. *Sheng Wu Gong Cheng Xue Bao*, 36(6), 1041–1050. <https://doi.org/10.13345/j.cjb.190431>

10. General conclusions and future work

The work presented in this thesis has been conducted with the aim of understanding the carbon metabolism related to the production acetate in bacteria, ethanol and glycerol in yeast and lactate in animal cells in order to improving the volumetric productivity when an industrial scale bioprocess is designed. With this goal, substantial contributions were made in both bioprocess engineering and systems biology fields. First, the carbon metabolism of *E.coli* M15, *E.coli* BL21, *S. cerevisiae*, *P. pastoris*, HEK293, hybridoma KB26.5 and hybridoma KB26.5-BHRF1 was characterized using genome scale metabolic models. These models were previously adapted in this thesis. All the knowledge gained in the metabolic study was applied to develop new robust monitoring and controlling tools to increase the volumetric productivity of fed-batch and perfusion strategies in bioreactor.

In relation with bacteria (*E. coli* BL21) and yeast (*S. cerevisiae*) bioprocesses, this tool was based on following the biomass profile through the monitor of biomass related variables. CER and the alkali buffer addition were used as a biomass-related variable. In the case of CER, it was related to the carbon dioxide produced by the glucose oxidation while the alkali buffer addition gave information about the products of the carbon metabolism that interacted with the pH, as acetate production in *E. coli*. However, as it was stated in metabolic studies of *E. coli* (**chapter 3**) and *S. cerevisiae* (**chapter 4**), due to the metabolic changes observed in the fed-batch phases, the prediction of the biomass concentration based on biomass-related variable became impossible, and consequently, controlling the culture's growth and its carbon demands. On this basis, a new tool was developed based on following the carbon dioxide response of the culture when a glucose pulse was added. Its use in fed-batch cultures was able to adapt the feeding profile to the carbon requirements and promoted the optimal growth depending on the environmental conditions.

Considering the animal cells (hybridoma KB26.5-BHRF1) bioprocess, to further increase the biomass obtained in a batch culture, a fed-batch based on a theoretical growth was carried out. Even if the biomass concentration was increased, the application of the feeding profile based on biomass-related variables were avoid due to the inconsistency of the carbon metabolism observed coupled with the appearance of a growth inhibition conditions at the mid stages of the fed-batch phase. However, a new culture strategy was carried in order to overcome these problematics, the perfusion strategy. The use of perfusion grants a constant metabolic phase due to the environmental conditions remain constant, moreover, it limits the accumulation of

growth inhibition products. The application of the perfusion brought a huge increase in the biomass concentration even if the specific growth was reduced in comparison with the reference biomass.

From the work developed and the obtained results, it can be conducted in relation with each chapter that:

Chapter 3. Physiology and metabolism of *Escherichia coli*

- The acetate production is based on an unbalance in acetyl-coA generated by an uncoupling between the flux through glycolytic pathway and TCA cycle. The origin of decoupling is hypothesized to be caused by a high glycolytic pathway that repress TCA's gene expression and the oversize of flux carbon acceptance of the TCA by means of using the anaplerotic reactions (glyoxylate and PEP-OAA shunts) as a "relief valve".
- The metabolic analysis of the proportion of ATP suggests that oxidative phosphorylation pathway is more active in *E. coli* BL21 than in *E. coli* M15. In addition, *E. coli* M15 generates more ATP via glycolytic pathway than *E. coli* BL21 and the cell maintenance of *E. coli* BL21 is higher than *E. coli* M15.
- The specific consumption rate of glucose can be modified through changing the environmental conditions, as it was observed in the *E. coli* BL21 continuous culture where the increase in the glucose availability provoked an increase the flux through the glycolytic pathway and TCA cycle until a limit is reached. Consequently, when TCA cannot metabolize all the acetyl-coA generated by the glycolytic pathway, acetate is produced.
- An improvement in the glucose conversion towards biomass was obtained when the glucose availability was decreased during the course of the continuous culture.

Chapter 4. Physiology and metabolism of *Saccharomyces cerevisiae*

- The ethanol production is related to an unbalance in the cytoplasmic NADH pool generated by three pathways regulated by the glucose availability:
 - the overexpression of the glucose transporters under excess glucose conditions in order to maximize the glucose consumption rate

- the regulation of the flux through the glycolytic pathway in order to be able to obtain high glucose consumption rates
 - the repression of the aerobic pathway under high external glucose concentrations
- *P. pastoris* is described as a low-ethanol producer yeast because the cytoplasmic NADH from the flux through the glycolytic pathway was able to be completely regenerated through mitochondrial shuttles.
- As it was observed in the *S. cerevisiae* continuous culture, the specific consumption rate of glucose can be modified through changing the environmental conditions. Specifically, the decrease in the extracellular glucose performed a metabolic restructuring based on decreasing the flux through the glycolytic and the ethanol pathways, while flux through the TCA remained unaffected.
- The specific production rate of ethanol was reduced due to a decrease in the glucose availability. Moreover, a metabolic threshold was observed where a minimum relation between the specific consumption rate of glucose consumed and the specific production rate of ethanol had a value revolving around 1,9.
- An improvement in the glucose conversion towards biomass was obtained when the glucose availability was decreased, owing to a decrease in the ethanol produced.
- Regarding the energy metabolism during the course of the continuous culture, the analysis of the ATP produced and consumed showed an interesting feature: the change in the glycolic flux did not affect the total ATP available and the distribution of ATP produced and consumed. This might be a peculiar trait of how the production of partially oxidized products due to a NADH cytoplasmic unbalance did not disturb the aerobic metabolism (the OP) and had a slightly impact in the ATP from the substrate level phosphorylation owing to a decrease in the flux through the glycolytic pathway.

Chapter 5. Physiology and metabolism of *animal cells*

- The lactate production, no matter which animal cell is studied, was related to a perturbation in the redox potential caused by an unbalance in the cytoplasmic NADH. It was caused by a difference between the fluxes through the glycolytic pathway and the flux through the mitochondrial shuttles.

- The transfection of the BHRF1 gene to hybridoma KB26.5 provoked a restructuring of the carbon metabolism. Specifically, the conversion of glucose to lactate was reduced while the specific growth rate was improved. The metabolic analysis concluded that the reduction in the lactate produced was correlated with a decrease in the flux through the glycolytic pathway that could be caused by the interaction between the BHRF1 gene and the mitochondrial metabolism. As a result, this interaction could modify the cellular redox compartmentalization. Moreover, the increase of the specific growth could be related to a slightly increase in the biomass precursors from the mitochondria and also to an increase in the total ATP that might be produced due to the modification of the mitochondrial energy metabolism by the expression of an anti-apoptotic gene.
- When HEK293 was cultured on fructose used as carbon source, a non-lactate producer metabolism was obtained due to a low flux through the glycolytic pathway. It provoked a low availability of cytoplasmic NADH that was completely oxidized by mitochondrial shuttles. However, a reduction in the growth rate was observed due to a carbon rate limitation.
- When HEK293 was cultured on fructose supplemented with sodium lactate, the specific rate was recovered while fructose was consumed simultaneously with lactate. Moreover, the addition of lactate only increased the mitochondrial metabolism because all the lactate consumption was oxidized to NADH and pyruvate.

Chapter 7. *Escherichia coli* bioprocess definition

- A new batch media was designed based on increasing the concentration of all the media components until a growth inhibition was reached. As a result, the biomass concentration increased by 2,48-fold in comparison with the reference batch.
- The application of a fed-batch strategy based on the estimation of the culture's growth as an exponential function, produced an increase in the biomass concentration of 5,75-fold compared with the reference batch. However, a slightly constant glucose accumulation was present due to the incapacity to predict modifications in the growth rate.
- The carbon exchange rate (CER) and the alkali buffer addition were used in order to develop a feeding profile that was able to predict the biomass concentration on-line during early stages of the FDB phase. When the biomass-based feeding profile was applied, the biomass concentration was increased in comparison with the reference

batch by 4,72-fold and 6,56-fold, respectively. However, due to the inability to predict modifications in the carbon metabolism depending on the changes in the environmental conditions was impossible to predict the metabolic parameters used by the feeding profiles, as a consequence, glucose was accumulated in the case of the alkali buffer addition or became a growth-limiting condition in the case of CER.

- A new automatic fed-batch strategy was developed that did not depend on the metabolic state of *E. coli* to calculate the feeding rate. This strategy was successfully applied, and at the end of the culture there was no glucose accumulation and the biomass concentration increased by compared with the reference batch. Even if the application of the new methodology did not produce an increase in the biomass concentration in comparison with the other FDB strategies, a fully automatic fed-batch that did not depended on metabolic data or any other experimental data was develop.
- The new methodology was tested in the induction via IPTG of an *E. coli* fed-batch culture. First, the induction conditions were defined where two concentrations (150 μM and 500 μM) and two addition methodologies (lineal addition and step addition) were analysed. The optimal condition for the induction were defined as a single pulse of 150 μM of IPTG because this method acquired the highest GFP-biomass yield. When the induction-FDB was carried out, the results obtained stated that the algorithm fitted the *E. coli* BL21-GFP growth-related demands letting the culture to grow during the growth phase of the FDB and, thus, in the induction phase, the feeding profile was adapted without neither oversizing the glucose feeding nor limiting the protein production.

Chapter 8. *Saccharomyces cerevisiae* bioprocess definition

- A new batch media was designed based on increasing the concentration of all the media components until a growth inhibition was reached. As a result, the biomass concentration increased by 3,43-fold in comparison with the reference batch.
- The application of a fed-batch strategy based on the estimation of the culture's growth as an exponential function produced an increase in the biomass concentration of 3,69-fold compared with the reference batch. The use of the metabolic data obtained in **chapter 4**, reduced the ethanol specific rate in a 56%, and the conversion of glucose towards biomass was optimized. Moreover, the incapability of the carbon metabolism to keep a steady metabolic phase during the course of the feeding addition was observed. Therefore, the next strategy to further increase the biomass concentration

was the non-metabolic methodology used in **chapter 7** due to it was able to carry out the optimal metabolic conditions during the course of the experiment without using any metabolic data.

- The application of the non-metabolic methodology to calculate the feeding profile did not increase the biomass concentration obtained in the previous one. However, it was possible to increase the biomass concentration as in previous FDB without performing a metabolic analysis in order to find the optimal specific consumption rate that granted the optimal conversion of glucose to biomass. Therefore, this strategy was carried without any previous data.
- The next experimental proposed was an induction experiment with the *S. cerevisiae* in order to evaluate how the feeding strategy might affect the protein production. The model protein selected was GFP with an auxotroph marker to grant the synthesis of histidine. However, due to the growth limitation and the improvement of the production of ethanol owing to the auxotrophies expressed in *S. cerevisiae*, the auxotrophic study was abandoned even if the GFP was correctly expressed. In addition, a new strategy to overcome the metabolic issues was described, even if it was not implemented. The expression of an antibiotic as a marker using as a platform *S. cerevisiae* wild type.

Chapter 9. Animal cell bioprocess definition

- The definition of the feeding solution was carried out via a shake-flask experiment testing two solutions based on a chemical defined supplement (Cell boost 5 and Cell boost 6). Due to there was no grow difference between; the feeding media based on cell boost 5 was selected as the reference feeding solution.
- A fed-batch based on theoretical profile of the growth rate in order to calculate the feeding profile was carried out using the reference feeding solution. As a result, the biomass concentration increased 1,43-fold in comparison with the reference batch culture. However, it was observed that the metabolic data changed during the course of the FDB phase in an abruptly manner leading the feeding profile to be not representative regarding the culture growth requirements that could be caused by the apparition of growth inhibition conditions.
- A perfusion strategy was carried out in order to solve the metabolic issues described in the fed-batch culture. OUR was used to predict the biomass profile in order to grant the

optimal feeding profile. Its application presented an 6,46-fold increase in the biomass concentration while the growth limiting conditions observed in FDB was overcome. In addition, a 30 % reduction in the lactate production was achieved while the specific growth rate was reduced by near 25 %. The use of a dilution rate profile lower than the required one in order to avoid a growth inhibition was the responsible for the reduction in the growth rate. However, even if the specific growth rate was reduced, the complete inhibition observed in FDB was avoided.

- The use of alkali buffer addition as a control variable should be possible if the feeding media pH is adjusted to the culture physiological conditions, then its use as a biomass-related variable might be possible.

The work developed in this thesis pretend to be a starting point to understand the carbon metabolism in culture in order to increase the volumetric productivity of bioprocesses. Thus, some future work detailed down below is proposed:

Multi-Omics Data Integration approach in metabolic models:

In this work, only exometabolomics (extracellular metabolites profile concentration) has been used to characterize different carbon metabolisms (acetate production, ethanol production and lactate production) using FBA. Although this approach has been widely used in the literature and it has generated valuable results for the case of the work presented, to improve the understanding of the metabolic adaptation to specific environmental conditions a combination of transcriptomics, metabolomics (meaning intracellular metabolites concentrations) and proteomics is proposed to be included in the metabolic model. This approach will allow a better characterization of all the microorganism described, as well as will be useful to detect the differences in protein expression and concentration depending on the extracellular conditions. Furthermore, the intracellular concentrations of the different metabolites directly involved in the carbon metabolisms could open the door to determine why the different proton and lactate extracellular concentration triggers one or other metabolic phase.

¹³C analysis:

Although the metabolic models used for studying the cells in culture normally contains very few degrees of freedom, not all the metabolic fluxes of the system can be determined solely by

measurement of extracellular metabolites concentration. This leads to obtain a range of possible solutions in some of the fluxes of the model, even if some reactions are maximized in order to obtain only one solution. For example, it is not possible to determine the ratio of the NADPH generation between the oxidative pentose-phosphate pathway and cytosolic malic enzyme. For this, experiments in which glucose or glutamine are labelled to reveal how these substrates are distributed into the model are strongly recommended to resolved those fluxes.

Study of concomitant fructose and lactate consumption in other mammalian cell lines:

In order to stablish a general assumption regarding the fructose and lactate co-consumption, a similar study that was performed in this work in HEK293 should be done in other mammalian cell lines, as CHO. It is particularly interesting to see if similar results might be obtained in other different mammalian cell lines, to clearly make a general assumption in relation with the lactate metabolism depending on the carbon source consumed.

Application of the non-metabolic methodology in all the available bioprocess, specifically, in animal cell cultures:

As stated, the application of this new methodology in fed-batch cultures brought a feeding profile able to grant an optimal conversion of the carbon source to biomass while the specific growth rate was at its optimal value. However, due to the analytical device used, its application in animal cells was impossible. If another analytic methodology was used, it could be possible its application.

11. Appendix

APPENDIX A: *E. coli* M15 and *E. coli* BL21 metabolic model

The *E. coli* M15 and *E. coli* BL21 modelling used the same metabolic model for all p-FBA presented in the chapter 3. The resulting model used for the metabolic flux calculation, that contains 455 reactions and 438 metabolites, is detailed in **Table A**.

Table A. List of reactions included in the *E. coli* M15 and *E. coli* BL21 reduced model developed and used for all Flux Balance Analysis in the Chapter 3.

Bio_T	Bio	----->	Bio_ext_b
R_3HAD100	M_3hdecACP_c	----->	M_h2o_c + M_tdec2eACP_c
R_3HAD120	M_3hddecACP_c	----->	M_h2o_c + M_tdddec2eACP_c
R_3HAD121	M_3hcddec5eACP_c	----->	M_h2o_c + M_t3c5ddeceACP_c
R_3HAD140	M_3hmrsACP_c	----->	M_h2o_c + M_tmrs2eACP_c
R_3HAD141	M_3hcmrs7eACP_c	----->	M_h2o_c + M_t3c7mrseACP_c
R_3HAD160	M_3hpalmACP_c	----->	M_h2o_c + M_tpalm2eACP_c
R_3HAD161	M_3hcpalm9eACP_c	----->	M_h2o_c + M_t3c9palmeACP_c
R_3HAD40	M_3haACP_c	----->	M_h2o_c + M_but2eACP_c
R_3HAD60	M_3hhexACP_c	----->	M_h2o_c + M_thex2eACP_c
R_3HAD80	M_3hoctACP_c	----->	M_h2o_c + M_toct2eACP_c
R_3OAR100	M_h_c + M_nadph_c + M_3odecACP_c	<----->	M_nadp_c + M_3hdecACP_c
R_3OAR120	M_h_c + M_nadph_c + M_3oddecACP_c	<----->	M_nadp_c + M_3hddecACP_c
R_3OAR121	M_h_c + M_nadph_c + M_3ocdddec5eACP_c	----->	M_nadp_c + M_3hcddec5eACP_c
R_3OAR140	M_h_c + M_nadph_c + M_3omrsACP_c	<----->	M_nadp_c + M_3hmrsACP_c
R_3OAR141	M_h_c + M_nadph_c + M_3ocmrs7eACP_c	----->	M_nadp_c + M_3hcmrs7eACP_c
R_3OAR160	M_h_c + M_nadph_c + M_3opalmACP_c	<----->	M_nadp_c + M_3hpalmACP_c
R_3OAR161	M_h_c + M_nadph_c + M_3ocpalm9eACP_c	----->	M_nadp_c + M_3hcpalm9eACP_c
R_3OAR40	M_h_c + M_nadph_c + M_actACP_c	<----->	M_nadp_c + M_3haACP_c
R_3OAR60	M_h_c + M_nadph_c + M_3ohexACP_c	<----->	M_nadp_c + M_3hhexACP_c

R_3OAR80	M_h_c + M_nadph_c + M_3oocACP_c	<---->	M_nadp_c + M_3hoctACP_c
R_3OAS100	M_h_c + M_ocACP_c + M_malACP_c	----->	M_co2_c + M_ACP_c + M_3odecACP_c
R_3OAS120	M_h_c + M_malACP_c + M_dcaACP_c	----->	M_co2_c + M_ACP_c + M_3oddecACP_c
R_3OAS121	M_h_c + M_malACP_c + M_cdec3eACP_c	----->	M_co2_c + M_ACP_c + M_3ocdddec5eACP_c
R_3OAS140	M_h_c + M_malACP_c + M_ddcaACP_c	----->	M_co2_c + M_3omrsACP_c + M_ACP_c
R_3OAS141	M_h_c + M_malACP_c + M_cddec5eACP_c	----->	M_co2_c + M_3ocmrs7eACP_c + M_ACP_c
R_3OAS160	M_h_c + M_myrsACP_c + M_malACP_c	----->	M_co2_c + M_3opalmACP_c + M_ACP_c
R_3OAS161	M_h_c + M_tdeACP_c + M_malACP_c	----->	M_co2_c + M_3ocpalm9eACP_c + M_ACP_c
R_3OAS60	M_h_c + M_butACP_c + M_malACP_c	----->	M_co2_c + M_ACP_c + M_3ohexACP_c
R_3OAS80	M_h_c + M_hexACP_c + M_malACP_c	----->	M_co2_c + M_ACP_c + M_3oocACP_c
R_5DOAN	M_h2o_c + M_dad_5_c	----->	M_ade_c + M_5drib_c
R_A5PISO	M_ru5p_D_c	<---->	M_ara5p_c
R_ACALD	M_nad_c + M_coa_c + M_acald_c	<---->	M_h_c + M_nadh_c + M_accoa_c
R_ACALDtex	M_acald_e	<---->	M_acald_p
R_ACALDtp	M_acald_p	<---->	M_acald_c
R_ACCOAC	M_atp_c + M_accoa_c + M_hco3_c	----->	M_h_c + M_pi_c + M_adp_c + M_malcoa_c
R_ACGK	M_atp_c + M_acglu_c	----->	M_adp_c + M_acg5p_c
R_ACGS	M_glu_L_c + M_accoa_c	----->	M_h_c + M_coa_c + M_acglu_c
R_ACHBS	M_h_c + M_2obut_c + M_pyr_c	----->	M_co2_c + M_2ahbut_c
R_ACKr	M_atp_c + M_ac_c	<---->	M_adp_c + M_actp_c
R_ACLS	M_h_c + 2.0*M_pyr_c	----->	M_co2_c + M_alac_S_c
R_ACODA	M_h2o_c + M_acorn_c	----->	M_orn_c + M_ac_c
R_ACONTa	M_cit_c	<---->	M_h2o_c + M_acon_C_c
R_ACONTb	M_h2o_c + M_acon_C_c	<---->	M_icit_c
R_ACOTA	M_akg_c + M_acorn_c	<---->	M_glu_L_c + M_acg5sa_c
R_AcT2rpp	M_h_p + M_ac_p	<---->	M_h_c + M_ac_c
R_AcTex	M_ac_e	<---->	M_ac_p

R_ADCL	M_4adcho_c	----->	M_h_c + M_pyr_c + M_4abz_c
R_ADCS	M_gln_L_c + M_chor_c	----->	M_glu_L_c + M_4adcho_c
R_ADK1	M_amp_c + M_atp_c	<----->	2.0*M_adp_c
R_ADNK1	M_atp_c + M_adn_c	----->	M_h_c + M_amp_c + M_adp_c
R_ADSK	M_atp_c + M_aps_c	----->	M_h_c + M_adp_c + M_paps_c
R_ADSL1r	M_dcamp_c	<----->	M_amp_c + M_fum_c
R_ADSL2r	M_25aics_c	<----->	M_fum_c + M_aicar_c
R_ADSS	M_imp_c + M_asp_L_c + M_gtp_c	----->	2.0*M_h_c + M_pi_c + M_dcamp_c + M_gdp_c
R_AGPAT160	M_1hdecg3p_c + M_palmACP_c	----->	M_ACP_c + M_pa160_c
R_AGPAT161	M_hdeACP_c + M_1hdec9eg3p_c	----->	M_pa161_c + M_ACP_c
R_AGPR	M_pi_c + M_nadp_c + M_acg5sa_c	<----->	M_h_c + M_nadph_c + M_acg5p_c
R_AHCYSNS	M_h2o_c + M_ahcys_c	----->	M_ade_c + M_rhcys_c
R_AICART	M_10fthf_c + M_aicar_c	<----->	M_fprica_c + M_thf_c
R_AIRC2	M_atp_c + M_hco3_c + M_air_c	----->	M_h_c + M_pi_c + M_adp_c + M_5caiz_c
R_AIRC3	M_5aizc_c	<----->	M_5caiz_c
R_AKGDH	M_nad_c + M_akg_c + M_coa_c	----->	M_nadh_c + M_co2_c + M_succoa_c
R_AKGt2rpp	M_h_p + M_akg_p	<----->	M_h_c + M_akg_c
R_AKGtex	M_akg_e	<----->	M_akg_p
R_ALAALAR	M_atp_c + 2.0*M_ala_D_c	<----->	M_h_c + M_pi_c + M_adp_c + M_alaala_c
R_ALAR	M_ala_L_c	<----->	M_ala_D_c
R_ALATA_L	M_akg_c + M_ala_L_c	<----->	M_glu_L_c + M_pyr_c
R_ALCD2x	M_nad_c + M_etoh_c	<----->	M_h_c + M_nadh_c + M_acald_c
R_AMPMS2	M_h2o_c + M_nad_c + M_air_c	----->	3.0*M_h_c + M_nadh_c + 2.0*M_for_c + M_4ampm_c
R_ANPRT	M_prpp_c + M_anth_c	----->	M_ppi_c + M_pran_c
R_ANS	M_gln_L_c + M_chor_c	----->	M_h_c + M_glu_L_c + M_pyr_c + M_anth_c
R_APRAUR	M_h_c + M_nadph_c + M_5apru_c	----->	M_nadp_c + M_5aprbu_c
R_ARGSL	M_argsuc_c	<----->	M_fum_c + M_arg_L_c

R_ARGSS	$M_{\text{atp_c}} + M_{\text{asp_L_c}} + M_{\text{citr_L_c}}$	----->	$M_{\text{h_c}} + M_{\text{amp_c}} + M_{\text{ppi_c}} + M_{\text{argsuc_c}}$
R_ASAD	$M_{\text{pi_c}} + M_{\text{nadp_c}} + M_{\text{aspsa_c}}$	<----->	$M_{\text{h_c}} + M_{\text{nadph_c}} + M_{\text{4pasp_c}}$
R_ASNS2	$M_{\text{atp_c}} + M_{\text{asp_L_c}} + M_{\text{nh4_c}}$	----->	$M_{\text{h_c}} + M_{\text{amp_c}} + M_{\text{ppi_c}} + M_{\text{asn_L_c}}$
R_ASP1DC	$M_{\text{h_c}} + M_{\text{asp_L_c}}$	----->	$M_{\text{ala_B_c}} + M_{\text{co2_c}}$
R_ASPCT	$M_{\text{cbp_c}} + M_{\text{asp_L_c}}$	----->	$M_{\text{h_c}} + M_{\text{cbasp_c}} + M_{\text{pi_c}}$
R_ASPK	$M_{\text{atp_c}} + M_{\text{asp_L_c}}$	<----->	$M_{\text{adp_c}} + M_{\text{4pasp_c}}$
R_ASPO5	$M_{\text{asp_L_c}} + M_{\text{fum_c}}$	----->	$M_{\text{h_c}} + M_{\text{succ_c}} + M_{\text{iasp_c}}$
R_ASPTA	$M_{\text{asp_L_c}} + M_{\text{akg_c}}$	<----->	$M_{\text{glu_L_c}} + M_{\text{oaa_c}}$
R_ATPM	$M_{\text{h2o_c}} + M_{\text{atp_c}}$	----->	$M_{\text{h_c}} + M_{\text{pi_c}} + M_{\text{adp_c}}$
R_ATPPRT	$M_{\text{atp_c}} + M_{\text{prpp_c}}$	----->	$M_{\text{ppi_c}} + M_{\text{prbatp_c}}$
R_ATPS4rpp	$M_{\text{pi_c}} + M_{\text{adp_c}} + 4.0 * M_{\text{h_p}}$	<----->	$M_{\text{h2o_c}} + 3.0 * M_{\text{h_c}} + M_{\text{atp_c}}$
R_BPNT	$M_{\text{h2o_c}} + M_{\text{pap_c}}$	----->	$M_{\text{amp_c}} + M_{\text{pi_c}}$
R_CA2tex	$M_{\text{ca2_e}}$	<----->	$M_{\text{ca2_p}}$
R_Cat6pp	$M_{\text{ca2_c}} + M_{\text{na1_p}}$	<----->	$M_{\text{na1_c}} + M_{\text{ca2_p}}$
R_CBMKr	$M_{\text{atp_c}} + M_{\text{nh4_c}} + M_{\text{co2_c}}$	<----->	$2.0 * M_{\text{h_c}} + M_{\text{cbp_c}} + M_{\text{adp_c}}$
R_CDPMEK	$M_{\text{atp_c}} + M_{\text{4c2me_c}}$	----->	$M_{\text{h_c}} + M_{\text{adp_c}} + M_{\text{2p4c2me_c}}$
R_CHORM	$M_{\text{chor_c}}$	----->	$M_{\text{pphn_c}}$
R_CHORS	$M_{\text{3psme_c}}$	----->	$M_{\text{pi_c}} + M_{\text{chor_c}}$
R_CHRPL	$M_{\text{chor_c}}$	----->	$M_{\text{pyr_c}} + M_{\text{4hbz_c}}$
R_CLt3_2pp	$M_{\text{h_c}} + 2.0 * M_{\text{cl_p}}$	----->	$M_{\text{h_p}} + 2.0 * M_{\text{cl_c}}$
R_CLtex	$M_{\text{cl_e}}$	<----->	$M_{\text{cl_p}}$
R_CO2tex	$M_{\text{co2_e}}$	<----->	$M_{\text{co2_p}}$
R_CO2tpp	$M_{\text{co2_p}}$	<----->	$M_{\text{co2_c}}$
R_COBALT2tex	$M_{\text{cobalt2_e}}$	<----->	$M_{\text{cobalt2_p}}$
R_COBALT2tpp	$M_{\text{cobalt2_p}}$	----->	$M_{\text{cobalt2_c}}$
R_CPPPGO2	$M_{\text{cpppg3_c}} + 2.0 * M_{\text{amet_c}}$	----->	$2.0 * M_{\text{co2_c}} + 2.0 * M_{\text{met_L_c}} + M_{\text{pppg9_c}} + 2.0 * M_{\text{dad_5_c}}$
R_CS	$M_{\text{h2o_c}} + M_{\text{accoa_c}} + M_{\text{oaa_c}}$	----->	$M_{\text{h_c}} + M_{\text{coa_c}} + M_{\text{cit_c}}$

R_CTPS2	$M_{h2o_c} + M_{atp_c} + M_{glu_L_c} + M_{utp_c}$	----->	$2.0 * M_{h_c} + M_{pi_c} + M_{glu_L_c} + M_{adp_c} + M_{ctp_c}$
R_CU2tex	M_{cu2_e}	<----->	M_{cu2_p}
R_CU2tpp	M_{cu2_p}	----->	M_{cu2_c}
R_CYSS	$M_{h2s_c} + M_{acser_c}$	----->	$M_{h_c} + M_{cys_L_c} + M_{ac_c}$
R_CYSTL	$M_{h2o_c} + M_{cyst_L_c}$	----->	$M_{nh4_c} + M_{pyr_c} + M_{hcys_L_c}$
R_CYTBDpp	$2.0 * M_{h_c} + M_{q8h2_c} + 0.5 * M_{o2_c}$	----->	$M_{h2o_c} + 2.0 * M_{h_p} + M_{q8_c}$
R_CYTBO3_4pp	$4.0 * M_{h_c} + M_{q8h2_c} + 0.5 * M_{o2_c}$	----->	$M_{h2o_c} + 4.0 * M_{h_p} + M_{q8_c}$
R_CYTK1	$M_{atp_c} + M_{cmp_c}$	<----->	$M_{adp_c} + M_{cdp_c}$
R_D_LACt2pp	$M_{lac_D_p} + M_{h_p}$	<----->	$M_{h_c} + M_{lac_D_c}$
R_D_LACtex	$M_{lac_D_e}$	<----->	$M_{lac_D_p}$
R_DALAt2pp	$M_{h_p} + M_{ala_D_p}$	----->	$M_{h_c} + M_{ala_D_c}$
R_DAPDC	$M_{h_c} + M_{26dap_M_c}$	----->	$M_{co2_c} + M_{lys_L_c}$
R_DAPE	$M_{26dap_LL_c}$	<----->	$M_{26dap_M_c}$
R_DASYN160	$M_{h_c} + M_{pa160_c} + M_{ctp_c}$	----->	$M_{ppi_c} + M_{cdpdhdecg_c}$
R_DASYN161	$M_{h_c} + M_{pa161_c} + M_{ctp_c}$	----->	$M_{ppi_c} + M_{cdpdhdec9eg_c}$
R_DB4PS	$M_{ru5p_D_c}$	----->	$M_{h_c} + M_{for_c} + M_{db4p_c}$
R_DDPA	$M_{h2o_c} + M_{e4p_c} + M_{pep_c}$	----->	$M_{pi_c} + M_{2dda7p_c}$
R_DHAD1	M_{23dhmb_c}	----->	$M_{h2o_c} + M_{3mob_c}$
R_DHAD2	M_{23dhmp_c}	----->	$M_{h2o_c} + M_{3mop_c}$
R_DHDPRy	$M_{h_c} + M_{nadph_c} + M_{23dhdp_c}$	----->	$M_{nadp_c} + M_{thdp_c}$
R_DHDPS	$M_{pyr_c} + M_{aspsa_c}$	----->	$2.0 * M_{h2o_c} + M_{h_c} + M_{23dhdp_c}$
R_DHFR	$M_{h_c} + M_{nadph_c} + M_{dhf_c}$	<----->	$M_{nadp_c} + M_{thf_c}$
R_DHFS	$M_{atp_c} + M_{glu_L_c} + M_{dhpt_c}$	----->	$M_{h_c} + M_{pi_c} + M_{adp_c} + M_{dhf_c}$
R_DHNPA2	M_{dhnpt_c}	----->	$M_{gcald_c} + M_{6hnhpt_c}$
R_DHORD5	$M_{mqn8_c} + M_{dhor_S_c}$	----->	$M_{mql8_c} + M_{orot_c}$
R_DHORTS	$M_{h2o_c} + M_{dhor_S_c}$	<----->	$M_{h_c} + M_{cbasp_c}$
R_DHPPDA2	$M_{h2o_c} + M_{h_c} + M_{25drapp_c}$	----->	$M_{nh4_c} + M_{5apru_c}$

R_DHPS2	M_6hmhptpp_c + M_4abz_c	----->	M_ppi_c + M_dhpt_c
R_DHPTDCs	M_dhptd_c	----->	M_h2o_c + M_hmfurn_c
R_DHQS	M_2dda7p_c	----->	M_pi_c + M_3dhq_c
R_DHQTi	M_3dhq_c	----->	M_h2o_c + M_3dhsk_c
R_DM_4HBA	M_4hba_c	----->	M_4hba_b
R_DM_5DRIB	M_5drib_c	----->	M_5drib_b
R_DM_HMFURN	M_hmfurn_c	----->	M_hmfurn_b
R_DMATT	M_dmpp_c + M_ipdp_c	----->	M_ppi_c + M_grdp_c
R_DNMPPA	M_h2o_c + M_dhpmp_c	----->	M_pi_c + M_dhnpt_c
R_DNTPPA	M_h2o_c + M_ahdt_c	----->	M_h_c + M_ppi_c + M_dhpmp_c
R_DPCOAK	M_atp_c + M_dpcoa_c	----->	M_h_c + M_adp_c + M_coa_c
R_DPR	M_h_c + M_nadph_c + M_2dhp_c	----->	M_pant_R_c + M_nadp_c
R_DTMPK	M_atp_c + M_dtmp_c	<----->	M_adp_c + M_dtdp_c
R_DXPRIi	M_h_c + M_nadph_c + M_dxyl5p_c	----->	M_nadp_c + M_2me4p_c
R_DXPS	M_h_c + M_pyr_c + M_g3p_c	----->	M_co2_c + M_dxyl5p_c
R_E4PD	M_h2o_c + M_nad_c + M_e4p_c	<----->	2.0*M_h_c + M_nadh_c + M_4per_c
R_EAR100x	M_h_c + M_nadh_c + M_tdec2eACP_c	----->	M_nad_c + M_dcaACP_c
R_EAR120x	M_h_c + M_nadh_c + M_tdddec2eACP_c	----->	M_nad_c + M_ddcaACP_c
R_EAR121x	M_h_c + M_nadh_c + M_t3c5ddeceACP_c	----->	M_nad_c + M_cddec5eACP_c
R_EAR140x	M_h_c + M_nadh_c + M_tmrs2eACP_c	----->	M_nad_c + M_myrsACP_c
R_EAR141x	M_h_c + M_nadh_c + M_t3c7mrseACP_c	----->	M_nad_c + M_tdeACP_c
R_EAR160x	M_h_c + M_nadh_c + M_tpalm2eACP_c	----->	M_nad_c + M_palmACP_c
R_EAR161x	M_h_c + M_nadh_c + M_t3c9palmeACP_c	----->	M_nad_c + M_hdeACP_c
R_EAR40x	M_h_c + M_nadh_c + M_but2eACP_c	----->	M_nad_c + M_butACP_c
R_EAR60x	M_h_c + M_nadh_c + M_thex2eACP_c	----->	M_nad_c + M_hexACP_c
R_EAR80x	M_h_c + M_nadh_c + M_toct2eACP_c	----->	M_nad_c + M_ocACP_c

R_Ec_biomass_iAF1260_core_59p81M	54.462*M_h2o_c + 0.001831*M_nad_c + 59.984*M_atp_c + 0.2411*M_asp_L_c + 0.011843*M_nh4_c + 4.47E-4*M_nadp_c + 0.2632*M_glu_L_c + 0.5137*M_ala_L_c + 2.23E-4*M_10fthf_c + 2.23E-4*M_mlthf_c + 0.2537*M_thr_L_c + 0.2158*M_ser_L_c + 5.76E-4*M_coa_c + 0.09158*M_cys_L_c + 0.007895*M_mg2_c + 0.01945*M_kdo2lipid4_e + 0.003948*M_so4_c + 0.004737*M_ca2_c + 5.5E-5*M_udcpdp_c + 0.2905*M_ile_L_c + 0.003158*M_cobalt2_c + 0.1335*M_ctp_c + 0.007106*M_fe3_c + 0.1379*M_tyr_L_c + 0.2632*M_gln_L_c + 0.02617*M_dttp_c + 0.1441*M_utp_c + 0.2151*M_gtp_c + 0.003158*M_mn2_c + 0.2211*M_pro_L_c + 0.01389*M_murein5px4p_p + 2.23E-4*M_thf_c + 0.003158*M_mobd_c + 0.1537*M_met_L_c + 0.2411*M_asn_L_c + 0.003158*M_cu2_c + 0.2958*M_arg_L_c + 2.23E-4*M_thmpp_c + 2.23E-4*M_fad_c + 0.007106*M_fe2_c + 0.02632*M_pe161_c + 0.02233*M_pe160_c + 2.23E-4*M_ribflv_c + 2.23E-4*M_amet_c + 0.4232*M_val_L_c + 2.23E-4*M_pheme_c + 0.6126*M_gly_c + 2.23E-4*M_2ohph_c + 0.003158*M_zn2_c + 0.09474*M_his_L_c + 0.05684*M_trp_L_c + 2.23E-4*M_sheme_c + 0.1759*M_phe_L_c + 0.02702*M_dctp_c + 0.02617*M_datp_c + 0.3432*M_lys_L_c + 0.4505*M_leu_L_c + 2.23E-4*M_pydx5p_c + 0.004737*M_cl_c + 0.04148*M_pe160_p + 0.02702*M_dgtp_c + 0.1776*M_k_c + 0.04889*M_pe161_p	----->	59.81*M_h_c + 0.7739*M_ppi_c + 59.806*M_pi_c + 59.81*M_adp_c + Bio
R_ENO	M_2pg_c	<----->	M_h2o_c + M_pep_c
R_ETOHt2rpp	M_h_p + M_etoh_p	<----->	M_h_c + M_etoh_c
R_ETOHtex	M_etoh_e	<----->	M_etoh_p
R_EX_ac_e_	M_ac_e	----->	M_ac_b
R_EX_acald_e_	M_acald_e	----->	M_acald_b
R_EX_akg_e_	M_akg_e	----->	M_akg_b
R_EX_ca2_e_	M_ca2_e	<----->	M_ca2_b
R_EX_cl_e_	M_cl_e	<----->	M_cl_b
R_EX_co2_e_	M_co2_e	<----->	M_co2_b
R_EX_cobalt2_e_	M_cobalt2_e	<----->	M_cobalt2_b
R_EX_cu2_e_	M_cu2_e	<----->	M_cu2_b
R_EX_etoh_e_	M_etoh_e	----->	M_etoh_b
R_EX_fe2_e_	M_fe2_e	<----->	M_fe2_b
R_EX_fe3_e_	M_fe3_e	<----->	M_fe3_b
R_EX_for_e_	M_for_e	----->	M_for_b

R_EX_glc_e_	M_glc_D_b	----->	M_glc_D_e
R_EX_glu_L_e_	M_glu_L_e	----->	M_glu_L_b
R_EX_h_e_	M_h_e	<----->	M_h_b
R_EX_h2_e_	M_h2_e	----->	M_h2_b
R_EX_h2o_e_	M_h2o_e	<----->	M_h2o_b
R_EX_k_e_	M_k_e	<----->	M_k_b
R_EX_lac_D_e_	M_lac_D_e	----->	M_lac_D_b
R_EX_mg2_e_	M_mg2_e	<----->	M_mg2_b
R_EX_mn2_e_	M_mn2_e	<----->	M_mn2_b
R_EX_mobd_e_	M_mobd_e	<----->	M_mobd_b
R_EX_nh4_e_	M_nh4_e	<----->	M_nh4_b
R_EX_o2_e_	M_o2_e	<----->	M_o2_b
R_EX_pi_e_	M_pi_e	<----->	M_pi_b
R_EX_pyr_e_	M_pyr_e	----->	M_pyr_b
R_EX_so4_e_	M_so4_e	<----->	M_so4_b
R_EX_succ_e_	M_succ_e	----->	M_succ_b
R_EX_zn2_e_	M_zn2_e	<----->	M_zn2_b
R_FBA	M_fdp_c	<----->	M_g3p_c + M_dhap_c
R_FBP	M_h2o_c + M_fdp_c	----->	M_pi_c + M_f6p_c
R_FCLT	M_fe2_c + M_ppp9_c	----->	2.0*M_h_c + M_pheme_c
R_FE2tex	M_fe2_e	<----->	M_fe2_p
R_FE2tpp	M_fe2_p	----->	M_fe2_c
R_FE3abcpp	M_h2o_c + M_atp_c + M_fe3_p	----->	M_h_c + M_pi_c + M_adp_c + M_fe3_c
R_FE3tex	M_fe3_e	<----->	M_fe3_p
R_FHL	M_h_c + M_for_c	----->	M_co2_c + M_h2_c
R_FLDR	M_h_c + M_nadph_c + M_fldox_c	----->	M_nadp_c + M_fldr_c
R_FMNAT	M_h_c + M_atp_c + M_fmn_c	----->	M_ppi_c + M_fad_c

R_FORt2pp	M_h_p + M_for_p	----->	M_h_c + M_for_c
R_FORtex	M_for_e	<----->	M_for_p
R_FORtppi	M_for_c	----->	M_for_p
R_FRD2	M_fum_c + M_mql8_c	----->	M_succ_c + M_mqn8_c
R_FRD3	M_fum_c + M_2dmmql8_c	----->	M_succ_c + M_2dmmq8_c
R_FUM	M_h2o_c + M_fum_c	<----->	M_mal_L_c
R_G1PACT	M_accoa_c + M_gam1p_c	----->	M_h_c + M_coa_c + M_acgam1p_c
R_G1SAT	M_glu1sa_c	<----->	M_5aop_c
R_G3PAT160	M_palmACP_c + M_glyc3p_c	----->	M_ACP_c + M_1hdecg3p_c
R_G3PAT161	M_hdeACP_c + M_glyc3p_c	----->	M_ACP_c + M_1hdec9eg3p_c
R_G3PD2	M_nadp_c + M_glyc3p_c	<----->	M_h_c + M_nadph_c + M_dhap_c
R_G5SADs	M_glu5sa_c	----->	M_h2o_c + M_h_c + M_1pyr5c_c
R_G5SD	M_h_c + M_nadph_c + M_glu5p_c	----->	M_pi_c + M_nadp_c + M_glu5sa_c
R_G6PDH2r	M_nadp_c + M_g6p_c	<----->	M_h_c + M_nadph_c + M_6pgl_c
R_GAPD	M_nad_c + M_pi_c + M_g3p_c	<----->	M_h_c + M_nadh_c + M_13dpg_c
R_GARFT	M_10fthf_c + M_gar_c	<----->	M_h_c + M_thf_c + M_fgam_c
R_GART	M_atp_c + M_for_c + M_gar_c	----->	M_h_c + M_pi_c + M_adp_c + M_fgam_c
R_GCALDD	M_h2o_c + M_nad_c + M_gcald_c	----->	2.0*M_h_c + M_nadh_c + M_glyclt_c
R_GF6PTA	M_f6p_c + M_gln_L_c	----->	M_glu_L_c + M_gam6p_c
R_GHMT2r	M_ser_L_c + M_thf_c	<----->	M_h2o_c + M_mlthf_c + M_gly_c
R_GK1	M_atp_c + M_gmp_c	<----->	M_adp_c + M_gdp_c
R_GLCptspp	M_pep_c + M_glc_D_p	----->	M_g6p_c + M_pyr_c
R_GLCtex	M_glc_D_e	<----->	M_glc_D_p
R_GLNS	M_atp_c + M_nh4_c + M_glu_L_c	----->	M_h_c + M_pi_c + M_adp_c + M_gln_L_c
R_GLU5K	M_atp_c + M_glu_L_c	----->	M_adp_c + M_glu5p_c
R_GLUDy	M_h2o_c + M_nadp_c + M_glu_L_c	<----->	M_h_c + M_nh4_c + M_nadph_c + M_akg_c
R_GLUN	M_h2o_c + M_gln_L_c	----->	M_nh4_c + M_glu_L_c

R_GLUPRT	M_h2o_c + M_gln_L_c + M_prpp_c	----->	M_ppi_c + M_glu_L_c + M_pram_c
R_GLUR	M_glu_D_c	<----->	M_glu_L_c
R_GLUSy	M_h_c + M_nadph_c + M_akg_c + M_gln_L_c	----->	M_nadp_c + 2.0*M_glu_L_c
R_GLUt2rpp	M_h_p + M_glu_L_p	<----->	M_h_c + M_glu_L_c
R_GLUtex	M_glu_L_e	<----->	M_glu_L_p
R_GLUTRR	M_h_c + M_nadph_c + M_glutrna_c	----->	M_nadp_c + M_trnaglu_c + M_glu1sa_c
R_GLUTRS	M_atp_c + M_glu_L_c + M_trnaglu_c	----->	M_amp_c + M_ppi_c + M_glutrna_c
R_GLYCTO4	M_2dmmq8_c + M_glyclt_c	----->	M_2dmmql8_c + M_glx_c
R_GMPS2	M_h2o_c + M_xmp_c + M_atp_c + M_gln_L_c	----->	2.0*M_h_c + M_amp_c + M_ppi_c + M_glu_L_c + M_gmp_c
R_GND	M_nadp_c + M_6pgc_c	----->	M_nadph_c + M_co2_c + M_ru5p_D_c
R_GRTT	M_ipdp_c + M_grdp_c	----->	M_ppi_c + M_frdp_c
R_GRXR	2.0*M_gthrd_c + M_grxox_c	----->	M_gthox_c + M_grxrd_c
R_GTHOr	M_h_c + M_nadph_c + M_gthox_c	<----->	M_nadp_c + 2.0*M_gthrd_c
R_GTPCI	M_h2o_c + M_gtp_c	----->	M_h_c + M_for_c + M_ahdt_c
R_GTPCII2	3.0*M_h2o_c + M_gtp_c	----->	2.0*M_h_c + M_ppi_c + M_25drapp_c + M_for_c
R_H2Otex	M_h2o_e	<----->	M_h2o_p
R_H2Otp	M_h2o_p	<----->	M_h2o_c
R_H2tex	M_h2_e	<----->	M_h2_p
R_H2tp	M_h2_p	<----->	M_h2_c
R_HBZOPT	M_octdp_c + M_4hbz_c	----->	M_ppi_c + M_3ophb_c
R_HCO3E	M_h2o_c + M_co2_c	<----->	M_h_c + M_hco3_c
R_HISTD	M_h2o_c + 2.0*M_nad_c + M_histd_c	----->	3.0*M_h_c + 2.0*M_nadh_c + M_his_L_c
R_HISTP	M_h2o_c + M_hisp_c	----->	M_pi_c + M_histd_c
R_HMBS	M_h2o_c + 4.0*M_ppbng_c	----->	4.0*M_nh4_c + M_hmbil_c
R_HPPK2	M_atp_c + M_6hnhpt_c	----->	M_h_c + M_amp_c + M_6hnhpttp_c
R_HSDy	M_nadp_c + M_hom_L_c	<----->	M_h_c + M_nadph_c + M_aspsa_c
R_HSK	M_atp_c + M_hom_L_c	----->	M_h_c + M_adp_c + M_phom_c

R_HSST	M_succoa_c + M_hom_L_c	----->	M_coa_c + M_suchms_c
R_HSTPT	M_glu_L_c + M_imacp_c	----->	M_akg_c + M_hisp_c
R_Htex	M_h_e	<----->	M_h_p
R_ICDHyr	M_nadp_c + M_icit_c	<----->	M_nadph_c + M_akg_c + M_co2_c
R_ICL	M_icit_c	----->	M_succ_c + M_glx_c
R_IG3PS	M_gln_L_c + M_prlp_c	----->	M_h_c + M_glu_L_c + M_aicar_c + M_eig3p_c
R_IGPDH	M_eig3p_c	----->	M_h2o_c + M_imacp_c
R_IGPS	M_h_c + M_2cpr5p_c	----->	M_h2o_c + M_co2_c + M_3ig3p_c
R_ILETA	M_akg_c + M_ile_L_c	<----->	M_glu_L_c + M_3mop_c
R_IMPC	M_imp_c + M_h2o_c	<----->	M_fprica_c
R_IMPD	M_imp_c + M_h2o_c + M_nad_c	----->	M_h_c + M_nadh_c + M_xmp_c
R_IPDDI	M_ipdp_c	<----->	M_dmpp_c
R_IPDPS	M_h_c + M_nadh_c + M_h2mb4p_c	----->	M_h2o_c + M_nad_c + M_ipdp_c
R_IPMD	M_nad_c + M_3c2hmp_c	----->	M_h_c + M_nadh_c + M_3c4mop_c
R_IPPMIa	M_3c2hmp_c	<----->	M_h2o_c + M_2ippm_c
R_IPPMIb	M_h2o_c + M_2ippm_c	<----->	M_3c3hmp_c
R_IPPS	M_h2o_c + M_accoa_c + M_3mob_c	----->	M_h_c + M_coa_c + M_3c3hmp_c
R_K2L4Aabcpp	M_h2o_c + M_atp_c + M_kdo2lipid4_c	----->	M_h_c + M_pi_c + M_adp_c + M_kdo2lipid4_p
R_K2L4Atex	M_kdo2lipid4_p	----->	M_kdo2lipid4_e
R_KARA1	M_nadp_c + M_23dhmb_c	<----->	M_h_c + M_nadph_c + M_alac_S_c
R_KARA2	M_h_c + M_nadph_c + M_2ahbut_c	<----->	M_nadp_c + M_23dhmp_c
R_KAS15	M_h_c + M_accoa_c + M_malACP_c	----->	M_co2_c + M_coa_c + M_actACP_c
R_KDOCT2	M_kdo_c + M_ctp_c	----->	M_ppi_c + M_ckdo_c
R_KDOPP	M_h2o_c + M_kdo8p_c	----->	M_pi_c + M_kdo_c
R_KDOPS	M_h2o_c + M_pep_c + M_ara5p_c	----->	M_pi_c + M_kdo8p_c
R_Kt2pp	M_h_p + M_k_p	----->	M_h_c + M_k_c
R_Ktex	M_k_e	<----->	M_k_p

R_LDH_D	M_nad_c + M_lac_D_c	<---->	M_h_c + M_nadh_c + M_pyr_c
R_LEUTai	M_glu_L_c + M_4mop_c	----->	M_akg_c + M_leu_L_c
R_LPADSS	M_u23ga_c + M_lipidX_c	----->	M_h_c + M_udp_c + M_lipidAds_c
R_MALS	M_h2o_c + M_accoa_c + M_glx_c	----->	M_h_c + M_coa_c + M_mal_L_c
R_MCOATA	M_ACP_c + M_malcoa_c	<---->	M_coa_c + M_malACP_c
R_MCTP1App	M_murein5p5p_p	----->	M_ala_D_p + M_murein5px4p_p
R_MDH	M_nad_c + M_mal_L_c	<---->	M_h_c + M_nadh_c + M_oaa_c
R_ME1	M_nad_c + M_mal_L_c	----->	M_nadh_c + M_co2_c + M_pyr_c
R_ME2	M_nadp_c + M_mal_L_c	----->	M_nadph_c + M_co2_c + M_pyr_c
R_MECDPDH2	M_nadh_c + M_2mecdp_c	----->	M_h2o_c + M_nad_c + M_h2mb4p_c
R_MECDPS	M_2p4c2me_c	----->	M_cmp_c + M_2mecdp_c
R_MEPECT	M_h_c + M_2me4p_c + M_ctp_c	----->	M_ppi_c + M_4c2me_c
R_METAT	M_h2o_c + M_atp_c + M_met_L_c	----->	M_ppi_c + M_pi_c + M_amet_c
R_METS	M_5mthf_c + M_hcys_L_c	----->	M_h_c + M_thf_c + M_met_L_c
R_MG2t3_2pp	2.0*M_h_c + M_mg2_p	<---->	2.0*M_h_p + M_mg2_c
R_MG2tex	M_mg2_e	<---->	M_mg2_p
R_MN2tpp	M_mn2_p	----->	M_mn2_c
R_MNtex	M_mn2_e	<---->	M_mn2_p
R_MOAT	M_ckdo_c + M_lipidA_c	----->	M_h_c + M_cmp_c + M_kdolipid4_c
R_MOAT2	M_ckdo_c + M_kdolipid4_c	----->	M_h_c + M_kdo2lipid4_c + M_cmp_c
R_MOBDabcpp	M_h2o_c + M_atp_c + M_mobd_p	----->	M_h_c + M_pi_c + M_adp_c + M_mobd_c
R_MOBDtex	M_mobd_e	<---->	M_mobd_p
R_MOHMT	M_h2o_c + M_mlthf_c + M_3mob_c	----->	M_2dhp_c + M_thf_c
R_MPTG	2.0*M_uaagmda_c	----->	2.0*M_h_c + 2.0*M_udcpdp_c + M_murein5p5p_p
R_MTHFC	M_h2o_c + M_methf_c	<---->	M_h_c + M_10fthf_c
R_MTHFD	M_nadp_c + M_mlthf_c	<---->	M_nadph_c + M_methf_c
R_MTHFR2	2.0*M_h_c + M_nadh_c + M_mlthf_c	----->	M_nad_c + M_5mthf_c

R_NADH16pp	$4.0 \cdot M_{h_c} + M_{nadh_c} + M_{q8_c}$	----->	$M_{nad_c} + 3.0 \cdot M_{h_p} + M_{q8h2_c}$
R_NADK	$M_{nad_c} + M_{atp_c}$	----->	$M_{h_c} + M_{nadp_c} + M_{adp_c}$
R_NADS1	$M_{atp_c} + M_{nh4_c} + M_{dnad_c}$	----->	$M_{h_c} + M_{nad_c} + M_{amp_c} + M_{ppi_c}$
R_NADTRHD	$M_{nad_c} + M_{nadph_c}$	----->	$M_{nadh_c} + M_{nadp_c}$
R_NDPK1	$M_{atp_c} + M_{gdp_c}$	<----->	$M_{adp_c} + M_{gtp_c}$
R_NDPK2	$M_{atp_c} + M_{udp_c}$	<----->	$M_{adp_c} + M_{utp_c}$
R_NDPK3	$M_{atp_c} + M_{cdp_c}$	<----->	$M_{adp_c} + M_{ctp_c}$
R_NDPK4	$M_{atp_c} + M_{dtdp_c}$	<----->	$M_{adp_c} + M_{dttp_c}$
R_NDPK6	$M_{atp_c} + M_{dudp_c}$	<----->	$M_{adp_c} + M_{dutp_c}$
R_NH4tex	M_{nh4_e}	<----->	M_{nh4_p}
R_NH4tpp	M_{nh4_p}	<----->	M_{nh4_c}
R_NNATr	$M_{h_c} + M_{atp_c} + M_{nicrnt_c}$	<----->	$M_{ppi_c} + M_{dnad_c}$
R_NNDPR	$2.0 \cdot M_{h_c} + M_{prpp_c} + M_{quln_c}$	----->	$M_{ppi_c} + M_{co2_c} + M_{nicrnt_c}$
R_O2tex	M_{o2_e}	<----->	M_{o2_p}
R_O2tpp	M_{o2_p}	<----->	M_{o2_c}
R_OCBT	$M_{cbp_c} + M_{orn_c}$	<----->	$M_{h_c} + M_{pi_c} + M_{citr_L_c}$
R_OCTDPS	$5.0 \cdot M_{ipdp_c} + M_{frdp_c}$	----->	$5.0 \cdot M_{ppi_c} + M_{octdp_c}$
R_OHPBAT	$M_{glu_L_c} + M_{ohpb_c}$	<----->	$M_{akg_c} + M_{phthr_c}$
R_OMCDC	$M_{h_c} + M_{3c4mop_c}$	----->	$M_{co2_c} + M_{4mop_c}$
R_OMPDC	$M_{h_c} + M_{orot5p_c}$	----->	$M_{co2_c} + M_{ump_c}$
R_OPHBDC	$M_{h_c} + M_{3ophb_c}$	----->	$M_{co2_c} + M_{2oph_c}$
R_OPHHX3	$3.0 \cdot M_{h2o_c} + M_{nad_c} + 2.0 \cdot M_{atp_c} + M_{2oph_c}$	----->	$3.0 \cdot M_{h_c} + M_{nadh_c} + 2.0 \cdot M_{pi_c} + 2.0 \cdot M_{adp_c} + M_{2ohph_c}$
R_ORPT	$M_{ppi_c} + M_{orot5p_c}$	<----->	$M_{prpp_c} + M_{orot_c}$
R_P5CR	$2.0 \cdot M_{h_c} + M_{nadph_c} + M_{1pyr5c_c}$	----->	$M_{nadp_c} + M_{pro_L_c}$
R_PANTS	$M_{pant_R_c} + M_{ala_B_c} + M_{atp_c}$	----->	$M_{h_c} + M_{amp_c} + M_{ppi_c} + M_{pnto_R_c}$
R_PAPPT3	$M_{ugmda_c} + M_{udcpp_c}$	----->	$M_{ump_c} + M_{uagmda_c}$
R_PAPSR2	$M_{paps_c} + M_{grxrd_c}$	----->	$2.0 \cdot M_{h_c} + M_{so3_c} + M_{pap_c} + M_{grxox_c}$

R_PDH	M_nad_c + M_pyr_c + M_coa_c	----->	M_nadh_c + M_co2_c + M_accoa_c
R_PDX5PO2	M_nad_c + M_pdx5p_c	----->	M_h_c + M_nadh_c + M_pydx5p_c
R_PDX5PS	M_nad_c + M_dxyl5p_c + M_phthr_c	----->	2.0*M_h2o_c + M_h_c + M_nadh_c + M_pi_c + M_co2_c + M_pdx5p_c
R_PE160abcpp	M_h2o_c + M_atp_c + M_pe160_c	----->	M_h_c + M_pi_c + M_adp_c + M_pe160_p
R_PE161abcpp	M_h2o_c + M_atp_c + M_pe161_c	----->	M_h_c + M_pi_c + M_adp_c + M_pe161_p
R_PERD	M_nad_c + M_4per_c	<----->	M_h_c + M_nadh_c + M_ohpb_c
R_PFK	M_atp_c + M_f6p_c	----->	M_h_c + M_adp_c + M_fdp_c
R_PFL	M_pyr_c + M_coa_c	----->	M_accoa_c + M_for_c
R_PGAMT	M_gam1p_c	<----->	M_gam6p_c
R_PGCD	M_nad_c + M_3pg_c	----->	M_h_c + M_nadh_c + M_3php_c
R_PGI	M_g6p_c	<----->	M_f6p_c
R_PGK	M_atp_c + M_3pg_c	<----->	M_adp_c + M_13dpg_c
R_PGL	M_h2o_c + M_6pgl_c	----->	M_h_c + M_6pgc_c
R_PGM	M_2pg_c	<----->	M_3pg_c
R_PHETA1	M_akg_c + M_phe_L_c	<----->	M_glu_L_c + M_phpyr_c
R_Plt2rpp	M_h_p + M_pi_p	<----->	M_h_c + M_pi_c
R_Pltex	M_pi_e	<----->	M_pi_p
R_PMDPHT	M_h2o_c + M_5aprbu_c	----->	M_pi_c + M_4r5au_c
R_PMPK	M_atp_c + M_4ampm_c	----->	M_adp_c + M_2mahmp_c
R_PNTK	M_pnto_R_c + M_atp_c	----->	M_h_c + M_adp_c + M_4ppan_c
R_PPBNGS	2.0*M_5aop_c	----->	2.0*M_h2o_c + M_h_c + M_ppbng_c
R_PPC	M_h2o_c + M_co2_c + M_pep_c	----->	M_h_c + M_pi_c + M_oaa_c
R_PPCDC	M_h_c + M_4ppcys_c	----->	M_co2_c + M_pan4p_c
R_PPCK	M_atp_c + M_oaa_c	----->	M_adp_c + M_co2_c + M_pep_c
R_PPKr	M_atp_c + M_pi_c	<----->	M_ppi_c + M_adp_c
R_PPM	M_r1p_c	<----->	M_r5p_c
R_PPNCL2	M_cys_L_c + M_ctp_c + M_4ppan_c	----->	M_h_c + M_ppi_c + M_cmp_c + M_4ppcys_c

R_PPND	M_nad_c + M_pphn_c	----->	M_nadh_c + M_co2_c + M_34hpp_c
R_PPNDH	M_h_c + M_pphn_c	----->	M_h2o_c + M_co2_c + M_phpyr_c
R_PPPGO3	3.0*M_fum_c + M_pppg9_c	----->	3.0*M_succ_c + M_ppp9_c
R_PPS	M_h2o_c + M_atp_c + M_pyr_c	----->	2.0*M_h_c + M_amp_c + M_pi_c + M_pep_c
R_PRAGSr	M_atp_c + M_pram_c + M_gly_c	<----->	M_h_c + M_pi_c + M_adp_c + M_gar_c
R_PRAli	M_pran_c	----->	M_2cpr5p_c
R_PRAIS	M_atp_c + M_fpram_c	----->	2.0*M_h_c + M_pi_c + M_adp_c + M_air_c
R_PRAMPC	M_h2o_c + M_prbamp_c	----->	M_prfp_c
R_PRASCSi	M_atp_c + M_asp_L_c + M_5aizc_c	----->	M_h_c + M_pi_c + M_adp_c + M_25aics_c
R_PRATPP	M_h2o_c + M_prbatp_c	----->	M_h_c + M_ppi_c + M_prbamp_c
R_PRFGS	M_h2o_c + M_atp_c + M_gln_L_c + M_fgam_c	----->	M_h_c + M_pi_c + M_glu_L_c + M_adp_c + M_fpram_c
R_PRMICI	M_prfp_c	<----->	M_prlp_c
R_PRPPS	M_atp_c + M_r5p_c	<----->	M_h_c + M_amp_c + M_prpp_c
R_PSCVT	M_pep_c + M_skm5p_c	<----->	M_pi_c + M_3psme_c
R_PSD160	M_h_c + M_ps160_c	----->	M_co2_c + M_pe160_c
R_PSD161	M_h_c + M_ps161_c	----->	M_co2_c + M_pe161_c
R_PSERT	M_glu_L_c + M_3php_c	----->	M_akg_c + M_pser_L_c
R_PSP_L	M_h2o_c + M_pser_L_c	----->	M_pi_c + M_ser_L_c
R_PSSA160	M_ser_L_c + M_cdpdhdecg_c	----->	M_h_c + M_cmp_c + M_ps160_c
R_PSSA161	M_ser_L_c + M_cdpdhdec9eg_c	----->	M_h_c + M_cmp_c + M_ps161_c
R_PTAr	M_pi_c + M_accoa_c	<----->	M_coa_c + M_actp_c
R_PTPATi	M_h_c + M_atp_c + M_pan4p_c	----->	M_ppi_c + M_dpcoa_c
R_PUNP1	M_pi_c + M_adn_c	<----->	M_ade_c + M_r1p_c
R_PYK	M_h_c + M_adp_c + M_pep_c	----->	M_atp_c + M_pyr_c
R_PYRt2rpp	M_pyr_p + M_h_p	<----->	M_h_c + M_pyr_c
R_PYRtex	M_pyr_e	<----->	M_pyr_p
R_QULNS	M_dhap_c + M_iasp_c	----->	2.0*M_h2o_c + M_pi_c + M_quln_c

R_RBFK	M_atp_c + M_ribflv_c	----->	M_h_c + M_adp_c + M_fmn_c
R_RBFSa	M_db4p_c + M_4r5au_c	----->	2.0*M_h2o_c + M_pi_c + M_dmlz_c
R_RBFSb	2.0*M_dmlz_c	----->	M_4r5au_c + M_ribflv_c
R_RFD_new	M_fum_c + M_q8h2_c	----->	M_q8_c + M_succ_c
R_RHCCE	M_rhcys_c	----->	M_dhptd_c + M_hcys_L_c
R_RNTR1c	M_atp_c + M_fldrd_c	----->	M_h2o_c + M_datp_c + M_fldox_c
R_RNTR2c	M_gtp_c + M_fldrd_c	----->	M_h2o_c + M_dgtp_c + M_fldox_c
R_RNTR3c	M_ctp_c + M_fldrd_c	----->	M_h2o_c + M_dctp_c + M_fldox_c
R_RNTR4c	M_utp_c + M_fldrd_c	----->	M_h2o_c + M_dutp_c + M_fldox_c
R_RPE	M_ru5p_D_c	<----->	M_xu5p_D_c
R_RPI	M_r5p_c	<----->	M_ru5p_D_c
R_SADT2	M_h2o_c + M_atp_c + M_so4_c + M_gtp_c	----->	M_ppi_c + M_pi_c + M_gdp_c + M_aps_c
R_SDPDS	M_h2o_c + M_sl26da_c	----->	M_succ_c + M_26dap_LL_c
R_SDPTA	M_akg_c + M_sl26da_c	<----->	M_glu_L_c + M_sl2a6o_c
R_SERAT	M_ser_L_c + M_accoa_c	<----->	M_coa_c + M_acser_c
R_SHCHD2	M_nad_c + M_dscl_c	----->	M_h_c + M_nadh_c + M_scl_c
R_SHCHF	M_scl_c + M_fe2_c	----->	3.0*M_h_c + M_sheme_c
R_SHK3Dr	M_h_c + M_nadph_c + M_3dhsk_c	<----->	M_nadp_c + M_skm_c
R_SHKK	M_atp_c + M_skm_c	----->	M_h_c + M_adp_c + M_skm5p_c
R_SHSL1	M_cys_L_c + M_suchms_c	----->	M_h_c + M_succ_c + M_cyst_L_c
R_SO4tex	M_so4_e	<----->	M_so4_p
R_SUCct2_2pp	2.0*M_h_p + M_succ_p	----->	2.0*M_h_c + M_succ_c
R_SUCct3pp	M_h_p + M_succ_c	----->	M_h_c + M_succ_p
R_SUCctex	M_succ_e	<----->	M_succ_p
R_SUCDi	M_q8_c + M_succ_c	----->	M_fum_c + M_q8h2_c
R_SUCOAS	M_atp_c + M_succ_c + M_coa_c	<----->	M_pi_c + M_adp_c + M_succoa_c
R_SULabcpp	M_h2o_c + M_atp_c + M_so4_p	----->	M_h_c + M_pi_c + M_adp_c + M_so4_c

R_SULRi	$5.0 \cdot M_{h_c} + 3.0 \cdot M_{nadph_c} + M_{so3_c}$	----->	$3.0 \cdot M_{h2o_c} + 3.0 \cdot M_{nadp_c} + M_{h2s_c}$
R_T2DECAI	$M_{tdec2eACP_c}$	<----->	$M_{cdec3eACP_c}$
R_TALA	$M_{g3p_c} + M_{s7p_c}$	<----->	$M_{e4p_c} + M_{f6p_c}$
R_TDSK	$M_{atp_c} + M_{lipidAds_c}$	----->	$M_{h_c} + M_{adp_c} + M_{lipidA_c}$
R_THD2pp	$M_{nadh_c} + M_{nadp_c} + 2.0 \cdot M_{h_p}$	----->	$2.0 \cdot M_{h_c} + M_{nad_c} + M_{nadph_c}$
R_THDPS	$M_{h2o_c} + M_{succoa_c} + M_{thdp_c}$	----->	$M_{coa_c} + M_{sl2a6o_c}$
R_THRD_L	$M_{thr_L_c}$	----->	$M_{nh4_c} + M_{2obut_c}$
R_THRS	$M_{h2o_c} + M_{phom_c}$	----->	$M_{pi_c} + M_{thr_L_c}$
R_THRt2rpp	$M_{h_p} + M_{thr_L_p}$	<----->	$M_{h_c} + M_{thr_L_c}$
R_THRt4pp	$M_{na1_p} + M_{thr_L_p}$	----->	$M_{thr_L_c} + M_{na1_c}$
R_THZPSN	$M_{atp_c} + M_{dxyl5p_c} + M_{cys_L_c} + M_{tyr_L_c}$	----->	$M_{h2o_c} + M_{h_c} + M_{amp_c} + M_{ppi_c} + M_{co2_c} + M_{ala_L_c} + M_{4hba_c} + M_{4mpetz_c}$
R_TKT1	$M_{xu5p_D_c} + M_{r5p_c}$	<----->	$M_{g3p_c} + M_{s7p_c}$
R_TKT2	$M_{e4p_c} + M_{xu5p_D_c}$	<----->	$M_{f6p_c} + M_{g3p_c}$
R_TMDS	$M_{mlthf_c} + M_{dump_c}$	----->	$M_{dtmp_c} + M_{dhf_c}$
R_TMPK	$M_{atp_c} + M_{thmmp_c}$	----->	$M_{adp_c} + M_{thmpp_c}$
R_TMPPP	$M_{h_c} + M_{4mpetz_c} + M_{2mahmp_c}$	----->	$M_{ppi_c} + M_{thmmp_c}$
R_TPI	M_{dhap_c}	<----->	M_{g3p_c}
R_TRPS2	$M_{ser_L_c} + M_{indole_c}$	----->	$M_{h2o_c} + M_{trp_L_c}$
R_TRPS3	M_{3ig3p_c}	----->	$M_{g3p_c} + M_{indole_c}$
R_TYRTA	$M_{akg_c} + M_{tyr_L_c}$	<----->	$M_{glu_L_c} + M_{34hpp_c}$
R_U23GAAT	$M_{3hmrsACP_c} + M_{u3hga_c}$	----->	$M_{h_c} + M_{ACP_c} + M_{u23ga_c}$
R_UAAGDS	$M_{atp_c} + M_{uamag_c} + M_{26dap_M_c}$	----->	$M_{h_c} + M_{pi_c} + M_{adp_c} + M_{ugmd_c}$
R_UAGAAT	$M_{3hmrsACP_c} + M_{uacgam_c}$	<----->	$M_{ACP_c} + M_{u3aga_c}$
R_UAGCVT	$M_{pep_c} + M_{uacgam_c}$	----->	$M_{pi_c} + M_{uaccg_c}$
R_UAGDP	$M_{h_c} + M_{utp_c} + M_{acgam1p_c}$	----->	$M_{ppi_c} + M_{uacgam_c}$
R_UAGPT3	$M_{uacgam_c} + M_{uagmda_c}$	----->	$M_{h_c} + M_{uaagmda_c} + M_{udp_c}$

R_UAMAGS	$M_{\text{atp_c}} + M_{\text{uama_c}} + M_{\text{glu_D_c}}$	----->	$M_{\text{h_c}} + M_{\text{pi_c}} + M_{\text{adp_c}} + M_{\text{uamag_c}}$
R_UAMAS	$M_{\text{atp_c}} + M_{\text{uamr_c}} + M_{\text{ala_L_c}}$	----->	$M_{\text{h_c}} + M_{\text{pi_c}} + M_{\text{adp_c}} + M_{\text{uama_c}}$
R_UAPGR	$M_{\text{h_c}} + M_{\text{nadph_c}} + M_{\text{uaccg_c}}$	----->	$M_{\text{nadp_c}} + M_{\text{uamr_c}}$
R_UDCPDP	$M_{\text{h2o_c}} + M_{\text{udcpdp_c}}$	----->	$M_{\text{h_c}} + M_{\text{pi_c}} + M_{\text{udcpp_c}}$
R_UDCPDPS	$8.0 * M_{\text{ipdp_c}} + M_{\text{frdp_c}}$	----->	$8.0 * M_{\text{ppi_c}} + M_{\text{udcpdp_c}}$
R_UGMDDS	$M_{\text{atp_c}} + M_{\text{alaala_c}} + M_{\text{ugmd_c}}$	----->	$M_{\text{h_c}} + M_{\text{pi_c}} + M_{\text{adp_c}} + M_{\text{ugmda_c}}$
R_UHGADA	$M_{\text{h2o_c}} + M_{\text{u3aga_c}}$	----->	$M_{\text{ac_c}} + M_{\text{u3hga_c}}$
R_UMPK	$M_{\text{atp_c}} + M_{\text{ump_c}}$	<----->	$M_{\text{adp_c}} + M_{\text{udp_c}}$
R_UPP3MT	$2.0 * M_{\text{amet_c}} + M_{\text{uppg3_c}}$	----->	$M_{\text{h_c}} + 2.0 * M_{\text{ahcys_c}} + M_{\text{dscl_c}}$
R_UPP3S	$M_{\text{hmbil_c}}$	----->	$M_{\text{h2o_c}} + M_{\text{uppg3_c}}$
R_UPPDC1	$4.0 * M_{\text{h_c}} + M_{\text{uppg3_c}}$	----->	$4.0 * M_{\text{co2_c}} + M_{\text{cpppg3_c}}$
R_URIDK2r	$M_{\text{atp_c}} + M_{\text{dump_c}}$	<----->	$M_{\text{adp_c}} + M_{\text{dudp_c}}$
R_USHD	$M_{\text{h2o_c}} + M_{\text{u23ga_c}}$	----->	$2.0 * M_{\text{h_c}} + M_{\text{ump_c}} + M_{\text{lipidX_c}}$
R_VALTA	$M_{\text{akg_c}} + M_{\text{val_L_c}}$	<----->	$M_{\text{glu_L_c}} + M_{\text{3mob_c}}$
R_Zn2tex	$M_{\text{zn2_e}}$	<----->	$M_{\text{zn2_p}}$
R_ZN2tp	$M_{\text{zn2_p}}$	----->	$M_{\text{zn2_c}}$

APPENDIX B: *S. cerevisiae* metabolic model

The *S. cerevisiae* metabolic model used for all the *p*-FBA presented in the chapter 4. The resulting model used for the metabolic flux calculation, that contains 221 reactions and 206 metabolites, is detailed in **Table B**.

Table B. List of reactions included in the HEK293 reduced model developed and used for all Flux Balance Analysis in the Chapter 4.

R_13BDglnSYN	M_g6p_c + M_atp_c	<---->	M_adp_c + M_ppi_c + M_13BDgln_c
R_2OBUTtm	M_2obut_c	----->	M_2obut_m
R_2OXOADPtim	M_akg_c + M_2oxoadp_m	<---->	M_2oxoadp_c + M_akg_m
R_3MOBtm	M_3mob_c	<---->	M_3mob_m
R_3MOPtm	M_3mop_c	<---->	M_3mop_m
R_AASAD1	M_h_c + M_nadph_c + M_atp_c + M_L2aadp_c	<---->	M_nadp_c + M_ppi_c + M_amp_c + M_L2aadp6sa_c
R_AATA	M_glu_DASH_L_c + M_2oxoadp_c	----->	M_akg_c + M_L2aadp_c
R_ACALDtm	M_acald_c	----->	M_acald_m
R_ACGKm	M_atp_m + M_acglu_m	<---->	M_adp_m + M_acg5p_m
R_ACHBSm	M_pyr_m + M_2obut_m + M_h2o_m + M_h_m	<---->	M_co2tot_m + M_2ahbut_m
R_ACLSm	2.0*M_pyr_m + M_h2o_m + M_h_m	<---->	M_co2tot_m + M_alac_DASH_S_m
R_ACOAH	M_h_c + M_coa_c + M_ac_c	----->	M_h2o_c + M_accoa_c
R_ACONT	M_cit_c	----->	M_icit_c
R_ACONTm	M_cit_m	----->	M_icit_m
R_ACOTAim	M_glu_DASH_L_m + M_acg5sa_m	<---->	M_akg_m + M_acorn_m
R_ACS	M_atp_c + M_coa_c + M_ac_c	<---->	M_ppi_c + M_accoa_c + M_amp_c
R_ACSm	M_atp_m + M_coa_m + M_ac_m	<---->	M_accoa_m + M_amp_m + M_ppi_m

R_Act2r	M_ac_e	----->	M_ac_c
R_Actm	M_ac_c	----->	M_ac_m
R_ADK1	M_atp_c + M_amp_c	<----->	2.0*M_adp_c
R_ADK1m	M_atp_m + M_amp_m	<----->	2.0*M_adp_m
R_ADSK	M_atp_c + M_aps_c	<----->	M_h_c + M_adp_c + M_paps_c
R_AGPRIm	M_h_m + M_nadph_m + M_acg5p_m	<----->	M_nadp_m + M_pi_m + M_acg5sa_m
R_AGTm	M_ala_DASH_L_m + M_glx_m	----->	M_pyr_m + M_gly_m
R_AHSERL2	M_achms_c + M_h2s_c	<----->	M_h_c + M_ac_c + M_hcys_DASH_L_c
R_aicarSYN	5.0*M_atp_c + M_h2o_c + M_asp_DASH_L_c + M_10fthf_c + M_co2tot_c + 2.0*M_gln_DASH_L_c + M_gly_c + M_r5p_c	<----->	8.0*M_h_c + 4.0*M_adp_c + M_ppi_c + 4.0*M_pi_c + 2.0*M_glu_DASH_L_c + M_amp_c + M_fum_c + M_thf_c + M_aicar_c
R_AKGDam	M_h2o_m + M_akg_m + M_coa_m + M_nad_m	----->	M_co2tot_m + M_succoa_m + M_nadh_m
R_ALAt2m	M_ala_DASH_L_c	----->	M_ala_DASH_L_m
R_ALATA_L	M_glu_DASH_L_c + M_pyr_c	----->	M_akg_c + M_ala_DASH_L_c
R_ALATA_Lm	M_pyr_m + M_glu_DASH_L_m	<----->	M_akg_m + M_ala_DASH_L_m
R_ALCD2m	M_nad_m + M_etoh_m	<----->	M_h_m + M_acald_m + M_nadh_m
R_ALCD2x	M_nad_c + M_etoh_c	----->	M_h_c + M_nadh_c + M_acald_c
R_ALDD2xm	M_h2o_m + M_acald_m + M_nad_m	<----->	2.0*M_h_m + M_nadh_m + M_ac_m
R_ALDD2y	M_nadp_c + M_h2o_c + M_acald_c	<----->	2.0*M_h_c + M_nadph_c + M_ac_c
R_ALDD2ym	M_h2o_m + M_nadp_m + M_acald_m	<----->	2.0*M_h_m + M_nadph_m + M_ac_m
R_ampSYN	M_atp_c + M_asp_DASH_L_c + M_aicar_c + M_10fthf_c	<----->	2.0*M_h_c + M_adp_c + M_pi_c + M_h2o_c + M_amp_c + M_fum_c + M_thf_c
R_ANPRT	M_anth_c + M_prpp_c	<----->	M_ppi_c + M_pran_c
R_ANS	M_gln_DASH_L_c + M_chor_c	<----->	M_h_c + M_glu_DASH_L_c + M_pyr_c + M_anth_c
R_ARGSL	M_argsuc_c	----->	M_fum_c + M_arg_DASH_L_c
R_ARGSSr	M_atp_c + M_asp_DASH_L_c + M_citr_DASH_L_c	----->	M_h_c + M_ppi_c + M_amp_c + M_argsuc_c
R_ASADi	M_h_c + M_nadph_c + M_4pasp_c	<----->	M_nadp_c + M_pi_c + M_aspsa_c
R_ASNS1	M_atp_c + M_h2o_c + M_asp_DASH_L_c + M_gln_DASH_L_c	<----->	M_h_c + M_ppi_c + M_glu_DASH_L_c + M_amp_c + M_asn_DASH_L_c
R_AspGlut	M_glu_DASH_L_c + M_asp_DASH_L_m	<----->	M_glu_DASH_L_m + M_asp_DASH_L_c

R_ASPIK	M_atp_c + M_asp_DASH_L_c	<---->	M_adp_c + M_4pasp_c
R_ASPTA	M_akg_c + M_asp_DASH_L_c	----->	M_glu_DASH_L_c + M_oaa_c
R_ATPPRT	M_atp_c + M_prpp_c	<---->	M_ppi_c + M_prbatp_c
R_ATPS	M_atp_c + M_h2o_c	----->	M_h_c + M_adp_c + M_pi_c
R_ATPS3m	3.0*M_h_c + M_adp_m + M_pi_m	<---->	M_h2o_m + 2.0*M_h_m + M_atp_m
R_ATPtm_DASH_H	M_adp_c + M_atp_m	<---->	M_atp_c + M_adp_m
R_bio2r	M_bio_e	<---->	M_bio_c
R_biomass	5.3E-5*M_ptd1ino_SC_c + 59.276*M_atp_c + 6.0E-6*M_pa_SC_c + 59.276*M_h2o_c + 0.3018*M_glu_DASH_L_c + 0.02*M_so4_c + 6.6E-5*M_triglyc_SC_c + 0.046*M_amp_c + 0.2975*M_asp_DASH_L_c + 0.1054*M_gln_DASH_L_c + 0.0036*M_damp_c + 0.1854*M_ser_DASH_L_c + 0.2862*M_lys_DASH_L_c + 0.1914*M_thr_DASH_L_c + 0.2646*M_val_DASH_L_c + 0.2904*M_gly_c + 0.102*M_tyr_DASH_L_c + 0.0599*M_ump_c + 1.1348*M_13BDgln_c + 0.1339*M_phe_DASH_L_c + 0.1927*M_ile_DASH_L_c + 0.1647*M_pro_DASH_L_c + 1.7E-5*M_ps_SC_c + 0.0663*M_his_DASH_L_c + 6.0E-5*M_pc_SC_c + 0.0507*M_met_DASH_L_c + 0.0284*M_trp_DASH_L_c + 0.0015*M_zymst_c + 0.0024*M_dcmp_c + 0.1017*M_asn_DASH_L_c + 0.4588*M_ala_DASH_L_c + 0.0447*M_cmp_c + 0.046*M_gmp_c + 0.0066*M_cys_DASH_L_c + 7.0E-4*M_ergst_c + 4.5E-5*M_pe_SC_c + 0.1607*M_arg_DASH_L_c + 0.0024*M_dgmp_c + 0.0036*M_dtmp_c + 0.2964*M_leu_DASH_L_c + 0.8079*M_mannan_c	<---->	58.7162*M_h_c + 59.276*M_adp_c + 59.305*M_pi_c + M_bio_c
R_BPNT	M_h2o_c + M_pap_c	<---->	M_pi_c + M_amp_c
R_CBPS	2.0*M_atp_c + M_h2o_c + M_co2tot_c + M_gln_DASH_L_c	<---->	2.0*M_h_c + 2.0*M_adp_c + M_pi_c + M_glu_DASH_L_c + M_cbp_c
R_CHORM	M_chor_c	<---->	M_pphn_c
R_CHORS	M_3psme_c	<---->	M_pi_c + M_chor_c
R_CITtam	M_mal_DASH_L_m + M_cit_c	<---->	M_mal_DASH_L_c + M_cit_m
R_CITtcm	M_cit_c + M_icit_m	----->	M_icit_c + M_cit_m
R_cmpSYN	M_atp_c + M_nh4_c + M_ump_c	<---->	2.0*M_h_c + M_adp_c + M_pi_c + M_cmp_c
R_CO2t	M_co2tot_e	<---->	M_co2tot_c
R_CO2tm	M_co2tot_c	<---->	M_co2tot_m
R_CSc	M_h2o_c + M_accoa_c + M_oaa_c	<---->	M_h_c + M_coa_c + M_cit_c
R_CSm	M_h2o_m + M_oaa_m + M_accoa_m	----->	M_h_m + M_coa_m + M_cit_m

R_CYOom	$6.0 \cdot M_{h_m} + M_{o2_m} + 4.0 \cdot M_{focytc_m}$	<---->	$6.0 \cdot M_{h_c} + 2.0 \cdot M_{h2o_m} + 4.0 \cdot M_{ficytc_m}$
R_CYOR_u6m	$1.5 \cdot M_{h_m} + M_{q6h2_m} + 2.0 \cdot M_{ficytc_m}$	<---->	$1.5 \cdot M_{h_c} + M_{q6_m} + 2.0 \cdot M_{focytc_m}$
R_CYSTGL	$M_{h2o_c} + M_{cyst_DASH_L_c}$	<---->	$M_{nh4_c} + M_{2obut_c} + M_{cys_DASH_L_c}$
R_CYSTS	$M_{ser_DASH_L_c} + M_{hcys_DASH_L_c}$	<---->	$M_{h2o_c} + M_{cyst_DASH_L_c}$
R_dampSYN	$M_{h_c} + M_{nadph_c} + M_{amp_c}$	<---->	$M_{nadp_c} + M_{h2o_c} + M_{damp_c}$
R_dcmpSYN	$M_{h_c} + M_{nadph_c} + M_{cmp_c}$	<---->	$M_{nadp_c} + M_{h2o_c} + M_{dcmp_c}$
R_DDPA	$M_{h2o_c} + M_{pep_c} + M_{e4p_c}$	<---->	$M_{pi_c} + M_{2dda7p_c}$
R_dgmpSYN	$M_{h_c} + M_{nadph_c} + M_{gmp_c}$	<---->	$M_{nadp_c} + M_{h2o_c} + M_{dgmp_c}$
R_DHAD1m	M_{23dhmb_m}	<---->	$M_{h2o_m} + M_{3mob_m}$
R_DHAD2m	M_{23dhmp_m}	<---->	$M_{h2o_m} + M_{3mop_m}$
R_DHQS	M_{2dda7p_c}	<---->	$M_{pi_c} + M_{3dhq_c}$
R_DHQTi	M_{3dhq_c}	<---->	$M_{h2o_c} + M_{3dhsk_c}$
R_dtmpSYN	$2.0 \cdot M_{h_c} + M_{nadph_c} + M_{h2o_c} + M_{mlthf_c} + M_{dcmp_c}$	<---->	$M_{nadp_c} + M_{nh4_c} + M_{thf_c} + M_{dtmp_c}$
R_ENO	M_{2pg_c}	----->	$M_{h2o_c} + M_{pep_c}$
R_ergstSYN	$M_{h_c} + 3.0 \cdot M_{nadph_c} + 2.0 \cdot M_{atp_c} + 2.0 \cdot M_{o2_c} + M_{met_DASH_L_c} + M_{zymst_c}$	<---->	$3.0 \cdot M_{nadp_c} + M_{adp_c} + M_{ppi_c} + M_{pi_c} + 2.0 \cdot M_{h2o_c} + M_{amp_c} + M_{ergst_c} + M_{hcys_DASH_L_c}$
R_ETOHt	M_{etoh_e}	<---->	M_{etoh_c}
R_ETOHtm	M_{etoh_c}	<---->	M_{etoh_m}
R_FBA	M_{fdp_c}	----->	$M_{dhap_c} + M_{g3p_c}$
R_FBP	$M_{h2o_c} + M_{fdp_c}$	----->	$M_{pi_c} + M_{f6p_c}$
R_FDHI	$M_{nad_c} + M_{h2o_c} + M_{for_c}$	<---->	$M_{nadh_c} + M_{co2tot_c}$
R_FTHFL	$M_{atp_c} + M_{thf_c} + M_{for_c}$	----->	$M_{adp_c} + M_{pi_c} + M_{10thf_c}$
R_FUM	$M_{h2o_c} + M_{fum_c}$	----->	$M_{mal_DASH_L_c}$
R_FUMm	$M_{h2o_m} + M_{fum_m}$	----->	$M_{mal_DASH_L_m}$
R_G3PD1ir	$M_{h_c} + M_{nadh_c} + M_{dhap_c}$	<---->	$M_{nad_c} + M_{glyc3p_c}$
R_G3PT	$M_{glyc3p_c} + M_{h2o_c}$	<---->	$M_{pi_c} + M_{glyc_c}$
R_G5SADr	M_{glu5sa_c}	----->	$M_{h_c} + M_{h2o_c} + M_{1pyr5c_c}$

R_G5SD	M_h_c + M_nadph_c + M_glu5p_c	<---->	M_nadp_c + M_pi_c + M_glu5sa_c
R_G6PDH2	M_nadp_c + M_g6p_c	<---->	M_h_c + M_nadph_c + M_6pgl_c
R_GAPD	M_nad_c + M_pi_c + M_g3p_c	----->	M_h_c + M_nadh_c + M_13dpg_c
R_GHMT2r	M_thf_c + M_ser_DASH_L_c	----->	M_h2o_c + M_mlthf_c + M_gly_c
R_GLCt1	M_glc_DASH_D_e	<---->	M_glc_DASH_D_c
R_GLNS	M_atp_c + M_nh4_c + M_glu_DASH_L_c	<---->	M_h_c + M_adp_c + M_pi_c + M_gln_DASH_L_c
R_GLnt2m	M_gln_DASH_L_c	----->	M_gln_DASH_L_m
R_GLU5K	M_atp_c + M_glu_DASH_L_c	<---->	M_adp_c + M_glu5p_c
R_GLUDy	M_nadp_c + M_h2o_c + M_glu_DASH_L_c	----->	M_h_c + M_nadph_c + M_nh4_c + M_akg_c
R_GLUDym	M_h2o_m + M_glu_DASH_L_m + M_nadp_m	----->	M_h_m + M_akg_m + M_nadph_m + M_nh4_m
R_GLUSxm	M_h_m + M_akg_m + M_gln_DASH_L_m + M_nadh_m	<---->	2.0*M_glu_DASH_L_m + M_nad_m
R_GLUt2m	M_h_c + M_glu_DASH_L_c	<---->	M_h_m + M_glu_DASH_L_m
R_Glutakg	M_glu_DASH_L_m + M_oaa_m	<---->	M_akg_m + M_asp_DASH_L_m
R_GLXtm	M_glx_c	----->	M_glx_m
R_GLYCt	M_glyc_c	<---->	M_glyc_e
R_GLYK	M_atp_c + M_glyc_c	<---->	M_glyc3p_c + M_h_c + M_adp_c
R_GLYt2m	M_gly_c	<---->	M_gly_m
R_gmpSYN	M_nad_c + M_atp_c + M_h2o_c + M_aicar_c + M_10fthf_c + M_gln_DASH_L_c	<---->	3.0*M_h_c + M_nadh_c + M_ppi_c + M_glu_DASH_L_c + M_amp_c + M_thf_c + M_gmp_c
R_GND	M_nadp_c + M_h2o_c + M_6pgc_c	----->	M_nadph_c + M_co2tot_c + M_ru5p_DASH_D_c
R_H2Ot	M_h2o_e	<---->	M_h2o_c
R_H2Otm	M_h2o_c	<---->	M_h2o_m
R_HACNHm	M_h2o_m + M_b124tc_m	----->	M_hicit_m
R_HCITS	M_h2o_c + M_akg_c + M_accoa_c	----->	M_h_c + M_coa_c + M_hcit_c
R_HCITtm	M_hcit_c	----->	M_hcit_m
R_HEX1	M_atp_c + M_glc_DASH_D_c	<---->	M_h_c + M_g6p_c + M_adp_c
R_HICITDm	M_nad_m + M_hicit_m	----->	M_h_m + M_nadh_m + M_oxag_m

R_HISTD	$2.0 \cdot M_{nad_c} + M_{h2o_c} + M_{histd_c}$	<---->	$3.0 \cdot M_{h_c} + 2.0 \cdot M_{nadh_c} + M_{his_DASH_L_c}$
R_HISTP	$M_{h2o_c} + M_{hisp_c}$	<---->	$M_{pi_c} + M_{histd_c}$
R_HSDyi	$M_{h_c} + M_{nadph_c} + M_{aspsa_c}$	<---->	$M_{nadp_c} + M_{hom_DASH_L_c}$
R_HSERTA	$M_{accoa_c} + M_{hom_DASH_L_c}$	----->	$M_{coa_c} + M_{achms_c}$
R_HSK	$M_{atp_c} + M_{hom_DASH_L_c}$	<---->	$M_{h_c} + M_{adp_c} + M_{phom_c}$
R_HSTPT	$M_{glu_DASH_L_c} + M_{imacp_c}$	<---->	$M_{akg_c} + M_{hisp_c}$
R_ICDHxm	$M_{h2o_m} + M_{nad_m} + M_{icit_m}$	<---->	$M_{co2tot_m} + M_{akg_m} + M_{nadh_m}$
R_ICDHy	$M_{nadp_c} + M_{h2o_c} + M_{icit_c}$	<---->	$M_{nadph_c} + M_{akg_c} + M_{co2tot_c}$
R_ICL	M_{icit_c}	<---->	$M_{succ_c} + M_{glx_c}$
R_IG3PS	$M_{glu_DASH_L_c} + M_{prlp_c}$	<---->	$M_{h_c} + M_{glu_DASH_L_c} + M_{aicar_c} + M_{eig3p_c}$
R_IGPDH	M_{eig3p_c}	<---->	$M_{h2o_c} + M_{imacp_c}$
R_IGPS	$M_{h_c} + M_{2cpr5p_c}$	<---->	$M_{co2tot_c} + M_{3ig3p_c}$
R_ILETA	$M_{akg_c} + M_{ile_DASH_L_c}$	<---->	$M_{glu_DASH_L_c} + M_{3mop_c}$
R_IPMD	$M_{nad_c} + M_{3c2hmp_c}$	<---->	$M_{h_c} + M_{nadh_c} + M_{3c4mop_c}$
R_IPPMIa	M_{3c2hmp_c}	<---->	$M_{h2o_c} + M_{2ippm_c}$
R_IPPMIb	$M_{h2o_c} + M_{2ippm_c}$	<---->	M_{3c3hmp_c}
R_IPPS	$M_{h2o_c} + M_{accoa_c} + M_{3mob_c}$	<---->	$M_{h_c} + M_{coa_c} + M_{3c3hmp_c}$
R_KARA1im	$M_{h_m} + M_{alac_DASH_S_m} + M_{nadph_m}$	<---->	$M_{23dhmb_m} + M_{nadp_m}$
R_KARA2im	$M_{2ahbut_m} + M_{h_m} + M_{nadph_m}$	<---->	$M_{nadp_m} + M_{23dhmp_m}$
R_LEUTA	$M_{akg_c} + M_{leu_DASH_L_c}$	<---->	$M_{glu_DASH_L_c} + M_{4mop_c}$
R_malateakg	$M_{akg_m} + M_{mal_DASH_L_c}$	----->	$M_{akg_c} + M_{mal_DASH_L_m}$
R_MALS	$M_{h2o_c} + M_{accoa_c} + M_{glx_c}$	----->	$M_{h_c} + M_{coa_c} + M_{mal_DASH_L_c}$
R_MALtm	$M_{mal_DASH_L_c} + M_{pi_m}$	<---->	$M_{pi_c} + M_{mal_DASH_L_m}$
R_mannanSYN	$M_{atp_c} + M_{f6p_c}$	<---->	$M_{adp_c} + M_{ppi_c} + M_{mannan_c}$
R_MCITDm	M_{hcit_m}	----->	$M_{h2o_m} + M_{b124tc_m}$
R_MDH	$M_{nad_c} + M_{mal_DASH_L_c}$	<---->	$M_{h_c} + M_{nadh_c} + M_{oaa_c}$
R_MDHm	$M_{mal_DASH_L_m} + M_{nad_m}$	----->	$M_{h_m} + M_{nadh_m} + M_{oaa_m}$

R_ME2m	M_h2o_m + M_mal_DASH_L_m + M_nadp_m	<---->	M_co2tot_m + M_pyr_m + M_nadph_m
R_METS	M_5mthf_c + M_hcys_DASH_L_c	<---->	M_thf_c + M_met_DASH_L_c
R_MTHFC	M_h2o_c + M_methf_c	----->	M_10fthf_c
R_MTHFD	M_nadp_c + M_mlthf_c	----->	M_h_c + M_nadph_c + M_methf_c
R_MTHFR3	M_h_c + M_nadph_c + M_mlthf_c	<---->	M_nadp_c + M_5mthf_c
R_NADH2_DASH_u6 cm	M_h_c + M_nadh_c + M_q6_m	<---->	M_nad_c + M_q6h2_m
R_NADH2_DASH_u6 m	M_h_m + M_q6_m + M_nadh_m	<---->	M_q6h2_m + M_nad_m
R_NH4t	M_nh4_e	----->	M_nh4_c
R_NH4tm	M_nh4_c	<---->	M_nh4_m
R_O2t	M_o2_e	----->	M_o2_c
R_O2tm	M_o2_c	----->	M_o2_m
R_OAAt2m	2.0*M_h_c + M_oaa_c	<---->	2.0*M_h_m + M_oaa_m
R_OCBTi	M_orn_c + M_cbp_c	<---->	M_h_c + M_pi_c + M_citr_DASH_L_c
R_OMCDC	M_h_c + M_h2o_c + M_3c4mop_c	<---->	M_co2tot_c + M_4mop_c
R_ORNt3m	M_orn_m	----->	M_orn_c
R_ORNTACim	M_glu_DASH_L_m + M_acorn_m	<---->	M_acglu_m + M_orn_m
R_OXAGm	M_h2o_m + M_h_m + M_oxag_m	----->	M_co2tot_m + M_2oxoadp_m
R_P5CR	2.0*M_h_c + M_nadph_c + M_1pyr5c_c	<---->	M_nadp_c + M_pro_DASH_L_c
R_PAPSR	M_nadph_c + M_paps_c	<---->	2.0*M_h_c + M_nadp_c + M_so3_c + M_pap_c
R_paSYN	M_glyc3p_c + 15.38*M_h_c + 29.58*M_nadph_c + 14.2*M_atp_c + 16.2*M_accoa_c + 1.18*M_o2_c	<---->	29.58*M_nadp_c + 14.2*M_adp_c + 14.2*M_pi_c + M_pa_SC_c + 2.36*M_h2o_c + 16.2*M_coa_c
R_PC	M_atp_c + M_co2tot_c + M_pyr_c	----->	M_h_c + M_adp_c + M_pi_c + M_oaa_c
R_pcSYN	6.0*M_atp_c + 6.0*M_h2o_c + 3.0*M_met_DASH_L_c + M_pe_SC_c	<---->	6.0*M_h_c + 3.0*M_adp_c + 3.0*M_ppi_c + 3.0*M_pi_c + 3.0*M_amp_c + M_pc_SC_c + 3.0*M_hcys_DASH_L_c
R_PDHm	M_pyr_m + M_h2o_m + M_coa_m + M_nad_m	<---->	M_co2tot_m + M_nadh_m + M_accoa_m
R_peSYN	M_h_c + M_h2o_c + M_ps_SC_c	<---->	M_co2tot_c + M_pe_SC_c
R_PFK	M_atp_c + M_f6p_c	----->	M_h_c + M_adp_c + M_fdp_c

R_PGCD	M_nad_c + M_3pg_c	<---->	M_h_c + M_nadh_c + M_3php_c
R_PGI	M_g6p_c	----->	M_f6p_c
R_PGK	M_atp_c + M_3pg_c	<---->	M_adp_c + M_13dpg_c
R_PGL	M_6pgl_c + M_h2o_c	<---->	M_h_c + M_6pgc_c
R_PGM	M_2pg_c	<---->	M_3pg_c
R_PHETA1	M_akg_c + M_phe_DASH_L_c	<---->	M_glu_DASH_L_c + M_phpyr_c
R_Plt2m	M_h_c + M_pi_c	<---->	M_h_m + M_pi_m
R_Plt2r	M_h_e + M_pi_e	----->	M_h_c + M_pi_c
R_PPA	M_ppi_c + M_h2o_c	<---->	M_h_c + 2.0*M_pi_c
R_PPAm	M_h2o_m + M_ppi_m	<---->	M_h_m + 2.0*M_pi_m
R_PPCK	M_atp_c + M_h2o_c + M_oaa_c	----->	M_adp_c + M_co2tot_c + M_pep_c
R_PPND2	M_nadp_c + M_h2o_c + M_pphn_c	<---->	M_nadph_c + M_co2tot_c + M_34hpp_c
R_PPNDH	M_h_c + M_pphn_c	<---->	M_co2tot_c + M_phpyr_c
R_PRAli	M_pran_c	<---->	M_2cpr5p_c
R_PRAMPC	M_h2o_c + M_prbamp_c	<---->	M_prfp_c
R_PRATPP	M_h2o_c + M_prbatp_c	<---->	M_h_c + M_ppi_c + M_prbamp_c
R_PRMICli	M_prfp_c	<---->	M_prlp_c
R_PRPPS	M_atp_c + M_r5p_c	----->	M_h_c + M_amp_c + M_prpp_c
R_PSCVTi	M_skm5p_c + M_pep_c	<---->	M_pi_c + M_3psme_c
R_PSERT	M_glu_DASH_L_c + M_3php_c	<---->	M_akg_c + M_pser_DASH_L_c
R_PSP_L	M_h2o_c + M_pser_DASH_L_c	<---->	M_pi_c + M_ser_DASH_L_c
R_psSYN	2.0*M_atp_c + M_pa_SC_c + M_ser_DASH_L_c	<---->	2.0*M_adp_c + M_ppi_c + M_ps_SC_c
R_ptd1inoSYN	M_g6p_c + 2.0*M_atp_c + M_pa_SC_c + M_h2o_c	<---->	2.0*M_adp_c + M_ppi_c + M_pi_c + M_ptd1ino_SC_c
R_PYK	M_h_c + M_adp_c + M_pep_c	----->	M_atp_c + M_pyr_c
R_PYRDC	M_h_c + M_h2o_c + M_pyr_c	<---->	M_acald_c + M_co2tot_c
R_PYRt2	M_pyr_e	----->	M_pyr_c
R_PYRt2m	M_h_c + M_pyr_c	----->	M_pyr_m + M_h_m

R_RPE	M_ru5p_DASH_D_c	<---->	M_xu5p_DASH_D_c
R_RPI	M_r5p_c	<---->	M_ru5p_DASH_D_c
R_SACCD1	M_h_c + M_nadph_c + M_glu_DASH_L_c + M_L2aadp6sa_c	----->	M_nadp_c + M_h2o_c + M_sacchrp_DASH_L_c
R_SACCD2	M_nad_c + M_h2o_c + M_sacchrp_DASH_L_c	----->	M_h_c + M_nadh_c + M_akg_c + M_lys_DASH_L_c
R_SHK3D	M_h_c + M_nadph_c + M_3dhsk_c	<---->	M_nadp_c + M_skm_c
R_SHKK	M_atp_c + M_skm_c	<---->	M_h_c + M_adp_c + M_skm5p_c
R_SLFAT	M_h_c + M_adp_c + M_so4_c	----->	M_pi_c + M_aps_c
R_SO4ti	M_so4_e	<---->	M_so4_c
R_SUCct2r	M_h_e + M_succ_e	<---->	M_h_c + M_succ_c
R_SUCctm	M_succ_c + M_pi_m	<---->	M_pi_c + M_succ_m
R_SUCD2_u6m	M_q6_m + M_succ_m	----->	M_fum_m + M_q6h2_m
R_SUCFUMtm	M_succ_c + M_fum_m	<---->	M_fum_c + M_succ_m
R_SUCOAS1m	M_succ_m + M_atp_m + M_coa_m	<---->	M_adp_m + M_succoa_m + M_pi_m
R_SULR	3.0*M_nadp_c + 3.0*M_h2o_c + M_h2s_c	<---->	5.0*M_h_c + 3.0*M_nadph_c + M_so3_c
R_TALA	M_g3p_c + M_s7p_c	<---->	M_f6p_c + M_e4p_c
R_THRA	M_acald_c + M_gly_c	----->	M_thr_DASH_L_c
R_THRD_Lm	M_thr_DASH_L_m	<---->	M_2obut_m + M_nh4_m
R_THRS	M_h2o_c + M_phom_c	<---->	M_pi_c + M_thr_DASH_L_c
R_THRt2m	M_thr_DASH_L_c	----->	M_thr_DASH_L_m
R_TKT1	M_r5p_c + M_xu5p_DASH_D_c	<---->	M_g3p_c + M_s7p_c
R_TKT2	M_e4p_c + M_xu5p_DASH_D_c	----->	M_f6p_c + M_g3p_c
R_TPI	M_dhap_c	----->	M_g3p_c
R_triglycSYN	7.69*M_h_c + 14.79*M_nadph_c + 7.1*M_atp_c + M_pa_SC_c + 8.1*M_accoa_c + 0.59*M_o2_c	<---->	14.79*M_nadp_c + 7.1*M_adp_c + 8.1*M_pi_c + 0.18*M_h2o_c + M_triglyc_SC_c + 8.1*M_coa_c
R_TRPS1	M_ser_DASH_L_c + M_3ig3p_c	<---->	M_h2o_c + M_g3p_c + M_trp_DASH_L_c
R_TYRTA	M_akg_c + M_tyr_DASH_L_c	<---->	M_glu_DASH_L_c + M_34hpp_c
R_umpSYN	3.0*M_atp_c + 0.5*M_o2_c + M_asp_DASH_L_c + M_gln_DASH_L_c + M_r5p_c	<---->	2.0*M_h_c + 2.0*M_adp_c + M_ppi_c + 2.0*M_pi_c + M_glu_DASH_L_c + M_amp_c + M_ump_c

R_VALTA	$M_{\text{akg_c}} + M_{\text{val_DASH_L_c}}$	<---->	$M_{\text{glu_DASH_L_c}} + M_{\text{3mob_c}}$
R_zymstSYN	$2.0 * M_{\text{nad_c}} + 11.0 * M_{\text{h_c}} + 26.0 * M_{\text{nadph_c}} + 18.0 * M_{\text{atp_c}} + M_{\text{h2o_c}} + 18.0 * M_{\text{accoa_c}} + 10.0 * M_{\text{o2_c}}$	<---->	$2.0 * M_{\text{nadh_c}} + 26.0 * M_{\text{nadp_c}} + 18.0 * M_{\text{adp_c}} + 6.0 * M_{\text{ppi_c}} + 6.0 * M_{\text{pi_c}} + 18.0 * M_{\text{coa_c}} + 8.0 * M_{\text{co2tot_c}} + M_{\text{for_c}} + M_{\text{zymst_c}}$

APPENDIX C: *P. pastoris* metabolic model.

The *P. pastoris* metabolic model used for all the p-FBA presented in the chapter 4. The resulting model used for the metabolic flux calculation, that contains 221 reactions and 205 metabolites, is detailed in **Table C**.

Table C. List of reactions included in the HEK293 reduced model developed and used for all Flux Balance Analysis in the Chapter 4.

R_13BDglnSYN	M_atp_c + M_g6p_c	<---->	M_adp_c + M_ppi_c + M_13BDgln_c
R_2OBUtm	M_2obut_c	----->	M_2obut_m
R_2OXOADPtim	M_2oxoadp_m + M_akg_c	<---->	M_akg_m + M_2oxoadp_c
R_3MOBtm	M_3mob_c	<---->	M_3mob_m
R_3MOPtm	M_3mop_c	<---->	M_3mop_m
R_AASAD1	M_h_c + M_atp_c + M_nadph_c + M_L2aadp_c	<---->	M_nadp_c + M_ppi_c + M_amp_c + M_L2aadp6sa_c
R_AATA	M_glu_DASH_L_c + M_2oxoadp_c	----->	M_akg_c + M_L2aadp_c
R_ACALDtm	M_acald_c	----->	M_acald_m
R_ACGKm	M_atp_m + M_acglu_m	<---->	M_adp_m + M_acg5p_m
R_ACHBSm	M_h_m + M_h2o_m + M_pyr_m + M_2obut_m	<---->	M_co2tot_m + M_2ahbut_m
R_ACLSm	M_h_m + M_h2o_m + 2.0*M_pyr_m	<---->	M_co2tot_m + M_alac_DASH_S_m
R_ACOAH	M_h_c + M_coa_c + M_ac_c	----->	M_h2o_c + M_accoa_c
R_ACONT	M_cit_c	----->	M_icit_c
R_ACONTm	M_cit_m	----->	M_icit_m
R_ACOTAim	M_glu_DASH_L_m + M_acg5sa_m	<---->	M_akg_m + M_acorn_m
R_ACS	M_atp_c + M_coa_c + M_ac_c	----->	M_accoa_c + M_ppi_c + M_amp_c
R_ACSm	M_coa_m + M_atp_m + M_ac_m	----->	M_accoa_m + M_amp_m + M_ppi_m
R_Act2r	M_ac_e	----->	M_ac_c

R_ACTm	M_ac_c	----->	M_ac_m
R_ADK1	M_atp_c + M_amp_c	<----->	2.0*M_adp_c
R_ADK1m	M_atp_m + M_amp_m	<----->	2.0*M_adp_m
R_ADSK	M_atp_c + M_aps_c	<----->	M_h_c + M_adp_c + M_paps_c
R_AGPRim	M_h_m + M_nadph_m + M_acg5p_m	<----->	M_pi_m + M_nadp_m + M_acg5sa_m
R_AGTm	M_glx_m + M_ala_DASH_L_m	<----->	M_gly_m + M_pyr_m
R_AHSERL2	M_h2s_c + M_achms_c	<----->	M_h_c + M_hcys_DASH_L_c + M_ac_c
R_aicarSYN	5.0*M_atp_c + M_h2o_c + M_co2tot_c + M_r5p_c + M_asp_DASH_L_c + 2.0*M_gln_DASH_L_c + M_gly_c + M_10fthf_c	<----->	8.0*M_h_c + 4.0*M_pi_c + 4.0*M_adp_c + M_ppi_c + M_amp_c + 2.0*M_glu_DASH_L_c + M_thf_c + M_aicar_c + M_fum_c
R_AKGDam	M_nad_m + M_akg_m + M_h2o_m + M_coa_m	----->	M_nadh_m + M_co2tot_m + M_succoa_m
R_ALAt2m	M_ala_DASH_L_c	----->	M_ala_DASH_L_m
R_ALATA_L	M_glu_DASH_L_c + M_pyr_c	<----->	M_akg_c + M_ala_DASH_L_c
R_ALATA_Lm	M_glu_DASH_L_m + M_pyr_m	----->	M_akg_m + M_ala_DASH_L_m
R_ALCD2m	M_nad_m + M_etoh_m	----->	M_nadh_m + M_h_m + M_acald_m
R_ALCD2x	M_nad_c + M_etoh_c	<----->	M_h_c + M_nadh_c + M_acald_c
R_ALDD2xm	M_nad_m + M_h2o_m + M_acald_m	<----->	M_nadh_m + 2.0*M_h_m + M_ac_m
R_ALDD2y	M_h2o_c + M_nadp_c + M_acald_c	<----->	2.0*M_h_c + M_nadph_c + M_ac_c
R_ALDD2ym	M_h2o_m + M_acald_m + M_nadp_m	<----->	2.0*M_h_m + M_nadph_m + M_ac_m
R_ampSYN	M_atp_c + M_asp_DASH_L_c + M_10fthf_c + M_aicar_c	<----->	2.0*M_h_c + M_pi_c + M_adp_c + M_h2o_c + M_amp_c + M_thf_c + M_fum_c
R_ANPRT	M_anth_c + M_prpp_c	<----->	M_ppi_c + M_pran_c
R_ANS	M_gln_DASH_L_c + M_chor_c	<----->	M_h_c + M_glu_DASH_L_c + M_anth_c + M_pyr_c
R_ARGSL	M_argsuc_c	----->	M_arg_DASH_L_c + M_fum_c
R_ARGSSr	M_atp_c + M_asp_DASH_L_c + M_citr_DASH_L_c	----->	M_h_c + M_ppi_c + M_amp_c + M_argsuc_c
R_ASADi	M_h_c + M_nadph_c + M_4pasp_c	<----->	M_pi_c + M_nadp_c + M_aspsa_c
R_ASNS1	M_atp_c + M_h2o_c + M_asp_DASH_L_c + M_gln_DASH_L_c	<----->	M_h_c + M_ppi_c + M_amp_c + M_glu_DASH_L_c + M_asn_DASH_L_c
R_AspGlut	M_glu_DASH_L_c + M_asp_DASH_L_m	<----->	M_glu_DASH_L_m + M_asp_DASH_L_c
R_ASPIKi	M_atp_c + M_asp_DASH_L_c	<----->	M_adp_c + M_4pasp_c

R_ASPTA	M_asp_DASH_L_c + M_akg_c	----->	M_oaa_c + M_glu_DASH_L_c
R_ATPPRT	M_atp_c + M_prpp_c	<----->	M_ppi_c + M_prbatp_c
R_ATPS	M_atp_c + M_h2o_c	----->	M_h_c + M_pi_c + M_adp_c
R_ATPS3m	3.0*M_h_c + M_adp_m + M_pi_m	<----->	2.0*M_h_m + M_h2o_m + M_atp_m
R_ATPtm_DASH_H	M_adp_c + M_atp_m	<----->	M_atp_c + M_adp_m
R_bio2r	M_bio_e	<----->	M_bio_c
R_biomass	20.4*M_atp_c + 20.4*M_h2o_c + 0.21*M_ser_DASH_L_c + 0.002*M_zymst_c + 0.051*M_amp_c + 0.067*M_ump_c + 0.303*M_glu_DASH_L_c + 0.143*M_asp_DASH_L_c + 0.303*M_gln_DASH_L_c + 0.00118*M_dtmp_c + 8.22E-4*M_dcmp_c + 0.189*M_thr_DASH_L_c + 0.233*M_gly_c + 0.207*M_lys_DASH_L_c + 0.0039*M_pe_SC_c + 8.0E-5*M_ps_SC_c + 1.701*M_13BDglicn_c + 0.05*M_cmp_c + 0.025*M_met_DASH_L_c + 0.0585*M_his_DASH_L_c + 0.349*M_ala_DASH_L_c + 8.0E-5*M_pa_SC_c + 8.22E-4*M_dgmp_c + 0.051*M_gmp_c + 0.143*M_asn_DASH_L_c + 0.00118*M_damp_c + 0.22*M_arg_DASH_L_c + 0.0388*M_ergst_c + 0.099*M_phe_DASH_L_c + 0.182*M_val_DASH_L_c + 0.0457*M_trp_DASH_L_c + 0.0356*M_triglyc_SC_c + 2.0E-4*M_ptd1ino_SC_c + 0.135*M_ile_DASH_L_c + 0.12*M_pro_DASH_L_c + 0.0696*M_tyr_DASH_L_c + 0.228*M_leu_DASH_L_c + 0.0049*M_cys_DASH_L_c + 0.0072*M_pc_SC_c	<----->	20.4*M_h_c + 20.4*M_pi_c + 20.4*M_adp_c + M_bio_c
R_BPNT	M_h2o_c + M_pap_c	<----->	M_pi_c + M_amp_c
R_CBPS	2.0*M_atp_c + M_h2o_c + M_co2tot_c + M_gln_DASH_L_c	<----->	2.0*M_h_c + M_pi_c + 2.0*M_adp_c + M_glu_DASH_L_c + M_cbp_c
R_CHORM	M_chor_c	<----->	M_pphn_c
R_CHORS	M_3psme_c	<----->	M_pi_c + M_chor_c
R_CITtam	M_cit_c + M_mal_DASH_L_m	<----->	M_cit_m + M_mal_DASH_L_c
R_CITcm	M_cit_c + M_icit_m	----->	M_cit_m + M_icit_c
R_cmpSYN	M_atp_c + M_ump_c + M_nh4_c	<----->	2.0*M_h_c + M_pi_c + M_adp_c + M_cmp_c
R_CO2t	M_co2tot_e	<----->	M_co2tot_c
R_CO2tm	M_co2tot_c	<----->	M_co2tot_m
R_CSc	M_h2o_c + M_oaa_c + M_accoa_c	----->	M_h_c + M_cit_c + M_coa_c
R_CSm	M_h2o_m + M_accoa_m + M_oaa_m	----->	M_h_m + M_cit_m + M_coa_m
R_CYOOm	M_o2_m + 6.0*M_h_m + 4.0*M_focytc_m	<----->	6.0*M_h_c + 2.0*M_h2o_m + 4.0*M_ficytc_m

R_CYOR_u6m	$1.5 \cdot M_{h_m} + M_{q6h2_m} + 2.0 \cdot M_{ficytc_m}$	<---->	$1.5 \cdot M_{h_c} + M_{q6_m} + 2.0 \cdot M_{focytc_m}$
R_CYSTGL	$M_{h2o_c} + M_{cyst_DASH_L_c}$	<---->	$M_{nh4_c} + M_{cys_DASH_L_c} + M_{2obut_c}$
R_CYSTS	$M_{ser_DASH_L_c} + M_{hcys_DASH_L_c}$	<---->	$M_{h2o_c} + M_{cyst_DASH_L_c}$
R_dampSYN	$M_{h_c} + M_{nadph_c} + M_{amp_c}$	<---->	$M_{h2o_c} + M_{nadp_c} + M_{damp_c}$
R_dcmpSYN	$M_{h_c} + M_{nadph_c} + M_{cmp_c}$	<---->	$M_{h2o_c} + M_{nadp_c} + M_{dcmp_c}$
R_DDPA	$M_{h2o_c} + M_{e4p_c} + M_{pep_c}$	<---->	$M_{pi_c} + M_{2dda7p_c}$
R_dgmpSYN	$M_{h_c} + M_{nadph_c} + M_{gmp_c}$	<---->	$M_{h2o_c} + M_{nadp_c} + M_{dgmp_c}$
R_DHAD1m	M_{23dhmb_m}	<---->	$M_{h2o_m} + M_{3mob_m}$
R_DHAD2m	M_{23dhmp_m}	<---->	$M_{h2o_m} + M_{3mop_m}$
R_DHQS	M_{2dda7p_c}	<---->	$M_{pi_c} + M_{3dhq_c}$
R_DHQTi	M_{3dhq_c}	<---->	$M_{h2o_c} + M_{3dhsk_c}$
R_dtmpSYN	$2.0 \cdot M_{h_c} + M_{h2o_c} + M_{nadph_c} + M_{dcmp_c} + M_{mlthf_c}$	<---->	$M_{nadp_c} + M_{nh4_c} + M_{thf_c} + M_{dtmp_c}$
R_ENO	M_{2pg_c}	----->	$M_{h2o_c} + M_{pep_c}$
R_ergstSYN	$2.0 \cdot M_{o2_c} + M_{h_c} + 2.0 \cdot M_{atp_c} + 3.0 \cdot M_{nadph_c} + M_{zymst_c} + M_{met_DASH_L_c}$	<---->	$M_{pi_c} + M_{adp_c} + 2.0 \cdot M_{h2o_c} + M_{hcys_DASH_L_c} + 3.0 \cdot M_{nadp_c} + M_{ppi_c} + M_{amp_c} + M_{ergst_c}$
R_ETOHt	M_{etoh_e}	<---->	M_{etoh_c}
R_ETOHtm	M_{etoh_c}	----->	M_{etoh_m}
R_FBA	M_{fdp_c}	----->	$M_{g3p_c} + M_{dhap_c}$
R_FBP	$M_{h2o_c} + M_{fdp_c}$	----->	$M_{pi_c} + M_{f6p_c}$
R_FDH	$M_{h2o_c} + M_{for_c} + M_{nad_c}$	<---->	$M_{co2tot_c} + M_{nadh_c}$
R_FTHFL	$M_{atp_c} + M_{for_c} + M_{thf_c}$	----->	$M_{pi_c} + M_{adp_c} + M_{10fthf_c}$
R_FUM	$M_{h2o_c} + M_{fum_c}$	----->	$M_{mal_DASH_L_c}$
R_FUMm	$M_{h2o_m} + M_{fum_m}$	----->	$M_{mal_DASH_L_m}$
R_G3PD1ir	$M_{h_c} + M_{nadh_c} + M_{dhap_c}$	<---->	$M_{nad_c} + M_{glyc3p_c}$
R_G3PT	$M_{h2o_c} + M_{glyc3p_c}$	<---->	$M_{pi_c} + M_{glyc_c}$
R_G5SADr	M_{glu5sa_c}	----->	$M_{h_c} + M_{h2o_c} + M_{1pyr5c_c}$
R_G5SD	$M_{h_c} + M_{glu5p_c} + M_{nadph_c}$	<---->	$M_{pi_c} + M_{glu5sa_c} + M_{nadp_c}$

R_G6PDH2	M_nadp_c + M_g6p_c	<---->	M_h_c + M_nadph_c + M_6pgl_c
R_GAPD	M_pi_c + M_nad_c + M_g3p_c	----->	M_h_c + M_nadh_c + M_13dpg_c
R_GHMT2r	M_ser_DASH_L_c + M_thf_c	----->	M_h2o_c + M_mlthf_c + M_gly_c
R_GLCt1	M_glc_DASH_D_e	<---->	M_glc_DASH_D_c
R_GLNS	M_atp_c + M_glu_DASH_L_c + M_nh4_c	<---->	M_h_c + M_pi_c + M_adp_c + M_gln_DASH_L_c
R_GLNt2m	M_gln_DASH_L_c	----->	M_gln_DASH_L_m
R_GLU5K	M_atp_c + M_glu_DASH_L_c	<---->	M_adp_c + M_glu5p_c
R_GLUDy	M_h2o_c + M_nadp_c + M_glu_DASH_L_c	<---->	M_h_c + M_nadph_c + M_nh4_c + M_akg_c
R_GLUDym	M_glu_DASH_L_m + M_h2o_m + M_nadp_m	<---->	M_akg_m + M_h_m + M_nh4_m + M_nadph_m
R_GLUSxm	M_gln_DASH_L_m + M_nadh_m + M_akg_m + M_h_m	<---->	2.0*M_glu_DASH_L_m + M_nad_m
R_GLUt2m	M_h_c + M_glu_DASH_L_c	<---->	M_glu_DASH_L_m + M_h_m
R_Glutakg	M_glu_DASH_L_m + M_oaa_m	<---->	M_akg_m + M_asp_DASH_L_m
R_GLXtm	M_glx_c	----->	M_glx_m
R_GLYCt	M_glyc_c	<---->	M_glyc_e
R_GLYK	M_atp_c + M_glyc_c	----->	M_h_c + M_adp_c + M_glyc3p_c
R_GLYt2m	M_gly_c	<---->	M_gly_m
R_gmpSYN	M_atp_c + M_h2o_c + M_nad_c + M_gln_DASH_L_c + M_10fthf_c + M_aicar_c	<---->	3.0*M_h_c + M_ppi_c + M_nadh_c + M_amp_c + M_glu_DASH_L_c + M_thf_c + M_gmp_c
R_GND	M_h2o_c + M_nadp_c + M_6pgc_c	----->	M_co2tot_c + M_nadph_c + M_ru5p_DASH_D_c
R_H2Ot	M_h2o_e	<---->	M_h2o_c
R_H2Otm	M_h2o_c	<---->	M_h2o_m
R_HACNHm	M_h2o_m + M_b124tc_m	----->	M_hcit_m
R_HCITS	M_h2o_c + M_accoa_c + M_akg_c	----->	M_h_c + M_coa_c + M_hcit_c
R_HCITtm	M_hcit_c	----->	M_hcit_m
R_HEX1	M_atp_c + M_glc_DASH_D_c	<---->	M_h_c + M_adp_c + M_g6p_c
R_HICITDm	M_nad_m + M_hcit_m	----->	M_nadh_m + M_h_m + M_oxag_m
R_HISTD	M_h2o_c + 2.0*M_nad_c + M_histd_c	<---->	3.0*M_h_c + 2.0*M_nadh_c + M_his_DASH_L_c

R_HISTP	M_h2o_c + M_hisp_c	<---->	M_pi_c + M_histd_c
R_HSDyi	M_h_c + M_nadph_c + M_aspsa_c	<---->	M_nadp_c + M_hom_DASH_L_c
R_HSERTA	M_accoa_c + M_hom_DASH_L_c	----->	M_coa_c + M_achms_c
R_HSK	M_atp_c + M_hom_DASH_L_c	<---->	M_h_c + M_adp_c + M_phom_c
R_HSTPT	M_glu_DASH_L_c + M_imacp_c	<---->	M_akg_c + M_hisp_c
R_ICDHxm	M_nad_m + M_h2o_m + M_icit_m	<---->	M_nadh_m + M_akg_m + M_co2tot_m
R_ICDH_y	M_h2o_c + M_nadp_c + M_icit_c	<---->	M_co2tot_c + M_nadph_c + M_akg_c
R_ICL	M_icit_c	<---->	M_glx_c + M_succ_c
R_IG3PS	M_gln_DASH_L_c + M_prlp_c	<---->	M_h_c + M_glu_DASH_L_c + M_eig3p_c + M_aicar_c
R_IGPDH	M_eig3p_c	<---->	M_h2o_c + M_imacp_c
R_IGPS	M_h_c + M_2cpr5p_c	<---->	M_3ig3p_c + M_co2tot_c
R_ILETA	M_akg_c + M_ile_DASH_L_c	<---->	M_glu_DASH_L_c + M_3mop_c
R_IPMD	M_nad_c + M_3c2hmp_c	<---->	M_h_c + M_nadh_c + M_3c4mop_c
R_IPPMIa	M_3c2hmp_c	<---->	M_h2o_c + M_2ippm_c
R_IPPMIb	M_h2o_c + M_2ippm_c	<---->	M_3c3hmp_c
R_IPPS	M_h2o_c + M_accoa_c + M_3mob_c	<---->	M_h_c + M_coa_c + M_3c3hmp_c
R_KARA1im	M_h_m + M_nadph_m + M_alac_DASH_S_m	<---->	M_nadp_m + M_23dhmb_m
R_KARA2im	M_h_m + M_nadph_m + M_2ahbut_m	<---->	M_nadp_m + M_23dhmp_m
R_LEUTA	M_akg_c + M_leu_DASH_L_c	<---->	M_glu_DASH_L_c + M_4mop_c
R_malateakg	M_akg_m + M_mal_DASH_L_c	----->	M_akg_c + M_mal_DASH_L_m
R_MALS	M_h2o_c + M_accoa_c + M_glx_c	----->	M_h_c + M_coa_c + M_mal_DASH_L_c
R_MALtm	M_pi_m + M_mal_DASH_L_c	----->	M_pi_c + M_mal_DASH_L_m
R_MCITDm	M_hcit_m	----->	M_h2o_m + M_b124tc_m
R_MDH	M_nad_c + M_mal_DASH_L_c	<---->	M_h_c + M_oaa_c + M_nadh_c
R_MDHm	M_nad_m + M_mal_DASH_L_m	----->	M_nadh_m + M_h_m + M_oaa_m
R_ME2m	M_h2o_m + M_mal_DASH_L_m + M_nadp_m	----->	M_co2tot_m + M_pyr_m + M_nadph_m
R_METS	M_hcys_DASH_L_c + M_5mthf_c	<---->	M_thf_c + M_met_DASH_L_c

R_MTHFC	M_h2o_c + M_methf_c	----->	M_10fthf_c
R_MTHFD	M_nadp_c + M_mlthf_c	----->	M_h_c + M_nadph_c + M_methf_c
R_MTHFR3	M_h_c + M_nadph_c + M_mlthf_c	<----->	M_nadp_c + M_5mthf_c
R_NADH2_DASH_u6cm	M_h_c + M_nadh_c + M_q6_m	-----	M_nad_c + M_q6h2_m
R_NADH2_DASH_u6m	M_nadh_m + M_h_m + M_q6_m	<----->	M_nad_m + M_q6h2_m
R_NH4t	M_nh4_e	----->	M_nh4_c
R_NH4tm	M_nh4_c	<----->	M_nh4_m
R_O2t	M_o2_e	----->	M_o2_c
R_O2tm	M_o2_c	----->	M_o2_m
R_OAAt2m	2.0*M_h_c + M_oaa_c	-----	2.0*M_h_m + M_oaa_m
R_OCBTi	M_orn_c + M_cbp_c	<----->	M_h_c + M_pi_c + M_citr_DASH_L_c
R_OMCDC	M_h_c + M_h2o_c + M_3c4mop_c	<----->	M_co2tot_c + M_4mop_c
R_ORNt3m	M_orn_m	----->	M_orn_c
R_ORNTACim	M_glu_DASH_L_m + M_acorn_m	<----->	M_acglu_m + M_orn_m
R_OXAGm	M_h_m + M_oxag_m + M_h2o_m	----->	M_2oxoadp_m + M_co2tot_m
R_P5CR	2.0*M_h_c + M_1pyr5c_c + M_nadph_c	<----->	M_nadp_c + M_pro_DASH_L_c
R_PAPSR	M_nadph_c + M_paps_c	<----->	2.0*M_h_c + M_nadp_c + M_so3_c + M_pap_c
R_paSYN	1.18*M_o2_c + 15.38*M_h_c + 14.2*M_atp_c + 29.58*M_nadph_c + 16.2*M_accoa_c + M_glyc3p_c	<----->	14.2*M_pi_c + 14.2*M_adp_c + 2.36*M_h2o_c + 29.58*M_nadp_c + 16.2*M_coa_c + M_pa_SC_c
R_PC_c	M_atp_c + M_co2tot_c + M_pyr_c	----->	M_h_c + M_pi_c + M_adp_c + M_oaa_c
R_PC_m	M_co2tot_m + M_pyr_m + M_atp_m	----->	M_h_m + M_oaa_m + M_adp_m + M_pi_m
R_pcSYN	6.0*M_atp_c + 6.0*M_h2o_c + M_pe_SC_c + 3.0*M_met_DASH_L_c	<----->	6.0*M_h_c + 3.0*M_pi_c + 3.0*M_adp_c + 3.0*M_hcys_DASH_L_c + 3.0*M_ppi_c + 3.0*M_amp_c + M_pc_SC_c
R_PDHm	M_nad_m + M_h2o_m + M_coa_m + M_pyr_m	<----->	M_nadh_m + M_co2tot_m + M_accoa_m
R_peSYN	M_h_c + M_h2o_c + M_ps_SC_c	<----->	M_co2tot_c + M_pe_SC_c
R_PFK	M_atp_c + M_f6p_c	----->	M_h_c + M_adp_c + M_fdp_c
R_PGCD	M_nad_c + M_3pg_c	<----->	M_h_c + M_nadh_c + M_3php_c

R_PGI	M_g6p_c	----->	M_f6p_c
R_PGK	M_atp_c + M_3pg_c	<----->	M_adp_c + M_13dpg_c
R_PGL	M_h2o_c + M_6pgl_c	<----->	M_h_c + M_6pgc_c
R_PGM	M_2pg_c	<----->	M_3pg_c
R_PHETA1	M_akg_c + M_phe_DASH_L_c	<----->	M_glu_DASH_L_c + M_phpyr_c
R_Plt2m	M_h_c + M_pi_c	<----->	M_h_m + M_pi_m
R_Plt2r	M_h_e + M_pi_e	----->	M_h_c + M_pi_c
R_PPA	M_h2o_c + M_ppi_c	<----->	M_h_c + 2.0*M_pi_c
R_PPAm	M_h2o_m + M_ppi_m	<----->	M_h_m + 2.0*M_pi_m
R_PPCK	M_atp_c + M_h2o_c + M_oaa_c	----->	M_adp_c + M_co2tot_c + M_pep_c
R_PPND2	M_h2o_c + M_nadp_c + M_pphn_c	<----->	M_co2tot_c + M_nadph_c + M_34hpp_c
R_PPNDH	M_h_c + M_pphn_c	<----->	M_co2tot_c + M_phpyr_c
R_PRAli	M_pran_c	<----->	M_2cpr5p_c
R_PRAMPC	M_h2o_c + M_prbamp_c	<----->	M_prfp_c
R_PRATPP	M_h2o_c + M_prbatp_c	<----->	M_h_c + M_prbamp_c + M_ppi_c
R_PRMICli	M_prfp_c	<----->	M_prlp_c
R_PRPPS	M_atp_c + M_r5p_c	----->	M_h_c + M_amp_c + M_prpp_c
R_PSCVTi	M_skm5p_c + M_pep_c	<----->	M_pi_c + M_3psme_c
R_PSERT	M_glu_DASH_L_c + M_3php_c	<----->	M_akg_c + M_pser_DASH_L_c
R_PSP_L	M_h2o_c + M_pser_DASH_L_c	<----->	M_pi_c + M_ser_DASH_L_c
R_psSYN	2.0*M_atp_c + M_ser_DASH_L_c + M_pa_SC_c	<----->	2.0*M_adp_c + M_ppi_c + M_ps_SC_c
R_ptd1inoSYN	2.0*M_atp_c + M_h2o_c + M_g6p_c + M_pa_SC_c	<----->	M_pi_c + 2.0*M_adp_c + M_ppi_c + M_ptd1ino_SC_c
R_PYK	M_h_c + M_adp_c + M_pep_c	----->	M_atp_c + M_pyr_c
R_PYRDC	M_h_c + M_h2o_c + M_pyr_c	<----->	M_co2tot_c + M_acald_c
R_PYRt2	M_pyr_e	----->	M_pyr_c
R_PYRt2m	M_h_c + M_pyr_c	----->	M_h_m + M_pyr_m
R_RPE	M_ru5p_DASH_D_c	<----->	M_xu5p_DASH_D_c

R_RPI	M_r5p_c	<---->	M_ru5p_DASH_D_c
R_SACCD1	M_h_c + M_nadph_c + M_glu_DASH_L_c + M_L2aadp6sa_c	----->	M_h2o_c + M_nadp_c + M_sacchrp_DASH_L_c
R_SACCD2	M_h2o_c + M_nad_c + M_sacchrp_DASH_L_c	----->	M_h_c + M_nadh_c + M_lys_DASH_L_c + M_akg_c
R_SHK3D	M_h_c + M_nadph_c + M_3dhsk_c	<---->	M_nadp_c + M_skm_c
R_SHKK	M_atp_c + M_skm_c	<---->	M_h_c + M_adp_c + M_skm5p_c
R_SLFAT	M_h_c + M_adp_c + M_so4_c	----->	M_pi_c + M_aps_c
R_SO4ti	M_so4_e	<---->	M_so4_c
R_SUCct2r	M_h_e + M_succ_e	<---->	M_h_c + M_succ_c
R_SUCctm	M_pi_m + M_succ_c	<---->	M_pi_c + M_succ_m
R_SUCD2_u6m	M_q6_m + M_succ_m	----->	M_q6h2_m + M_fum_m
R_SUCFUMtm	M_succ_c + M_fum_m	<---->	M_succ_m + M_fum_c
R_SUCOAS1m	M_coa_m + M_atp_m + M_succ_m	<---->	M_adp_m + M_pi_m + M_succoa_m
R_SULR	3.0*M_h2o_c + 3.0*M_nadp_c + M_h2s_c	<---->	5.0*M_h_c + 3.0*M_nadph_c + M_so3_c
R_TALA	M_s7p_c + M_g3p_c	<---->	M_f6p_c + M_e4p_c
R_THRA	M_acald_c + M_gly_c	----->	M_thr_DASH_L_c
R_THRD_Lm	M_thr_DASH_L_m	<---->	M_2obut_m + M_nh4_m
R_THRS	M_h2o_c + M_phom_c	<---->	M_pi_c + M_thr_DASH_L_c
R_THRt2m	M_thr_DASH_L_c	----->	M_thr_DASH_L_m
R_TKT1	M_r5p_c + M_xu5p_DASH_D_c	<---->	M_s7p_c + M_g3p_c
R_TKT2	M_xu5p_DASH_D_c + M_e4p_c	----->	M_f6p_c + M_g3p_c
R_TPI	M_dhap_c	----->	M_g3p_c
R_triglycSYN	0.59*M_o2_c + 7.69*M_h_c + 7.1*M_atp_c + 14.79*M_nadph_c + 8.1*M_accoa_c + M_pa_SC_c	<---->	8.1*M_pi_c + 7.1*M_adp_c + 0.18*M_h2o_c + 14.79*M_nadp_c + 8.1*M_coa_c + M_triglyc_SC_c
R_TRPS1	M_ser_DASH_L_c + M_3ig3p_c	<---->	M_h2o_c + M_trp_DASH_L_c + M_g3p_c
R_TYRTA	M_akg_c + M_tyr_DASH_L_c	<---->	M_glu_DASH_L_c + M_34hpp_c
R_umpSYN	0.5*M_o2_c + 3.0*M_atp_c + M_r5p_c + M_asp_DASH_L_c + M_gln_DASH_L_c	<---->	2.0*M_h_c + 2.0*M_pi_c + 2.0*M_adp_c + M_ppi_c + M_amp_c + M_ump_c + M_glu_DASH_L_c
R_VALTA	M_akg_c + M_val_DASH_L_c	<---->	M_glu_DASH_L_c + M_3mob_c

R_zymstSYN	$10.0 \cdot M_{o2_c} + 11.0 \cdot M_{h_c} + 18.0 \cdot M_{atp_c} + M_{h2o_c} + 26.0 \cdot M_{nadph_c} + 18.0 \cdot M_{accoa_c} + 2.0 \cdot M_{nad_c}$	<---->	$6.0 \cdot M_{pi_c} + 18.0 \cdot M_{adp_c} + 8.0 \cdot M_{co2tot_c} + 26.0 \cdot M_{nadp_c} + 18.0 \cdot M_{coa_c} + 6.0 \cdot M_{ppi_c} + M_{for_c} + 2.0 \cdot M_{nadh_c} + M_{zymst_c}$
------------	--	--------	---

APPENDIX D.: Hybridoma KB26.5 and hybridoma KB26.5-BHRF1 metabolic model

The hybridoma KB26.5 and hybridoma KB26.5-BHRF1 modelling used the same metabolic model for all p-FBA presented in the chapter 5. The resulting model used for the metabolic flux calculation, that contains 362 reactions and 359 metabolites, is detailed in **Table D**.

Table D. List of reactions included in the hybridoma KB26.5 and hybridoma KB26.5-BHRF1 reduced model developed and used for all Flux Balance Analysis in the Chapter 5.

BIOM_AA	4.306*M_ATP_cytosol + 3.306*M_H2O_cytosol + 0.0646*M_LGlutamate_cytosol + 0.0525*M_LGlutamine_cytosol + 0.0061*M_LTryptophan_cytosol + 0.0202*M_LTyrosine_cytosol + 0.0212*M_LPhenylalanine_cytosol + 0.0576*M_LSerine_cytosol + 0.0636*M_LArginine_cytosol + 0.0485*M_LAspartate_cytosol + 0.0283*M_LCysteine_cytosol + 0.0202*M_LMethionine_cytosol + 0.0616*M_LThreonine_cytosol + 0.0899*M_LLysine_cytosol + 0.0222*M_LHistidine_cytosol + 0.0788*M_Glycine_cytosol + 0.0596*M_LValine_cytosol + 0.0525*M_LIsoleucine_cytosol + 0.0889*M_LLLeucine_cytosol + 0.0283*M_LProline_cytosol + 0.0394*M_LAsparagine_cytosol + 0.096*M_LAlanine_cytosol	----->	4.306*M_ADG_cytosol + 4.306*M_Orthophosphate_cytosol + M_PROT_cytosol
BIOM_AMP	M_ATP_cytosol + 2.0*M_H2O_cytosol	----->	2.0*M_Orthophosphate_cytosol + M_AMP_cytosol
BIOM_CARBO	M_Amylose_cytosol	----->	M_CAcytosol
BIOM_CMP	2.0*M_H2O_cytosol + M_CTP_cytosol	----->	2.0*M_Orthophosphate_cytosol + M_CMP_cytosol
BIOM_dAMP	2.0*M_H2O_cytosol + M_dATP_cytosol	----->	2.0*M_Orthophosphate_cytosol + M_dAMP_cytosol
BIOM_dCMP	2.0*M_H2O_cytosol + M_dCTP_cytosol	----->	2.0*M_Orthophosphate_cytosol + M_dCMP_cytosol
BIOM_dGMP	2.0*M_H2O_cytosol + M_dGTP_cytosol	----->	2.0*M_Orthophosphate_cytosol + M_dGMP_cytosol
BIOM_DNA	1.372*M_ATP_cytosol + 1.372*M_H2O_cytosol + 0.2*M_dGMP_cytosol + 0.3*M_dTMP_cytosol + 0.2*M_dCMP_cytosol + 0.3*M_dAMP_cytosol	----->	1.372*M_ADG_cytosol + 1.372*M_Orthophosphate_cytosol + M_DNA_cytosol
BIOM_dTMP	2.0*M_H2O_cytosol + M_dTTP_cytosol	----->	2.0*M_Orthophosphate_cytosol + M_dTMP_cytosol
BIOM_GMP	2.0*M_H2O_cytosol + M_GTP_cytosol	----->	2.0*M_Orthophosphate_cytosol + M_GMP_cytosol

BIOM_LIP	0.0605*M_Sphingomyelin_cytosol + 0.5006*M_Phosphatidylcholine_cytosol + 0.1315*M_Cholesterol_cytosol + 0.0096*M_Phosphatidylglycerol_cytosol + 0.0204*M_Cardiolipin_cytosol + 0.1898*M_Phosphatidylethanolamine_cytosol + 0.0688*M_1PhosphatidylDmyoinositol_cytosol + 0.0189*M_Phosphatidylserine_cytosol	----->	M_LIP_cytosol
BIOM_RNA	0.4*M_ATP_cytosol + 0.4*M_H2O_cytosol + 0.3*M_CMP_cytosol + 0.34*M_GMP_cytosol + 0.18*M_AMP_cytosol + 0.18*M_UMP_cytosol	----->	0.4*M_ADG_cytosol + 0.4*M_Orthophosphate_cytosol + M_RNA_cytosol
BIOM_T	0.188*M_RNA_cytosol + 0.465*M_CAcytosol + 0.114*M_LIP_cytosol + 0.061*M_DNA_cytosol + 6.902*M_PROT_cytosol	----->	M_BIOMASS_cytosol
BIOM_UMP	2.0*M_H2O_cytosol + M_UTP_cytosol	----->	2.0*M_Orthophosphate_cytosol + M_UMP_cytosol
DEGARG_added	M_H_mitoc + M_LOrnithine_cytosol	----->	M_LOrnithine_mitoc
DEGCYS1_added	M_Oxygen_cytosol + M_LCysteine_cytosol	----->	M_3SulfinolAlanine_cytosol
DEGCYS2_added	M_2Oxoglutarate_cytosol + M_3SulfinolAlanine_cytosol	----->	M_LGlutamate_cytosol + M_3Sulfinylpyruvate_cytosol
DEGCYS3_added	M_3Sulfinylpyruvate_cytosol	----->	M_Pyruvate_cytosol + M_SO2_cytosol
DEGCYS4_added	M_SO2_cytosol	----->	M_SO2_ext
DEGMET1_added	M_ATP_cytosol + M_LMethionine_cytosol	----->	M_Pyrophosphate_cytosol + M_Orthophosphate_cytosol + M_SAdenosylLMethionine_cytosol
DEGMET2_added	M_Tetrahydrofolate_cytosol + M_SAdenosylLMethionine_cytosol	----->	M_5Methyltetrahydrofolate_cytosol + M_SAdenosylLhomocysteine_cytosol
DEGMET3_added	M_5Methyltetrahydrofolate_cytosol + M_NAD_cytosol	<----->	M_H_cytosol + M_510Methylenetetrahydrofolate_cytosol + M_NADH_cytosol
DEGMET4_added	M_SAdenosylLhomocysteine_cytosol	<----->	M_Homocysteine_cytosol + M_Adenosine_cytosol
DEGMET5_added	M_LSerine_cytosol + M_Homocysteine_cytosol	----->	M_Lcystathionine_cytosol
DEGMET6_added	M_Lcystathionine_cytosol	----->	M_NH3_cytosol + M_2Oxobutanoate_cytosol + M_LCysteine_cytosol
DEGMET7_added	M_ATP_cytosol + M_Adenosine_cytosol	----->	M_ADG_cytosol + M_AMP_cytosol
DEGMET8_added	M_NAD_mitoc + M_CoA_mitoc + M_2Oxobutanoate_cytosol	----->	M_NADH_mitoc + M_PropanoylCoA_mitoc
EF0002	M_ATP_cytosol + M_H2O_cytosol	<----->	M_ADG_cytosol + M_Orthophosphate_cytosol
gCat03	M_Oxygen_cytosol + M_Hydantoin5propionate_cytosol	----->	M_NCarbamylLglutamate_cytosol
gCat04	M_NCarbamylLglutamate_cytosol	----->	M_LGlutamate_cytosol + M_CO2_cytosol + M_NH3_cytosol
gCat06_added	M_LGlutamate5semialdehyde_cytosol	<----->	M_S1Pyrroline5carboxylate_cytosol
gCat06mitoc	M_LGlutamate5semialdehyde_mitoc	<----->	M_S1Pyrroline5carboxylate_mitoc
gCat07	M_H2O_cytosol + M_CO2_cytosol	<----->	M_H_cytosol + M_HCO3_cytosol

gCat07mitoc	M_H2O_mitoc + M_CO2_mitoc	<---->	M_H_mitoc + M_HCO3_mitoc
Glutaminolisis	M_LGlutamine_cytosol	<---->	M_LGlutamate_cytosol + M_NH3_cytosol
K00006mitoc	M_H_mitoc + M_NADH_mitoc + 2.5*M_ADP_mitoc + 2.5*M_Orthophosphate_mitoc + 0.5*M_Oxygen_mitoc	----->	M_NAD_mitoc + 3.5*M_H2O_mitoc + 2.5*M_ATP_mitoc
K00007mitoc	M_FADH2_mitoc + 1.5*M_ADP_mitoc + 1.5*M_Orthophosphate_mitoc + 0.5*M_Oxygen_mitoc	----->	2.5*M_H2O_mitoc + M_FAD_mitoc + 1.5*M_ATP_mitoc
K00008	M_9ZOctadecenoicacid_cytosol	<---->	M_Fattyacid_cytosol
K00009	M_ATP_cytosol + M_CoA_cytosol + M_Fattyacid_cytosol	----->	M_Pyrophosphate_cytosol + M_AMP_cytosol + M_AcylCoA_cytosol
K00010	M_FADH2_cytosol + M_Acceptocytosol	<---->	M_Reducedacceptocytosol + M_FAD_cytosol
K00010mitoc	M_FADH2_mitoc + M_Acceptomitoc	<---->	M_FAD_mitoc + M_Reducedacceptomitoc
K00011	2.0*M_NADPH_cytosol + M_Hexadecanoylcp_cytosol + M_Malonylacylcarrierprotein_cytosol	----->	M_H2O_cytosol + 2.0*M_NADP_cytosol + M_CO2_cytosol + M_Acylcarrierprotein_cytosol + M_Octadecanoylacylcarrierprotein_cytosol
MEMB0001	M_alphaDGlucose_ext	<---->	M_alphaDGlucose_cytosol
MEMB0003	M_CO2_ext	<---->	M_CO2_cytosol
MEMB0004	M_SLactate_ext	<---->	M_SLactate_cytosol
MEMB0005	M_Oxygen_ext	<---->	M_Oxygen_cytosol
MEMB0006	M_LAlanine_cytosol	----->	M_LAlanine_ext
MEMB0007	M_LAspartate_ext	----->	M_LAspartate_cytosol
MEMB0008	M_LAsparagine_cytosol	<---->	M_LAsparagine_ext
MEMB0009	M_LGlutamine_ext	<---->	M_LGlutamine_cytosol
MEMB0010	M_LGlutamate_ext	----->	M_LGlutamate_cytosol
MEMB0011	M_LSerine_ext	----->	M_LSerine_cytosol
MEMB0012	M_NH3_ext	<---->	M_NH3_cytosol
MEMB0013	M_Glycine_cytosol	<---->	M_Glycine_ext
MEMB0014	M_H_ext	<---->	M_H_cytosol
MEMB0016	M_LProline_ext	----->	M_LProline_cytosol
MEMB0017	M_LValine_ext	----->	M_LValine_cytosol
MEMB0018	M_LIsoleucine_ext	----->	M_LIsoleucine_cytosol
MEMB0019	M_LLeucine_ext	----->	M_LLeucine_cytosol

MEMB0020	M_LArginine_ext	----->	M_LArginine_cytosol
MEMB0021	M_LThreonine_ext	----->	M_LThreonine_cytosol
MEMB0022	M_LLysine_ext	----->	M_LLysine_cytosol
MEMB0023	M_LCysteine_ext	----->	M_LCysteine_cytosol
MEMB0024	M_LMethionine_ext	----->	M_LMethionine_cytosol
MEMB0025	M_LPhenylalanine_ext	----->	M_LPhenylalanine_cytosol
MEMB0026	M_LTyrosine_ext	----->	M_LTyrosine_cytosol
MEMB0027	M_LTryptophan_ext	----->	M_LTryptophan_cytosol
MEMB0028	M_LHistidine_ext	----->	M_LHistidine_cytosol
MEMB0030	M_Formate_ext	<----->	M_Formate_cytosol
MEMB0033	M_Choline_ext	----->	M_Choline_cytosol
MEMB0034	M_myoinositol_ext	----->	M_myoinositol_cytosol
MEMB0035	M_Ethanolamine_ext	----->	M_Ethanolamine_cytosol
MEMB0039	M_Orthophosphate_ext	<----->	M_Orthophosphate_cytosol
MEMBBIO	M_BIOMASS_cytosol	----->	M_BIOMASS_ext
MEMBH2O	M_H2O_ext	<----->	M_H2O_cytosol
MEMBUREA	M_Urea_ext	<----->	M_Urea_cytosol
R00004	M_H2O_cytosol + M_Pyrophosphate_cytosol	----->	2.0*M_Orthophosphate_cytosol
R00009	2.0*M_H2O2_cytosol	----->	2.0*M_H2O_cytosol + M_Oxygen_cytosol
R00069	M_Oxygen_cytosol + 2.0*M_4Imidazolone5propanoate_cytosol	----->	2.0*M_Hydantoin5propionate_cytosol
R00127	M_ATP_cytosol + M_AMP_cytosol	----->	2.0*M_ADG_cytosol
R00156	M_ATP_cytosol + M_UDP_cytosol	<----->	M_ADG_cytosol + M_UTP_cytosol
R00158	M_ATP_cytosol + M_UMP_cytosol	<----->	M_ADG_cytosol + M_UDP_cytosol
R00200	M_Phosphoenolpyruvate_cytosol + M_ADG_cytosol	----->	M_ATP_cytosol + M_Pyruvate_cytosol
R00209mitoc	M_NAD_mitoc + M_Pyruvate_mitoc + M_CoA_mitoc	----->	M_H_mitoc + M_NADH_mitoc + M_CO2_mitoc + M_AcetylCoA_mitoc
R00214mitoc	M_NAD_mitoc + M_SMalate_mitoc	----->	M_NADH_mitoc + M_Pyruvate_mitoc + M_CO2_mitoc
R00216	M_NADP_cytosol + M_SMalate_cytosol	----->	M_Pyruvate_cytosol + M_NADPH_cytosol + M_CO2_cytosol

R00216mitoc	M_SMalate_mitoc + M_NADP_mitoc	----->	M_Pyruvate_mitoc + M_CO2_mitoc + M_NADPH_mitoc
R00220	M_LSerine_cytosol	----->	M_Pyruvate_cytosol + M_NH3_cytosol
R00238	2.0*M_AcetylCoA_cytosol	<----->	M_CoA_cytosol + M_AcetoacetylCoA_cytosol
R00238mitoc	2.0*M_AcetylCoA_mitoc	<----->	M_CoA_mitoc + M_AcetoacetylCoA_mitoc
R00239_added	M_ATP_cytosol + M_LGlutamate_cytosol	----->	M_ADP_cytosol + M_LGlutamyl5phosphate_cytosol
R00243mitoc	M_LGlutamate_mitoc + M_NAD_mitoc + M_H2O_mitoc	<----->	M_H_mitoc + M_NADH_mitoc + M_NH3_mitoc + M_2Oxoglutarate_mitoc
R00256mitoc	M_H2O_mitoc + M_LGlutamine_mitoc	----->	M_LGlutamate_mitoc + M_NH3_mitoc
R00258	M_LAlanine_cytosol + M_2Oxoglutarate_cytosol	<----->	M_Pyruvate_cytosol + M_LGlutamate_cytosol
R00258mitoc	M_2Oxoglutarate_mitoc + M_LAlanine_mitoc	<----->	M_LGlutamate_mitoc + M_Pyruvate_mitoc
R00289	M_UTP_cytosol + M_alphaDGlucose1phosphate_cytosol	----->	M_Pyrophosphate_cytosol + M_UDPglucose_cytosol
R00292	M_UDPglucose_cytosol	----->	M_UDP_cytosol + M_Amylose_cytosol
R00330	M_ATP_cytosol + M_GDP_cytosol	<----->	M_ADP_cytosol + M_GTP_cytosol
R00332	M_ATP_cytosol + M_GMP_cytosol	----->	M_ADP_cytosol + M_GDP_cytosol
R00342	M_NAD_cytosol + M_SMalate_cytosol	<----->	M_H_cytosol + M_NADH_cytosol + M_Oxaloacetate_cytosol
R00342mitoc	M_NAD_mitoc + M_SMalate_mitoc	<----->	M_H_mitoc + M_NADH_mitoc + M_Oxaloacetate_mitoc
R00351mitoc	M_H2O_mitoc + M_AcetylCoA_mitoc + M_Oxaloacetate_mitoc	----->	M_CoA_mitoc + M_Citrate_mitoc
R00352	M_ATP_cytosol + M_CoA_cytosol + M_Citrate_cytosol	----->	M_ADP_cytosol + M_Orthophosphate_cytosol + M_Oxaloacetate_cytosol + M_AcetylCoA_cytosol
R00355	M_LAspartate_cytosol + M_2Oxoglutarate_cytosol	<----->	M_LGlutamate_cytosol + M_Oxaloacetate_cytosol
R00355mitoc	M_2Oxoglutarate_mitoc + M_LAspartate_mitoc	<----->	M_LGlutamate_mitoc + M_Oxaloacetate_mitoc
R00371mitoc	M_CoA_mitoc + M_L2Amino3oxobutanoicacid_mitoc	----->	M_AcetylCoA_mitoc + M_Glycine_mitoc
R00405mitoc	M_CoA_mitoc + M_Succinate_mitoc + M_ATP_mitoc	<----->	M_SuccinylCoA_mitoc + M_ADP_mitoc + M_Orthophosphate_mitoc
R00410mitoc	M_Acetoacetate_mitoc + M_SuccinylCoA_mitoc	<----->	M_Succinate_mitoc + M_AcetoacetylCoA_mitoc
R00412mitoc	M_FAD_mitoc + M_Succinate_mitoc	<----->	M_FADH2_mitoc + M_Fumarate_mitoc
R00431	M_GTP_cytosol + M_Oxaloacetate_cytosol	----->	M_Phosphoenolpyruvate_cytosol + M_GDP_cytosol + M_CO2_cytosol
R00485	M_H2O_cytosol + M_LAsparagine_cytosol	<----->	M_NH3_cytosol + M_LAspartate_cytosol
R00512	M_ATP_cytosol + M_CMP_cytosol	<----->	M_ADP_cytosol + M_CDP_cytosol

R00551	M_H2O_cytosol + M_Arginine_cytosol	----->	M_LOrnithine_cytosol + M_Urea_cytosol
R00570	M_ATP_cytosol + M_CDP_cytosol	<----->	M_ADG_cytosol + M_CTP_cytosol
R00573	M_ATP_cytosol + M_H2O_cytosol + M_LGlutamine_cytosol + M_UTP_cytosol	----->	M_ADG_cytosol + M_CTP_cytosol + M_Orthophosphate_cytosol + M_LGlutamate_cytosol
R00575	2.0*M_ATP_cytosol + M_H2O_cytosol + M_LGlutamine_cytosol + M_HCO3_cytosol	----->	2.0*M_ADG_cytosol + M_Orthophosphate_cytosol + M_LGlutamate_cytosol + M_Carbamoylphosphate_cytosol
R00582_added	M_H2O_cytosol + M_OPhosphoLserine_cytosol	----->	M_Orthophosphate_cytosol + M_LSerine_cytosol
R00621mitoc	M_NAD_mitoc + M_CoA_mitoc + M_2Oxoglutarate_mitoc	----->	M_NADH_mitoc + M_CO2_mitoc + M_SuccinylCoA_mitoc
R00658	M_2PhosphoDglycerate_cytosol	<----->	M_Phosphoenolpyruvate_cytosol + M_H2O_cytosol
R00667mitoc	M_LOrnithine_mitoc + M_2Oxoglutarate_mitoc	<----->	M_LGlutamate_mitoc + M_LGlutamate5semialdehyde_mitoc
R00678	M_LTryptophan_cytosol + M_Oxygen_cytosol	----->	M_LFormylkynurenine_cytosol
R00702	2.0*M_transtransFarnesyldiphosphate_cytosol	----->	M_H_cytosol + M_Pyrophosphate_cytosol + M_Presqualenediphosphate_cytosol
R00703	M_NAD_cytosol + M_SLactate_cytosol	<----->	M_Pyruvate_cytosol + M_H_cytosol + M_NADH_cytosol
R00703_added_2_1	M_NAD_mitoc + M_SLactate_mitoc	<----->	M_H_mitoc + M_NADH_mitoc + M_Pyruvate_mitoc
R00707mitoc	M_NAD_mitoc + M_H2O_mitoc + M_LGlutamate5semialdehyde_mitoc	----->	M_H_mitoc + M_NADH_mitoc + M_LGlutamate_mitoc
R00709mitoc	M_NAD_mitoc + M_Isocitrate_mitoc	----->	M_H_mitoc + M_NADH_mitoc + M_CO2_mitoc + M_2Oxoglutarate_mitoc
R00716mitoc	M_H_mitoc + M_NADPH_mitoc + M_LLysine_mitoc + M_2Oxoglutarate_mitoc	----->	M_N6L13DicarboxypropylLysine_mitoc + M_H2O_mitoc + M_NADP_mitoc
R00734	M_LTyrosine_cytosol + M_2Oxoglutarate_cytosol	<----->	M_LGlutamate_cytosol + M_34Hydroxyphenylpyruvate_cytosol
R00742	M_ATP_cytosol + M_AcetylCoA_cytosol + M_HCO3_cytosol	----->	M_ADG_cytosol + M_Orthophosphate_cytosol + M_MalonylCoA_cytosol
R00833mitoc	M_R2Methyl3oxopropanoylCoA_mitoc	<----->	M_SuccinylCoA_mitoc
R00842	M_NAD_cytosol + M_snGlycerol3phosphate_cytosol	<----->	M_H_cytosol + M_NADH_cytosol + M_Glyceronephosphate_cytosol
R00848	M_FAD_cytosol + M_snGlycerol3phosphate_cytosol	<----->	M_FADH2_cytosol + M_Glyceronephosphate_cytosol
R00851	M_AcylCoA_cytosol + M_snGlycerol3phosphate_cytosol	----->	M_CoA_cytosol + M_1AcylsnGlycerol3phosphate_cytosol
R00927mitoc	M_CoA_mitoc + M_2MethylacetoacetylCoA_mitoc	----->	M_AcetylCoA_mitoc + M_PropanoylCoA_mitoc
R00935mitoc	M_NAD_mitoc + M_CoA_mitoc + M_SMethylmalonatesemialdehyde_mitoc	----->	M_H_mitoc + M_NADH_mitoc + M_CO2_mitoc + M_PropanoylCoA_mitoc
R00939	M_H_cytosol + M_NADPH_cytosol + M_Dihydrofolate_cytosol	----->	M_NADP_cytosol + M_Tetrahydrofolate_cytosol
R00945	M_H2O_cytosol + M_510Methylenetetrahydrofolate_cytosol + M_Glycine_cytosol	<----->	M_LSerine_cytosol + M_Tetrahydrofolate_cytosol
R00959	M_alphaDGlucose1phosphate_cytosol	<----->	M_alphaDGlucose6phosphate_cytosol

R00965	M_Orotidine5phosphate_cytosol	----->	M_CO2_cytosol + M_UMP_cytosol
R01015	M_2R2Hydroxy3phosphonooxypropanal_cytosol	<----->	M_Glyceronephosphate_cytosol
R01021	M_ATP_cytosol + M_Choline_cytosol	<----->	M_ADG_cytosol + M_Cholinephosphate_cytosol
R01049	M_ATP_cytosol + M_DRibose5phosphate_cytosol	----->	M_AMP_cytosol + M_5PhosphoalpaDribose1diphosphate_cytosol
R01056	M_DRibose5phosphate_cytosol	<----->	M_DRibulose5phosphate_cytosol
R01061	M_NAD_cytosol + M_Orthophosphate_cytosol + M_2R2Hydroxy3phosphonooxypropanal_cytosol	<----->	M_H_cytosol + M_NADH_cytosol + M_3PhosphoDglyceroylphosphate_cytosol
R01070	M_betaDfructose16bisphosphate_cytosol	<----->	M_2R2Hydroxy3phosphonooxypropanal_cytosol + M_Glyceronephosphate_cytosol
R01072	M_H2O_cytosol + M_LGlutamine_cytosol + M_5PhosphoalpaDribose1diphosphate_cytosol	----->	M_Pyrophosphate_cytosol + M_LGlutamate_cytosol + M_5Phosphoribosylamine_cytosol
R01082	M_SMalate_cytosol	<----->	M_H2O_cytosol + M_Fumarate_cytosol
R01082mitoc	M_SMalate_mitoc	<----->	M_H2O_mitoc + M_Fumarate_mitoc
R01083	M_N612DicarboxyethylAMP_cytosol	<----->	M_AMP_cytosol + M_Fumarate_cytosol
R01090mitoc	M_2Oxoglutarate_mitoc + M_LLeucine_mitoc	<----->	M_LGlutamate_mitoc + M_4Methyl2oxopentanoate_mitoc
R01121	M_ATP_cytosol + M_R5Diphosphomevalonate_cytosol	----->	M_ADG_cytosol + M_Isopentenylidiphosphate_cytosol + M_Orthophosphate_cytosol + M_CO2_cytosol
R01123	M_Isopentenylidiphosphate_cytosol	<----->	M_Dimethylallyldiphosphate_cytosol
R01127	M_H2O_cytosol + M_IMP_cytosol	<----->	M_15Phosphoribosyl5formamido4imidazolecarboxamide_cytosol
R01130	M_H2O_cytosol + M_NAD_cytosol + M_IMP_cytosol	----->	M_H_cytosol + M_NADH_cytosol + M_Xanthosine5phosphate_cytosol
R01135	M_GTP_cytosol + M_LAspartate_cytosol + M_IMP_cytosol	<----->	M_GDP_cytosol + M_Orthophosphate_cytosol + M_N612DicarboxyethylAMP_cytosol
R01137	M_ATP_cytosol + M_dADP_cytosol	<----->	M_ADG_cytosol + M_dATP_cytosol
R01168	M_LHistidine_cytosol	<----->	M_NH3_cytosol + M_Urocanate_cytosol
R01214mitoc	M_2Oxoglutarate_mitoc + M_LValine_mitoc	<----->	M_LGlutamate_mitoc + M_3Methyl2oxobutanoicacid_mitoc
R01220	M_NADP_cytosol + M_510Methylenetetrahydrofolate_cytosol	<----->	M_H_cytosol + M_510Methenyltetrahydrofolate_cytosol + M_NADPH_cytosol
R01221	M_NAD_cytosol + M_Glycine_cytosol + M_Tetrahydrofolate_cytosol	<----->	M_H_cytosol + M_510Methylenetetrahydrofolate_cytosol + M_NADH_cytosol + M_CO2_cytosol + M_NH3_cytosol
R01231	M_ATP_cytosol + M_H2O_cytosol + M_LGlutamine_cytosol + M_Xanthosine5phosphate_cytosol	----->	M_Pyrophosphate_cytosol + M_LGlutamate_cytosol + M_GMP_cytosol + M_AMP_cytosol

R01251_added	M_H_cytosol + M_NADPH_cytosol + M_S1Pyrroline5carboxylate_cytosol	----->	M_NADP_cytosol + M_LProline_cytosol
R01253mitoc	M_Acceptomitoc + M_LProline_mitoc	----->	M_Reducedacceptomitoc + M_S1Pyrroline5carboxylate_mitoc
R01280	M_ATP_cytosol + M_CoA_cytosol + M_Hexadecanoicacid_cytosol	----->	M_Pyrophosphate_cytosol + M_AMP_cytosol + M_PalmitoylCoA_cytosol
R01281	M_LSerine_cytosol + M_PalmitoylCoA_cytosol	----->	M_CO2_cytosol + M_3Dehydrosphinganine_cytosol + M_CoA_cytosol
R01321	M_CDPcholine_cytosol + M_12Diacylsnglycerol_cytosol	----->	M_CMP_cytosol + M_Phosphatidylcholine_cytosol
R01324mitoc	M_Citrate_mitoc	<----->	M_Isocitrate_mitoc
R01360mitoc	M_S3Hydroxy3methylCO2_mitoc	----->	M_AcetylCoA_mitoc + M_Acetoacetate_mitoc
R01364	M_H2O_cytosol + M_4Fumarylacetoacetate_cytosol	----->	M_Fumarate_cytosol + M_Acetoacetate_cytosol
R01397	M_Carbamoylphosphate_cytosol + M_LAspartate_cytosol	----->	M_Orthophosphate_cytosol + M_NCarbamoylLaspartate_cytosol
R01456	M_H_cytosol + M_NADPH_cytosol + M_Cholesta57dien3betaol_cytosol	----->	M_NADP_cytosol + M_Cholesterol_cytosol
R01465mitoc	M_NAD_mitoc + M_LThreonine_mitoc	----->	M_H_mitoc + M_NADH_mitoc + M_L2Amino3oxobutanoicacid_mitoc
R01468	M_ATP_cytosol + M_Ethanolamine_cytosol	----->	M_ADP_cytosol + M_Ethanolaminephosphate_cytosol
R01512	M_ATP_cytosol + M_3PhosphoDglycerate_cytosol	<----->	M_ADP_cytosol + M_3PhosphoDglyceroylphosphate_cytosol
R01513_added	M_NAD_cytosol + M_3PhosphoDglycerate_cytosol	<----->	M_H_cytosol + M_NADH_cytosol + M_3Phosphonoxypruvate_cytosol
R01518	M_2PhosphoDglycerate_cytosol	<----->	M_3PhosphoDglycerate_cytosol
R01528	M_NADP_cytosol + M_6PhosphoDgluconate_cytosol	<----->	M_H_cytosol + M_NADPH_cytosol + M_CO2_cytosol + M_DRibulose5phosphate_cytosol
R01529	M_DRibulose5phosphate_cytosol	<----->	M_DXylulose5phosphate_cytosol
R01624	M_Acylcarrierprotein_cytosol + M_AcetylCoA_cytosol	----->	M_CoA_cytosol + M_Acetylacylcarrierprotein_cytosol
R01626	M_Acylcarrierprotein_cytosol + M_MalonylCoA_cytosol	<----->	M_Malonylacylcarrierprotein_cytosol + M_CoA_cytosol
R01641	M_2R2Hydroxy3phosphonoxypropanal_cytosol + M_DSedoheptulose7phosphate_cytosol	<----->	M_DXylulose5phosphate_cytosol + M_DRibose5phosphate_cytosol
R01655	M_H2O_cytosol + M_510Methenyltetrahydrofolate_cytosol	<----->	M_10Formyltetrahydrofolate_cytosol + M_H_cytosol
R01658	M_Isopentenylidiphosphate_cytosol + M_Dimethylallyldiphosphate_cytosol	----->	M_Pyrophosphate_cytosol + M_Geranyldiphosphate_cytosol
R01706	M_H2O_cytosol + M_Hexadecanoylcp_cytosol	----->	M_Acylcarrierprotein_cytosol + M_Hexadecanoicacid_cytosol
R01786_added	M_ATP_cytosol + M_alphaDGlucose_cytosol	----->	M_ADP_cytosol + M_alphaDGlucose6phosphate_cytosol
R01794	M_H_cytosol + M_NADPH_cytosol + M_Dihydrobiopterin_cytosol	----->	M_NADP_cytosol + M_Tetrahydrobiopterin_cytosol
R01795	M_Oxygen_cytosol + M_Tetrahydrobiopterin_cytosol + M_LPhenylalanine_cytosol	----->	M_H2O_cytosol + M_LTyrosine_cytosol + M_Dihydrobiopterin_cytosol

R01799	M_CTP_cytosol + M_Phosphatidate_cytosol	----->	M_Pyrophosphate_cytosol + M_CDPdiacylglycerol_cytosol
R01801	M_CDPdiacylglycerol_cytosol + M_snGlycerol3phosphate_cytosol	----->	M_CMP_cytosol + M_Phosphatidylglycerophosphate_cytosol
R01802	M_CDPdiacylglycerol_cytosol + M_myoinositol_cytosol	----->	M_CMP_cytosol + M_1PhosphatidylDmyoinositol_cytosol
R01827	M_2R2Hydroxy3phosphonooxypropanal_cytosol + M_DSedoheptulose7phosphate_cytosol	<----->	M_betaDfructose6phosphate_cytosol + M_DErythrose4phosphate_cytosol
R01830	M_2R2Hydroxy3phosphonooxypropanal_cytosol + M_betaDfructose6phosphate_cytosol	<----->	M_DXylulose5phosphate_cytosol + M_DErythrose4phosphate_cytosol
R01857	M_ATP_cytosol + M_dGDP_cytosol	<----->	M_ADG_cytosol + M_dGTP_cytosol
R01859mitoc	M_PropanoylCoA_mitoc + M_ATP_mitoc + M_HCO3_mitoc	----->	M_ADG_mitoc + M_Orthophosphate_mitoc + M_S2Methyl3oxopropanoylCoA_mitoc
R01867	M_Oxygen_cytosol + M_SDihydroorotate_cytosol	<----->	M_Orotate_cytosol + M_H2O2_cytosol
R01870	M_Orotate_cytosol + M_5PhosphoalphanRibose1diphosphate_cytosol	----->	M_Pyrophosphate_cytosol + M_Orotidine5phosphate_cytosol
R01890	M_CTP_cytosol + M_Cholinephosphate_cytosol	----->	M_Pyrophosphate_cytosol + M_CDPcholine_cytosol
R01891	M_CDPcholine_cytosol + M_NAcylsphingosine_cytosol	----->	M_Sphingomyelin_cytosol + M_CMP_cytosol
R01933mitoc	M_NAD_mitoc + M_2Oxoadipate_mitoc + M_CoA_mitoc	----->	M_H_mitoc + M_NADH_mitoc + M_CO2_mitoc + M_GlutarylCoA_mitoc
R01938	M_H_cytosol + M_H2O_cytosol + M_NADPH_cytosol + M_2Aminomuconate_cytosol	----->	M_NADP_cytosol + M_NH3_cytosol + M_2Oxoadipate_cytosol
R01939	M_L2Aminoadipate_cytosol + M_2Oxoglutarate_cytosol	<----->	M_LGlutamate_cytosol + M_2Oxoadipate_cytosol
R01959	M_H2O_cytosol + M_LFormylkynurenine_cytosol	----->	M_LKynurenine_cytosol + M_Formate_cytosol
R01960	M_H_cytosol + M_NADPH_cytosol + M_Oxygen_cytosol + M_LKynurenine_cytosol	----->	M_H2O_cytosol + M_NADP_cytosol + M_3HydroxyLkynurenine_cytosol
R01975mitoc	M_NAD_mitoc + M_S3HydroxybutanoylCoA_mitoc	<----->	M_H_mitoc + M_NADH_mitoc + M_AcetoacetylCoA_mitoc
R01978	M_H2O_cytosol + M_AcetylCoA_cytosol + M_AcetoacetylCoA_cytosol	----->	M_CoA_cytosol + M_S3Hydroxy3methylglutarylCoA_cytosol
R01993	M_H2O_cytosol + M_SDihydroorotate_cytosol	<----->	M_NCarbamoylLAspartate_cytosol
R02003	M_Geranyldiphosphate_cytosol + M_Isopentenylidiphosphate_cytosol	----->	M_Pyrophosphate_cytosol + M_transtransFarnesylidiphosphate_cytosol
R02016	M_H_cytosol + M_NADPH_cytosol + M_Oxidizedthioredoxin_cytosol	----->	M_NADP_cytosol + M_Thioredoxin_cytosol
R02017	M_ADG_cytosol + M_Thioredoxin_cytosol	----->	M_H2O_cytosol + M_dADG_cytosol + M_Oxidizedthioredoxin_cytosol
R02018	M_UDP_cytosol + M_Thioredoxin_cytosol	----->	M_H2O_cytosol + M_dUDP_cytosol + M_Oxidizedthioredoxin_cytosol
R02019	M_GDP_cytosol + M_Thioredoxin_cytosol	----->	M_H2O_cytosol + M_dGDP_cytosol + M_Oxidizedthioredoxin_cytosol
R02024	M_CDP_cytosol + M_Thioredoxin_cytosol	----->	M_H2O_cytosol + M_dCDP_cytosol + M_Oxidizedthioredoxin_cytosol
R02029	M_H2O_cytosol + M_Phosphatidylglycerophosphate_cytosol	----->	M_Orthophosphate_cytosol + M_Phosphatidylglycerol_cytosol

R02030	M_CDPdiacylglycerol_cytosol + M_Phosphatidylglycerol_cytosol	----->	M_CMP_cytosol + M_Cardiolipin_cytosol
R02035	M_H2O_cytosol + M_DGlucono15lactone6phosphate_cytosol	----->	M_6PhosphoDgluconate_cytosol
R02038	M_CTP_cytosol + M_Ethanolaminephosphate_cytosol	----->	M_Pyrophosphate_cytosol + M_CDPethanolamine_cytosol
R02057	M_12Diacylsnglycerol_cytosol + M_CDPethanolamine_cytosol	----->	M_CMP_cytosol + M_Phosphatidylethanolamine_cytosol
R02082	2.0*M_H_cytosol + 2.0*M_NADPH_cytosol + M_S3Hydroxy3methylglutarylCoA_cytosol	----->	2.0*M_NADP_cytosol + M_CoA_cytosol + M_RMevalonate_cytosol
R02085mitoc	M_S3Hydroxy3methylCO2_mitoc	<----->	M_H2O_mitoc + M_3MethylglutaconylCoA_mitoc
R02093	M_ATP_cytosol + M_dTDP_cytosol	<----->	M_ADP_cytosol + M_dTTP_cytosol
R02094	M_ATP_cytosol + M_dTMP_cytosol	<----->	M_ADP_cytosol + M_dTDP_cytosol
R02098	M_ATP_cytosol + M_dUMP_cytosol	<----->	M_ADP_cytosol + M_dUDP_cytosol
R02101	M_510Methylenetetrahydrofolate_cytosol + M_dUMP_cytosol	<----->	M_dTMP_cytosol + M_Dihydrofolate_cytosol
R02198mitoc	M_2Oxoglutarate_mitoc + M_LIsoleucine_mitoc	----->	M_LGlutamate_mitoc + M_3Methyl2oxopentanoate_mitoc
R02239	M_H2O_cytosol + M_Phosphatidate_cytosol	----->	M_Orthophosphate_cytosol + M_12Diacylsnglycerol_cytosol
R02241	M_AcylCoA_cytosol + M_1Acylsnglycerol3phosphate_cytosol	----->	M_Phosphatidate_cytosol + M_CoA_cytosol
R02245	M_ATP_cytosol + M_RMevalonate_cytosol	----->	M_ADP_cytosol + M_R5Phosphomevalonate_cytosol
R02313mitoc	M_N6L13DicarboxypropylLlysine_mitoc + M_NAD_mitoc + M_H2O_mitoc	<----->	M_H_mitoc + M_L2Amino adipate6semialdehyde_mitoc + M_NADH_mitoc + M_LGlutamate_mitoc
R02326	M_ATP_cytosol + M_dCDP_cytosol	<----->	M_ADP_cytosol + M_dCTP_cytosol
R02487mitoc	M_FAD_mitoc + M_GlutarylCoA_mitoc	----->	M_FADH2_mitoc + M_CO2_mitoc + M_CrotonoylCoA_mitoc
R02519	M_Oxygen_cytosol + M_Homogentisate_cytosol	----->	M_4Maleylacetoacetate_cytosol
R02521	M_Oxygen_cytosol + M_34Hydroxyphenylpyruvate_cytosol	----->	M_CO2_cytosol + M_Homogentisate_cytosol
R02661mitoc	M_FAD_mitoc + M_2MethylpropanoylCoA_mitoc	----->	M_FADH2_mitoc + M_2Methylprop2enoylCoA_mitoc
R02662mitoc	M_NAD_mitoc + M_CoA_mitoc + M_3Methyl2oxobutanoicacid_mitoc	----->	M_H_mitoc + M_NADH_mitoc + M_CO2_mitoc + M_2MethylpropanoylCoA_mitoc
R02665	M_Oxygen_cytosol + M_3Hydroxyanthranilate_cytosol	----->	M_2Amino3carboxymuconatesemialdehyde_cytosol
R02668	M_H2O_cytosol + M_3HydroxyLkynurenine_cytosol	----->	M_LAlanine_cytosol + M_3Hydroxyanthranilate_cytosol
R02736	M_NADP_cytosol + M_betaDGlucose6phosphate_cytosol	----->	M_H_cytosol + M_NADPH_cytosol + M_DGlucono15lactone6phosphate_cytosol
R02739	M_alphaDGlucose6phosphate_cytosol	<----->	M_betaDGlucose6phosphate_cytosol
R02740	M_alphaDGlucose6phosphate_cytosol	<----->	M_betaDFructose6phosphate_cytosol

R02765mitoc	M_R2Methyl3oxopropanoylCoA_mitoc	<---->	M_S2Methyl3oxopropanoylCoA_mitoc
R02814	M_H2O_cytosol + M_Oleoylacylcarrierprotein_cytosol	----->	M_Acylcarrierprotein_cytosol + M_9ZOctadecenoicacid_cytosol
R02872	M_H_cytosol + M_Presqualenediphosphate_cytosol + M_NADPH_cytosol	----->	M_Pyrophosphate_cytosol + M_NADP_cytosol + M_Squalene_cytosol
R02874	M_H_cytosol + M_Squalene_cytosol + M_NADPH_cytosol + M_Oxygen_cytosol	----->	M_H2O_cytosol + M_NADP_cytosol + M_S23Epoxyssqualene_cytosol
R02914	M_H2O_cytosol + M_Urocanate_cytosol	----->	M_4Imidazolone5propanoate_cytosol
R02918	3.3*M_ATP_cytosol + M_LTyrosine_cytosol + M_tRNATyctyosol	----->	2.3*M_ADG_cytosol + M_Pyrophosphate_cytosol + 2.3*M_Orthophosphate_cytosol + M_AMP_cytosol + M_LTyrosyltRNATyctyosol
R02978	M_H_cytosol + M_NADPH_cytosol + M_3Dehydrosphinganine_cytosol	----->	M_NADP_cytosol + M_Sphinganine_cytosol
R03026mitoc	M_S3HydroxybutanoylCoA_mitoc	<---->	M_H2O_mitoc + M_CrotonoylCoA_mitoc
R03038	3.3*M_ATP_cytosol + M_LAlanine_cytosol + M_tRNAAla_cytosol	----->	2.3*M_ADG_cytosol + M_Pyrophosphate_cytosol + 2.3*M_Orthophosphate_cytosol + M_AMP_cytosol + M_LAlanylRNA_cytosol
R03103	M_H2O_cytosol + M_NADP_cytosol + M_L2Aminoadipate6semialdehyde_cytosol	----->	M_H_cytosol + M_NADPH_cytosol + M_L2Aminoadipate_cytosol
R03172mitoc	M_S2MethylbutanoylCoA_mitoc + M_FAD_mitoc	----->	M_FADH2_mitoc + M_2Methylbut2enoylCoA_mitoc
R03174mitoc	M_NAD_mitoc + M_CoA_mitoc + M_3Methyl2oxopentanoate_mitoc	----->	M_H_mitoc + M_NADH_mitoc + M_S2MethylbutanoylCoA_mitoc + M_CO2_mitoc
R03181	M_4Maleylacetoacetate_cytosol	----->	M_4Fumarylacetoacetate_cytosol
R03199	M_S23Epoxyssqualene_cytosol	----->	M_Lanosterol_cytosol
R03245	M_ATP_cytosol + M_R5Phosphomevalonate_cytosol	----->	M_ADG_cytosol + M_R5Diphosphomevalonate_cytosol
R03310	M_H_cytosol + M_NADH_cytosol + M_Oxygen_cytosol + M_5alphaCholest7en3betaol_cytosol	----->	2.0*M_H2O_cytosol + M_NAD_cytosol + M_Cholesta57dien3betaol_cytosol
R03313_added	M_H_cytosol + M_NADPH_cytosol + M_LGlutamyl5phosphate_cytosol	----->	M_NADP_cytosol + M_Orthophosphate_cytosol + M_LGlutamate5semialdehyde_cytosol
R03370	M_Oxygen_cytosol + M_Reducedacceptocytosol + M_Octadecanoylacylcarrierprotein_cytosol	----->	2.0*M_H2O_cytosol + M_Acceptocytosol + M_Oleoylacylcarrierprotein_cytosol
R03646	3.3*M_ATP_cytosol + M_LArginine_cytosol + M_tRNAArg_cytosol	----->	2.3*M_ADG_cytosol + M_Pyrophosphate_cytosol + 2.3*M_Orthophosphate_cytosol + M_AMP_cytosol + M_LArginyltRNAArg_cytosol
R03647	3.3*M_ATP_cytosol + M_LAspartate_cytosol + M_tRNAAsn_cytosol	----->	2.3*M_ADG_cytosol + M_Pyrophosphate_cytosol + 2.3*M_Orthophosphate_cytosol + M_AMP_cytosol + M_LAspartyltRNAAsn_cytosol

R03648	3.3*M_ATP_cytosol + M_LAsparagine_cytosol + M_tRNAAsn_cytosol	----->	2.3*M_ADG_cytosol + M_Pyrophosphate_cytosol + 2.3*M_Orthophosphate_cytosol + M_AMP_cytosol + M_LAsparaginyItRNAAsn_cytosol
R03650	3.3*M_ATP_cytosol + M_LCysteine_cytosol + M_tRNACys_cytosol	----->	2.3*M_ADG_cytosol + M_Pyrophosphate_cytosol + 2.3*M_Orthophosphate_cytosol + M_AMP_cytosol + M_LCysteinyItRNACys_cytosol
R03651	3.3*M_ATP_cytosol + M_LGlutamate_cytosol + M_tRNAGln_cytosol	----->	2.3*M_ADG_cytosol + M_Pyrophosphate_cytosol + 2.3*M_Orthophosphate_cytosol + M_AMP_cytosol + M_LGlutamyltRNAGln_cytosol
R03652	3.3*M_ATP_cytosol + M_LGlutamine_cytosol + M_tRNAGln_cytosol	----->	2.3*M_ADG_cytosol + M_Pyrophosphate_cytosol + 2.3*M_Orthophosphate_cytosol + M_AMP_cytosol + M_GlutaminyItRNA_cytosol
R03654	3.3*M_ATP_cytosol + M_Glycine_cytosol + M_tRNAGl_cytosol	----->	2.3*M_ADG_cytosol + M_Pyrophosphate_cytosol + 2.3*M_Orthophosphate_cytosol + M_AMP_cytosol + M_GlycyltRNAGly_cytosol
R03655	3.3*M_ATP_cytosol + M_LHistidine_cytosol + M_tRNAHis_cytosol	----->	2.3*M_ADG_cytosol + M_Pyrophosphate_cytosol + 2.3*M_Orthophosphate_cytosol + M_AMP_cytosol + M_LHistidyltRNAHis_cytosol
R03656	3.3*M_ATP_cytosol + M_LIsoleucine_cytosol + M_tRNAIle_cytosol	----->	2.3*M_ADG_cytosol + M_Pyrophosphate_cytosol + 2.3*M_Orthophosphate_cytosol + M_AMP_cytosol + M_LIsoleucyltRNAIle_cytosol
R03657	3.3*M_ATP_cytosol + M_LLeucine_cytosol + M_tRNALeu_cytosol	----->	2.3*M_ADG_cytosol + M_Pyrophosphate_cytosol + 2.3*M_Orthophosphate_cytosol + M_AMP_cytosol + M_LLeucyltRNA_cytosol
R03658	3.3*M_ATP_cytosol + M_LLysine_cytosol + M_tRNALys_cytosol	----->	2.3*M_ADG_cytosol + M_Pyrophosphate_cytosol + 2.3*M_Orthophosphate_cytosol + M_AMP_cytosol + M_LLysyltRNA_cytosol
R03659	3.3*M_ATP_cytosol + M_LMethionine_cytosol + M_tRNAMet_cytosol	----->	2.3*M_ADG_cytosol + M_Pyrophosphate_cytosol + 2.3*M_Orthophosphate_cytosol + M_AMP_cytosol + M_LMethionyltRNA_cytosol
R03660	3.3*M_ATP_cytosol + M_LPhenylalanine_cytosol + M_tRNAPhe_cytosol	----->	2.3*M_ADG_cytosol + M_Pyrophosphate_cytosol + 2.3*M_Orthophosphate_cytosol + M_AMP_cytosol + M_LPhenylalanylItRNAPhe_cytosol
R03661	3.3*M_ATP_cytosol + M_LProline_cytosol + M_tRNAPro_cytosol	----->	2.3*M_ADG_cytosol + M_Pyrophosphate_cytosol + 2.3*M_Orthophosphate_cytosol + M_AMP_cytosol + M_LProlyItRNAPro_cytosol

R03662	3.3*M_ATP_cytosol + M_LSerine_cytosol + M_tRNA ^{Sec} cytosol	----->	2.3*M_AD ^P _cytosol + M_Pyrophosphate_cytosol + 2.3*M_Orthophosphate_cytosol + M_AMP_cytosol + M_LSer ^{yl} tRNA ^{Sec} cytosol
R03663	3.3*M_ATP_cytosol + M_LThreonine_cytosol + M_tRNA ^{Thc} cytosol	----->	2.3*M_AD ^P _cytosol + M_Pyrophosphate_cytosol + 2.3*M_Orthophosphate_cytosol + M_AMP_cytosol + M_LThreonyl ^t tRNA ^{Thc} cytosol
R03664	3.3*M_ATP_cytosol + M_LTryptophan_cytosol + M_tRNA ^{Trp} cytosol	----->	2.3*M_AD ^P _cytosol + M_Pyrophosphate_cytosol + 2.3*M_Orthophosphate_cytosol + M_AMP_cytosol + M_LTryptophanyl ^t tRNA ^{Trp} cytosol
R03665	3.3*M_ATP_cytosol + M_LValine_cytosol + M_tRNA ^{Val} cytosol	----->	2.3*M_AD ^P _cytosol + M_Pyrophosphate_cytosol + 2.3*M_Orthophosphate_cytosol + M_AMP_cytosol + M_LValyl ^t tRNA ^{Val} cytosol
R03889	M_H ₂ O_cytosol + M_NAD_cytosol + M_2Aminomuconatesemialdehyde_cytosol	----->	M_H_cytosol + M_NADH_cytosol + M_2Aminomuconate_cytosol
R04095mitoc	M_FAD_mitoc + M_3MethylbutanoylCoA_mitoc	----->	M_FADH ₂ _mitoc + M_3MethylcrotonylCoA_mitoc
R04097mitoc	M_NAD_mitoc + M_CoA_mitoc + M_4Methyl2oxopentanoate_mitoc	----->	M_H_mitoc + M_NADH_mitoc + M_CO ₂ _mitoc + M_3MethylbutanoylCoA_mitoc
R04138mitoc	M_ATP_mitoc + M_HCO ₃ _mitoc + M_3MethylcrotonylCoA_mitoc	----->	M_AD ^P _mitoc + M_Orthophosphate_mitoc + M_3MethylglutaconylCoA_mitoc
R04144	M_ATP_cytosol + M_Glycine_cytosol + M_5Phosphoribosylamine_cytosol	----->	M_AD ^P _cytosol + M_Orthophosphate_cytosol + M_5Phosphoribosylglycinamide_cytosol
R04173_added	M_2Oxoglutarate_cytosol + M_OPhosphoLserine_cytosol	<----->	M_LGlu ^t amate_cytosol + M_3Phosphonooxypyruvate_cytosol
R04203mitoc	M_NAD_mitoc + M_2S3S3Hydroxy2methylbutanoylCoA_mitoc	<----->	M_H_mitoc + M_NADH_mitoc + M_2MethylacetoacetylCoA_mitoc
R04204mitoc	M_H ₂ O_mitoc + M_2Methylbut2enoylCoA_mitoc	----->	M_2S3S3Hydroxy2methylbutanoylCoA_mitoc
R04208	M_ATP_cytosol + M_2FormamidoN15phosphoribosylacetamidine_cytosol	----->	M_AD ^P _cytosol + M_Orthophosphate_cytosol + M_Aminoimidazoleribotide_cytosol
R04209	M_15PhosphoDribosyl5amino4imidazolecarboxylate_cytosol	<----->	M_CO ₂ _cytosol + M_Aminoimidazoleribotide_cytosol
R04224mitoc	M_H ₂ O_mitoc + M_2Methylprop2enoylCoA_mitoc	----->	M_S3HydroxyisobutyrylCoA_mitoc
R04323	M_2Amino3carboxymuconatesemialdehyde_cytosol	----->	M_CO ₂ _cytosol + M_2Aminomuconatesemialdehyde_cytosol
R04325	M_10Formyltetrahydrofolate_cytosol + M_5Phosphoribosylglycinamide_cytosol	----->	M_Tetrahydrofolate_cytosol + M_5PhosphoribosylNformylglycinamide_cytosol
R04355	M_Malonylacylcarrierprotein_cytosol + M_Acetylacylcarrierprotein_cytosol	----->	M_CO ₂ _cytosol + M_Acylcarrierprotein_cytosol + M_Acetoacetylacp_cytosol
R04428	M_3R3Hydroxybutanoylacylcarrierprotein_cytosol	<----->	M_H ₂ O_cytosol + M_But2enoylacylcarrierprotein_cytosol
R04430	M_H_cytosol + M_NADPH_cytosol + M_But2enoylacylcarrierprotein_cytosol	----->	M_NADP_cytosol + M_Butyryl ^{acp} _cytosol

R04463	M_ATP_cytosol + M_H2O_cytosol + M_LGlutamine_cytosol + M_5PhosphoribosylNformylglycinamide_cytosol	----->	M_ADG_cytosol + M_Orthophosphate_cytosol + M_LGlutamate_cytosol + M_2FormamidoN15phosphoribosylacetamide_cytosol
R04533	M_H_cytosol + M_NADPH_cytosol + M_Acetoacetylacp_cytosol	----->	M_NADP_cytosol + M_3R3Hydroxybutanoylacylcarrierprotein_cytosol
R04534	M_NADPH_cytosol + M_3Oxodecanoylacylcarrierprotein_cytosol	----->	M_NADP_cytosol + M_3R3Hydroxydecanoylacylcarrierprotein_cytosol
R04535	M_3R3Hydroxydecanoylacylcarrierprotein_cytosol	<----->	M_H2O_cytosol + M_transDec2enoylacylcarrierprotein_cytosol
R04536	M_H_cytosol + M_NADPH_cytosol + M_3Oxooctanoylacylcarrierprotein_cytosol	----->	M_NADP_cytosol + M_3R3Hydroxyoctanoylacylcarrierprotein_cytosol
R04537	M_3R3Hydroxyoctanoylacylcarrierprotein_cytosol	<----->	M_H2O_cytosol + M_transOct2enoylacylcarrierprotein_cytosol
R04543	M_H_cytosol + M_NADPH_cytosol + M_3Oxohexadecanoylacylcarrierprotein_cytosol	----->	M_NADP_cytosol + M_3R3Hydroxypalmitoylacylcarrierprotein_cytosol
R04544	M_3R3Hydroxypalmitoylacylcarrierprotein_cytosol	<----->	M_H2O_cytosol + M_transHexadec2enoylacylcarrierprotein_cytosol
R04559	M_15Phosphoribosyl5amino4Nsuccinocarboxamideimidazole_cytosol	<----->	M_Fumarate_cytosol + M_15Phosphoribosyl5amino4imidazolecarboxamide_cytosol
R04560	M_10Formyltetrahydrofolate_cytosol + M_15Phosphoribosyl5amino4imidazolecarboxamide_cytosol	<----->	M_15Phosphoribosyl5formamido4imidazolecarboxamide_cytosol + M_Tetrahydrofolate_cytosol
R04566	M_NADPH_cytosol + M_3Oxotetradecanoylacylcarrierprotein_cytosol	----->	M_NADP_cytosol + M_3R3Hydroxytetradecanoylacylcarrierprotein_cytosol
R04568	M_3R3Hydroxytetradecanoylacylcarrierprotein_cytosol	<----->	M_H2O_cytosol + M_transTetradec2enoylacylcarrierprotein_cytosol
R04591	M_ATP_cytosol + M_LAspartate_cytosol + M_15Phosphoribosyl5amino4imidazolecarboxylate_cytosol	<----->	M_ADG_cytosol + M_Orthophosphate_cytosol + M_15Phosphoribosyl5amino4Nsuccinocarboxamideimidazole_cytosol
R04725	M_H_cytosol + M_NADPH_cytosol + M_transDodec2enoylacylcarrierprotein_cytosol	----->	M_NADP_cytosol + M_Dodecanoylacylcarrierprotein_cytosol
R04726	M_Malonylacylcarrierprotein_cytosol + M_Dodecanoylacylcarrierprotein_cytosol	----->	M_CO2_cytosol + M_Acylcarrierprotein_cytosol + M_3Oxotetradecanoylacylcarrierprotein_cytosol
R04779_added	M_ATP_cytosol + M_betaDfructose6phosphate_cytosol	----->	M_ADG_cytosol + M_betaDfructose16bisphosphate_cytosol
R04780	M_H2O_cytosol + M_betaDfructose16bisphosphate_cytosol	----->	M_Orthophosphate_cytosol + M_betaDfructose6phosphate_cytosol
R04804	M_Zymosterol_cytosol	----->	M_5alphaCholesta724dien3betaol_cytosol
R04952	M_Malonylacylcarrierprotein_cytosol + M_Butyrylacylcarrierprotein_cytosol	----->	M_CO2_cytosol + M_Acylcarrierprotein_cytosol + M_3Oxohexanoylacylcarrierprotein_cytosol
R04953	M_NADPH_cytosol + M_3Oxohexanoylacylcarrierprotein_cytosol	----->	M_NADP_cytosol + M_R3Hydroxyhexanoylacylcarrierprotein_cytosol
R04954	M_R3Hydroxyhexanoylacylcarrierprotein_cytosol	<----->	M_H2O_cytosol + M_transHex2enoylacylcarrierprotein_cytosol
R04956	M_NADPH_cytosol + M_transHex2enoylacylcarrierprotein_cytosol	----->	M_NADP_cytosol + M_Hexanoylacylcarrierprotein_cytosol
R04957	M_Malonylacylcarrierprotein_cytosol + M_Hexanoylacylcarrierprotein_cytosol	----->	M_CO2_cytosol + M_Acylcarrierprotein_cytosol + M_3Oxooctanoylacylcarrierprotein_cytosol
R04959	M_NADPH_cytosol + M_transOct2enoylacylcarrierprotein_cytosol	----->	M_NADP_cytosol + M-Octanoylacylcarrierprotein_cytosol

R04960	M_Malonylacylcarrierprotein_cytosol + M_Octanoylacc_cytosol	----->	M_CO2_cytosol + M_Acylcarrierprotein_cytosol + M_3Oxododecanoylacc_cytosol
R04962	M_NADPH_cytosol + M_transDec2enoylacc_cytosol	----->	M_NADP_cytosol + M_Decanoylacc_cytosol
R04963	M_Malonylacylcarrierprotein_cytosol + M_Decanoylacc_cytosol	----->	M_CO2_cytosol + M_Acylcarrierprotein_cytosol + M_3Oxododecanoylacc_cytosol
R04964	M_NADPH_cytosol + M_3Oxododecanoylacc_cytosol	----->	M_NADP_cytosol + M_R3Hydroxydodecanoylacc_cytosol
R04965	M_R3Hydroxydodecanoylacc_cytosol	<----->	M_H2O_cytosol + M_transDodec2enoylacc_cytosol
R04967	M_NADPH_cytosol + M_transTetradec2enoylacc_cytosol	----->	M_NADP_cytosol + M_Tetradecanoylacc_cytosol
R04968	M_Malonylacylcarrierprotein_cytosol + M_Tetradecanoylacc_cytosol	----->	M_CO2_cytosol + M_Acylcarrierprotein_cytosol + M_3Oxohexadecanoylacc_cytosol
R04970	M_NADPH_cytosol + M_transHexadec2enoylacc_cytosol	----->	M_NADP_cytosol + M_Hexadecanoylacc_cytosol
R05064mitoc	M_H2O_mitoc + M_S3HydroxyisobutyrylCoA_mitoc	----->	M_CoA_mitoc + M_S3Hydroxyisobutyrate_mitoc
R05066mitoc	M_NAD_mitoc + M_S3Hydroxyisobutyrate_mitoc	<----->	M_H_mitoc + M_NADH_mitoc + M_SMethylmalonatesemialdehyde_mitoc
R05639	M_NADP_cytosol + M_14Demethyllanosterol_cytosol	<----->	M_H_cytosol + M_NADPH_cytosol + M_44Dimethyl5alphacholesta81424trien3betaol_cytosol
R05640	3.0*M_H_cytosol + 3.0*M_NADPH_cytosol + 3.0*M_Oxygen_cytosol + M_Lanosterol_cytosol	----->	4.0*M_H2O_cytosol + 3.0*M_NADP_cytosol + M_Formate_cytosol + M_44Dimethyl5alphacholesta81424trien3betaol_cytosol
R05703	M_H_cytosol + M_5alphaCholesta724dien3betaol_cytosol + M_NADPH_cytosol	----->	M_NADP_cytosol + M_5alphaCholest7en3betaol_cytosol
R06517	M_Sphinganine_cytosol + M_AcylCoA_cytosol	----->	M_CoA_cytosol + M_Dihydroceramide_cytosol
R06519	M_Oxygen_cytosol + M_Reducedacceptocytosol + M_Dihydroceramide_cytosol	----->	2.0*M_H2O_cytosol + M_NAcylsphingosine_cytosol + M_Acceptocytosol
R07377	M_Phosphatidylcholine_cytosol + M_LSerine_cytosol	----->	M_Choline_cytosol + M_Phosphatidylserine_cytosol
R07494	M_NADP_cytosol + M_4alphaMethylzymosterol4carboxylate_cytosol	----->	M_H_cytosol + M_NADPH_cytosol + M_CO2_cytosol + M_3Keto4methylzymosterol_cytosol
R07495	M_NADP_cytosol + M_3Keto4methylzymosterol_cytosol	----->	M_H_cytosol + M_NADPH_cytosol + M_4alphaMethylzymosterol_cytosol
R07496	M_4alphaMethylzymosterol_cytosol	----->	M_Zymosterol_cytosol
R07509	M_H_cytosol + M_NADPH_cytosol + M_CO2_cytosol + M_14Demethyllanosterol_cytosol	----->	M_H2O_cytosol + M_NADP_cytosol + M_4alphaMethylzymosterol4carboxylate_cytosol
RGTXDE	M_Glutamax_cytosol	----->	M_LGlutamine_cytosol + M_LAlanine_cytosol
RGTXM	M_Glutamax_ext	----->	M_Glutamax_cytosol
TF0001	M_Pyruvate_cytosol	<----->	M_Pyruvate_mitoc
TF0002	M_Citrate_cytosol	<----->	M_Citrate_mitoc

TF0003	M_LGlutamate_cytosol	<---->	M_LGlutamate_mitoc
TF0004	M_LGlutamine_cytosol	<---->	M_LGlutamine_mitoc
TF0005	M_LAlanine_cytosol	<---->	M_LAlanine_mitoc
TF0006	M_SMalate_cytosol + M_2Oxoglutarate_mitoc	<---->	M_SMalate_mitoc + M_2Oxoglutarate_cytosol
TF0007	M_LGlutamate_cytosol + M_LAspartate_mitoc	<---->	M_LGlutamate_mitoc + M_LAspartate_cytosol
TF0008	M_Oxygen_cytosol	<---->	M_Oxygen_mitoc
TF0009	M_CO2_cytosol	<---->	M_CO2_mitoc
TF0010	M_ATP_cytosol + M_ADG_mitoc	<---->	M_ADG_cytosol + M_ATP_mitoc
TF0012	M_H_cytosol	<---->	M_H_mitoc
TF0013	M_H2O_cytosol	<---->	M_H2O_mitoc
TF0014	M_NH3_cytosol	<---->	M_NH3_mitoc
TF0017	M_LValine_cytosol	<---->	M_LValine_mitoc
TF0018	M_LLeucine_cytosol	<---->	M_LLeucine_mitoc
TF0019	M_LIsoleucine_cytosol	<---->	M_LIsoleucine_mitoc
TF0020	M_LProline_cytosol	<---->	M_LProline_mitoc
TF0023	M_Glycine_cytosol	<---->	M_Glycine_mitoc
TF0024	M_LThreonine_cytosol	<---->	M_LThreonine_mitoc
TF0025	M_LLysine_cytosol	<---->	M_LLysine_mitoc
TF0026	M_L2Aminoadipate6semialdehyde_cytosol	<---->	M_L2Aminoadipate6semialdehyde_mitoc
TF0027	M_2Oxadipate_cytosol	<---->	M_2Oxadipate_mitoc
TF0028	M_Acetoacetate_cytosol	<---->	M_Acetoacetate_mitoc
TF0032	M_Orthophosphate_cytosol	<---->	M_Orthophosphate_mitoc
TF00703_added_2_1	M_SLactate_cytosol	----->	M_SLactate_mitoc

APPENDIX E: HEK293 metabolic models.

The HEK293 metabolic model used for all the p-FBA presented in the chapter 5. The resulting model used for the metabolic flux calculation, that contains 322 reactions and 302 metabolites, is detailed in **Table E**.

Table E. List of reactions included in the HEK293 reduced model developed and used for all Flux Balance Analysis in the Chapter 5.

R_10FTHFtm	M_10fthf_c	<---->	M_10fthf_m
R_2AMACHYD	M_h2o_c + M_2amac_c	----->	M_pyr_c + M_nh4_c
R_2OXOADOXm	M_nad_m + M_coa_m + M_2oxoadp_m	----->	M_nadh_m + M_co2_m + M_glutcoa_m
R_2OXOADPTm	M_akg_m + M_2oxoadp_c	<---->	M_akg_c + M_2oxoadp_m
R_3DSPHR	M_h_c + M_nadph_c + M_3dsphgn_c	----->	M_nadp_c + M_sphgn_c
R_3HAO	M_o2_c + M_3hanthrn_c	----->	M_h_c + M_cmusa_c
R_3HBCOAHlm	M_h2o_m + M_3hibutcoa_m	----->	M_h_m + M_coa_m + M_3hmp_m
R_3HCO3_NAt	M_na1_e + 3.0*M_hco3_e	<---->	M_na1_c + 3.0*M_hco3_c
R_AASAD3m	M_h2o_m + M_nad_m + M_L2aadp6sa_m	----->	2.0*M_h_m + M_nadh_m + M_L2aadp_m
R_ACACT10m	M_coa_m + M_2maacoa_m	<---->	M_accoa_m + M_ppcoa_m
R_ACACT1r	2.0*M_accoa_c	<---->	M_coa_c + M_aacoa_c
R_ACACT1rm	2.0*M_accoa_m	----->	M_coa_m + M_aacoa_m
R_ACCOAC	M_atp_c + M_accoa_c + M_hco3_c	----->	M_h_c + M_pi_c + M_adp_c + M_malcoa_c
R_ACITL	M_atp_c + M_coa_c + M_cit_c	----->	M_oaa_c + M_pi_c + M_adp_c + M_accoa_c
R_ACOAD10m	M_fad_m + M_2mbcoa_m	----->	M_fadh2_m + M_2mb2coa_m
R_ACOAD8m	M_ivcoa_m + M_fad_m	----->	M_fadh2_m + M_3mb2coa_m
R_ACOAD9m	M_fad_m + M_ibcoa_m	----->	M_fadh2_m + M_2mp2coa_m
R_ACONTm	M_cit_m	<---->	M_icit_m

R_ADK1	M_atp_c + M_amp_c	<---->	2.0*M_adp_c
R_ADNK1	M_atp_c + M_adn_c	----->	M_h_c + M_adp_c + M_amp_c
R_ADSL1	M_dcamp_c	----->	M_fum_c + M_amp_c
R_ADSL2	M_25aics_c	----->	M_fum_c + M_aicar_c
R_ADSS	M_gtp_c + M_asp_L_c + M_imp_c	----->	2.0*M_h_c + M_gdp_c + M_pi_c + M_dcamp_c
R_AGPAT1	M_alpa_hs_c + M_Rtotalcoa_c	----->	6.0*M_h_c + M_coa_c + M_pa_hs_c
R_AHC	M_h2o_c + M_ahcys_c	<---->	M_hcys_L_c + M_adn_c
R_AHCYStd	M_ahcys_m	<---->	M_ahcys_c
R_AICART	M_aicar_c + M_10fthf_c	<---->	M_thf_c + M_fprica_c
R_AIRC_r_PRASCS	M_co2_c + M_atp_c + M_asp_L_c + M_air_c	<---->	2.0*M_h_c + M_pi_c + M_adp_c + M_25aics_c
R_AKGDm	M_nad_m + M_coa_m + M_akg_m	----->	M_nadh_m + M_co2_m + M_succoa_m
R_AKGMALtm	M_mal_L_c + M_akg_m	<---->	M_akg_c + M_mal_L_m
R_ALATA_L	M_akg_c + M_ala_L_c	<---->	M_glu_L_c + M_pyr_c
R_AMCOXO	M_h2o_c + M_h_c + M_nadph_c + M_amuco_c	----->	M_nh4_c + M_nadp_c + M_2oxoadp_c
R_AMETtd	M_amet_c	<---->	M_amet_m
R_ARGN	M_h2o_c + M_arg_L_c	----->	M_orn_c + M_urea_c
R_ARGtiDF	M_arg_L_e	----->	M_arg_L_c
R_ARTPLM3	M_Rtotalcoa_c	<---->	4.0*M_h_c + M_pmtcoa_c
R_ASPECTr	M_asp_L_c + M_cbp_c	<---->	M_h_c + M_pi_c + M_cbasp_c
R_ASPLUm	M_glu_L_c + M_h_i + M_asp_L_m	----->	M_h_m + M_glu_L_m + M_asp_L_c
R_ASPTA	M_asp_L_c + M_akg_c	<---->	M_glu_L_c + M_oaa_c
R_ASPTAm	M_akg_m + M_asp_L_m	<---->	M_glu_L_m + M_oaa_m
R_ASPTe	M_asp_L_c	----->	M_asp_L_e
R_ATPS4m	M_adp_m + 4.0*M_h_i + M_pi_m	----->	3.0*M_h_m + M_h2o_m + M_atp_m
R_ATPTm	M_atp_m + M_adp_c	----->	M_atp_c + M_adp_m
R_biomass_carbohy drate	3.87591549295775*M_g6p_c	----->	M_biomass_carbohydrate_c

R_biomass_DNA	$0.707 * M_{\text{dntp_n}} + 0.674428571428572 * M_{\text{dctp_n}} + 0.935071428571429 * M_{\text{dttp_n}} + 0.941642857142857 * M_{\text{datp_n}}$	----->	M_biomass_DNA_c
R_biomass_lipid	$0.570865979381443 * M_{\text{pe_hs_c}} + 0.0300412371134021 * M_{\text{pglyc_hs_c}} + 0.0600927835051546 * M_{\text{ps_hs_c}} + 1.59237113402062 * M_{\text{pchol_hs_c}} + 0.210319587628866 * M_{\text{chsterol_c}} + 0.240360824742268 * M_{\text{pail_hs_c}} + 0.180268041237113 * M_{\text{sphmyln_hs_c}} + 0.120185567010309 * M_{\text{clpn_hs_c}}$	----->	M_biomass_lipid_c
R_biomass_protein	$0.546558073654391 * M_{\text{glu_L_c}} + 0.461756373937677 * M_{\text{gln_L_c}} + 29.2504249291785 * M_{\text{h2o_c}} + 0.0188470254957507 * M_{\text{trp_L_c}} + 0.77271954674221 * M_{\text{leu_L_c}} + 0.0659645892351275 * M_{\text{cys_L_c}} + 0.367521246458923 * M_{\text{phe_L_c}} + 0.555991501416431 * M_{\text{ser_L_c}} + 29.2504249291785 * M_{\text{atp_c}} + 0.584249291784703 * M_{\text{pro_L_c}} + 0.405212464589235 * M_{\text{ile_L_c}} + 0.763300283286119 * M_{\text{gly_c}} + 0.499447592067989 * M_{\text{asp_L_c}} + 0.216742209631728 * M_{\text{met_L_c}} + 0.716189801699717 * M_{\text{ala_L_c}} + 0.179050991501416 * M_{\text{his_L_c}} + 0.508866855524079 * M_{\text{arg_L_c}} + 0.499447592067989 * M_{\text{val_L_c}} + 0.226161473087819 * M_{\text{tyr_L_c}} + 0.838682719546742 * M_{\text{lys_L_c}} + 0.442903682719547 * M_{\text{thr_L_c}} + 0.395779036827196 * M_{\text{asn_L_c}}$	----->	$29.2504249291785 * M_{\text{h_c}} + M_{\text{biomass_protein_c}} + 29.2504249291785 * M_{\text{pi_c}} + 29.2504249291785 * M_{\text{adp_c}}$
R_biomass_reaction	$0.058 * M_{\text{biomass_RNA_c}} + 0.097 * M_{\text{biomass_lipid_c}} + 0.071 * M_{\text{biomass_carbohydrate_c}} + 0.014 * M_{\text{biomass_DNA_c}} + 0.054 * M_{\text{biomass_other_c}} + 0.706 * M_{\text{biomass_protein_c}}$	----->	M_biomass_c
R_biomass_RNA	$0.622706896551724 * M_{\text{gtp_c}} + 0.925862068965503 * M_{\text{atp_c}} + 0.673034482758621 * M_{\text{ctp_c}} + 0.92148275862069 * M_{\text{utp_c}}$	----->	M_biomass_RNA_c
R_C14STRr	$M_{\text{h_r}} + M_{\text{nadph_r}} + M_{\text{44mctr_r}}$	----->	$M_{\text{nadp_r}} + M_{\text{44mzym_r}}$
R_C3STDH1Pr	$M_{\text{nadp_r}} + M_{\text{4mzym_int1_r}}$	----->	$M_{\text{h_r}} + M_{\text{nadph_r}} + M_{\text{4mzym_int2_r}} + M_{\text{co2_r}}$
R_C40CPT1	$M_{\text{btcoa_c}} + M_{\text{crn_c}}$	<----->	$M_{\text{coa_c}} + M_{\text{c4crn_c}}$
R_C4CRNCPT2	$M_{\text{coa_m}} + M_{\text{c4crn_m}}$	<----->	$M_{\text{crn_m}} + M_{\text{btcoa_m}}$
R_C4STMO1r	$3.0 * M_{\text{h_r}} + 3.0 * M_{\text{nadph_r}} + M_{\text{44mzym_r}} + 3.0 * M_{\text{o2_r}}$	----->	$3.0 * M_{\text{nadp_r}} + M_{\text{4mzym_int1_r}} + 4.0 * M_{\text{h2o_r}}$
R_CBPS	$M_{\text{gln_L_c}} + M_{\text{h2o_c}} + 2.0 * M_{\text{atp_c}} + M_{\text{hco3_c}}$	----->	$M_{\text{glu_L_c}} + 2.0 * M_{\text{h_c}} + M_{\text{pi_c}} + 2.0 * M_{\text{adp_c}} + M_{\text{cbp_c}}$
R_CDIPTTr	$M_{\text{inost_c}} + M_{\text{cdpdag_hs_c}}$	<----->	$M_{\text{h_c}} + M_{\text{cmp_c}} + M_{\text{pail_hs_c}}$
R_CDS	$M_{\text{h_c}} + M_{\text{pa_hs_c}} + M_{\text{ctp_c}}$	----->	$M_{\text{ppi_c}} + M_{\text{cdpdag_hs_c}}$
R_CHSTEROLtrc	$M_{\text{chsterol_r}}$	<----->	$M_{\text{chsterol_c}}$
R_CITRtm	$M_{\text{citr_L_m}}$	<----->	$M_{\text{citr_L_c}}$
R_CITtam	$M_{\text{mal_L_m}} + M_{\text{cit_c}}$	<----->	$M_{\text{cit_m}} + M_{\text{mal_L_c}}$

R_CLS_hs	M_h_c + M_pglyc_hs_c + M_cdpdag_hs_c	----->	M_cmp_c + M_clpn_hs_c
R_CO2t	M_co2_e	<----->	M_co2_c
R_CO2ter	M_co2_c	<----->	M_co2_r
R_CO2tm	M_co2_c	<----->	M_co2_m
R_COAtm	M_coa_c	<----->	M_coa_m
R_CSm	M_h2o_m + M_accoa_m + M_oaa_m	----->	M_h_m + M_coa_m + M_cit_m
R_CTPS2	M_gln_L_c + M_h2o_c + M_atp_c + M_utp_c	----->	M_glu_L_c + 2.0*M_h_c + M_pi_c + M_adp_c + M_ctp_c
R_CYOOm3	8.0*M_h_m + 4.0*M_focytC_m + M_o2_m	----->	2.0*M_h2o_m + 4.0*M_h_i + 4.0*M_ficytC_m
R_CYOR_u10m	2.0*M_h_m + M_q10h2_m + 2.0*M_ficytC_m	----->	M_q10_m + 4.0*M_h_i + 2.0*M_focytC_m
R_CYStec	M_cys_L_e	<----->	M_cys_L_c
R_CYSTGL	M_h2o_c + M_cyst_L_c	----->	M_nh4_c + M_cys_L_c + M_2obut_c
R_CYSTS	M_hcys_L_c + M_ser_L_c	----->	M_h2o_c + M_cyst_L_c
R_CYTK1	M_atp_c + M_cmp_c	<----->	M_adp_c + M_cdp_c
R_DAGK_hs	M_atp_c + M_dag_hs_c	<----->	M_h_c + M_adp_c + M_pa_hs_c
R_DATPtn	M_datp_c	<----->	M_datp_n
R_DCTPtn	M_dctp_c	<----->	M_dctp_n
R_DGTPtn	M_dgtp_c	<----->	M_dgtp_n
R_DHCR71r	M_h_r + M_nadph_r + M_ddsmssterol_r	----->	M_nadp_r + M_dsmsterol_r
R_DHCRD1	M_nadp_c + M_dhcrm_hs_c	----->	M_h_c + M_nadph_c + M_crm_hs_c
R_DHFR	M_h_c + M_nadph_c + M_dhf_c	<----->	M_thf_c + M_nadp_c
R_DHORD9	M_q10_m + M_dhor_S_c	----->	M_q10h2_m + M_orot_c
R_DHORTS	M_h2o_c + M_dhor_S_c	<----->	M_h_c + M_cbasp_c
R_DM_atp_c_	M_h2o_c + M_atp_c	----->	M_h_c + M_pi_c + M_adp_c
R_DMATT	M_ipdp_c + M_dmpp_c	----->	M_ppi_c + M_grdp_c
R_DPMVDC	M_atp_c + M_5dpmev_c	----->	M_co2_c + M_pi_c + M_adp_c + M_ipdp_c
R_DSAT	M_sphgn_c + M_Rtotalcoa_c	----->	5.0*M_h_c + M_coa_c + M_dhcrm_hs_c
R_DSREDUCr	M_h_r + M_nadph_r + M_dsmsterol_r	----->	M_nadp_r + M_chsterol_r

R_DTMPK	M_atp_c + M_dtmp_c	----->	M_adp_c + M_dtdp_c
R_DTTptn	M_dttp_c	<----->	M_dttp_n
R_EBP1r	M_zymst_r	----->	M_chlstol_r
R_ECOAH12m	M_h2o_m + M_2mp2coa_m	<----->	M_3hibutcoa_m
R_ECOAH1m	M_3hbcoa_m	<----->	M_h2o_m + M_b2coa_m
R_ECOAH9m	M_h2o_m + M_2mb2coa_m	<----->	M_3hmbcoa_m
R_ENO	M_2pg_c	<----->	M_h2o_c + M_pep_c
R ETF	M_etfox_m + M_fadh2_m	----->	M_etfrd_m + M_fad_m
R ETFQO	M_q10_m + M_etfrd_m	----->	M_q10h2_m + M_etfox_m
R_EX_GLTX_hydrolysis	M_GLTX_e	----->	M_gln_L_e + M_ala_L_e
R_FAS100COA	3.0*M_h_c + 2.0*M_nadph_c + M_malcoa_c + M_occoa_c	----->	M_h2o_c + M_co2_c + 2.0*M_nadp_c + M_coa_c + M_dcacoa_c
R_FAS120COA	3.0*M_h_c + 2.0*M_nadph_c + M_malcoa_c + M_dcacoa_c	----->	M_h2o_c + M_co2_c + 2.0*M_nadp_c + M_coa_c + M_ddcacoa_c
R_FAS140COA	3.0*M_h_c + 2.0*M_nadph_c + M_malcoa_c + M_ddcacoa_c	----->	M_h2o_c + M_co2_c + 2.0*M_nadp_c + M_coa_c + M_tdcoa_c
R_FAS160COA	3.0*M_h_c + 2.0*M_nadph_c + M_tdcoa_c + M_malcoa_c	----->	M_h2o_c + M_co2_c + 2.0*M_nadp_c + M_coa_c + M_pmtcoa_c
R_FAS80COA_L	9.0*M_h_c + 6.0*M_nadph_c + 3.0*M_malcoa_c + M_accoa_c	----->	3.0*M_h2o_c + 3.0*M_co2_c + 6.0*M_nadp_c + 3.0*M_coa_c + M_occoa_c
R_FBA	M_fdp_c	<----->	M_dhap_c + M_g3p_c
R_FBA_fructose	M_f1p_c	<----->	M_gdh_c + M_dhap_c
R_FBP	M_h2o_c + M_fdp_c	----->	M_pi_c + M_f6p_c
R_FDH	M_nad_c + M_for_c	----->	M_co2_c + M_nadh_c
R_FKYNH	M_h2o_c + M_Lfmkynr_c	----->	M_h_c + M_Lkynr_c + M_for_c
R_FORtr	M_for_c	<----->	M_for_r
R_FRDPctr	M_frdp_c	<----->	M_frdp_r
R_fru_f1p	M_atp_c + M_fru_c	<----->	M_adp_c + M_f1p_c
R_FTCD	2.0*M_h_c + M_5forthf_c	----->	M_nh4_c + M_methf_c
R_FUMm	M_h2o_m + M_fum_m	<----->	M_mal_L_m
R_FUMtm	M_fum_c + M_pi_m	<----->	M_pi_c + M_fum_m

R_G3PD1	M_nad_c + M_glyc3p_c	<---->	M_h_c + M_nadh_c + M_dhap_c
R_G5SADrm	M_glu5sa_m	----->	M_1pyr5c_m + M_h_m + M_h2o_m
R_G6PDH2r	M_nadp_c + M_g6p_c	<---->	M_h_c + M_nadph_c + M_6pgl_c
R_GAPD	M_pi_c + M_nad_c + M_g3p_c	<---->	M_h_c + M_nadh_c + M_13dpg_c
R_GARFT	M_10fthf_c + M_gar_c	<---->	M_h_c + M_fgam_c + M_thf_c
R_GHMT2r	M_ser_L_c + M_thf_c	<---->	M_h2o_c + M_gly_c + M_m1thf_c
R_GK1	M_atp_c + M_gmp_c	<---->	M_gdp_c + M_adp_c
R_GLCt4	M_na1_e + M_glc_D_e	<---->	M_na1_c + M_glc_D_c
R_GLNS	M_glu_L_c + M_nh4_c + M_atp_c	----->	M_gln_L_c + M_h_c + M_pi_c + M_adp_c
R_GLNtm	M_gln_L_c	----->	M_gln_L_m
R_GLUDxm	M_h2o_m + M_glu_L_m + M_nad_m	<---->	M_h_m + M_nadh_m + M_nh4_m + M_akg_m
R_GLUDym	M_h2o_m + M_glu_L_m + M_nadp_m	<---->	M_h_m + M_nh4_m + M_akg_m + M_nadph_m
R_GluForTx	M_h_c + M_thf_c + M_forglu_c	----->	M_glu_L_c + M_5forthf_c
R_GLUNm	M_h2o_m + M_gln_L_m	----->	M_glu_L_m + M_nh4_m
R_GLUPRT	M_gln_L_c + M_h2o_c + M_prpp_c	----->	M_glu_L_c + M_ppi_c + M_pram_c
R_GLUTCOADHm	M_h_m + M_fad_m + M_glutcoa_m	----->	M_co2_m + M_fadh2_m + M_b2coa_m
R_GLUVESSEC	M_glu_L_c + M_h2o_c + M_atp_c	----->	M_h_c + M_pi_c + M_adp_c + M_glu_L_e
R_GLYtm	M_gly_c	<---->	M_gly_m
R_GNDc	M_nadp_c + M_6pgc_c	----->	M_co2_c + M_nadph_c + M_ru5p_D_c
R_GPAM_hs	M_Rtotalcoa_c + M_glyc3p_c	----->	2.0*M_h_c + M_coa_c + M_alpa_hs_c
R_GRTT	M_grdp_c + M_ipdp_c	----->	M_ppi_c + M_frdp_c
R_GUAPRT	M_prpp_c + M_gua_c	----->	M_ppi_c + M_gmp_c
R_H2CO3D	M_h2o_c + M_co2_c	<---->	M_h_c + M_hco3_c
R_H2CO3Dm	M_h2o_m + M_co2_m	<---->	M_h_m + M_hco3_m
R_H2Ot	M_h2o_e	<---->	M_h2o_c
R_H2Oter	M_h2o_c	<---->	M_h2o_r
R_H2Otm	M_h2o_c	<---->	M_h2o_m

R_HACD1m	M_h_m + M_nadh_m + M_aacoa_m	<---->	M_nad_m + M_3hbcoa_m
R_HACD9m	M_nad_m + M_3hmbcoa_m	<---->	M_h_m + M_nadh_m + M_2maacoa_m
R_HEX1	M_atp_c + M_glc_D_c	----->	M_h_c + M_adp_c + M_g6p_c
R_HIBDm	M_nad_m + M_3hmp_m	<---->	M_h_m + M_nadh_m + M_2mop_m
R_HISD	M_his_L_c	----->	M_nh4_c + M_urcan_c
R_HISiDF	M_his_L_e	----->	M_his_L_c
R_HKYNH	M_h2o_c + M_hLkynr_c	----->	M_3hanthrn_c + M_ala_L_c
R_HMGCOARc	2.0*M_h_c + 2.0*M_nadph_c + M_hmgcoa_c	----->	2.0*M_nadp_c + M_coa_c + M_mev_R_c
R_HMGCOASi	M_h2o_c + M_accoa_c + M_aacoa_c	----->	M_h_c + M_coa_c + M_hmgcoa_c
R_HMGCOASim	M_h2o_m + M_accoa_m + M_aacoa_m	----->	M_h_m + M_coa_m + M_hmgcoa_m
R_HMGCOAtm	M_hmgcoa_c	<---->	M_hmgcoa_m
R_Htr	M_h_c	<---->	M_h_r
R_ICDHxm	M_nad_m + M_icit_m	----->	M_nadh_m + M_co2_m + M_akg_m
R_ILEt5m	M_ile_L_c	<---->	M_ile_L_m
R_ILETAm	M_ile_L_m + M_akg_m	<---->	M_glu_L_m + M_3mop_m
R_ILEtec	M_ile_L_e	<---->	M_ile_L_c
R_IMPC	M_h2o_c + M_imp_c	<---->	M_fprica_c
R_IMPD	M_h2o_c + M_nad_c + M_imp_c	----->	M_h_c + M_nadh_c + M_xmp_c
R_IPDDI	M_ipdp_c	<---->	M_dmpc_c
R_IZPN	M_h2o_c + M_4izp_c	----->	M_h_c + M_forglu_c
R_KHte	M_h_c + M_k_e	<---->	M_h_e + M_k_c
R_KYN3OX	M_o2_c + M_h_c + M_nadph_c + M_Lkynr_c	----->	M_h2o_c + M_nadp_c + M_hLkynr_c
R_L_LACt2r	M_h_e + M_lac_L_e	<---->	M_h_c + M_lac_L_c
R_L_LACtm	M_h_c + M_lac_L_c	<---->	M_h_m + M_lac_L_m
R_LDH_L	M_nad_c + M_lac_L_c	<---->	M_h_c + M_pyr_c + M_nadh_c
R_LDH_Lm	M_nad_m + M_lac_L_m	<---->	M_h_m + M_nadh_m + M_pyr_m
R_LEUt5m	M_leu_L_c	<---->	M_leu_L_m

R_LEUTAm	M_akg_m + M_leu_L_m	<---->	M_glu_L_m + M_4mop_m
R_LEUtec	M_leu_L_e	<---->	M_leu_L_c
R_LNSTLSr	M_Ssq23epx_r	----->	M_lanost_r
R_LSTO1r	M_h_r + M_nadph_r + M_o2_r + M_chlstol_r	----->	M_nadp_r + 2.0*M_h2o_r + M_ddsminsterol_r
R_LYStiDF	M_lys_L_e	----->	M_lys_L_c
R_LYStm	M_h_m + M_lys_L_c	<---->	M_h_c + M_lys_L_m
R_MCCCrM	M_atp_m + M_hco3_m + M_3mb2coa_m	<---->	M_h_m + M_adp_m + M_3mgcoa_m + M_pi_m
R_MDH	M_mal_L_c + M_nad_c	<---->	M_h_c + M_oaa_c + M_nadh_c
R_MDHm	M_nad_m + M_mal_L_m	<---->	M_h_m + M_nadh_m + M_oaa_m
R_ME1m	M_nad_m + M_mal_L_m	----->	M_nadh_m + M_co2_m + M_pyr_m
R_ME2	M_nadp_c + M_mal_L_c	----->	M_co2_c + M_pyr_c + M_nadph_c
R_ME2m	M_mal_L_m + M_nadp_m	----->	M_co2_m + M_pyr_m + M_nadph_m
R_METAT	M_h2o_c + M_atp_c + M_met_L_c	----->	M_ppi_c + M_pi_c + M_amet_c
R_METS	M_hcys_L_c + M_5mthf_c	----->	M_h_c + M_thf_c + M_met_L_c
R_METtec	M_met_L_e	<---->	M_met_L_c
R_MEVK1c	M_atp_c + M_mev_R_c	----->	M_h_c + M_adp_c + M_5pmev_c
R_MGCHrm	M_h2o_m + M_3mgcoa_m	<---->	M_hmgcoa_m
R_MI1PP	M_h2o_c + M_mi1p_D_c	----->	M_pi_c + M_inost_c
R_MI1PS	M_g6p_c	----->	M_mi1p_D_c
R_MMEEm	M_mmcoa_R_m	<---->	M_mmcoa_S_m
R_MMMm	M_mmcoa_R_m	<---->	M_succoa_m
R_MMSAD1m	M_nad_m + M_coa_m + M_2mop_m	----->	M_nadh_m + M_ppcoa_m + M_co2_m
R_MTHFC	M_h2o_c + M_methf_c	<---->	M_h_c + M_10fthf_c
R_MTHFCm	M_h2o_m + M_methf_m	<---->	M_h_m + M_10fthf_m
R_MTHFD	M_nadp_c + M_mlthf_c	<---->	M_methf_c + M_nadph_c
R_MTHFD2m	M_nad_m + M_mlthf_m	<---->	M_nadh_m + M_methf_m
R_MTHFR3	2.0*M_h_c + M_nadph_c + M_mlthf_c	----->	M_nadp_c + M_5mthf_c

R_NADH2_u10m	$5.0 * M_{h_m} + M_{nadh_m} + M_{q10_m}$	----->	$M_{nad_m} + M_{q10h2_m} + 4.0 * M_{h_i}$
R_NADPHtru	M_{nadph_c}	----->	M_{nadph_r}
R_NADPtru	M_{nadp_r}	----->	M_{nadp_c}
R_NaKt	$M_{h2o_c} + M_{na1_c} + M_{atp_c} + M_{k_e}$	----->	$M_{h_c} + M_{pi_c} + M_{na1_e} + M_{adp_c} + M_{k_c}$
R_NDP8	$M_{h2o_c} + M_{dudp_c}$	----->	$M_{h_c} + M_{pi_c} + M_{dump_c}$
R_NDPK1	$M_{gdp_c} + M_{atp_c}$	<----->	$M_{gtp_c} + M_{adp_c}$
R_NDPK3	$M_{atp_c} + M_{cdp_c}$	<----->	$M_{adp_c} + M_{ctp_c}$
R_NDPK4	$M_{atp_c} + M_{dtdp_c}$	<----->	$M_{adp_c} + M_{dttp_c}$
R_NDPK5	$M_{atp_c} + M_{dgdpc_c}$	<----->	$M_{adp_c} + M_{dgtp_c}$
R_NDPK7	$M_{atp_c} + M_{dcdp_c}$	<----->	$M_{adp_c} + M_{dctp_c}$
R_NDPK8	$M_{atp_c} + M_{dadp_c}$	<----->	$M_{adp_c} + M_{datp_c}$
R_NH4t3r	$M_{nh4_c} + M_{h_e}$	<----->	$M_{h_c} + M_{nh4_e}$
R_NTD10	$M_{h2o_c} + M_{xmp_c}$	----->	$M_{pi_c} + M_{xtsn_c}$
R_O2t	M_{o2_e}	<----->	M_{o2_c}
R_O2ter	M_{o2_c}	<----->	M_{o2_r}
R_O2tm	M_{o2_c}	<----->	M_{o2_m}
R_OBDHc	$M_{nad_c} + M_{coa_c} + M_{2obut_c}$	----->	$M_{co2_c} + M_{nadh_c} + M_{ppcoa_c}$
R_OIVD1m	$M_{nad_m} + M_{coa_m} + M_{4mop_m}$	----->	$M_{nadh_m} + M_{co2_m} + M_{ivcoa_m}$
R_OIVD2m	$M_{nad_m} + M_{coa_m} + M_{3mob_m}$	----->	$M_{nadh_m} + M_{co2_m} + M_{ibcoa_m}$
R_OIVD3m	$M_{nad_m} + M_{coa_m} + M_{3mop_m}$	----->	$M_{nadh_m} + M_{co2_m} + M_{2mbcoa_m}$
R_OMPDC	$M_{h_c} + M_{orot5p_c}$	----->	$M_{co2_c} + M_{ump_c}$
R_ORNTArm	$M_{akg_m} + M_{orn_m}$	<----->	$M_{glu5sa_m} + M_{glu_L_m}$
R_ORNTiDF	M_{orn_e}	----->	M_{orn_c}
R_ORPT	$M_{ppi_c} + M_{orot5p_c}$	<----->	$M_{prpp_c} + M_{orot_c}$
R_P5CDm	$M_{1pyr5c_m} + 2.0 * M_{h2o_m} + M_{nad_m}$	----->	$M_{h_m} + M_{nadh_m} + M_{glu_L_m}$
R_P5CRm	$M_{1pyr5c_m} + 2.0 * M_{h_m} + M_{nadph_m}$	----->	$M_{nadp_m} + M_{pro_L_m}$
R_PCFLOPm	$M_{h2o_c} + M_{atp_c} + M_{pchol_hs_m}$	----->	$M_{h_c} + M_{pi_c} + M_{adp_c} + M_{pchol_hs_c}$

R_PCHOL_HSter	M_pchol_hs_c	<---->	M_pchol_hs_r
R_PCLAD	M_h_c + M_cmusa_c	----->	M_co2_c + M_am6sa_c
R_PCm	M_atp_m + M_pyr_m + M_hco3_m	----->	M_h_m + M_adp_m + M_oaa_m + M_pi_m
R_PDHm	M_nad_m + M_coa_m + M_pyr_m	----->	M_nadh_m + M_accoa_m + M_co2_m
R_PE_HSter	M_pe_hs_c	<---->	M_pe_hs_r
R_PE_HStm	M_pe_hs_c	<---->	M_pe_hs_m
R_PEPCK	M_oaa_c + M_gtp_c	----->	M_co2_c + M_gdp_c + M_pep_c
R_PETOHHm_hs	M_pe_hs_m + 3.0*M_amet_m	----->	3.0*M_h_m + M_pchol_hs_m + 3.0*M_ahcys_m
R_PETOHMr_hs	M_pe_hs_r + 3.0*M_amet_r	----->	3.0*M_h_r + M_pchol_hs_r + 3.0*M_ahcys_r
R_PFK	M_atp_c + M_f6p_c	----->	M_h_c + M_adp_c + M_fdp_c
R_PGI	M_g6p_c	<---->	M_f6p_c
R_PGK	M_atp_c + M_3pg_c	<---->	M_adp_c + M_13dpg_c
R_PGL	M_h2o_c + M_6pgl_c	----->	M_h_c + M_6pgc_c
R_PGM	M_2pg_c	<---->	M_3pg_c
R_PGPP_hs	M_h2o_c + M_pgp_hs_c	----->	3.0*M_h_c + M_pi_c + M_pglyc_hs_c
R_PGPPT	2.0*M_h_c + M_glyc3p_c + M_cdpdag_hs_c	----->	M_pgp_hs_c + M_cmp_c
R_PHEtec	M_phe_L_e	<---->	M_phe_L_c
R_Plt2m	M_h_c + M_pi_c	----->	M_h_m + M_pi_m
R_Plter	M_pi_r	<---->	M_pi_c
R_PMEVKc	M_atp_c + M_5pmev_c	----->	M_adp_c + M_5dpmev_c
R_PPA	M_ppi_c + M_h2o_c	----->	M_h_c + 2.0*M_pi_c
R_PPAer	M_h2o_r + M_ppi_r	----->	M_h_r + 2.0*M_pi_r
R_PPAP	M_h2o_c + M_pa_hs_c	----->	M_pi_c + M_dag_hs_c
R_PPCOACm	M_atp_m + M_ppcoa_m + M_hco3_m	----->	M_h_m + M_adp_m + M_pi_m + M_mmcoa_S_m
R_PPM	M_r1p_c	<---->	M_r5p_c
R_PRAGSr	M_pram_c + M_atp_c + M_gly_c	<---->	M_h_c + M_pi_c + M_adp_c + M_gar_c
R_PRFGS	M_gln_L_c + M_h2o_c + M_atp_c + M_fgam_c	----->	M_glu_L_c + M_h_c + M_pi_c + M_adp_c + M_fpram_c

R_PROPAT4te	M_pro_L_e	<---->	M_pro_L_c
R_PROt2r	M_pro_L_e + M_h_e	<---->	M_h_c + M_pro_L_c
R_PROtm	M_pro_L_c	<---->	M_pro_L_m
R_PRPPS	M_atp_c + M_r5p_c	----->	M_prpp_c + M_h_c + M_amp_c
R_PSDm_hs	M_h_m + M_ps_hs_m	----->	M_pe_hs_m + M_co2_m
R_PSLIPm	M_h2o_c + M_atp_c + M_ps_hs_c	----->	M_h_c + M_pi_c + M_adp_c + M_ps_hs_m
R_PUNP3	M_pi_c + M_gsn_c	<---->	M_r1p_c + M_gua_c
R_PYK	M_h_c + M_pep_c + M_adp_c	----->	M_pyr_c + M_atp_c
R_PYRt2m	M_h_c + M_pyr_c	----->	M_h_m + M_pyr_m
R_r0074	M_h2o_m + M_glu5sa_m + M_nad_m	<---->	2.0*M_h_m + M_nadh_m + M_glu_L_m
R_r0127	M_h2o_c + M_asn_L_c	----->	M_nh4_c + M_asp_L_c
R_r0165	M_h_c + M_pep_c + M_udp_c	----->	M_pyr_c + M_utp_c
R_r0193	M_h2o_c + M_cys_L_c	<---->	M_h_c + M_HC00250_c + M_pyr_c + M_nh4_c
R_r0295	M_nadh_m + M_nh4_m + M_co2_m + M_mlthf_m	----->	M_nad_m + M_thf_m + M_gly_m
R_r0450	M_akg_m + M_L2aadb_m	<---->	M_glu_L_m + M_2oxoadp_m
R_r0525	M_h2o_m + M_nad_m + M_sacccp_L_m	<---->	M_h_m + M_nadh_m + M_glu_L_m + M_L2aadb6sa_m
R_r0645	M_h2o_c + M_am6sa_c + M_nad_c	<---->	2.0*M_h_c + M_nadh_c + M_amuco_c
R_r0666	M_atp_c + M_fpram_c	<---->	2.0*M_h_c + M_pi_c + M_adp_c + M_air_c
R_r0781	2.0*M_h_r + 3.0*M_nadph_r + 3.0*M_o2_r + M_lanost_r	<---->	3.0*M_nadp_r + 4.0*M_h2o_r + M_for_r + M_44mctr_r
R_r0838	M_nh4_c	<---->	M_nh4_m
R_r0911	M_glu_L_m + M_pro_L_c	<---->	M_glu_L_c + M_pro_L_m
R_r0940	M_HC00250_c	<---->	M_HC00250_e
R_r0941	M_hco3_c	<---->	M_hco3_m
R_r0947	M_citr_L_c + M_orn_m	<---->	M_citr_L_m + M_orn_c
R_r1135	M_h_r + M_nadph_r + M_4mzym_int2_r	<---->	M_nadp_r + M_HC02110_r
R_r1143	M_na1_e + M_asp_L_e	----->	M_na1_c + M_asp_L_c
R_r1144	M_na1_e + M_glu_L_e	----->	M_glu_L_c + M_na1_c

R_r1146	M_h_r + M_ahcys_r + M_HC02110_r	<---->	M_zymst_r + M_amet_r
R_r1384	M_h2o_c + M_h_c + M_gsn_c	<---->	M_nh4_c + M_xtsn_c
R_r1400	M_crn_m + M_ppcoa_c	----->	M_ppcoa_m + M_crn_c
R_r1401	M_btcoa_m + M_crn_c	----->	M_crn_m + M_btcoa_c
R_r1418	M_h_e + M_hco3_e	<---->	M_co2_e + M_h2o_e
R_r1554	M_gly_e + M_val_L_c	<---->	M_gly_c + M_val_L_e
R_r1566	M_pro_L_c + M_ala_L_e	<---->	M_pro_L_e + M_ala_L_c
R_r2136	M_na1_e + M_pi_e	----->	M_na1_c + M_pi_c
R_r2419	M_pi_m + M_akg_c	----->	M_pi_c + M_akg_m
R_r2438	M_crn_m + M_c4crn_c	----->	M_c4crn_m + M_crn_c
R_r2525	M_gln_L_e	<---->	M_gln_L_c
R_r2526	M_ser_L_e	<---->	M_ser_L_c
R_r2532	M_asn_L_e	<---->	M_asn_L_c
R_r2534	M_thr_L_e	<---->	M_thr_L_c
R_RE2954C	M_h_c + M_pep_c + M_dtdp_c	<---->	M_pyr_c + M_dttp_c
R_RE3301C	M_h2o_c + M_ps_hs_c	<---->	M_h_c + M_ser_L_c + M_pa_hs_c
R_RNDR1	M_adp_c + M_trdrd_c	----->	M_h2o_c + M_dadp_c + M_trdox_c
R_RNDR2	M_gdp_c + M_trdrd_c	----->	M_h2o_c + M_dgdp_c + M_trdox_c
R_RNDR3	M_cdp_c + M_trdrd_c	----->	M_h2o_c + M_dcdp_c + M_trdox_c
R_RNDR4	M_trdrd_c + M_udp_c	----->	M_h2o_c + M_dudp_c + M_trdox_c
R_RPE	M_ru5p_D_c	<---->	M_xu5p_D_c
R_RPI	M_r5p_c	<---->	M_ru5p_D_c
R_SACCD3m	M_h_m + M_akg_m + M_nadph_m + M_lys_L_m	----->	M_h2o_m + M_nadp_m + M_saccrp_L_m
R_SERHL	M_ser_L_c	----->	M_h2o_c + M_2amac_c
R_SERPT	M_h_c + M_ser_L_c + M_pmtcoa_c	----->	M_co2_c + M_3dsphgn_c + M_coa_c
R_SMS	M_h_c + M_pchol_hs_c + M_crm_hs_c	----->	M_dag_hs_c + M_sphmyln_hs_c
R_SQLer	M_h_r + M_nadph_r + M_o2_r + M_sql_r	----->	M_nadp_r + M_h2o_r + M_Ssq23epx_r

R_SQLSr	$M_{h_r} + M_{nadph_r} + 2.0 * M_{frdp_r}$	----->	$M_{nadp_r} + M_{sql_r} + 2.0 * M_{ppi_r}$
R_SUCD1m	$M_{succ_m} + M_{fad_m}$	<----->	$M_{fadh2_m} + M_{fum_m}$
R_SUCOASm	$M_{atp_m} + M_{coa_m} + M_{succ_m}$	<----->	$M_{adp_m} + M_{pi_m} + M_{succoa_m}$
R_TALA	$M_{s7p_c} + M_{g3p_c}$	<----->	$M_{f6p_c} + M_{e4p_c}$
R_THFtm	M_{thf_c}	<----->	M_{thf_m}
R_TKN	$M_{atp_c} + M_{gdh_c}$	<----->	$M_{h_c} + M_{adp_c} + M_{g3p_c}$
R_TKT1	$M_{r5p_c} + M_{xu5p_D_c}$	<----->	$M_{s7p_c} + M_{g3p_c}$
R_TKT2	$M_{xu5p_D_c} + M_{e4p_c}$	<----->	$M_{f6p_c} + M_{g3p_c}$
R_TMDS	$M_{dump_c} + M_{mlthf_c}$	----->	$M_{dhf_c} + M_{dtmp_c}$
R_TPI	M_{dhap_c}	<----->	M_{g3p_c}
R_TRDR	$M_{h_c} + M_{nadph_c} + M_{trdox_c}$	----->	$M_{nadp_c} + M_{trdrd_c}$
R_TRPO2	$M_{trp_L_c} + M_{o2_c}$	----->	$M_{Lfmkynr_c}$
R_TRPt	$M_{trp_L_e}$	<----->	$M_{trp_L_c}$
R_TYRt	$M_{tyr_L_e}$	<----->	$M_{tyr_L_c}$
R_UMPK	$M_{atp_c} + M_{ump_c}$	<----->	$M_{adp_c} + M_{udp_c}$
R_URCN	$M_{h2o_c} + M_{urcan_c}$	----->	M_{4izp_c}
R_UREAt5	$M_{h2o_e} + M_{urea_e}$	<----->	$M_{h2o_c} + M_{urea_c}$
R_VALt5m	$M_{val_L_c}$	<----->	$M_{val_L_m}$
R_VALTAm	$M_{akg_m} + M_{val_L_m}$	<----->	$M_{glu_L_m} + M_{3mob_m}$
R_VALtec	$M_{val_L_e}$	<----->	$M_{val_L_c}$